For Reference

NOT TO BE TAKEN FROM THIS ROOM

Ex libris
universitatis
albertaensis




Digitized by the Internet Archive
in 2019 with funding from
University of Alberta Libraries

https://archive.org/details/Sobkowicz1982

THE UNIVERSITY OF ALBERTA

RELEASE FORM

NAME OF AUTHOR JOHN C. SOBKOWICZ

TITLE OF THESIS THE MECHANICS OF GASSY SEDIMENTS

DEGREE FOR WHICH THESIS WAS PRESENTED PhD

YEAR THIS DEGREE GRANTED Fall 1982

Permission is hereby granted to THE UNIVERSITY OF ALBERTA LIBRARY to reproduce single copies for private, scholarly or scientific research purposes only.

The author reserves other publication rights, and neither the thesis nor extensive extracts from it may be printed or otherwise reproduced without the author's written permission.

THE UNIVERSITY OF ALBERTA

THE MECHANICS OF GASSY SEDIMENTS

by

JOHN C. SOBKOWICZ

A THESIS

SUBMITTED TO THE FACULTY OF GRADUATE STUDIES AND RESEARCH

IN PARTIAL FULFILMENT OF THE REQUIREMENTS FOR THE DEGREE

OF DOCTOR OF PHILOSOPHY

in

. GEOTECHNIQUE

DEPARTMENT OF CIVIL ENGINEERING

EDMONTON, ALBERTA

FALL, 1982

82F-62D

THE UNIVERSITY OF ALBERTA

FACULTY OF GRADUATE STUDIES AND RESEARCH

The undersigned certify that they have read, and recommend to the Faculty of Graduate Studies and Research, for acceptance, a thesis entitled THE MECHANICS OF GASSY SEDIMENTS, submitted by JOHN C. SOBKOWICZ in partial fulfilment of the requirements for the degree of Doctor of Philosophy in Geotechnique.

No other success can compensate for

failure in the home...

David O. McKay

To my family,

past,

present,

and future.

ABSTRACT

This thesis examines the mechanics of gassy sediments. The term "mechanics" is used in its classical sense to refer to the study of the behaviour of a system when subjected to the action of external forces or stresses.

A gassy soil (or sediment) is defined as an assemblage of solid particles, imbued with a pore fluid which contains a large amount of gas, either dissolved in the pore liquid phase, or existing in the free state.

There are two grossly observable transient processes which are normally operative in a gassy soil. One is consolidation, which is due to the movement of the pore fluid through the solid matrix. The other is gas exsolution, which is defined in a macroscopic sense as the observed ability of the gaseous phase to move into or out of solution in the liquid phase. At the microscopic level, gas exsolution must comprise several processes, amongst which are gas sorption and bubble nucleation.

Gassy soil behaviour may be subdivided into two general categories, equilibrium and non-equilibrium. Equilibrium behaviour is that behaviour which is (or has become) independent of time. Non-equilibrium behaviour includes both transient processes and is time-dependent. The behaviour may be further described by the terms drained or undrained, referring to the flow of pore fluid through the

soil, and by immediate or long term, referring to the gas exsolution process.

The theory concerning the undrained equilibrium behaviour of gassy soils is discussed, and its predictive capabilities verified by laboratory tests. Using this theory, a distinction between gassy soil and unsaturated soil is made on the basis of:

(a) the amount of gas in the pore space.

(b) the observed behaviour of the soil.

The gas exsolution process is observed in the laboratory, both for undrained and totally drained boundary conditions. A macroscopic theory of gas exsolution is proposed for the drained case, which is compared to theories describing the behaviour of simple models subjected to the single processes of gas sorption and bubble nucleation. A finite difference solution (based on the macroscopic theory) is then developed for the undrained case, and its predictions are compared to observed behaviour.

The consolidation and gas exsolution processes are combined into one general theory of transient behaviour, which incorporates a linear elastic constitutive relationship for the soil. The resulting differential equation is non-linear, for which a finite difference solution is presented.

Pore fluid pressure changes around a shaft or borehole in a gassy soil are then examined, for the case of changing fluid pressure at the boundary, and for the case of changing total stress at the boundary, (the soil response during the undrained unloading phase is modelled in an elastic - perfectly plastic manner). The response of the shaft wall is characterized by a ground reaction curve for the soil.

RÉSUMÉ

Le sujet de cette thèse est l'étude de la mécanique des sols riches en gaz. Le terme "mécanique" est employé dans le sens classique car il réfère à l'étude des comportement d'un système soumis à l'action de forces ou de contraintes exterieures.

Un sol riche en gaz comprend un assemblage de particules solides et un liquide intersticiel contenant une grande quantité de gaz soit à l'état libre soit dissouts.

En général, on peut distinguer deux processus transitoires dans les sols riches en gaz: la consolidation et l'exsolution. La consolidation résulte du mouvement du liquide intersticiel à traver la matrice solide. L'exsolution définie au sens macroscopique comme la quantité de la phase gazeuse se dissolvant ou s'évaporant de la phase liquide. Au niveau microscopique ce processus d'"exsolution" englobe plusieurs procédés physiques tels l'absorption gazeuse et la nucleation des bulles.

Le comportement des sols riches en gaz peut se subdiviser en deux categories : l'état d'équilibre et l'état de non-équilibre. L'état d'équilibre est caractérisé par un comportement indépendent du temps. Le comportement de l'état de non-équilibre inclus l'état transitoire et la dépendence du temps. Ensuite cet état de "non-équilibre" peut être décrit en terme de comportement drainé ou non drainé

concernant l'écoulement liquide à travers le sol et en terme de comportement instantanné ou différé lorsqu'il s'agit du processus d'exsolution.

La théorie décrivant le comportement d'équilibre non drainé des sols "gazeux" est discutée et son potentiel est vérifié par la simulation de tests en laboratoire. Cette théorie permet de distinguer les sols "gazeux" des sols non saturés suite à

(a) la quantité de gaz dans les pores.

(b) le comportement observé du sol.

Le processus d'exsolution est observé en laboratoire pour les conditions aux limites non drainé et drainé. On propose une théorie macroscopique d'exsolution des gaz pour le cas drainé et on la compare à des modeles simples décrivant le processus d'absorption des gaz et de nucleation en bulles. Une solution par la méthode des différences finies est aussi développe pour le cas non drainé et les résultats sont comparés aux comportements observés.

La consolidation et le processus d'exsolution sont combinés dans une théorie générale de comportement transitoire incorporant une loi de comportement élastique et linéaire pour le sol. L'équation différentielle résultante est non linéaire et la solution est obtenue par la méthode des différences finies. Le changement des pressions intersticielles autour des puits ou des forages dans les sédiments gazeux est analysé. On examine également les changements de pressions aux limites et les changements de

contraintes totales aux limites en simulant le comportement du sol pendant le chargement non drainé par une loi elasto-plastique parfaite. Le comportement de la paroi du puit est caracterisé par une courbe de réaction du sol.

ACKNOWLEDGMENTS

I entered the University of Alberta for graduate studies in Civil Engineering in the fall of 1977, several months before the birth of our first child, Shawna Lynn. The intervening years have seen her grow into a bright and humane daughter, and have also witnessed the birth of a son, Eric Douglas. It is against this setting of a warm and loving family, and of a kind, encouraging, and loving companion, that any accomplishment here must be appreciated.

I must express my love to my parents, who have always been a motivational force in my education. I owe a deep respect for learning to them.

My thanks are extended to Murray Harris, who during my early years at Hardy Assoc. was a friend and teacher in many ways. My interest in this subject was largely stirred by discussions with him.

It is difficult to communicate my feelings for my friends and peers at the University. Learning and research in the Civil Engineering Department is conducted in a remarkably nuturing and challenging environment. Dr. Morgenstern has been a true mentor. I have stood in awe of his ability to guide my efforts in this research, and to infect me with his enthusiasm for the subject. He has

maintained a perfect balance in allowing me to seek my own direction and experience the excitement of discovery, and yet has incisively penetrated to the heart of any problem that arose. I have experienced his joy and excitement in the understanding of a new subject as acutely as my own, and sensed his respect for and dedication to this field of research.

I have also appreciated discussions with many other professors in the Department, including Dr. Eisenstein, Dr. Murray, Dr. Sego, and Dr. Kaiser. A special acknowledgment is due Dr. Forest of the Mechanical Engineering Department, who spent numerous hours educating me in the concepts of bubble nucleation and gas sorption, and who reviewed Chapter 5 of this thesis. Advice and direction was also provided in this area by Dr. Ward of the University of Toronto.

I have very fond feelings for those fellow graduate students with whom I have shared office space, and enjoyed many hours of friendship. Particular thanks must be given to Jean-Marie Konrad, Bryan Watts, Oldrich Hungr and John Agar. I will never forget the intense discussions, the table-banging and arm-waving that accompanied almost any subject, be it geotechnique or life in general. Happy hours were spent running through the beautiful trails along the river with these friends. There were many other graduate students who partook of this life, and to them all I am grateful for the experience.

The support staff at the University have been extremely helpful and friendly. My thanks are extended to O. Wood and G. Cyre for their assistance in the laboratory, A. Muir for work in the machine shop and for running the best congregating spot on campus, and R. Howells and A. Dunbar for their computing expertise.

A. Vermette very ably drafted the figures for this thesis.

It was critically reviewed by Bryan Watts and Jan Sobkowicz, both of whom performed an extra-ordinary effort.

My thanks are extended to the University, which provided financial support through various graduate assistantships, and to the Alberta Oil Sands Technology and Research Authority, which supported me by scholarships over a period of four years.

I hope to have communicated a feeling for the remarkable environment in which I have worked for the past five years. And yet I have not painted the full picture, for much friendship and guidance has been given by friends outside the University. Perhaps the most important lesson I have learned is that a man does not climb alone, nor on the backs of others, but is lifted and borne along by, and in his own turn uplifts, his fellow men. I thank God it is so, for he is the Author of all good things.

"Now the Lord had shown unto me, Abraham,
the intelligences that were organized
before the world was;
and among all these there were many
of the noble and great ones;
And God saw these souls that they were good,
and he stood in the midst of them...
and he said unto those who were with him:
We will go down, for there is space there,
and we will take of these materials,
and we will make an earth whereon these may dwell;
And we will prove them herewith,
to see if they will do all things
whatsoever the Lord their God shall command them...

Abraham 3: 22-25

TABLE OF CONTENTS

CHAPTER 1 - INTRODUCTION..... 1

1.1 GENERAL..... 1

1.2 A NEW CLASS OF SOIL..... 4

1.2.1 Oilsands..... 4

1.2.2 Deep Sea Deposits..... 6

1.2.3 Geopressure Reservoirs..... 6

1.2.4 Alto Lazio Nuclear Power Plant, Italy.... 7

1.3 NOMENCLATURE..... 8

1.4 SCOPE OF THESIS..... 12

CHAPTER 2 - EQUILIBRIUM BEHAVIOUR OF GASSY SOILS..... 15

2.1 GENERAL..... 15

2.2 LITERATURE REVIEW..... 17

2.3 BOYLES & HENRY'S LAWS..... 22

2.4 COMPRESSIBILITY OF THE PORE FLUIDS..... 25

2.4.1 Compressibility of a gas..... 25

2.4.2 Compressibility of a pure liquid..... 27

2.4.3 Compressibility of an immiscible gas - liquid mixture..... 27

2.4.4 Compressibility of a partly miscible gas-liquid mixture..... 27

2.5 THEORETICAL PORE PRESSURE RESPONSE..... 29

2.6 EQUILIBRIUM UNDRAINED PORE PRESSURE RESPONSE..... 34

2.7 UNSATURATED OR GASSY?..... 39

2.8 SUMMARY..... 46

CHAPTER 3 - THE LABORATORY INVESTIGATION..... 47

3.1 GENERAL..... 47

3.2 CONSIDERATIONS FOR THE DESIGN OF TEST EQUIPMENT.... 49

3.3 DEVELOPMENT OF EQUIPMENT..... 50

3.3.1 Membrane and cell fluid considerations... 51

3.3.2 Measuring strains or volume changes..... 66

3.3.3 Measuring pressures..... 76

3.3.4 Measuring Deviator Stress..... 78

3.3.5 Saturating water with CO_2 gas..... 79

3.3.6 General cell design considerations..... 79

3.4 TESTING PROGRAM..... 87

3.5 TESTING PRELIMINARIES..... 89

3.5.1 Sample preparation..... 89

3.5.2 Saturation with water..... 92

3.5.3 Isotropic compressibility..... 93

3.5.4 Test for full saturation..... 93

3.5.5 Saturation with water and dissolved CO_2 gas..... 94

3.6 TESTING PROCEDURE..... 94

3.7 TEST RESULTS..... 95

3.7.1 Isotropic Tests..... 99

3.7.2 Anisotropic Tests.....102

3.7.3 Tests to failure.....125

3.8 SUMMARY.....137

CHAPTER 4 - EVALUATION OF LABORATORY TESTS -
UNDRAINED EQUILIBRIUM RESULTS..... 139
4.1 GENERAL..... 139
4.2 EQUILIBRIUM BEHAVIOUR..... 140
4.2.1 Effects of gas diffusion and leakage..... 142
4.2.2 Evaluating non-isotropic tests..... 143
4.2.3 Non-equilibrium at the start of a test... 148
4.2.4 Modification of test results due to dissolved air..... 152
4.3 PORE PRESSURE RESPONSE..... 154
4.3.1 Isotropic tests..... 154
4.3.2 Constant K tests..... 154
4.3.3 Tests to failure..... 163
4.4 COMPARISON OF OBSERVED AND PREDICTED BEHAVIOUR..... 163
4.5 NON-EQUILIBRIUM BEHAVIOUR..... 176
4.6 SUMMARY..... 188
CHAPTER 5 - GAS EXSOLUTION..... 189
5.1 GENERAL..... 189
5.1.1 Previous work on gas exsolution..... 192
5.2 GAS SORPTION..... 193
5.3 SINGLE BUBBLE IN AN INFINITE MEDIUM..... 195
5.3.1 Surface tension, pressure and equilibrium bubble size..... 196
5.3.2 The time variation of bubble size..... 200
5.4 SINGLE BUBBLE IN A FINITE VOLUME OF LIQUID..... 206
5.4.1 Equilibrium Bubble Size..... 206
5.4.2 Bubble size as a function of time..... 212

5.5 BUBBLE NUCLEATION..... 217
5.6 OBSERVED BEHAVIOUR & A MACROSCOPIC THEORY OF EXSOLUTION..... 223
5.7 AN EVALUATION OF THE GENERAL GAS EXSOLUTION RELATIONSHIP..... 240
5.8 SUMMARY..... 241
CHAPTER 6 - EVALUATION OF LABORATORY RESULTS - UNDRAINED TRANSIENT RESPONSE..... 243
6.1 GENERAL..... 243
6.2 THEORETICAL CONSIDERATIONS, TRANSIENT UNDRAINED BEHAVIOUR..... 244
6.2.1 Uncoupled solution..... 245
6.2.2 "Coupled" solution..... 248
6.3 ANALYSIS..... 251
6.4 COMPARISON OF PREDICTED AND OBSERVED BEHAVIOUR..... 253
6.4.1 An Evaluation of Henry's constant..... 164
6.4.2 Variation of E with initial saturation... 170
6.5 SUMMARY..... 274
CHAPTER 7 - A COMBINED, GENERAL THEORY OF CONSOLIDATION AND GAS EXSOLUTION..... 276
7.1 INTRODUCTION..... 276
7.2 A GENERAL THEORY..... 278
7.3 NUMERICAL SOLUTION..... 284
7.4 APPLICATION OF THE NUMERICAL SOLUTION..... 288
7.4.1 Consolidation/gas exsolution around a borehole..... 291
7.5 SUMMARY..... 307

CHAPTER 8 - FLUID RESPONSE AROUND A BOREHOLE OR SHAFT IN A GASSY SOIL..... 308
8.1 INTRODUCTION..... 308
8.2 IMMEDIATE AND UNDRAINED RESPONSE..... 311
8.2.1 Stresses..... 312
8.2.1.1 Stresses in the elastic zone..... 312
8.2.1.2 Stresses in the Plastic Zone..... 313
8.2.1.3 Radius of the Plastic Zone..... 313
8.2.1.4 Stress in the z-direction..... 314
8.2.2 Strains..... 316
8.2.2.1 Strains & displacements due to unloading..... 318
8.2.2.2 Volumetric strains..... 319
8.2.3 Undrained, immediate pressure response.... 321
8.3 ANALYSIS OF THE TRANSIENT FLUID PRESSURE PROFILE... 322
8.4 IMPLICATIONS OF THE TRANSIENT ANALYSES..... 334
8.5 GROUND REACTION CURVES & STAND-UP TIMES..... 335
8.5.1 Drained, or undrained?..... 338
8.5.2 Time-dependent ground reaction curves..... 343
8.6 SUMMARY..... 345
CHAPTER 9 - SUMMARY & CONCLUSIONS..... 346
9.1 GENERAL..... 346
9.2 RESTATEMENT OF OBJECTIVES..... 346
9.3 HIGHLIGHTS OF THE RESEARCH..... 346
9.4 SUGGESTIONS FOR FURTHER RESEARCH..... 353
BIBLIOGRAPHY..... 355

APPENDIX A - GAS EXSOLUTION IN AN UNDRAINED ELEMENT OF SOIL - COMPUTER PROGRAM..... 371

APPENDIX B - PLOTS FOR GAS DIFFUSION THROUGH SAMPLE MEMBRANE..... 374

APPENDIX C - ISOTROPIC TEST RESULTS - TESTS 7, 9, 23... 390

APPENDIX D - CONSTANT STRESS RATIO TEST RESULTS - TESTS 12, 15, 22..... 430

APPENDIX E - TESTS TO FAILURE - TESTS 12, 22, 13, 14... 460

APPENDIX F - COMPUTER PROGRAM TO MODEL UNDRAINED LABORATORY TESTS..... 494

APPENDIX G - P vs t BEHAVIOUR FOR ALL UNDRAINED TESTS - COMPARISON OF ACTUAL AND PREDICTED BEHAVIOUR..... 502

APPENDIX H - COMPUTER PROGRAM FOR CONSOLIDATION - GAS EXSOLUTION MODEL..... 524

LIST OF TABLES

Table		Page
2.1	Theoretical undrained equilibrium pore pressure response in a gassy soil	37
2.2	Theoretical undrained equilibrium pore pressure response in an unsaturated soil	41
3.1	Summary of gas diffusion tests	58
4.1	Summary of all undrained tests	141
4.2	Initial conditions for Test No. 11	168
4.3	Test No. 11 - Predicted results (Analysis #1)	170
4.4	Test No. 11 - Predicted results (Analysis #2)	171
4.5	Summary of non-linear regression parameter on all undrained tests	187
6.1	E vs S_g for all undrained tests	271
7.1	Insitu conditions for F.D. analysis of consolidation/gas exsolution problem	294
7.2	Parameters for consolidation/gas exsolution analysis	298
8.1	Input parameters for Borehole analysis	323
8.2	Input parameters for Borehole analysis	324
8.3	Undrained ground reaction curve calculations	341

LIST OF FIGURES

Figure		Page
2.1	Element of soil	16
2.2	Soil mechanics terminology	18
2.3	Henry's constant vs temperature for CO_2 & N_2	26
2.4	Spring analogy for unsaturated soils	31
2.5	Theoretical undrained equilibrium response, gassy soil	38
2.6	Theoretical undrained equilibrium response, unsaturated soil	42
2.7	Relationship between gassy and unsaturated soil behaviour	45
3.1	Lateral and axial strain response, Sample 18	62
3.2	Lateral and axial strain response, Sample 21	63
3.3	Gas diffusion through membrane, Sample 15	65
3.4	Original deformation gauges	69
3.5	Detail of vertical deformation gauge	69
3.6	Detail of horizontal deformation gauge	70
3.7	Modified horizontal gauge, detail of point contact	73
3.8	Modified horizontal gauge, detail of LVDT mounting	73
3.9	Comparison of vertical and horizontal strains, Test 21	75
3.10	Design of light weight Lateral Strain indicator	77
3.11	Triaxial loading frame	80
3.12	Calibration for ram friction	81
3.13	Hourly temperatures at Edmonton	84

Figure		Page
3.14	Testing station	86
3.15	Stress paths for undrained tests on gassy soil	88
3.16	Typical grain size analysis	90
3.17	Compaction curve, Ottawa sand	91
3.18	Isotropic undrained loading test on a gassy soil	96
3.19	Isotropic stress-strain behaviour, Test 11	100
3.20	Stress-strain behaviour, Test 11	101
3.21-3.32	Transient pore pressure response, Test 11, Phases A to M	103-114
3.33	Deviatoric stress-strain response, Test 21	116
3.34	Constant K stress path, Test 21	116
3.35	Stress-strain behaviour, Test 21	117
3.36	Volumetric vs axial strain, Test 21	118
3.37	Stress ratio vs strain, Test 21	118
3.38-3.43	Transient pore pressure response, Test 21, Phases A to F	119-124
3.44	Stress path to failure, Test 21	126
3.45	Stress-strain response to failure, Test 21	128
3.46	Volumetric vs axial strain, Test 21 (failure)	130
3.47	Stress ratio vs axial strain, Test 21	130
3.48-3.53	Transient pore pressure response, Test 21, Phases G to L, (failure)	131-136
4.1-4.4	Total stress vs pore pressure, isotropic undrained tests	155-158
4.5-4.8	Total stress vs pore pressure, constant stress ratio undrained tests	159-162

Figure		Page
4.9-4.10	Total stress vs pore pressure, undrained tests to failure	164-165
4.11	Predicted and observed pore pressure, Test 11	172
4.12-4.15	Pressure - time data, Test 11D	178-179
4.16-4.24	Non-linear regression, pore pressure vs time, Test 11A to 11J	181-185
5.1	Volumetric strain vs time for psuedo-drained tests	230
5.2	Relationship between V_{fg} and time in psuedo-drained tests	232
5.3-5.7	Non-linear regression on volumetric strain vs time for psuedo-drained tests	234-238
6.1	Flowchart for computer program to analyze undrained transient response of a gassy soil	254
6.2-6.11	Analysis of undrained equilibrium and transient response, Test 11B to 11M	255-259
6.12-6.13	Analysis of transient response, Test 11B to 11C	263
6.14-6.19	Undrained analysis, Test 11E, varying H	266-268
6.20	Undrained analysis, Test 11C, H=0.02, K'=4410	269
7.1	Idealized consolidation/gas exsolution problem	293
7.2	Finite difference mesh for consolidation/ gas exsolution problem	295
7.3	Comparison between theoretical and F.D. solutions to consolidation problem	297

Figure		Page
7.4-7.14	Transient pore pressure response for consolidation/gas exsolution problem	299-304
8.1	Flow chart for iteration technique for effective stress at borehole or shaft wall	325
8.2	Stress path for point on borehole wall during unloading	327
8.3-8.10	Transient pore pressure profiles, borehole analyses	329-332
8.11	Ground and support reaction curves	337
8.12	Ground reaction curve, drained analysis	339
8.13	Ground reaction curves, undrained analyses	342

LIST OF SYMBOLS

The following is a list of the commonly used symbols in this thesis. It has not been possible to avoid the multiple use of several symbols, particularly when the equations and theory cited have originated from several different fields of engineering and science. Where the use of symbols differs from that listed below, the symbol will be defined in the text, immediately following its first occurrence.

SYMBOL	MEANING
A,B,C	Constants used in undrained pore pressure response equation
a_v	Coefficient of compressibility
c	Gas concentration
D	Partial differential
d	Exact differential
E	Gas exsolution constant
	Young's modulus (Chapter 8)
e	Void ratio
H	Henry's constant
I	Radius of plastic zone
$\underline{H}$	Non-equilibrium ratio of dissolved gas/water volume
J	Rate of bubble formation
K	Coefficient of diffusion (Chapter 5)
	Hydraulic conductivity (Chapter 6 ff)
K'	Total volume of gas * Pressure
k	Constant
m	Mass
N	Number of bubbles
n	Porosity
P	Pressure (absolute)

LIST OF SYMBOLS (CONT.)

SYMBOL	MEANING
R	Radius of borehole or shaft
r	Radius (usually, of bubble)
r_c	Critical radius
r_e	Equilibrium radius
r_m	Maximum radius
S	Saturation
T	Temperature
T_s	Surface tension
t	Time
U	Radial displacement
u	Fluid pressure (gauge)
V	Volume
v	Velocity
W	Weight of water
W_s	Weight of solids
w	Water content
x,y,z	Spacial coordinates
β	Compressibility
Δ	Finite change
σ	Normal stress
ϕ	Angle of internal friction
∞	Infinity
ρ	Density
γ	Unit weight
θ	Angular coordinate
ε	Strain
τ	Shear stress
ν	Poisson's ratio
$\fallingdotseq$	Approximately equal to
$\sim$	Is proportional to

Subscripts and superscripts on following page

LIST OF SYMBOLS (CONT.)

SUBSCRIPTS

SYMBOL	MEANING
a	Atmospheric
av	Average
dg	Dissolved gas
f	Fluid
g	Gas
fg	Free gas
i	Liquid/gas interface
h	Horizontal
L or l	Liquid
l/g	Liquid/gas saturation
s	Saturated (gas in liquid)
Tg	Total gas
T	Tunnel, or
	Total
v	Vertical
w	Water
0	Initial

SUPERSCRIPTS

0	Initial
1	Final
'	Effective
e	Elastic
p	Plastic
t	Total (stress)

CHAPTER 1 - INTRODUCTION

1.1 GENERAL

Soil mechanics is the study of the fluid conductivity, volume change and strength behaviour of an assemblage of particles, and may be rightly thought of as particulate mechanics. It is normally subdivided into three broad groups: dry soil, wet soil with no flow or constant flow (undrained and fully drained cases) and wet soil with transient flow.

Initially, the study of wet soils was confined to soils saturated with water. Terzaghi's hypothesis of "effective stress" was based upon the observed deformation and strength behaviour of saturated soils. It is saturated soil that the practising engineer in temperate climates deals with in the majority of soil mechanics problems.

However, there are also two classes of unsaturated soil which have been recognized. The first class is related to the construction of earth fill dams, road beds, airport runways and backfill for earth-retaining structures, using remolded, compacted material which is partially saturated; or to many dry areas of the earth that have not experienced active erosional or depositional processes over recent geological time, and have developed deep layers of residual soils which are partially saturated. In both these instances, the practising engineer has developed methods of designing structures built of or on such soils, and the

theoretical engineer has conducted research into ways of extending classical soil mechanics theories to incorporate these materials.

This class of unsaturated soil, which is now commonly recognized and understood reasonably well, has been described as a three phase system consisting of solid particles, water and air. The pore fluids have a distinct characteristic, in that the gas phase is only slightly soluble in the liquid phase. This has a profound effect on the observed soil behaviour.

More recently, however, and mostly associated with the exploration for and exploitation of new energy resources, another class of unsaturated soil has been recognized. This class possesses two characteristics which dominate the soil behaviour:

(a) There is a large amount of gas dissolved in the pore fluid, either because:

(i) the gas is very soluble, such as is the case for methane or CO_2 in water or bitumen, or

(ii) the insitu fluid pressures are initially very high, so that even with low solubility the reduction to near atmospheric pressures causes the production of large volumes of gas.

In both of these instances, it is not uncommon to have the potential of producing a volume of gas several to tens of times larger than the initial volume of voids in the soil.

(b) The soil exhibits a low hydraulic conductivity, either because:

(i) the absolute permeability is low, such as is seen in lacustrine and marine deposits, or

(ii) one or several of the pore fluids has a high viscosity. The oilsands found in the Athabasca, Cold Lake and Peace River areas of Alberta are typical of this class of material. They comprise a dense aggregate of coarse silt to fine sand size particles, of very uniform grading. Water saturated samples may exhibit hydraulic conductivities in the order of 10^{-3} to 10^{-4} cm/sec.,(Agar, 1982). However, the exploitable oil-rich samples have hydraulic conductivities as low as 10^{-8} to 10^{-9} cm/sec. at in-situ temperatures, (Dusseault, 1980).

As a consequence of the large volumes of dissolved gas in such materials, undrained pore pressures are high, and are only reduced to near atmospheric values if either:

(a) a long time is available for consolidation and diffusion of gas from the system, or

(b) effective stresses are reduced to such a small value that actual disruption of the soil fabric occurs, with an increase of permeability and a venting of the gas phase.

Commonly for such soils, the pore size, the pore pressure and the gas saturation are high enough that differences in fluid pressure in the gas and liquid phases are insignificant and can be ignored. This idea will be addressed further in Chapter 2.

This class of material will be referred to as a "gassy" soil. The term "gassy" is meant to have a very specific meaning in the context of this thesis, which will be developed further in this chapter, and in Chapter 2. The following section discusses several instances where such a soil has been recognized in the literature, and the observed behaviour correctly attributed to the phenomenon of large volumes of dissolved gas.

1.2 A NEW CLASS OF SOIL

1.2.1 Oilsands

The oilsands of the Athabasca region in Alberta have been under study by engineers and scientists since the early 1920's. Ells(1926) reported on the escape of gas from oilsands during drilling and excavation. Hardy and Hemstock (1963) were the first to recognize the significant geotechnical implications of gas in the oilsands, describing both the loss of strength and change in deformation properties accompanying gas exsolution. Sample disturbance and insitu vs disturbed strength in the oilsands has been discussed thoroughly by Dusseault (1977,1980).

Insitu, oilsand is an extremely dense, uncemented fine-grained sand. It exhibits low compressibilities and high strengths (Dusseault & Morgenstern, 1978a,b). As mentioned above, hydraulic conductivities for samples with no bitumen are on the order of 10^{-4} cm/sec. However, the presence of a highly viscous bitumen reduces the hydraulic conductivity of oil-rich samples to 10^{-8} to 10^{-10} cm/sec. Hardy & Hemstock reported a bitumen viscosity of $1.3 * 10^{5}$ mPas (1mPas = 1 centipoise) and Carrigy (1967) reports insitu viscosities from several hundred to several tens of thousands of Pascal-seconds.

Upon reduction of confining stress (and thus pore pressure) dissolved gas tends to come out of solution in large quantities. Both methane and CO_2 are present in substantial amounts in the pore water and bitumen. In the undrained case, this leads to the maintenance of insitu pressures or alternatively to the production of large volume changes, which cause a loss of strength and an increase in compressibility.

Particular observations of this phenomenon have included:

(a) disturbance of core samples: swelling, splitting longitudinally and diametrically, effervescence, and corrugation (Hardy & Hemstock, 1963).

(b) excavations for foundations: excessive swelling (heave) and softening of materials at the base of the excavation, followed by settlement on reloading.

(c) slopes: swelling, softening and surficial "slabbing" of material leading to retrogression and overall flattening of steep slopes in oilsand.

(d) pore pressures within slopes: initial decrease in pore pressures due to unloading followed by time-dependent increases in part due to gas exsolution.

1.2.2 Deep Sea Deposits

Okumura (1977) reported on the disturbance of samples taken just below the sea floor, but subjected to initial pore pressures equivalent to 100 to 10,000 meters of overlying water. These marine sediments were of low permeability and saturated with water and dissolved air. Although the solubility of air in water is small, he calculated that the large decreases in pressure on retrieval of the sample would lead to substantial decreases in effective stress.

1.2.3 Geopressure Reservoirs

A conference was held on the "Geotechnical and Environmental Aspects of Geopressure Energy" in 1980 (Saxena, 1980) which discussed the possibility of exploiting deeply buried gas reserves in the Gulf Coast.

These reserves are found in upper Cretaceous and Tertiary sediments, buried to depths of 3300 to 4400 meters. The reservoirs are wedge-shaped and faulted, and contain saline waters with dissolved methane gas. Reduction of insitu fluid pressures (57 to 80 Mpa) to atmospheric would

produce 20 to 30 SCF of gas per barrel of water, a volume 4 to 6 times the insitu void volume.

1.2.4 Alto Lazio Nuclear Power Plant, Italy

From 1978 to 1981, excavations were made at the sites for ENEL VI & VIII Nuclear Power Plants in Alto Lazio, Italy (D'Appolonia, 1981). The excavation was approximately 320 meters by 380 meters in size and progressed in stages to a depth of approximately 10 meters.

The site is underlain by about 25 m of sands and gravels (unit II), 30 m of silty clay (unit III), 15 m of silty sand (unit IV), and at least 130 m of clay (unit V). Units III and IV were found to contain CO_2 gas in solution in the pore fluids, which exsolved with a reduction in total stress and pore water pressure. Unit IV was relatively permeable and showed little pore pressure response to either unloading or dewatering processes. Unit III, however, was relatively impermeable and pore pressures in this zone responded well to changes in total stress due to excavation. During the early part of the excavation, before the upper aquifer (Unit II) was dewatered, Unit III showed an immediate response to unloading. B values (Skempton, 1954) in the order of 0.4 to 0.6 were measured. The initial water saturations in this layer were greater than 95%, and based on measured soil compressibility, B > .90 was expected. Hence there was an indication of a less sensitive pore pressure response due to the exsolution of gas during the excavation period. The measured heaves were limited to about 15 cm

(total) and 5 cm due to units III & IV, since the reduction in effective stress at this depth was not large. The development of this deformation in layer III may have been speeded up by the exsolution of gas, however.

1.3 NOMENCLATURE

It is necessary at this point to mention several items of nomenclature to avoid future confusion.

Saturation

In soil mechanics, the term saturation has been used exclusively to describe the proportion of the pore space occupied by a particular fluid. For example, a sample of oilsand may have a void volume of 100 cm^3, distributed as 5 cm^3 of free gas, 75 cm^3 of bitumen and 20 cm^3 of water. The terms 5% gas saturation, 75% bitumen saturation and 20% water saturation are then applicable. If the term "saturation" is not modified by some adjective, it is understood to imply saturation of water in the voids.

In speaking of mixtures of liquid and gas, however, it is also possible to use the term saturation in referring to the amount of gas dissolved in the liquid divided by the maximum amount dissolvable, at a particular pressure and temperature. Thus, water is saturated with air at atmosperic pressure and room temperature when it contains two per cent by volume of dissolved air. It is possible for the water to be undersaturated, and if it is at equilibrium, no free gas will be present in the system; or if there is some free

gas present, it will be dissolving in time and a state of disequilibrium will prevail. It is also possible for water to be momentarily oversaturated with air, which again is a disequilibrium state.

The terms "saturation", "gas saturation", "water saturation", etc. where used alone in this thesis will refer to the former meaning, (i.e. the condition of the pore spaces), whilst use of the terms in referring to liquid-gas equilibrium will be indicated by appropriate modifiers.

Liquid-gas saturation pressure

An additional term, the "liquid-gas saturation pressure", ($P_{l/g}$) will be used in reference to a closed system of liquid and gas. It will mean that pressure at which the liquid in the system is just saturated with gas - no free gas exists and the system is at equilibrium. This is equivalent to the term "bubble pressure" used in petroleum engineering.

It is clear that for an undrained system the liquid-gas saturation pressure is dependent upon only two variables, the ratio of volume of total gas to volume of liquid, and the temperature. For any natural soil, the insitu (equilibrium) conditions may be of three types:

(a) liquid and free gas; $p < p_{l/g}$

(b) liquid saturated with gas; $p = p_{l/g}$

(c) undersaturated liquid; $p > p_{l/g}$

Undrained, Drained, Short and Long Term Behaviour

The terms "undrained" and "drained", "short" and "long" term behaviour also need clarification. It is common, when evaluating a problem in soil mechanics, to bound the anticipated behaviour of soil by looking at the extremes of undrained and drained boundary conditions. An undrained condition refers to that situation where no pore fluids are permitted to move across the boundaries of a soil element, and is practically only achievable either where the boundary condition can be imposed (such as in a laboratory test) or where the permeability of the soil is so low that no measurable drainage may occur over a specified time interval. Total stress changes at the soil boundary result in both pore and effective stress changes in the soil element, and depending on the relative compressibilities of the soil skeleton and the pore fluid, some volume change may occur. For most saturated soils, it is a reasonable assumption to say that the volume change is zero and that the total stress changes are almost completely transformed into changes in pore fluid pressure. At the other extreme, "drained" behaviour refers to the soil element which provides no hindrance to movement of pore fluids, so that any changes in total stress at a boundary are supported completely by changes in effective stress. Any intermediate condition of partial drainage is also possible.

For saturated soils, it is common to equate the terms "undrained" and "short term" behaviour, and "drained" and "long term" behaviour, since the only operative transient process is consolidation. For a gassy soil, however, they are not equivalent. It is most important to recognize that a second transient process of gas exsolution exists, which will also cause changes in pore pressure with time, so that it is possible to have both short and long term undrained responses, if the exsolution process is much faster than the consolidation process, or if the undrained boundary condition is enforced.

Gas Exsolution

The term gas exsolution, introduced above, will be used in a general way in this thesis to refer to all those processes going on at a microscopic scale that lead to our macroscopic observation that gas is either "dissolving" or "coming out of solution". These microscopic processes include, (but are not limited to), gas sorption, (i.e. absorption or desorption), which refers to the transfer of gas from the free (bubble) state to the dissolved state across a liquid-gas interface (or vice versa); and bubble nucleation, that physical phenomenon which determines where, how many, at what size and at what rate gas bubbles will form in the soil. The concept of gas exsolution is discussed in more detail in Chapter 5.

Gassy Soils

Lastly, the term "gassy soil" will be used throughout this thesis to refer specifically to that material which contains a relatively large volume of gas either dissolved in the pore liquids or existing in the free state. The determination of what constitutes a "large" volume is somewhat subjective, but for general purposes may be defined as a volume which, measured at atmospheric pressure, is at least several times the saturated void volume.

The definition of a gassy soil is fairly complex. The concepts are treated further in Chapter 2, and a practical means of distinguishing between "gassy" and "unsaturated" soils is given in Section 2.7.

The word "gassy" is used to avoid the confusion inherent in the word "gas-saturated", which already has several specific meanings.

1.4 SCOPE OF THESIS

It is the purpose of this thesis to discuss the mechanics of the behaviour of gassy soils subjected to changes in boundary stresses. This behaviour may be divided into two groups, equilibrium and non-equilibrium.

Equilibrium behaviour is the simplest to formulate analytically, as there are no rate processes involved. The physics describing the pressure-volume relationship for free gas and the relationship between volume of dissolved gas and pressure is well understood and has been treated

theoretically in the literature. This information will be summarized in Chapter 2.

Although the equilibrium behaviour has been discussed and modelled to explain field behaviour, it has not (for gassy soils) been verified quantitatively in the laboratory. Chapter 3 will describe the laboratory investigation undertaken to provide such verification, and the results will be discussed in Chapter 4.

Less is known about the non-equilibrium case, and no attempt has been made to formulate a proper theory. There are several reasons for this. Although it is possible to speculate on the microscopic processes responsible for gas exsolution, these are not completely catalogued nor well understood for soils. Those processes which are thought to have a dominant role, gas sorption and nucleation, can be modelled only for the simplest of boundary conditions, and indeed currently form the frontiers for research in several fields of mechanical and chemical engineering. Application of these ideas to soil problems is difficult because of our incomplete knowledge of the complex boundary conditions in soils.

Hence this research approaches the non-equilibrium behaviour from an observational point of view. Laboratory investigations of the transient behaviour for both the undrained and drained cases are presented in Chapter 3. A physical "law" is postulated for the exsolution process on

the basis of the observed (macroscopic) behaviour in Chapter 5, and an attempt is made to support this hypothesis by considering the dominant microscopic processes.

The laboratory results for non-equilibrium behaviour are analyzed in Chapter 6, first for the drained case, on which the macroscopic gas exsolution hypothesis is based, and then for the undrained case.

A general theory of partially-drained behaviour is then developed in Chapter 7 which incorporates consolidation, gas expansion and gas exsolution. Finally, this is applied to the problem of fluid pressure responses around a borehole, shaft, or tunnel in Chapter 8. Immediate pore fluid response is determined in the plastic zone surrounding a shaft, and then the transient response due to consolidation/exsolution is examined. The determination of ground reaction curves for a shaft in a gassy soil is also discussed.

CHAPTER 2 - EQUILIBRIUM BEHAVIOUR OF GASSY SOILS

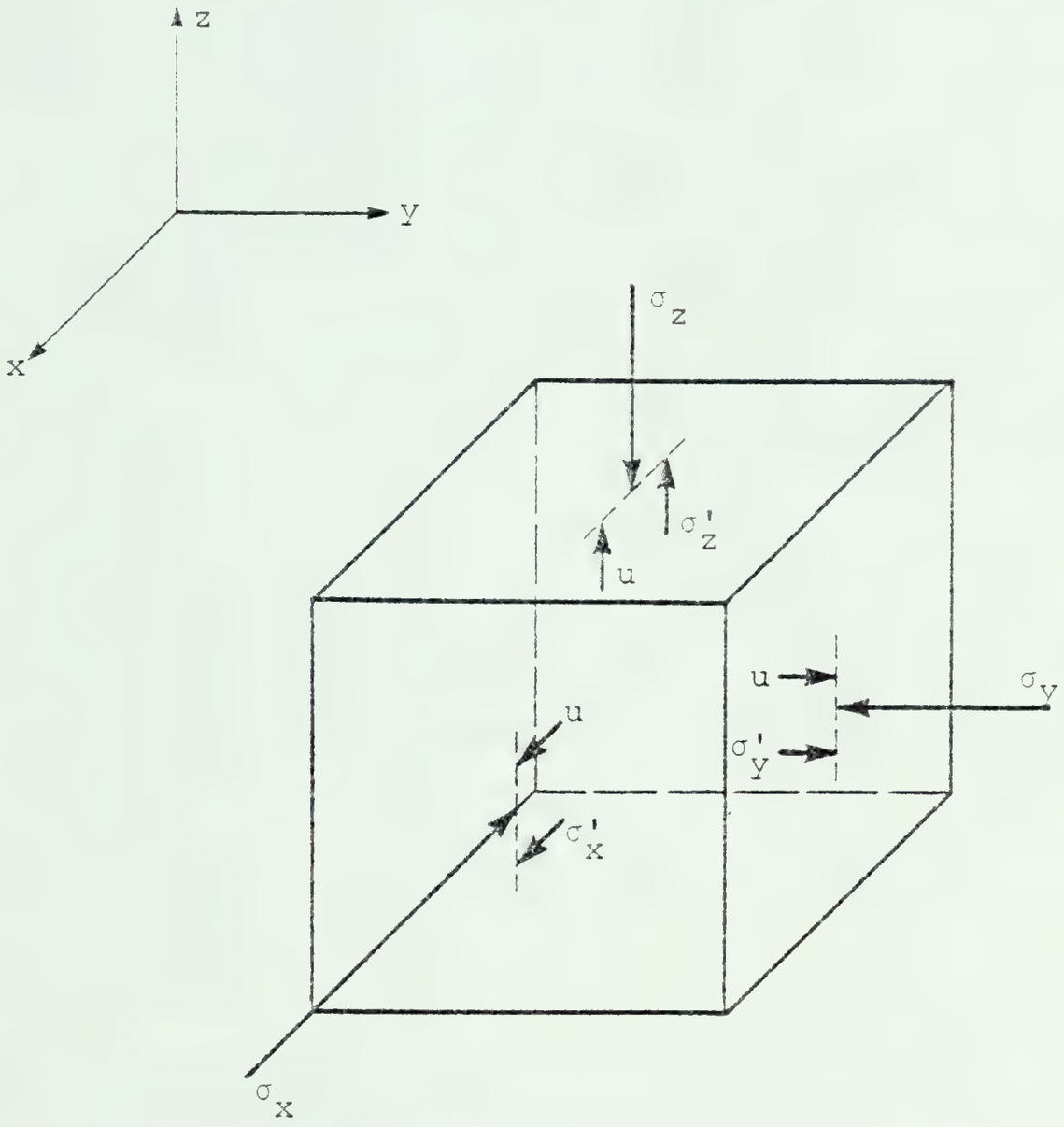
2.1 GENERAL

It is the intent of this chapter to provide a general introduction to the physical behaviour of unsaturated and gassy soils. Only the equilibrium behaviour of such soils will be considered, which means that behaviour which is governed by processes which are or have become independent of time.

Consider an element of soil (Figure 2.1) which has an undrained boundary and which is subjected to known total stresses along that boundary. The soil itself consists of solid particles which are in contact with each other and form a continuous, 3-dimensional network referred to as the "soil skeleton". The interstices, or pores, are occupied by one or several fluids, which may be either a gas or a liquid or a mixture of several gases and/or liquids.

The total stress applied at the boundaries of this element are carried internally by a stress acting in the soil skeleton and a stress acting in the pore fluid. The latter is referred to as the pore pressure; the former is characterized by the "effective stress", which is that portion of the average intergranular stress in excess of the pore pressure multiplied by the areal porosity.

Any change in total stress on the boundary of this element will be accompanied by a change in both the pore pressure and the effective stress, and also by a change in



Single arrows represent a stress acting on the full face of the element

Figure 2.1 - Undrained element of soil - External total stresses supported internally by an effective stress and a pore pressure.

the volume of the element. It will be desirable to describe this behaviour both in the short term, before gas exsolution processes have time to act, and in the long term, after gas exsolution is complete. (The discussion of the transient or non-equilibrium response is left until Chapter 5).

The standard soil mechanics terminology will be applied in describing the volume and weight relationships for this element of soil (Figure 2.2).

First, a review of the literature on the strength and volume changes in unsaturated soils will be made. This will be followed by a brief discussion of the physical laws governing free and dissolved gas behaviour and how this influences the compressibility of pore fluids. Fredlund (1973) has treated this subject in detail, and only a summary of the important points will be given here. The implications of such undrained behaviour will then be investigated for an element of gassy soil.

2.2 LITERATURE REVIEW

Engineers have long appreciated the fact that in the absence of drainage, considerable pore pressures may develop in compacted earth fills and dams. The soil comprising the fill is remolded and thus unsaturated due to its initial excavation and handling. The magnitude of the pore pressure response is dependent mainly upon the degree of compaction, the initial water content, and the self-weight of the soil.

	Property		Saturated sample (W_s, W_w, G, are known)	Unsaturated sample (W_s, W_w, G, V are known)	Supplementary formulas relating measured and computed factors			
Volume components	V_s	volume of solids	$\frac{W_s}{G\gamma_w}$		$V-(V_a+V_w)$	$V(1-n)$	$\frac{V}{(1+e)}$	$\frac{V_v}{e}$
	V_w	volume of water	$\frac{W_w}{\gamma_w}$		V_v-V_a	SV_v	$\frac{SV_s}{(1-e)}$	$SV_s e$
	V_a	volume of air or gas	zero	$V-(V_s+V_w)$	V_v-V_w	$(1-S)V_v$	$\frac{(1-S)V_s}{(1-e)}$	$(1-S)V_s e$
	V_v	volume of voids	$\frac{W_w}{\gamma_w}$	$V-\frac{W_s}{G\gamma_w}$	$V-V_s$	$\frac{V_s n}{1-n}$	$\frac{V_s e}{(1-e)}$	$V_s e$
	V	total volume of sample	V_s+V_w	measured	$V_s+V_a+V_w$	$\frac{V_s}{1-n}$	$V_s(1+e)$	$\frac{V_v(1+e)}{e}$
	n	porosity	$\frac{V_v}{V}$		$\frac{1-V_s}{V}$	$1-\frac{V_s}{GV\gamma_w}$	$\frac{e}{1+e}$	
	e	void ratio	$\frac{V_v}{V_s}$		$\frac{V}{V_s-1}$	$\frac{GV\gamma_w}{W_s}-1$	$\frac{wG}{S}$	$\frac{n}{1-n}$ | $\frac{wG}{S}$
Weights for specific sample	W_s	weight of solids	measured		$\frac{V_t}{(1+w)}$	$GV\gamma_w(1-n)$	$\frac{wV_v G}{eS}$	
	W_w	weight of water	measured		wW_s	$SV_w V_v$	$\frac{eW_s S}{G}$	
	W_t	total weight of sample	W_s+W_w		$W_s(1+w)$			
Weights for sample of unit volume	γ_D	dry unit weight	$\frac{W_s}{V_s+V_a}$	$\frac{W_s}{V}$	$\frac{W_t}{V(1+w)}$	$\frac{G\gamma_w}{(1+e)}$	$\frac{G\gamma_w}{1+wG\ S}$	
	γ_T	wet unit weight	$\frac{W_s+W_w}{V_s+V_a}$	$\frac{W_s+W_w}{V}$	$\frac{W_t}{V}$	$\frac{(G+Se)\gamma_w}{(1+e)}$	$\frac{(1+w)\gamma_w}{w/S+1/G}$	
	γ_{SAT}	saturated unit weight	$\frac{W_s+W_w}{V_s+V_w}$	$\frac{W_s+V_v\gamma_w}{V}$	$\frac{W_s}{V}+\left(\frac{e}{1+e}\right)\gamma_w$	$\frac{(G+e)\gamma_w}{(1+e)}$	$\frac{(1+w)\gamma_w}{w+1/G}$	
	γ_{SUB}	submerged (buoyant) unit weight	$\gamma_{SAT}-\gamma_w$		$\frac{W_s}{V}-\left(\frac{1}{1+e}\right)\gamma_w$	$\left(\frac{G-e}{1+e}-1\right)\gamma_w$	$\left(\frac{1-1/G}{w+1/G}\right)\gamma_w$	
Combined relations	w	moisture content	$\frac{W_w}{W_s}$		$\frac{W_t}{W_s}-1$	$\frac{Se}{G}$	$S\left[\frac{\gamma_w}{\gamma_D}-\frac{1}{G}\right]$	
	S	degree of saturation	1.00	$\frac{V_w}{V_v}$	$\frac{W_w}{V_v\gamma_w}$	$\frac{wG}{e}$	$\frac{w}{\frac{\gamma_w}{\gamma_D}-\frac{1}{G}}$	
	G	specific gravity	$\frac{\gamma_s}{\gamma_w}$		$\frac{Se}{w}$			

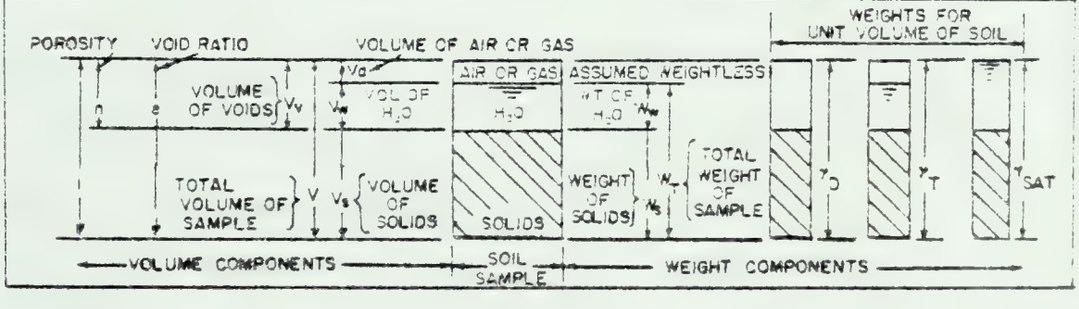


Figure 2.2 - Soil volume and weight relationships (after NAVFAC DM-7, 1971)

Several early publications from the U.S. Bureau of Reclamation, appearing in the II International Conference on Soil Mechanics and Foundation Engineering, (Hilf, 1948; Walker and Daehn, 1948), emphasized this fact. In particular, Hilf developed an expression relating pore fluid pressure after compaction to initial pressure, volumes of air and water, Henry's constant for solubility of a gas in a liquid, and the volume change in the soil. These ideas were further developed by Bishop and Eldin (1950), and by Bishop (1957), who examined the influence of free and dissolved gas on pore fluid compressibility, and noted that "the pore pressure set up by an increase in total stress under undrained conditions is a function of the relative compressibilities of the soil structure and of the fluid occupying the pore space". Bishop also derived an expression relating change in pore pressure to initial pressure, saturation, Henry's constant, porosity and volume change. He noted that this relationship was only valid as long as some free gas remained. When the pore fluid became saturated, the fluid compressibility would decrease drastically and B, ($= \Delta u/\Delta \sigma$), would approach 1.

During the 1960's, a number of researchers investigated the behaviour of unsaturated soils, working primarily with clays having small air saturations. Bishop et al. (1960) and Bishop & Blight (1963) looked at the effective shear strength of partly saturated soils and were the first to propose a modified form of the effective stress

equation, incorporating both pore air and water pressures, and later to use two separate stress state variables, $(\sigma - u_a)$ and $(u_a - u_w)$. In the same period, Jennings & Burland (1962), Blight (1965), Burland (1965), Matyas & Radhakrishna (1968) and Barden et al. (1969) were examining volume changes in unsaturated soil and proposing the use of these same stress variables. Research in this area culminated in extensive PhD theses by Fredlund (1973), and Verma (1976), and a number of papers elaborating on the volume change, strength and consolidation of unsaturated soils followed: Fredlund (1976); Fredlund & Morgenstern (1976); Fredlund & Morgenstern (1977); Fredlund (1978); Fredlund, Morgenstern & Widger (1978); and Fredlund (1979).

During this period, a significant paper was given by Schuurman (1966). He discussed the compressibility of unsaturated soils ($0.85 < S < 1.0$) containing occluded gas bubbles, taking into account the difference between air and water pressure due to surface tension, and developed an expression both for fluid compressibility and for the air and water pressures. Fredlund (1973) questioned the validity of Schuurman's equation because he (Fredlund) felt that surface tension effects were only operative in the presence of a solid, and that therefore the pressure in an occluded gas bubble would be equal to the surrounding liquid pressure. Fredlund's criticism was ill-founded. Schuurman's ideas were correct, as far as his assumptions allowed. If anything, they needed only to be modified to reflect real gas behaviour

at high pressures (Epstein, 1975), and to incorporate concepts of critical bubble radius (Mori et al., 1977). A discussion of these ideas will be postponed until the literature review in Chapter 5.

A further interesting contribution to the subject of fluid compressibility in unsaturated soils was made by Black & Lee (1973). They investigated the saturation of laboratory samples by back pressure and presented several equations relating saturation to the pore pressure response parameter B, for no gas solution and for total gas solution. However, they were more interested in the non-equilibrium behaviour of the soil, and their discussion of equilibrium conditions offered no new physical hypotheses.

An excellent review of the development of the concepts discussed above has been provided by Wood (1979).

All of this work was performed as part of an ongoing research effort into the equilibrium behaviour of unsaturated soils. By the mid-1970's, both the laboratory investigations and the theoretical concepts were well developed, but they had only been applied to soils with small amounts of gas dissolved in the pore fluid. The logical extention of the concepts to gassy soils awaited the actual observation and recognition of these soils in nature. The first application was made by Harris & Sobkowicz (1977), who investigated the geotechnical implications of such behaviour. They gave a

physical rationale for the behaviour of a gassy soil, and extending the analytical concepts, developed:

(a) an expression for the compressibility of the total pore fluid as a function of pressure and temperature, and

(b) a closed form solution relating the change in pore pressure to the change in total stress. This solution incorporated a linear constitutive relationship for the soil.

Dusseault (1979) also investigated and modelled the equilibrium behaviour of gassy soils. He developed a differential equation for the relationship between $du/d\sigma$, and u and σ, incorporating a non-linear constitutive law, which was then solved by a finite difference technique. As will be discussed later, there is a distinct advantage to retaining the linear form of the constitutive law in this solution, as the concepts may be applied in a tractable way to the transient problem. The behaviour of non-linear materials may be treated by a step-wise linear analysis.

2.3 BOYLES & HENRY'S LAWS

Pore fluids may be totally miscible, totally immiscible, or a combination of the two. That is, if several liquids are present, they may form a complete solution, and act as one liquid, or they may be mutually insoluble (as is the case for water and bitumen in the oilsands). If several

gases are present, they will be completely miscible. For simplicity, in this thesis we will deal exclusively with the case of a single liquid and a single gas. The gas will be soluble to some extent in the liquid, and depending upon the weight ratio of gas to liquid in a soil element and the pore pressure, there may or may not be any free gas in the pores.

If the pore liquid is undersaturated or just saturated with gas, the pore fluid compressibility will be low and close to the compressibility of the pure liquid. Fredlund (1973) presented some experimental data which confirmed that the dissolved air only increased the fluid compressibility slightly.

However, if there is both free gas and liquid present, the pore fluid compressibility may be much higher (by several orders of magnitude), and will be pressure dependent. If the gas and liquid are immiscible, the physical laws governing compression of gas will determine the fluid compressibility, whereas if the gas is soluble to some extent in the liquid, the fluid compressibility will also be influenced by the solubility relationship.

The two physical laws governing these volume and pressure relationships are Boyle's law and Henry's law:

(a) Boyle's law: If the temperature of a given gas is held constant, its density is proportional to the absolute pressure. For the undrained case, where the mass of gas does not vary, this is equivalent to stating:

$$P * V = k \qquad (2.1)$$

P=absolute pressure, V=volume, k=constant.

(b) Henry's law: The weight of gas dissolved in a fixed quantity of a liquid, at constant temperature, is directly proportional to the absolute pressure of the gas above the solution. This may also be worded in another way. Suppose there is a fixed quantity of liquid subjected to a constant temperature and to a confining pressure P. The volume of dissolved gas is constant when the volume is measured at P (sec. 2.4.4).

$$V_{dg} = H * V_w \qquad (2.2)$$

V_{dg} = Volume of dissolved gas, V_w = Volume of water, H = Henry's constant.

Henry's constant varies for different gas/liquid combinations. For air/water, H = 0.02; for CO_2/water, H = 0.85; for methane/bitumen, H = 0.25.

H is temperature dependent, and over a wide range of pressures is also pressure dependent, particularly for natural gases in hydrocarbons (Burcik, 1956). (Verma (1976) discusses the possible deviations from Henry's law, as it applies to a gas in a free liquid, for gases and liquids in the pore space of a soil.)

For the purposes of this thesis, it will be assumed that H is independent of pressure. The variation of H with temperature for both CO_2 and N_2 in water is given in Figure 2.3.

2.4 COMPRESSIBILITY OF THE PORE FLUIDS

Pore fluid compressibility, β_f, is defined as follows:

$$\beta_f = -1/V_f * dV_f/dP_f$$

where V_f is the volume of the pore fluid and P_f is the absolute pressure. Assuming that $P_L = P_g = P_f = P$, then:

$$\beta_f = -1/V_f * dV_f/dP \qquad (2.3)$$

2.4.1 Compressibility of a gas

The compressibility of a gas is defined as:

$$\beta_g = -1/V_g * dV_g/dP \qquad (2.4)$$

But from Boyle's law,

$$V_g = k/P$$

$$dV_g/dP = -k/P\text{^}2$$

$$\beta_g = -P/k * -k/P\text{^}2 = 1/P \qquad (2.5)$$

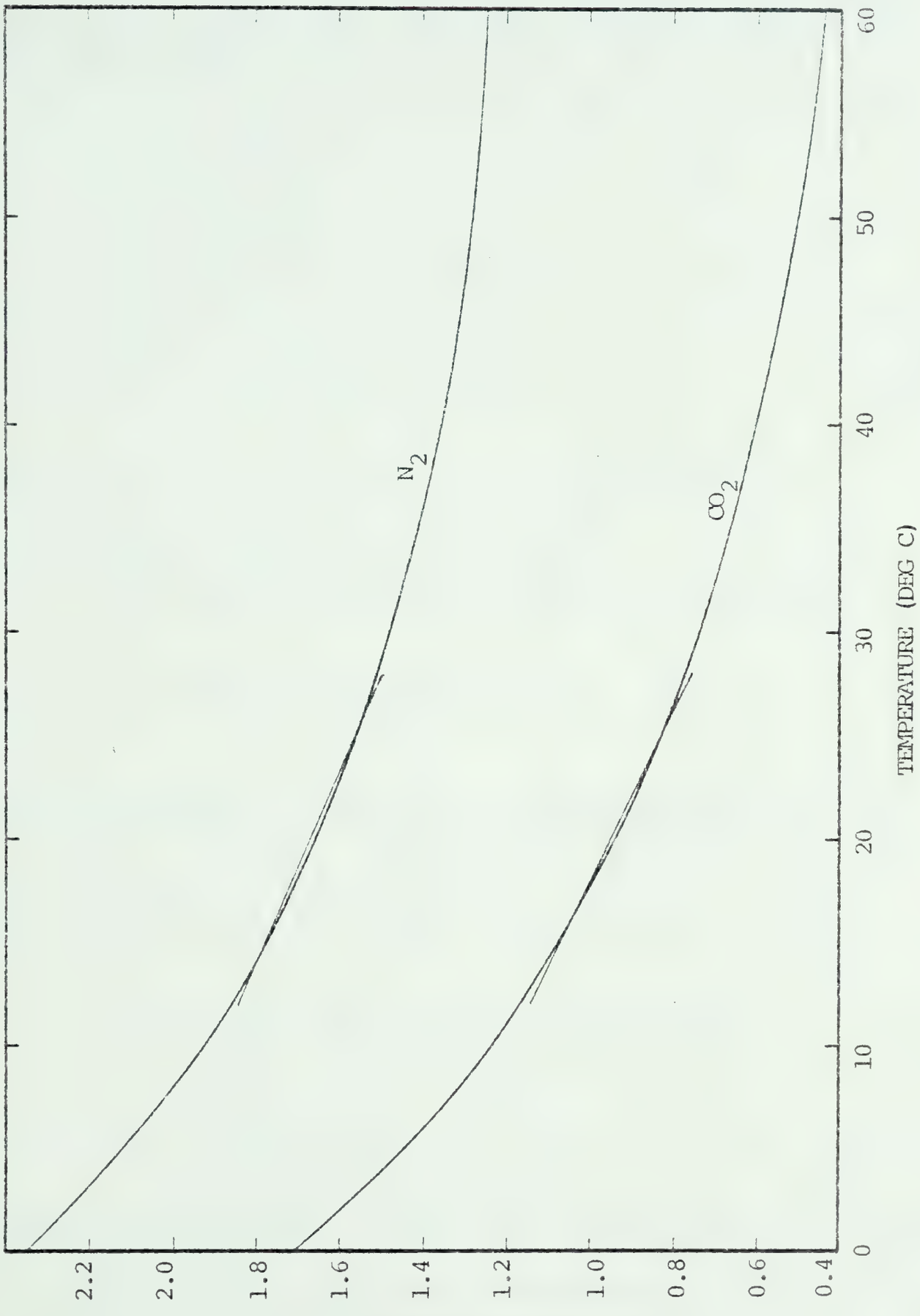


Figure 2.3 - Henry's constant vs temperature for CO_2 and N_2

It is also useful to develop the finite difference form of this relationship, from:

$$P_1 * V_1 = P_2 * V_2$$

$$V_2 = P_1 * V_1 / P_2$$

$$\Delta V_g = V_2 - V_1 = V_1 * (P_1/P_2 - 1)$$

$$\Delta V_g = V_1 * (-\Delta P) / (P + \Delta P) \qquad (2.6)$$

$$\beta_g = -1/V_g * \Delta V_g/\Delta P = 1/(P+\Delta P) \qquad (2.7)$$

In the limit, as ΔP approaches 0, β_g approaches $1/P$.

2.4.2 Compressibility of a pure liquid

The compressibility of a liquid is defined as:

$$\beta_L = -1/V_L * dV_L/dP \qquad (2.8)$$

2.4.3 Compressibility of an immiscible gas/liquid mixture

In a similar manner, the compressibility of an immiscible gas/liquid mixture may be defined as follows:

$$\beta_f = -1/V_f * dV_f/dP = -1/V_f * d/dP(V_g + V_L)$$
$$= -1/V_f * (-V_g/P - V_L * \beta_L)$$
$$= (1-S)/P + S * \beta_L \qquad (2.9)$$

2.4.4 Compressibility of a partly miscible gas/liquid mixture

This relationship may be conveniently developed as a finite difference formulation. Consider first the

compressibility of the gas due to free gas compression and solution.[1]

Let the initial volumes of gas and water in an element of soil be:

$$V_{fg}^{0} \text{ and } V_{w}$$

Then the total volume of free and dissolved gas is:

$$V_{Tg}^{0} = V_{fg}^{0} + H * V_{w}$$

It will be assumed that the compressibility of the water is small enough that the volume of water can be considered constant insofar as determining the amount of dissolved gas is concerned. Fredlund (1973) demonstrates that Boyle's law for free gas and Henry's law for dissolved gas may be combined by applying Boyle's law to the total volume of gas in the system, both free and dissolved. Thus, for an increase in pressure from P_0 to P_1, we have:

$$V_{Tg}^{1} = V_{Tg}^{0} * P_0/P_1 = (V_{fg}^{0} + H*V_{w}) * P_0/P_1$$

The volume of dissolved gas is still $H * V_w$ (measured now at P_1; the total <u>weight</u> of dissolved gas has increased according to Henry's law), so that the new volume of free gas is:

---

[1]The subscripts fg, dg, and Tg will be used throughout the text to denote free gas, dissolved gas and total gas respectively.

$$V_{fg}^{1} = V_{Tg}^{1} - V_{dg}^{1} = (V_{fg}^{0} + H*V_w) * P_0/P_1 - H*V_w$$

and then

$$\Delta V_{fg} = V_{fg}^{1} - V_{fg}^{0} = (V_{fg}^{0} + H*V_w) * (-\Delta P)/(P_0+\Delta P) \quad (2.10)$$

and

$$\beta_g = -1/V_{fg}^{0}*\Delta V_{fg}/\Delta P = (V_{fg}^{0}+H*V_w)/V_{fg}^{0} *1/(P_0+\Delta P) \quad (2.11)$$

Then

$$\begin{aligned}\beta_f &= -1/V_f* V_f/ P \\ &= -1/V_f * \{-(V_{fg}^{0}+H*V_w)/(P_0+\Delta P) - V_L* {}_L\} \\ &= (1-S+S*H)/(P_0+\Delta P) + S*\beta_L \end{aligned} \quad (2.12a)$$

which, in the limit as ΔP approaches 0, becomes:

$$\beta_f = (1-S+S*H)/P + S*\beta_L \quad (2.12b)$$

2.5 THEORETICAL PORE PRESSURE RESPONSE

Let us return to consider an element of gassy soil, (Figure 2.1). With an application of a change in total stress $\Delta\sigma$ on the boundaries of this element, what will be the change in the pore pressure, Δu,[2] and the change in effective stress $\Delta\sigma'$? As previously noted by Bishop (1957), the

---

[2]Throughout this thesis, a differentiation will be made between the gauge pore pressure, u, and the absolute pore pressure, P, such that:

$$P = u + P_{atmospheric}$$

magnitude of the pore pressure response will depend upon the relative values of the pore fluid and soil skeleton compressibilities, and may be computed by invoking strain compatibility between the pore volume and the total soil volume.

The response of the soil (skeleton and pore fluid) may be physically modelled by a set of springs as illustrated in Figure 2.4. For saturated soils with no dissolved gas, $\beta_f << \beta_T$,[3] so that for all practical purposes the total stress change is taken up wholly in the pore fluid. For unsaturated soils, where some free gas is present but where there is very little dissolved gas, $\beta_f \mp \beta_T$, and the change in total stress is roughly, equally distributed between the pore fluid and the soil skeleton. For gassy soils, however, not only is the saturation less than 1, but there is a large volume of gas dissolved in the pore liquids, so that with decreasing , $\beta_f >> \beta_T$. The total stress change is almost entirely taken up in the soil skeleton and the pore pressure change is very small. This phenomenon will be examined quantitatively in the next section.

Harris & Sobkowicz (1977) developed a closed-form solution for Δu in terms of $\Delta\sigma$ and ΔT, assuming a linear constitutive relationship for the soil skeleton. The temperature-independent solution is elaborated below, (notice that finite differences are used in this analysis).

---

[3] β_T is the compressibility of the soil skeleton, i.e. the compressibility of the soil in the totally drained mode.

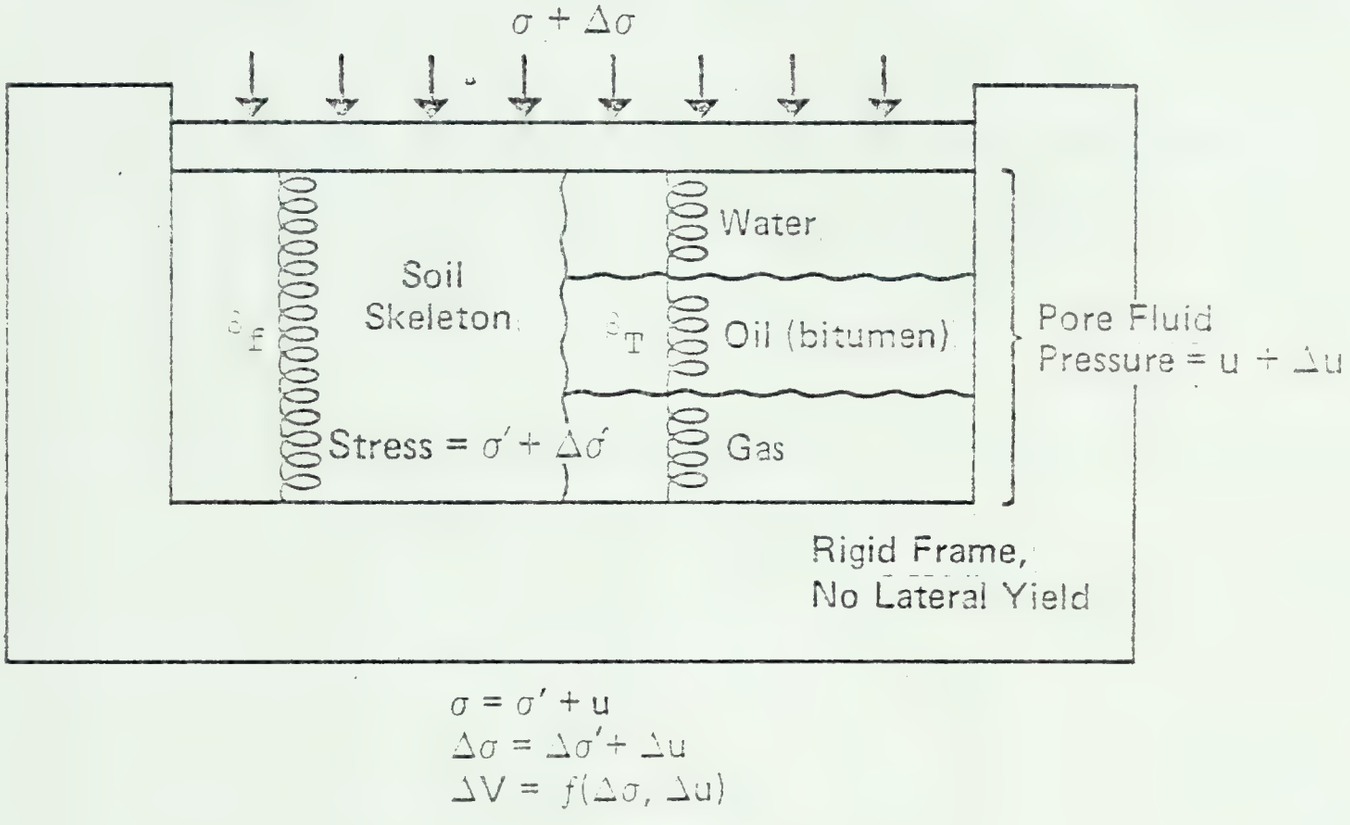


Figure 2.4 - Spring analogy for unsaturated soils

(After Dusseault, 1979)

Consider again the element of gassy soil (Figure 2.1) subjected to a change in total stress $\Delta\sigma$. If we allow that there will be a corresponding change in pore pressure Δu and in effective stress $\Delta\sigma'$, then we have that:

$$\Delta\sigma = \Delta u + \Delta\sigma' \tag{2.13}$$

The relationship between Δu and $\Delta\sigma$ may be developed by examining the volume changes in each of the phases.

From equation 2.10:

$$\Delta V_{fg} = (V_{fg}^{0}+H*V_L)*(-\Delta P)/(P_0+\Delta P)$$
$$= (V_{fg}^{0}+H*V_L)*(-\Delta u)/(u_0+P_a+\Delta u)$$

and from equation 2.8,

$$\Delta V_L = -\beta_L * V_L * \Delta u \tag{2.8b}$$

If we define an overall element compressibility β_T (soil skeleton compressibility) such that:

$$\beta_T = -1/V_T * dV_T/d\sigma' \tag{2.14a}$$

then

$$\Delta V_T = -\beta_T * V_T * \Delta\sigma' \tag{2.14b}$$

Substituting for $\Delta\sigma'$ from equation 2.13,

$$\Delta V_T = -\beta_T * V_T * (\Delta\sigma - \Delta u) \qquad (2.14c)$$

But for compatibility of volume change, (assuming the volume change of the solid particles is negligible),

$$\Delta V_T = \Delta V_f = \Delta V_L + \Delta V_g \qquad (2.15c)$$

such that

$$-\beta_T * V_T * (\Delta\sigma - \Delta u) = -\beta_L * V_L * \Delta u - \Delta u * (V_{fg}^0 + H * V_L) / (u_0 + P_a + \Delta u) \qquad (2.15a)$$

Rearranging, a quadratic equation is found for Δu,

$$A * \Delta u^2 + B * \Delta u + C = 0 \qquad (2.15b)$$

where

$$A = \beta_T + n * S * \beta_L$$

$$B = \beta_T * (P_0 - \Delta\sigma) + n * (\beta_L * S * P_0 + 1 - S + S * H)$$

$$C = -\beta_T * \Delta\sigma * P_0$$

and n, S and p_0 are initial values taken at the beginning of the stress increment. This solution assumes that the element is at equilibrium both before and after the stress change is applied, and is an exact solution as long as β_T = constant.

A modified solution to account for disequilibrium at the beginning of the stress increment will be presented in Chapter 4, during the evaluation of the laboratory tests.

Thus a closed form solution for Δu has been found which is dependent only on the total stress change on the element, the soil skeleton and liquid compressibilities, the initial element porosity and saturation, the initial absolute pore pressure and the solubility (Henry's) constant for the gas in the liquid.

The behaviour of this gassy element of soil subjected to a decreasing total stress path will be examined in the following section.

2.6 EQUILIBRIUM UNDRAINED PORE PRESSURE RESPONSE

Harris & Sobkowicz (1977) examined the behaviour of a foundation on a gassy soil during excavation and reloading, and the response of a tunnel excavated in the same material. Dusseault (1979) investigated the pore pressure response and volume change in an element of gassy soil upon total stress unloading from initial conditions of $S < 1$, i.e. for a sample whose pore fluid was initially saturated with gas and in which there was also some free gas in the pore space.

However, the pore fluid of many gassy soils is undersaturated (with gas) insitu. It is instructive, in considering the total response of such soils, to investigate the undrained equilibrium behaviour of a soil element when it is initially saturated with water, and when the pore liquid

is undersaturated with respect to gas. The soil element illustrated in Figure 2.1 will be used, and subjected to a continually decreasing total isotropic stress along its boundaries. Initial soil properties are shown on Figure 2.1 and are representative of one of the laboratory tests, which will be discussed in more detail in Chapter 4. The analysis will use the theoretical relationships established in section 2.5, but will assume the soil is non-linear elastic, the void ratio (e) being a linear function of log σ'. The analysis is made with step decrements in σ of arbritrary size. For each $\Delta\sigma$ there is an iteration for Δu, due to the fact that β_T is a function of Δu, but is also a term in equation 2.15.

Two responses of the soil will be examined, the immediate (short term) and the long term ones. Immediately after the step decrease in total stress is applied to the soil element, there will be some change in pore pressure and in effective stress. The fluid compressibility will be influenced by the compressibility of the free gas, but not by any gas exsolution. Strictly speaking this is not an equilibrium response for the soil unless the gas is totally insoluble in the pore liquid (H = 0), but even for partly miscible fluids it is worthwhile examining this behaviour as it is observable in the laboratory and in the field. The true equilibrium response of the soil is that behaviour observed after all gas exsolution has been completed.

In summary, the theoretical undrained pore pressure response of a soil element, subjected to a number of step decreases in total stress, will be predicted. For each decrement, both the short and long term behaviour will be calculated before the next decrease in total stress is applied.

The response of the soil is summarized in Table 2.1 and presented graphically in Figure 2.5. Starting with an initial total stress of 1600 KPa and a pore pressure of 850 KPa (Figure 2.5, Graph A), the pore liquid is undersaturated with gas ($P_{l/g}$ = 650 KPa). Small decreases in total stress produce nearly equivalent decreases in pore pressure, since $\beta_L << \beta_T$, and thus $B = \Delta u/\Delta\sigma \mp 1$. As soon as the pore pressure drops below 650 KPa, however, several changes in behaviour may be observed:

(a) Gas begins to exsolve and thus the saturation of the element decreases.

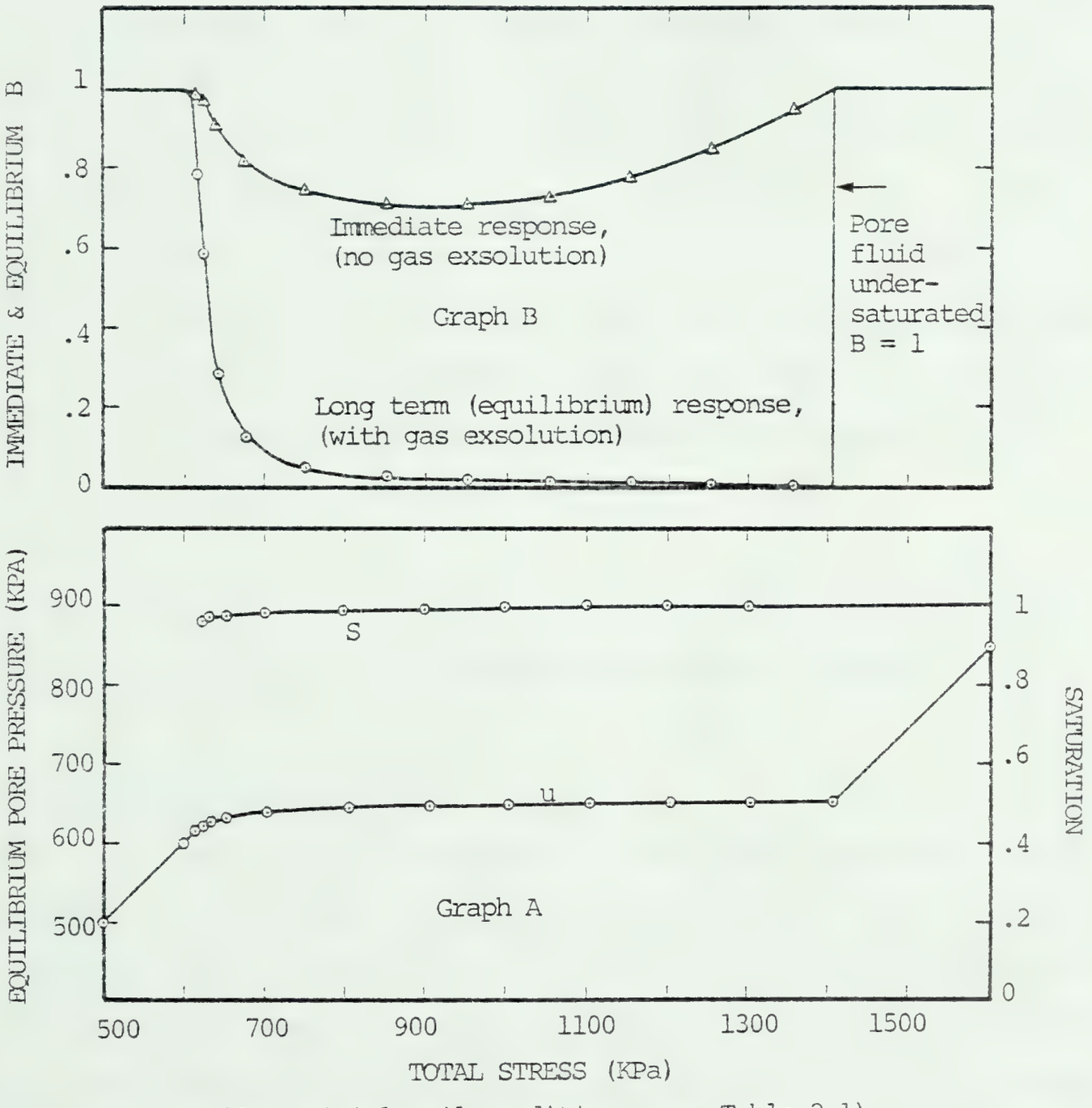
(b) With decreasing saturation, the immediate pore pressure response becomes less than the change in total stress, i.e. $B_{st} < 1$. This is due to increasing fluid compressibility. Note however that there is a limiting value for B_{st}, below which it will not drop. With continued decreasing saturation, B_{st} increases because $\Delta\sigma'$ is approaching zero.

(c) Initially, σ' is quite high and thus β_T is low. For equilibrium at the end of a time interval associated with one total stress decrement, $P \mp P_{l/g}$.

TABLE 2.1

THEORETICAL UNDRAINED EQUILIBRIUM PORE PRESSURE RESPONSE FOR AN ELEMENT OF GASSY SOIL SUBJECTED TO AN ISOTROPIC TOTAL STRESS DECREASE ON ITS BOUNDARY
($H = 0.86$, $C_C = 0.0073$)

STEP NO.	$\frac{\Delta U_{ST}}{B_{ST}}$	$\frac{\Delta U_{LT}}{B_{LT}}$	N_{end}	S_{end}	U_{end}	σ	σ'_{end}
0			.3228	100.0	652.34	1403.31	750.97
1	-95.2	-.82	.3230	99.91	651.51	1303.31	651.79
2	-84.68	-.96	.3232	99.80	650.56	1203.31	552.75
3	-77.76	-1.14	.3235	99.67	649.42	1103.31	453.89
4	-73.71	-1.41	.3239	99.50	648.00	1003.31	355.30
5	-70.92	-1.86	.3244	99.29	646.14	903.31	257.16
6	-70.61	-2.72	.3250	98.98	643.43	803.31	159.88
7	-74.25	-5.14	.3263	98.40	638.29	703.31	65.02
7a $\Delta\sigma$=-50	-40.89	-6.46	.32789	97.692	631.83	653.31	21.48
7b $\Delta\sigma$=- 20	-18.13	-5.78	.32944	97.008	626.06	633.31	7.253
7c $\Delta\sigma$=-5	-4.78	-2.43	.33006	96.735	623.63	628.31	4.68
7d	-3.88	-2.37	.33067	96.469	621.26	624.31	3.05
-4	(.969)	(.593)					
-3	-2.93	-2.05	.33120	96.238	619.21	621.31	2.10
	(.978)	(.683)					
-2	-1.97	-1.49	.33159	96.067	617.72	619.31	1.59
-1.55	-1.53	-1.22	.33192	95.927	616.50	617.76	1.26
	(.987)	(.790)					



(for initial soil conditions, see Table 2.1)

Figure 2.5 - Theoretical undrained equilibrium pore pressure response
Gassy Soil

Because the soil is so stiff, and because there is so much gas in solution, relatively little gas need be generated to maintain high pore pressures (Graph A). Thus B_{Lt} is close to zero. As σ' decreases, however, β_T increases and thus greater volumes of gas must be generated to achieve equilibrium. As a consequence, P decreases slowly to a value slightly less than $P_{l/g}$.

(d) For a real soil, σ' at some point reduces to zero, since σ is decreasing but u is not. For this example, this occurs when $\sigma_T = u = 600$ KPa. Any further decrease in σ_T will produce an equivalent decrease in u, hence $B_{st} = B_{Lt} = 1$. Significantly larger volumes of gas will be produced in the soil element, leading to a disruption of the soil skeleton and eventual venting of the gas.

The analysis described above was coded for a hand-held computer in BASIC. The program is located in Appendix A.

2.7 UNSATURATED OR GASSY?

A correct understanding of the ideas discussed in this chapter is crucial to the recognition of the peculiar behaviour of a gassy soil. It must be understood that this behaviour is attributable to large volumes of gas dissolved in the pore fluid. It may be argued that the distinction between an unsaturated and a gassy soil is one of degree, and that the transition between the two is gradational. However,

the concept unifying the two, i.e. the solubility of the pore gas in the pore liquid, is for a particular soil and a particular problem, unique. The soil behaviour usually conforms to one of the two categories. It is thus useful to consider the extremes of behaviour, and to make the distinction between two different types of soil.

For example, consider Table 2.2 and Figure 2.6, which illustrate the response of an unsaturated soil (H = 0.02, typical of air in water) given the same initial conditions as for the previous analysis. Recalling from Bishop that the pore pressure response is a function of the relative compressibilities of the pore fluid and the soil skeleton, and examining equation 2.15, it is clear that the distinction between gassy and unsaturated soil is intensified not only by a higher fluid compressibility but also a lower soil skeleton compressibility in the gassy soil. Thus the example in Figure 2.6 also uses a relatively high compression index (and porosity), representative of a clay soil.

Figure 2.6 illustrates the behaviour that is normally associated with an unsaturated soil, (e.g. Skempton, 1954), and which may be contrasted with gassy soil behaviour in Figure 2.5. The soil element is initially completely saturated at a total stress of 1600 KPa and a pore pressure of 850 KPa, and behaves that way under decreasing total stress (B = 1) until $P = P_{lg}$. At this point, gas begins to exsolve from the pore fluid and the soil becomes unsaturated.

TABLE 2.2

THEORETICAL UNDRAINED EQUILIBRIUM PORE PRESSURE RESPONSE FOR AN ELEMENT OF UNSATURATED SOIL SUBJECTED TO AN ISOTROPIC TOTAL STRESS DECRESE ON ITS BOUNDARY
(H = 0.02, C_C = 0.47)

STEP NO.	ΔU_{ST}	ΔU_{LT}	N	S	U	σ	σ'
0			.4300	100.0	652.34	1403.31	750.97
1	-99.88	-99.20	.4307	99.72	560.14	1303.31	743.17
2	-98.53	-90.07	.43158	99.358	470.07	1203.31	733.24
3	-96.36	-87.09	.43275	98.86	382.98	1103.31	720.33
4	-92.83	-82.84	.4343	98.25	300.14	1003.31	703.17
5	-87.17	-76.83	.4365	97.38	223.31	903.31	680.00
6	-78.53	-68.60	.4396	96.19	154.70	803.31	648.61
7	-66.70	-58.20	.4438	94.55	96.50	703.31	606.81
8	-53.00	-46.65	.4495	92.37	49.85	603.31	553.46
9	-39.92	-36.70	.4570	89.65	13.15	503.31	490.16
10	-30.30	-27.70	.4664	86.31	-14.54	403.31	417.85
11	-22.52	-20.95	.4784	82.28	-35.49	303.31	338.80
12	-17.18	-16.23	.4937	77.39	-51.72	203.31	255.03
13	-13.76	-13.19	.5145	71.19	-64.91	103.31	168.22
14	-12.14	-11.80	.5478	62.28	-76.71	3.31	80.02

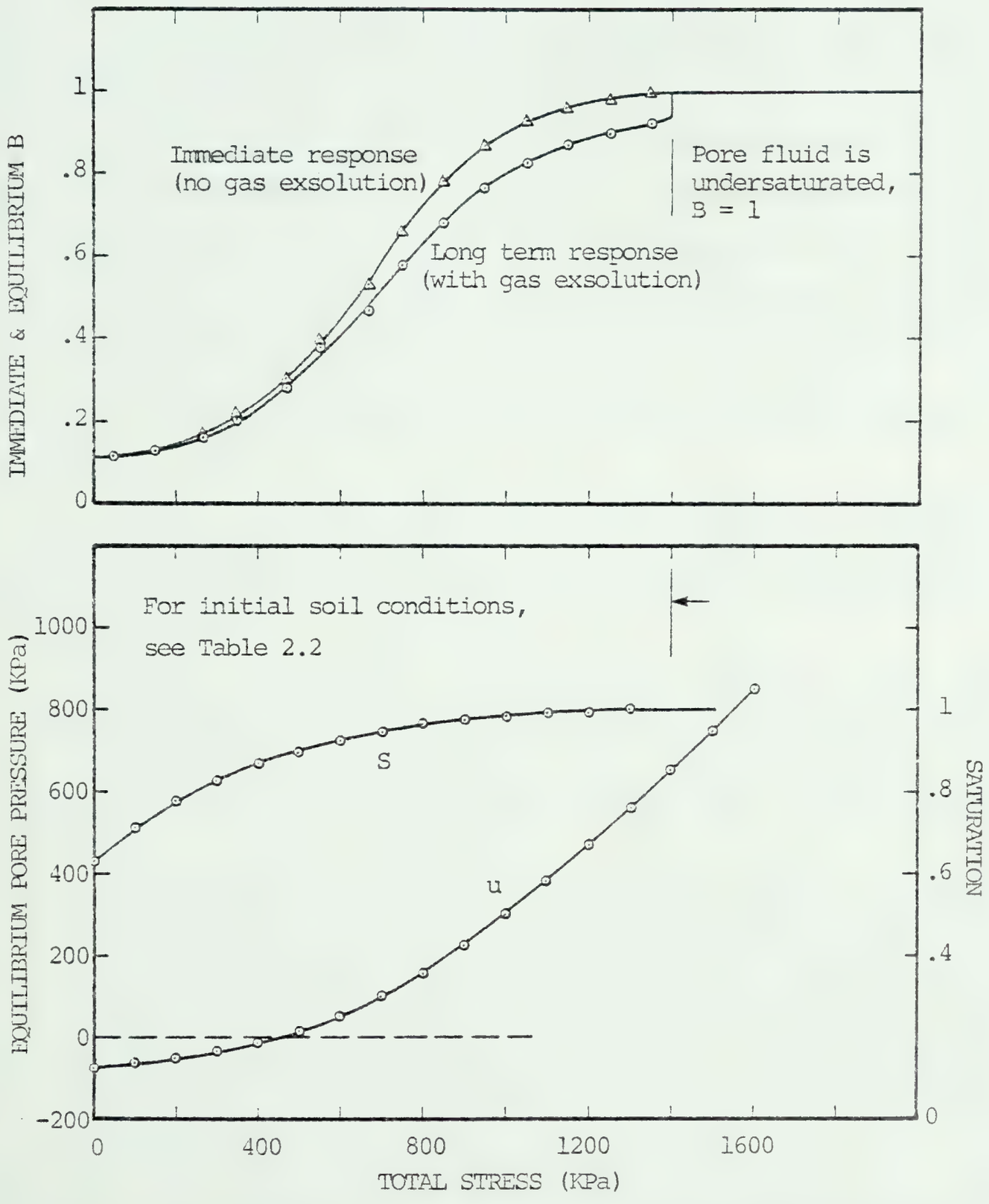


Figure 2.6 - Theoretical undrained equilibrium pore pressure response Unsaturated Soil

However, because the soil skeleton is quite compressible, and because there is not much gas in solution, the pore fluid compressibility does not increase too drastically and remains of the same order of magnitude as β_T. With decreasing total stress and saturation, B_{st} and B_{Lt} gradually decrease from 1 and become asymptotic to a value close to 0, (0.15 in this case). Note that B does not level out and then increase at lower total stresses, as in the gassy case. This is because σ' remains greater than zero. During the unloading process, the pore pressure decreases montonically, becoming negative at some point, (for this example, when σ_T = 450 KPa), and becoming asymptotic to a value of 0 atmosphere absolute or -1 atmosphere gauge.

There are some important differences, then, between the gassy and the unsaturated soil behaviour. For decreasing total stress,

(a) B_{st} and B_{Lt} monotonically decrease for the unsaturated soil, whereas for the gassy soil, they decrease, level off, then increase back to a value of 1.

(b) The pore pressure decreases monotonically and often becomes negative for an unsaturated soil, whereas for a gassy soil, it levels off at a value close to $P_{l/g}$, and only begins to decrease when the effective stress approaches 0.

(c) Effective stress remains positive for an unsaturated soil, and oftentimes is larger than the total stress at the end of the unloading sequence. For a gassy soil, the effective stress reduces to zero at an intermediate point in the unloading process, when $\sigma > 0$ and $u = \sigma$. Any further unloading causes the generation of large volumes of gas and a disruption of the soil structure.

(d) Saturation decreases monotonically for both soils, but at a quicker rate for the unsaturated soil. This is mainly a function of the higher soil compressibility used for the unsaturated soil.

It is tempting to try to develop an analytical expression which would define the boundary between gassy and undersaturated soils, perhaps in terms of the gas solubility constant, H, and the soil compressibility β_T or compression index C_c. An examination of Figure 2.7 will illustrate that this is a futile endeavor, however. This figure demonstrates diagramatically the relationship between the two types of soil behaviour, and the location of their mutual boundary. It is evident that the soil response for behaviour near the transition zone is not just a function of the compressibilities β_T and β_f, and thus also of C_c, β_L, and H, but is also a function of the insitu state of stress σ_0 and u_0, and of the liquid/gas saturation pressure $P_{l/g}$. The

LEGEND

A - Response of totally saturated soil

B,C - Possible responses for gassy soil

D - Boundary between gassy and unsaturated soil

E,F - Possible responses for unsaturated soil

G - Soil response if B = 1

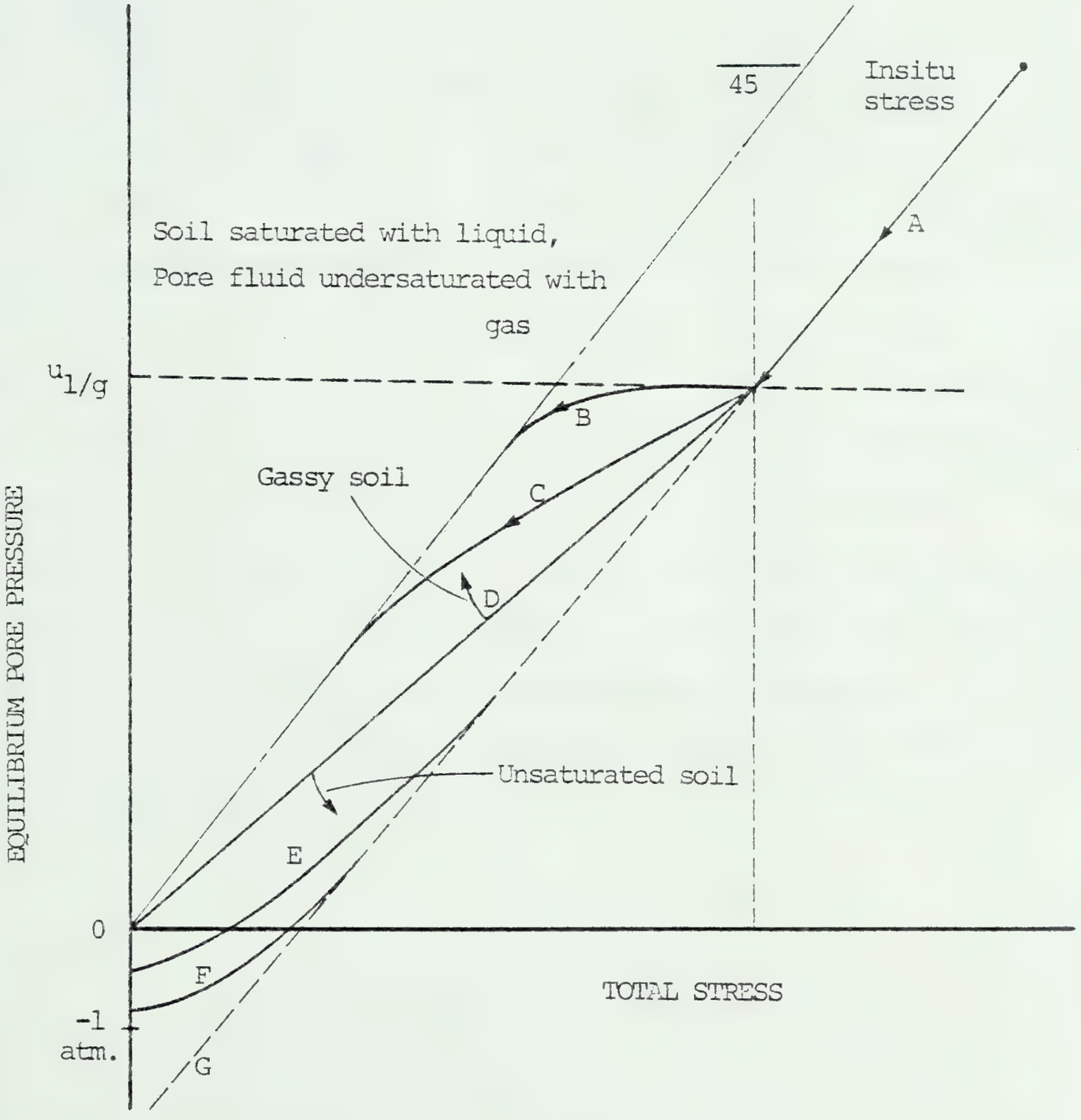


Figure 2.7 - Relationship between gassy and unsaturated soil behaviour

exact u - σ stress path followed by an element of soil on unloading is a complex function of these variables and may only be defined analytically in a step-wise manner. Thus there is no simple analytical expression defining the boundary between the two types of soil behaviour.

2.8 SUMMARY

This chapter has defined the general behaviour of unsaturated and gassy soils, discussing the distinction to be made between the two classes in terms of undrained pore-pressure response. A review of the concepts and analytical work on unsaturated soil has been presented. This was followed by a discussion of the physical laws governing gas expansion and exsolution, followed by a derivation of the expressions for compressibility of each of the phases in an element of unsaturated soil. The theoretical pore pressure response for an undrained element of soil was then derived for decreasing total stress on the element boundary, and this behaviour was examined and compared for both the unsaturated and gassy soil.

CHAPTER 3 - THE LABORATORY INVESTIGATION

3.1 GENERAL

The laboratory investigation formed an essential part of the study of the behaviour of gassy soils, both in confirming and extending currently understood theory, and in providing hypotheses for the development of new theory. Several objectives were set at the beginning of the investigation to provide an overall and continuing perspective to the work:

(a) The first objective was to demonstrate the equilibrium behaviour of gassy soils in the laboratory, and to verify that the predictive models developed (Section 2.5) were quantitatively accurate.

(b) The second objective was to observe the transient, or non-equilibrium behaviour of a gassy soil, and to determine what initial soil conditions or boundary conditions had an influence on this behaviour.

(c) It was planned to initially follow a simple isotropic stress path using undrained boundary conditions so that there were as few variables complicating the soil response as possible. As this simple response was defined, other undrained stress paths were also envisioned, for example, a constant ratio of effective principal stresses σ_1'/σ_3', and several stress paths to failure. It was recognized

that for the theoretical work on consolidation in gassy soils to proceed, the drained behaviour of a laboratory sample would also have to be observed. The manner in which this was achieved was somewhat fortuitous, and certainly propitious, as will be discussed in section 3.4.

(d) It was desirable, in addition to observing the gassy soil behaviour, to determine if the exsolution process itself had any direct influence on the strength or stress-strain response of the soil. As discussed in section 2.6, an undrained test on a gassy soil is very similar to a drained test on a saturated soil, at least during the initial stages of unloading, (i.e. pore pressure approximately constant, soil volume change responding to changes in effective stress). Thus conventional drained tests were planned for saturated soils using similar initial conditions and stress paths, to establish this fact.

The choice of soil materials for the test was made mainly by considering the observed natural soils exhibiting gassy behaviour (Section 1.2), and also partly on the basis of testing convenience. The dense nature (and low compressibility) of the Athabasca oilsands could be modelled well by densely compacted cohesionless samples in the laboratory. Using a reasonably permeable cohesionless material ensured ease of proper pore pressure measurements during the undrained tests. Good sample permeability was

also important in the initial stages of each test to first allow total saturation of the pore space with water, and then later total saturation with water and dissolved gas.

A large volume of dissolved gas in the pore fluid could be achieved by either using high pore pressures and a gas with low to moderate solubility, or low pore pressures and a highly soluble gas. Since the combination of water and carbon dioxide gas had been encountered at Alto Lazio, Italy, it was decided to use this combination of pore fluids. They had the advantages of being non-corrosive, easy to handle, easy to control during sample preparation, and CO_2 had a high solubility in water which permitted working at low test pressures.

3.2 CONSIDERATIONS FOR THE DESIGN OF TEST EQUIPMENT

Experimental work on the behaviour of unsaturated soil was pursued quite intensively during the 1960's and early 1970's. Fredlund (1973) reviews the experimental aspects of this work in detail. Particular attributes of previous workers' equipment that have proven useful in the study of gassy soils will be discussed in the following section.

Before doing this, however, it is worthwhile considering several general problems which were encountered in the design of the laboratory equipment. Two characteristics of gassy soils provide special design consideration:

(a) low skeleton compressibility, and

(b) large volumes of gas in the sample

The low soil skeleton compressibility results in extremely small strains and volume changes, with changes in stress. A typical, densely packed sand has a volumetric compressibility of 5 to 10 * 10^{-6} KPa^{-1} in the 100 to 500 KPa stress range. Dusseault (1979) reported compressibilities as low as 0.1 to 1 * 10^{-6} Kpa^{-1} for "locked" sands, (i.e. sands with an insitu relative density much greater than 100%), which is nearly equivalent to the compressibility of pure water. The desire to test dense materials in the laboratory exists because of a need to further exacerbate the gassy soil behaviour, but it must be tempered by an ability to accurately measure small sample strains.

The large volumes of gas to be initially dissolved in the pore fluid present several problems:

(a) How is this fluid brought into the soil in a controlled fashion?

(b) How is the gas confined to the sample?

(c) What influence will gas leakage or diffusion have on the measurement of pore pressures and volume changes?

3.3 DEVELOPMENT OF EQUIPMENT

All of the laboratory tests were performed in a triaxial cell, with several modifications, as described in the following sections.

3.3.1 Membrane & cell fluid considerations

It is difficult to separate the design considerations for the membrane and cell fluid from those for measuring volume change, because the two are so interdependent. However, because of gas-diffusion restrictions, the choice of membrane and cell fluid is the more important one.

A typical laboratory sample held 1100 cc of gas, (measured at 1 atmosphere pressure), dissolved in 250 cc of pore liquid, ($S = 1$, $p_{l/g} = 510$ KPa). A correct observation of undrained soil response required containing this gas in the soil for the duration of a test, which was several days to 1 week. Because of high differences in dissolved gas concentration between the pore liquid and the cell liquid, however, there was a tendency for gas to diffuse out of the soil sample, through the membrane and into the cell.

Limiting diffusion

This diffusion process can be limited in one of two ways:

(a) by providing a membrane that is nearly impermeable to the gas, i.e. one that has a low diffusivity coefficient, or

(b) by surrounding the membrane with a liquid in which the gas has a low solubility. Even if the gas can diffuse quickly through the membrane and possibly also through the cell liquid, the mass transfer process will stop when the cell liquid becomes saturated with gas.

Izydorczyk et.al. (1977) discuss the diffusion of CO_2 gas through thin polymer membranes into a closed volume of liquid, and present a solution (after Holstein, 1951) showing that the time rate of change of CO_2 concentration on the liquid side of the membrane becomes asymptotic to zero at infinite time.

If there are free gas bubbles in the cell liquid, (as may occur in later stages of an incremental unloading test), the argument is slightly more complex but the conclusions are the same. There is still a stable equilibrium volume of gas that can exist both in the free and dissolved states in the cell liquid, and hence there is a limit to the amount of gas that can be lost from the sample. The rate of diffusion of gas through the membrane is then limited both by the gases' solubility and its diffusivity characteristics in the cell liquid. (Diffusion of gas through liquids and into bubbles is discussed further in Chapter 5).

Bishop and Donald (1961) and Fredlund (1973) both used method b) to prevent gas diffusion. They constructed a triaxial cell which had a double perspex wall. The inner wall contained a volume of mercury, which surrounded the sample and prevented gas diffusion through the membrane. The mercury was initially placed to a level just above the top cap on the sample, and the remaining cell volume was filled with water. Sample volume changes were monitored by measuring the vertical displacement of a steel ball floating

on the surface of the mercury with a cathetometer. Dunn (1964) employed method a) to prevent gas diffusion, using a double latex rubber membrane, with two sheets of slotted aluminum foil sandwiched between them, and lubricated with silicone grease.

Secondary design requirements

Besides preventing loss of gas from the sample, the membrane and cell fluid have several other design requirements:

(a) The membrane should be as thin as possible to minimize error in measuring the lateral strain, if a direct contact strain indicator is used. If volumetric and vertical strains only are measured, this requirement is not as stringent. In fact, the membrane then needs some ability to resist penetration of the pore spaces at the boundary of the soil sample (under high cell pressures) to minimize errors in the volume change readings.

(b) The membrane should be stretchable. During the early portions of an undrained test, the lateral and axial strains are small, but as σ' approaches zero (or the sample approaches failure) strains of 10 to 15% may occur.

(c) The membrane must resist being punctured by the soil grains at higher cell pressures.

(d) The cell fluid should be non-conductive, in the event that any strain-measuring transducers are used inside the cell.

(e) It is also preferrable that the cell fluid be non-corrosive to any of the materials comprising the interior of the cell and the transducers, that it be safe to work with (non-volatile, non-toxic), and be easy to handle during sample preparation.

The search for an acceptable membrane/cell fluid combination

A study of the literature on membrane science (e.g. Izydorczyk et.al., 1977) provided some information on the relative "permeability" characteristics of various membranes to CO_2 gas, but it was clear to the author that an acceptable combination of membrane and cell liquid would have to be found by direct testing in the laboratory. A tentative decision had been made to utilize direct contact transducers inside the cell for measuring lateral and axial deformations (see section 3.3.3 following) so that, because of its electrical conductivity, the use of mercury as a cell fluid was not feasible. Mercury is not an ideal cell fluid, (independent of its electrical properties), as it is corrosive to aluminum, difficult to handle properly, and potentially dangerous to health if used over extended periods of time in the laboratory.

The search for an acceptable membrane/cell fluid combination then proceeded in both directions mentioned previously. The work by Dunn(1964) suggested several modifications that could be made to the standard latex membrane to restrict gas diffusion. A thin film of known low diffusivity material could be used between two latex membranes, although it was thought that this material would need to be continuous and properly sealed, both at its overlapping section and at the end caps. Several possible materials were aluminum foil, polyethylene, and mylar. This arrangement would have the disadvantage of drastically reducing membrane stretchability, and thus would probably only be useful during the early stages of testing. Some volume change could be accommodated by the movement of the film at its overlapping section if this were properly lubricated, but the seal at each end cap would restrict this movement, and it was not likely that movement along the overlap was compatible with the objective of preventing gas diffusion.

Law (1975) discusses the use of 1/32" thick neoprene membranes to prevent diffusion of air, which suggested the testing of other rubber-like materials for fabrication of a membrane. It was discovered that the physical characteristics necessary to inhibit gas diffusion also resulted in a less stretchable membrane, although this was not as serious a restriction as with the use of foil or plastic films. Two such membranes were tested for use, a

1 mm thick neoprene membrane used by Sterne (1981) for hollow cylinder tests on oilsands at the University of Alberta, and a 1.5 mm thick butyl rubber membrane, (fabricated from a large tractor tire inner tube).

During this same period, several cell fluids were tested for their ability to inhibit gas diffusion. Both water and mercury were unacceptable because of their electrical conductivity. Law (1975) mentions the use of a non-conductive hydraulic fluid, and the use of non-conductive oils manufactured for cooling transformers was also a possibility. The author had previously had experience in the use of a non-conductive, chemically stable fluid, trifluoropropylmethysiloxane (trade name "Silicone Oil"). All three of these fluids were unacceptable because they had too high a solubility for CO_2, (e.g. Wedlake & Robinson, 1979 for solubility of CO_2 in silicone oil). The discovery of a fluid that satisfied both conditions of low affinity for CO_2 and low electrical conductivity proved elusive. Several compilations of solubility data were consulted, (Gerrard, 1976; Stephen & Stephen, 1963), and it was found that there was one liquid with a solubility constant for CO_2 significantly lower than that of CO_2 in water. This liquid was glycerol, (or glycerin, $C_3H_8O_3$), with H = 0.03 at T = 25 degrees C. Glycerol also proved to have an electrical conductivity much lower than water. Using a Beckman RB3 SoluBridge and a G01 conductivity cell, the volume conductivity of glycerol was not measurable on the scale

provided, and from the equipment sensitivity must have been less than 0.1 micromhos/cm. This may be compared to measured values of 250 micromhos/cm for tap water, 7 micromhos/cm for distilled water, and 4 micromhos/cm for a 50/50 mixture of glycerol and distilled water.

Preliminary tests on sample membranes

Table 3.1 summarizes the results of tests to measure gas diffusion through various combinations of sample membrane and cell fluid. Unless otherwise specified, the tests were performed by setting up a dry sample of sand in the triaxial cell, surrounded by the appropriate membrane and cell fluid, by pressurizing the sample with CO_2 gas, then turning off all valves to the sample so that it was undrained.[1] The cell fluid was maintained at a higher pressure, and the pressure drop in the sample was monitored with time. Some of the pressure drop in the sample may have been due to leakage either through the valves or through the seal between the membrane and the end-caps. These are discussed below. Both effects proved to be negligible compared to mass transfer by gas diffusion.

---

[1] Since the compressibility of a liquid/gas mixture $\beta_f = (1-S+S*H)/P + S*\beta_l$, and since for CO_2 in water $H \neq 1$, $\beta_l \neq 0$, $\beta_f \neq 1/P$. The pressure drop due to gas diffusion from the sample will then be approximately the same for a dry or a partly saturated sample. For this reason, dry samples were used in the diffusion tests.

TABLE 3.1 RESULTS OF TESTS TO MEASURE GAS DIFFUSION THROUGH SAMPLE MEMBRANE

TEST NUMBER	MEMBRANE TYPE	SAMPLE FLUID AND PRESSURE (KPa)	CELL FLUID AND PRESSURE (KPa)	VOLUME OF PORE SPACE (cc)	GAS DIFFUSING INTO	QUASI-STEADY DIFFUSION RATE (KPa/hour)	COMMENTS
M 4	Double latex	CO_2 (840-680)	Glyc. (1290)	250	Cell	-1.5	On disassembly, some CO_2 trapped between membranes and many bubbles seen in glycerol.
M 5	Double latex	CO_2 (0-850)	CO_2 (850)	250	Sample	+75 +6-	Initial rate Secant rate 0 - 10 hours
M 7	Double latex	CO_2 (420-320)	Glyc. (700)	270	Cell	-0.7	
M8	Double latex	CO_2 (510-440)	Glyc. (1100)	250	Cell	Similar to test 7 for first 15 hours	Test aborted due to ruptured membrane.
M10 a	Double latex	H_2O (546-537)	Glyc. (850)	280	N/A	-0.5 KPa/min.	This is pressure loss in a totally saturated sample due to valve leakage. (dm/m)/dt = 2 * 10(-5) hr(-1)
b	Double latex	CO_2 (400-300)	Glyc. (850)	280	Cell	-0.7 (2 tests)	(dm/m)/dt = 2*10(-3) hr(-1).Mass transfer by diffusion approx. 100 * mass loss by valve leakage.
M11	Double latex	CO_2 (400-300)	Glyc. (700)	250	Cell	-1.0	
M12	Double latex	CO_2 (670-510)	Glyc. (1110)	440	Cell	-1.3 (2 tests)	
M15 a	Double latex	CO_2 (730-620)	Glyc. (1000)	450	Cell	-2.0	
b	Double latex	CO_2 (500- H_2O 380)	Glyc. (1050)	450	Cell	-0.9	High temp. dependence - discussed in sec. 3.3.6
M16	Neoprene	CO_2 (0-400)	CO_2 (670)	450	Sample	+13 +9	Initial rate Secant rate 10 - 30 hours
M17 a	Butyl Rubber	CO_2 (0)	CO_2 (500)	450	Sample	+0.2	
b		CO_2 (670-540)	Air (1250)	450	Cell	-1.2	Some air trapped as bubbles within sealed joint membrane.
c	Double latex Aluminum foil	CO_2 (650-1250)	Air (1250)	450	Sample	+80 +66	Aluminum foil extended to end caps but not under O-ring seal. Foil ripped on dismantling. [Aluminum foil extended under first O-ring of double O-ring seal on each end cap.
M19 a	Double latex & Polyethylene	Air (0)	Air (420)	450	Sample	+49	Definite leak thru seal on end caps. Cf 19b.
b	Double latex	Air (0)	Air (420)	450	Sample	+4	Cf. 19a, 19c, 19d.
c		Air (0)	CO_2 (420)	450	Sample	+43	Cf. 19b.
d		Air (210)	Air (630)	450	Sample	+6	Cf. 19b.
e		CO_2 (210)	Air (630)	450	cell	-21	Note direction of flow despite pressure difference!
f	Double latex & Polyethylene	CO_2 (210)	Air (630)	450	Cell	-0.3	Same as above
M 20a	Double latex & Polyethylene	CO_2 (600)	Air (1200)	450	Cell, then sample	-13 0.8	Loss of pressure for approx. 15 minutes, then reversal to increase in pressure for 12 hours.
b		Air (0)	Air (1200)	450	Sample	0.9	Air diffusion only
c	Double latex	CO_2 (550)	Glyc.(1250)	450	Cell	-1.1	
M21	Double latex	CO_2 (630)	Glyc.(1250)	450	Cell	-1.1	

The plots of pressure vs time for all these tests are located in Appendix B. An attempt to calculate an effective diffusivity for each membrane/cell liquid combination could be pursued using the early time analysis outlined by Izydorczyk et.al. (1977). However, due to an uncertainty about the boundary conditions for his method compared with those in the test, as well as the uncertainty concerning the influence of diffusion in the cell liquid, this was not done. Instead, the relative merits of the various membrane/cell fluid combinations was assessed on the basis of the quasi-steady rate of pressure drop established after 5 to 10 hours of observation.

Table 3.1 contains a summary of all the gas diffusion tests. A perusal of this table will indicate several important points:

(a) Both the neoprene and the double latex with aluminum foil membranes proved to be unacceptable. They leaked at the seal with the end caps, and also ripped with only a small expansion of the sample. The neoprene membrane sealed properly at the end caps, but allowed moderate rates of gas diffusion. This would significantly influence the results of a single phase of a soil test, conducted over 1 to 3 hours, and would introduce a large cumulative error to a complete test lasting several days.

(b) Some problems were also encountered with the membrane/end cap seal for the latex and polyethylene film combination (M19a), but several such membranes were tested successfully (M19f, M20a & b). The ability of this membrane to prevent diffusion of air appeared to be good, but its ability to inhibit CO_2 diffusion was only moderate (M20a), similar to the neoprene membrane. An anisotropic undrained soil test (Test No. 20) was conducted using a latex and polyethylene film membrane, but was aborted due to a leak which developed during stress cycling of the sample. The ability of the polyethylene film to stretch or slide at its overlap, instead of ripping, was only marginally better than the aluminum foil.

(c) The butyl rubber membrane fabricated in the laboratory performed satisfactorily in limiting the diffusion of both air and CO_2 gas (M17a & b). Extreme care was necessary in establishing a proper seal between the end caps and that portion of the membrane that had been overlapped and joined. This part of the membrane was filed and feathered with a power wire brush to produce a smooth joint and a constant membrane thickness, and was smeared with a vacuum grease prior to installation. An isotropic undrained soil test (Test No. 18) was performed using this membrane, but two problems developed:

(i) The horizontal strain response was poor due to membrane thickness and compressibility. Figure 3.1 illustrates the axial (vertical) and lateral (horizontal) strain response of Sample 18 when subjected to a drained isotropic cycling of stress. It is obvious that the lateral strain measurement suffers a response lag on stress reversal which has led to a large hysteresis loop and a loss of accuracy. The superior performance of a double latex membrane in transmitting lateral strain to the strain-sensing device is shown in Figure 3.2 for comparison.

(ii) During the course of the test the membrane developed a leak at the end cap seal, and so the test was aborted.

(d) The double latex membrane used with glycerin proved to be the most reliable membrane/cell fluid combination. During 19 separate tests, only 1 leak developed, which was due to a punctured membrane. The double latex membrane alone (without the glycerin as a cell fluid) provided moderate inhibition of air diffusion but was extremely poor in limiting diffusion of CO_2 gas. Combined with the glycerin cell fluid, pressure drops in the sample due to gas diffusion were proportional to the gas pressure (and hence concentration) inside the sample and ranged from -0.7 KPa/hr at 400 KPa to -1.5 KPa/hr at 800 KPa. The

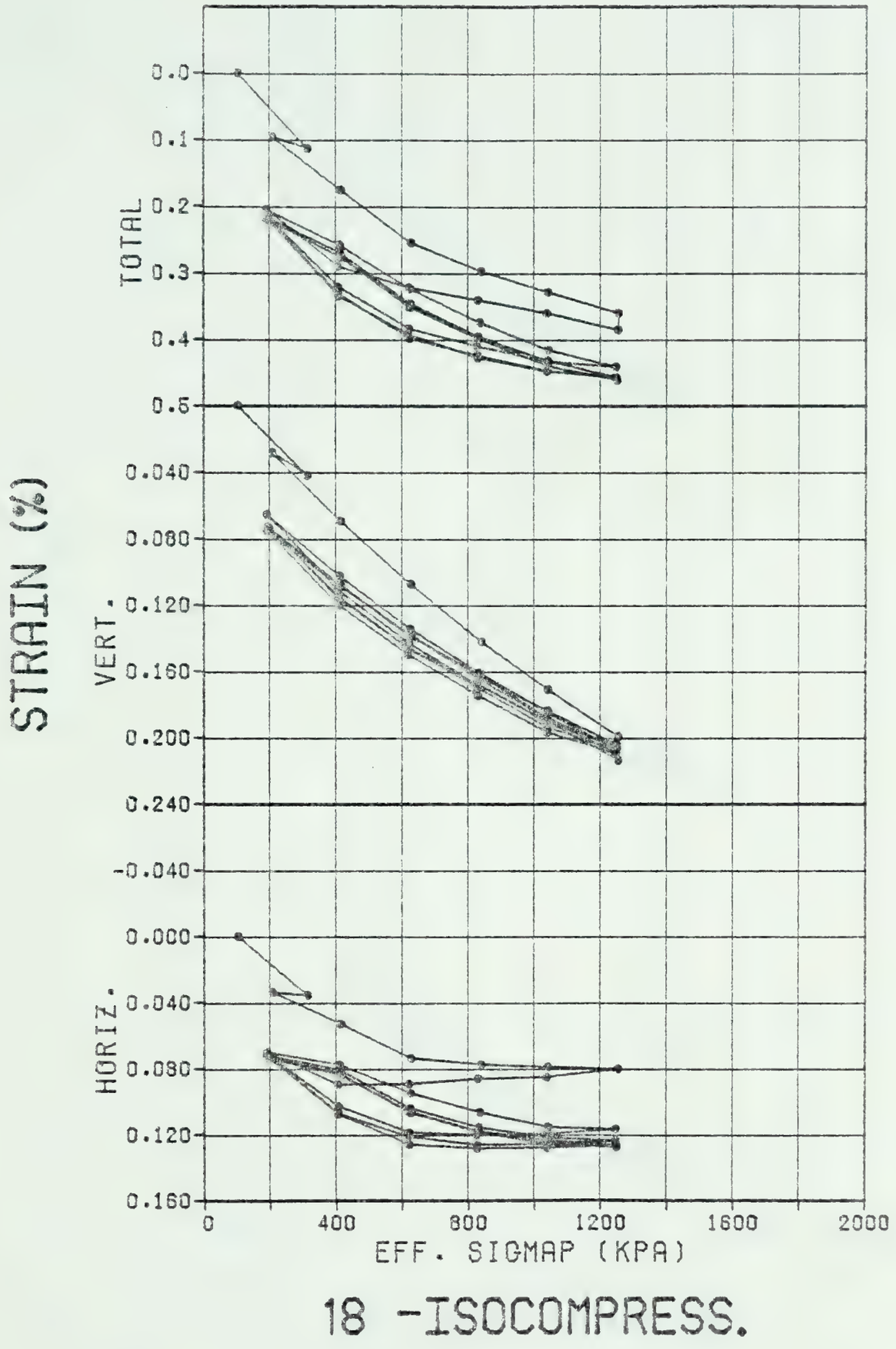


Figure 3.1 Lateral and axial strain response for sample 18. Isotropic stress cycling using Butyl rubber membrane.

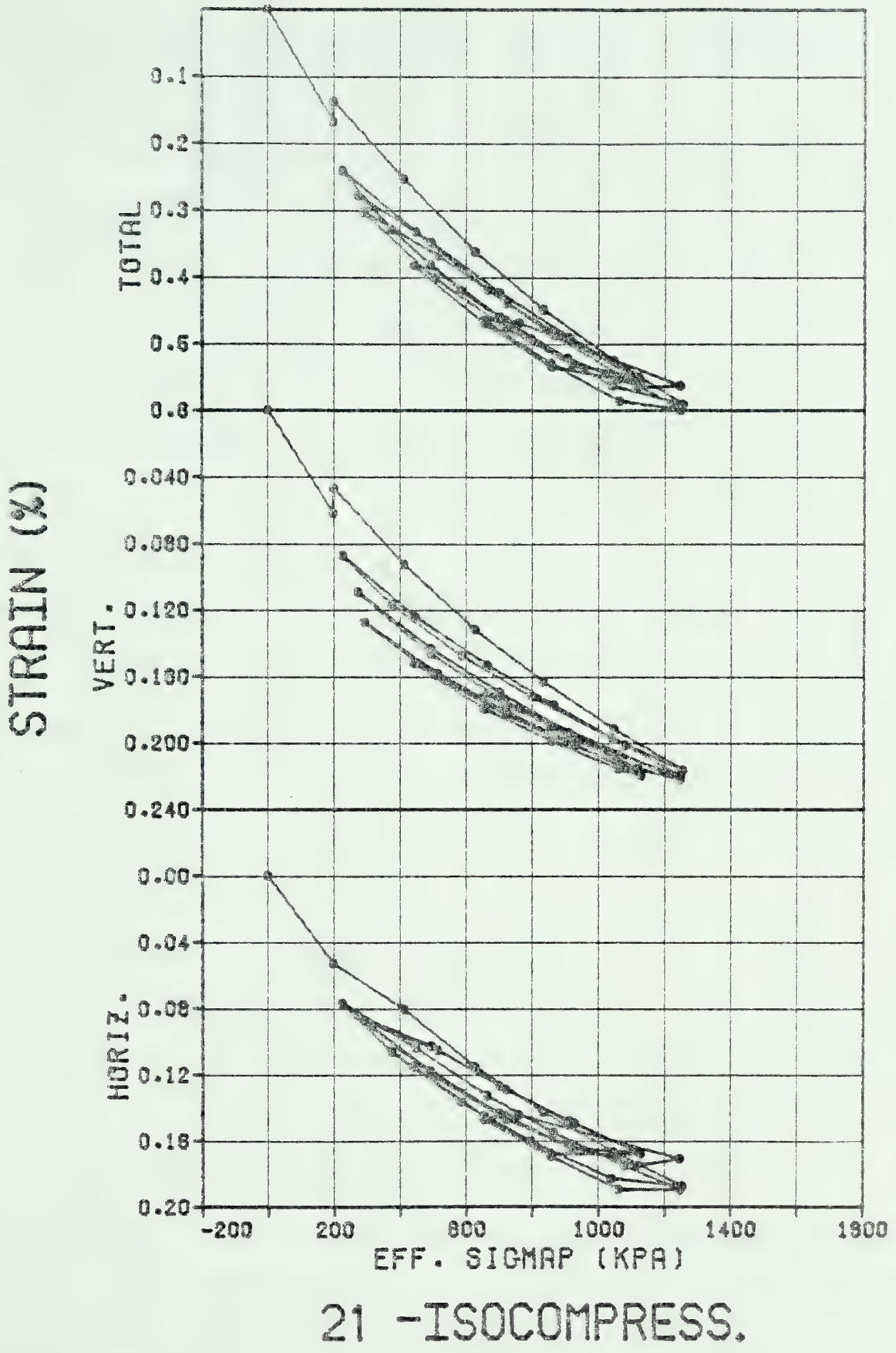


Figure 3.2 Lateral and axial strain response for sample 21. Isotropic stress cycling using double latex rubber membrane.

effects of gas diffusion on test results will be examined in Chapter 4.

(e) Tests M10a and b were performed to compare mass transfer rates due to gas diffusion and due to leakage through the external valves to the sample. The pressure drop for test M10a for a sample totally saturated with water and no gas was -0.5 KPa/min. Using a compressibility for water of 4.5E-7 KPa^{-1}, this can be converted to a rate of loss of mass, $(1/m * dm/dt)$ of $2 * 10^{-5}$ hr^{-1}. The equivalent mass loss rate for CO_2 diffusion, (test M10b), at dp/dt = -0.7 KPa/hr is $2 * 10^{-3}$ hr^{-1}, or 2 orders of magnitude faster. Thus, during an undrained soil test, the loss of gas by diffusion through the membrane would be the more important source of error in the fluid pressure readings.

(f) One gas diffusion test (M15b) was performed, using water and CO_2 as the pore fluid, to confirm the idea expressed in the last footnote, that the pressure response in the sample due to gas diffusion was independent of water saturation (since $H \neq 1$). The measured rate of pressure drop was -0.9 KPa/hr for p = 450 KPa, which compares favourably with the gas diffusion tests run on dry samples. It is interesting to note the strong temperature dependence of this response, (Figure 3.3; this will be discussed further in section 3.3.6).

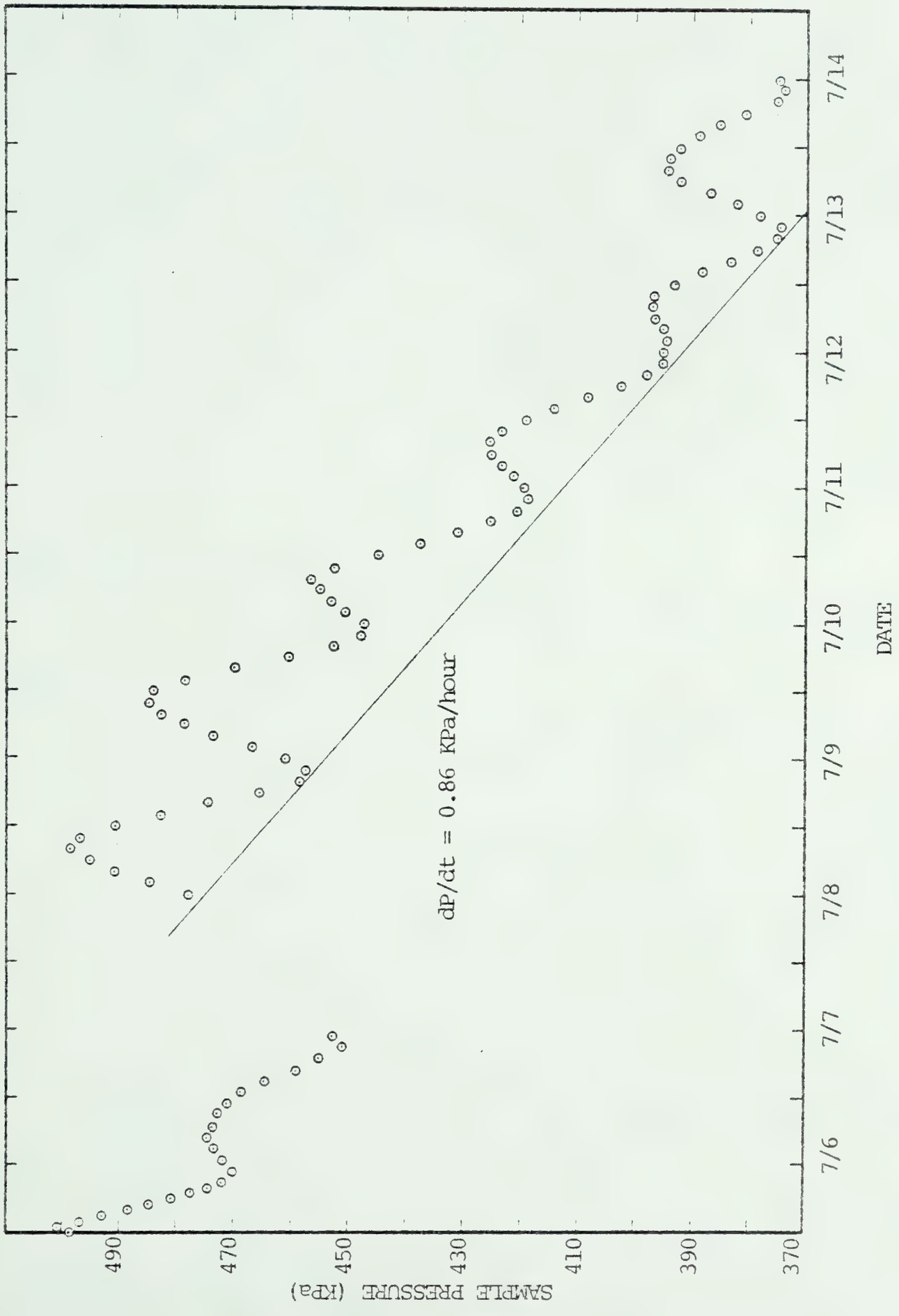


Figure 3. 3 - Gas diffusion from sample, for Test No. 15

As a result of the gas-diffusion tests outlined above, all undrained tests on gassy soils were executed with a standard double latex rubber membrane surrounded by glycerol. The glycerol, in addition to its low CO_2 solubility and low electrical conductivity, was non-toxic, easy to handle, non-volatile, non-corrosive, and totally miscible with water. This last attribute made clean-up much easier, but required that certain care be exercised in not contaminating the cell fluid with water and thus raising its conductivity (section 3.3.6)

3.3.2 Measuring strains or volume changes

Axial and lateral sample strains could be measured in one of two basic ways:

(a) By measuring the axial load ram displacement, and converting this into a vertical strain, measuring the volumetric strain of the sample, and then calculating the horizontal strain. The volumetric strain could be measured by the surface displacement and cathetometer method (Bishop & Donald, 1961) or by measuring the volume of liquid entering or leaving the cell.

(b) By measuring the vertical and horizontal strains independently, inside the cell, using either direct contact or non-contact transducers.

The choice of a strain-measuring device is somewhat arbitrary, as long as it meets the constraints of accuracy and stability. Accuracy requirements were assessed during an

initial drained isotropic test on a sample of dense Ottawa sand. The vertical strain in the sample was measured with an LVDT (Linear Voltage Displacement Transducer), monitoring displacements of the sample top cap inside the cell. An extremely sensitive model 24DCDT-100 (Hewlett-Packard) transducer was used, with an operating range of $\pm$ 2.5 mm. Over this range the maximum non-linearity is $\pm$ 0.5%, (a "least-squares" fit of transducer calibration data typically gives a correlation coefficient, r, of 0.99999). This transducer is a sealed unit with built-in signal conditioning equipment. Full-scale displacement is given by a $\pm$ 10VDC signal. Equipment sensitivity allowed signals to be measured reliably to $\pm$ 0.0005 Volts, giving a displacement accuracy of $\pm$ .00013 mm (or $\pm$ 5 * 10^{-6} inches). Using this transducer, a volumetric compressibility of 6 * 10^{-6} KPa^{-1} (for σ'= 300-700 KPa) was measured, or $C_1 = C_3 = \Delta\varepsilon / \Delta\sigma' = 2 * 10^{-6}$ KPa^{-1}. For a sample height of 100 mm, a minimum displacement of .00025 mm would correspond to a strain of 2.5 * 10^{-6}, which for this material would be the response to a change in stress of $\sigma' = \Delta\varepsilon/C_1$ = 1 KPa. The undrained soil tests were performed in increments of $\Delta\sigma'$ = 20 to 50 KPa; hence this transducer gave an acceptable accuracy for measuring vertical strains.

Fredlund (1973) reports an accuracy for volume change measurements of $\pm$ .09 cc, or for volumetric strains of $\pm$ 6 * 10^{-5}, using a steel ball and a cathetometer. This is an order of magnitude less accurate than the LVDT mentioned above, and was unacceptable for use with low compressibility

soils. It was decided not to use this method of measuring total volume change because of insufficient accuracy, and also because the measurements had to be collected manually. The measurement of the volume of liquid leaving or entering the cell by use of an external burette system suffered from the same limitations of accuracy, and also needed to be read manually. In addition, the cell fluid possessed a high compressibility because of the presence of tiny gas bubbles. These were caused by gas which diffused out of the sample and then exsolved upon a decrease in cell pressure. The measurement of cell fluid volume change, and thus sample volume change, was impossible.

Both Fredlund (1973) and Law (1975) had also used a caliper-operated, direct contact mechanism for measuring lateral deformations of the sample. Law reported measuring lateral deformations to an accuracy of 0.00004 inches (or 0.001 mm). Menzies (1976) similarly reported measuring lateral deformations to 0.003 mm. This is still an order of magnitude higher than the accuracy discussed above for the vertical LVDT. However, both Law and Fredlund used a model 24DCDT-500, which has 1/4 of the sensitivity of the model 24DCDT-100 transducer. A preliminary test was therefore performed using the more sensitive transducer with the caliper-arm direct contact mechanism.

Figure 3.4 illustrates the first generation of deformation transducers tested, (Figures 3.5 and 3.6 are

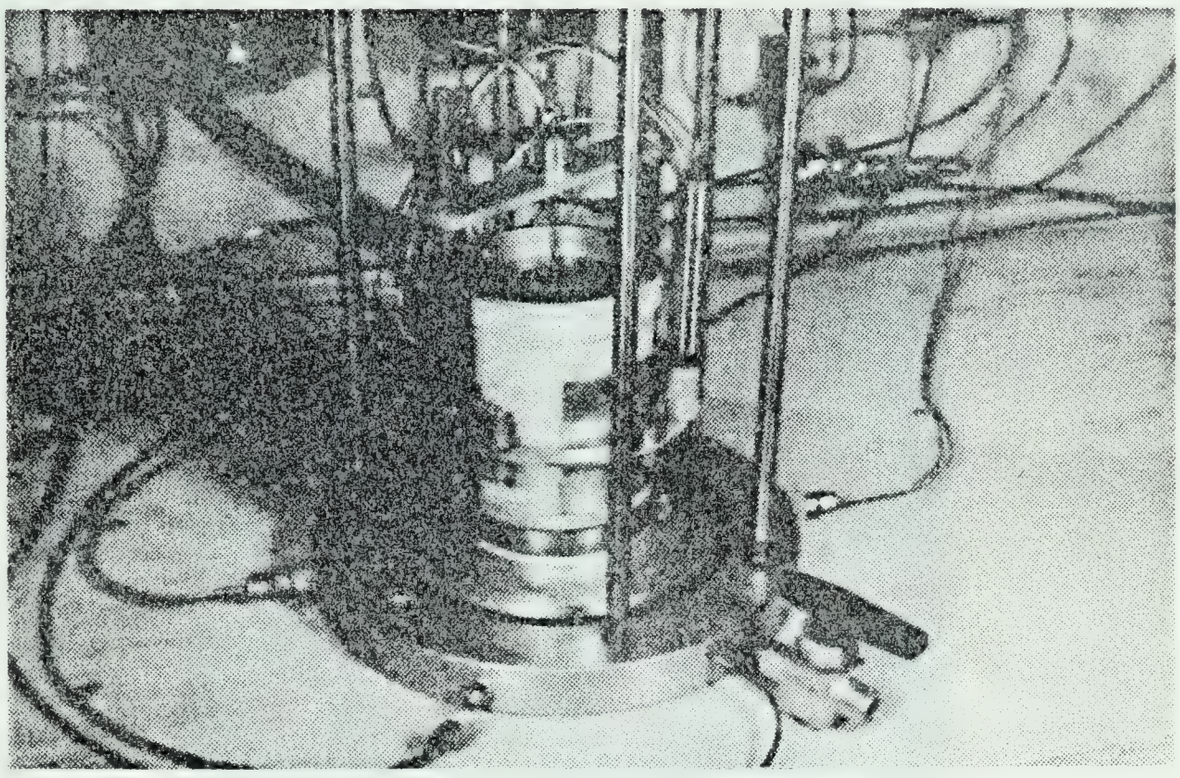


Figure 3.4 - Original Deformation Gauges

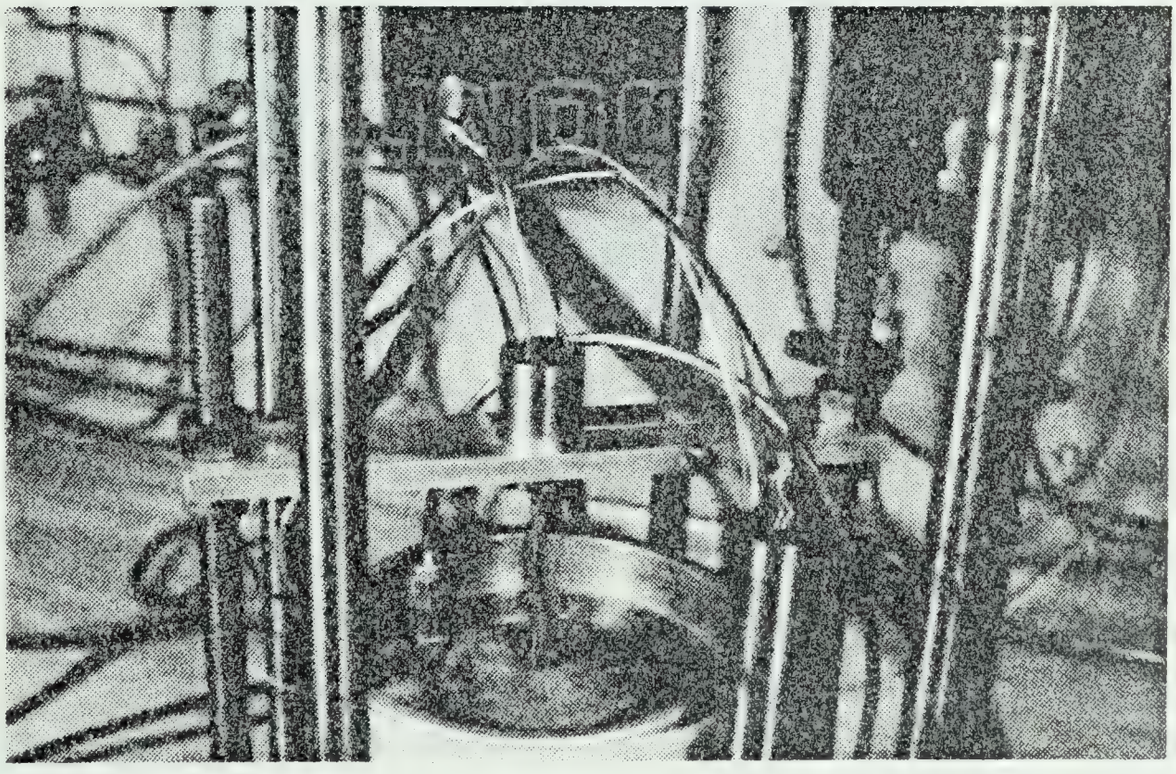


Figure 3.5 - Detail of vertical deformation gauge

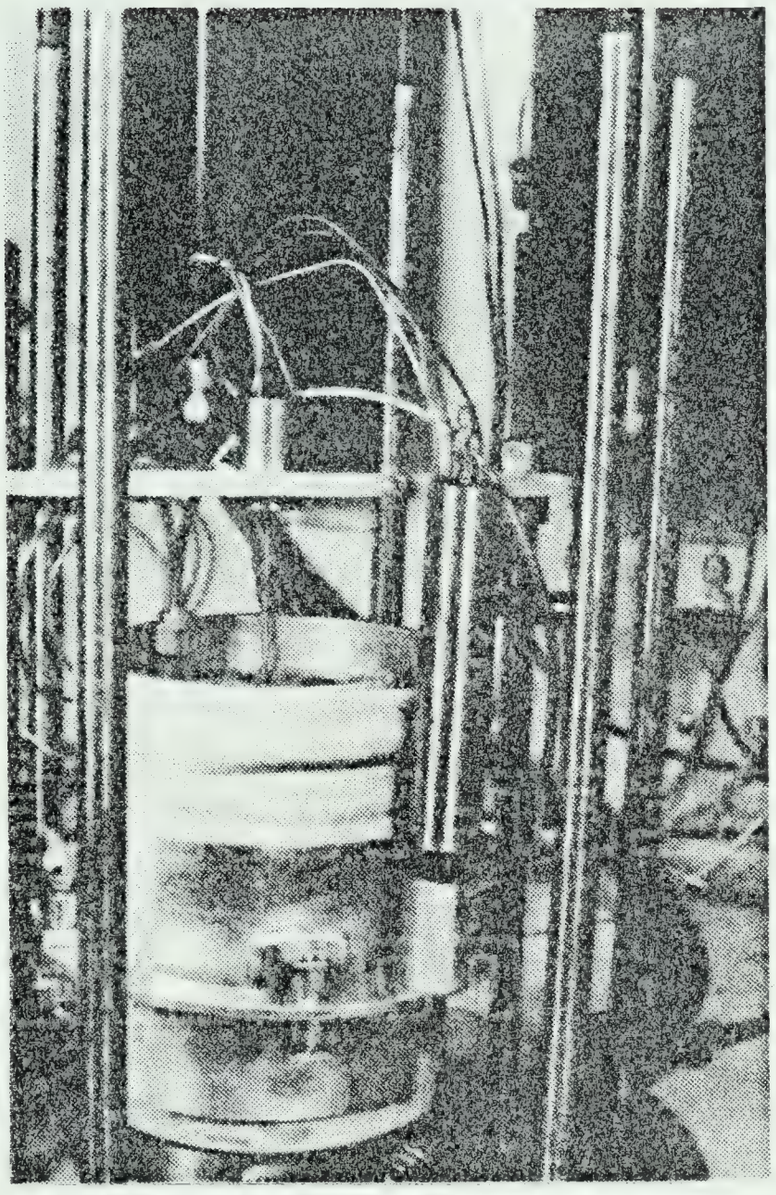


Figure 3.6
Detail, horizontal deformation gauge

closeups of the vertical and horizontal transducers, respectively). Several details of construction which reduced the lateral strain indicator accuracy are worth noting:

(a) The lateral strain indicator consists of a pair of circular-shaped calipers which rest against the sample at their midpoint, are hinged at the back, and joined at the front by an LVDT mechanism (not shown completely).

(b) The hinge-point at the back of the calipers is a source of small but measurable error on strain reversal.

(c) The original mechanism for establishing contact between the caliper and the sample was first a 2.5 cm square and then a 7.5 cm square brass plate (Figure 3.6) attached to the caliper by a hinge and given a curvature of about 12 cm, slightly greater than the sample. This proved to be a major source of inaccuracy in the measurement.

(d) The LVDT mechanism (Figure 3.6) consisted of an LVDT mounted vertically on one caliper. The core of the LVDT was attached to the opposite caliper by a thin steel wire and was spring-loaded. Again, this method introduced inaccuracy into the measurements.

Isotropic drained tests on dense samples of sand were performed to establish the accuracy of the lateral strain indicator, using a 24DCDT-100 transducer. It was found that

the poor level of accuracy reported by Law was due mostly to the caliper mechanism. This mechanism was improved in two ways:

(a) The contact point between the sample and the caliper was redesigned. The hinge and brass-plate was replaced by a solid point-contact. To prevent indentation of the sample, a 2.5 cm square brass plate (curved) was held against the sample on each side until the caliper mechanism was set in place (Figure 3.7).

(b) The LVDT was mounted horizontally, with the body attached directly to one caliper and the core attached directly to the other, (Figure 3.8). The core arm had to be bent slightly and the body adjusted to the proper angle to allow the caliper arms to move freely. Using this arrangement, movements of 10 - 15 mm were possible before the mechanism was restricted by non-compatible angular displacements of the core and transducer housing. The calipers were spring loaded at the front, parallel to the LVDT, as well as at the rear hinge point.

The improved lateral strain indicator provided an accuracy comparable to the vertical LVDT, except for some hysteresis in the stress-strain curve upon stress reversal. This was mainly due to the caliper pivot, (Figure 3.2).

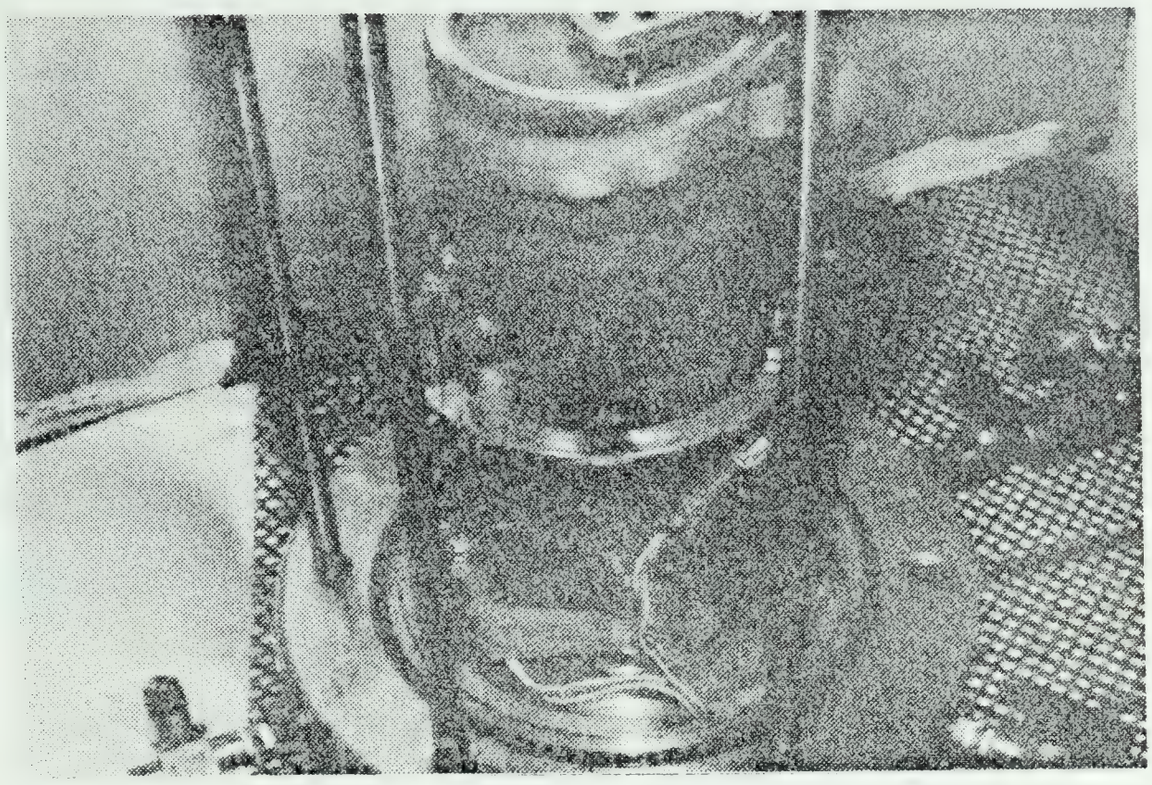


Figure 3.7 - Modified horizontal gauge
Detail of point contact

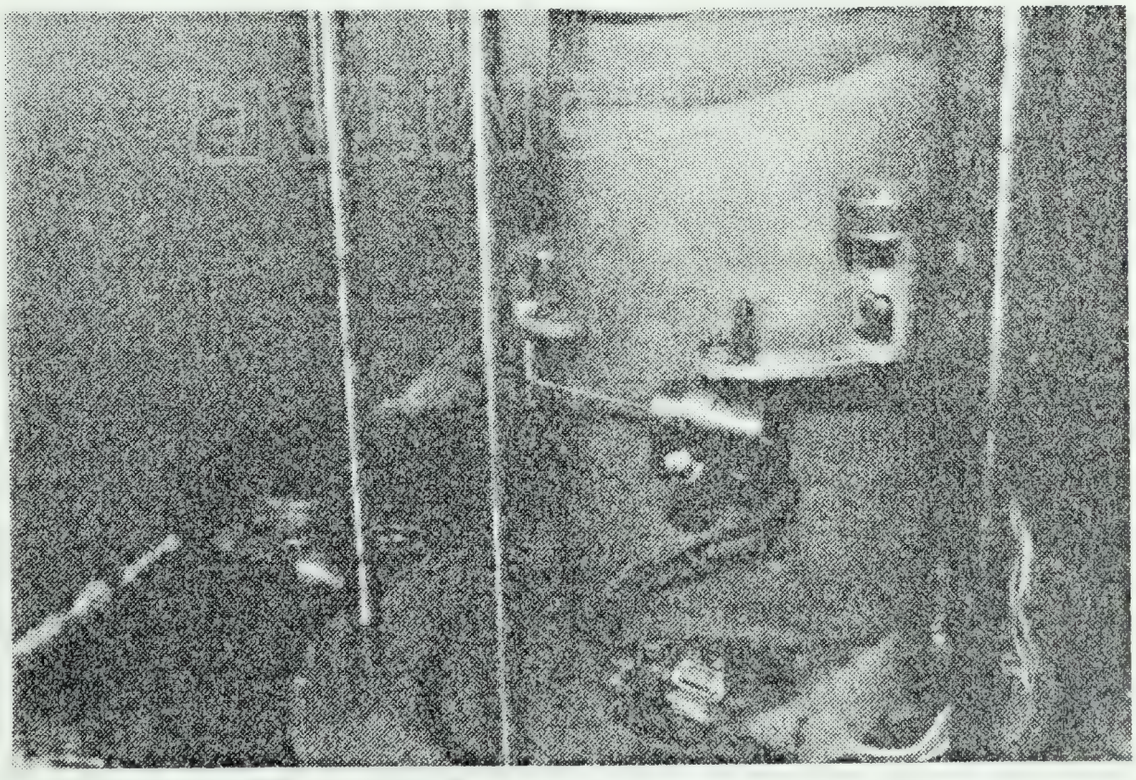


Figure 3.8 - Modified horizontal gauge
Detail of LVDT mounting

A test was also performed to measure the "stiffness" of the strain-measuring system itself. Typically, this is done with an incompressible sample, so that the deformations measured are those of the system components, i.e. the top cap, porous stones, membrane, caliper arms, etc. The system compressibility was $4 * 10^{-7}$ KPa^{-1} vertically, and was too small to measure horizontally. The vertical system compressibility may be attributed to deformations of the metal porous stone against the (steel) sample. It was felt that these deformations were not representative of the behaviour of the strain-measuring system in contact with a real, and considerably more compressible sample, and so they were not used as corrections for the laboratory test data.

A comparison of the performance of the vertical and horizontal strain indicators may also be made by examining the measured strains in an isotropic test. Figure 3.9 is a plot of axial strain vs volumetric strain for the isotropic stress-cycling portion of Test No. 21. Since $\varepsilon_{vol} = \varepsilon_{vert} + 2*\varepsilon_{horiz}$, if $\varepsilon_{vert} = \varepsilon_{horiz}$, then $\varepsilon_{vol} = 3*\varepsilon_{vert}$. The good correspondence between vertical and horizontal strains suggests that the vertical system compressibility correction mentioned above was indeed peculiar to the use of an incompressible sample.

The modified direct-contact Lateral Strain Indicator then provided an acceptable accuracy of $\pm$ .00013 mm. The design of the LSI inherently possessed one minor disadvantage, however. Since the caliper arms were attached

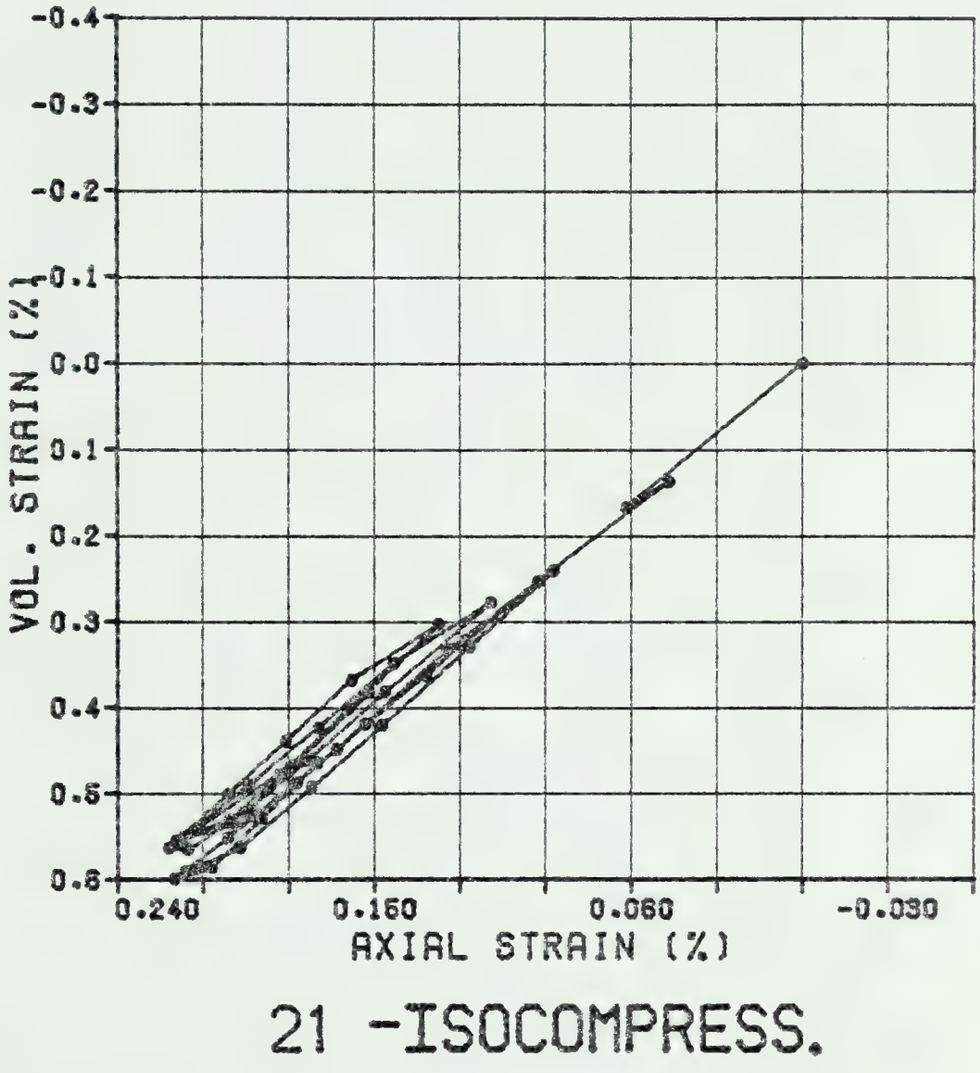


Figure 3.9 Comparison of vertical and horizontal strains, Test 21.

to an external post (Figure 3.4), any translation of the sample in a direction away from this post would cause spurious lateral strain readings. This disadvantage could be overcome by designing a LSI which was attached to the sample only. It would necessarily need to be light, as it would be held in place by frictional resistance at the point contacts. A light LSI was designed, consisting of two lengths of curved spring steel, attached to pads which contacted the sample, (Figure 3.10). Strain gauges were mounted on the spring steel. Tests on this device revealed a sensitivity of $\pm$ .01 mm. In addition, long term drift problems associated with this model limited the accuracy to $\pm$ 0.2 mm. Even assuming the problem of drift in the readings could be overcome, the maximum accuracy of $\pm$ .01 mm was unacceptable.

The caliper arm LSI could be used for measuring strains in the laboratory samples if sample translation was not large. Since all preliminary isotropic tests had demonstrated excellent agreement between measured vertical and horizontal strains, this horizontal LSI was chosen for all the subsequent testing.

3.3.3 Measuring pressures

Cell and sample pressures were measured using CELESCO 0 to 300 psi, (0 to 2000 KPa), strain-gauged diaphragm transducers, exhibiting an accuracy of $\pm$ 0.1 KPa. The transducer for monitoring sample pressure was mounted in the base of the cell, as close as possible to the bottom of the sample. When all valves to the sample were closed,

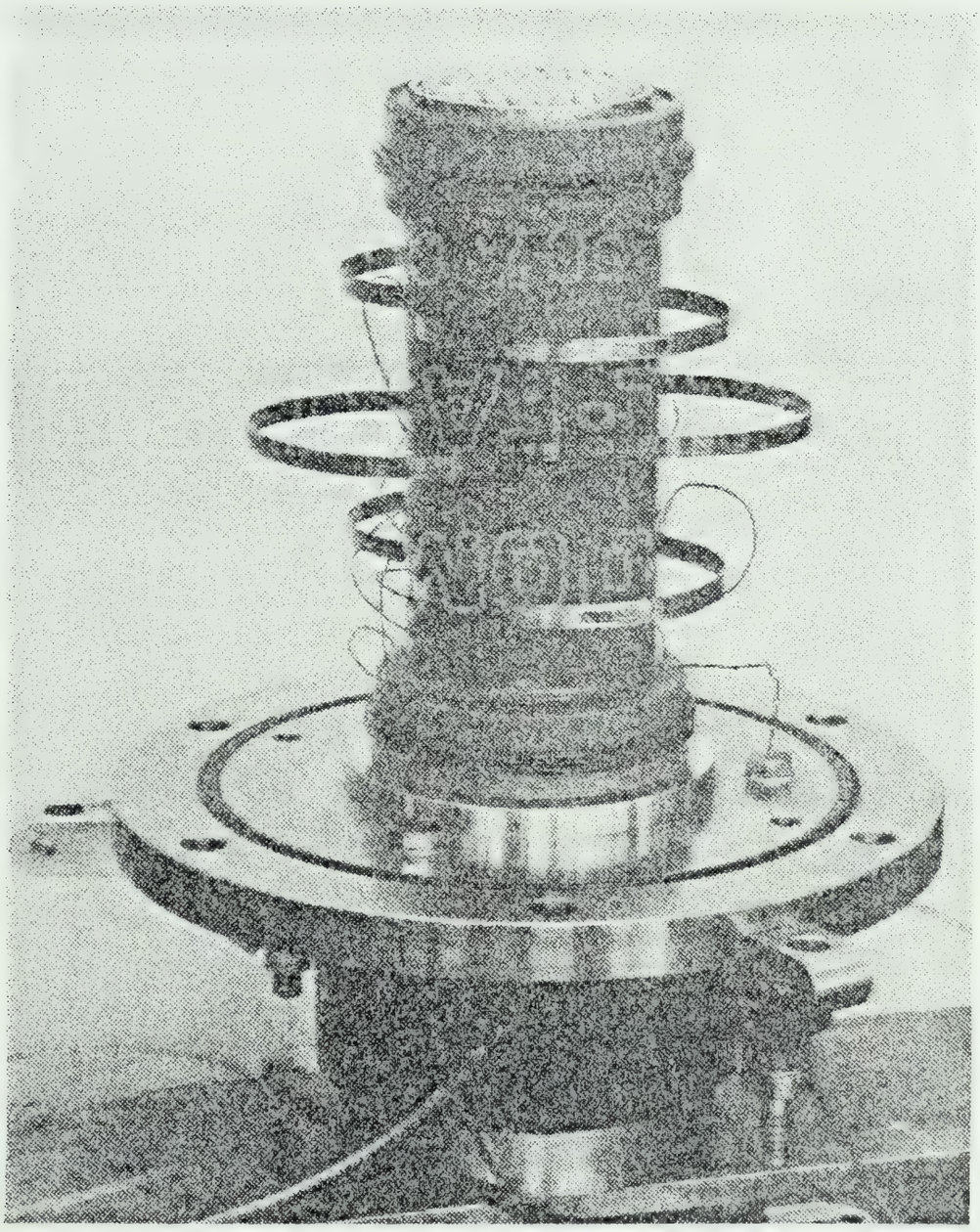


Figure 3.10 - Light-weight Lateral Strain Indicator
(illustrated from El-Ruwayih, 1976)

approximately 20 cc of fluid were contained in the lower porous stone, lines, and pressure transducer, and approximately 25 cc of fluid were contained in the upper porous stone and lines. This may be compared to a void volume of 250 cc for the 100 mm high samples and 500 cc for the 200 mm high samples.

The pore pressure transducer was connected to the sample via a coarse metallic filter stone. Although the use of coarse stones is associated with the measurement of pore gas pressures, it is likely that at the saturations measured during most of the tests, the air phase was occluded and the pressure measured was that of the liquid phase. The typical bubble radii for the material tested (see Chapter 5) probably lie in the range of 0.03 to 0.07 mm, and using an interfacial tension between CO_2 and H_2O of 70 dynes/cm, this implies a difference between the gas pressure and the liquid pressure of:

$$P = 2 * T_s / r$$

T_s = interfacial tension

r = bubble radius

$$= 90{,}000 \text{ dynes/cm}^2$$

$$= 4 \text{ to } 9 \text{ KPa}$$

3.3.4 Measuring Deviator Stress

All tests performed were stress-controlled. Deviator stresses were applied using a diaphragm-operated air cylinder (trade name Bellofram) and measured with an external load

cell placed in-line with the cell loading ram (Figure 3.11). Cell ram friction was initially measured with two load transducers, (one mounted external and one internal to the testing chamber), at a series of cell pressures. The calibrations applied to all test results are shown in Figure 3.12.

The application of these calibrations was somewhat uncertain when, during the course of the test, the sample underwent a vertical strain reversal. In this case, the plots of deviator stress appear to take a step increase or decrease, whereas the changeover from positive to negative ram friction (or vice versa) was actually more gradual.

3.3.5 Saturating water with CO_2 gas

Water was saturated with CO_2 gas in a bubble chamber (exterior to the test cell) and then moved into the sample under an appropriate back-pressure. A Linde commercial grade CO_2 was used (99% pure) with the main contaminant being air. The CO_2 gas was allowed to bubble slowly through the water in the chamber under a controlled and measured back pressure for a period of several hours to establish equilibrium between dissolved and free gas in the chamber.

3.3.6 General cell design considerations

Cell construction

The cell was constructed of aluminum and the drain lines were of copper tubing. This allowed the possibility of high pressure tests (up to 7000 KPa), although this facility

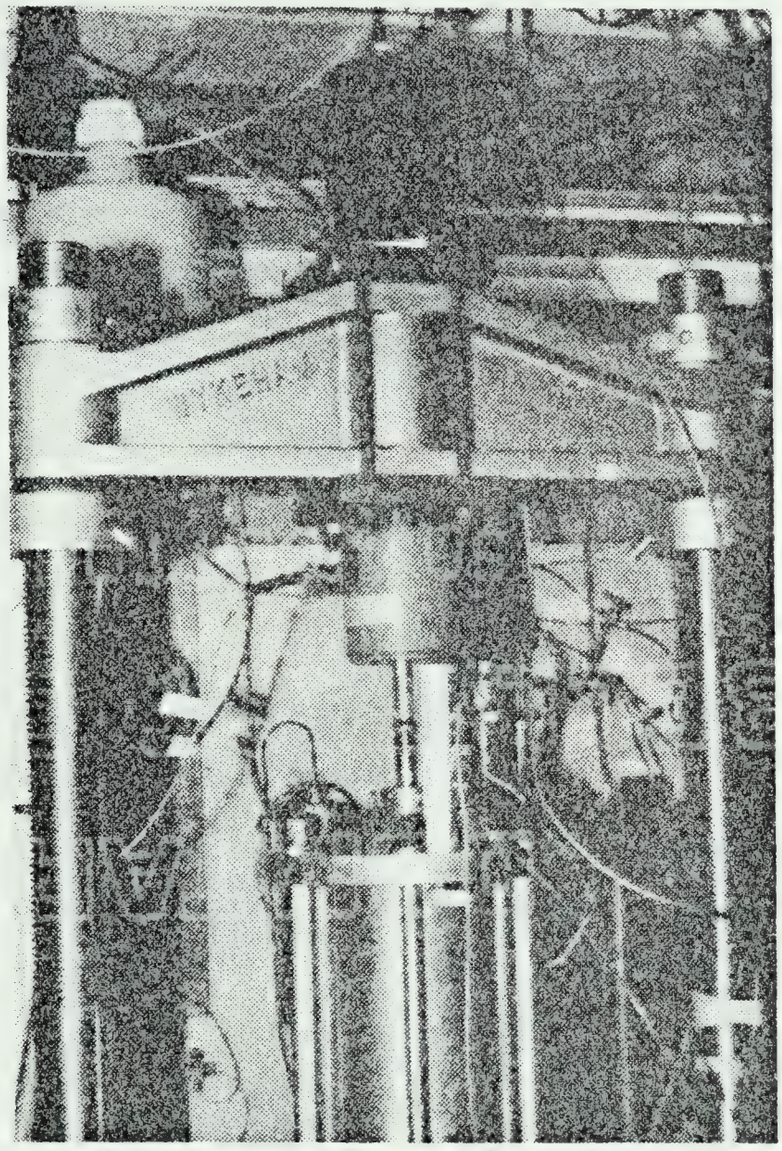
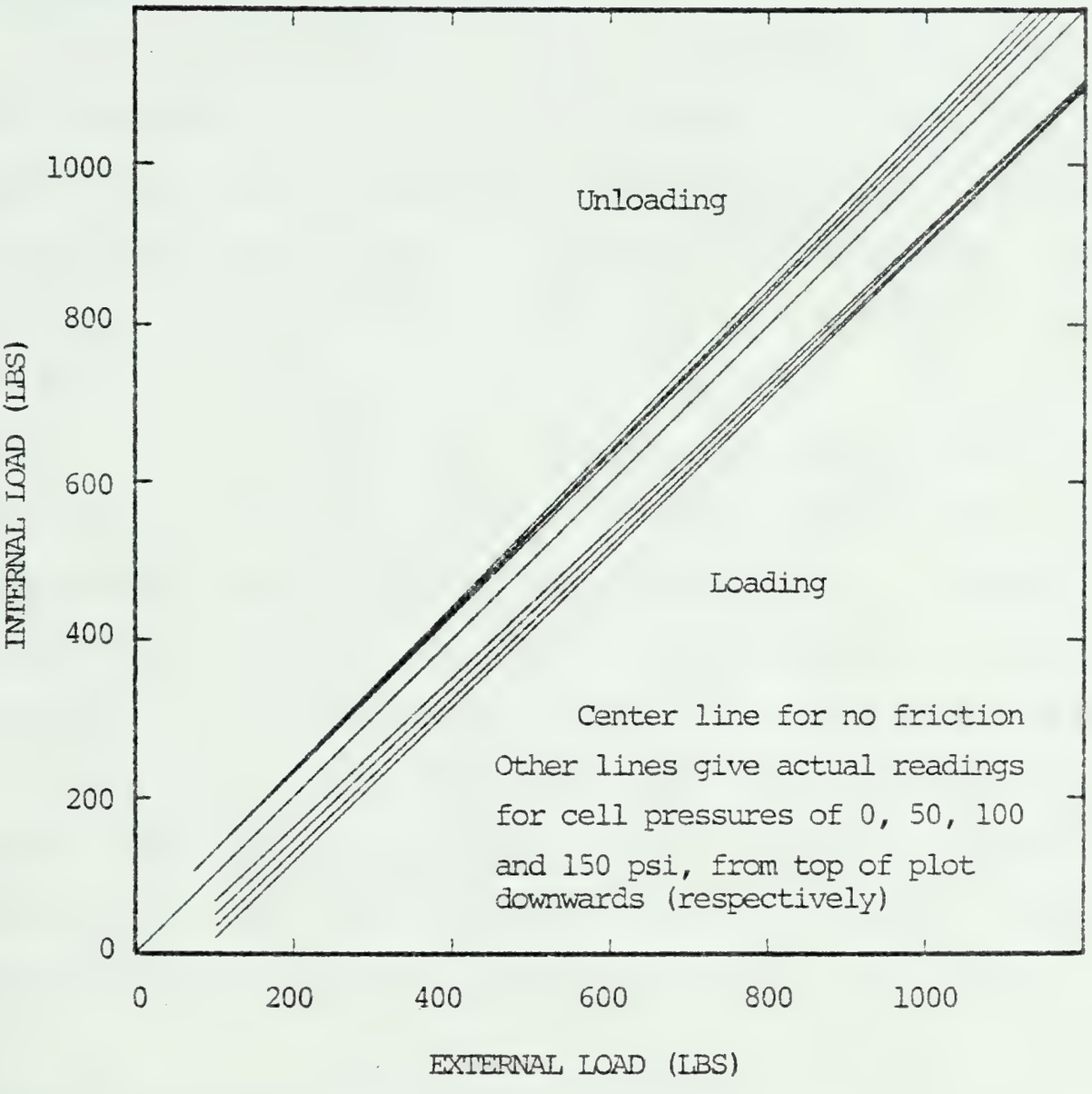


Figure 3.11 - Triaxial loading frame
Bellofram and load cell



For loading: Ram friction =
-30-(0.05*AL)-(0.32-[0.0002*AL])*cell pressure

unloading: Ram friction =
27+(0.03*AL)+(0.02-[0.0002*AL])*cell pressure

where: AL = axial load (lbs)
Ram friction in lbs
Cell pressure in psi

Figure 3.12 - Calibration for ram friction

was never exploited. The metal parts were used mainly to prevent gas diffusion from the lines or from the cell itself.

Diffusion through the end caps

Fredlund (1973) discusses the problems associated with the diffusion of gas from the sample, through the porous plates and into the area around the pore pressure transducer. Due to the present method of sample preparation, not only the sample, but the porous stones, end caps and all lines are initially filled with a CO_2-saturated water. During the test there is no reason for CO_2 concentration gradients to develop, and so it is unlikely that diffusion occurs through the porous stones, as encountered by Fredlund. However, with decreasing pore pressure, gas will exsolve from the fluid located in the lines, porous stones, etc. and will contribute to the sample volume change measured during the undrained test. This has an equivalent effect of testing a sample with about a 5 to 10% (depending on sample size) increased porosity over that actually established in the sample.

Temperature control

Both the pore pressure and the volume change measurements were found to be temperature dependent. The pore pressure dependence on temperature was first recognized at the end of Test No. 15. After completion of the test, the sample was left in an undrained state, and under constant cell pressure, for 10 days to monitor change in pore pressure

due to loss of gas by diffusion through the sample membrane (Test M15b). A general decrease in pore pressure was observed, but superimposed on this was a daily fluctuation in pressure (Figure 3.3). At the time there was no temperature monitoring equipment on the sample, but the pressure fluctuations were thought to be due to temperature changes. Figure 3.13 plots the outside temperature fluctuations for the same period of time, and it may be observed that there is a good correspondence between the two, both in time and amplitude.

Problems with temperature-induced pressure fluctuations had not been encountered in tests 1 to 14, since these were performed over the winter of 1979-80, when laboratory temperatures were maintained relatively constant. Temperature monitoring was carried out for subsequent tests in the cell itself, and the test apparatus was further insulated against temperature fluctuations. These were confined to $\pm$ 0.5 degrees F, and the temperatures changes for any particular phase of one test were limited to $\pm$ 0.1 degrees F.

It was also found that the volume change measurements were slightly temperature dependent due to temperature sensitivity of the LVDTs. Calibrations were then performed at the test temperature.

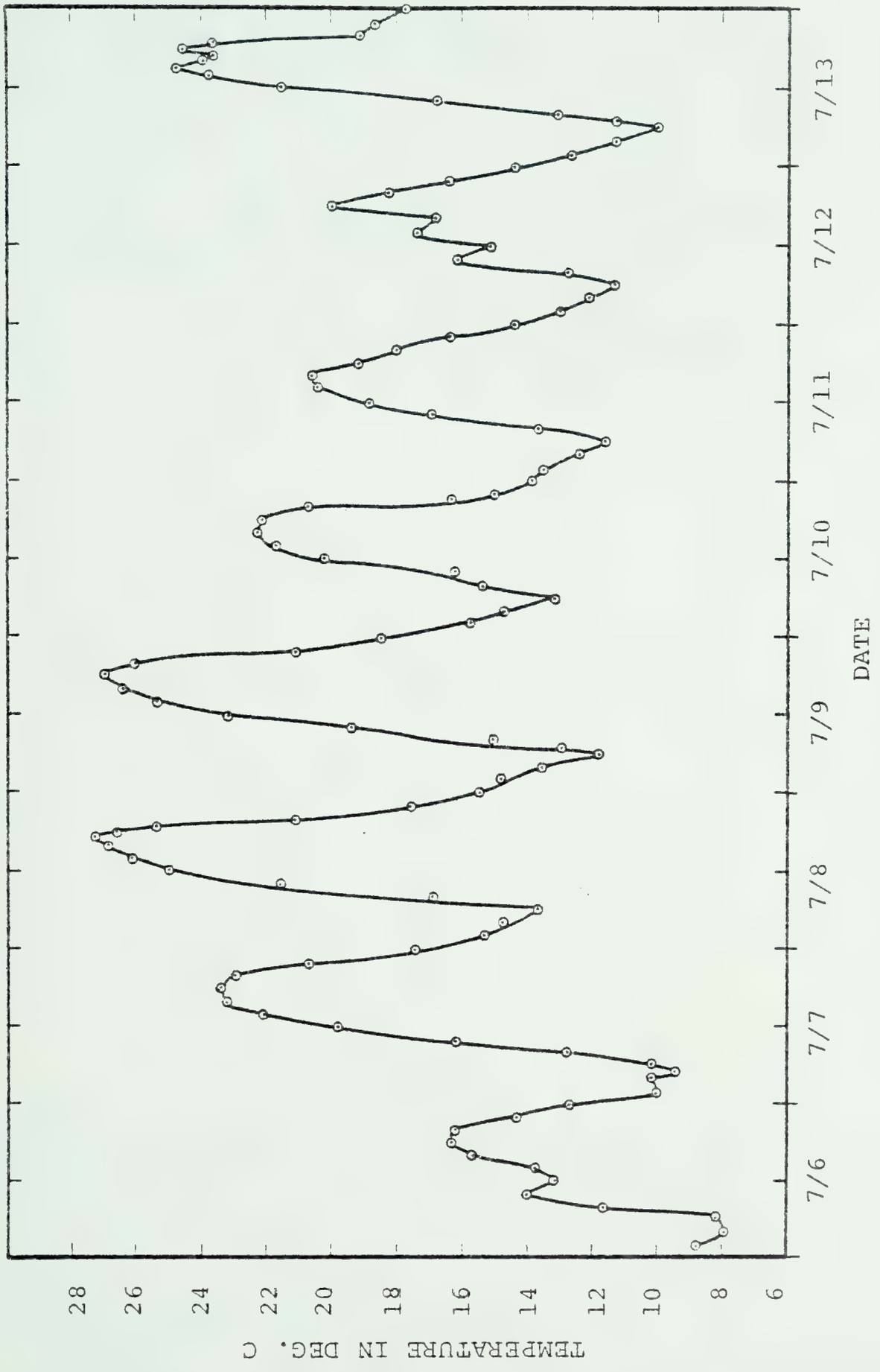


Figure 3.13 - Hourly temperatures at Edmonton

Sealing the electrical cables

It was necessary to pass the wires for all internal transducers through the cell in some manner. Several methods of sealing the wires were investigated. All methods attempting to seal around the insulation on the wire proved unsatisfactory, as invariably, in the course of preparing or dismantling a sample, this insulation would be damaged slightly and the cell fluid would leak out between the insulation and the wire. Finally, a bare-wire seal was devised. Each wire was individually passed through a hole in a short rod of teflon and this teflon was compressed by a standard tube fitting at the base of the cell. The method successfully sealed all wires leaving the cell, but required extreme care in preventing electrical leaks at the fitting. The fitting was located at the base of the cell, and on dismantling the cell, water was used to clean the sample and cell interior of glycerin. It was important to properly dry around these fittings, so that electrical short circuits would not develop during the next test.

Assembly

The cell was designed so that the sample could be set up on the base and the transducers attached and checked for operation. The top portion of the cell was attached just prior to starting the test.

Figure 3.14 shows the general testing equipment, including the sample on the cell base, the CO_2 cylinder and

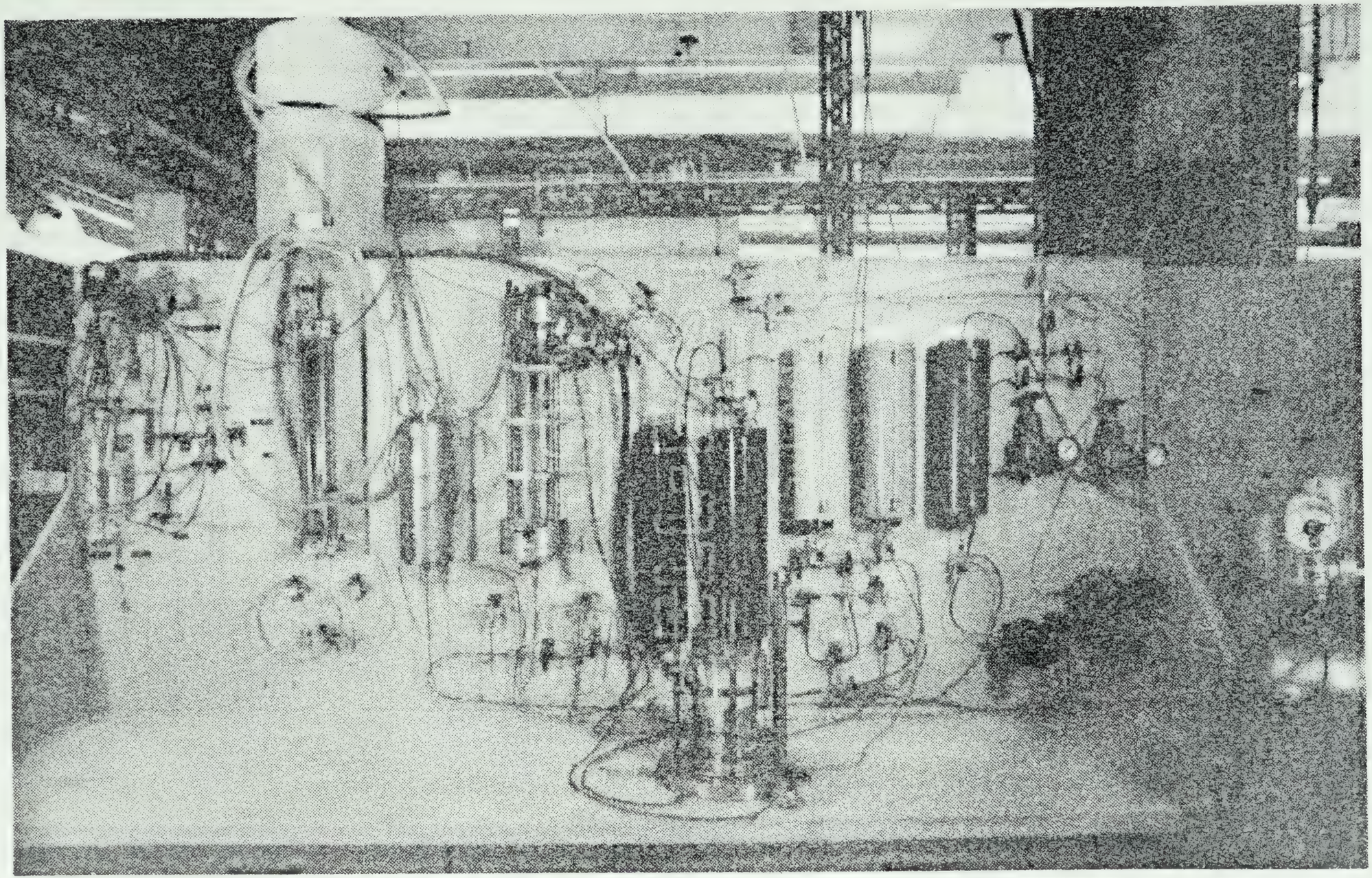


Figure 3.14 - Testing Apparatus

bubble chamber, several back-pressure chambers, a low and high pressure volume change indicator (not used), the glycerin storage container, air pressure regulators and associated plumbing.

3.4 TESTING PROGRAM

The laboratory program consisted of a series of undrained tests on dense samples of Ottawa Sand ($n_i = 0.32$). These samples were initially totally saturated with water ($S = 1$) which contained some dissolved CO_2 gas, (and minor amounts of air). All samples were initially unloaded to low effective confining pressures, and some experienced stress cycling. The stress paths investigated included isotropic unloading/loading, anisotropic unloading/loading, decreasing p' to failure, and increasing q to failure. These stress paths are illustrated in Figure 3.15.

All tests were performed by applying several increments of stress, and allowing the sample to come to equilibrium between stress increments. Transient behaviour, due to gas exsolution, typically lasted from 1 to 2 hours, so that a full test, comprising 10 to 15 phases, lasted from 1 to 2 days. Including sample preparation, initial testing for gas diffusion and deformation properties, the test proper, and dismantling, a test could last up to 1 week.

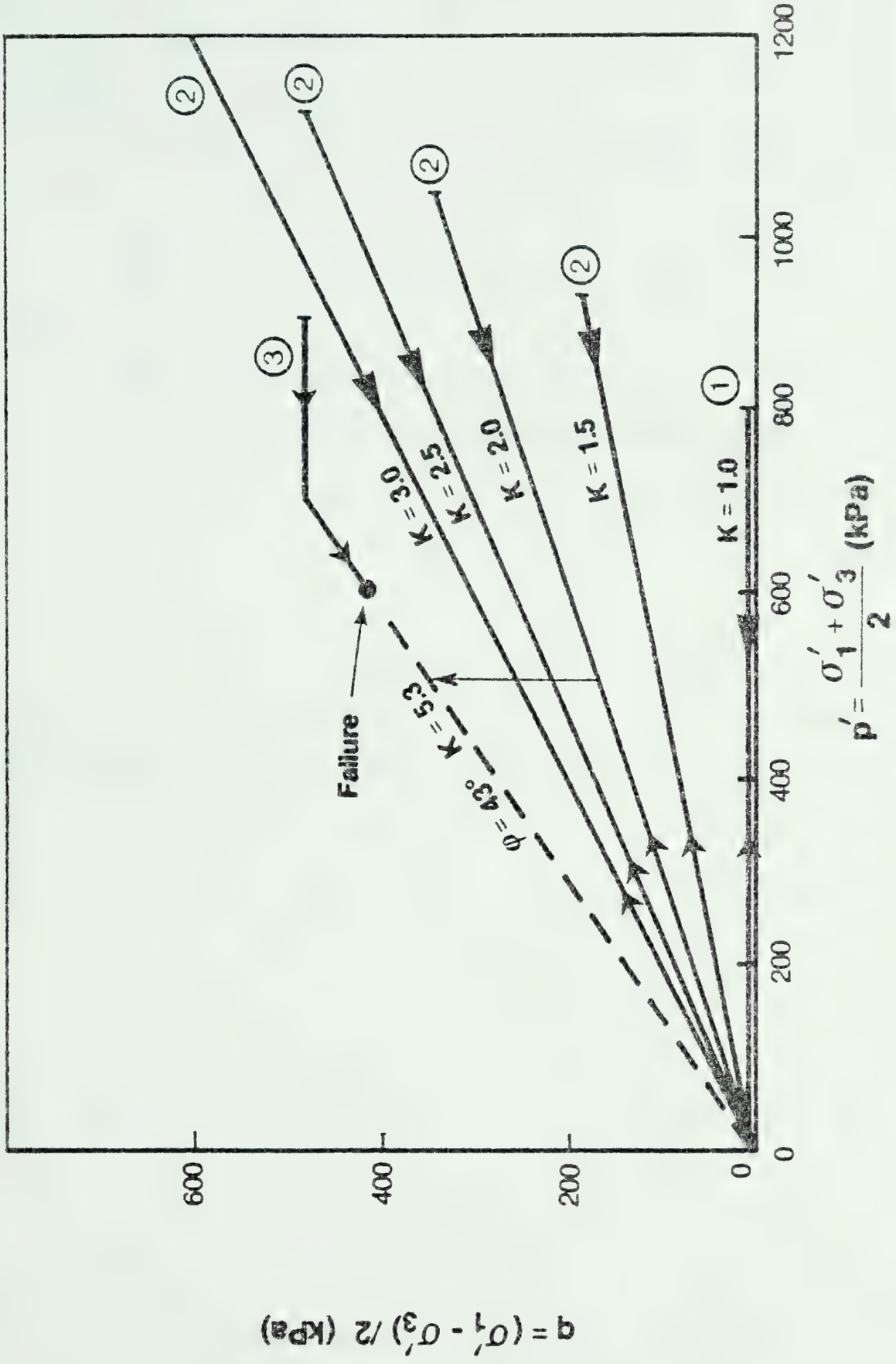


Figure 3.15 Stress paths for undrained tests on dense sand with H_2O/CO_2 pore fluid (Sw_i=100%)

3.5 TESTING PRELIMINARIES

3.5.1 Sample preparation

The soil used in all tests was Ottawa Sand, presieved so that 90% of its grains were between 0.6 and 0.25 mm (ASTM C109). Figure 3.16 illustrates a typical grain size analysis.

A compaction test was performed for this sand, using the actual sample mold and cell base from the test apparatus. The result is shown in Figure 3.17. A maximum dry density of 1.73 Mg/m^3 was obtained by this method, (or a minimum porosity of 0.353).

It was found, however, that a much denser sample could be obtained by placing the base and mold on a vibrating table, partially filling the mold with water, and placing and compacting the sand underwater. Dry densities of 1.81 Mg/m^3 (or n = 0.322) were consistently achieved using this method.

The sample was then prepared by placing a double latex membrane around the bottom cap and sealing with two O-rings. A split mold was strapped around the bottom cap and the sample compacted inside the membrane and mold as described previously. The top cap and top drainage line were attached and then a suction was applied to the sample and the compaction mold was removed. Sample dimensions were recorded and the strain indicators were attached and initial readings were taken. Then the top of the cell was assembled, the cell filled with glycerin, a nominal cell pressure applied, and the vacuum removed.

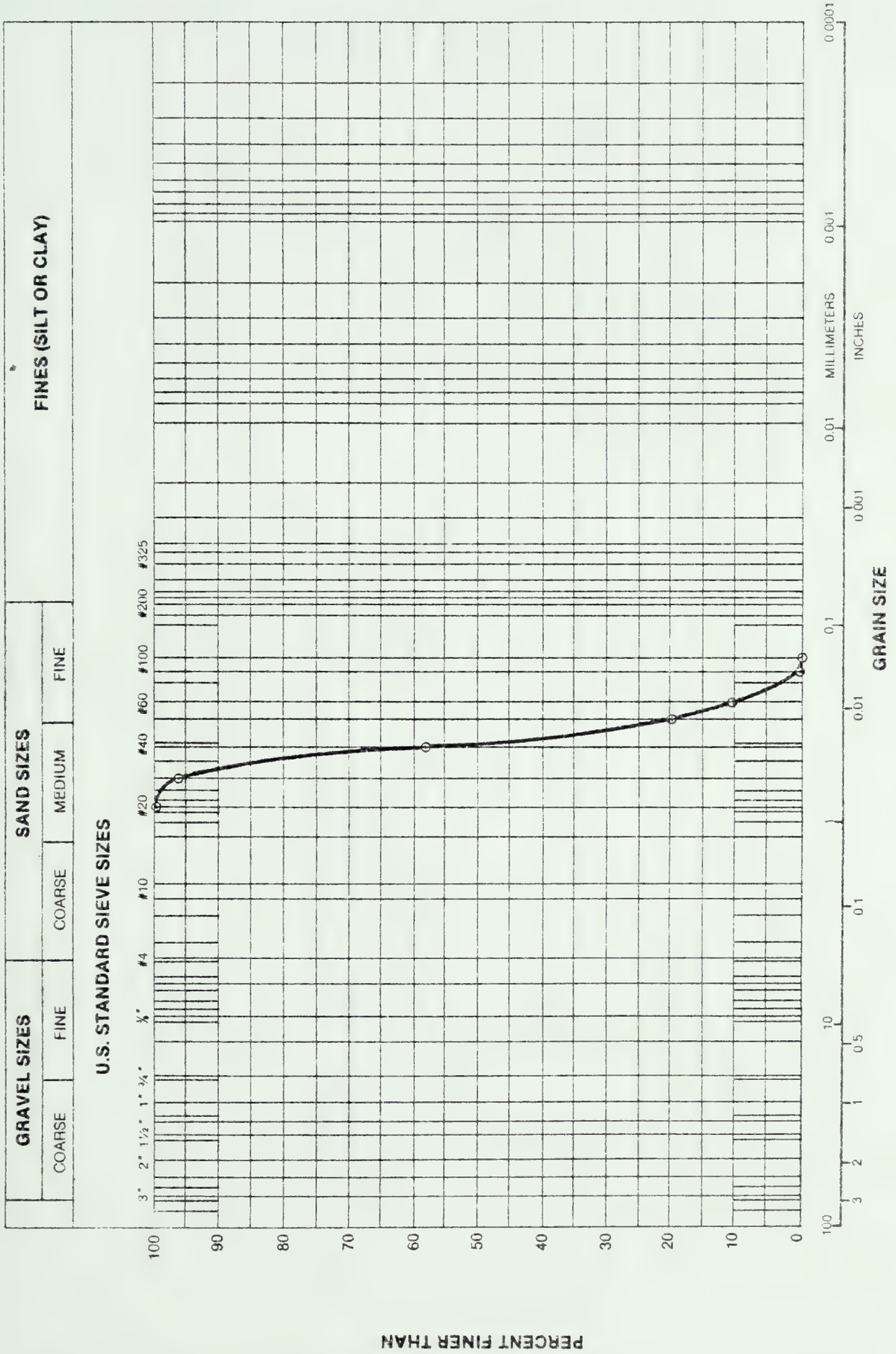


Figure 3.16 - Grain size analysis for typical sample

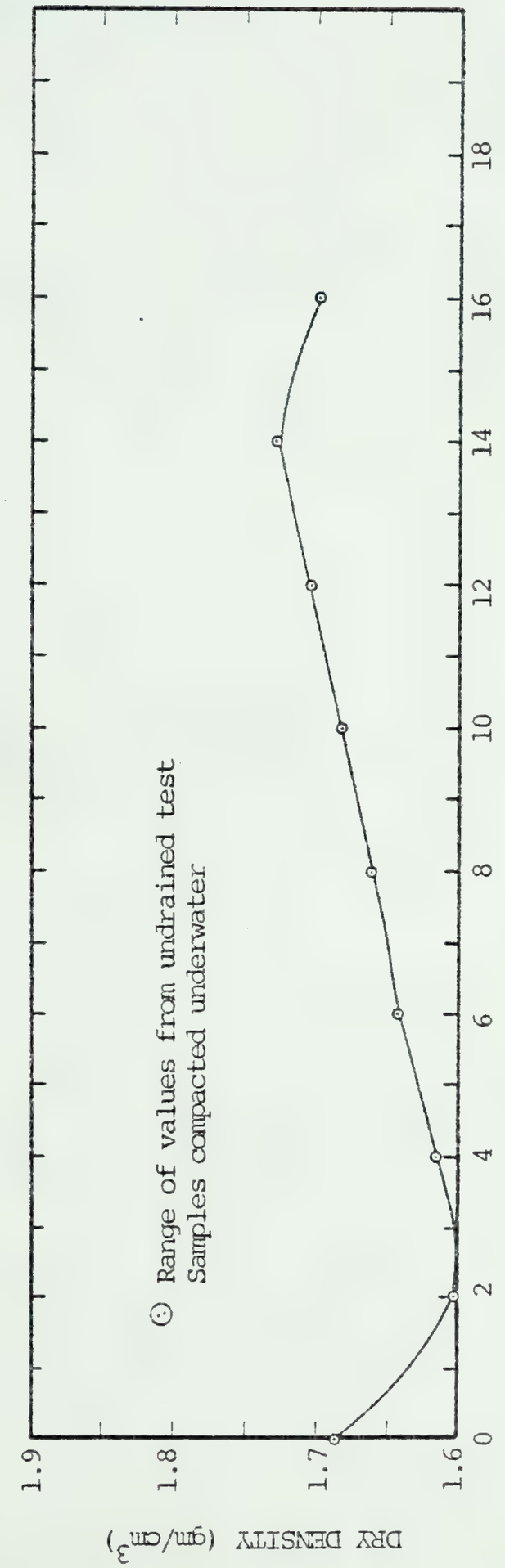


Figure 3.17 - Compaction curve, Ottawa Sand

3.5.2 Saturation with water

Even though the sample was prepared by placing and compacting underwater, it was found that it was not fully saturated due to the presence of entrapped air bubbles. Black and Lee (1973) have demonstrated that, depending upon the back pressure and initial saturation, the time to fully saturate such samples could take from several hours to several days (or even months).

A quicker and more consistent method of saturating these samples was discovered, however. Part of the reason for requiring high pressures and/or long times for saturating such samples containing air bubbles is the low solubility of air in water. Approximately one atmosphere back pressure is required to dissolve each 2% of initial gas saturation, since $H = 0.02$. The process of dissolution, at such pressures, will only be complete at infinite time. One method of increasing the rate of gas sorption, discussed by Black and Lee, is to increase the back pressure. Another method is to increase H, and possibly also the diffusivity constant, by replacing the air with a more soluble gas.

This was accomplished by displacing the water and air in the sample with CO_2 gas, allowing the CO_2 to drain through the sample for approximately 15 to 30 minutes, and then slowly displacing and dissolving the CO_2 gas with distilled water. This water contained some dissolved air, but all free

air bubbles had been removed. Left under a minimal back pressure for an additional 15 minutes, the sample would be totally saturated.

3.5.3 Isotropic compressibility

While the sample was being totally saturated (the last step discussed above) an isotropic compressibility test was performed by subjecting it to several drained stress cycles. This preliminary stress cycling further compacted the sample and provided information on the performance of the vertical and horizontal strain indicators. The results from such a test are shown in Figure 3.2. The volume compressibility for the sample could then be calculated, (e.g. for Test No. 21, $\beta_T = 3.5 * 10^{-6}$ KPa^{-1}).

3.5.4 Test for full saturation

When the compressibility tests were completed, a standard B-test was then performed by closing all drainage lines to the sample, increasing the cell pressure and measuring the pore pressure response. Black and Lee (1973) present a formula for calculating the initial degree of saturation in the sample knowing the pore pressure response B (=$du/d\sigma$):

$$S_i = \frac{1 - Z * (1 - B)}{1 - Z * Q} \qquad (3.1)$$

$Q = B*n*\beta_l/\beta_T$; $Z = Y/D$; $Y = \beta_T*\Delta\sigma/n$; $D = 1-(P/[P+\Delta u])$

Equation 3.1 may be obtained by solving equation 2.15a in terms of S instead of Δu, (with H = 0, since no time is allowed for gas exsolution). Calculations for initial saturation at this stage of the test typically yielded values of about 99.98%.

3.5.5 Saturation with water and dissolved CO_2 gas

The last step, prior to testing, and after full saturation of the sample with water had been established, was to replace the distilled water in the pore space with water and a known amount of dissolved CO_2 gas. This was accomplished by slowly draining the fluid out of the bubble chamber and into the sample. The displacement was done in 3 stages, using a volume of CO_2 saturated fluid equal to twice the pore volume during each stage, and letting the sample sit for 30 minutes between stages to allow the new, and any remaining old pore fluid to mix and equilibrate their dissolved CO_2 concentrations. This movement of pore fluid was driven by a low pressure gradient, of approximately 30 KPa, across the sample. The lowest pressure in the system was maintained at about 300 KPa above the previously established liquid/gas saturation pressure.

3.6 TESTING PROCEDURE

At the beginning of the undrained portion of the test, all the preliminary work discussed in Section 3.5 had been performed. The initial sample stresses were then set, with σ_3 usually about 1200-1300 KPa and u about 600 KPa. U was

initially greater than the liquid/gas saturation pressure, so that the sample was totally saturated with water. All drainage lines to the sample were closed and initial readings were taken for σ_3, σ_D, u, ε_h, and ε_v.

For the isotropic tests, σ_3 was then decreased by some amount, typically about 100 KPa, readings of u, ε_h, and ε_v were immediately noted and then monitored with time until no further change was measured. The next step decrease in σ_3 was then applied and the measurement sequence repeated. σ_3 was decreased until σ'_3 was close to zero, and in some cases equal to zero, and then increased in several stages back to its initial value.

The anisotropic tests were conducted in a similar manner, except that both σ_3 and σ_D were decreased (or increased) together and σ_D was further adjusted as u varied with time to maintain a constant ratio of σ'_1/σ'_3.

At the end of the isotropic and anisotropic tests, the sample was failed either by decreasing σ_3 or increasing σ_D. These stress changes were again applied in increments, and sample pore pressure and strain monitored with time during each increment.

3.7 TEST RESULTS

The process of gas exsolution dominated the observed behaviour in all tests and produced some general characteristics common to all, that may be understood by examining Figure 3.18, (Test No. 11). The unloading portion

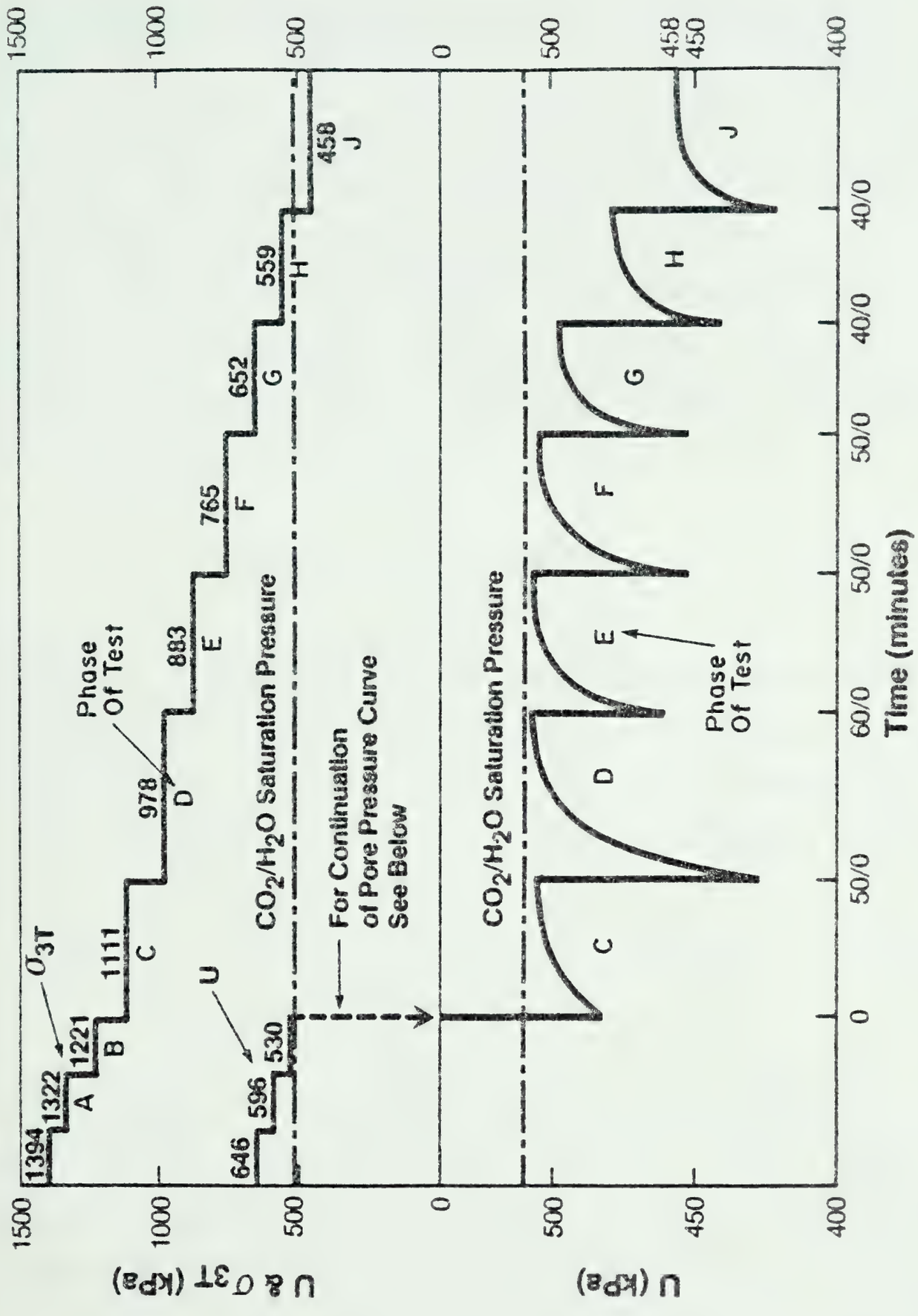


Figure 3.18 Isotropic undrained unloading test on dense sand with H_2O/CO_2 pore fluid (Sw_i=100%)

of this test was conducted in 9 stress decrements, (i.e. phases A - J). Initial stresses were σ_3 = 1394 KPa, u = 646 KPa, and the pore fluid was undersaturated with respect to gas, since the initial pore pressure was higher than the liquid/gas saturation pressure of 510 KPa.

For the first two phases of the test, the soil behaved as if it were totally saturated, with no gas in the pore space. For example, at the beginning of phase A the measured pore pressure response was:

$$B = du / d\sigma = -50/-72 = 0.69$$

Using n = 0.32, β_T = 5.8 E-6 KPa^{-1}, β_l = 4.5 E-7 KPa^{-1} and P = 746 KPa (absolute), equation 3.1 gives an initial saturation of 99.5%. The theoretical response for a fully-saturated soil using these compressibilities would be:

$$B = du / d\sigma = 1 / (1 + n*\beta_l/\beta_T) \qquad (3.2)$$
$$= 0.976$$

It is apparent what a marked effect a small amount of gas can have on the pore pressure response. This effect is particularly exacerbated in soils with a low compressibility, as was demonstrated by Black & Lee (1973).

The initial saturation of 99.5% obtained in this test appears to be somewhat low in comparison to other tests performed. However, some care must be exercised in

calculating a B-response in this manner at the beginning of one phase of the test, since a small period of time has elapsed (15 - 30 seconds) during which the cell pressure was decreased and the initial readings taken, and hence some exsolution may have occurred already. The B-response calculated may then be too low. This source of error is discussed more fully in Chapter 4. Actual B-tests performed above the liquid/gas saturation pressure for Test No. 11, and before the commencement of phase A, yielded B = 0.84, or S_i = 99.75%.

At the beginning of phase C of the test, a drop in σ_3 from 1220 to 1111 KPa induces an immediate change in pore pressure from 551 to 482 KPa.[2] This brings the pore pressure below the CO_2/H_2O saturation pressure of 510 KPa and hence CO_2 gas begins to exsolve. Note the distinctive shape of the pressure-time exsolution curve for all phases. The rate of exsolution is very high at zero time and decreases steadily towards zero as the pressure becomes asymptotic to some maximum value, P_{max}. P_{max} is the equilibrium pressure that would be calculated from equation 2.15b using the appropriate value of Henry's constant H. During the early portions of the test, P_{max} is very close to $P_{l/g}$. This is due to the fact that σ_3' is large and hence β_T is low. Volumetric strains to the end of phase E of the test are only 0.25%

---

[2]For simplicity, Figure 3-18 does not show minor increases in pore pressure during phase B of the test due to air exsolution. This will be discussed in Chapter 4.

(expansion). Hence, there has been an increase in void volume, and thus generation of free CO_2 gas, of approximately 2 cc, compared to a volume of dissolved gas of 215 cc at this same pressure. As the test progresses through phases F to J, σ_3' decreases from 375 KPa to 0 KPa, and the soil skeleton compressibility increases from 1 E-5 to 1 E-3 KPa^{-1}. Volumetric strain at the end of phase J is 1.1% (expansion), or 8.5 cc of gas have been produced. This increased soil skeleton compressibility and increased fluid compressibility (due to lower water saturation, S) cause P_{max} to gradually decrease (see equation 2.15b).[3] This type of behaviour was observed both in the isotropic and anisotropic tests, as σ_1' and σ_3' approached zero and thus β_T became larger, and in the tests to failure, as large volumetric strains occurred when the stress trajectory approached the failure envelope.

3.7.1 Isotropic Tests

The previous section has discussed the general nature of all the undrained tests, and has used an isotropic test (No. 11) to illustrate this behaviour (Figure 3.18).

Figures 3.19 and 3.20 illustrate the stress-strain behaviour of the sample observed during Test No. 11. The data for Figure 3.19 were collected during the preliminary isotropic stress-cycling phase, and the data for Figure 3.20 from phases A to M of the test proper.

---

[3] A small portion of the decrease in P_{max} with decreasing σ_3' during the test is due to the loss of gas from the sample by diffusion through the membrane. This effect is discussed in Chapter 4.

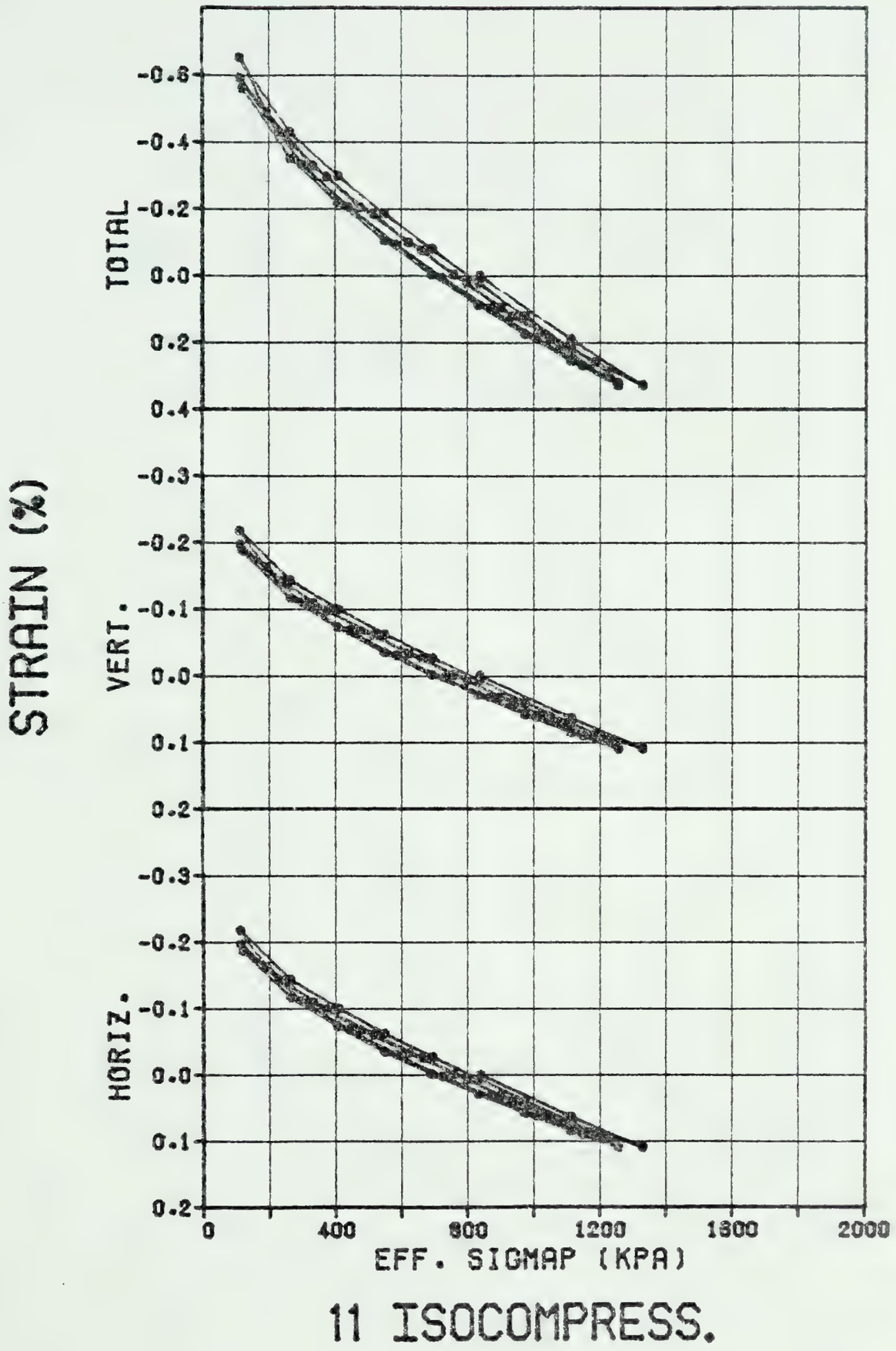

STRAIN (%)
TOTAL
VERT.
HORIZ.
-0.6
-0.4
-0.2
0.0
0.2
0.4
-0.3
-0.2
-0.1
0.0
0.1
0.2
-0.3
-0.2
-0.1
0.0
0.1
0.2
0
400
800
1200
1600
2000
EFF. SIGMAP (KPA)
11 ISOCOMPRESS.

Figure 3.19

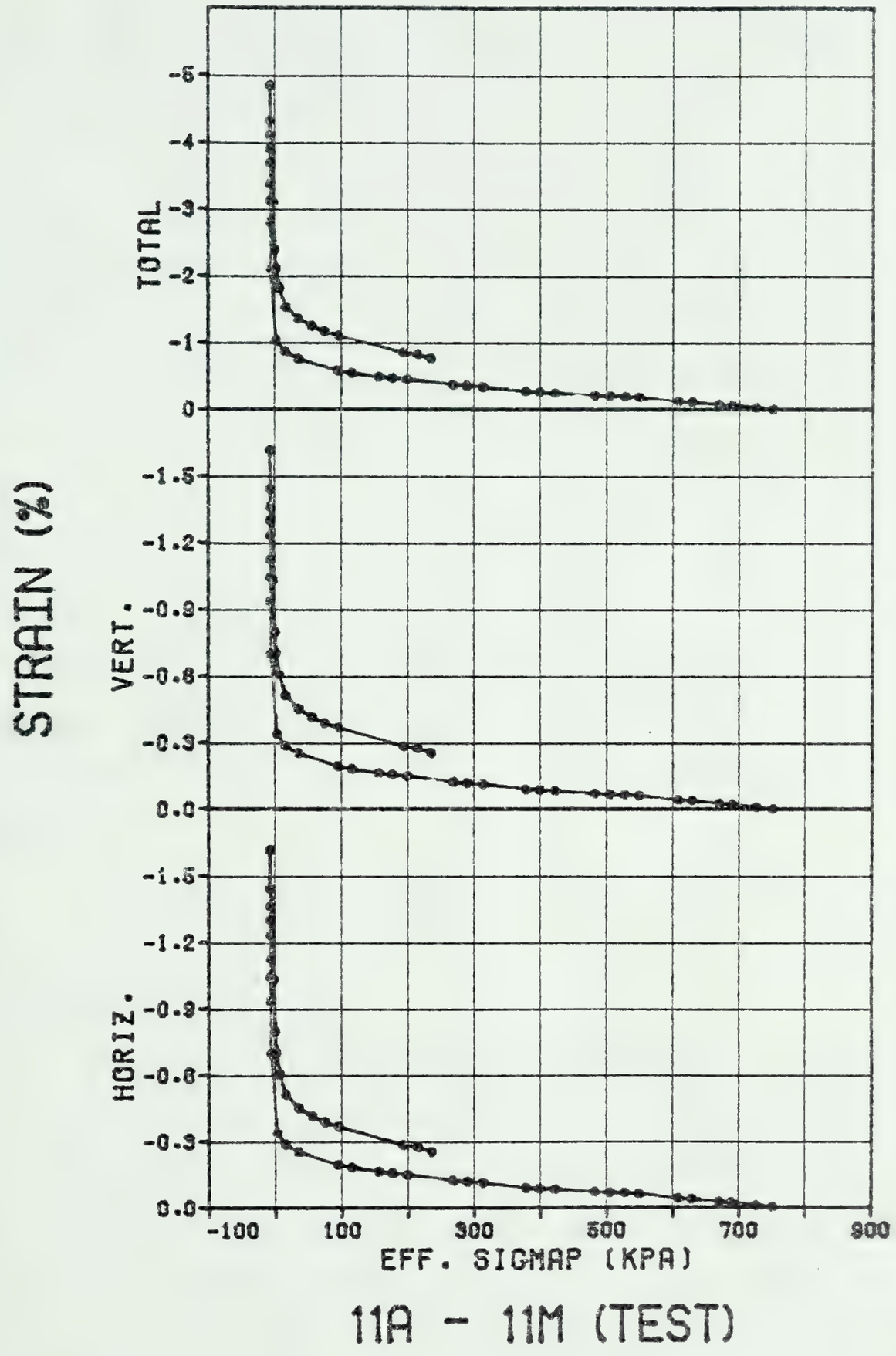

STRAIN (%)
TOTAL
VERT.
HORIZ.
-5
-4
-3
-2
-1
0
-1.5
-1.2
-0.9
-0.6
-0.3
0.0
-100
100
300
500
700
900
EFF. SIGMAP (KPA)
11A - 11M (TEST)

Figure 3.20

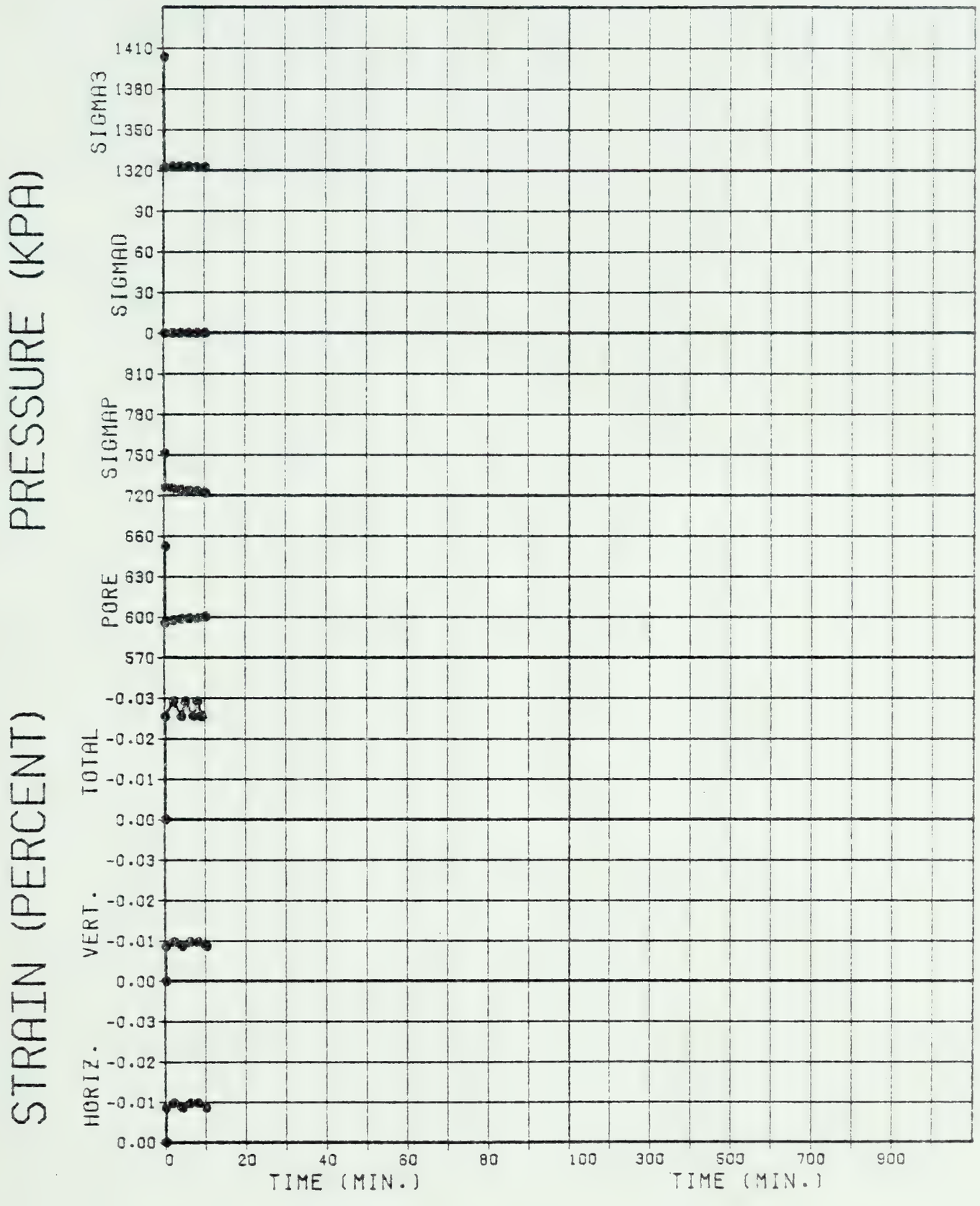
The transient response of pore pressure (and hence effective stress) and strain for each of the phases of the test are portrayed in more detail in Figures 3.21 to 3.32.

It should be noted that Test No. 11, (and other isotropic tests), were unloaded past the point of zero effective stress (phase K, Figure 3.30). Since σ' cannot decrease below 0, a decrease in σ forces an equivalent decrease in u, and u must remain at a value equivalent to σ. This causes the generation of large volumes of gas in the sample, and the measured volume change increases substantially. Actually, only the fluid behaviour is being measured during this phase, but a fluid that is responding to a change in external stress in the presence of the soil grains. Phase K is thus a psuedo-drained test. The significance of these results will be discussed further in Chapter 6.

The same data for the other isotropic tests performed is located in Appendix C.

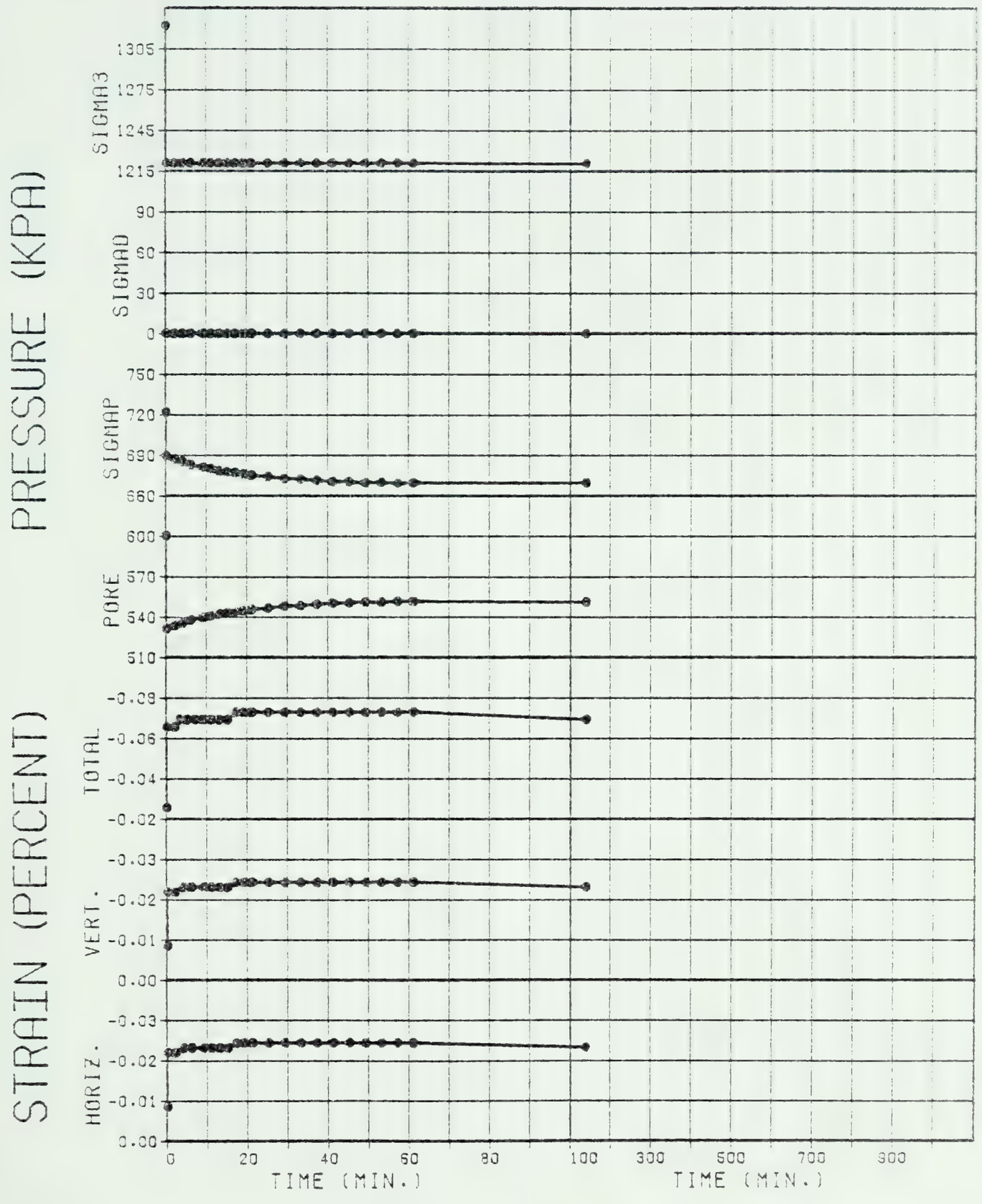
3.7.2 Anisotropic Tests

The isotropic stress-strain behaviour of sample No. 21 during preliminary stress cycling has already been presented in Figure 3.2. During preliminary tests the deviator stress was also cycled (with σ_3' maintained at a constant value). The strain response to this cycling is shown in Figure 3.33. It can be seen that the deviator stress alone has little influence on ε_v and almost no influence on ε_h at low values of σ_1'/σ_3', (the maximum value of k in test 21 is 2.0).



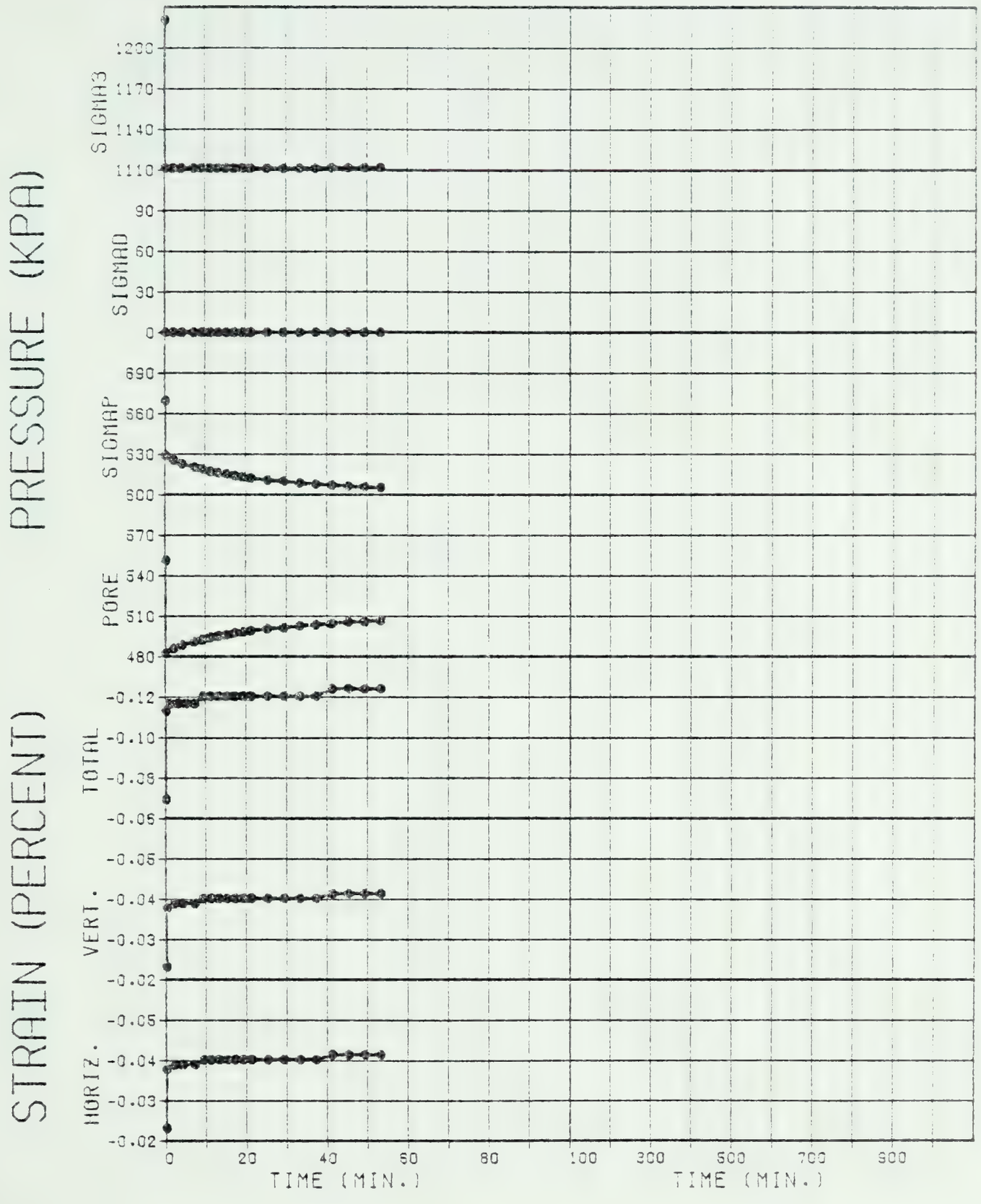
TEST NO. 11A

Figure 3.21



TEST NO. 11B

Figure 3.22



TEST NO. 11C

Figure 3.23

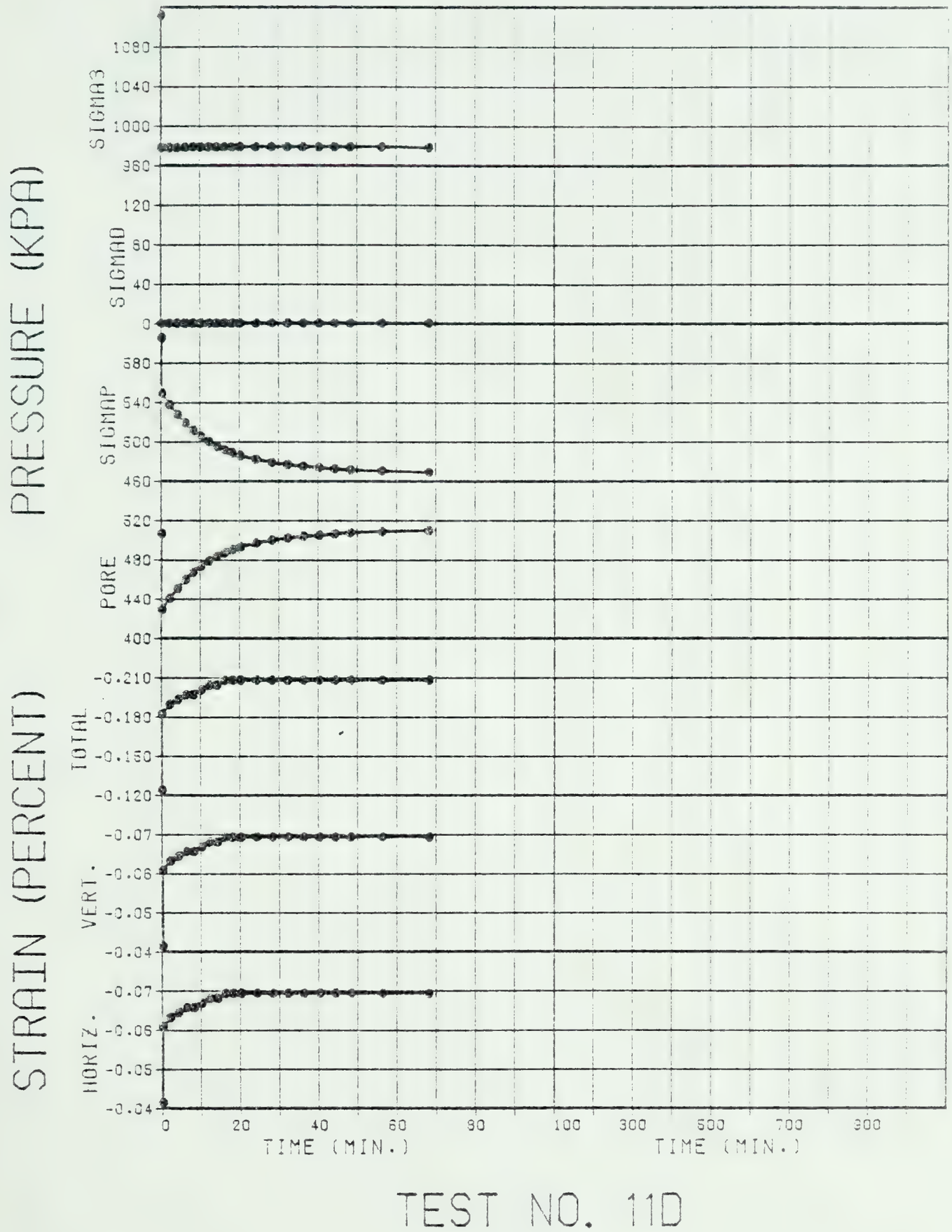

PRESSURE (KPA)
STRAIN (PERCENT)
SIGMA3
1080
1040
1000
960
SIGMAD
120
80
40
0
SIGMAP
580
540
500
460
PORE
520
480
440
400
TOTAL
-0.210
-0.180
-0.150
-0.120
VERT.
-0.07
-0.06
-0.05
-0.04
HORIZ.
-0.07
-0.06
-0.05
-0.04
0
20
40
60
80
100
300
500
700
900
TIME (MIN.)
TIME (MIN.)
TEST NO. 11D

Figure 3.24

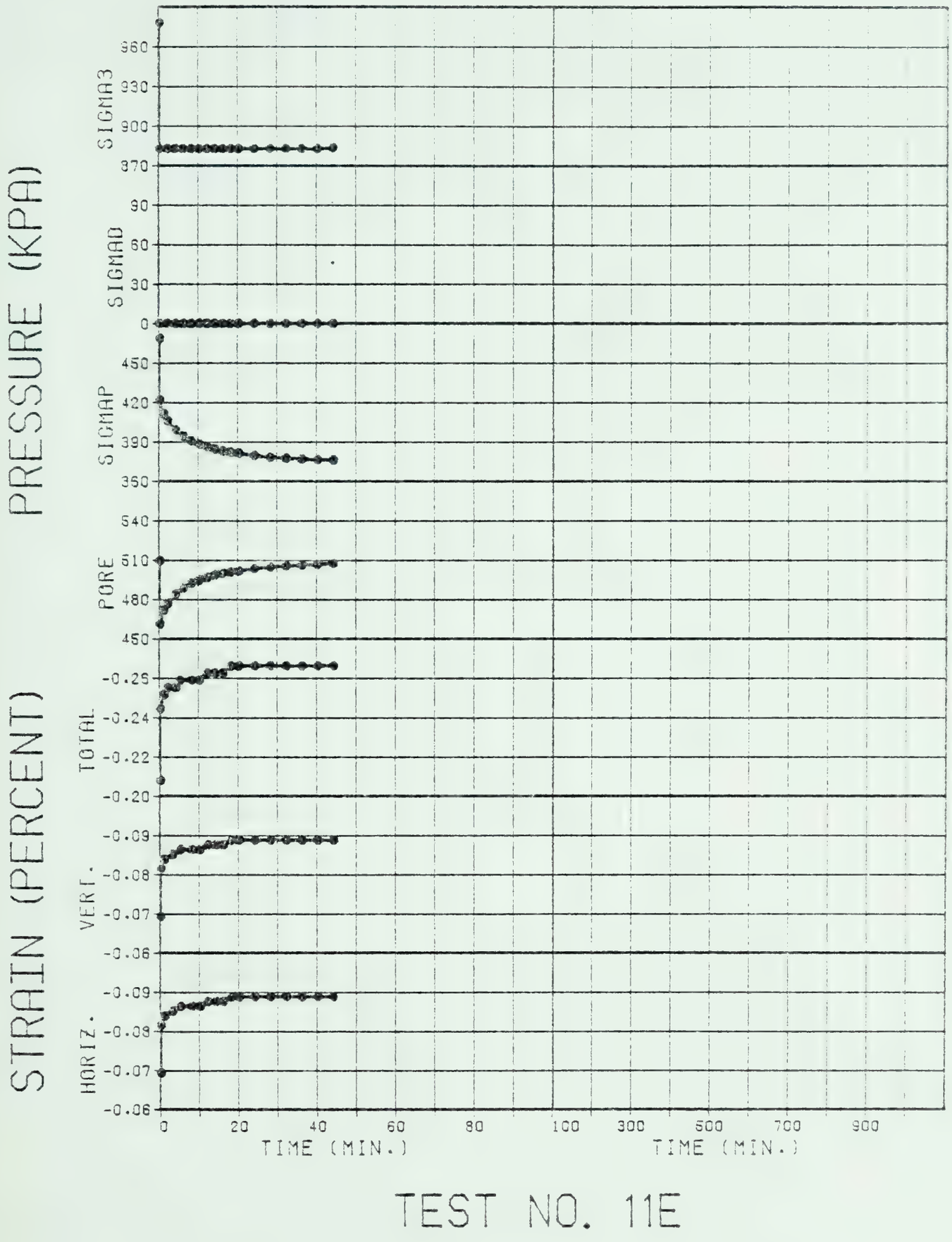

PRESSURE (KPA)
SIGMA3
960
930
900
870
SIGMAD
90
60
30
0
SIGMAP
450
420
390
360
PORE
540
510
480
450
STRAIN (PERCENT)
TOTAL
-0.25
-0.24
-0.22
-0.20
VERT.
-0.09
-0.08
-0.07
-0.06
HORIZ.
-0.09
-0.08
-0.07
-0.06
0
20
40
60
80
100
300
500
700
900
TIME (MIN.)
TIME (MIN.)
TEST NO. 11E

Figure 3.25

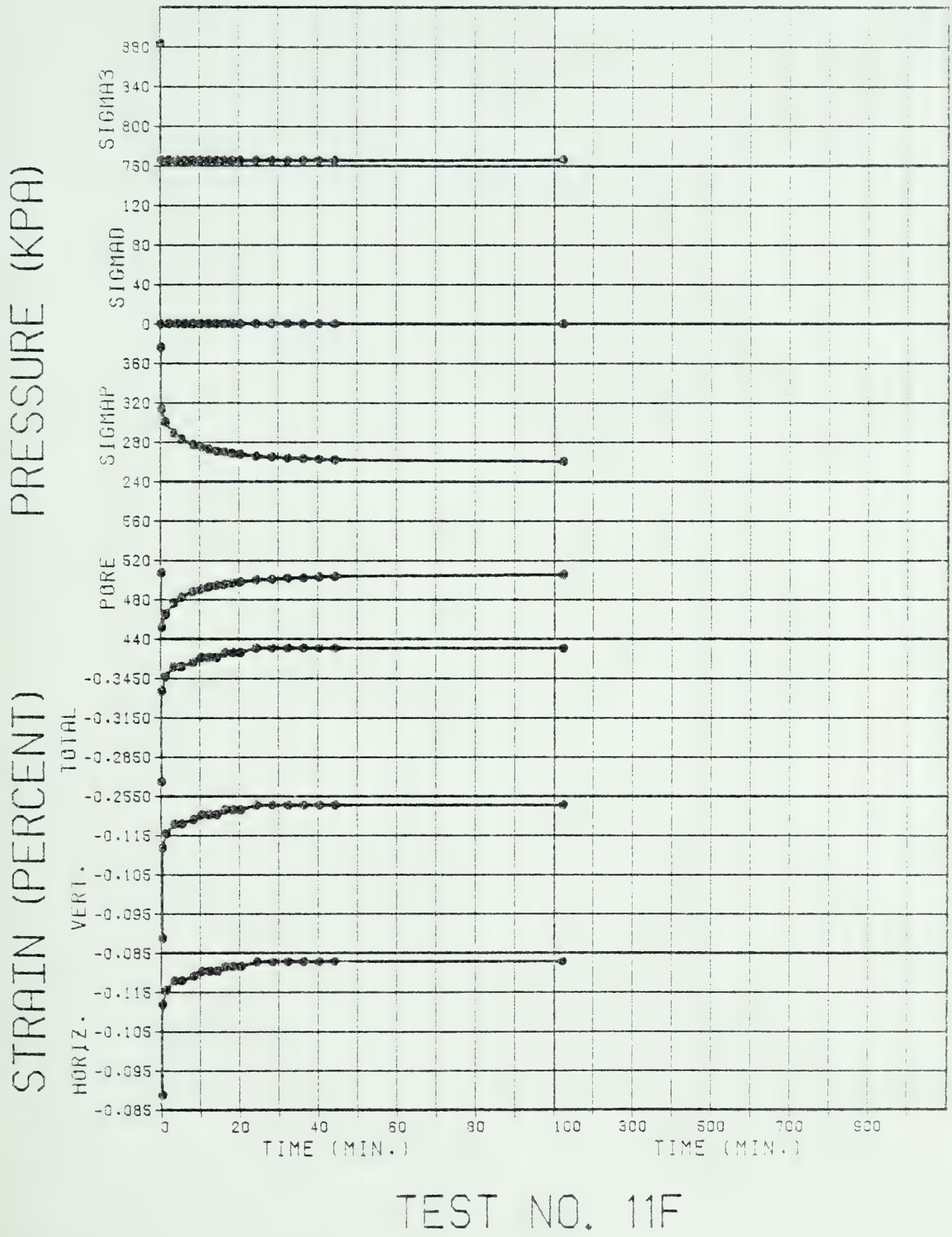
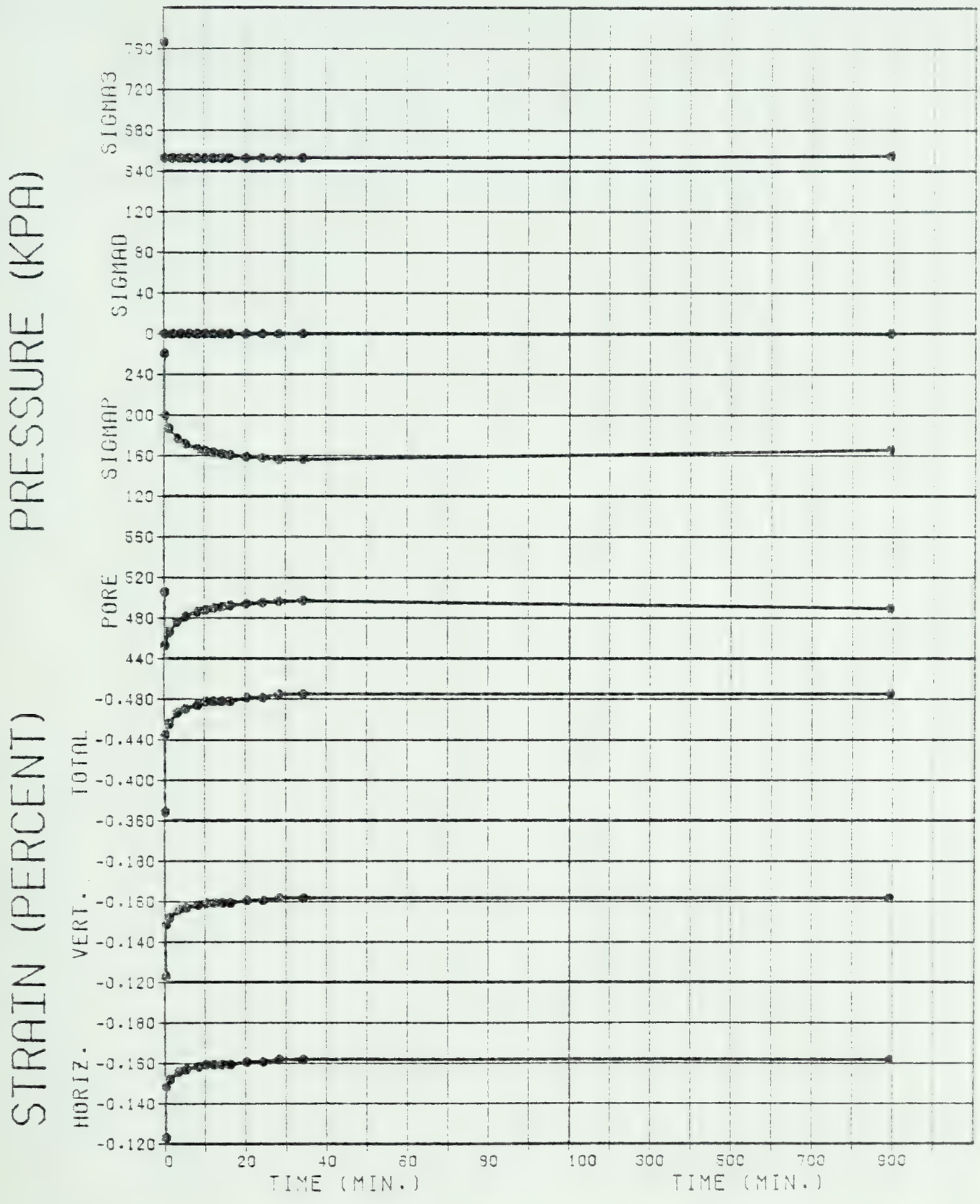

PRESSURE (KPA)
SIGMA3
SIGMAD
SIGMAP
PORE
880
840
800
760
120
80
40
0
360
320
280
240
660
620
580
540
500
460
420
STRAIN (PERCENT)
TOTAL
VERT.
HORIZ.
-0.3450
-0.3150
-0.2850
-0.2550
-0.115
-0.105
-0.095
-0.085
-0.115
-0.105
-0.095
-0.085
0
20
40
60
80
100
300
500
700
900
TIME (MIN.)
TIME (MIN.)
TEST NO. 11F

Figure 3.26



TEST NO. 11G

Figure 3.27

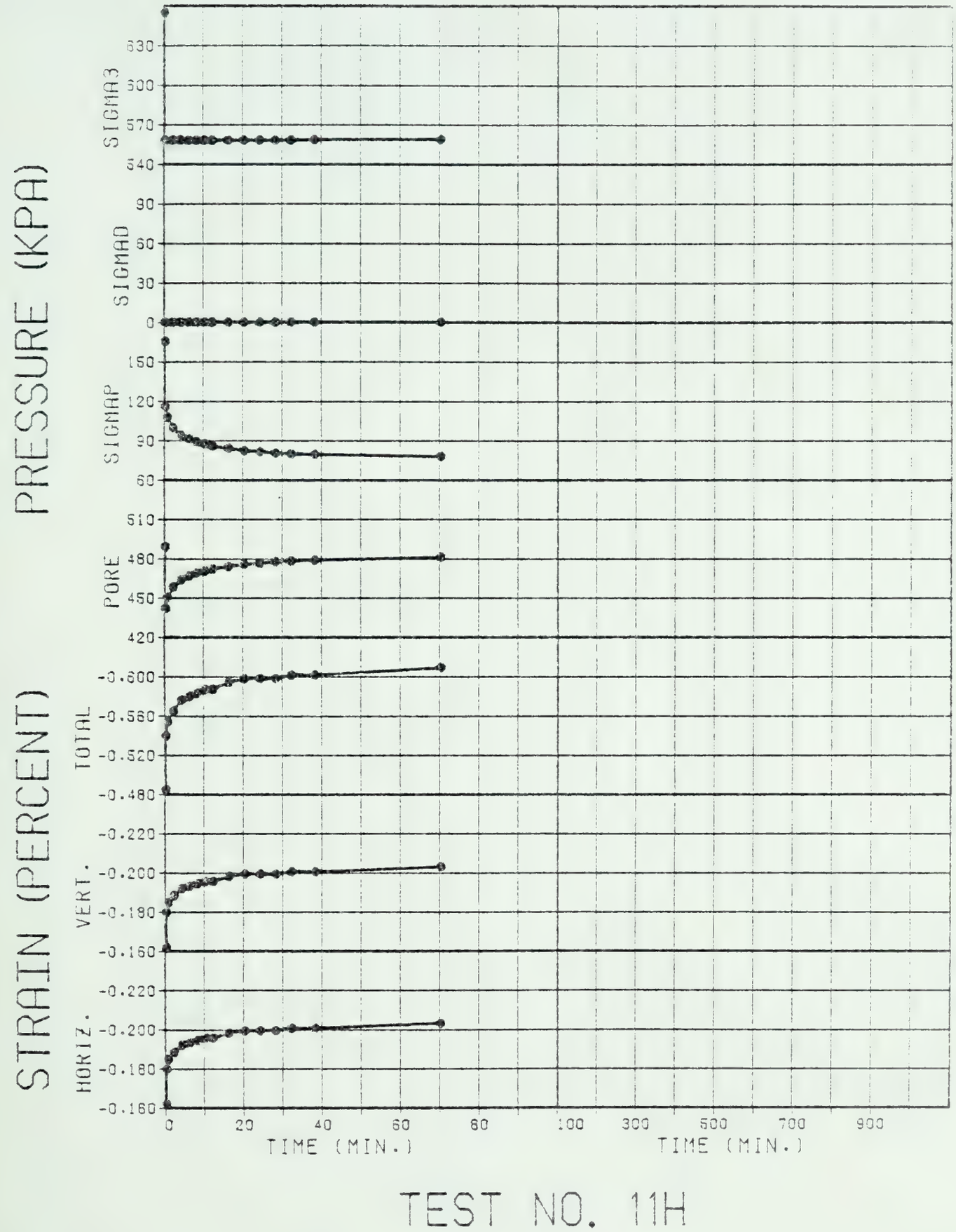

PRESSURE (KPA)
SIGMA3
630
600
570
540
SIGMAD
90
60
30
0
SIGMAP
150
120
90
60
PORE
510
480
450
420
STRAIN (PERCENT)
TOTAL
-0.600
-0.560
-0.520
-0.480
VERT.
-0.220
-0.200
-0.180
-0.160
HORIZ.
-0.220
-0.200
-0.180
-0.160
0
20
40
60
80
100
300
500
700
900
TIME (MIN.)
TIME (MIN.)
TEST NO. 11H

Figure 3.28

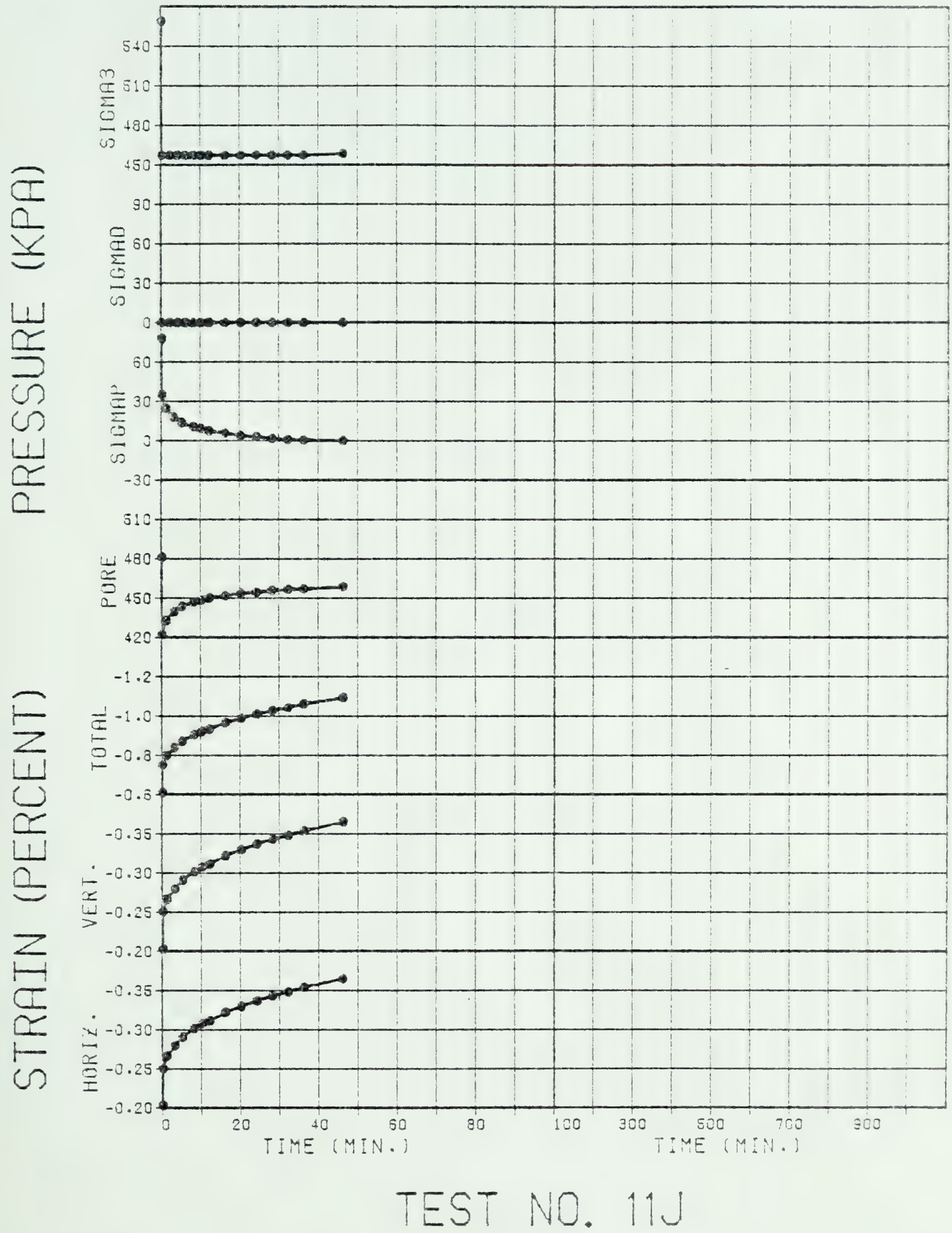

PRESSURE (KPA)
STRAIN (PERCENT)
SIGMA3
540
510
480
450
SIGMAD
90
60
30
0
SIGMAP
60
30
0
-30
PORE
510
480
450
420
TOTAL
-1.2
-1.0
-0.8
-0.6
VERT.
-0.35
-0.30
-0.25
-0.20
HORIZ.
-0.35
-0.30
-0.25
-0.20
0
20
40
60
80
100
300
500
700
900
TIME (MIN.)
TIME (MIN.)
TEST NO. 11J

Figure 3.29

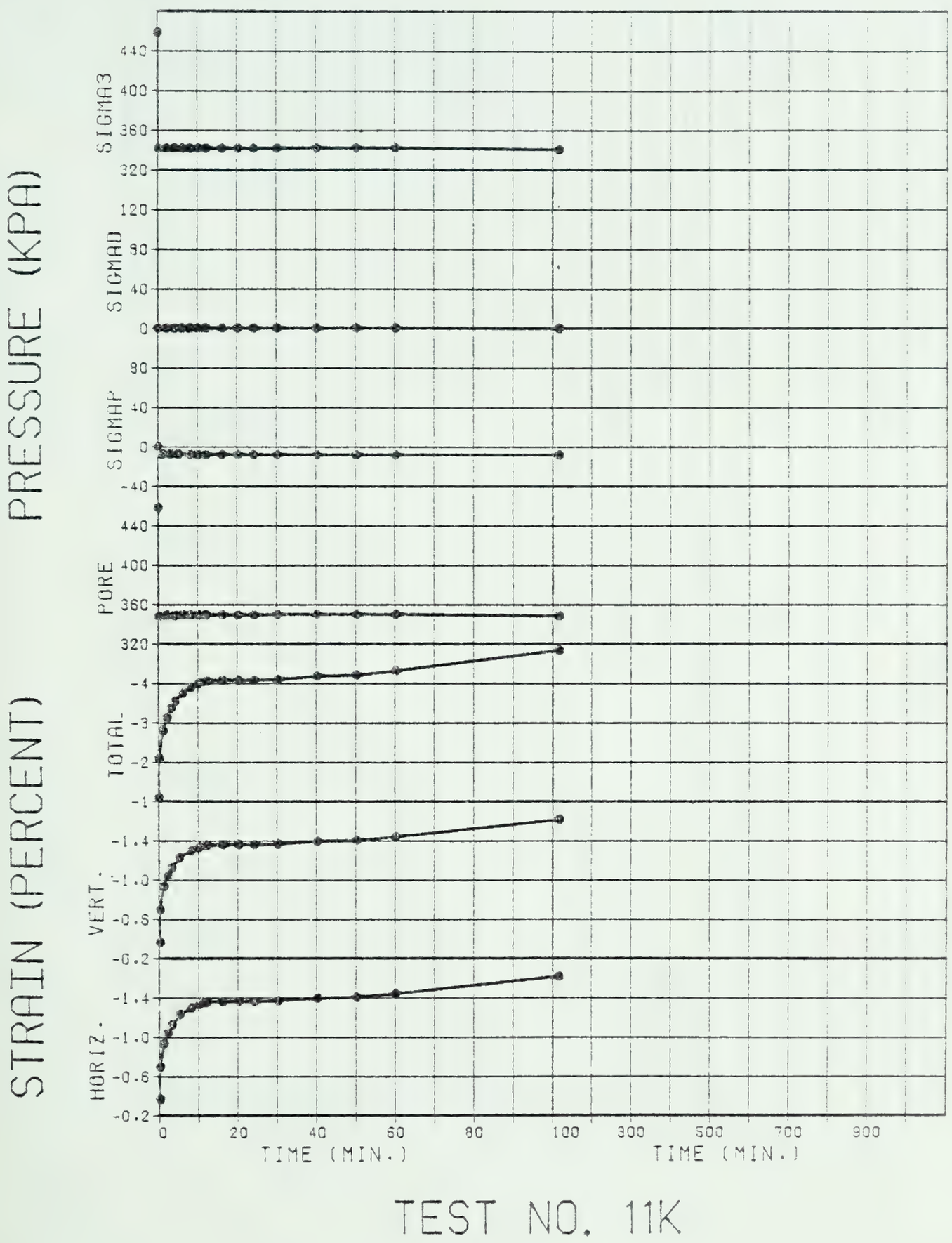
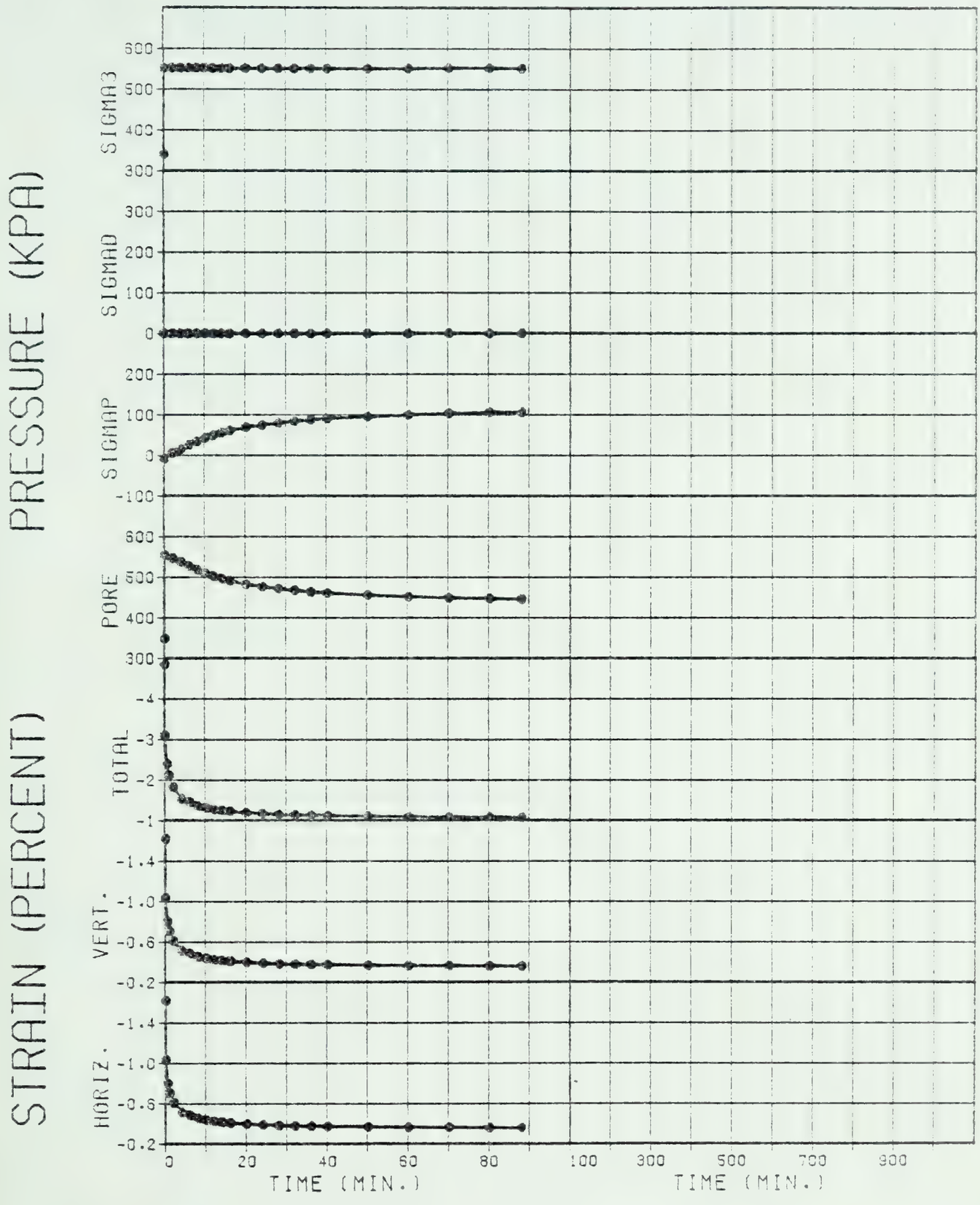

PRESSURE (KPA)
STRAIN (PERCENT)
SIGMA3
SIGMAD
SIGMAP
PORE
TOTAL
VERT.
HORIZ.
440
400
360
320
120
80
40
0
-40
-4
-3
-2
-1
-1.4
-1.0
-0.6
-0.2
0
20
40
60
80
100
300
500
700
900
TIME (MIN.)
TIME (MIN.)
TEST NO. 11K

Figure 3.30



TEST NO. 11L

Figure 3.31

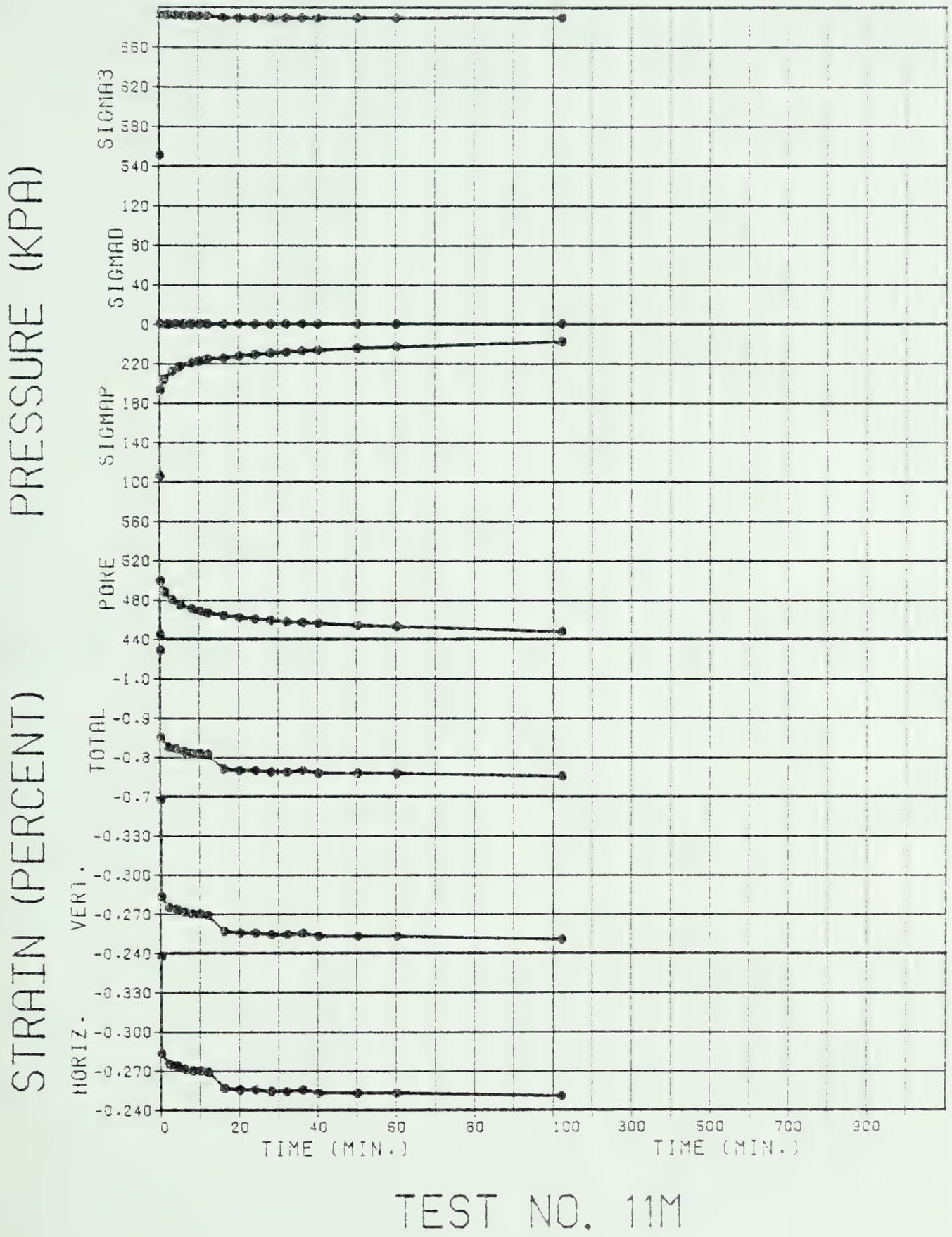
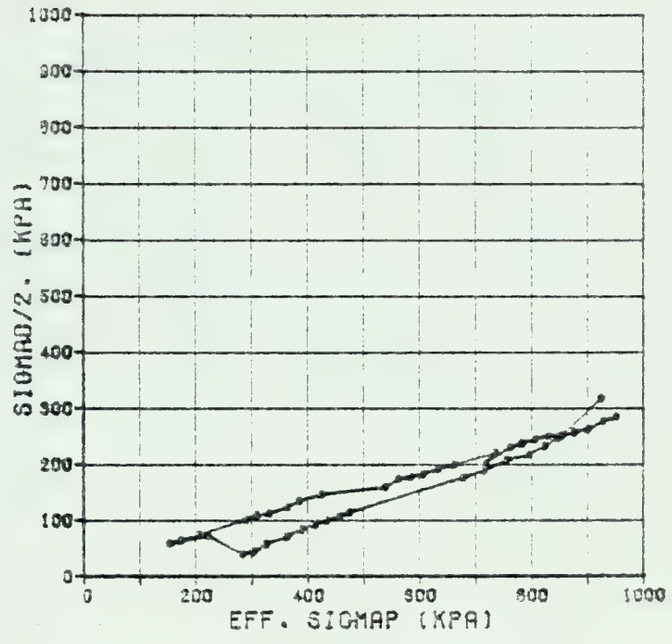

PRESSURE (KPA)
SIGMA3
560
520
480
SIGMAD
120
80
40
0
SIGMAP
220
180
140
100
PORE
560
520
480
440
STRAIN (PERCENT)
TOTAL
-1.0
-0.9
-0.8
-0.7
VERT.
-0.330
-0.300
-0.270
-0.240
HORIZ.
-0.330
-0.300
-0.270
-0.240
0
20
40
60
80
100
TIME (MIN.)
300
500
700
900
TIME (MIN.)
TEST NO. 11M

Figure 3.32

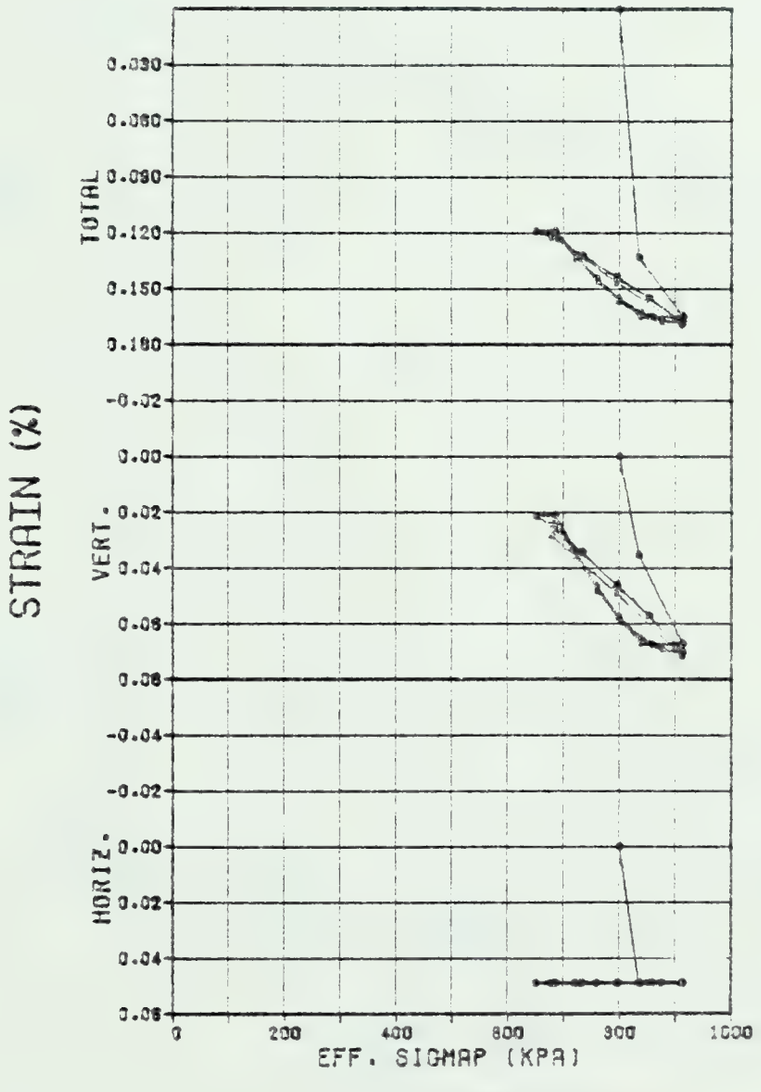
Houlebec (1968) also reported this predominance of the strain response by the cell pressure and noted that it seemed to be a peculiarity of the triaxial test.

The undrained portion of Test No. 21 was performed by unloading from initial stress conditions of σ_3 = 1041 KPa, σ_1 = 1676 KPa and u = 435 KPa, and maintaining K approximately constant at a value of 2. Figure 3.34 illustrates the stress path for the unloading and reloading portions of this test and Figures 3.35 & 3.36 show the stress-strain behaviour of the sample for all phases. Figure 3.37 is a plot of σ_D/σ_3' vs ε_v for the test, and gives an indication of how good the control on constant K was. For K = 2, σ_D/σ_3' = 1.0. It can be seen that during the unloading portion of the test 1.8 < K < 2.4. During the reloading portion, K initially seems to decrease to a value of 1.2. This is a problem associated with applying the correction for ram friction, which changes sign on vertical strain reversal. During this portion of the test, it is likely that 1.6 < K < 2.0.

Figures 3.38 to 3.43 illustrate the transient response of u, p', ε_h, ε_v, and ε_{vol} during phases A to F of Test No. 21, for both unloading and reloading. The behaviour is very similar to that for the isotropic tests. The variation of pore pressure and strain with time is identical to that discussed previously for Test No. 11. Note the value of p_{max} for each phase of the test in comparison to the CO_2/H_2O



21A-21F (TEST)



21-NISOCOMPRESS.

Figures 3.33 and 3.34

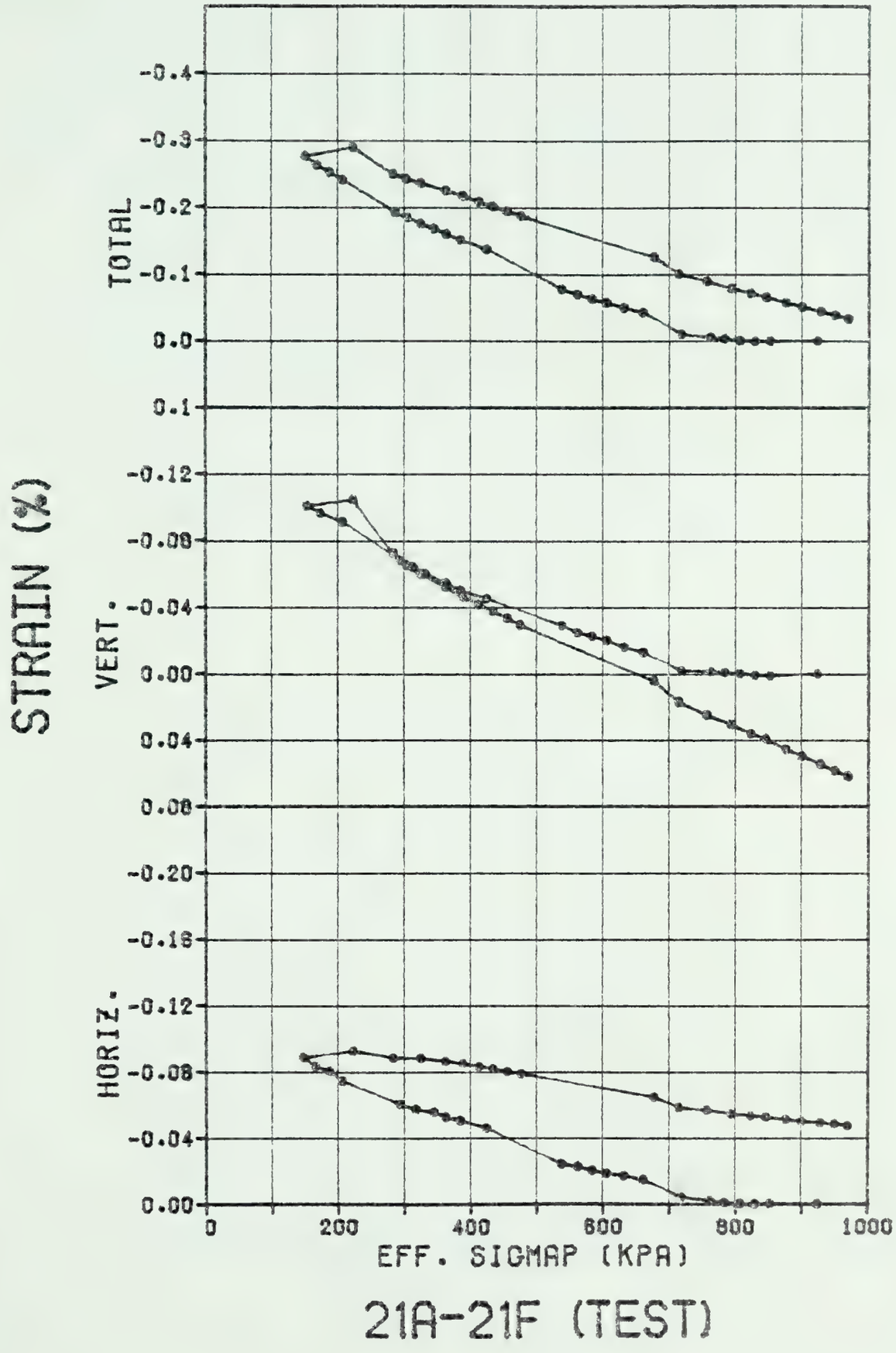
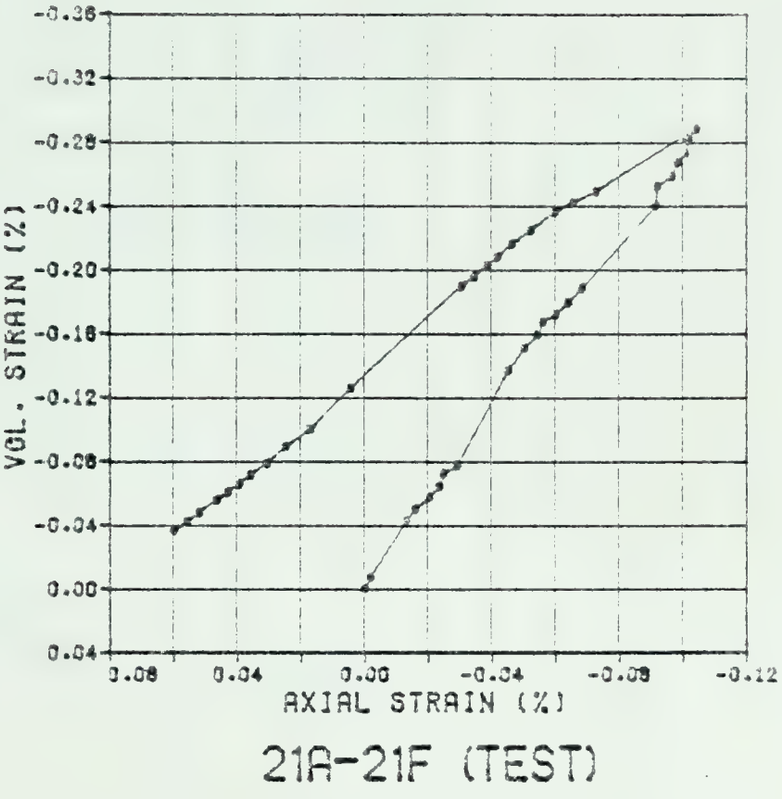
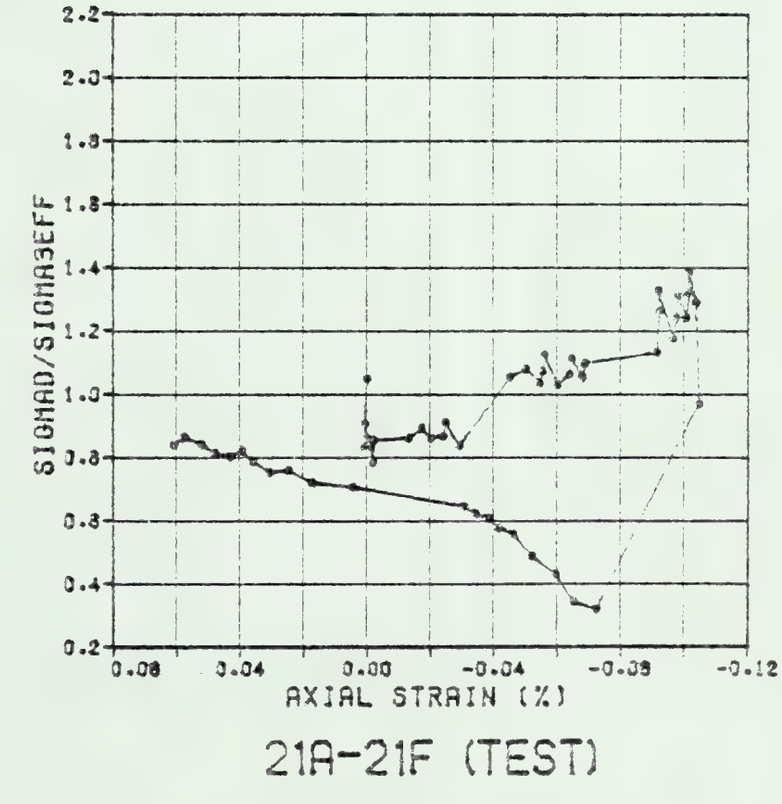

STRAIN (%)
TOTAL
VERT.
HORIZ.
-0.4
-0.3
-0.2
-0.1
0.0
0.1
-0.12
-0.08
-0.04
0.00
0.04
0.08
-0.20
-0.16
-0.12
-0.08
-0.04
0.00
0
200
400
600
800
1000
EFF. SIGMAP (KPA)
21A-21F (TEST)

Figure 3.35





Figures 3.36 and 3.37

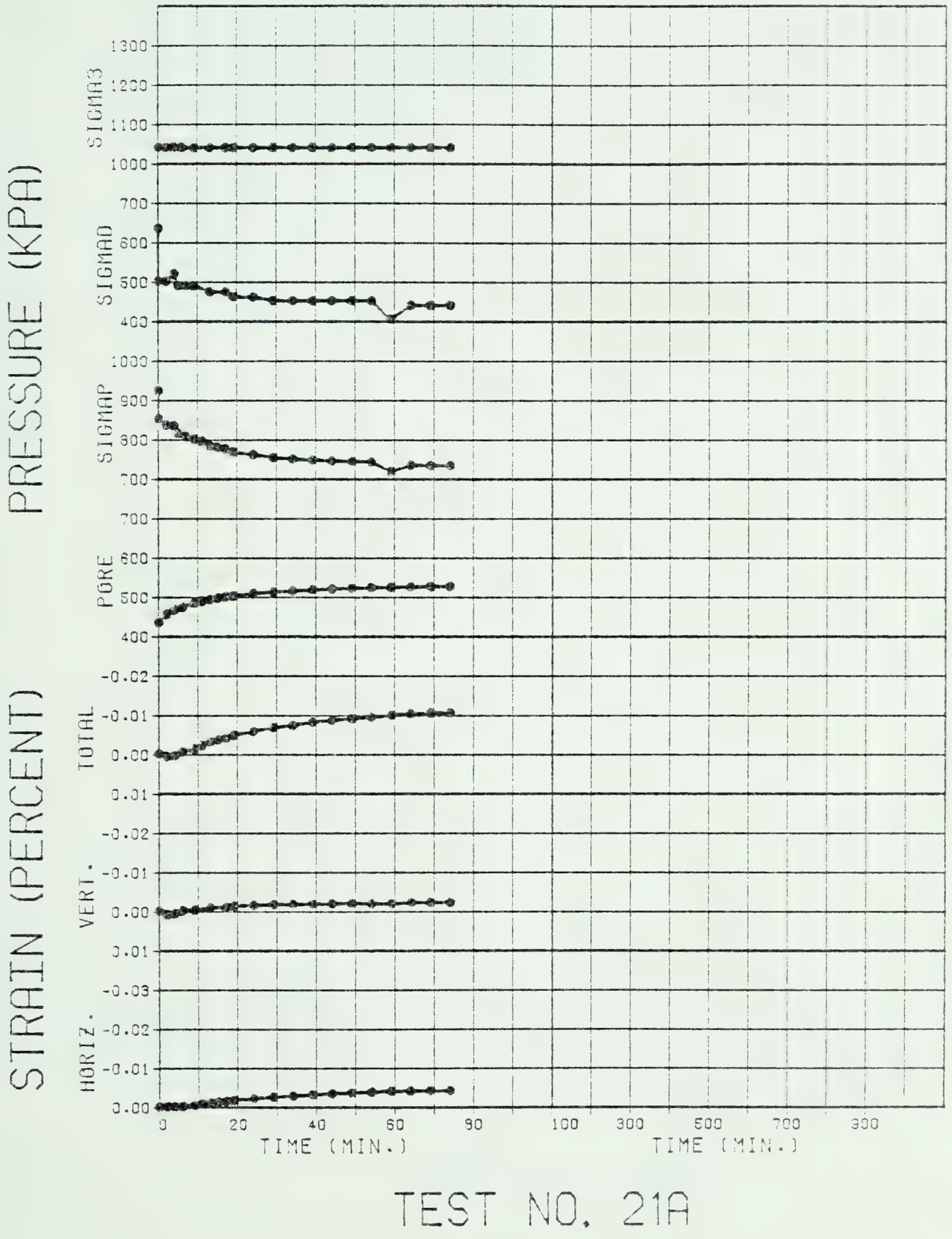

PRESSURE (KPA)
STRAIN (PERCENT)
SIGMA3
SIGMAD
SIGMAP
PORE
TOTAL
VERT.
HORIZ.
1300
1200
1100
1000
700
600
500
400
1000
900
800
700
700
600
500
400
-0.02
-0.01
0.00
0.01
-0.02
-0.01
0.00
0.01
-0.03
-0.02
-0.01
0.00
0
20
40
60
80
100
300
500
700
900
TIME (MIN.)
TIME (MIN.)
TEST NO. 21A

Figure 3.38

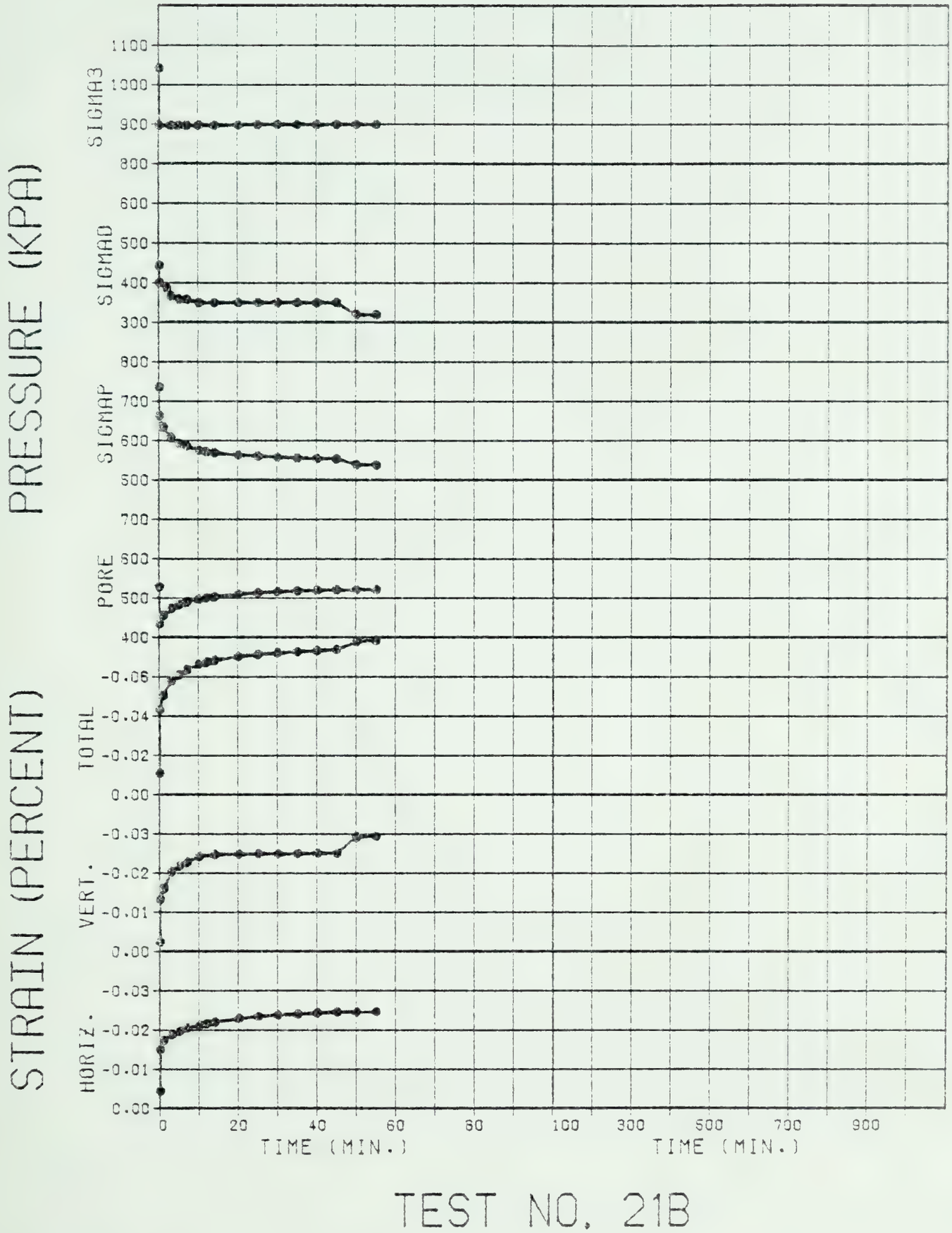

PRESSURE (KPA)
STRAIN (PERCENT)
SIGMA3
SIGMAD
SIGMAP
PORE
TOTAL
VERT.
HORIZ.
TIME (MIN.)
TIME (MIN.)
TEST NO. 21B

Figure 3.39

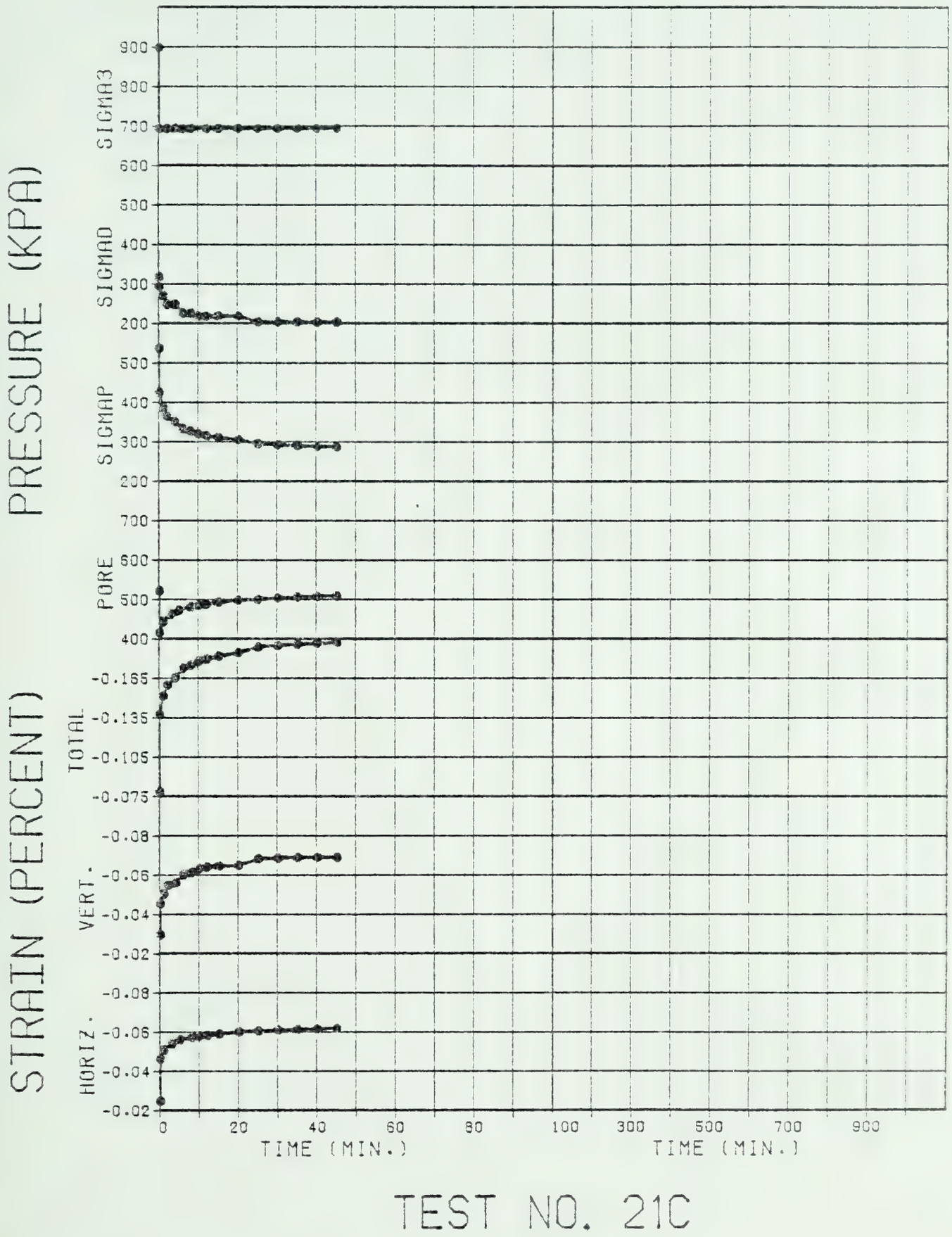

PRESSURE (KPA)
SIGMA3
SIGMAD
SIGMAP
PORE
STRAIN (PERCENT)
TOTAL
VERT.
HORIZ.
TIME (MIN.)
TIME (MIN.)
TEST NO. 21C

Figure 3.40

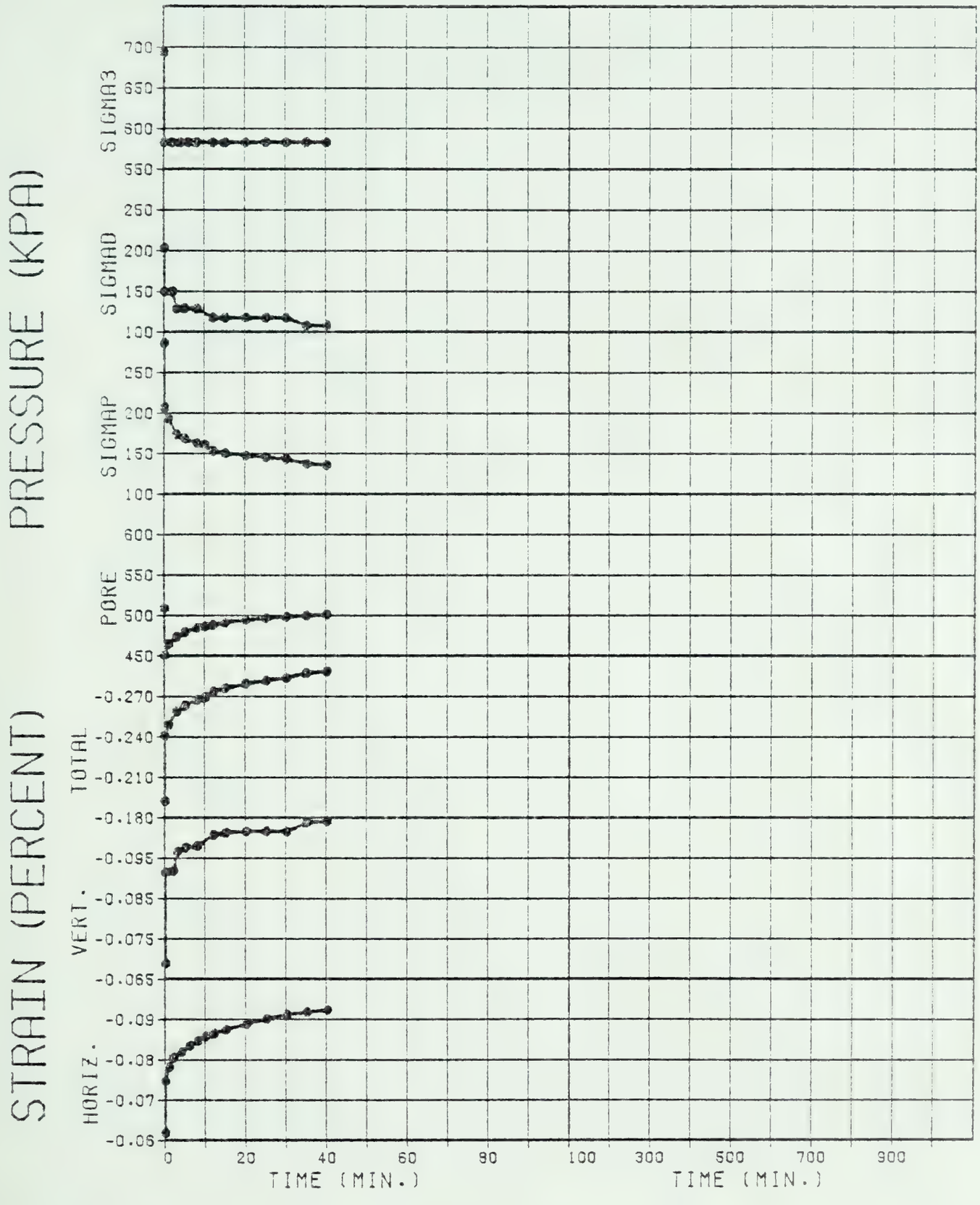
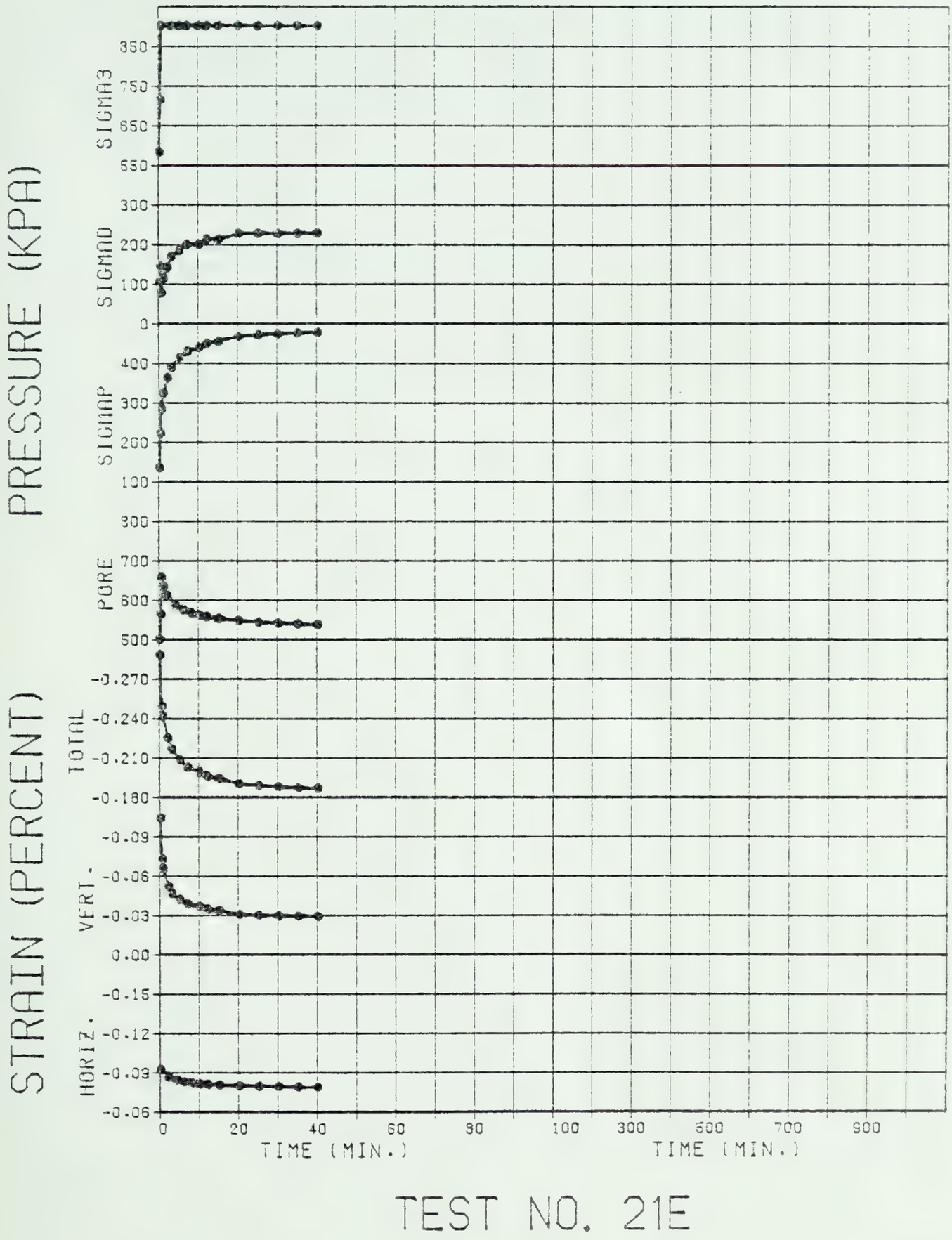
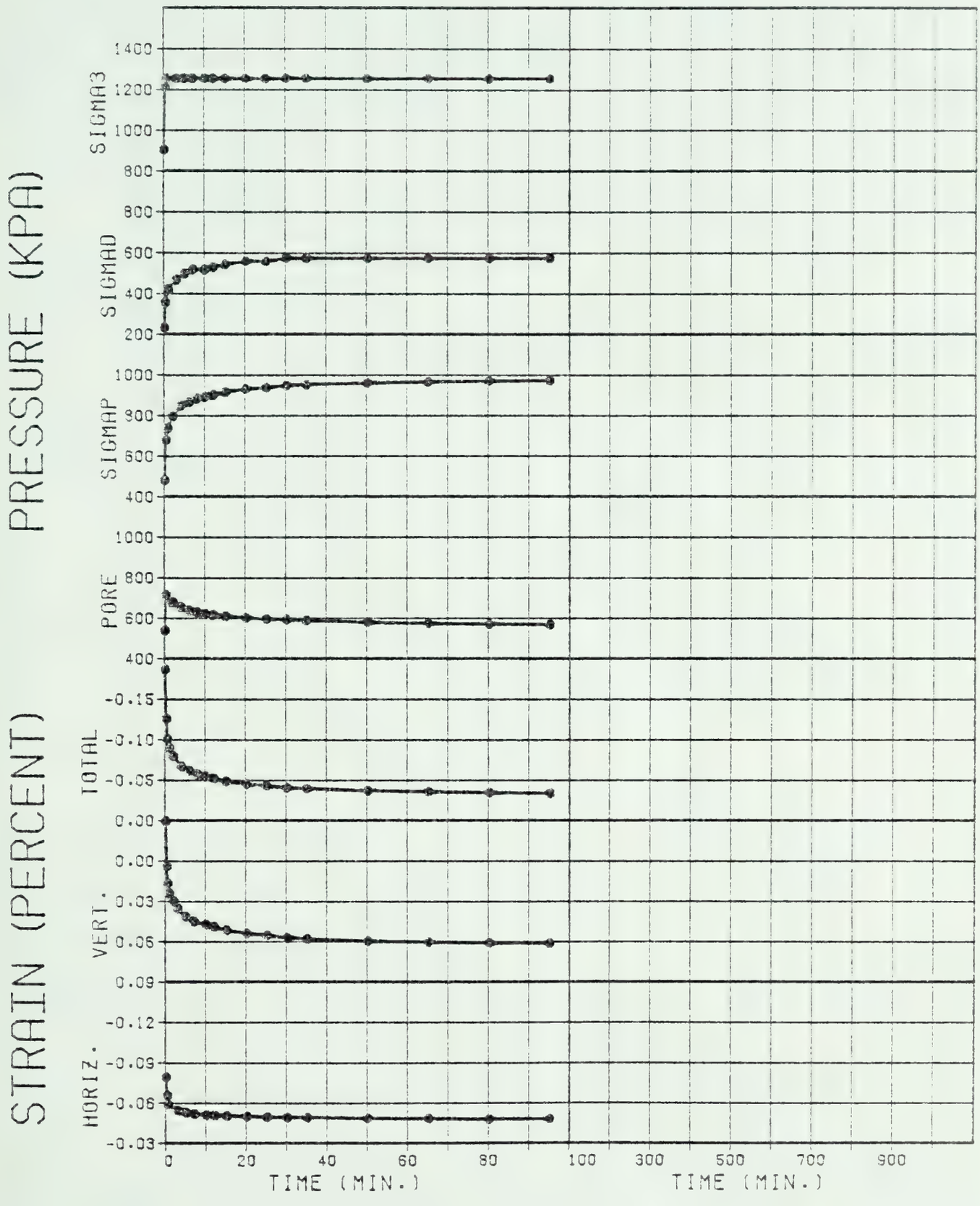

PRESSURE (KPA)
SIGMA3
SIGMAD
SIGMAP
PORE
STRAIN (PERCENT)
TOTAL
VERT.
HORIZ.
TIME (MIN.)
TIME (MIN.)
TEST NO. 21D

Figure 3.41



TEST NO. 21E

Figure 3.42



TEST NO. 21F

Figure 3.43

saturation pressure of 510 KPa. σ_D also varies during each phase of the test. This adjustment was made manually in an effort to maintain constant K, as u and hence σ_3' varied during each phase.

The results of other anisotropic tests are located in Appendix D.

3.7.3 Tests to failure

Phases A to F of Test No. 21 followed an anisotropic, constant K stress path. At the end of phase F, the sample stresses were σ_3 = 1251 KPa, σ_1 = 1135 KPa, and u = 566 KPa. The test was then continued as an undrained test to failure during phases G to L. At the beginning of phase G, σ_1 was increased to 1323 KPa, and then σ_3 was decreased in steps from 1250 to 513 KPa over the remaining phases. During the test σ_D was set to a constant value.

Figure 3.44 is a q vs p′ stress plot for the test, and is typical of all tests to failure. Note that the test proceeded for some distance along the failure envelope, i.e. q decreased during phases K and L. This was a most unexpected and unusual phenomenon, because the pressure to the bellofram controlling σ_D was maintained at a constant value, (q is measured by a load transducer external to the cell). Although it seems obvious that the stress path must follow the failure envelope, the author is unable to give a

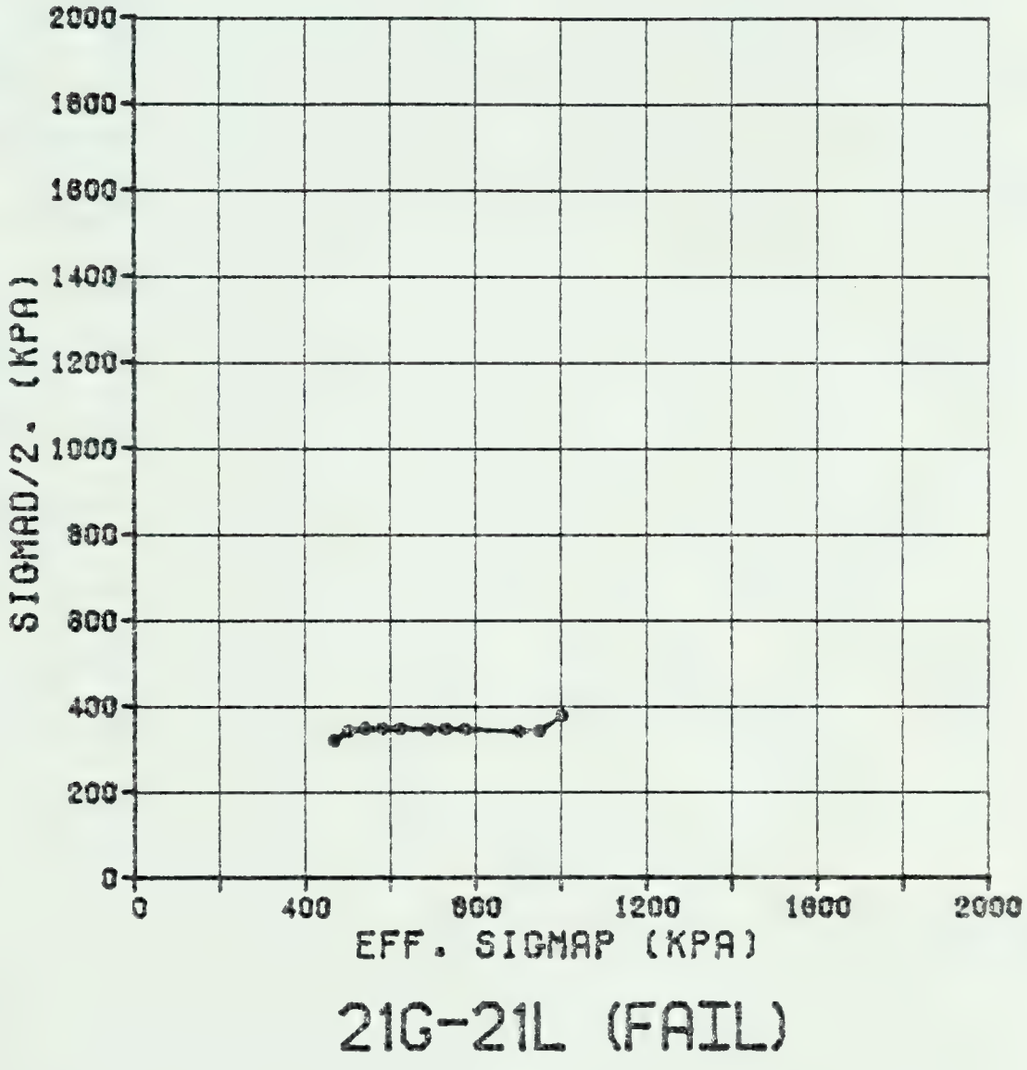

2000
1800
1600
1400
1200
1000
800
600
400
200
0
SIGMAD/2. (KPA)
0
400
800
1200
1600
2000
EFF. SIGMAP (KPA)
21G-21L (FAIL)

Figure 3.44

complete explanation of the mechanism that allows it to do so.[4] The bellofram was well within its range of operation throughout the test, so that the difference between the "applied" and measured loads cannot be attributed to energy lost in stretching the internal diaphragm in this device. Likewise, the rate of deformation of the sample, which is controlled by the rate of gas exsolution, was much too slow to attribute the difference to an energy associated with sample acceleration. Another possibility is that the difference in "applied" and measured loads, which is forced to exist because of an incompatibility between the boundary conditions of the test and the failure behaviour of the soil, is used as energy which modifies (i.e. increases) the natural rate of gas exsolution in the soil, and thus slightly increases the rate of soil deformation. This is an interesting area for consideration, but it was not pursued further during the course of this research.

Figures 3.45 & 3.46 illustrate the stress-strain behaviour of the sample as it was failed. Note that the rate of dilation of the sample ($d\varepsilon_{vol}/d\varepsilon_v$, Figure 3.46) is almost constant throughout the test, and particularly during failure. This constant rate of dilation was observed in all

---

[4]Castro (1969) reports on a series of load-controlled triaxial tests on saturated sand samples for an investigation of liquefaction. As soon as the stress trajectory in one of his samples touched the failure envelope, and then travelled down it, there was an immediate acceleration of the sample, due to the fact that the load on the vertical ram was not balanced by a resistance in the sample. No such acceleration of deformations was encountered in the present tests.

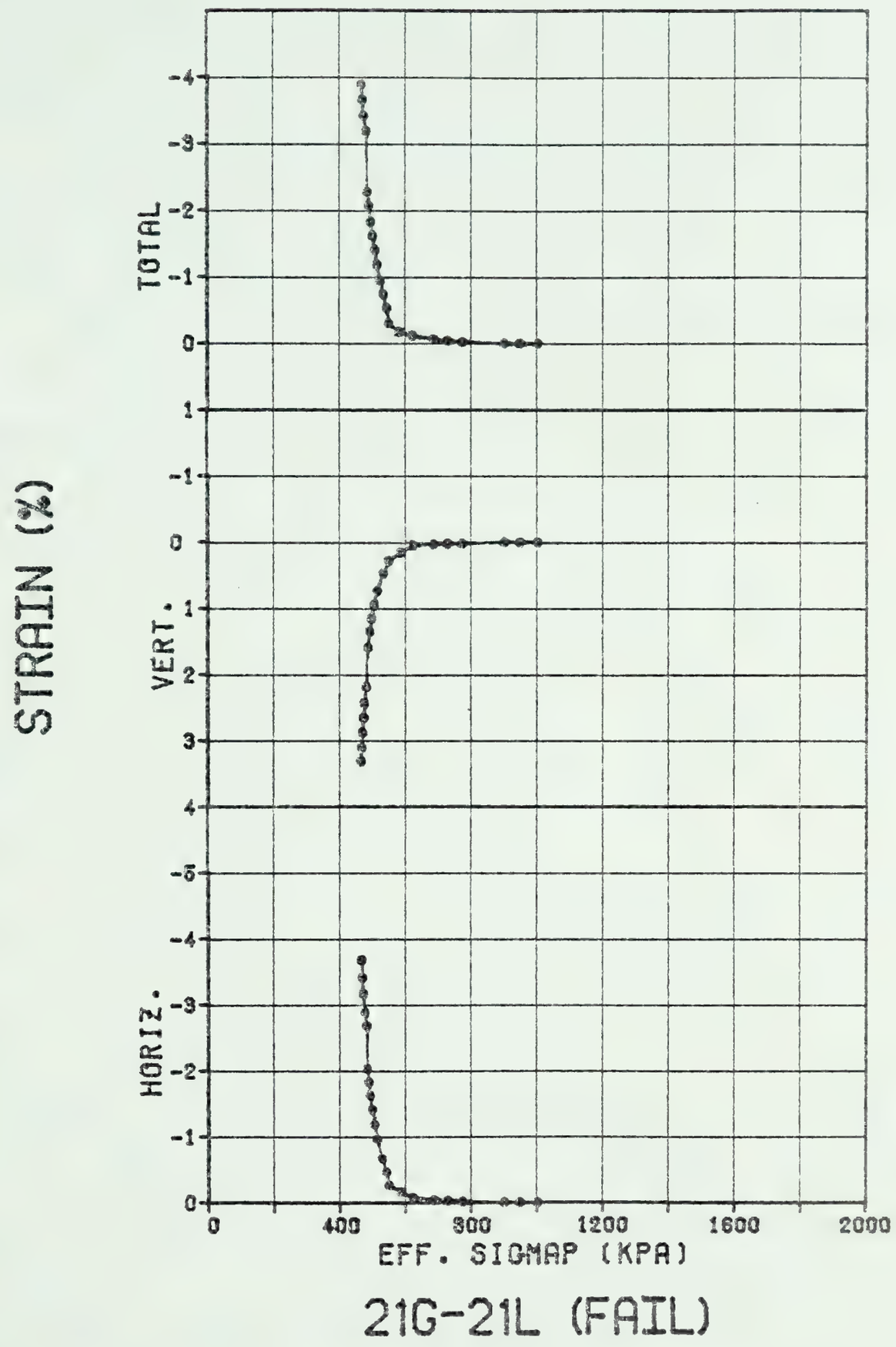

STRAIN (%)
TOTAL
VERT.
HORIZ.
-4
-3
-2
-1
0
1
-1
0
1
2
3
4
-5
-4
-3
-2
-1
0
0
400
800
1200
1600
2000
EFF. SIGMAP (KPA)
21G-21L (FAIL)

Figure 3.45

the tests to failure, that is, in both the gassy and gas-free undrained tests, and in the drained test.

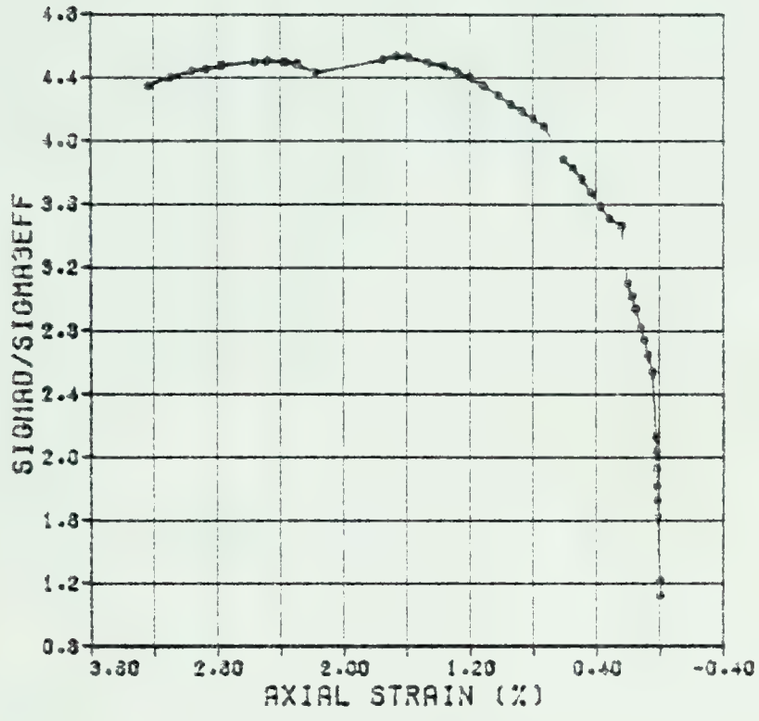
Figure 3.47 is a plot of σ_D/σ_3' vs ε_v. The maximum value for σ_D/σ_3' during Test No. 21 was 4.5, indicating a strength of ϕ' = 43.8 degrees.

Figures 3.48 to 3.53 show the transient behaviour of the soil during phases G to L of the test. Note that the stress path for the sample is moving closer to the failure envelope both when a step decrease in σ_3 is applied and when u increases in response to gas exsolution.

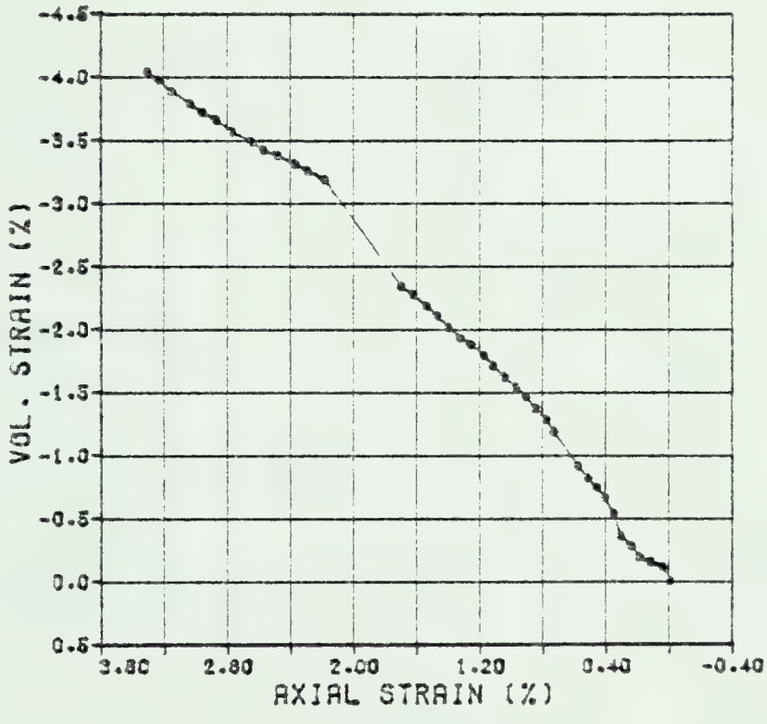
Again, the form of the transient response is similar to the isotropic and anisotropic cases, except that for Test No. 21, with decreasing p' to failure, vertical strains are compressive and horizontal strains expansive, (and the overall volume change is dilative).

The decrease in q with time during phases K and L, discussed previously, may be examined in Figures 3.52 & 3.53.

Three tests to failure were performed on undrained, gassy soils, two by decreasing σ_3 (Tests 21 & 12), and one by increasing σ_D (Test 22). For comparison one additional test was performed on an undrained, gas-free sample (Test 14) and one on a drained sample (Test 13) using similar stress paths to Test No. 12. The test results were comparable, except that Test 12 gave a slightly higher strength of ϕ' = 44.5 degrees compared to ϕ' = 41.8 degrees for the drained test. The ultimate strength for the undrained test with no gas (Test 14) could not be determined exactly, because the pore



21G-21L (FAIL)



21G-21L (FAIL)

Figures 3.46 and 3.47

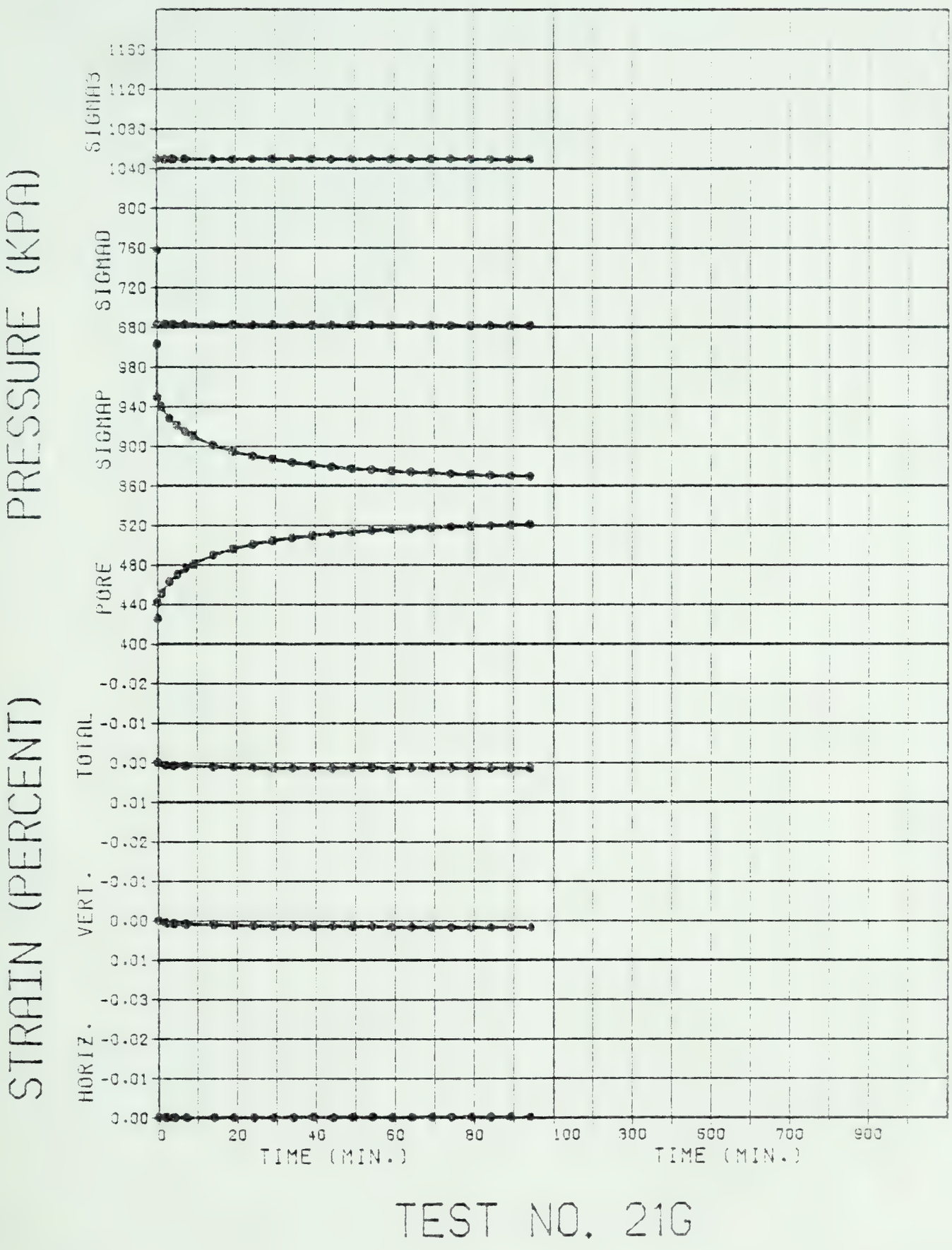

PRESSURE (KPA)
STRAIN (PERCENT)
SIGMA3
SIGMAD
SIGMAP
PORE
TOTAL
VERT.
HORIZ.
1160
1120
1080
1040
800
760
720
680
980
940
900
860
520
480
440
400
-0.02
-0.01
0.00
0.01
-0.02
-0.01
0.00
0.01
-0.03
-0.02
-0.01
0.00
0
20
40
60
80
100
300
500
700
900
TIME (MIN.)
TIME (MIN.)
TEST NO. 21G

Figure 3.48

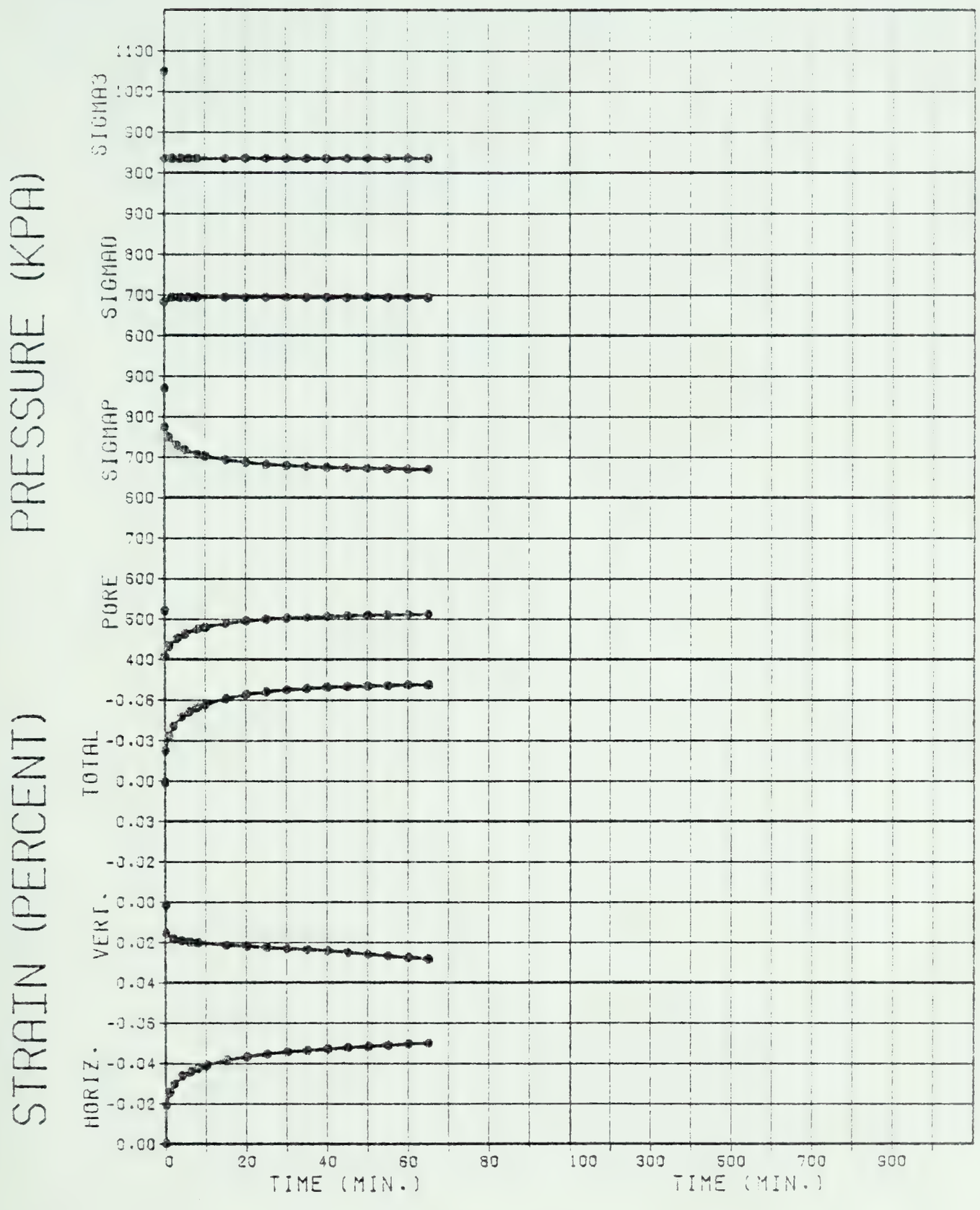
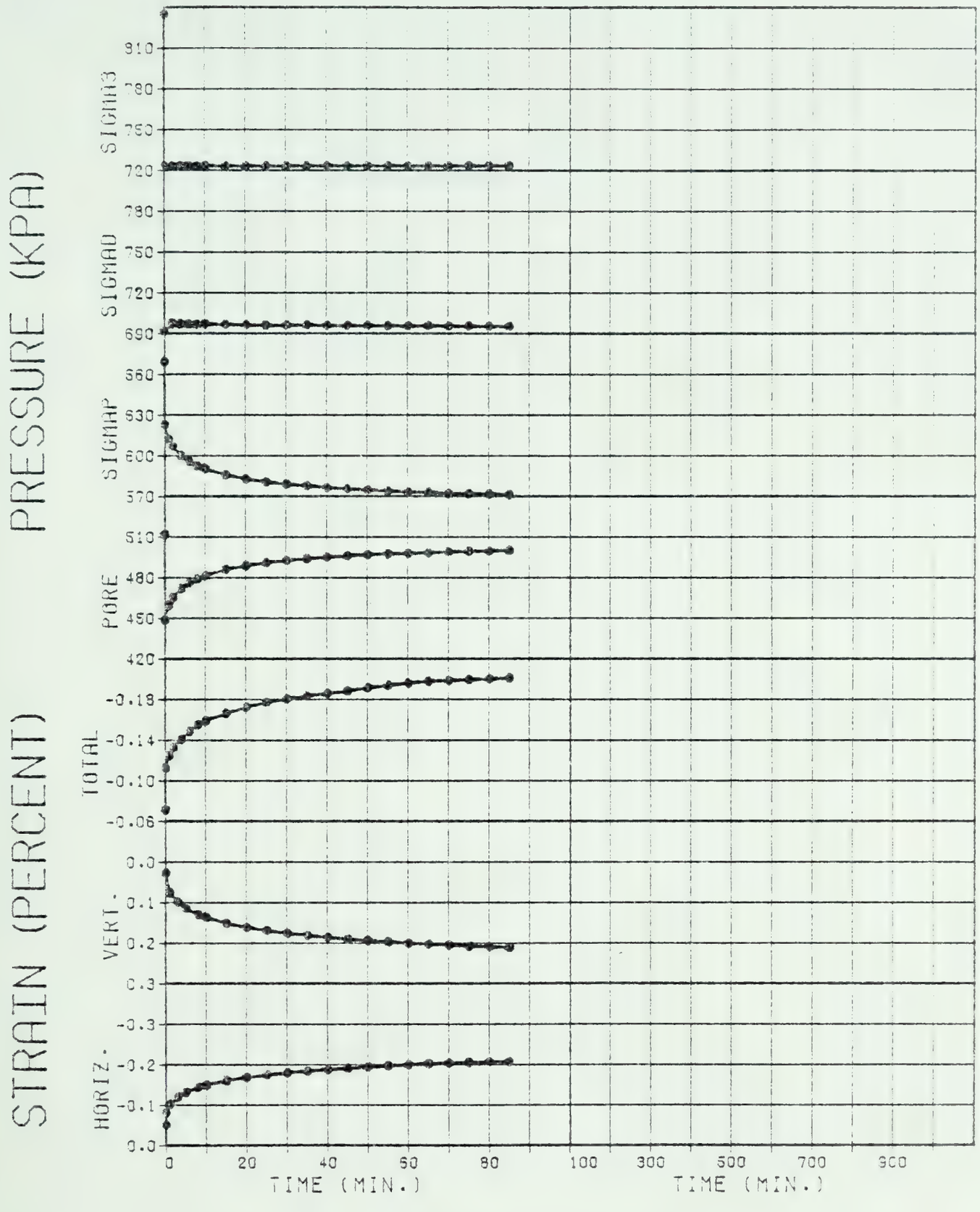
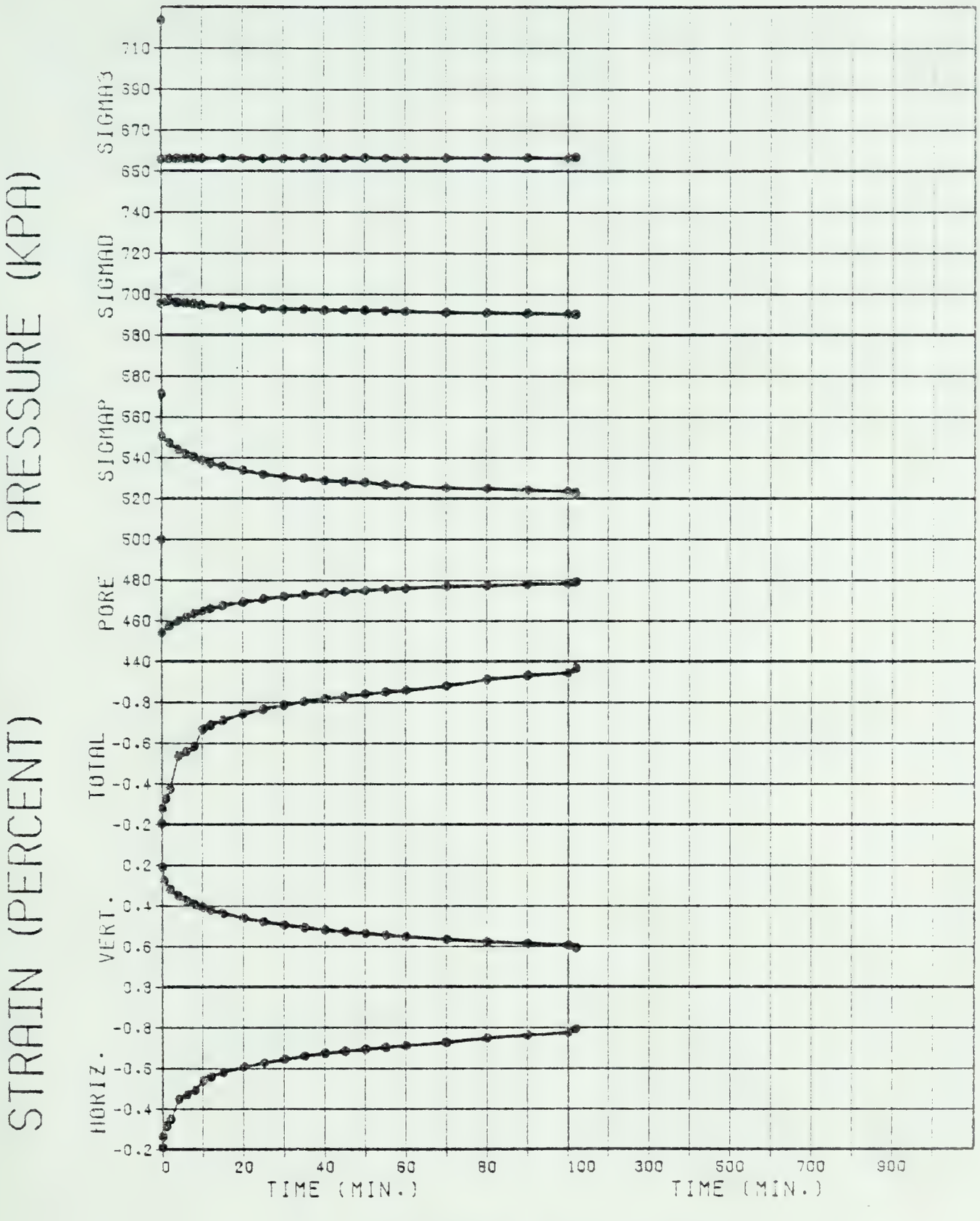

PRESSURE (KPA)
STRAIN (PERCENT)
SIGMA3
SIGMAO
SIGMAP
PORE
TOTAL
VERT.
HORIZ.
TIME (MIN.)
TIME (MIN.)
TEST NO. 21H

Figure 3.49



TEST NO. 21I

Figure 3.50



TEST NO. 21J

Figure 3.51

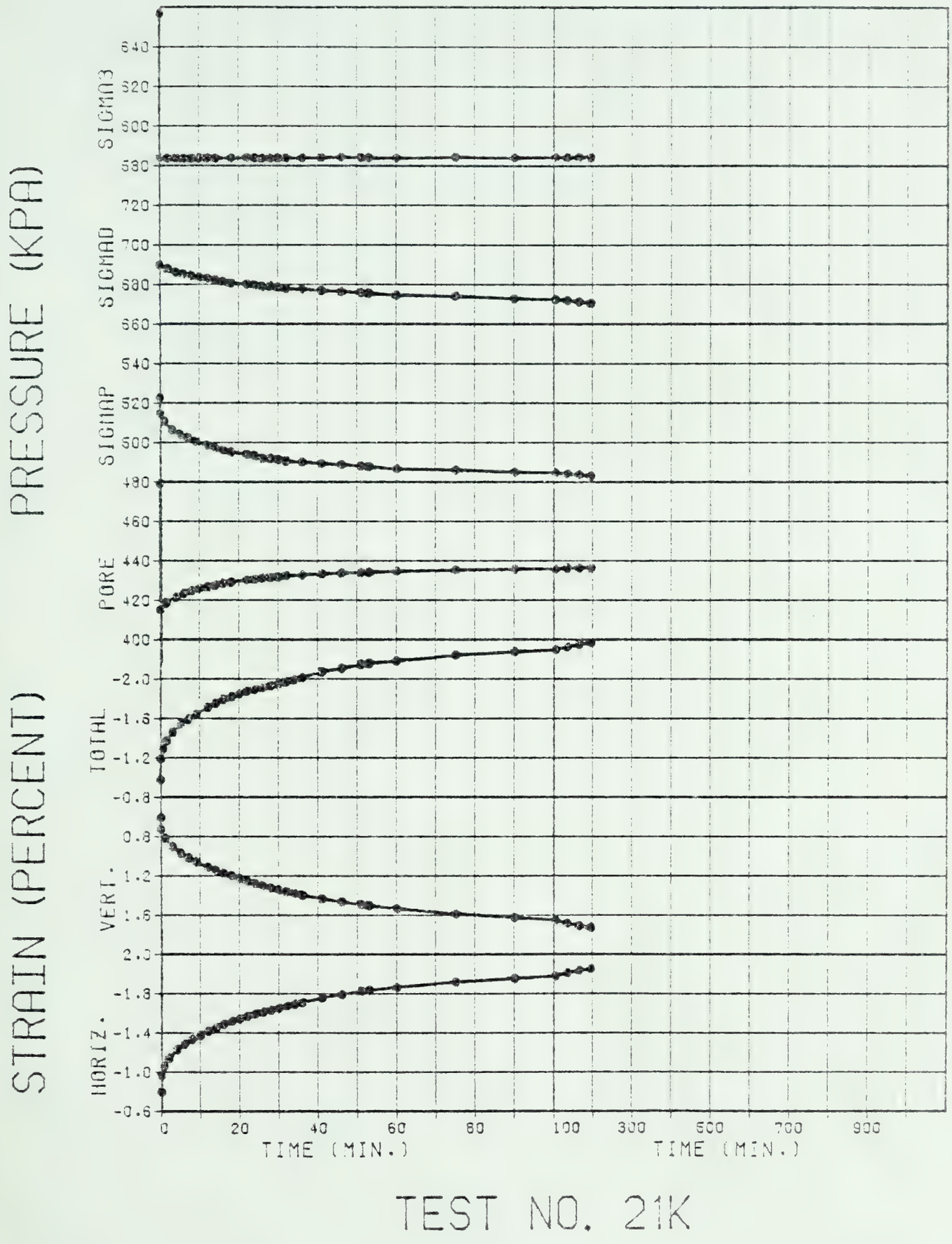

PRESSURE (KPA)
STRAIN (PERCENT)
SIGMA3
SIGMAD
SIGMAP
PORE
TOTAL
VERT.
HORIZ.
640
620
600
580
720
700
680
660
540
520
500
480
460
440
420
400
-2.0
-1.6
-1.2
-0.8
0.8
1.2
1.6
2.0
-1.8
-1.4
-1.0
-0.6
0
20
40
60
80
100
300
600
700
900
TIME (MIN.)
TIME (MIN.)
TEST NO. 21K

Figure 3.52

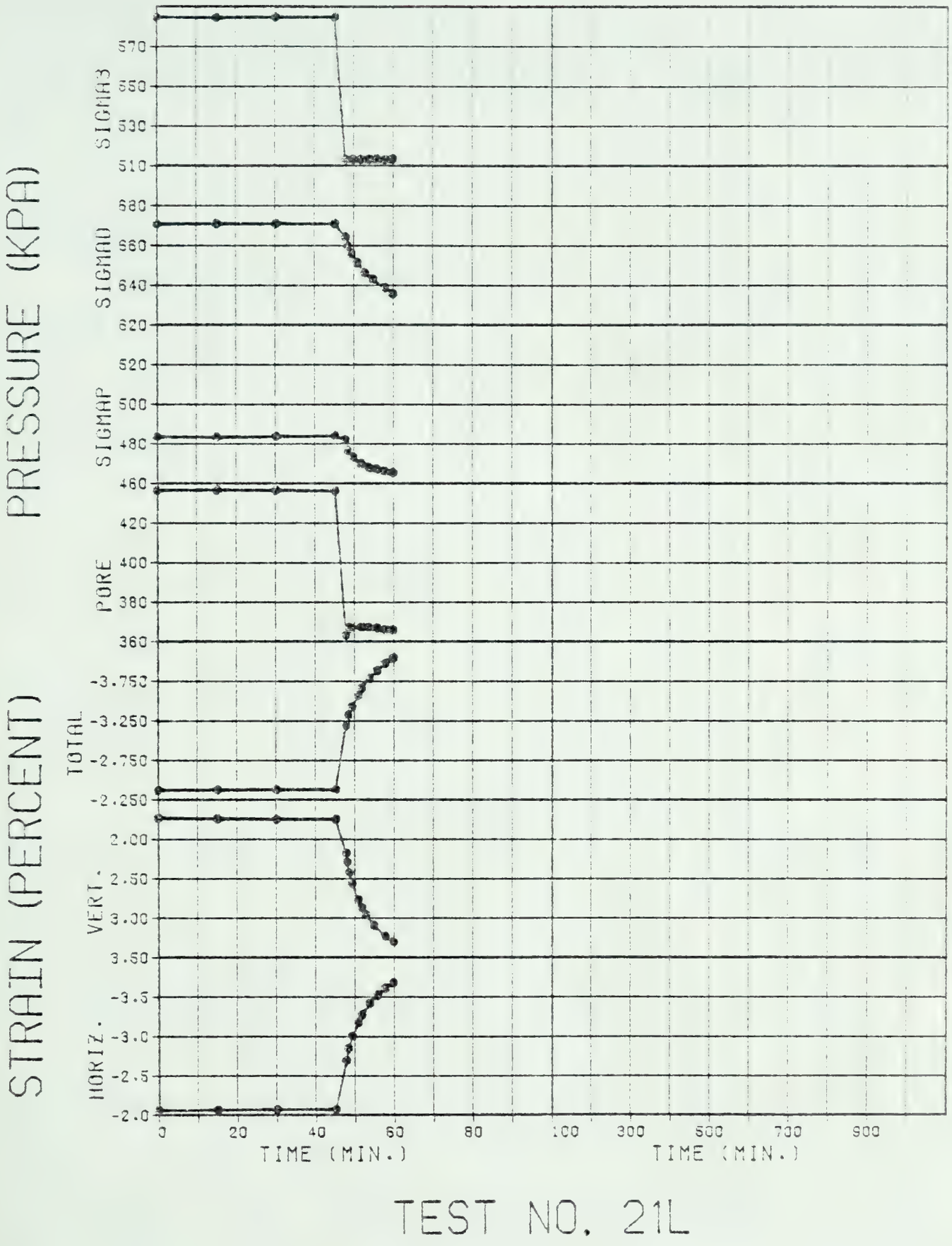

PRESSURE (KPA)
SIGMA3
SIGMAD
SIGMAP
PORE
570
550
530
510
680
660
640
620
520
500
480
460
420
400
380
360
STRAIN (PERCENT)
TOTAL
-3.750
-3.250
-2.750
-2.250
VERT.
2.00
2.50
3.00
3.50
HORIZ.
-3.5
-3.0
-2.5
-2.0
0
20
40
60
80
100
300
500
700
900
TIME (MIN.)
TIME (MIN.)
TEST NO. 21L

Figure 3.53

pressure became negative before the onset of failure. The results from all the tests to failure are located in Appendix E.

3.8 SUMMARY

This chapter has reviewed the development of the laboratory testing equipment and the performance of the tests, and has presented the test results. No analysis or interpretation of these results has been attempted, beyond those comments which can be made from visual inspection of the data, and those which are useful in understanding the general nature of the behaviour of gassy soils.

The existence and importance of the liquid-gas saturation pressure, $P_{l/g}$, (or bubble point) has been demonstrated in the observed pore pressure responses.

An evaluation of the equilibrium response of the soil and a preliminary analysis of the transient response will be made in Chapter 4. A complete discussion of the transient soil behaviour will be postponed until Chapter 6, to allow the theoretical considerations to be developed in Chapter 5.

It is appropriate to note here, however, that an examination of the stress-strain behaviour of gassy soils has indicated that such behaviour is identical to soils containing no or little gas. The presence of large quantities of gas in the sample has only caused a change in the nature of the pore pressure response, and introduced a

time-dependency of pore pressure and hence strain in the undrained behaviour of such soils. A discussion of the implications with respect to drained behaviour will be left until Chapter 7.

CHAPTER 4 - EVALUATION OF LABORATORY TESTS

UNDRAINED EQUILIBRIUM RESULTS

4.1 GENERAL

The theoretical considerations for the equilibrium response of a gassy soil have been discussed in Chapter 2, and the laboratory tests, conducted in part to demonstrate this behaviour, have been presented in Chapter 3. This chapter focuses on the evaluation of the equilibrium test results, in an attempt to verify the theoretical relationships.

Various soil conditions and boundary conditions that introduce "anomalies" into the soil behaviour are also described and modelled. These include the influence of diffusion of gas from the sample to the cell fluid, testing of the sample along non-isotropic stress paths, non-equilibrium in the pore fluid at the start of one phase of the test (when the change in boundary stress is applied), and modification of the test results due to the presence of dissolved air. Either the theory or the analytical technique is changed to incorporate these effects.

A typical test (No. 11) is analyzed and a comparison is made between predicted and observed pore pressures to evaluate the accuracy of the undrained equilibrium model.

A preliminary assessment of the observed non-equilibrium or transient behaviour will also be made, with the objective of more closely examining the form of the behaviour and of establishing a basis for the development of a more precise or mathematical statement of the exsolution process. The theoretical treatment of gas exsolution will then be developed in Chapter 5, and a complete evaluation of the observed transient response made in Chapter 6.

A summary of all the successful undrained tests is given for reference in Table 4.1.

4.2 EQUILIBRIUM BEHAVIOUR

For any particular phase of the undrained isotropic tests, the immediate and the final pore pressure responses may be predicted using equation 2.15b and the proper value of Henry's constant, H. For the immediate response, $H = 0$, since no time is allowed for gas exsolution. For the long term, or equilibrium response, H is set equal to the particular value appropriate for the gas and liquid involved, and the test temperature, (Figure 2.3).

An ability to predict the pore pressure is predicated upon a knowledge of the liquid and soil skeleton compressibilities, the initial porosity and saturation, the initial pore pressure and the change in total stress. The initial porosity, pore pressure, and change in total stress are all measured quantities. The soil skeleton compressibility may be obtained from the volume change

TABLE 4.1 - SUMMARY OF UNDRAINED TESTS

TEST NO.	DATE	STRESS RATIO	PSUEDO-DRAINED PHASE?	FAILURE ?
7	XI/16-23/79	1	yes	no
9	I /08-22/80	1	yes	no
11	III/04-07/80	1	yes	no
12	IV/11-20/80	3	no	yes
15	VII/4-20/80	1.5	no	no
21	II/13-20/81	2	no	yes
22	III/10-12/81	2.5	no	yes
23	IV/21-23/81	1	no	no

measurements. The saturation at the beginning of a test is calculated from a B-test performed after the water and dissolved CO_2 gas is drained into the sample, but before the commencement of the first phase of the test, and at a pressure above the CO_2/H_2O saturation pressure. Subsequent saturations at the beginning of each phase of the test are calculated using the initial saturation plus the measurements of volume change.

In these calculations the compressibility of water is assumed to be 4.5 E-7 KPa^{-1} (Fredlund, 1973).

An example has been given previously (Section 2.6) of the theoretical response for two samples with similar initial stress conditions to Test No. 11, one using H = 0.86 and one using H = 0.02, and both assuming S_i = 100%.

The following sub-sections will investigate various aspects of the testing technique, or of the sample itself, which caused the behaviour of the soil to vary from the "ideal" case discussed in Chapter 2. Modifications to incorporate these effects are suggested.

4.2.1 Effects of gas diffusion and leakage

It is to be expected that some gas will be lost due to diffusion through the sample membrane and into the cell fluid (Section 3.3.1). Loss of gas or liquid may also occur due to leakage, although tests to measure this source of mass loss yielded rates several orders of magnitude less than that due to gas diffusion (Table 3.1, Tests M10a & M10b).

Evidence for loss of gas from the sample exists in all tests performed. Each phase of the undrained tests was typically monitored for 50 - 100 minutes, until the transient pore pressure response was clearly becoming asymptotic to some maximum value. Usually, the next phase was commenced immediately, but in a few cases the sample was left overnight and the next phase was started in the morning. An example is phase G of Test No. 11 (Figure 3-27) which was monitored for a period of 900 minutes. During phase F of Test No. 15 (Appendix D), the pore pressure was monitored for a total period of 560 minutes. At zero time the pressure was 467 KPa, and this rose rapidly and then became asymptotic to a maximum value of 545.8 KPa at t = 125 minutes. The pressure stayed at this maximum value until t = 200 minutes and then gradually decreased to 523 KPa at t = 560 minutes, for an average $dp/dt = -3.7$ KPa/hour. A similar response at the end of Test 15 yielded a rate of decrease of pressure $dp/dt = -0.9$ KPa/hour.

A method of evaluating test results, allowing for gas diffusion, will be discussed in section 4.4.

4.2.2 Evaluating non-isotropic tests

The application of a non-isotropic stress change to an undrained sample of soil, such as in the case of the constant K tests or the tests to failure, requires the additional consideration of sample pore pressure changes caused by deviatoric stresses. This topic was first addressed by Skempton (1954), who developed the equation:

$$\Delta u = B * (\Delta\sigma_3 + A * (\Delta\sigma_1 - \Delta\sigma_3)) \qquad (4.1)$$

where Δu comprises two parts, Δu_a, the change in pore pressure due to an isotropic stress change, and Δu_d, the change in pore pressure due to a deviatoric stress, (Skempton's discussion was oriented towards the triaxial test, where $\Delta\sigma_2 = \Delta\sigma_3$).

Thus:

$$\Delta u = \Delta u_a + \Delta u_d \qquad (4.2a)$$

$$\Delta u_a = B * \Delta\sigma_3 \qquad (4.2b)$$

$$\Delta u_d = A * B * (\Delta\sigma_1 - \Delta\sigma_3) \qquad (4.2c)$$

Skempton (1954) also demonstrated that for a soil behaving in a linear, elastic manner, (and for the "triaxial case"),

$$A = 1/3$$

so that any deviation of A from a value of 1/3 is a measurement of the influence of <u>shear stress on volumetric strain</u>. As noted by Skempton, "from a physical point of view, the pore pressure equation is best written in the form:

$$\Delta u = B*\{1/3*(\Delta\sigma_1+2*\Delta\sigma_3)+(3A-1)/3*(\Delta\sigma_1-\Delta\sigma_3)\} \qquad (4.3)$$

since this shows that, for a material behaving in accordance

with elastic theory, with A = 1/3, the pore pressure depends solely on the mean principal stress, whereas in soils with A ≠ 1/3 the pure shear stress has a marked influence on the pore pressures".

Recalling that equations 2.15a & b were developed by combining equations 2.8b, 2.10 and 2.14c in the form:

$$\Delta V_T = \Delta V_l + \Delta V_g,$$

it is clear that the modifications necessary to derive a solution for Δu lie in the term ΔV_T, which depends on the constitutive relationship for the soil skeleton. ΔV_l and ΔV_g depend on Δu only and so are not affected by the stress path directly.

Harris & Sobkowicz (1977) used the approach of modifying the normal constitutive relationship for an elastic soil in the manner suggested by Skempton (op.cit.). Thus, for the triaxial test,

$$\begin{aligned}\Delta V_T &= V_T * \varepsilon_{vol} = -V_T * \varepsilon_{jj} \\ &= -V_T * ((1+\nu)/E * \sigma_{jj}' - \delta_{jj}*\nu*\sigma_{kk}'/E) \\ &= -V_T * (1-2\nu)/E * \sigma_{kk}'\end{aligned}$$

but since $\sigma_{22}' = \sigma_{33}'$

$$= -V_T * (1-2\nu)/E * (\sigma_{11}' + 2*\sigma_{33}')$$

and if $\beta_T = 3*(1-2\upsilon)/E$

$$= V_T * \beta_T * (\sigma_{3\acute{3}} + 1/3*(\sigma_{1\acute{1}} - \sigma_{3\acute{3}})$$

for the elastic case, or for the more general case:

$$= -V_T * \beta_T * (\sigma_{3\acute{3}} + A * (\sigma_{1\acute{1}} - \sigma_{3\acute{3}}) \qquad (4.4a)$$

Equation 4.4a is analagous to equation 2.14b (in terms of effective stresses) and can be written in terms of total stresses as:

$$\Delta V_T = -V_T * \beta_T * ((\Delta\sigma_3+A*(\Delta\sigma_1-\Delta\sigma_3))-\Delta u) \qquad (4.4b)$$

Combining equations 2.10,2.8b and 4.4b then produces a solution for Δu indentical to equation 2.15b, except that $\Delta\sigma$ is replaced by $\Delta\sigma_3 + A*(\Delta\sigma_1-\Delta\sigma_3)$.

For the stress path of $K = \sigma_{1\acute{1}}/\sigma_{3\acute{3}}$ = constant, equation 4.4a can be simplified further to:

$$\Delta V_T = -V_T * \beta_T * (1+A*(K-1))*(\Delta\sigma_3-\Delta u) \qquad (4.4c)$$

and again a solution for Δu is found equivalent to equation 2.15b, but replacing β_T by $\beta_T*(1+A*(K-1)$. The constant K tests can then be analyzed in a similar manner to the isotropic tests, but defining the compressibility as:

$$\beta_T' = \beta_T * (1+A*(K-1)$$
$$= (-1/V_T) * (\Delta V_T/\Delta\sigma_3') \qquad (4.5)$$

As discussed previously, for K < 2.5, $\beta_T' \neq \beta_T$, suggesting that A is close to zero. For the tests to failure, A was significantly different from zero.

The above discussion is based upon a knowledge of the parameter A. As has been shown, A can be measured directly during the constant K tests, and may also be determined as a function of K for the tests to failure.

An alternative and more sophisticated approach has been taken by Byrne et.al. (1980), who model the soil in a non-linear elastic manner. Shear dilatancy is incorporated by the use of a linear relationship between plastic volumetric strain and shear strain, for shear strains above that developed for ϕ_{cv}. Undrained pore pressure changes around a tunnel due to unloading at the tunnel face are solved using a finite element analysis and iterating on Δu.

For the purposes of this thesis, a comparison of predicted and observed pore pressure behaviour during the laboratory tests will be made using equation 2.15b, modified where necessary to include the parameter A. Non-linearity in the soil compressibility β_T, can also be modelled. It will be convenient to use a linear e vs log σ_3' relationship, with a constant value of C_c for any particular phase of the test. This means that β_T will vary continuously with σ_3', and hence indirectly with Δu. This effect will be included by assuming

a value of β_{T0}, solving for Δu, computing σ_3' and σ_1', and then β_{T1}, and then by comparing β_{T0} with β_{T1}. If the absolute value of the difference between the two lies within a specified tolerance, the solution will be deemed complete. If not, the new value of β_{T1} will be substituted into the equation for Δu, and the iteration on Δu continued until the convergence criteria is met.

4.2.3 Non equilibrium at the start of a test

The solutions discussed in sections 2.5 and 4.2.2 have both assumed that the pore fluid is at equilibrium with respect to dissolved gas concentration at the beginning of the analysis, when the total stress change is applied. In practical terms, this would require that sufficient time be given during one phase of a test, so that at the beginning of the ensuing phase, when a step decrease (or increase) in total stress was made, the exsolution process from the previous phase would have been completed. This is not always possible. Because of the asymptotic nature of the pore pressure response, this would require a time interval of long duration, which would not be compatible with the limitations of the testing apparatus.

However, if the liquid/gas saturation pressure is known for the pore fluid, or if measurements of pressure and saturation are made at some point of equilibrium, a solution to the expected equilibrium response can be found. The equilbrium solution outlined in section 2.5, and in

particular the equation relating the change in volume of free gas (equation 2.10), is modified to include the effect of initial gas disequilibrium. First, it is necessary to determine the total amount of gas in the system:

(a) If the pore fluid is at equilbrium with respect to dissolved gas at some pressure P, and the saturation is S, then the total equilibrium volume of dissolved and free gas at P is:

$$V_{tg} = (1 - S + H*S) * V_v \qquad (4.6a)$$

(b) If the liquid/gas saturation pressure is $P_{l/g}$ and the volume of water in the sample is V_w, then the total equilibrium volume of dissolved and free gas at $P = P_{l/g}$ is:

$$V_{tg} = H * V_w \qquad (4.6b)$$

Since P * V = constant, the constant K′ is defined as:

$$K' = P_{l/g} * H * V_w = P * (1-S+H*S) * V_v \qquad (4.6c)$$

Thus K′ is the total equilibrium volume of dissolved and free gas in the pore space at pressure P, multiplied by P.

Now, consider an element of soil with initial volumes of free gas V_{fg}^0 and water V_w (as in section 2.4.4). Notice now, however, that:

$$V_{tg}^{0} \neq V_{fg}^{0} + H * V_{w},$$

since the pore fluid is temporarily either undersaturated or oversaturated with gas. If the pressure in the pore fluids is P_0, then:

$$V_{tg}^{0} = K'/P_0$$

and if the soil element is to undergo a change in boundary stresses such that the <u>equilibrium</u> pressure P_1 is established, then:

$$V_{tg}^{1} = K'/P_1$$

and therefore the change in volume of free gas in the system is:

$$\begin{aligned} \Delta V_{fg} &= V_{fg}^{1} - V_{fg}^{0} \\ &= (K'/P_1 - H*V_w) - V_{fg}^{0} \end{aligned} \qquad (4.7)$$

Combining equations 4.7, 2.8b, and 2.14c (or 4.4b, or 4.4c):

$$\begin{aligned} K'/(P_0+\Delta u) - H*V_w - V_{fg}^{0} - \beta_l*V_l*\Delta u = \\ -\beta_T * V_T * (\Delta\sigma - \Delta u) \end{aligned} \qquad (4.8a)$$

Again, a quadratic solution is found for Δu:

$$A * \Delta u^2 + B * \Delta u + C = 0 \qquad (4.8b)$$

$$A = \beta_T + n * S * \beta_1$$

$$B = \beta_T*(P_0-\Delta\sigma) + n*(\beta_1*S*P_0+1-S+S*H)$$

$$C = P_0 * (-\beta_T*\Delta\sigma+n*(1-S+S*H))-K'/V_T$$

A comparison with equation 2.15b will confirm that the terms for A and B are equivalent. The term C is different, because it reflects the effect of the initial fluid/gas disequilibrium. Equation 2.15b may still be recovered from (4.8b) by specifying equilibrium at P_0. Then:

$$K' = P_0*(1-S+H*S)*V_v^0$$

and

$$C = P_0*(-\beta_T*\Delta\sigma+n*(1-S+S*H))-P_0*(1-S+S*H)*V_v^0/V_T$$

$$= -\beta_T* \quad *P_0$$

Note in general, however, that the terms n, S, and V_T in equation 4.8b refer to values measured at $P = P_0$ and $t = 0$, whereas the expression for K' in equation 4.6c incorporates the terms S and V_v measured at some pressure P when the system is at equilibrium. Hence the term K'/V_T cannot in general be simplified in equation 4.8b. In the special case where:

$$K' = P_{l/g} * H * V_w,$$

since V_w = constant

$$K'/V_T = n * S * H * P_{l/g}$$

where n refers to the porosity and S the saturation at $P = P_0$.

If the saturation is known at any pressure P_0 at which the pore fluid and free gas are in equilibrium, then the liquid/gas saturation pressure can be found from equation 2.10 by setting $V_{fg}^1 = 0$ and $\Delta V_{fg} = -V_{fg}^0$, to get:

$$P_{l/g} = P_0 + \Delta P = P_0 * (1-S+S*H)/(S*H) \qquad (4.9)$$

4.2.4 Modification of test results due to dissolved air

It was found that the pore fluids used during the tests were also saturated with air, and that the air/H_2O saturation pressure was generally higher than the CO_2/H_2O saturation pressure. The introduction of air into the pore fluid occurred in at least two stages of the pore fluid preparation:

(a) As the water was being saturated with CO_2 in the bubble chamber, minor amounts of air were also being introduced, because air was the main "contaminant" in the CO_2 source (approximately 1%). Since $H_{air} << H_{CO2}$,

it is quite likely that the water became saturated with both air and CO_2 in the bubble chamber.

(b) After the CO_2 saturation sequence was completed in the bubble chamber, the pressure of this fluid was normally raised 100 to 200 KPa to keep the CO_2 in solution and allow the movement of gas-saturated water into the sample. This pressure was applied using a regulated air source, so that some time was available to drive more air into solution, i.e. to make $P_{H2O/air} > P_{H2O/CO2}$.

The sample, then, at the beginning of the undrained portion of a test, is likely to be saturated with respect to air in water, and undersaturated with respect to CO_2 in water. The pore pressure response on unloading will be a composite of that behaviour illustrated in Figures 2.5 and 2.6. As long as $P_{CO2/H2O} < P < P_{air/H2O}$, the response is similar to that for an unsaturated soil, whereas when $P < P_{CO2/H2O}$, the response becomes that of a gassy soil. This phenomenon was observed in practically all tests performed, but was particularly noticeable in Test No. 9, (Figure 4.2).

4.3 PORE PRESSURE RESPONSE

4.3.1 Isotropic tests

Plots of pore pressure vs total stress and the pore pressure parameter B vs total stress are presented for Test No. 7, 9, 11, and 23 in Figures 4.1 to 4.4 respectively.

The results of Tests No. 11 and 23 are closely illustrative of the gassy behaviour circumscribed in Figure 2.5. Test No. 7 shows an apparent increase in long term pressure with decreasing total stress in the range $600 > \sigma > 450$ KPa. This is due to the fact that several phases of the test were started a substantial time before equilibrium had been established in the previous phase, so that the plot shown is not a true equilibrium curve. As mentioned above, Test No. 9 includes air exsolution rather than CO_2 exsolution in the first several phases of the test, so that the u vs curve for $1200 > \sigma > 900$ KPa does not form a plateau, but shows a gradual decrease in pressure.

4.3.2 Constant K tests

Similar plots for Tests No. 12, 15, 21 and 22 are given in Figures 4.5 to 4.8 inclusive. None of these tests were taken to zero effective stress, (because the samples were later to be failed), so that only a part of the gassy soil behaviour is portrayed. Tests 15 and 21 include the results of unloading and reloading the sample.

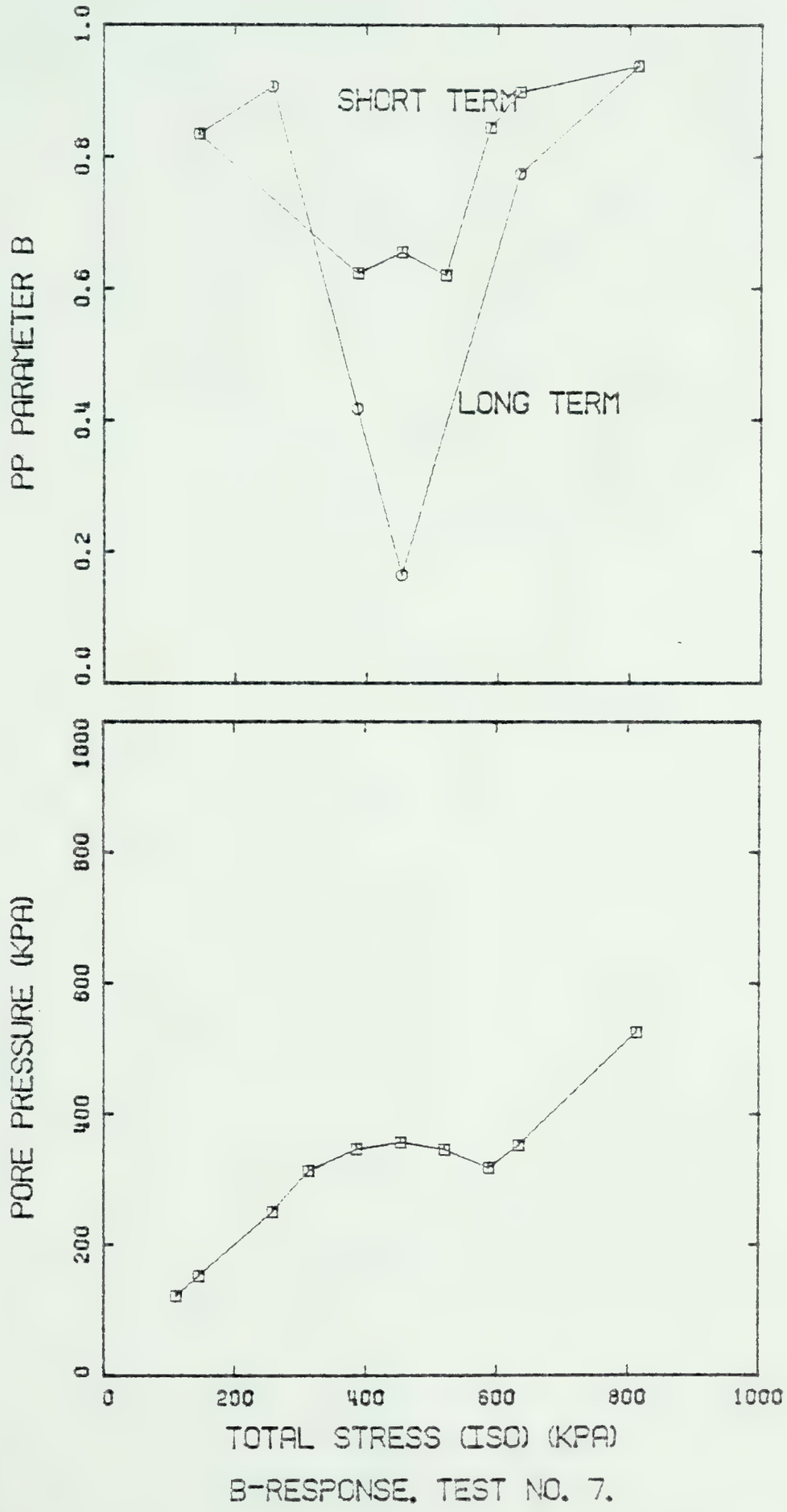

PP PARAMETER B
1.0
0.8
0.6
0.4
0.2
0.0
SHORT TERM
LONG TERM
PORE PRESSURE (KPA)
1000
800
600
400
200
0
0
200
400
600
800
1000
TOTAL STRESS (ISO) (KPA)
B-RESPONSE. TEST NO. 7.

Figure 4.1

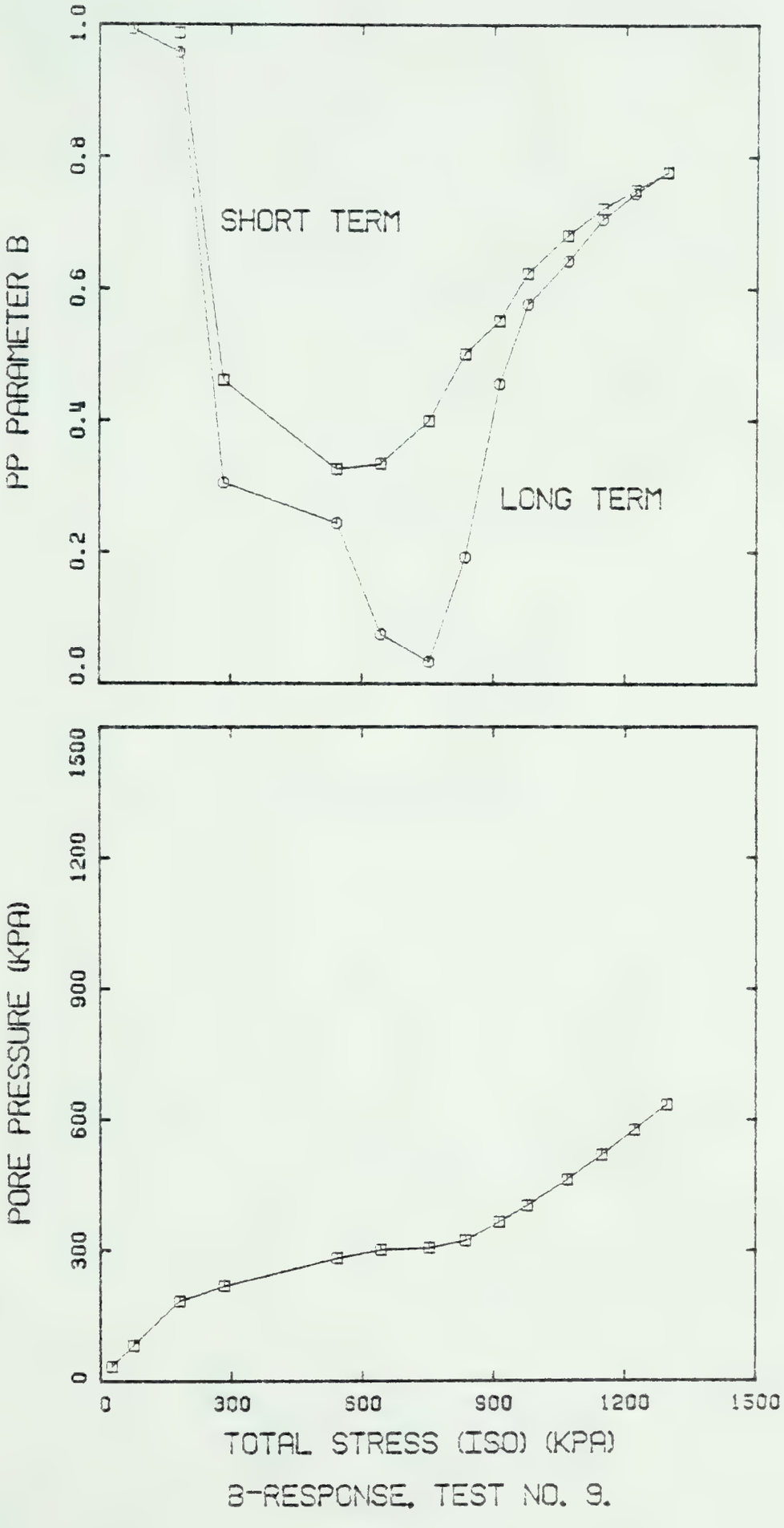

PP PARAMETER B
1.0
0.8
0.6
0.4
0.2
0.0
SHORT TERM
LONG TERM
PORE PRESSURE (KPA)
1500
1200
900
600
300
0
0
300
600
900
1200
1500
TOTAL STRESS (ISO) (KPA)
B-RESPONSE, TEST NO. 9.

Figure 4.2

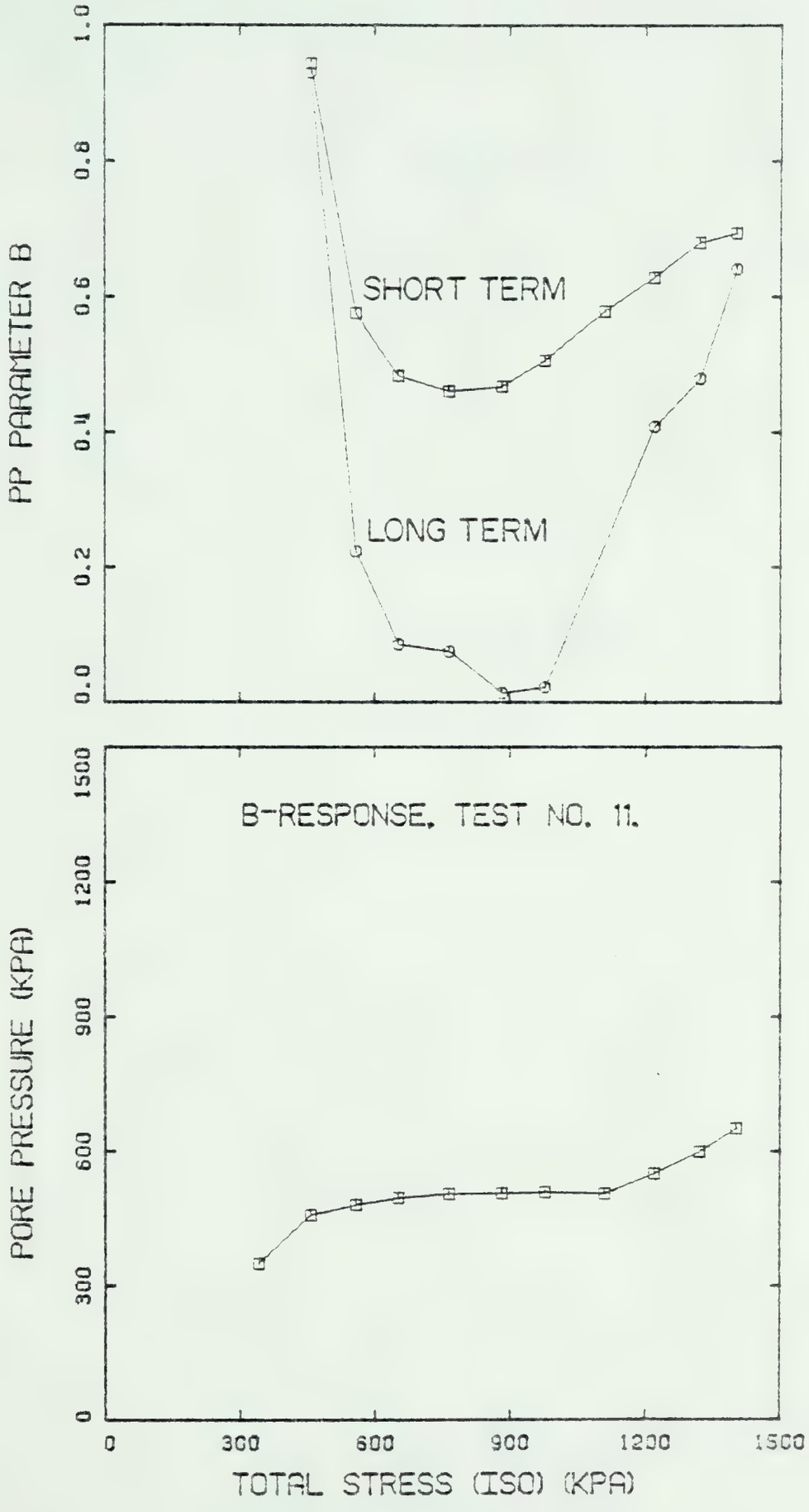

PP PARAMETER B
1.0
0.8
0.6
0.4
0.2
0.0
SHORT TERM
LONG TERM
B-RESPONSE, TEST NO. 11.
PORE PRESSURE (KPA)
1500
1200
900
600
300
0
0
300
600
900
1200
1500
TOTAL STRESS (ISO) (KPA)

Figure 4.3

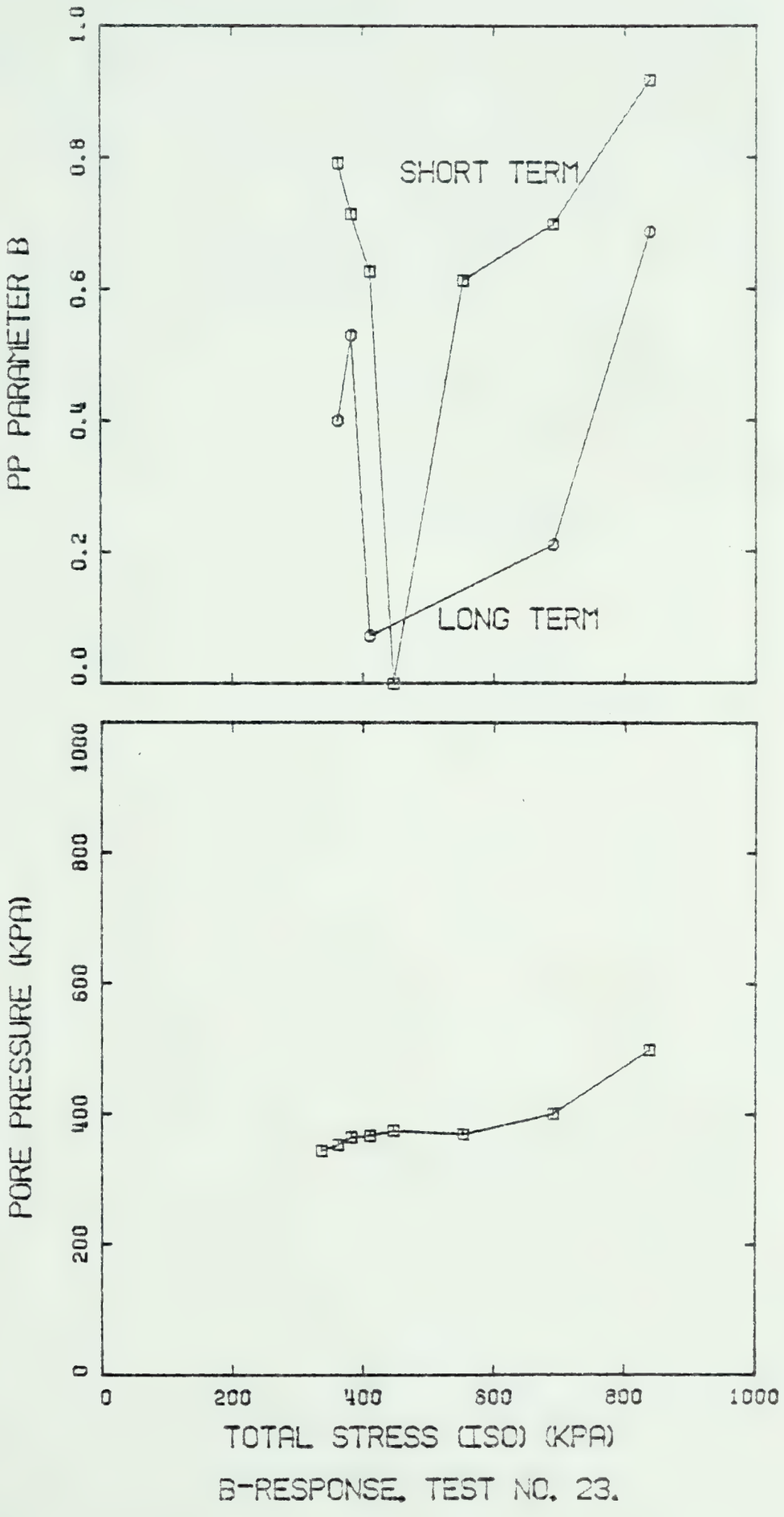

PP PARAMETER B
1.0
0.8
0.6
0.4
0.2
0.0
SHORT TERM
LONG TERM
PORE PRESSURE (KPA)
1000
800
600
400
200
0
0
200
400
600
800
1000
TOTAL STRESS (ISO) (KPA)
B-RESPONSE. TEST NO. 23.

Figure 4.4

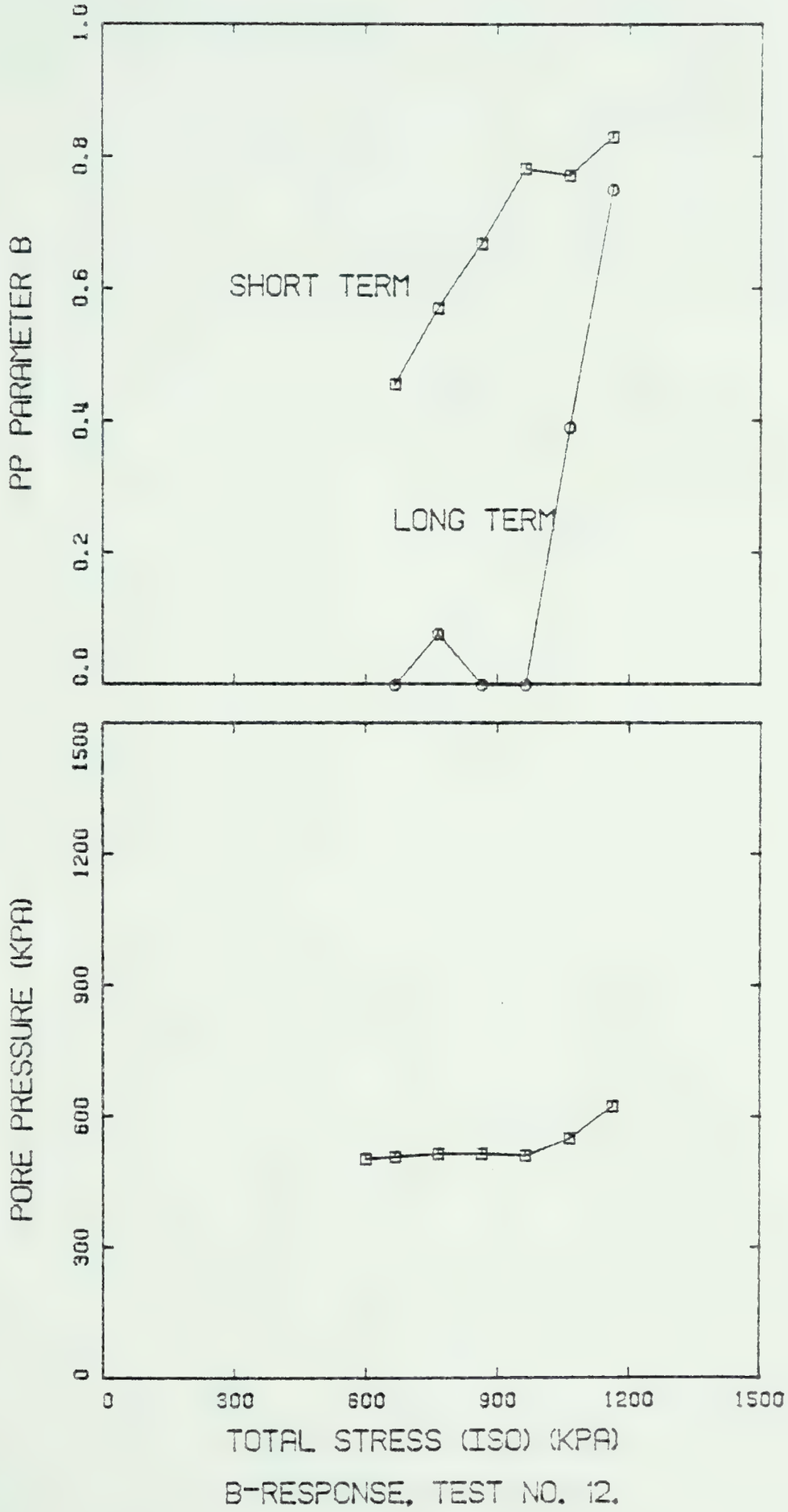

PP PARAMETER B
0.0
0.2
0.4
0.6
0.8
1.0
SHORT TERM
LONG TERM
PORE PRESSURE (KPA)
0
300
600
900
1200
1500
0
300
600
900
1200
1500
TOTAL STRESS (ISO) (KPA)
B-RESPONSE, TEST NO. 12.

Figure 4.5

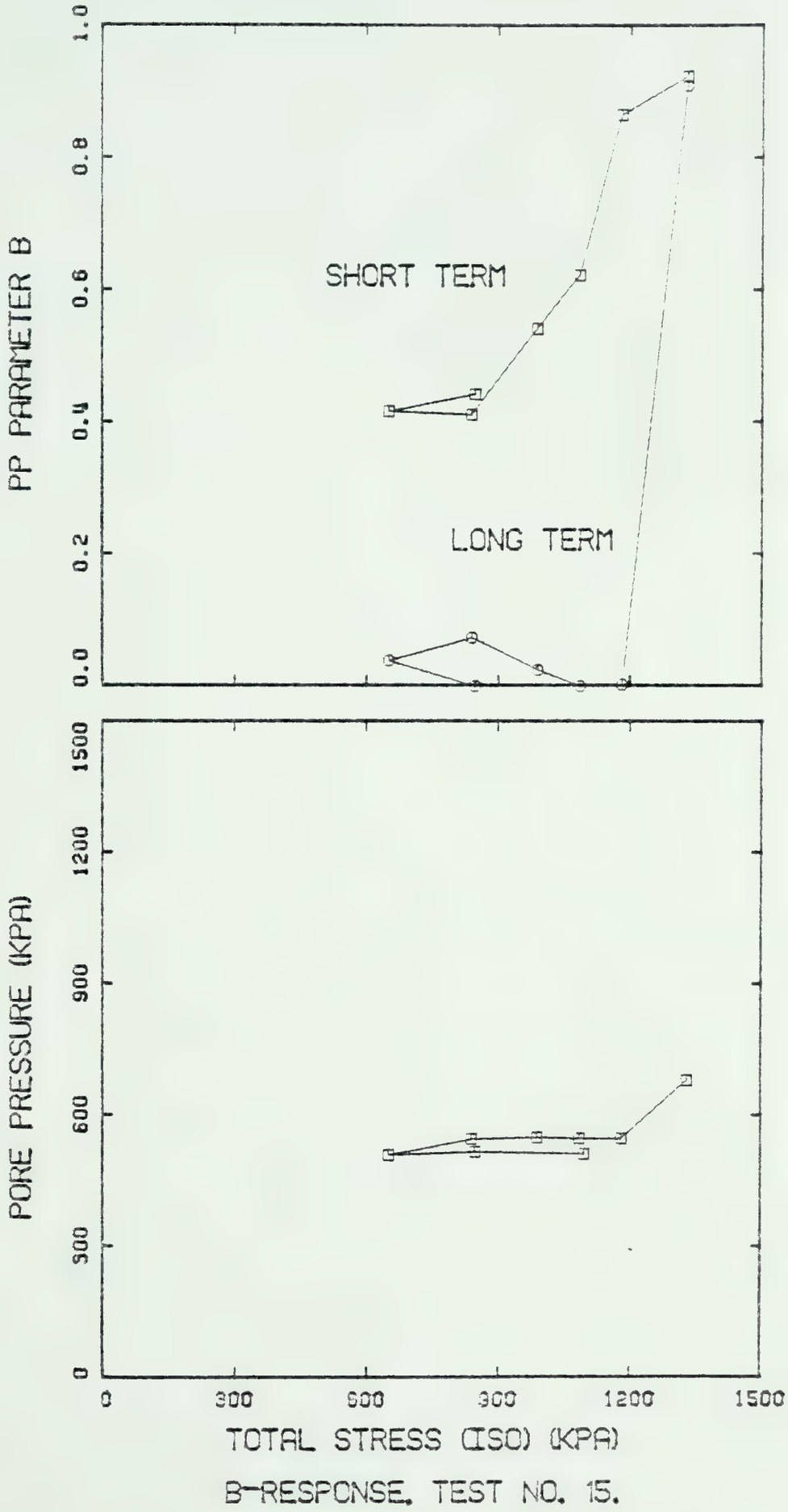

PP PARAMETER B
1.0
0.8
0.6
0.4
0.2
0.0
SHORT TERM
LONG TERM
PORE PRESSURE (KPA)
1500
1200
900
600
300
0
0
300
600
900
1200
1500
TOTAL STRESS (ISO) (KPA)
B-RESPONSE. TEST NO. 15.

Figure 4.6

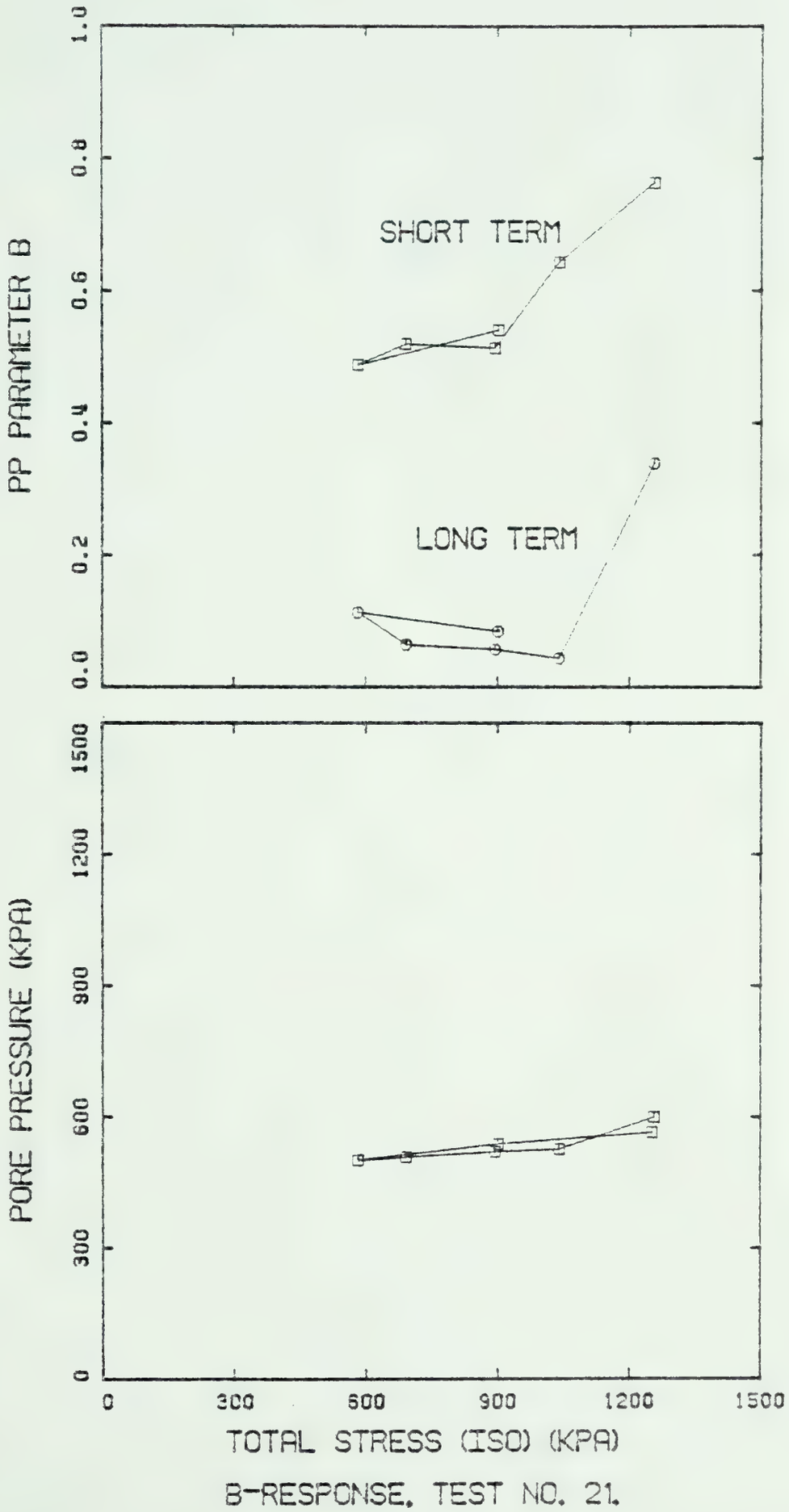

PP PARAMETER B
1.0
0.8
0.6
0.4
0.2
0.0
SHORT TERM
LONG TERM
PORE PRESSURE (KPA)
1500
1200
900
600
300
0
0
300
600
900
1200
1500
TOTAL STRESS (ISO) (KPA)
B-RESPONSE. TEST NO. 21.

Figure 4.7

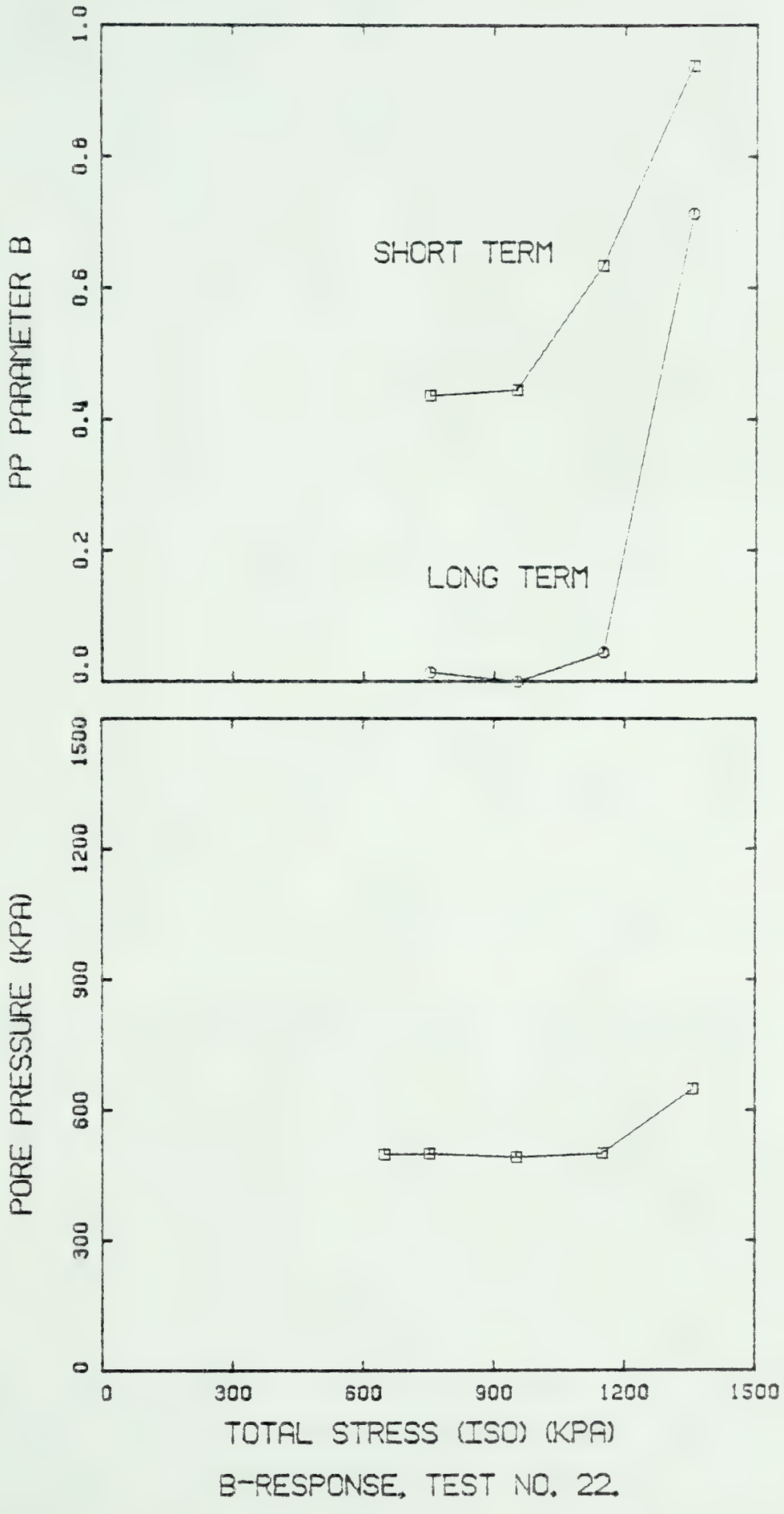

PP PARAMETER B
1.0
0.8
0.6
0.4
0.2
0.0
SHORT TERM
LONG TERM
PORE PRESSURE (KPA)
1500
1200
900
600
300
0
0
300
600
900
1200
1500
TOTAL STRESS (ISO) (KPA)
B-RESPONSE, TEST NO. 22.

Figure 4.8

4.3.3 Tests to failure

The variation of pore-pressure and the parameter B can be plotted against σ_3 in a similar manner to the previous tests, since failure was induced by decreasing the cell pressure, (for Tests No. 12 & 21). During the initial portions of these tests, the influence of shear strain on volumetric strain is small (A ≠ 1/3) and the behaviour is similar to an isotropic test. As K increases, however, and the sample approaches failure, shear dilation becomes more important, and the sample begins to undergo large volumetric strains. This is a similar response, in terms of volumetric strain and pore pressure, to when a sample subjected to isotropic stress changes approaches $\sigma' = 0$. Pore pressures begin to decrease and the B-parameter increases with continued unloading.

This behaviour is illustrated in Figures 4.9 to 4.10.

4.4 COMPARISON OF OBSERVED AND PREDICTED BEHAVIOUR

Using the theoretical relationships for undrained, gassy soil behaviour developed previously (Sections 2.5 & 4.2), it is possible to make a comparison between the predicted pore-pressure response and that observed in the laboratory. A typical undrained test (Test No. 11) will be analyzed and evaluated in this section. The examination of other test results will be postponed until Chapter 6, where a more comprehensive appraisal is made of the predictive capabilities of both the equilibrium and transient models.

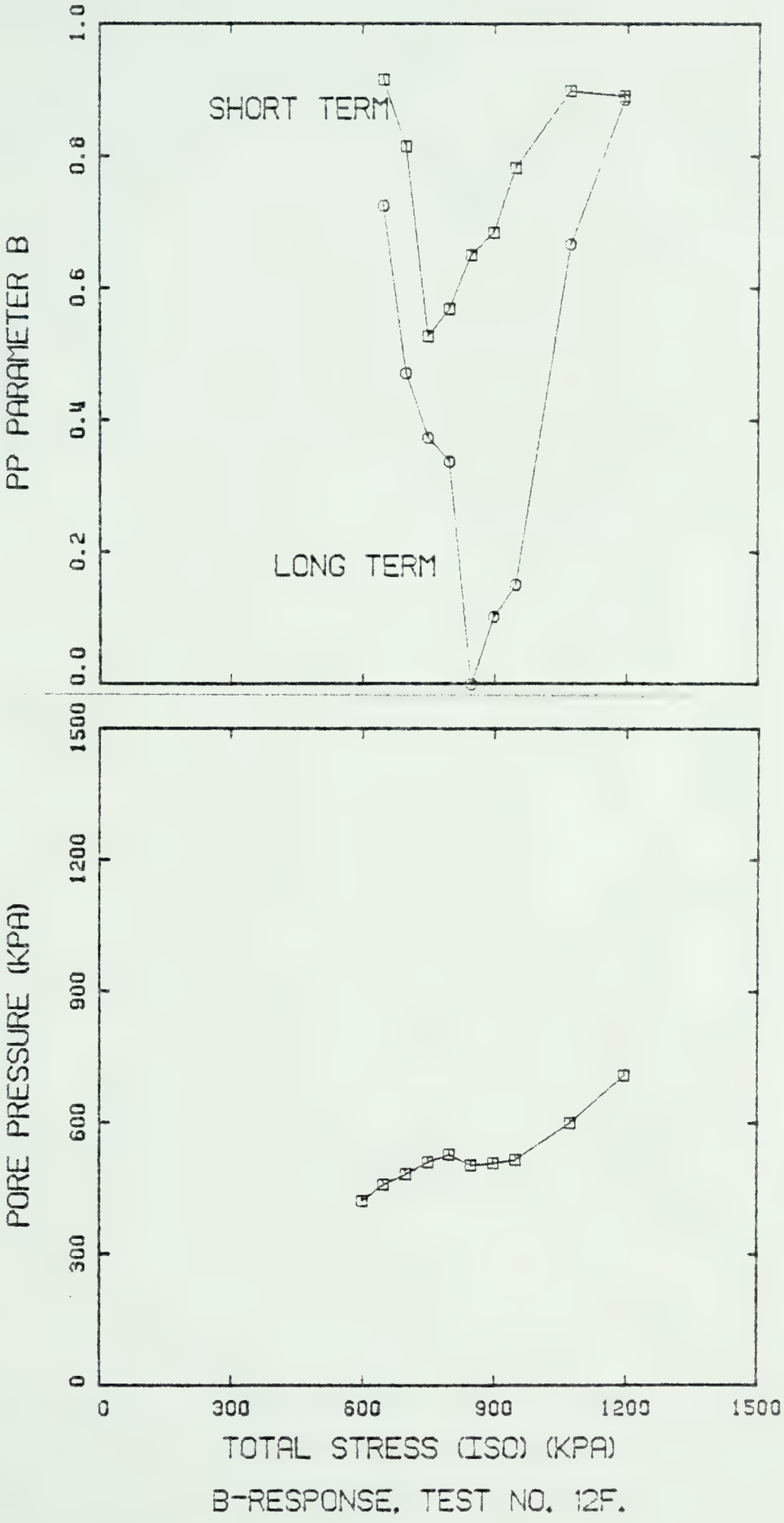

PP PARAMETER B
1.0
0.8
0.6
0.4
0.2
0.0
SHORT TERM
LONG TERM
PORE PRESSURE (KPA)
1500
1200
900
600
300
0
0
300
600
900
1200
1500
TOTAL STRESS (ISO) (KPA)
B-RESPONSE, TEST NO. 12F.

Figure 4.9

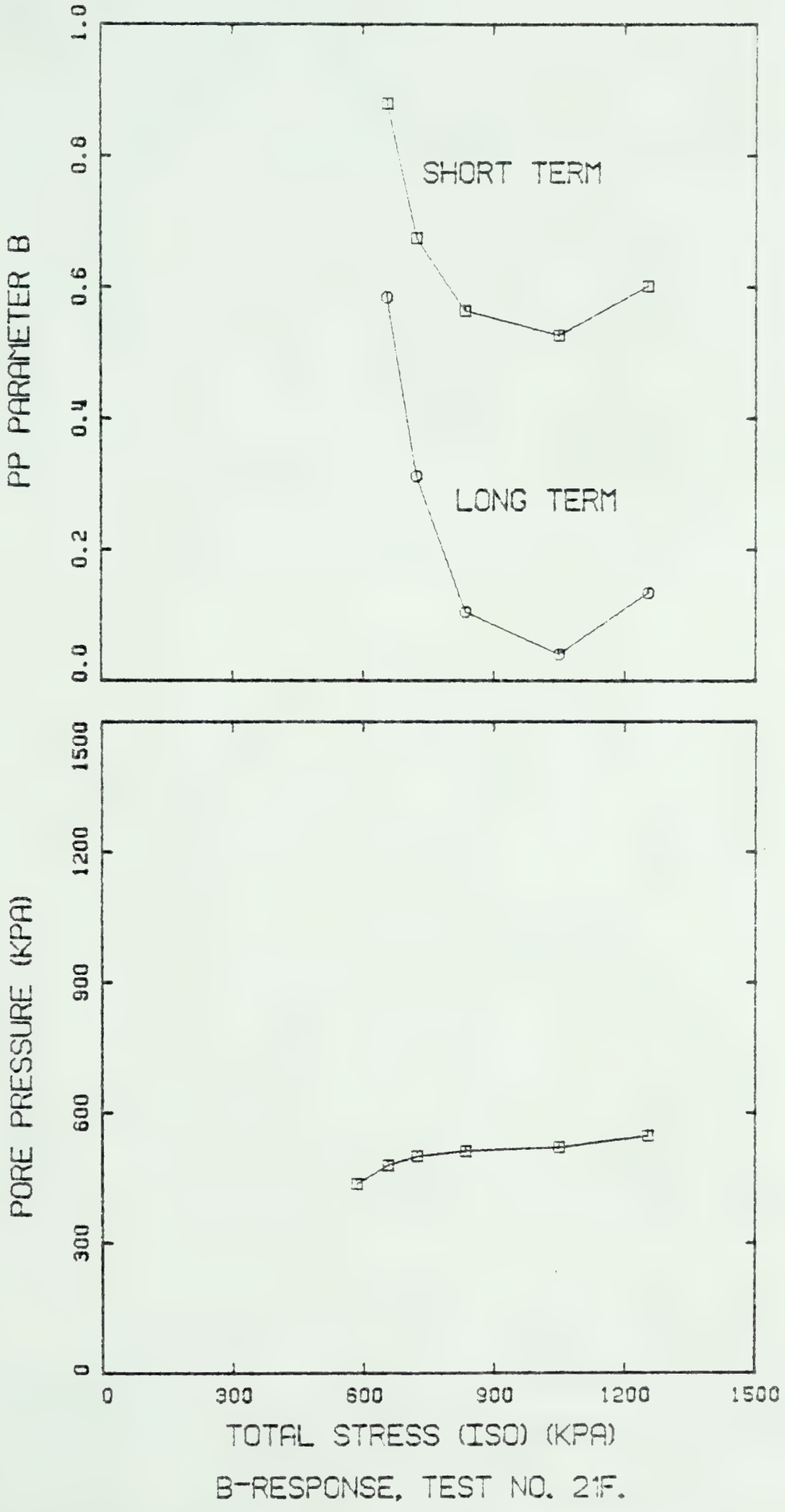

PP PARAMETER B
1.0
0.8
0.6
0.4
0.2
0.0
SHORT TERM
LONG TERM
PORE PRESSURE (KPA)
1500
1200
900
600
300
0
0
300
600
900
1200
1500
TOTAL STRESS (ISO) (KPA)
B-RESPONSE, TEST NO. 21F.

Figure 4.10

The analysis of equilibrium behaviour undertaken here will use the following two methods:

(a) Method #1 : The assumption will be made that no gas is lost from the sample by diffusion through its membrane. Given the initial conditions of the test and the change in total stress applied at the beginning of each phase, the analysis can proceed in a self-consistent manner, using computed values of pore pressure, porosity and saturation at the end of one phase as input parameters for the beginning of the next phase.

(b) Method #2 : This method attempts to incorporate the effects of loss of gas from the sample (by diffusion into the cell fluid). To do this, each phase is analyzed separately, using as input parameters for u, n and S the values actually measured during the test. Any loss of gas during a previous phase of the test is reflected in lower porosities and higher saturations than would normally be expected. These "adjusted" values can be used for the analysis of the pore pressure behaviour during the current phase of the test.

Since the pressure at the beginning of a phase is not actually an equilibrium pressure established from the previous phase, but has a value slightly lower, the p_{max} for the preceding phase is estimated by using a non-linear "least-squares" analysis of the pressure-

time data, (this is discussed in the next section). Then equation 4.9 is applied to calculate the current liquid/gas saturation pressure. (If gas is being lost from the sample, $P_{l/g}$ will decrease as the test proceeds.) Knowing u, n, S and $P_{l/g}$ at the beginning of the phase, P_{max} for the end of the phase can be calculated using equation 4.8b. To be meaningful, the calculated P_{max} must be compared to that value extrapolated from the laboratory pressure-time data.

An appraisal of the success of the numerical model may then be made by comparing predicted and observed values of the immediate pore pressure, the immediate value of B ($=\Delta u/\Delta\sigma$), the equilibrium pore pressure, the equilibrium value of B, and for Method #1, the values of saturation and porosity at the end of each phase.

Table 4.2 was compiled to assist in the analysis of the test results. It summarizes the initial values of porosity, saturation, total stress and pore pressure observed for each phase of Test 11, as well as the total stress change applied at the beginning of the phase and the compression index measured during the phase. The initial saturation for phase A was obtained from a B-test performed at a pore pressure above the liquid-gas saturation pressure, and for subsequent phases was calculated from the volume change data.

TABLE 4.2

INITIAL CONDITIONS FOR TEST NO. 11

PHASE	C_C	N (%)	S (%)	*****INITIAL VALUES******* σ(KPa)	U(KPa)	$\Delta\sigma$(KPa)
A	$\beta_T = 9^* 10^{-6}$ KPa^{-1}	32.28	99.75	1403.3	652.3	-81.3
B	.0233	32.30	99.67	1322.4	600.4	-101.4
C	.0159	32.33	99.54	1220.5	551.2	-109.3
D	.0138	32.36	99.38	1112.1	506.8	-133.9
E	.00912	32.42	99.11	978.2	509.6	-95.2
F	.00912	32.46	98.93	883.6	507.4	-117.7
G	.00766	32.53	98.62	766.4	505.7	-113.6
H	.00658	32.61	98.27	654.9	489.4	-96.7
J	.00658	32.69	97.90	559.0	481.1	-101.7

Analysis #1 was then performed using the initial conditions for Phase A of n = 32.28%, S = 99.75%, σ = 1403.3 KPa, u = 652.3 KPa and β_T = 9E-6 KPa^{-1}. The predicted values of Δu and B (immediate and equilibrium), as well as all other calculated quantities for phases B through J are shown in Table 4.3. During Phases A & B, only air was exsolving from the pore fluid and so a value of H = 0.02 was used. The sample was assumed to be at equilibrium at the beginning of phase A, yielding a $P_{air/H2O}$ = 746.7 KPa. During phase C, CO_2 began to exsolve and it was found that $P_{CO2/H2O}$ was close to 520 KPa, (this is slightly higher than the backpressure of 505 KPa maintained in the bubble chamber during sample preparation). It was not possible to finish the analysis of phase J, since the condition of zero effective stress was being approached. It is likely that the actual compressibility of the soil skeleton during the latter part of phase J is not being adequately modelled with a constant compression index.

The only additional input at the beginning of each phase in analysis #1 is the changing compression index, and the applied total stress change.

Analysis #2 was performed and the calculated pore pressure response is given in Table 4.4. This table also contains the measured pore pressures, and those predicted from analysis #1, for comparative purposes. The information summarized in Table 4.4 is presented graphically in Figure 4.11.

TABLE 4.3

TEST 11 - PREDICTED RESULTS - ANALYSIS #1
(NO LOSS OF GAS BY DIFFUSION THROUGH MEMBRANE)

PHASE	N (%)	S (%)	IMMEDIATE RESPONSE ΔU(KPa)	B	U(KPa)	EQUILIBRIUM RESPONSE ΔU(KPa)	B	U(KPa)	COMMENTS
A	32.28	99.75	-70.85	.872	581.45	-37.99	.467	614.31	N & S as given at beginning of test. For H=0.02 P_{air/H_2O} calculated to be 746.7 KPa.
B	32.322	99.560	-81.44	.803	532.87	-56.81	.560	557.50	
C	32.352	99.423	-74.34	.680	483.16	-42.70	.391	514.80	Using P_{CO_2/H_2O} = 520 KPa
D	32.385	99.271	-80.55	.602	434.25	-2.28	.017	512.52	
E	32.454	98.962	-46.54	.489	465.98	-1.32	.014	511.20	
F	32.494	98.779	-60.83	.517	450.37	-2.18	.018	509.02	
G	32.562	98.476	-59.18	.521	449.84	-2.77	.024	506.25	
H	32.468	98.092	-56.17	.581	450.08	-4.25	.044	502.00	
J_1	32.780	97.505	-40.89	.730	461.11	-7.69	.137	494.31	Since at beginning of this increment, σ'=57, these calcs. are for Δσ= -56
J_2	33.022	96.442	-7.91	.920	486.4	-3.39	.395	490.92	σ'=8.69 Δσ= -8.6
J_3	33.139	95.933	-3.27	.962	487.65	-2.07	.610	488.85	σ'=3.48 Δσ= -3.4

TABLE 4.4 - TEST 11 - PREDICTED RESULTS - ANALYSIS #2

(PLUS SUMMARY OF ANALYSIS #1 & OBSERVED PORE PRESSURES)

PHASE	$P_{1/g}$ USED for ANALYSIS #2 (KPa)	IMMEDIATE PORE PRESSURE (KPa)				EQUILIBRIUM PORE PRESSURE (KPa)			
		OBSERVED	ANALYSIS #2		ANALYSIS #1	Umax. estimated from p vs t plots	ANALYSIS #2		ANALYSIS #1
			U	B			U	B	
A	746.7	595.9	581.5	.872	581.5	>603(*1)	614.3	.467	614.3
B	719.6	531.4	518.1	.837	532.9	559(*1)	557.0	.454	557.5
C	520	482.4	472.5	.720	483.2	515(*2)	515.5	.326	514.8
D	519.5	429.2	422.4	.630	434.3	~513.5	512.7	-.044(*5)	512.5
E	519.5	461.3	459.9	.522	466.0	512	511.7	-.022	511.2
F	519.5	452.2	443.7	.541	450.4	508	509.6	-.018	509.0
G	517.9	453.2	444.8	.536	449.8	500	505.2	.004	506.3
H	512.3	442.5	435.2	.561	450.1	~485	496.0	-.068	502.0
J	499.6	422.4	N/A(*4)	N/A(*4)	N/A(*4)	459(*3)	~455	increasing to 1	455

Footnotes:
(*1) Air exsolution, pp data somewhat erratic, difficult to estimate Pmax.
(*2) Transition to CO_2 exsolution.
(*3) O' became O during this phase. Further increase in u thus not possible.
(*4) Calculations for phase J done in several steps -- short term response not applicable.
(*5) Negative values of B due to incomplete gas exsolution in previous phase.

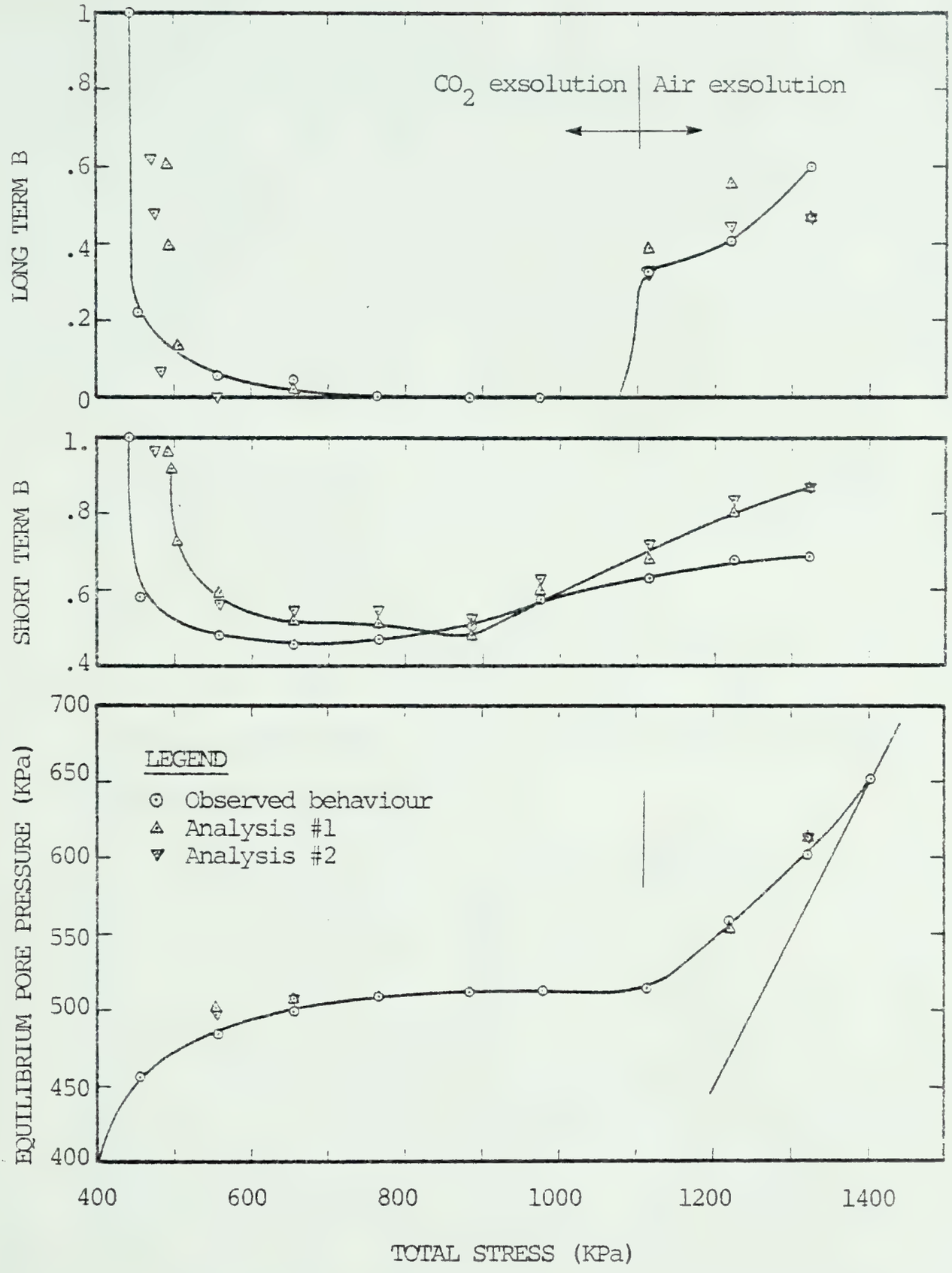


Figure 4.11 - Comparison of observed and predicted pore pressures for Test No. 11

A perusal of Figures 4.1 to 4.10, discussed previously, will have established already the veracity of the concept of gassy soil behaviour, and will have illustrated the general correspondence between the theoretical and the observed responses. A careful scruitiny of Tables 4.2 to 4.4, and Figure 4.11, will allow a quantitative assessment of the accuracy of the theory. The following points should be noted:

(a) The predictive capability of the theory is extremely good, particularly for the equilibrium (or long term) response.

(b) Analysis #1 predicts long term pressures slightly on the high side towards the end of the test. This would be expected if the sample had accumulated a measurable loss of gas.[1]

(c) There seems to be a better correlation for short term pore pressures between Analysis #1 and the observed values than with Analysis #2. Generally, analysis #1 predicts values equivalent, to a little high, whereas analysis #2 predicts values 7 - 10 KPa too low. The <u>better correlation for analysis #1 is probably fortuitous</u>, however. From an examination of Tables 4.2 and 4.3 it is evident that predicted values of n are too high and of S are too low for Analysis #1, indicating that the sample has indeed lost gas during

---

[1]In this discussion the loss of gas will be understood to be due to diffusion through the membrane into the cell fluid.

the test. The lower values of S input in analysis #1 are what force the initial pore pressure response to be higher than for analysis #2. It was expected, before any analyses had been undertaken, that the observed immediate pore pressures might be high compared to predicted values, because there was a time lapse of 15 - 30 seconds between reducing the total stress and taking the first reading at the beginning of a phase. Since the pressure vs time curve is quite steep at t = 0, it was possible that the true "immediate" response of the sample was not being accurately recorded.

(d) The existence of loss of gas from the sample has been clearly demonstrated by direct observation, i.e. the membrane-gas diffusion tests, and those phases of the undrained tests monitored for more than several hours, in which the pressure initially increases, plateaus, and then decreases. This is also implied in the observed values of P_{max} for each phase, which progressively become smaller than the calculated equilibrium values as the test proceeds. (Analysis #2, which partially accounts for gas loss, is more capable of predicting this behaviour.) This is reflected in a decreasing value of $P_{l/g}$ (column 2, Table 4.4), since $P_{l/g}$ is calculated from P_{max}.

It should be emphasized that the above critique of the theoretical model is not meant to detract from its remarkable capability to predict the immediate and equilibrium response of a gassy soil. The deviations of predicted from observed behaviour are of a secondary nature and are adequately explained by the peculiarities of the testing equipment and technique.

Analyses of the other isotropic tests, and of the anisotropic tests (using a modified β_T, as discussed in section 4.2.2), have been in complete agreement with the conclusions and criticisms discussed in this section. Recognizing as well that the theoretical model has demonstrated the ability to correctly assess the behaviour of soils containing air or CO_2, it is appropriate to state that the laboratory program has confirmed the predictive accuracy of the theoretical equilibrium model. This may seem to be a mute point, as it has implicitly been accepted by many authors in their work on unsaturated soils. The extention of the concepts from unsaturated to gassy soils has predicted remarkably different undrained soil behaviour, however, which has called for experimental verification in addition to field support. To the author's knowledge, the experimental approach adopted herein is the first direct method of quantitatively assessing the theory for either the unsaturated or gassy soil.

4.5 NON-EQUILIBRIUM BEHAVIOUR

While performing the equilibrium analyses for the undrained tests, it became evident that a method of estimating P_{max} for each phase of the test was necessary. Given a set of data relating the pore pressure u to time t, covering an interval of time Δt = 60 - 100 minutes, what was the value of u at infinite time? Although the tests had been performed for long enough intervals to establish the asymptotic nature of the response, a visual estimation of P_{max} was not sufficiently accurate for analytical purposes.

Engineers have a predilection for linear relationships, and often in seeking a functional correlation for two variables will first consider those functions that can be reduced to a linear form. Such functions include:

(a) $y = m * x + b$

(b) $y = m * \ln(x) + b$, or $a*x^m = e^y$

(c) $\ln(y) = m * \ln(x) + b$, or $y = a*x^m$

(d) $\ln(y) = m * x + b$, or $y = e^{(m*x+b)} = a*c^x$

Unfortunately, these functions are not useful in the analysis of the laboratory pressure-time data, since the pressure becomes asymptotic to some maximum value, whereas the functions (a)to (d) above are all continually increasing with x. It is interesting to note that for function (c), if $0<m<1$, then

$$dy/dx = a*m*x^{(m-1)}$$

$$\lim(x\to\infty)\ dy/dx = 0$$

However, the

$$\lim(x\to\infty)\ y = \infty$$

so that this function still does not possess a true asymptotic character. Attempts to fit the pressure-time data of phase 11D with functions (c) & (d) above, as well as to a polynomial, are illustrated in Figures 4.12-14. It may be seen that none of these functions produce a suitable fit to the observed data.

Two functions that have an asymptotic nature were used to fit the pressure-time and volumetric strain vs time data for all the undrained tests:

(a) Hyperbolic Tangent Function (Figure 4.15)

$$(u-u_{min})/(B'-u_{min})=\tanh(t/A')$$

(b) "Quotient + 1" Function:

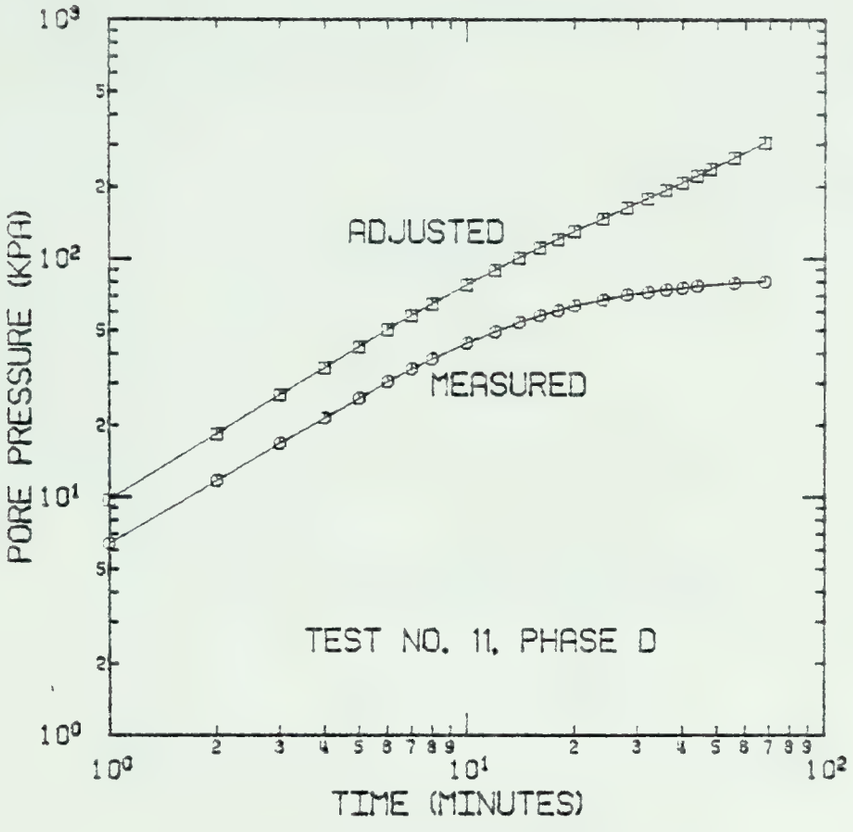
$$(u-u_{min})/(B'-u_{min})=t/(t+A')$$

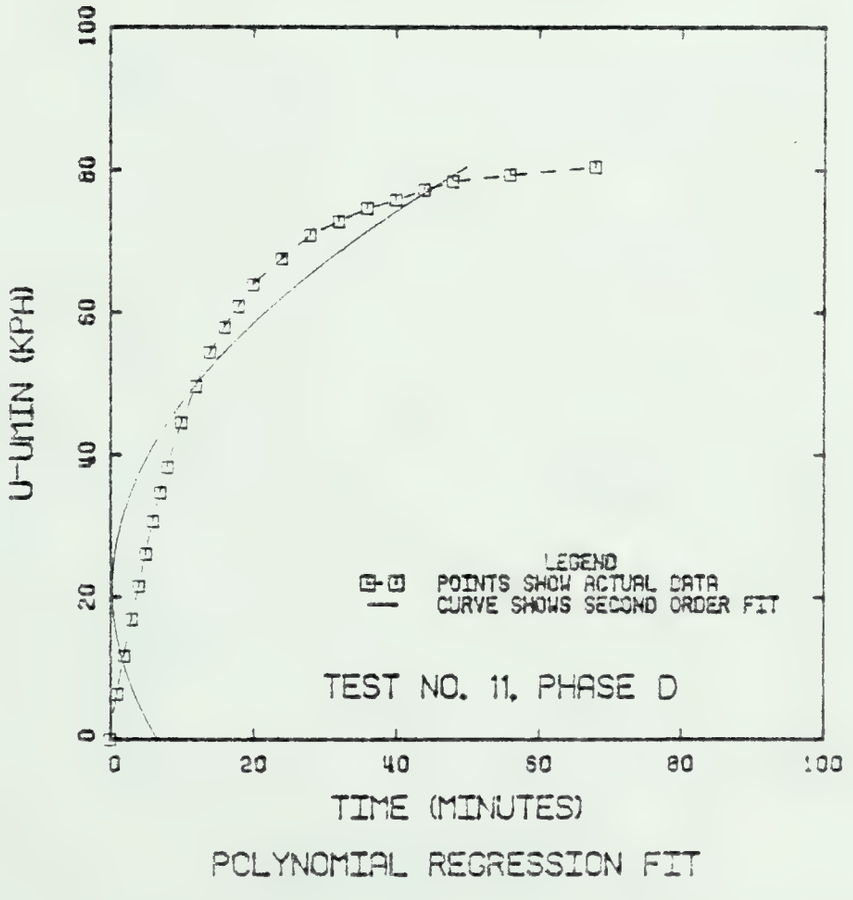
where u,t = current values of pore pressure and time

u_{min} = pore pressure at time = 0

$B' = u_{max}$ = pore pressure at infinite time

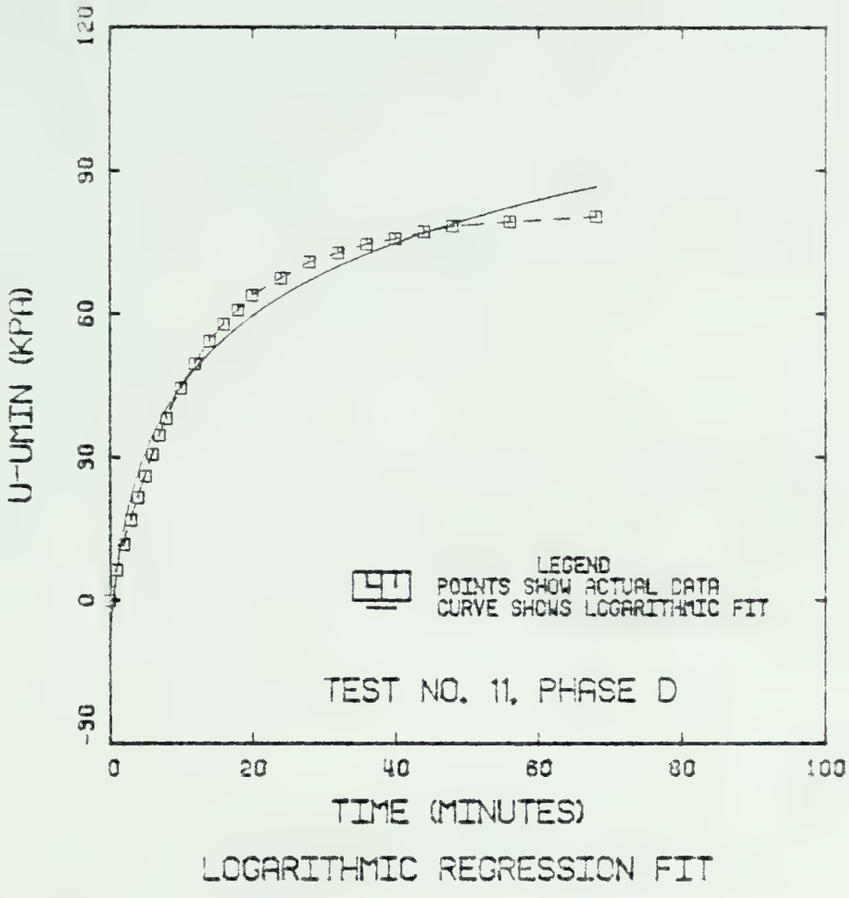
A' = scaling parameter



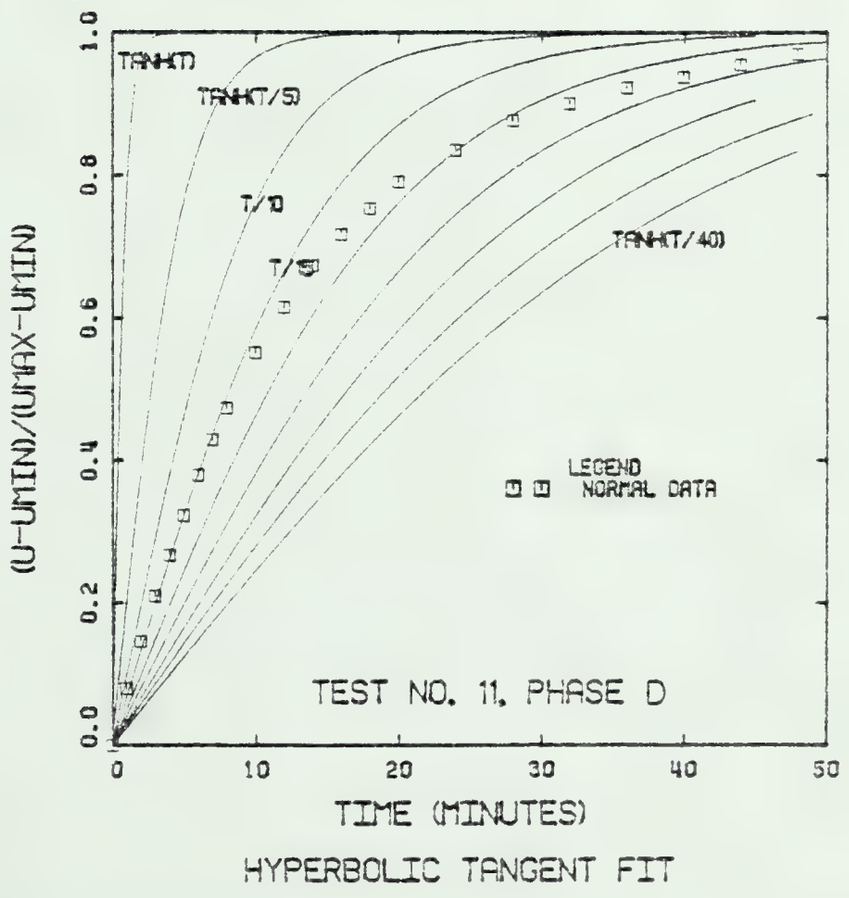


POLYNOMIAL REGRESSION FIT

Figures 4.12 and 4.13



LOGARITHMIC REGRESSION FIT



HYPERBOLIC TANGENT FIT

Figures 4.14 and 4.15

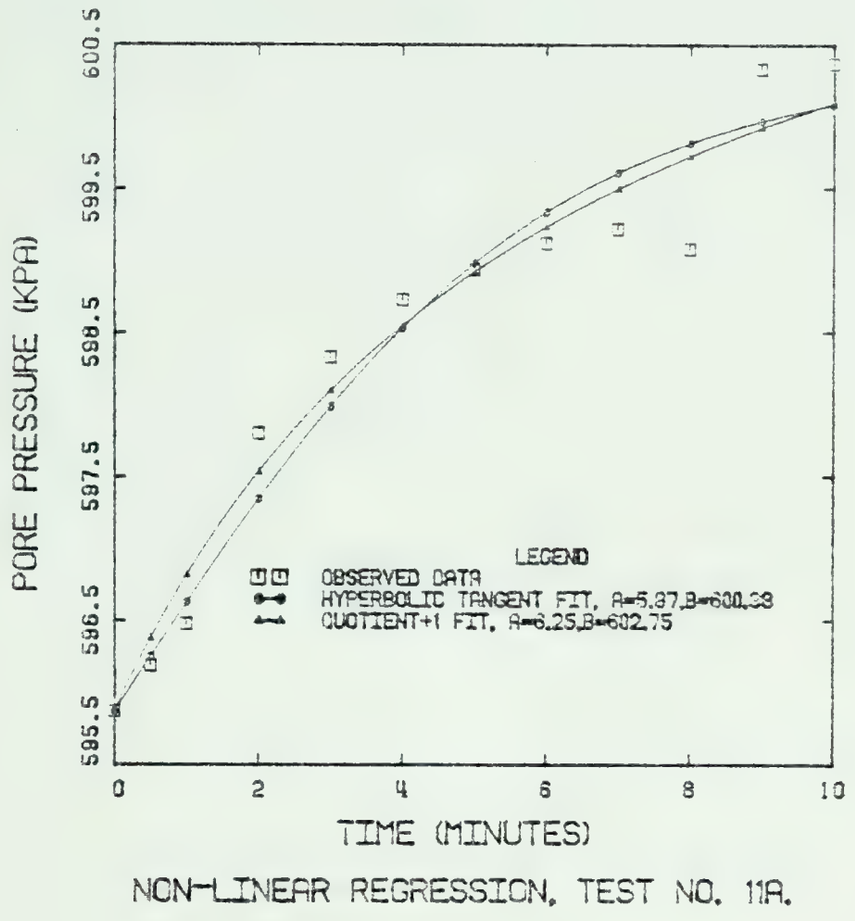
Figure 4.15 was generated to illustrate the nature of the hyperbolic tangent function. The test results could not be fit to either function (a) or (b) by this visual method, because a goodness-of-fit criteria was lacking, and also because B′ needed to be specified.

It was possible to fit either of these functions to the data using a non-linear least-squares analysis, where both A′ and B′ were allowed to vary to establish a "best fit". This was accomplished using the program BMDPAR, Derivative-free Nonlinear Regression, which is part of a statistical package of Biomedical Computer Programs (P-Series, 1979) developed at the Health Sciences Computing Facility, UCLA.[2]

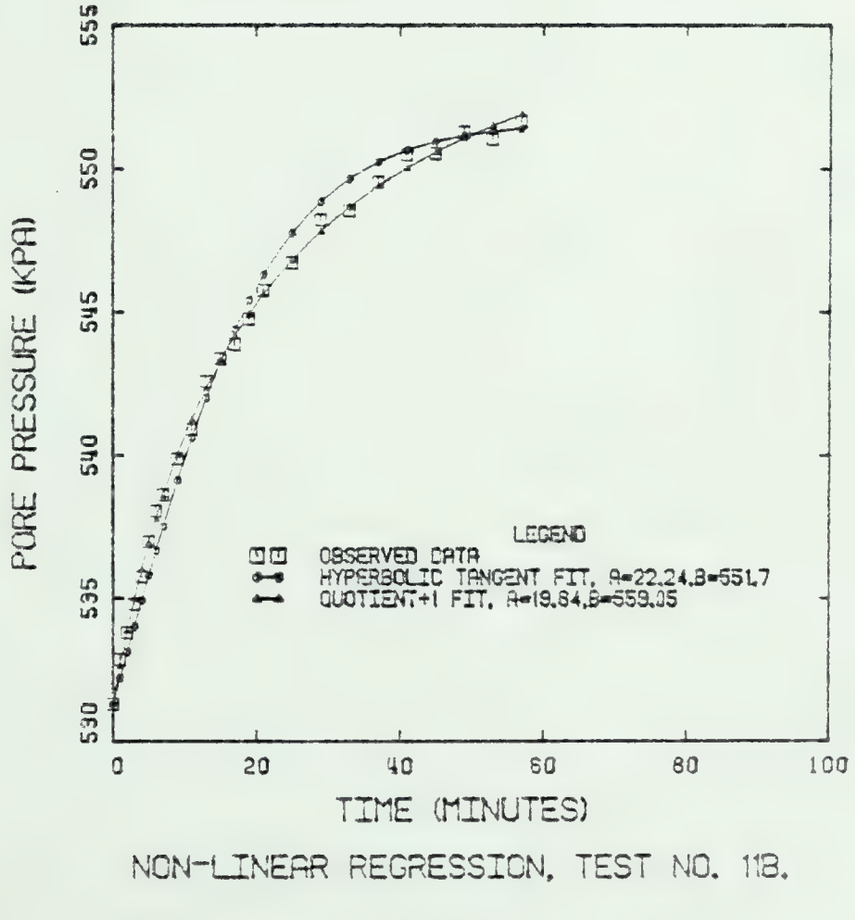
Figures 4.16-24 illustrate the best-fit curves for both functions obtained by this method for phases A to J of Test No. 11. It is clear that the "Quotient + 1" function provides a better fit than the hyperbolic tangent, and in most cases visually appears to have an almost perfect conformity with the data. Except in the unusual case where the agreement was not good (Phase D), or where the data was spurious (phase A), the "Quotient + 1" function was used to estimate the value of u_{max} (i.e. B′). (The values of u_{max} recorded in Table 4.4 were estimated in this manner.)

---

[2]Program revision November, 1979. The Health Sciences Computing Facility was sponsored by NIH Special Research Resources Grant RR-3.

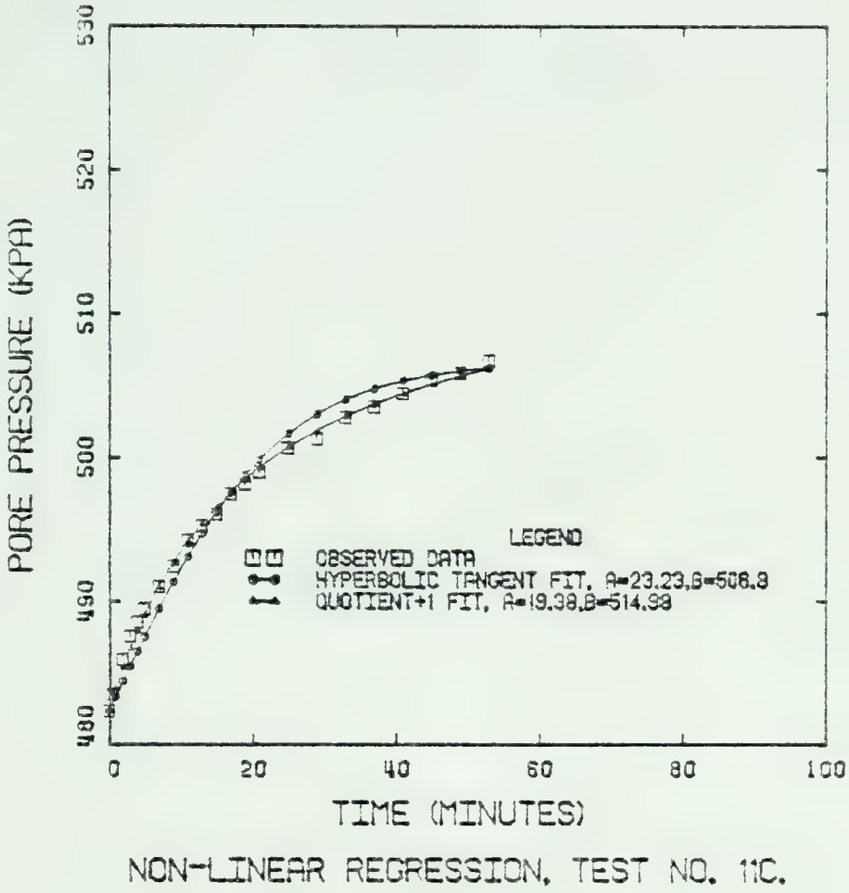


NON-LINEAR REGRESSION, TEST NO. 11A.

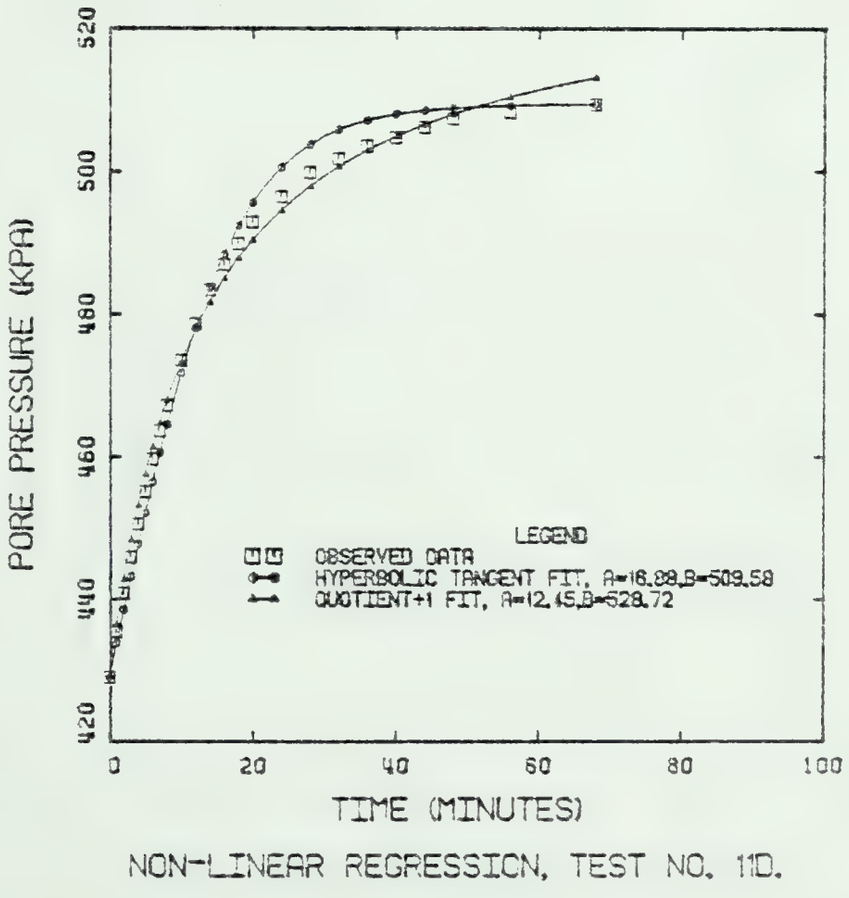


NON-LINEAR REGRESSION, TEST NO. 11B.

Figures 4.16 and 4.17

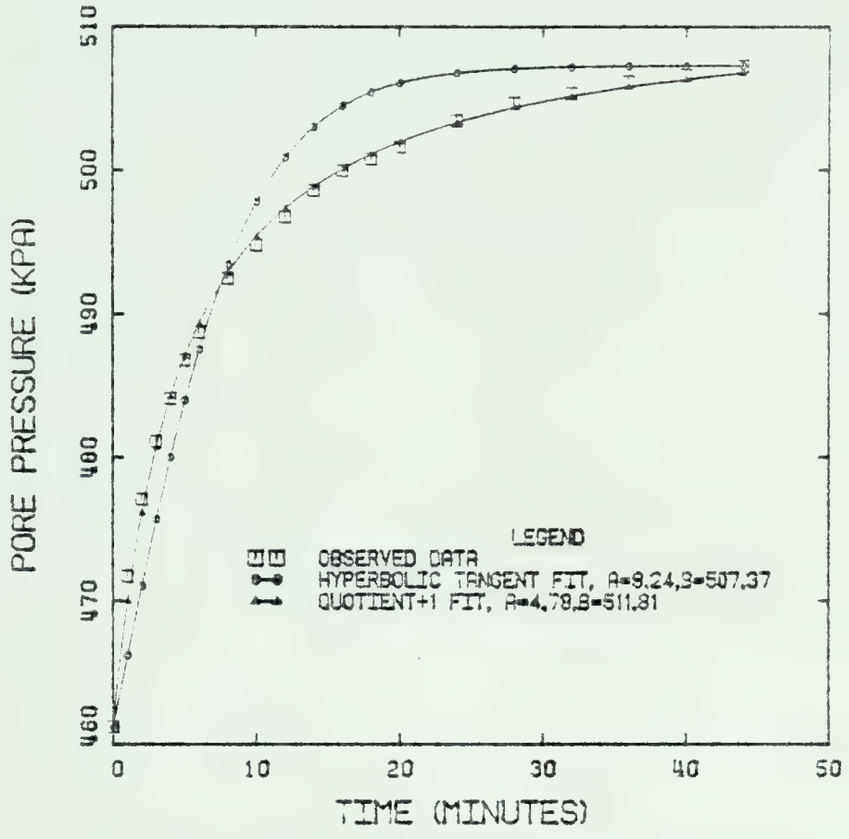


NON-LINEAR REGRESSION, TEST NO. 11C.

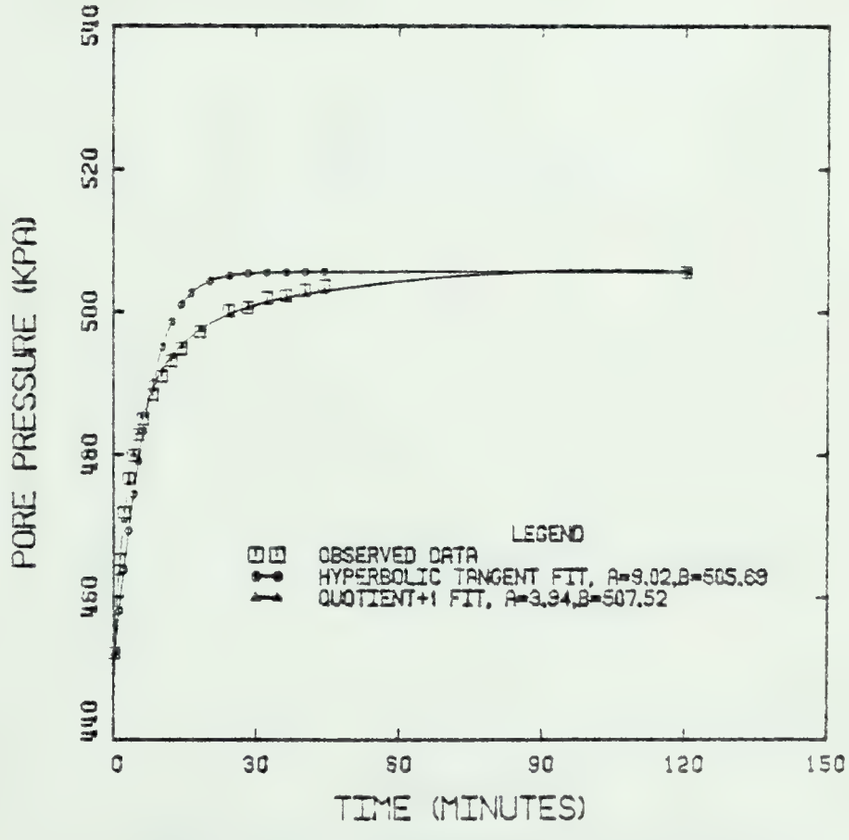


NON-LINEAR REGRESSION, TEST NO. 11D.

Figures 4.18 and 4.19

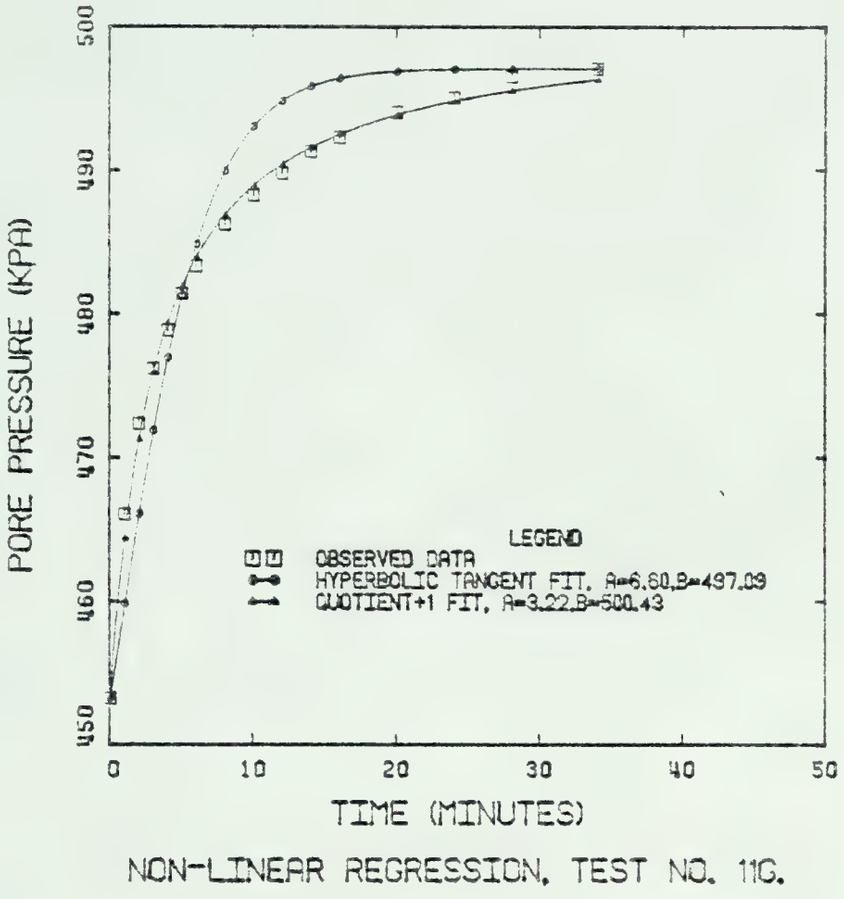


NON-LINEAR REGRESSION, TEST NO. 11E.

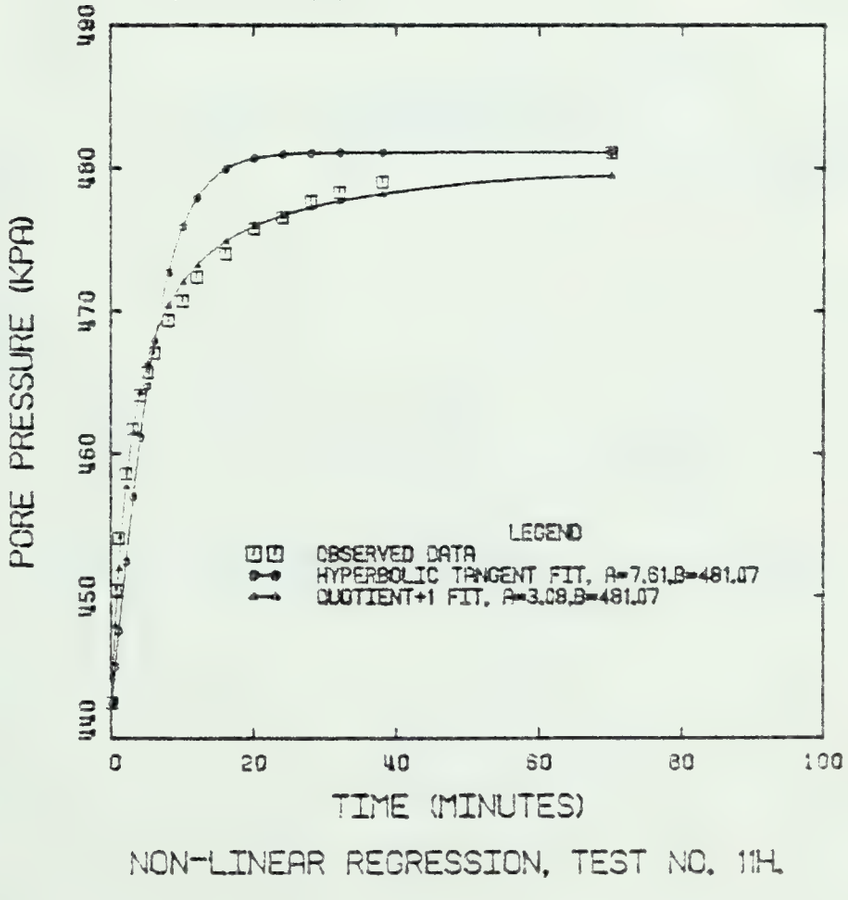


NON-LINEAR REGRESSION, TEST NO. 11F.

Figures 4.20 and 4.21



NON-LINEAR REGRESSION, TEST NO. 11G.



NON-LINEAR REGRESSION, TEST NO. 11H.

Figures 4.22 and 4.23

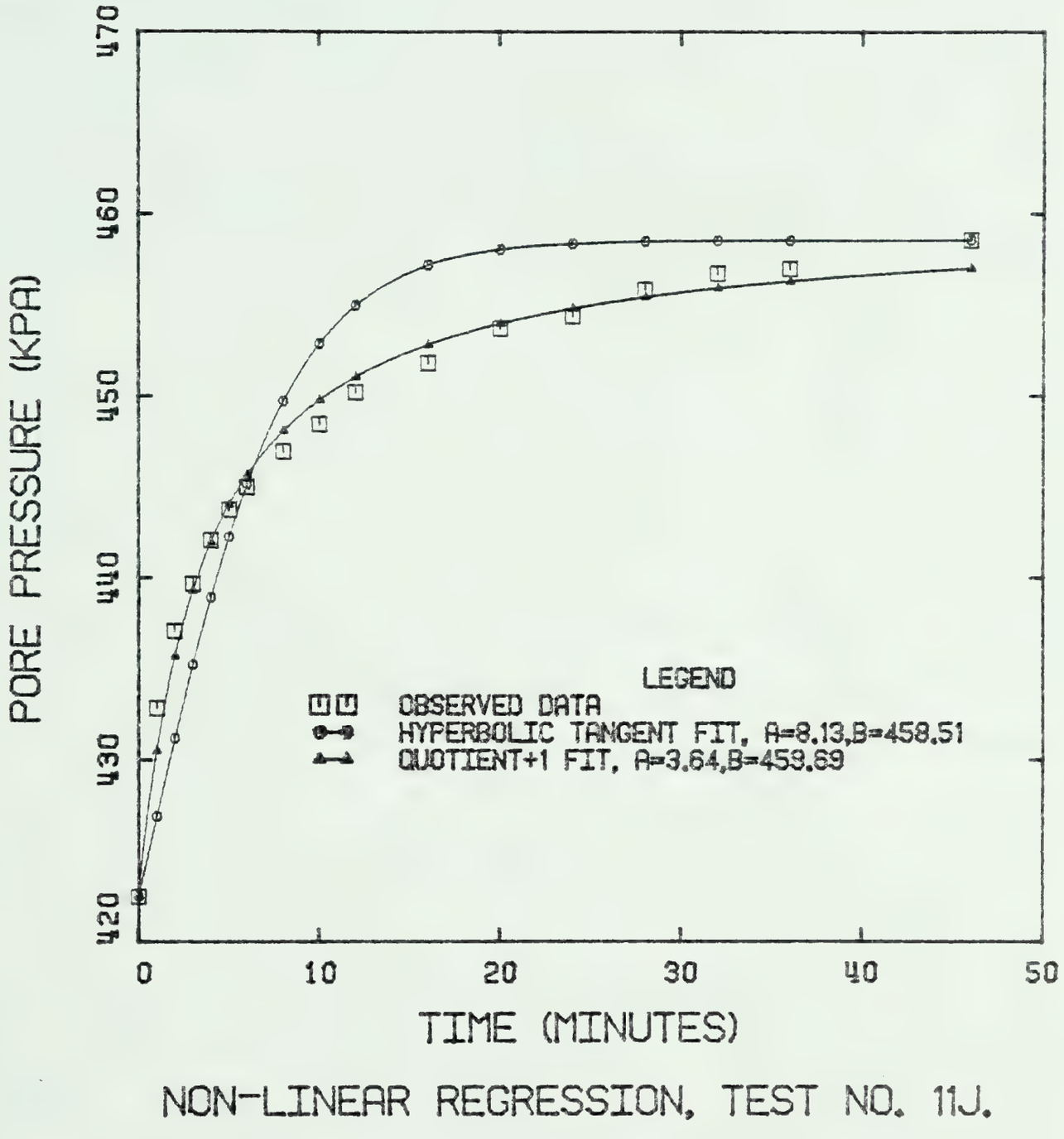

PORE PRESSURE (KPA)
420
430
440
450
460
470
0
10
20
30
40
50
TIME (MINUTES)
LEGEND
OBSERVED DATA
HYPERBOLIC TANGENT FIT, A=8.13,B=458.51
QUOTIENT+1 FIT, A=3.64,B=459.69
NON-LINEAR REGRESSION, TEST NO. 11J.

Figure 4.24

It is interesting as well to examine the value of A´ throughout the test, as it is this parameter that controls the steepness of the pressure-time curve, and thus may provide some information about the gas exsolution process. Discounting, for the moment, phases A & B (air exsolution), phase C (transition to CO_2 exsolution) and phase J (pore pressure response limited by σ' approaching zero), a remarkable pattern is observed in the value of A´. For phase D to H, respectively, A´ = 12.5, 4.8, 3.9, 3.2 and 3.1. As A´ decreases during the test, the pressure vs time curves are steepening, that is, the initial rates of gas exsolution are increasing.

This pattern of change in A´ was encountered in all the undrained tests, and is summarized in Table 4.5. Since the curve-fitting technique itself makes no statement about the gas exsolution process, it is important to only compare those phases with similar boundary conditions. Table 4.5 thus includes only those results for CO_2 exsolution, where the sample was saturated with gas and near equilibrium at the beginning of the phase, where $\sigma' > 0$ at the end of the phase, and for the reloading results, where $\sigma' > 0$ in all previous phases.

As a process model is hypothesized in Chapter 5, and the transient results evaluated in more detail in Chapter 6, this phenomenon of rate of exsolution will be examined again.

TABLE 4.5

SUMMARY OF RESULTS TO FIT TRANSIENT
PRESSURE RESPONSE WITH "QUOTIENT +1" FUNCTION

PHASE	TEST NUMBER							
	7	9	11	23	12	15	21	22
B							4.4	5.1
C	14.1						3.4	5.3
D	14.8		12.5	9.9	10.0	8.7	4.2	5.1
E	13.1		4.8	6.4	8.3	4.5	4.0(L)	
F			3.9	10.0	7.1	3.0	5.2(L)	
G		38.0	3.2		7.4	3.2		
H		22.7	3.1			3.3(L)		
I		9.8	n/a			n/a		
J		6.6	3.6			4.9(L)		

(L) Reloading sample after completion of unloading sequence.

4.6 SUMMARY

This chapter has reviewed the laboratory tests in light of the theory postulated for the equilibrium behaviour of gassy soils. An evaluation of the predictive capabilities of the model has been made, and this has been demonstrated to be quantitatively accurate. Several peculiarities of the test which have modified the boundary conditions, and thus influenced the test results, have been discussed. Where possible, these changed boundary conditions have been incorporated into the theoretical model.

A cursory examination of the transient response has been made, primarily to develop a method of predicting u_{max} from the pressure-time data, but also to investigate the form of the pressure-time curve.

CHAPTER 5 - GAS EXSOLUTION

5.1 GENERAL

The previous chapters in this thesis have dealt with the characteristic equilibrium, or time-independent, behaviour of gassy soils. A theoretical model has been developed, and this has been verified by laboratory tests and used to demonstrate the nature of gassy soil behaviour.

Beginning with this chapter, an investigation is made into the nature of the transient, or time-dependent response in gassy soils. An introduction to a new macroscopic process, gas exsolution, is given. The major objective of the chapter is to develop a general macroscopic theory of gas exsolution, which may then be applied to soil behaviour under various boundary conditions in later chapters. It will first be necessary to review the present state of knowledge on this subject, both within the geotechnical field, and from other fields of engineering, to establish a proper foundation on which to build the framework of the proposed theory.

The term "gas exsolution" as applied to soils refers to an observed or macroscopic behaviour. As the pore pressure in an element of gassy soil is reduced, the saturation in the soil decreases due to the production of gas. Gas is being transferred, in some manner, from the dissolved to the "free" state.

In using the term "gas exsolution", there is no implication that a specific microscopic process is operative in the pores. It is possible to observe, describe and even predict that aspect of transient soil behaviour due to gas exsolution, from a macroscopic perspective, without being limited by any particular process model or by an overly simple set of boundary conditions.

Gas exsolution may be attributed to several known microscopic processes, but our understanding of the processes, as well as the complex boundary conditions in the pore space of a soil, is too rudimentary to develop a general theory from them. Moreover, it is uncertain that all of the contributing processes have been identified. However, this should not preclude their study, as much of the general observed behaviour can be explained qualitatively with very little extrapolation, from simple boundary conditions and single microscopic processes. A study of the physical processes can only increase our understanding of gas exsolution. In addition, any general macroscopic theory proposed to fit the observed laboratory behaviour must also be compatible with what is perceived to be the predominant physical processes.

As a first step in the development of a general macroscopic theory, the physical processes that are thought to control the gas exsolution behaviour will be examined.

They are:

(a) sorption of a gas bubble in a liquid (i.e. absorption, or desorption, depending upon whether the liquid is over- or undersaturated with gas).

(b) bubble nucleation.

The gas exsolution behaviour observed in the laboratory tests will then be examined, and a general theory proposed which is dependent upon these observations only. Lastly, there will be a comparison of the general theory with the simple gas sorption and bubble nucleation models.

It is important to reiterate the distinction between undrained and drained boundary conditions, insofar as the gas exsolution behaviour is concerned. An undrained boundary on an element of soil is one through which there is no mass flow of gas, liquid, or soil particles. Consider such an element of gassy soil, whose pore liquid is super-saturated with gas. Over a period of time, gas will be produced, which will have two inter-related effects:

(a) The volume of the element will increase.

(b) The pore fluid pressure will increase.

Since a volume increase is caused by an effective stress decrease in the soil skeleton, it is also governed by fluid pressure increases. As discussed previously, for gassy soils the volume increase will be small, and the pressure increase relatively large.

A drained boundary is one across which an unhindered mass flow of gas or liquid occurs.[1] For a drained element of gassy soil with a super-saturated pore liquid, there will be:

(a) an element volume change dependent on the boundary stresses, i.e. if and u are constant, $_{vol} = 0$.

(b) a pore fluid pressure which is attempting to equilibrate with the fluid boundary conditions, (consolidation).

(c) the production of large amounts of gas which will, for a period of time, oppose the consolidation process.

5.1.1 Previous work on gas exsolution

There is a paucity of information on gas exsolution in the geotechnical literature. Most investigators have been primarily concerned with the investigation of the equilibrium behaviour of unsaturated soils. The apparent complexity of gas exsolution, combined with a lack of field problems warranting its consideration, seems to have led to a lack of research effort in this area.

Barden & Sides (1970) have measured the diffusivity of air in clay soils and discussed the marked difference from air in water. However, the only attempt to study the exsolution process seems to have been by Black & Lee (1973) in connection with establishing the time required to fully saturate samples in the laboratory. Lee & Black (1972)

---

[1]The element boundary is normally assumed to change shape with the soil skeleton, so that there is still no mass flow of soil particles.

observed the time to dissolve a bubble of gas in a large container of water, and in a tube of water, then (Black & Lee, 1973) extended these findings, developing a model to predict the time necessary to fully saturate a soil sample using a back pressure. As will be discussed in Section 5.3, Lee & Black's solution to the "single bubble in an infinite liquid" problem contains poorly posed approximations, and yet, somewhat fortuitously, is a reasonable solution. Their work was preceded by 20 years of research on that particular problem, the pioneering paper of which provides a more satisfactory approach.

The extention of their ideas to gas exsolution in soils of 85 to 100% saturation (occluded bubbles) will also be evaluated in section 5.4.

5.2 GAS SORPTION

Gas sorption is defined as the transfer of molecules of gas across a gas-liquid interface. As stated by Davies & Rideal (1961), "if a molecule passes across the gas-liquid interface, it encounters, in general, a total resistance R which is the sum of three separate diffusional resistances, due respectively to diffusion in the gas phase, across the monomolecular region constituting the interface, and through the liquid below (beyond) the interface. This may be expressed as:

$$R = R_g + R_i + R_l$$

Of these resistances, R_l is usually the highest, corresponding to molecular diffusion of the solute through a non-turbulent liquid layer adjacent to the surface."

Davies & Rideal are stating that the diffusion process is the measurement of the resistance to movement of a molecule through a medium. In the case of a gas molecule moving through a liquid, across an interface and into a bubble, diffusion in the liquid medium is usually the governing factor. They quote typical values of R_g, R_i, and R_l, e.g.:

(a) For ammonia or CO_2 in water, $R_l = 10^2$ to 10^3 sec/cm.

(b) For CO_2 passing from water to air, $R_g = 4$ sec/cm.

(c) For most cases where no contaminants are present at the interface, R_i is negligible.[2]

Thus for the sorption of gases such as CO_2 in water, R_l predominates. The problem is treated as that of a bubble of spatially constant gas concentration, (i.e. the gas density or concentration does not vary with radius inside the bubble), in a quiescent liquid, the sorption being controlled solely by the diffusion of gas molecules in the liquid phase. This is the classical treatment of the problem in the literature. As will be mentioned later, it has only been

---

[2]Harvey & Smith (1959) measured the absorption of CO_2 in a quiescent liquid and concluded that both R_i and R_g were negligible for CO_2 in water, and that R_l was the governing resistance. Manley (1960) examined the influence of an "organic skin" at the gas-liquid interface on R_i.

since an exact solution has been found for the problem of a single bubble dissolving (or growing) in an infinite liquid that the possibility of diffusion in the gas phase at small bubble radii and high gas pressures has been investigated. This is of peripheral concern in this thesis; the classical approach will be applied in the following discussions.

Gerrard (1976) has discussed the possible modification of the "normal" sorption process by a chemical reaction between the solute and the solvent. In the case of H_2O and CO_2, there is a relationship that:

$$H_2O + CO_2 \equiv\equiv\equiv HCO_3^- + H^+$$

This dissociation is very weak, however. Gerrard states that most of the CO_2 dissolved in the H_2O exists as free molecules and not as HCO_3^- ions, (<1% of the CO_2 reacts to form H_2CO_3), and thus the chemical reaction has little effect on the sorption process. For other gases and liquids, the chemical dissociation may have an equal or more important effect than diffusion in determining the rate of gas exsolution.

5.3 SINGLE BUBBLE IN AN INFINITE MEDIUM

A convenient starting point for the study of the gas sorption process is the case of a single bubble growing in an infinite liquid medium. These boundary conditions cannot be directly applied to the pore space in an element of soil, but

they are worth investigating as they form the basis for further hypotheses with more realistic boundary conditions.

Before considering the sorption process, however, it is necessary to study two related phenomena, the pressure inside gas bubbles, and the concept of an equilbrium bubble size.

5.3.1 Surface tension, pressure, and equilibrium bubble size

Terzaghi (1943) devoted one chapter to the discussion of capillary forces in soils and the pressure of gas in bubbles and voids. He presented the equation:

$$P_g = u + P_a + 2 * T_s / r \qquad (5.1)$$

P_a = atmospheric pressure

T_s = surface tension

r = bubble radius

which was already scientific doctrine. He stated further that "if r approaches zero, the gas pressure P_g approaches infinity. However, within the range of molecular dimensions, equation (5.1) loses its validity". The statement has generally been accepted as an established fact in the geotechnical community.

Recently, however, Fredlund (1973) has taken exception to the idea of surface tension acting on a bubble. He stated that "...air and water pressures cannot differ apart from the inclusion of a solid medium...the capillary model is pertinent only when a solid phase is in the presence of the

air and water. The comprehension of this fact is imperative to the study of the case under consideration. Its omission from the research literature has created considerable confusion (Hilf, 1956; Schuurman, 1966). The reasoning of Schuurman leads him to the conclusion that the air in minute bubbles must reach extremely high pressures just prior to collapsing and disappearing. This is absurd and contrary to observed behaviour."

It is this statement by Fredlund that is incorrect, and in fact contrary to observed behaviour. To demonstrate the validity of the surface tension concept as it applies to gas bubbles, the following discussion will outline the development and laboratory confirmation of the theory regarding this subject.

There has been a continued attempt in the scientific literature since 1950 to solve the differential equation governing gas sorption for the very simple boundary condition discussed previously. All of the authors have accepted the existence of surface tension, quite independent of any solid substance, and have discussed and observed the effects of surface tension on bubble behaviour.

Epstein & Plesset (1950) developed an approximate solution for a bubble growing (or dissolving) in an infinite liquid, solving both for the case of $T_s = 0$, and $T_s > 0$. They noted that for bubbles in a <u>saturated</u> solution, if $T_s = 0$, the bubble should be stable; if $T_s > 0$, the bubble would dissolve because of surface tension effects. This idea was

reiterated by Plesset (Davies, 1964). Keller (Davies, 1964) advanced this idea further by noting that:

(a) Bubbles in an undersaturated solution decay in size and disappear in a finite time.

(b) In a supersaturated solution, bubble behaviour depends on its initial radius r_0. For each concentration of gas c_0, (where $c_0 > c_s$, the saturated concentration), there is an equilibrium radius r_e such that if $r_0 = r_e$, the bubble is in unstable equilibrium. For $r_0 < r_e$ the bubble decays and disappears in finite time, (because of surface tension), while for $r_0 > r_e$ it grows indefinitely.

(c) If the solution is just saturated, every bubble will decay unless surface tension is absent, in which case it remains in neutral equilibrium.

(d) Bubbles may form spontaneously around nucleii, such as solid particles, a hole in the liquid (near the surface of a solid), etc. An unsaturated solution is stable against bubble formation. Supersaturated solutions are also stable against bubble formation, unless the bubble forms with $r_0 > r_e$.

Cable (1967) comments "finally, it must be remembered that the pressure inside a bubble increases significantly when it becomes very small and this accelerates its rate of shrinkage." These ideas are again reiterated by several other authors.

Tucker & Ward (1975) report on research for a doctoral dissertation by Tucker (1974), who investigated the measurement of diffusion coefficients by using the unstable equilibrium state of gas bubbles in supersaturated solutions. Their work confirmed experimentally Keller´s ideas, and they presented an equation for the critical radius r_c,

$$r_c = 2 * T_s / (n*P_{vap}+c_2/c_{2s}*P'-P') \qquad (5.2)$$

$$n = \exp(v_1*(P'-P_{vap})/K/T-c_2)$$

where T_s, P', K, T and c_2 are the surface tension of the liquid-gas interface, the pressure, Boltzmann constant, temperature and gas concentration (moles solute/moles solvent) in the solution surrounding the bubble; v_1 and P_{vap} are the specific volume and vapour pressure of the pure solvent; and c_{2s} is the equilibrium saturation concentration of the dissolved gas in the solvent when a flat surface of the solvent is exposed to the gas only at P', T.

The critical radius is defined as that radius a bubble must achieve upon nucleation to ensure its continued existence. As previously discussed, there is a single equilibrium bubble size for an unbounded liquid and that state is unstable. For the case of the infinite liquid the equilibrium and critical radii are equivalent.

Keller had given an earlier version of equation 5.2, but had neglected the term $\eta^* P_{vap}$, as he had not considered the presence of the solvent vapour in the bubble as well as the gaseous solute.

It is clear that the concept of interfacial tension (the correct term for fluid/fluid contacts) in gas bubbles, quite independent of any solid particles, has been given both theoretical support and experimental verification, and in fact has become the basis of a recognized method of measuring gas diffusion coefficients in liquids. The work of Schuurman (1966) then is very pertinent to the expression of fluid compressibilities. As recognized by Terzaghi, the postulated relationships may not apply at extremely small bubble radii. At this level, modifications may be necessary not only in the expression for interfacial tension, but also in the pressure-volume relationships for a dense gas (Epstein, 1975), and for inertial and viscous effects (Szekely & Martins, 1971).

5.3.2 The time variation of bubble size

In 1950, Epstein & Plesset presented an approximate solution to the problem of a single bubble growing (or shrinking) in a super (or under) saturated, infinite liquid. Refinements to their approximations, and numerical solutions to the more complete differential equations have been reported on by Birkhoff et.al.(1958), Scriven (1959), Manley (1960), Barlow & Langlois (1962), Davies (1964, including papers by Plesset, Keller, Westwater & Prigogine), Bankoff

(1966), Ready & Cooper (1966), Kreiger et.al.(1967), Cable & Evans (1967), and Cable (1967). Duda & Vrentas (1969) present an excellent list of references of previous work and a good discussion on the accuracy of previous approximate solutions. Later work includes that of Rosner & Epstein (1970), Szekely & Martins (1971), Duda & Vrentas (1971), Fogler & Verma (1971), Rosner & Epstein (1972), Yang (1972), Lee & Black (1972), Ward & Tucker (1975), and finally Tao (1978, 1979). The last papers by Tao are significant in that an exact solution is established for the problem, although the solutions are mathematically quite complex.

As will be discussed in section 5.4, the solution to the problem of a bubble growing in an infinite liquid cannot be applied directly to gas sorption in the pore space of a soil. The model might be refined somewhat by considering a single bubble growing in a liquid of finite extent, but still this is only part of a complex series of processes that govern the gas exsolution behaviour. Hence it is unlikely that an extremely complicated exact solution to either problem will be useful in evaluating the general soil behaviour.

A simple approximate solution, using reasonable simplifying assumptions, will later be developed for the finite problem. This will be based upon the method employed by Epstein & Plesset (1950), and so their paper will be

discussed here. A consideration of the infinite liquid problem will also allow a critique of the work by Lee and Black (1972).

Epstein & Plesset treated the problem of a single gas bubble of radius R_0, placed at time t=0 into an infinite liquid of initial saturation c_i. The solution is maintained at a constant pressure and temperature, and has a saturated gas concentration of c_s.

For any time t>0, the concentration c at distance r from the center of the bubble must satisfy the diffusion equation, which in spherical polar coordinates is:

$$Dc/Dt = K * (D^2c/Dr^2 + 2/r * Dc/Dr) \text{ (note)}^3 \qquad (5.3a)$$

It is assumed that the term for convection associated with bubble growth or shrinkage is small compared to diffusion, and can be ommitted. The solution to this equation must satisfy the boundary conditions that:

$$\begin{aligned} c(r,0) &= c_i, \quad r > R \\ \lim(r\to\infty)c(r,t) &= c_i, \quad t > 0 \\ c(R,t) &= c_s, \quad t > 0 \end{aligned} \qquad (5.3b)$$

---

[3]Throughout this thesis, the partial differential will be designated by a capital D and the exact differential by a small d.

A transformation to the linear one-dimensional problem is made by substituting $g = r * (c - c_s)$, so that 5.3a & b become:

$$Dg/Dt = K * D^2g/Dr^2$$
$$g(r,0) = r * (c_i - c_s) \qquad (5.3c)$$
$$g(R,t) = 0$$

A further shift in the r-coordinate by $z = r - R$ will make the problem identical to the problem in heat conduction of a semi-infinite solid with an initial temperature $T(z,0) = (z+R)*(c_i-c_s)$ and with $T(0,t)=0$. The solution is provided by Carslaw & Jaeger (1959):

$$g(r,t) = (c_i - c_s)/\{2*[\pi*K*t]\text{^}.5\} * \int_0^\infty (R+z)*\{\exp[-(z-z')\text{^}2/(4*K*t)]-\exp[-(z+z')\text{^}2/(4*K*t)]\}*dz' \qquad (5.4)$$

(note)[4]

The concentration gradient at r = R is then:

$$(Dg/Dr)_R = (c_i-c_s)*\{1+R/(\pi*K*t)\text{^}.5\} \qquad (5.5a)$$

or, substituting for g,

$$(Dc/Dr)_R = (c_i-c_s)*\{1/R + 1/(\pi*K*t)\text{^}.5\} \qquad (5.5b)$$

---

[4]Where the use of a superscript for a power notation would be confusing, the character "^" will be employed instead.

or $$dm/dt = 4*\pi*R^2*K*(Dc/Dr)_R$$

$$= 4*\pi*R^2*K*(c_i-c_s)*\{1/R + 1/(\pi*K*t)\hat{}.5\} \quad (5.5c)$$

where m is the mass of gas.

Equation 5.5c is only valid for a stationary bubble boundary. However, for problems in which the bubble volume change is small compared to the movement of the "diffusion front" through the liquid, it is a reasonable physical approximation to use (5.5c) to predict the variation of bubble size with time.

Then if ρ is the bubble density,

$$dm/dt = 4*\pi*R^2*\rho*(dR/dt) \quad (5.6a)$$

so that

$$dR/dt = K*(c_i-c_s)/\rho * \{1/R + 1/(\pi*K*t)\hat{}.5\} \quad (5.6b)$$

Epstein & Plesset then solve equation 5.6b for R for the cases of undersaturated and oversaturated solutions. They note that at small times, the complete equation must be treated, but that at larger times the term $1/(\pi*K*t)\hat{}.5$ becomes negligible, and so a further approximation can be made by solving:

$$dR/dt = K*(c_i-c_s)/\rho * 1/R \quad (5.7a)$$

or $R*dR = K*(c_i-c_s)/\rho * dt$ (5.7b)

whence

$$(R^2-R_0^2)/2 = K*(c_i-c_s)/\rho * t \quad (5.8)$$

It must be emphasized that this particular solution does not include the influence of surface tension. Epstein & Plesset present and compare solution (5.8) with the solution which includes the term $1/(\pi*K*t)^{.5}$, and also with the solution which includes surface tension effects.

For a growing bubble only, Epstein & Plesset also note that for:

$q = R/R_0$, and

$x^2 = 2*K*(c_i-c_s)*t/(\rho*R_0^2)$, and

$w = \{(c_i-c_s)/(2*\rho*\pi)\}^{.5}$

that if both q and x were large, q varied linearly with x,

$$\text{i.e. } q \mp \{w+(1+w^2)^{.5}\}*x \quad (5.9)$$

A comparison of Epstein & Plesset's work with that of Lee & Black (1972) would be appropriate at this point, (using the same notation as above). Lee & Black derive the following differential equation for the bubble radius:

$$dR/dt = -K*c_s/(\rho*R) \quad (5.10)$$

Equation 5.10 lacks the $1/(\pi*K*t)^{.5}$ term of equation 5.6b, and assumes that $c_i=0$. The absence of the time term is due to the manner in which Lee & Black posed the problem. Rather than conforming the diffusion process to Fick's second law, as Epstein & Plesset did, Lee & Black started with a quasi-steady state solution for the problem of a static sphere diffusing into a liquid. They assumed that Dc/Dr was a function of radius only, and not also of time.

5.4 SINGLE BUBBLE IN A FINITE VOLUME OF LIQUID

5.4.1 Equilibrium Bubble Size

A logical extention and application of Keller's ideas on the equilibrium bubble size for a bubble in an infinite liquid, presented in section 5.3.1, would lead to the hypothesis that there is a stable equilibrium size for a bubble in a liquid of finite volume. The reasoning for this hypothesis might follow as below:

(a) Growth of a bubble in a supersaturated solution will eventually result in the liquid becoming just saturated because the liquid only has a finite volume. If the bubble could somehow continue to grow, the liquid must become undersaturated. Continued bubble growth (past the point of saturation) is thus not possible because it is not a viable process in undersaturated solutions. One would expect that the bubble in the supersaturated solution would grow only

until the solution became just saturated, and that the rate of solution would decrease as the amount of supersaturation decreased.

(b) A bubble placed in an undersaturated solution would tend to shrink, which would cause an increase in saturation. Depending upon the volume of liquid and the original extent of undersaturation, the bubble may achieve stability as the solution becomes just saturated, or it may extinguish before the solution reaches saturation.

(c) A small bubble placed in a supersaturated solution may still shrink and extinguish because of surface tension effects.

Mori, Hijikata & Nagatani (1977) conducted some experiments to observe this phenomenon. They introduced a mixture of gaseous freon 21 with other non-condensable gases such as N_2, O_2 and CO_2 into a container of glycerin. As the pressure in the glycerin was raised, the freon 21 condensed into a liquid droplet, which contained a bubble of the non-condensable gas. Since the solubility of N_2, O_2 and CO_2 are all much higher in freon 21 liquid than glycerin, they had by this novel method isolated a fixed volume of solute (the freon 21) containing a bubble of gaseous solvent.

Starting at an equilibrium condition, Mori et.al. raised the pressure in the glycerin and hence also in the freon 21 and the gas bubble, and monitored bubble radius with time. They found that for each pressure P, there was a

stable equilibrium bubble size r_e, and that r_e varied inversely with P. For a particular set of initial conditions, i.e. volume of freon 21 and volume of non-condensable gas, there was a minimum radius r_m and maximum pressure P_m. For $P > P_m$, or $r < r_m$, the bubble would extinguish. Thus their experimental observations support the heuristic arguments for an equilibrium bubble size (given above) extremely well.

Mori et.al. (1977) also derived a theoretical relationship between the equilibrium radius of the bubble r_e and the pressure in the fluid surrounding the droplet (glycerin) P''', as:

$$P'''-P_1' = -2*\sigma/r_e - 2*\sigma_{gl}/r_{gl} + n_{20}/\{(n_1''+n_2'')*K + (4*\pi/3/R/T)\}/r_e^3 \qquad (5.17)$$

where P = pressure
σ = surface tension
r = radius
n = mole number
K = solubility
R = gas constant of 1 mole
T = temperature

1 = liquid component of droplet
2 = component of non-condensable gas
gl = gas-liquid interface
$'$ = gas phase
$''$ = freon 21 phase
$'''$ = liquid phase of glycerin
$n_{20} = n_2' + n_2''$

This equation predicts a decrease in r_e with increasing pressure P''' until some minimum radius r_m is reached, at

which point Dr/DP = ∞. Any further decrease in r would theoretically be accompanied by a <u>decrease</u> in P''', but since P''' is externally maintained at some (constant) value, the bubble extinguishes.

The agreement between theory and observed behaviour, for both the r_e vs P''' relationship and the value of r_m, was excellent.

The stability of gas bubbles in finite volumes of liquid was further considered by Tucker (1974) and later by Ward et.al. (1981,82).

Tucker (1974) pointed out that equation 5.2 for the critical radius of the bubble in an infinite medium was still valid for the bubble in a finite medium, because it was "derived from a consideration of the equality of the chemical potential of each component across the curved interface at the equilibrium condition". However, the change in boundary conditions could affect the <u>nature</u> of the stability of the equilibrium state. Tucker then examined this stability further. His work was extended by Ward, Tikuisis & Venter (1982). They present an equation for the critical radius similar to (5.2),

$$r_c = 2*T_s/\{\eta*P_{vap}+c_2/c_s*P'-P'\} \qquad (5.18a)$$

$$\eta = \exp[\nu_l*(P'-P_{vap})/K/T - c_2/c_1] \qquad (5.18b)$$

where all variables have been defined previously (for equation 5.2) except:

c_s = the saturation concentration of the gas in the liquid phase, and for a weak solution,

= $c_1 * P'/H$

c_i = the concentration of component i in the liquid phase.

component 1 = liquid and its vapour

component 2 = gas

Furthermore, for given values of pressure, temperature and volume of liquid, they find:

(a) If the total gas content in the volume is less than a certain number, there are no possible equilibrium states for a bubble in the system.[5]

(b) If the total gas content is equal to this minimum number there is one equilibrium state.

(c) If the total gas content is greater than this minimum number, there are two equilibrium states.

(d) If the radius of the equilibrium bubble described in (b) is denoted r_m, then r_m does not depend on the amount of gas in the volume but only on the type of gas, i.e. on H.

---

[5] A distinction must be made here between r_c and r_e. For an infinite liquid, $r_c = r_e$. For a finite volume of liquid this is not the case, i.e. r_c is not necessarily equal to r_e.

(e) The equilibrium state described in (b) is stable against growth but unstable against dissolution. This is referred to as a metastable equilibrium.

(f) There are two equilibrium states discussed in (c). The one with the smaller radius is unstable (similar to the single equilibrium size for an infinite liquid). The one with the larger radius is stable. A bubble initially at the unstable equilibrium radius can be predicted to grow in size to the stable equilibrium radius should a fluctuation perturb it to a size slightly larger than its initial value.

These results were confirmed experimentally.

Ward et.al. also examine the problem of a finite volume of liquid containing a number of bubbles at equilibrium. They find the same variation of equilibrium size with total gas content described in (a)-(c) above; the same modes of metastable, unstable and stable equilibrium (e & f); and also that r_m decreases with increasing number of bubbles. "For example, for a single bubble in the closed volume, the equilibrium radius must exceed approximately 207 μm for the bubble to be in stable equilibrium in 1 cc of a water-nitrogen solution maintained at room temperature and pressure. However, the equilibrium radius need only exceed 3.47 μm for the bubbles to be in a stable equilibrium state when the bubble number density is 10^7/cc under the same conditions of temperature and pressure."

This statement should have interesting implications for what constitutes a stable bubble size in the pore fluids of a soil. With the presence of innumerable soil grains, the number of bubble nucleation sites should also be extremely high, and thus the equilibrium bubble size very small.

It should be noted that all of Ward et.al.'s investigations applied to the case of a "well-stirred" fluid, i.e. one in which C_2 was constant throughout.

5.4.2 Bubble size as a function of time

From equations 5.7a and 5.8, the approximate solution to the problem of a bubble growing (or shrinking) in a fluid of infinite extent can be used to predict a rate of change of bubble radius,

$$dR/dt \sim 1/R \sim 1/(t)\hat{}.5 \quad \text{(note)}^6 \qquad (5.11a)$$

or $$dV/dt = 4*\pi*R^2*dR/dt \sim R \sim t\hat{}.5 \qquad (5.11b)$$

Any attempt to model gas sorption in pore fluids by a relationship of this type cannot be successful because the functional relationship does not possess an asymptotic characteristic. It is akin to the discussion in section 4.5 of attempting to fit asymptotic pressure-time relationships with improper functions.

---

[6]The character "~" will be used to denote "is proportional to"

Black & Lee (1973) attempted to generalize the results for a bubble in an infinite medium to a bubble in the pore space of a soil by the relationship:

$$V \sim t^x, \text{ or } dV/dt \sim t^{(x-1)}, \quad 0<x<1 \qquad (5.12)$$

Their experimental data, which was collected for periods up to 50,000 minutes (35 days), appear to give a good straight-line fit on a log-log plot. However, this is somewhat misleading. As discussed previously, although the limit as t approaches infinity of dV/dt is 0, for V the limit is infinite. Clearly, the amount of gas dissolved in the pore fluid must be limited to a finite amount, determined by the solubility coefficient H. Hence a relationship of the form expressed by (5.12) is theoretically unacceptable at longer times, even if its use appears to be reasonable at shorter time intervals. The "linear" relationship observed by Black & Lee must in truth deviate from linearity if taken to a sufficient length of time. (An evaluation of the laboratory data obtained in this research using equation 5.12 will be made in section 5.6).

A more reasonable model for gas sorption in the pore space is the single bubble in a container of fluid of finite size. An approximate solution to this problem for a liquid which is at constant pressure and temperature may be developed in a manner similar to Epstein & Plesset's (1950)

solution for a bubble in an infinite medium. This development is presented below.

Consider a single bubble in the center of a spherical container of finite size, which is full of some fluid. The container is completely flexible so that the fluid inside is maintained at a constant pressure despite changes in volume. Equation 5.3a governing the diffusion process is still valid, only now the boundary conditions become:

$$\begin{aligned} c(r,0) &= c_i, \quad R<r<S \\ c(R,t) &= c_s, \quad t>0 \\ Dc/Dr(S,t) &= 0 \quad t>0 \end{aligned} \tag{5.13}$$

where S is the radius of the container.

The substitution $g = r*(c-c_s)$ into (5.3a) and (5.13) produces:

$$\begin{aligned} Dg/Dt &= K * D^2g/Dr^2 \\ g(r,0) &= r*(c_i-c_s), \quad R<r<S \\ g(r,t) &= 0 \quad , \quad t>0 \\ Dg/Dr(S,t) &= 0 \quad , \quad t>0 \end{aligned} \tag{5.14}$$

which, again, is a linear (one-dimensional) problem, identical (with a coordinate transformation) to the problem of heat conduction in a plate, where one side of the plate is maintained at a constant temperature and the other side of

the plate is insulated. Using the coordinate transformation that:

$$x = S - r$$

the solution to this problem may be obtained from Carslaw & Jaeger (1959) as:

$$g(r,t) = 2*(c_s-c_i)/(S-R) * \sum_{n=0}^{\infty}\{\exp[-K*(2*n+1)^2*\pi^2*t/4/(S-R)^2] * \cos[(2*n+1)*\pi*(S-r)/2/(S-R)] * \int_S^R [r'*\cos((2*n+1)*\pi*(S-r')/2/(S-R))]dr'\} \quad (5.15a)$$

and if $a = (2*n+1)*\pi/2/(S-R)$

then $$g(r,t) = 2*(c_s-c_i)/(S-R) * \Sigma\{\exp[-K*a^2*t] * \cos[a*(S-r)] * [\cos(a*(S-R))/a^2 - R/a * \sin(a*(S-R))]\} \quad (5.15b)$$

whence

$$Dg/Dr(R,t) = 2 * (c_s-c_i)/(S-R) * \Sigma\{\exp[-K*a^2*t] * [\sin(a*(S-R))*\cos(a*(S-R))/a - R*\sin^2(a*(S-R))]\} \quad (5.15c)$$

This is a solution for Dg/Dr at r=R, assuming the bubble wall is stationary. If we introduce the same approximation as Epstein & Plesset, namely that the increase in the size of

the bubble is small in relation to the movement of the diffusion front, then the solution for Dg/Dr may be used to obtain an expression for DV/Dt, and this in turn could be integrated to obtain an expression for V = V(t). This requires that the solubility of the gas in the liquid be low to moderate in relation to the diffusivity of the gas in the liquid. An additional stipulation must be added that the volume of the container be relatively large in relation to the volume of the bubble (for the soil, say $S_w > 0.8$) so that as R increases, and hence S increases, the form of c(r,t) is not significantly influenced.

Then, recognizing that:

$$dV/dt = 1/\rho * dm/dt = K/\rho * 4*\pi*R\hat{}2*(Dc/Dr)_R$$

$$= 4*\pi*R*K/\rho * (Dg/Dr)_R$$

and if $H = c_s/\rho$ (Henry's constant), and

$f = c_i/c_s$, then

$$dV/dt = 8*\pi*K*H*(1-f)*R/(S-R) *$$

$$\Sigma\{\exp[-K*a\hat{}2*t] *$$

$$[\sin(\pi*(2*n+1))/2/a - R*\sin\hat{}2(\pi*(2*n+1)/2)]\} \qquad (5.16)$$

A comparison of equation 5.16 with the infinite fluid solution may be made by rearranging equation 5.7a to give:

$$dV/dt = 4*\pi*R*K*H*(f-1) \qquad (5.7c)$$

The solution to the case of a finite fluid then differs from the solution to the infinite fluid problem by:

(a) the inclusion of the term (S-R), representing the container size,

(b) and more importantly by a summation of exponential terms which quickly reduces dV/dt to near zero values. As will be demonstrated later, this form of the solution for dV/dt also gives an asymptotic character to the volume-time relationship.

5.5 BUBBLE NUCLEATION

Although one might speculate that sorption is the dominant process influencing the gas exsolution behaviour, an attempt to generalize the theory of a single bubble growing in a finite volume to gas bubbles growing in the pore space of a soil encounters several serious questions, related to our ignorance of the problem itself:

(a) In a particular soil sample, how many gas bubbles are there, or in other words, what is the volume of pore fluid associated with these bubbles?

(b) What is the distribution of pore fluid with respect to the bubbles? What influence does pore shape and bubble location have on the volume-time relationship?

(c) Are bubbles generated at any particular time in the sorption process, or do they just continue to grow after some initial formation?

(d) How are bubbles formed? Are there preferential nucleation sites?

(e) At what point does the gas phase change from occluded bubbles to a continuous fluid? How does this influence the sorption process?

These questions are particularly important to the investigator desiring to build a theory of gas exsolution from an understanding of the actual physical processes. Unfortunately, they cannot be answered in more than a conjectural manner at present.

The concept of critical bubble radius has already been introduced (5.3.1). To reiterate, it is that radius at which a bubble must form in a particular fluid, so that its continued existence will be ensured. Bubbles forming with radii less than r_c will decay and disappear, while bubbles forming with radii greater than r_c will generally increase in size, either indefinitely (as in the case of an infinite fluid) or until some stable equilibrium size is achieved (as in the case of a fluid of finite volume).

The formation of a bubble in a liquid is called bubble nucleation. There are various mechanisms which will cause bubble nucleation. A bubble may form due to local fluctuations in pressure (e.g. due to turbulence in the liquid), or at condensation nucleii, such as the imperfections in the surface of some solid particle. Nucleation in the latter case is due to gas adsorbed on the surface of the nucleus, which provides a liquid-gas interface

to which dissolved gas can diffuse. Considerations of the probability of a bubble of gas forming in a liquid in the former case lead to the development of homogeneous nucleation theory, which will be treated further below.

The rate at which gas will exsolve in the pore space of a soil is clearly related to the number of bubbles in the pore space and to the rate at which additional bubbles might form. Hunt & Berry (1956) discussed the problem of non-equilibrium effects in an oil reservoir subjected to a constant rate of pressure decline. They noted that both bubble formation rates and diffusion rates depend strongly upon the degree of supersaturation, that is, the difference between the current fluid pressure and the gas/liquid saturation pressure. They proposed a relationship from homogeneous nucleation theory relating the rate of bubble formation J to P and $P_{l/g}$ by:

$$\log J = V - W * (P_{l/g}-P)^{-2} \qquad (5.19)$$

where V,W are constants

Hunt & Berry then predicted the variation of supersaturation with time (after the pressure depletion process was started). They reasoned that at short times $(P_{l/g}-P)$ would be small, the number of bubbles present would be small, and thus, since diffusion could not keep up with pressure depletion, the supersaturation would increase. As it did increase, however, so would J and N, the number of bubbles. At some point the

influence of diffusion would just offset the rate of pressure decline, so that the magnitude of the supersaturation would level off, and then decrease. Due to the functional relationship for J and $(P_{l/g}-P)$, a small decrease in supersaturation would lead, practically speaking, to $J \neq 0$, after which time the production of free gas would be almost exclusively by diffusion to existing bubbles, with very few new bubbles formed.

Ward, Balakrishnan & Hooper (1970) studied the formation of gas-vapor nuclei in liquid-gas solutions. It was shown that "a nucleus which is created as a result of a fluctuation must exceed a certain critical radius if it is to grow to a macroscopic size, and...that this required radius can be considerably reduced by the presence of a dissolved gas." Their expression for the critical radius of a spherical nucleus in which the gas-vapour mixture is considered to behave as a non-ideal gas is:

$$r_c = 2*T_s \,/\, (n*P_{vap}/v_1' + c_2/c_{2s}*P'/v_2' - P') \qquad (5.20a)$$

where all variables have been defined previously (equation 5.2) except:

v_1' = modified activity coefficient of vapour

v_2' = modified activity coefficient of gas

This equation is very similar to equation 5.2. It is clear that an increased amount of dissolved gas (a higher c_2) will decrease the value of the critical radius, and hence expedite the nucleation process.

The term η^*P_{vap}/v_1' is the partial pressure of the vapour inside the nucleate bubble, while $(c_2/c_{2s})^*(P'/v_2')$ is the partial pressure of the gas, hence equation 5.20a can be rewritten in the form:

$$r_c = 2^*T_s/(P_g'-P') \qquad (5.20b)$$

where P_g' is the pressure in the bubble <u>at equilibrium</u>.

Ward et.al. (1970) also present an equation relating the rate of formation of nuclei per unit volume, J, as:

$$J = Z * \exp[-4^*\pi^*T_s^*r_c\hat{}2/(3^*K^*T)] \qquad (5.21a)$$

which was developed from statistical thermodynamics, by considering the probability that a fluctuation in the thermodynamic properties of the system would occur at any particular instant.[7]

---

[7]Note that this is the correct expression developed from homogeneous nucleation theory, and is akin to Hunt & Berry's equation 5.19. This equation only considers the nucleation of gas bubbles due to a random variation in the thermodynamic properites of the gas-fluid system, and does not include the equally important phenomenon of dissolved gas "nucleating" at imperfections on included solids, as discussed previously.

Using (5.20b), equation 5.21a may be written as:

$$J = Z * \exp[-16*\pi*T_s\hat{}3/(3*K*T)/(P_g'-P')\hat{}2] \qquad (5.21b)$$

This equation causes some reflection on the use of the term $P_{1/g}$, which has been defined as that pressure at which gas "begins to come out of solution". Ignoring the influence of the vapour in the gas phase for a moment, the expression for r_c would yield J = 0 only when $c_2 = c_{2s}$. Any $c_2 > c_{2s}$ will produce bubble nucleation, but the rate of formation is dependent on the ratio c_2/c_{2s}. Fortunately, the functional relationship given in (5.21b) produces an extremely quick increase in J with initial changes in c_2, so that a pressure very close to $P_{1/g}$ will cause observable rates of bubble nucleation.

Equation (5.21b) may be rearranged to give an expression for the "nucleation pressure" P', as:

$$P' = \eta*P_{vap}/v_1' + c_2/c_{2s} * P'/v_2' - [16*\pi*T_s\hat{}3/(3*K*T*\ln(Z/J))]\hat{}.5 \qquad (5.22)$$

The first and last terms on the right-hand side are those for a pure liquid, while the middle term reflects the contribution of a dissolved gas. As noted by Forest and Ward (1977), "this additional term always acts to raise the nucleation pressure", (for some assumed value of J), "and from equation (5.22) it has been predicted that the presence

of a dissolved gas can significantly change the pressure at which nucleation occurs."

Forest & Ward (1977) reported on experimental work to confirm this relationship. They performed several isothermal decompression tests to measure the nucleation pressure of ethyl ether - nitrogen, and found close agreement with the predictions from equation 5.22. Consistent with the form of (5.21b) they also found that "the nucleation event was very rapid and almost explosive in nature".

From the above discussion of bubble nucleation theory and observation, one must conclude that the gas exsolution process in soils is influenced both by the initial volume of free gas in the pores and its distribution, (i.e. number of bubbles), as well as by the magnitude of the supersaturation, expressed by the ratio c_2/c_{2s}.

5.6 OBSERVED BEHAVIOUR & A MACROSCOPIC THEORY OF EXSOLUTION

The study of gas sorption and bubble nucleation is an area of current research in the fields of chemical and mechanical engineering. The solutions to problems of the simplest boundary conditions are quite complex, and in most cases only approximate. Although a study of these processes would increase our comprehension of gas exsolution in soils, it would be difficult to build a general theory from the known processes, given our present state of ignorance. The intent of this section of the thesis is to examine a portion of the gas exsolution behaviour observed in the laboratory

and independently postulate a simple descriptive model, a "macroscopic" theory of gas exsolution. The discussion in the previous sections has been largely to introduce background material; this section is where the major objective of the chapter is addressed. Once the macroscopic theory of gas exsolution has been established, it will be compared, in section 5.7, to the theories developed for gas sorption and bubble nucleation. The ability of the model to predict other test results will be discussed in Chapter 6.

To be properly applicable to a number of different problems, the model of gas exsolution must incorporate the appropriate boundary conditions. It should be independent of the soil skeleton behaviour, so that the undrained boundary condition, which is the easiest to maintain in the laboratory, will not suffice. From a consideration of how a general, combined theory of consolidation and gas exsolution might be developed, it is clear that the proper boundary conditions are those of full drainage. The model must consider an element of soil, with a constant void volume (and hence effective stress), and a constant pore pressure, and be able to predict the mass flow of fluid across the element boundary.

If the model is to be developed empirically, then this fully drained boundary condition must also be obtained in the laboratory. Unfortunately, this is not a simple task. The case of a pore fluid undersaturated with gas, such that the

bubbles in the pores are dissolving and water is flowing into the sample, is possible. This is the problem addressed by Black & Lee (1973), although their experimental method was not ideal for studying a sample with homogeneous conditions. They prepared a sample of Ottawa sand at 100% relative density, and allowed a measured quantity of water to percolate into the bottom of the sample, to reach a pre-determined saturation. Then, after closing the bottom drain line, a back pressure was applied to the top drain line, which allowed a further quantity of water to surge into the top of the sample. After 1 minute the top line was closed and the back pressure and sample drainage was reapplied to the bottom drain. This method can not guaranty an homogeneous distribution of gas and liquid throughout the voids of one sample, and it cannot produce a consistent distribution from one sample to the next, nor can this distribution be determined for any one sample. This is a serious shortcoming of the test technique, since the distribution of pore gas and liquid must have an influence on the test results.

This testing technique can be improved by changing the method of sample preparation. If a fully saturated sample containing dissolved gas was prepared in a manner similar to that described in Chapter 3, and unloaded with an undrained boundary condition, then a relatively homogeneous nucleation of gas bubbles should occur throughout the sample. Drained tests could then be performed by adjusting the external

pressure to a value equivalent to the sample pore pressure, opening a drainage line to the sample, measuring an initial volume on an in-line burette, applying a step increase in back pressure and then monitoring the volume of fluid draining into the sample with time.

The method still suffers at least two disadvantages, the second one rather severe:

(a) Any fluid draining into the sample would presumably be bubble free and have a lower gas concentration than the pore fluid. This would create a change in the total gas concentration in the system, which would change the equilibrium and hence transient pore volume response. In addition, it would introduce an inhomogeneity in the bubble distribution at the ends of the sample, which would further modify the transient response.

(b) The test technique may work reasonably well for a step increase in pore pressure, with fluid draining into the sample, but would not be amenable to a step decrease in pore pressure with flow of pore fluid out of the sample. The latter would introduce problems of two-phase fluid flow as well as bubble nucleation outside the sample, both of which would not be controllable, and both of which would influence, perhaps drastically, the nature of the transient response. It would also be difficult simply to measure the volume of pore fluid expelled from the sample.

Perhaps the restrictions on monitoring the behaviour of supersaturated pore fluids would not be so severe if this behaviour were similar to the response of a sample with an undersaturated pore fluid. However, in the former case the bubble nucleation process has a definite influence whereas in the latter it is probably not operative at all.

Fortunately, it is possible to observe the drained behaviour of a gassy sample in another way. This will be referred to as the "psuedo-drained" response, for reasons which will be presently apparent.

Consider again Test No. 11, which was described in some detail in Chapter 3. This was an isotropic undrained test on an initially fully saturated sample, with initial conditions of σ = 1400 KPa, u = 650 KPa, and σ' = 750 KPa. The sample was unloaded in steps of $\Delta\sigma$ = -100 KPa in phases A to J of the test, (the sample response may be seen in Figures 3.20 to 3.29). At the end of phase J, σ' had just reduced to 0 KPa, σ = u = 458 KPa, and the sample had undergone a volumetric strain of approximately 1% (expansion). During the next phase, K, a further step decrease in σ was applied from 458 to 342 KPa. Because σ' = 0, u also decreased from 458 to 342 KPa (B = 1), and for the duration of that phase of the test σ' = 0 and u = constant. These are the boundary

conditions for a drained test, (even though the sample appeared to be undrained). Since there was no change in effective stress during this phase of the test, the void ratio of the sample must also have remained constant. Volumetric strains measured external to the membrane were due solely to drainage of fluid out of the actual sample, which acted to "balloon" the membrane and top cap. During phase K of Test 11, an additional 3.8% of volume expansion was measured due simply to gas exsolution.

As an aside, it is interesting to note that during all the psuedo-drained tests, the sample maintained its shape and did not "liquify" or otherwise act in a viscous manner. This was true despite measured volume changes of the pore fluid equivalent to up to 15% of the total sample volume, and elapsed times of several hours. One might speculate on the reason for this. One possibility is that a small positive effective stress is maintained in the sample due to surface tension effects despite the fact that pressures in both the gas and liquid phases are high, and their difference is relatively small.

All the psuedo-drained tests (phases 7H, 11K, 9L, 9M, 9N) were performed before the development of the lateral strain indicator, discussed in Chapter 3, so that sample

deformations were measured only by displacement of the top cap.[8] Since the sample was unencumbered by the lateral strain indicator, which was stiff compared to the pore fluid compressibility at this stage of the test, the membrane was free to expand in a relatively uniform manner. The measured vertical strains may be expected to be slightly low due to a "ballooning" of the membrane at sample mid-height, but the measured time variation of V_v is expected to represent the actual pore volume changes in form if not exactly in value.

A comparison of measured cell and pore fluid pressures when $\sigma' = 0$ also indicates a confining influence of the membrane of 8 to 10 KPa.

The volumetric strain vs time plot for phase 11K is found in Figure 3.30, and similar plots for phases 7H, and 9L to 9N are located in Appendix C. This data is summarized also on a plot of log ε_{vol} vs log t in Figure 5.1. The data is presented in this fashion to test the applicability of Black & Lee's (1973) relationship:

$$\varepsilon_{vol} = t^x, \quad 0<x<1 \tag{5.12}$$

---

[8]It would have been useful, during these phases of the tests, to also measure sample volume changes using the volume change of the cell fluid. As discussed in Chapter 3, however, this was not possible due to exsolution of gas in the cell fluid itself.

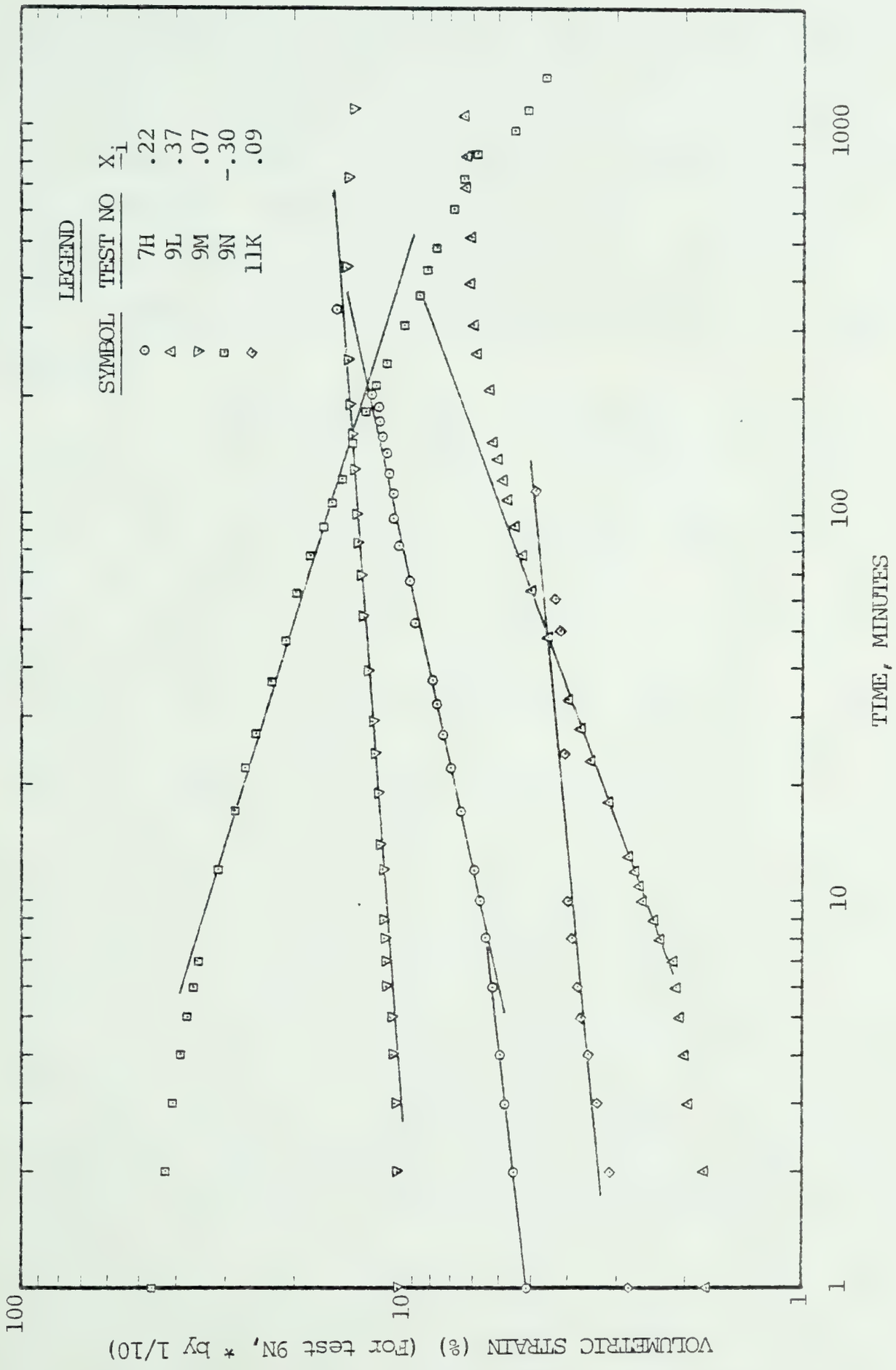


Figure 5.1 - Volumetric strain vs time for psuedo-drained tests

As may be seen in Figure 5.1, this relationship is approximately valid for $10<t<100$ minutes. For $t<10$ minutes, the data is consistently flatter (i.e. a smaller x) than for later times. For $t>100$ minutes, the curves again deviate from a straight line relationship. This is due partly to the asymptotic nature of the pressure-time response and partly due to loss of gas from the sample by diffusion through the membrane.

The measurement of volumetric strain in the psuedo-drained tests is actually a measurement of the volume of free gas, V_{fg}, produced in the pore space. The form of the relationship between V_{fg} and t is illustrated diagrammatically in Figure 5.2. It is characterized by an initial volume V_1 at t=0; a relatively quick rate of increase dV/dt at low t, diminishing to 0 at infinite time; and V becoming asymptotic to some value V_2. For an unloading phase of a psuedo-drained test (e.g. phase 11K), V_1 is the equilibrium volume from the previous phase (11J) adjusted for the pressure decrease (according to Boyle's law) at the beginning of phase K, and V_2 is the equilibrium volume of free gas for the current phase calculated from Henry's law.

The V_{fg} vs t response is similar to the p vs t response in the undrained tests, and one might therefore postulate a similar relationship to that given in section 4.2:

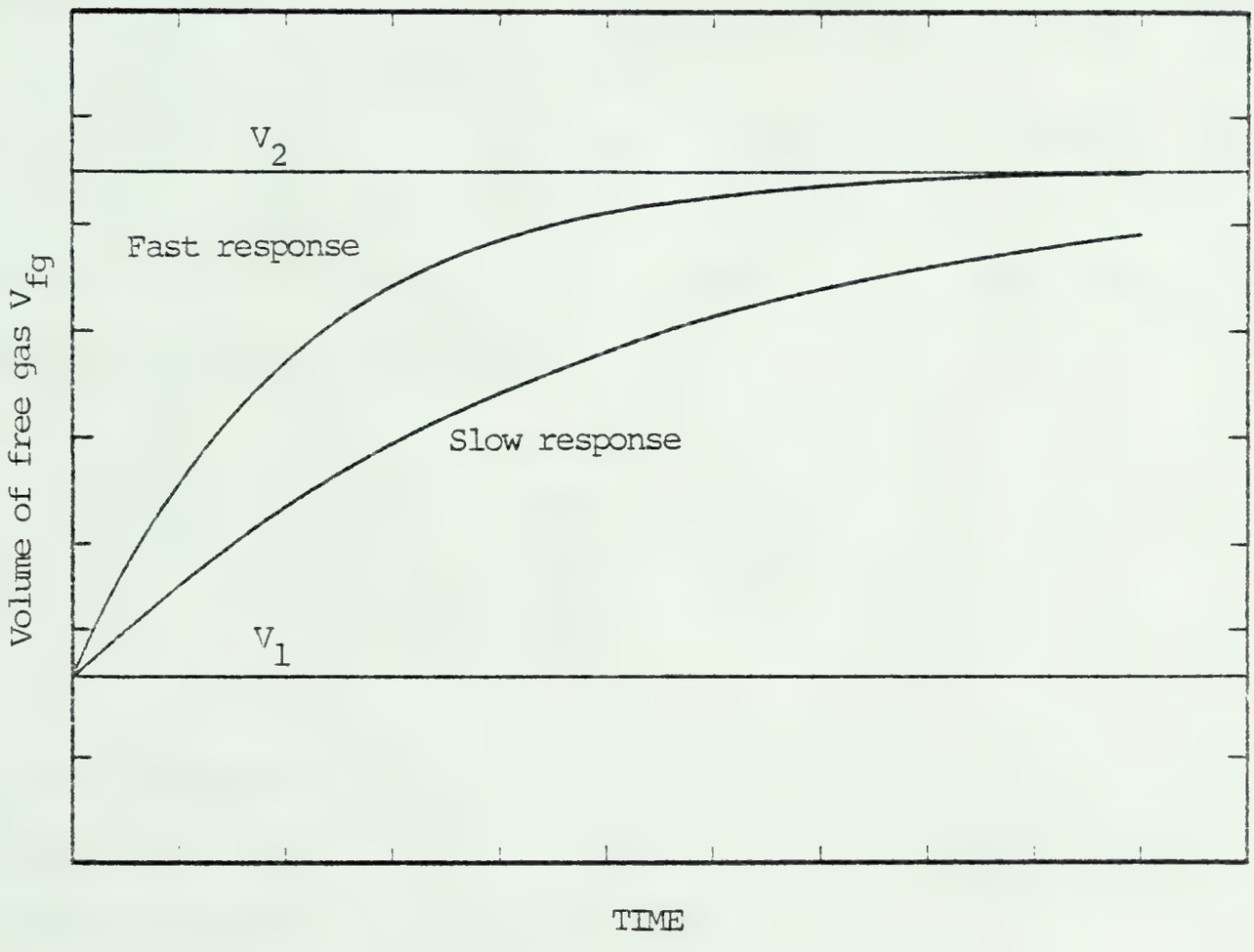


Figure 5.2 - Diagrammatic relationship between volume of free gas in the pores and time for a drained test on a gassy soil. Pore fluid supersaturated with gas.

$$(V-V_1)/(V_2-V_1) = t/(t+A')$$

or $$V = V_1 + (V_2-V_1) * t / (t+A') \qquad (5.23)$$

A non-linear "least squares" fit using this function is shown for tests 7H, 11K and 9L-N in Figures 5.3 to 5.7 (curve labelled "quotient+1 fit"). The agreement between observed and predicted values is excellent.

This function suffers one disadvantage, however. To develop the more general consolidation equation, it will be necessary to provide an expression for DV_{fg}/Dt. Differentiating 5.23, we get:

$$\begin{aligned} DV_{fg}/Dt &= (V_2-V_1)/(t+A') - (V_2-V_1)*t/(t+A')^2 \\ &= (V_2-V_1)*A'/(t+A')^2 \\ &= (V_2-V_{fg})/(t+A') \end{aligned} \qquad (5.24)$$

Although equation 5.23 provides a good fit to the data, it is cumbersome because (5.24) contains t in the denominator. A functional relationship of the form:

$$DV_{fg}/Dt = E*(V_2 - V_{fg}) \qquad (5.25a)$$

would be much more tractable. Equation (5.25a) may be obtained from (5.24) by ignoring the t term in the denominator and setting $E = 1/A'$. Equation 5.25a is a

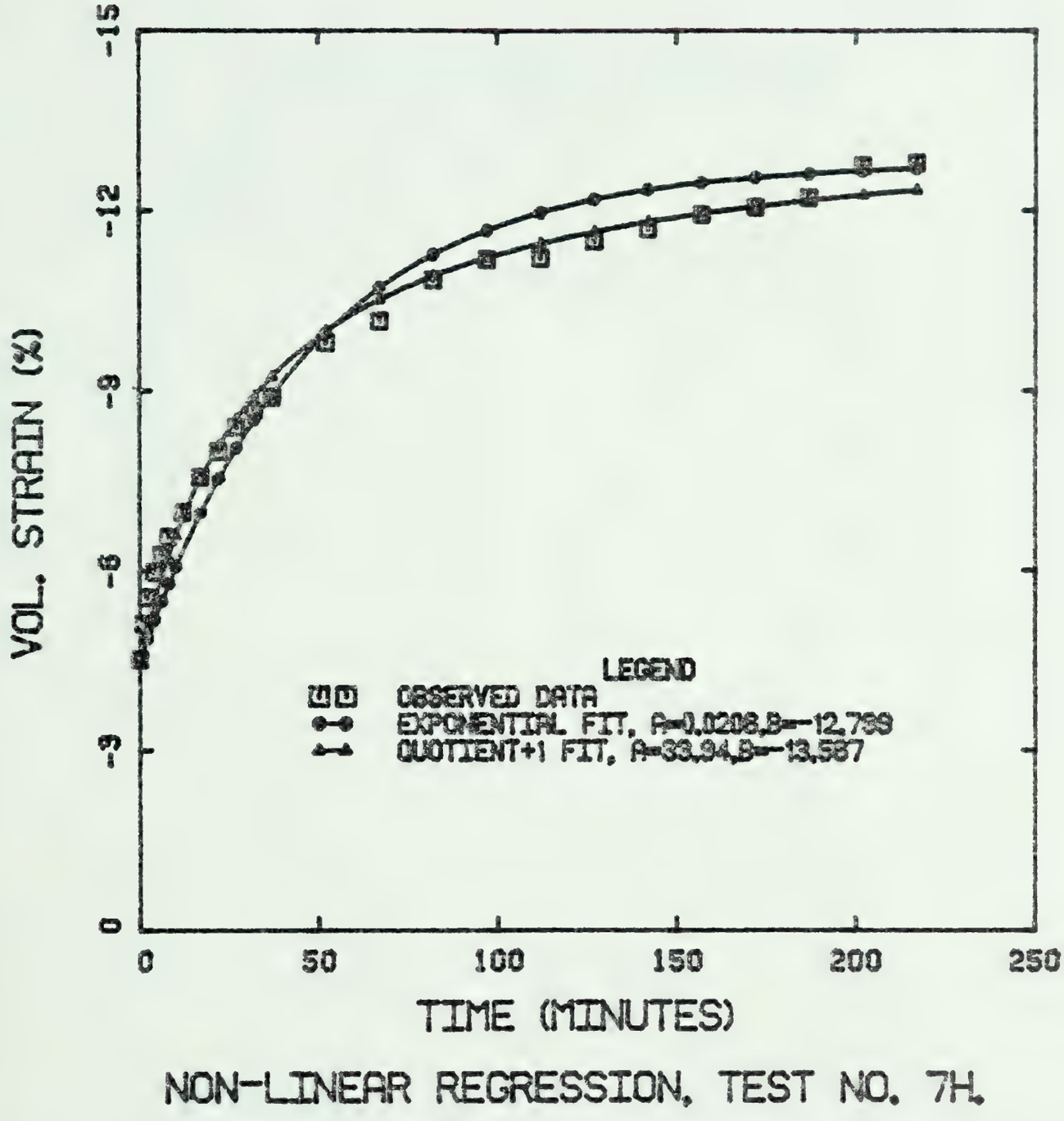

VOL. STRAIN (%)
0
-3
-6
-9
-12
-15
0
50
100
150
200
250
TIME (MINUTES)
LEGEND
OBSERVED DATA
EXPONENTIAL FIT, A=0.0208,B=-12.799
QUOTIENT+1 FIT, A=33.94,B=-13.567
NON-LINEAR REGRESSION, TEST NO. 7H.

Figure 5.3

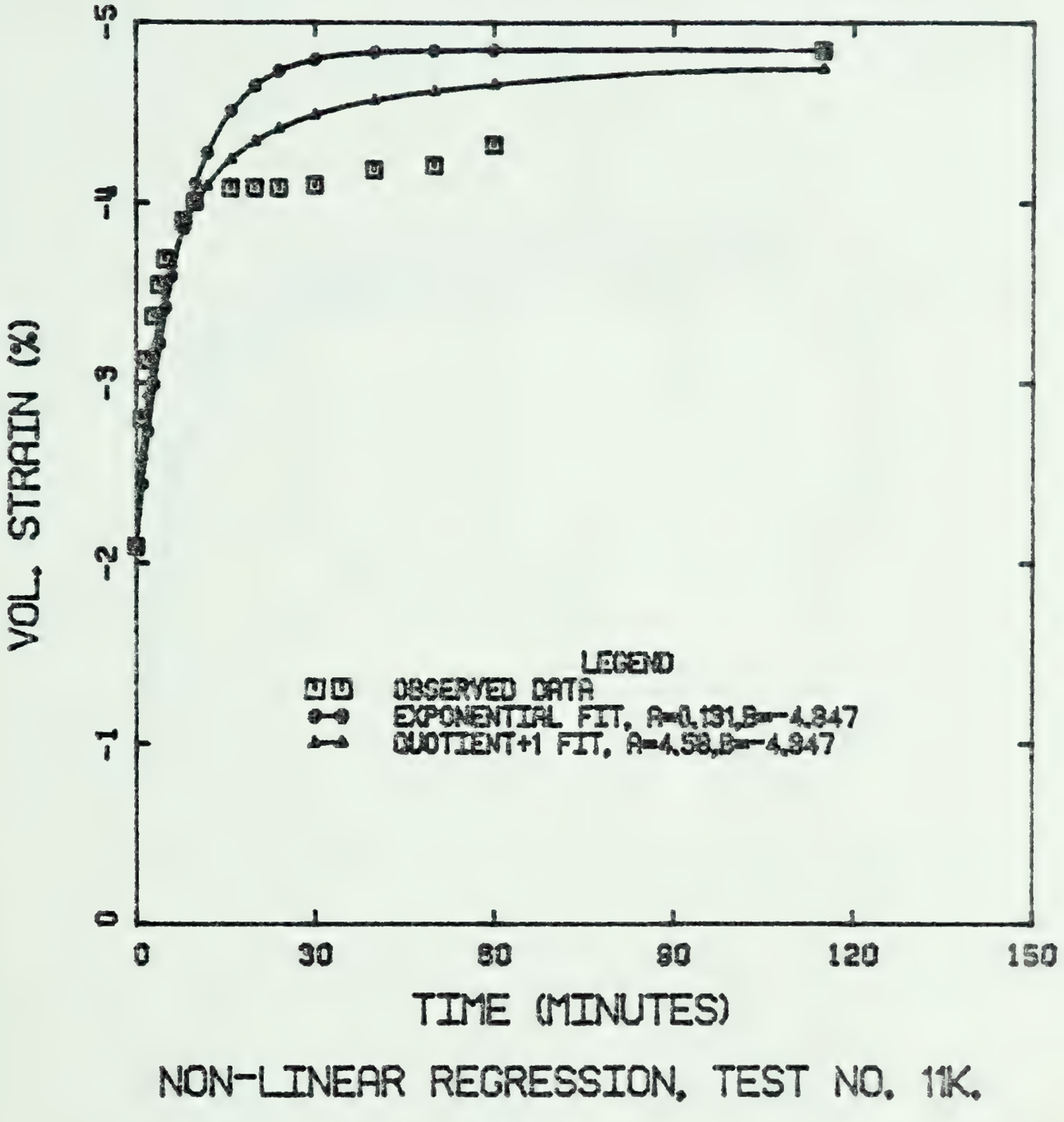

VOL. STRAIN (%)
-5
-4
-3
-2
-1
0
0
30
60
90
120
150
TIME (MINUTES)
LEGEND
OBSERVED DATA
EXPONENTIAL FIT, A=0.131,B=-4.847
QUOTIENT+1 FIT, A=4.58,B=-4.947
NON-LINEAR REGRESSION, TEST NO. 11K.

Figure 5.4

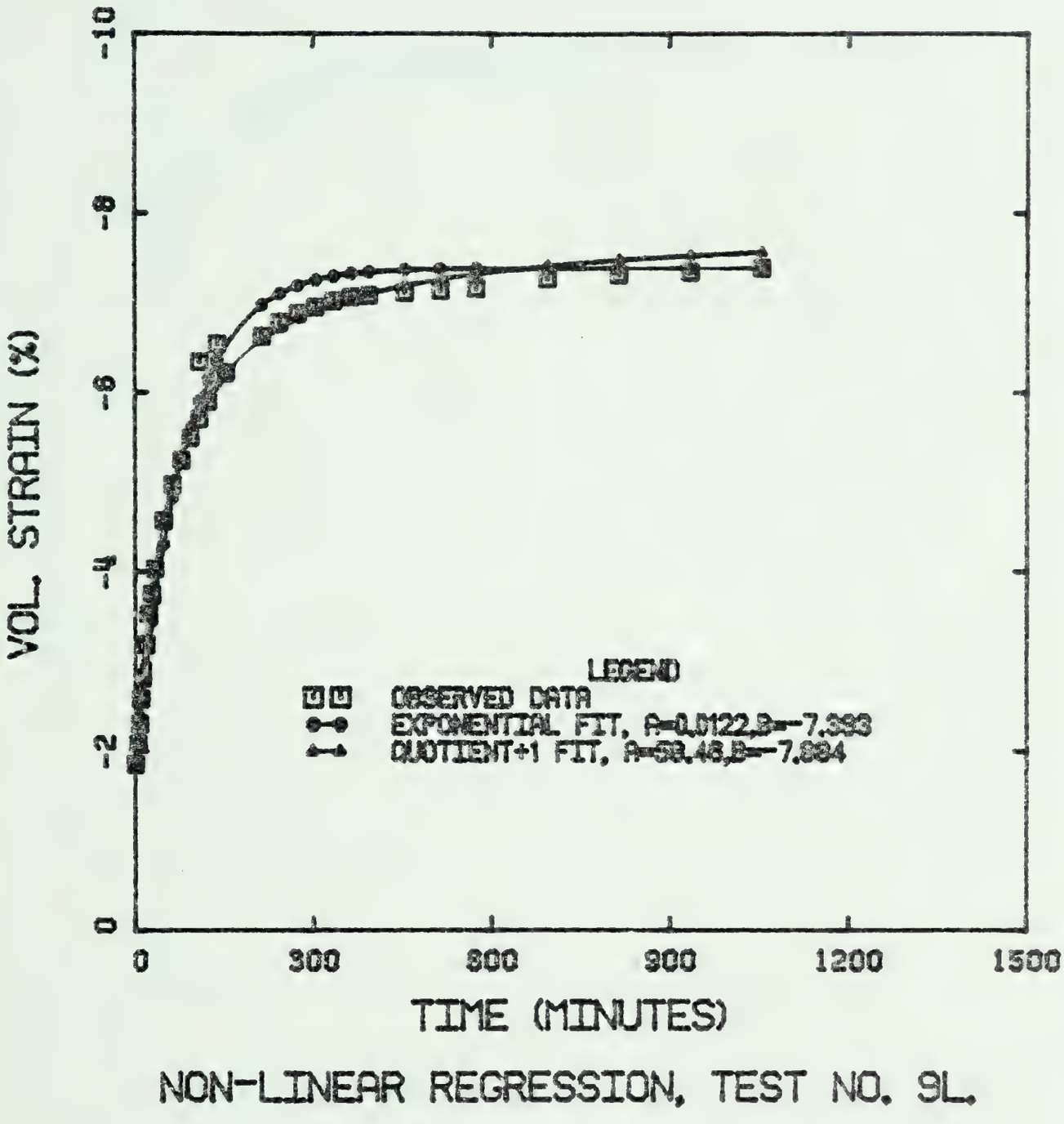

VOL. STRAIN (%)
-10
-8
-6
-4
-2
0
0
300
600
900
1200
1500
TIME (MINUTES)
LEGEND
OBSERVED DATA
EXPONENTIAL FIT, A=0.0122,B=-7.393
QUOTIENT+1 FIT, A=58.48,B=-7.894
NON-LINEAR REGRESSION, TEST NO. 9L.

Figure 5.5

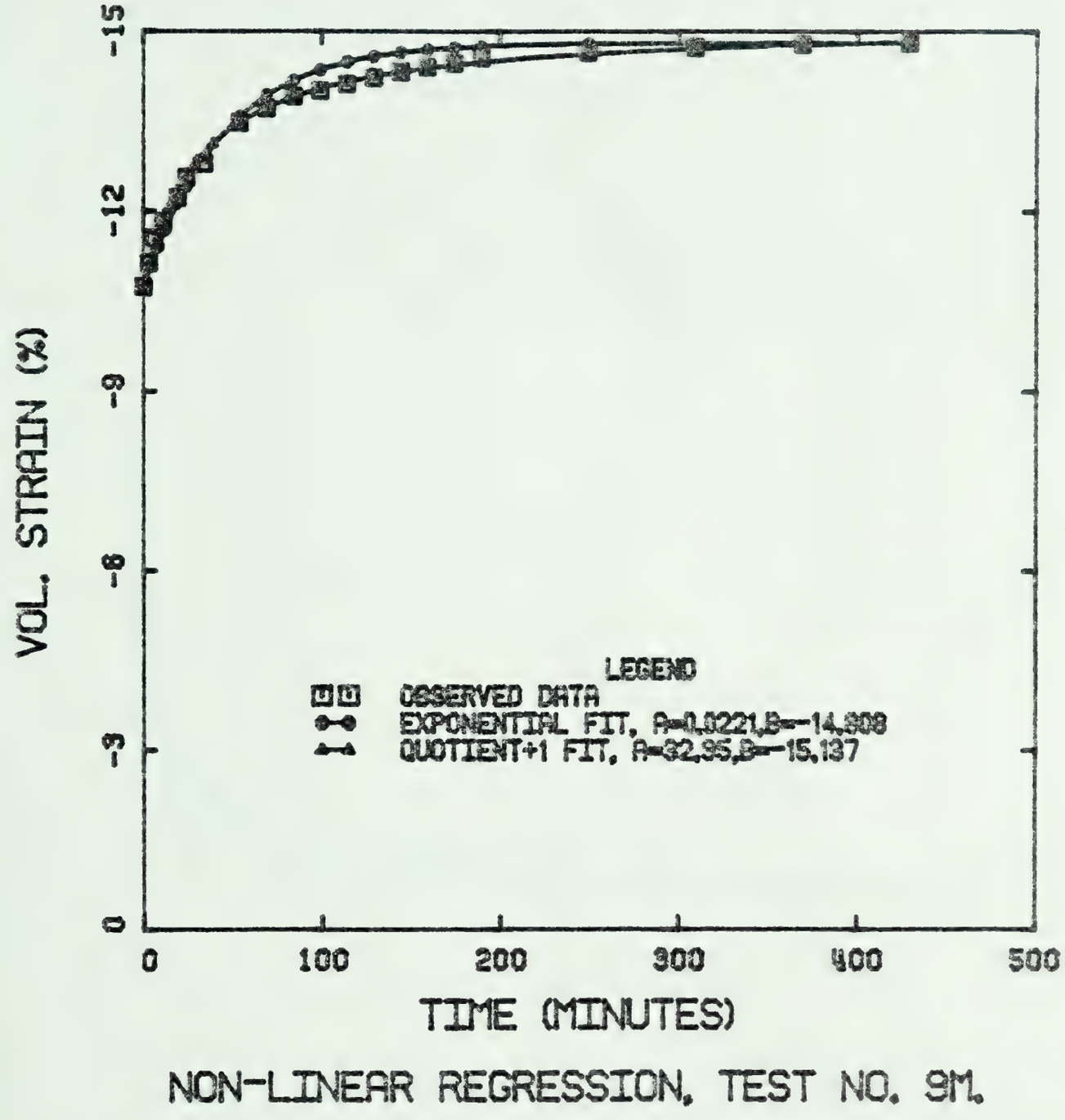

VOL. STRAIN (%)
0
-3
-6
-9
-12
-15
0
100
200
300
400
500
TIME (MINUTES)
LEGEND
OBSERVED DATA
EXPONENTIAL FIT, A=-1.0221,B=-14.308
QUOTIENT+1 FIT, A=-32.95,B=-15.137
NON-LINEAR REGRESSION, TEST NO. 9M.

Figure 5.6

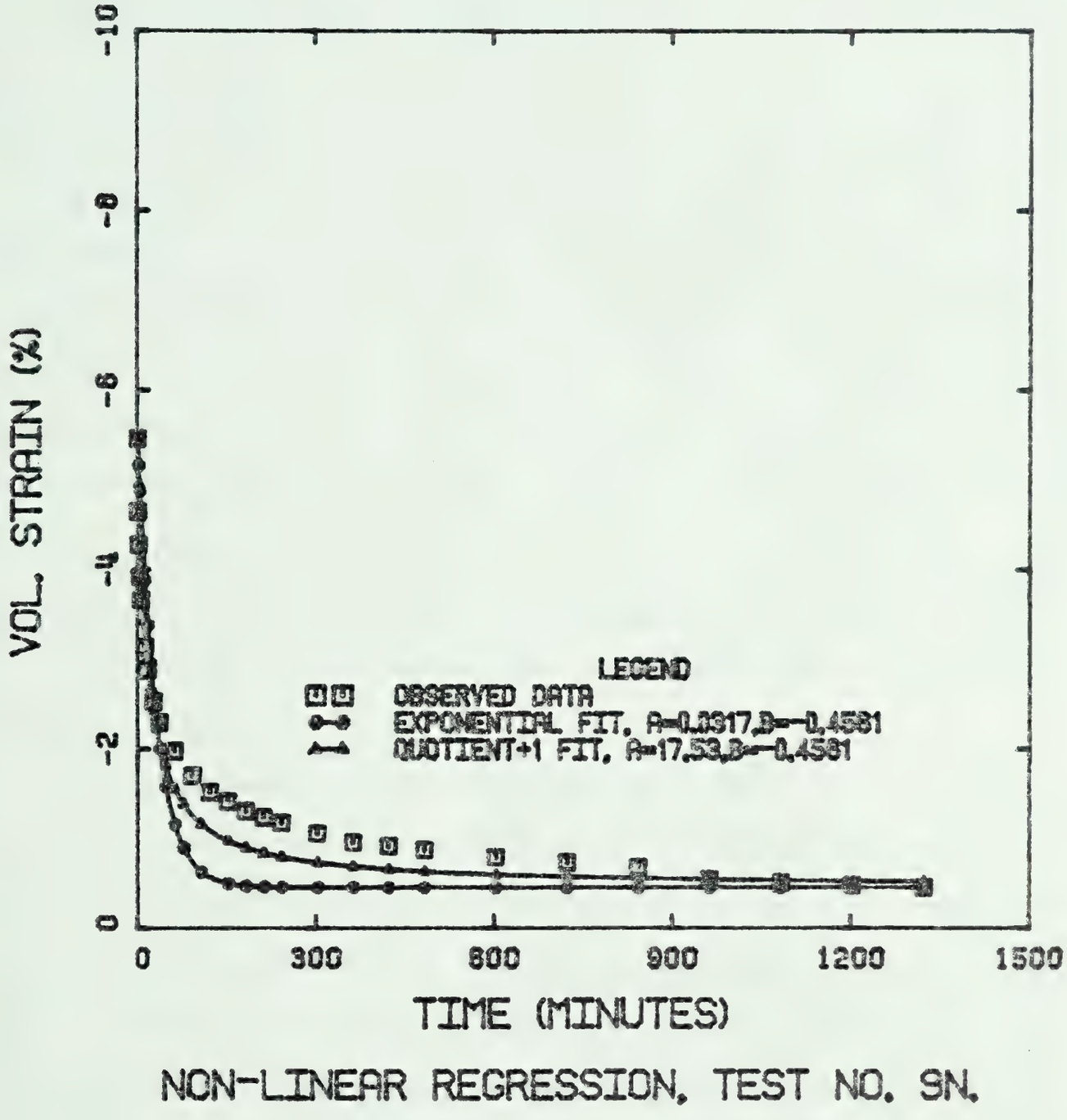

VOL. STRAIN (%)
-10
-8
-6
-4
-2
0
LEGEND
OBSERVED DATA
EXPONENTIAL FIT, A=0.0917,B=-0.4581
QUOTIENT+1 FIT, A=17.53,B=-0.4581
0
300
600
900
1200
1500
TIME (MINUTES)
NON-LINEAR REGRESSION, TEST NO. SN.

Figure 5.7

first-order ordinary differential equation that can be solved to give:

$$V_{fg} = V_2 - (V_2-V_1)*\exp[-E*t] \qquad (5.25b)$$

The term $t/(t+A')$ in equation 5.23 has thus been replaced by $(1-\exp[-E*t])$. A non-linear least squares fit for this function on the observed data is also shown on Figures 5.3-7, (labelled "exponential fit"). The agreement between observed and predicted points is good, but not quite as good as for equation 5.23. As would be expected, the neglect of the term t in the denominator of (5.24) yields a slightly higher value of DV_{fg}/Dt at larger values of t, with the result that the exponential curve slightly over-estimates the data for larger t. At lower values of t the two theoretical curves are nearly identical.

The psuedo-drained test results, then, will be deemed to have been acceptably modelled by equations (5.25a & b). The fit between observed and predicted values is reasonable, and the expression for DV_{fg}/Dt is independent of time, which makes the function very useful in further analyses. The advantages of using equation 5.25a over 5.24 will become apparent as the combined theory of consolidation and gas exsolution is developed in Chapter 7.

The ability of equation 5.25 to predict <u>undrained</u> test results will be discussed in Chapter 6.

5.7 AN EVALUATION OF THE GENERAL GAS EXSOLUTION RELATIONSHIP

In the preceeding section an empirical relationship has been proposed to model gas exsolution:

$$V_{fg} = V_2 - (V_2-V_1)*\exp[-E*t] \qquad (5.25b)$$

$$DV_{fg}/Dt = E * (V_2 - V_{fg}) \qquad (5.25a)$$

$$= E * (V_2 - V_1) * \exp[-e*t] \qquad (5.25c)$$

It is interesting to compare the general relationship (5.25c) with the theoretical relationships previously derived for gas sorption:

$$dV/dt = 8*\pi*K*H*(1-f)*R/(S-R) * \Sigma\{\exp[-K*a\hat{}2*t] * [\text{sin and sin}\hat{}2 \text{ terms}]\} \qquad (5.16)$$

and for bubble nucleation:

$$J = Z * \exp[-4*\pi*T_s*r_c\hat{}2/(3*k*T)] \qquad (5.21a)$$

All three of these equations have a similar form. The correspondence between (5.25c) and (5.16) is obvious. Indeed, for the case of an undersaturated pore fluid, where the sorption process is probably the only major contributor to gas exsolution, it would be very tempting to equate E with gas diffusivity. Equation 5.21a does not contain time explicitly, but it does contain the magnitude of the supersaturation c_2/c_{2s} through the term r_c. For a higher

degree of supersaturation, c_2/c_{2s} is large and hence r_c is small. The smaller r_c is, the larger is the bubble nucleation rate J, which must have a direct influence on increasing DV_{fg}/Dt. From (5.25a) DV_{fg}/Dt is seen to be higher for higher supersaturations (i.e. for larger values of V_2-V_{fg}). Another way to view this correspondence is to realize that at t=0, r_c is extremely small (due to a high c_2/c_{2s}), but that at t approaches infinity, c_2/c_{2s} approaches 1 and hence r_c also approaches infinity. r_c is therefore directly proportional to t.

The intent of the above comments is not to suggest that (5.25c) can be derived from either or both of (5.16) and (5.21a), but to point out that the observed behaviour corresponds in form to what is perceived to be the dominant processes in the pore space.[9]

5.8 SUMMARY

A definition of gas exsolution has been presented, which is that gas exsolution in soils is the observed production of gas in the pore space upon reduction in fluid pressure. Several contributing processes, gas sorption and bubble nucleation, have been discussed. A general

---

[9] It should also be noted here that the additional process of bubbles forming at nucleation sites on included solids has yet to be modelled (mathematically) in a suitable way. This contribution to bubble nucleation is also seen as important.

relationship between the volume of free gas in the pores and time has been proposed, based on observed behaviour in the laboratory. This relationship has been compared to the theoretical relationships governing gas sorption and bubble nucleation, and found to possess a similar form.

CHAPTER 6 - EVALUATION OF LABORATORY RESULTS

UNDRAINED TRANSIENT RESPONSE

6.1 GENERAL

An appraisal has been made of the observed undrained equilibrium behaviour of a gassy soil in Chapter 4 in relation to the theoretical model presented in Chapter 2. It is desirable to extend this evaluation of the laboratory data to the undrained transient response. This may be accomplished given an appropriate, non-equilibrium volume-time relationship.

Transient behaviour in an undrained element of gassy soil is due to gas exsolution. An empirical relationship was proposed in Chapter 5 of the form:

$$DV_{fg}/Dt = E * (V_2 - V_{fg}) \qquad (5.25a)$$

A finite difference solution to the transient undrained response is formulated directly in this chapter, using the above relationship plus the theoretical developments of Chapter 2. The results of some analyses are then presented; a comparison is made between predicted and observed behaviour, and the ability of the transient model to converge on the equilibrium solution is assessed.

6.2 THEORETICAL CONSIDERATIONS, TRANSIENT UNDRAINED BEHAVIOUR

The transient nature of the undrained response in a gassy soil is caused by gas exsolution. Exsolution forces the compressibility of the gaseous component of the pore fluid to become time dependent. The compressibility of the liquid component of the pore fluid, as well as that of the soil skeleton, is not influenced by gas exsolution and so remains independent of time.

In developing a theoretical model for the undrained response of an element of gassy soil, equation 2.15c must then be modified as follows:

$$\Delta V_T = \Delta V_l + \Delta V_{fg}(\Delta t) \qquad (6.1)$$

Equation 2.14c

$$\Delta V_T = -\beta_T * V_T * (\Delta\sigma - \Delta u)$$

and equation 2.8b

$$\Delta V_l = -\beta_l * V_l * \Delta u$$

are still applicable, but the expression for ΔV_{fg} in (6.1) must incorporate the influence of:

(a) a non-equilibrium condition at the beginning of the time-interval for which Δu is to be calculated, and

(b) a ΔV_{fg} which is a function of Δt.

Consider, then, an element of gassy soil, with an undrained boundary and with the boundary condition that:

$$\sigma_1 = \sigma_3 = \text{constant}$$

At time t=0, there is a non-equilibrium condition with respect to gas dissolved in the pore fluid, i.e. the pore liquid is either undersaturated or oversaturated with dissolved gas, and hence some of the free gas in the pore space will either dissolve or exsolve. This will result both in a volume change in the element and a change in the fluid pressure.

Consider as well an increment of time, Δt, during which there will be a change in volume of free gas, ΔV_{fg}, and a change in pressure Δu, (or $\Delta P = \Delta u$). Two methods will be used to calculate ΔV_{fg}, a simple approach which uncouples gas compression and gas exsolution, and a more refined approach which attempts to account for the influence of free gas compression on the nature of the dissolved gas disequilibrium, and thus on gas exsolution.

6.2.1 Uncoupled solution

The change in volume of free gas ΔV_{fg} is assumed to occur because of two independent processes:

(a) a compression or expansion of the free gas according to Boyle's law:

$$(\Delta V_{fg})_1 = -V_{fg} * \Delta P/(P+\Delta P) \qquad (2.6)$$

(b) exsolution. In calculating this volume it is assumed that P = constant over Δt, (even though ΔV_{fg} is being derived to calculate ΔP), i.e. that ΔP does not affect either the rate or volume of gas produced due to exsolution. This approximation becomes exact in the limit as Δt approaches 0, so that for small Δt it should be a reasonable assumption.

Then:

$$\Delta V_{fg}/\Delta t = E^*(V_2 - V_{fg}) \qquad (5.25a)$$

where V_2 = equilibrium volume of free gas at pressure P.

Recalling from section 4.2.3 the definition of K′,

K′ = the total equilibrium volume of dissolved and free gas in the pore space at any pressure P′, multiplied by P′.

Then

V_2 = Total volume of gas - volume of dissolved gas

$$V_2 = K'/P - H^*V_w \qquad (6.2a)$$

so that, from equation 5.25a,

$$(\Delta V_{fg})_2 = E*\Delta t*(K'/P - H*V_w - V_{fg}) \qquad (6.2b)$$

Combining (2.6) and (6.2b)

$$\Delta V_{fg} = (\Delta V_{fg})_1 + (\Delta V_{fg})_2$$
$$= -V_{fg}*\Delta P/(P+\Delta P) + E*\Delta t*(K'/P-H*V_w-V_{fg}) \qquad (6.3)$$

Substituting equations 2.8b, 2.14c, and 6.3 into equation 6.1, the expression for compatibility of volume change in the pore fluid and soil skeleton, gives ($\Delta\sigma$=0):

$$\beta_T*V_T*\Delta u = -\beta_l*V_l*\Delta u - V_{fg}*\Delta P/(P+\Delta P) +$$
$$E*\Delta t*(K'/P - H*V_w - V_{fg}) \qquad (6.4a)$$

Multiplying both sides by $(P+\Delta P)/V_T$ and collecting terms for Δu ($=\Delta P$), a quadratic equation is again found for Δu:

$$A * \Delta u^2 + B * \Delta u + C = 0 \qquad (6.4b)$$

$$A = \beta_T + n*S*\beta_l$$

$$D = E*\Delta t*(K'/P/V_T - n*[1-S+S*H])$$

$$B = n*(1-S) + P*A - D$$

$$C = -P * D$$

This is the uncoupled solution for Δu over a time interval Δt, given values of n, S, V_T and P at the beginning of the interval.[1]

6.2.2 "Coupled" Solution

The method used to couple the gas compression and exsolution effects in one time step may appear to be slightly arbitrary. There is a logical basis for it, however, which leads to a much more efficient algorithm for Δu.

Suppose, for a moment, that ΔV_{fg} was calculated in the following manner:

(a) $(\Delta V_{fg})_1$ was calculated on the basis of equation 6.2b, i.e. $(\Delta V_{fg})_1$ = volume of gas generated over Δt due to gas exsolution, assuming P = constant.

(b) A pressure change ΔP was applied to $(V_{fg}+(\Delta V_{fg})_1)$.

This procedure would modify $(\Delta V_{fg})_1$ according to the anticipated pressure change, (Boyle's law), but would not account for that portion of the gas exsolution process that changes because of a changing solubility imbalance (due to ΔP). A further computational modification will incorporate this effect. Suppose a pressure change is allowed in the pore fluid, with no gas exsolution. The solubility imbalance at pressure P is:

---

[1] It is interesting to compare this solution to equation 4.8b. Referring to coefficients in equation 4.8b with primes, it may be seen that, ($\Delta\sigma$=0):
A=A', B=B'-n*S*H-D, C=E* t*C'

$$(V_2-V_{fg})_1 = K'/P - H*V_w - V_{fg} \qquad (6.5a)$$

The solubility imbalance at pressure P+ P is:

$$(V_2-V_{fg})_2 = K'/(P+\Delta P) - H*V_w - V_{fg}*P/(P+\Delta P)$$
$$= P/(P+\Delta P) * \{K'/P - (P+\Delta P)/P*H*V_w - V_{fg}) \qquad (6.5b)$$

If the computational procedure outlined in (a) & (b) above is used, then a modification that recognizes a changing solubility imbalance could be introduced in step (a) by defining an average solubility imbalance for the interval:

$$(V_2-V_{fg})_{av} = \{(V_2-V_{fg})_1 + (V_2-V_{fg})_2\}/2 \qquad (6.5c)$$

However, since the influence of changing pressure [P/(P+ΔP)] will be applied in step (b), this term must be dropped from the expression for $(V_2-V_{fg})_2$, so that 6.5c becomes:

$$(V_2-V_{fg})_{av} = \{(K'/P-H*V_w-V_{fg})+(K'/P-[P+\Delta P]/P*H*V_w-V_{fg})\}/2$$
$$= K'/P - V_{fg} - H*V_w*(1+\Delta P/[2*P]) \qquad (6.5d)$$

Then at the end of step (a), the volume of free gas in the pores is:

$$(V_{fg})_1 = V_{fg} + (\Delta V_{fg})_1$$
$$= V_{fg} + E*\Delta t*(K'/P-V_{fg}-H*V_w*[1+\Delta P/2/P]) \qquad (6.6a)$$

and at the end of step (b), the volume of free gas is:

$$(V_{fg})_2 = P/(P+\Delta P) * (V_{fg}+(\Delta V_{fg})_1) \qquad (6.6b)$$

so that

$$\Delta V_{fg} = (V_{fg})_2 - V_{fg}$$
$$= -\Delta P*V_{fg}/(P+\Delta P) + P*(\Delta V_{fg})_1/(P+\Delta P) \qquad (6.6c)$$

Again, substituting equations 2.8b, 2.14c, and 6.6c into 6.1, an expression for Δu may be derived:

$$\beta_T*V_T*\Delta u = -\beta_1*V_1*\Delta u - \Delta u*V_{fg}/(P+\Delta u) +$$
$$P*E*\Delta t*\{K'/P-V_{fg}-H*V_w*[1+\Delta P/(2*P)]\}/(P+\Delta u) \qquad (6.7a)$$

or $$A * \Delta u^2 + B * \Delta u + C = 0 \qquad (6.7b)$$

A,D,C as previously defined in (6.4b)

$$B = P*A + n*(1-S+S*H*[E*\Delta t/2])$$

Note that both equation 6.4a and 6.7a give the same expression, in the limit (as Δu, Δt approach 0) for:

$$du/dt = E * \{K'/(P*V_T) - n*[1-S+S*H]\} /$$
$$\{ _T + n*(S* _1+[1-S]/P)\} \qquad (6.8)$$

A comparison of the computational efficiency of the uncoupled and "coupled" solutions has shown that for a particular level of accuracy, equation 6.4b requires a time

step 1/4 the size of equation 6.7b. Thus the coupled solution is more efficient. However, it must be understood that, unlike the theoretical equations for equilibrium behaviour, both solutions are approximate and only become exact as Δt approaches 0. This is due to the assumptions made in combining the gas compression and exsolution effects.

6.3 ANALYSIS

Equation 6.7b provides an efficient, but approximate algorithm for calculating the change in pressure in an undrained element of gassy soil over a time interval Δt, given a non-equilibrium condition at the beginning of the time interval.

This solution is incorporated into a transient analysis of the undrained laboratory tests, in the following manner:

(a) At the beginning of the laboratory test, a sample has been prepared which has a measured set of initial conditions, i.e. values of V_{fg}, V_l, V_s, C_c, β_w, H, E, P and σ are known. The sample is at equilibrium, so that no time-dependent processes are active.

(b) A decrease in boundary stress, $\Delta\sigma$, is applied to the element, causing an immediate change in V_{fg} and P due to fluid compressibility. This response can be modelled using equation 2.15b with H=0.

(c) The pressure in the fluid has changed due to the change in boundary stress, but immediately afterwards, the weight of dissolved gas is the same as it was before the stress change occurred. Since W_{dg} is proportional to P (at equilibrium), there is now an imbalance of dissolved gas in the pore fluid. The pore liquid is either undersaturated or supersaturated with dissolved gas depending upon whether the boundary stress (and pore pressure) has increased or decreased. The amount of solubility imbalance may also be expressed by the term (V_2-V_{fg}), where V_2 is the equilibrium volume of free gas at the current pressure and V_{fg} is the actual volume of free gas.

(d) The value of K′ for the sample may be computed from the initial conditions, an interval of time Δt may be selected, and equation 6.7b applied to predict the change in pressure Δu for the time interval. Knowing Δu, the initial conditions outlined in (a) may be adjusted to the end of the time interval using equations 2.8b, 2.14c, and 6.3.

(e) In this manner the analysis may proceed, time step by time step, until equilibrium conditions are again established.

(f) The equilibrium solution for u and V_{fg} obtained from the transient analysis, (at "infinite" time), may

be compared to the equilibrium equation (2.15b, $H \neq 0$) and an assessment made of the convergence of the transient analysis.

(g) Both solutions (equilibrium and transient) may then be compared with the actual sample response. It is necessary to make the transient predictions using several values of E to bracket the observed behaviour.

This analytical procedure was coded for the computer, and the program is located in Appendix F. Figure 6.1 provides a flowchart of the program logic.

6.4 COMPARISON OF PREDICTED AND OBSERVED BEHAVIOUR

A comparison between predicted and observed "pressure vs time" behaviour for Test Number 11 will be presented in this section. The results of analyses for all the other isotropic tests and constant K tests were of a similar nature. They are located in Appendix G, and summarized later in this section.

Initially, an analysis of Test No. 11 was performed assuming S=100% at the beginning of the test, or S=99.92% at the start of Phase B, where air exsolution begins to occur. The results of these analyses are presented in Figures 6.2 to 6.11. A perusal of these figures will allow an evaluation of the analytical method. The following points are noteworthy:

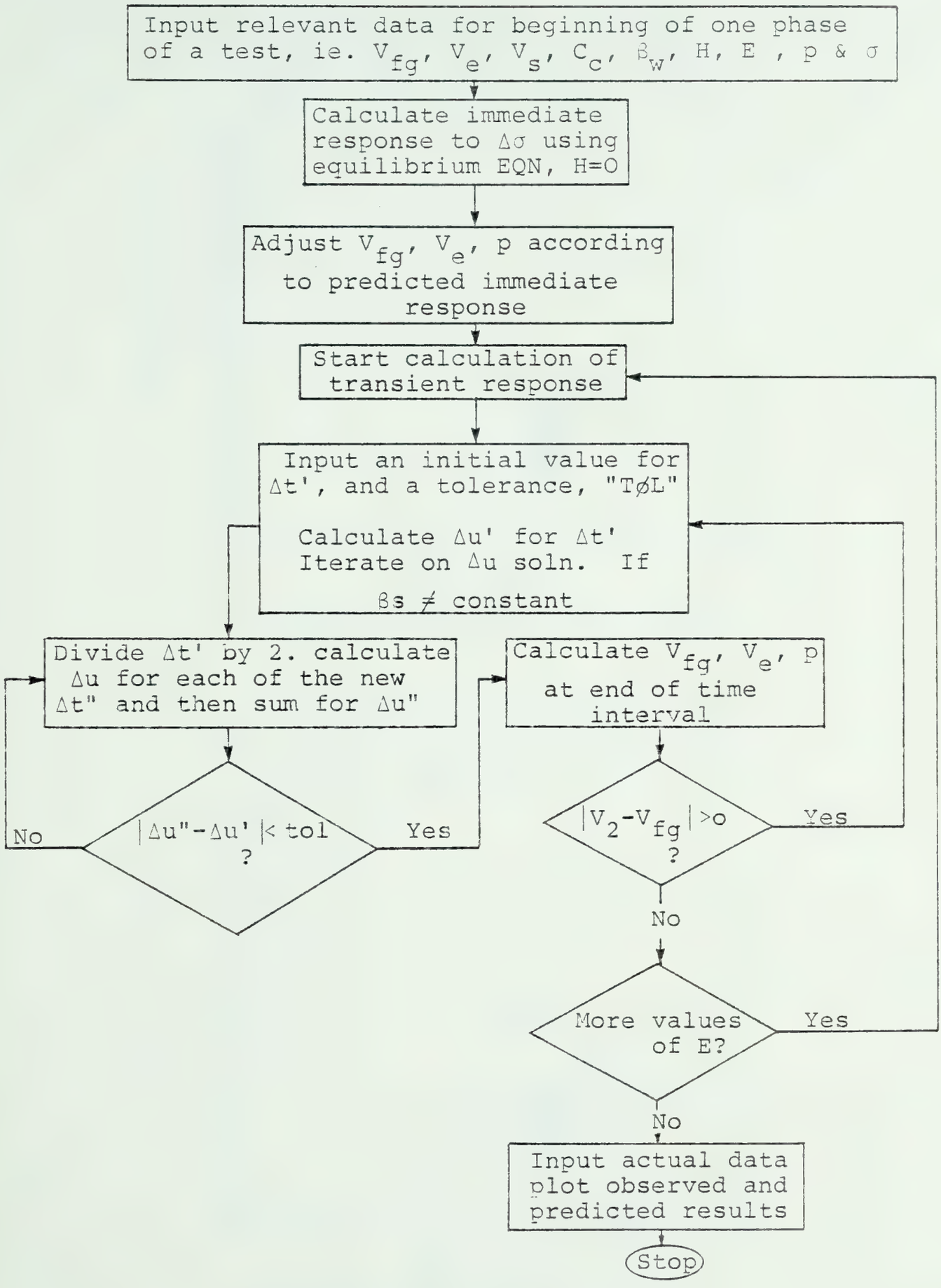
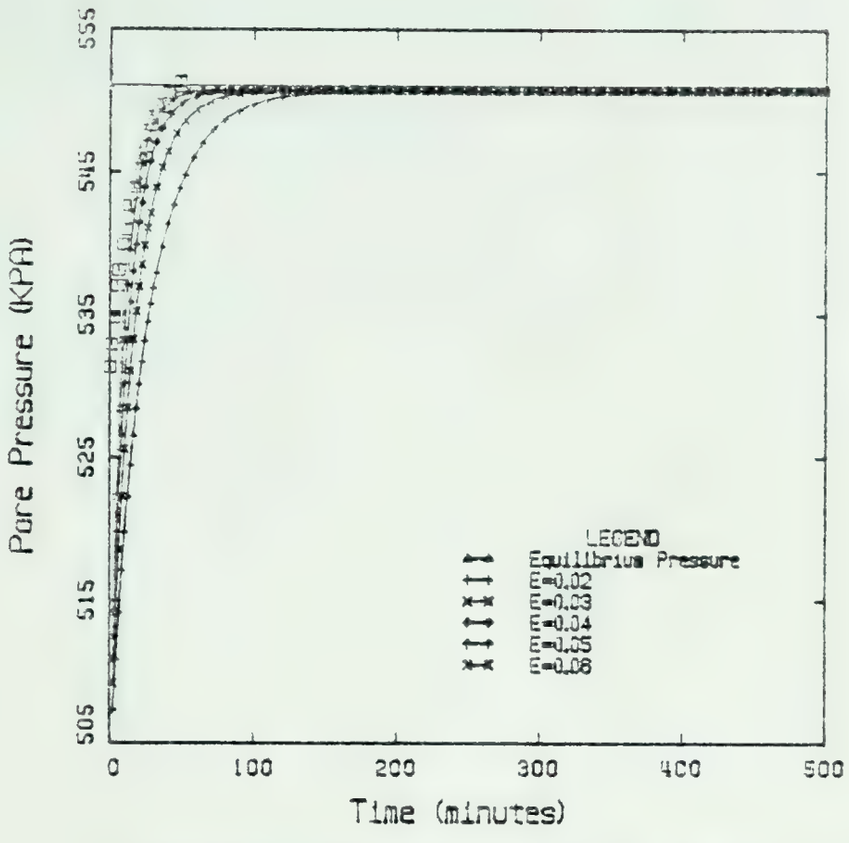
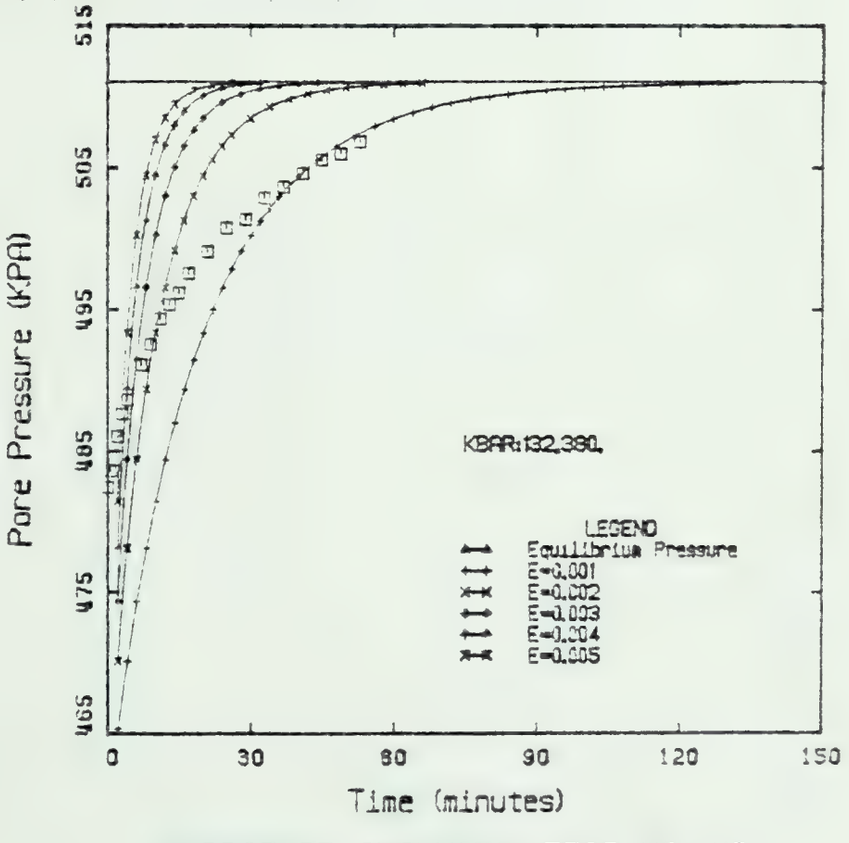


Figure 6.1
Flowchart for computer program to analyze undrained transient response of gassy soil

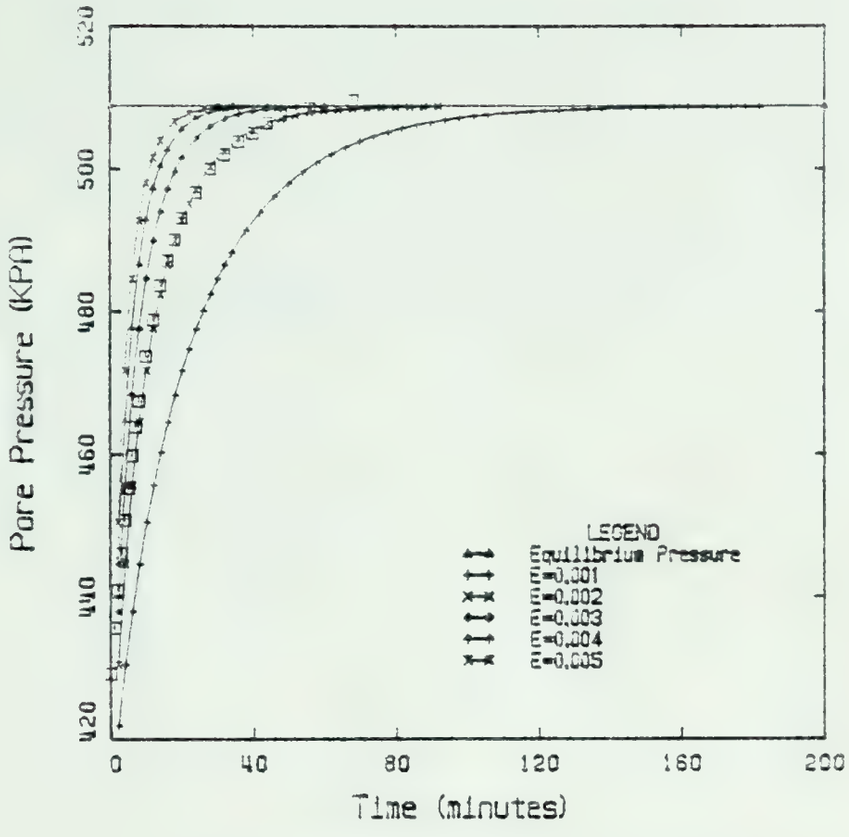


UNDRAINED ANALYSIS, TEST NO. 11B (AIR)

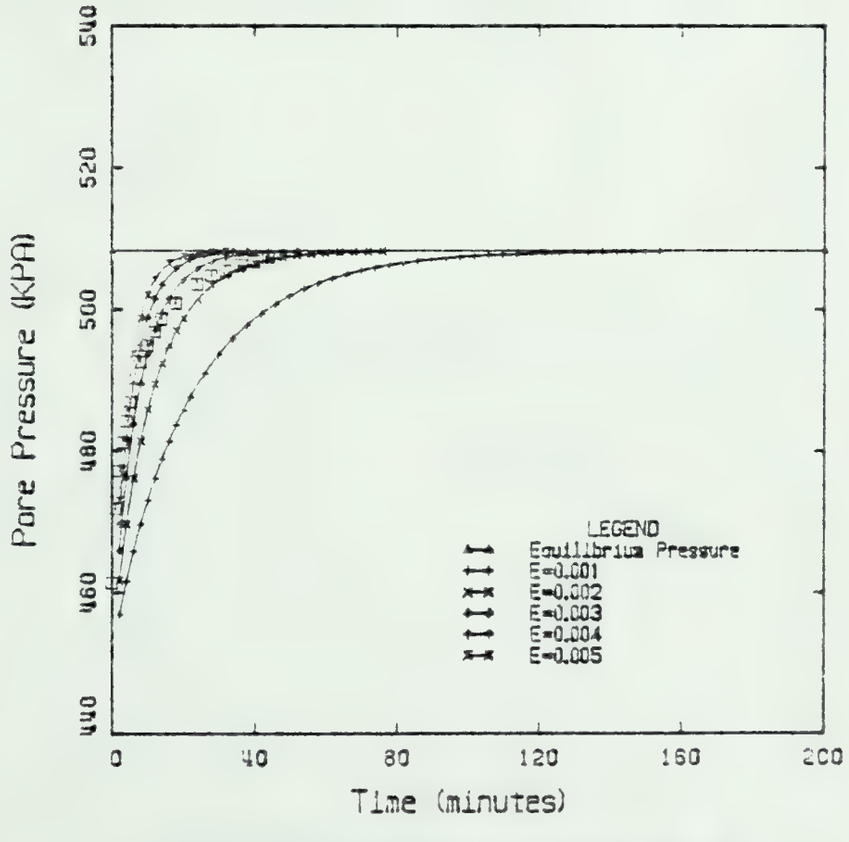


UNDRAINED ANALYSIS, TEST NO. 11C

Figures 6.2 and 6.3

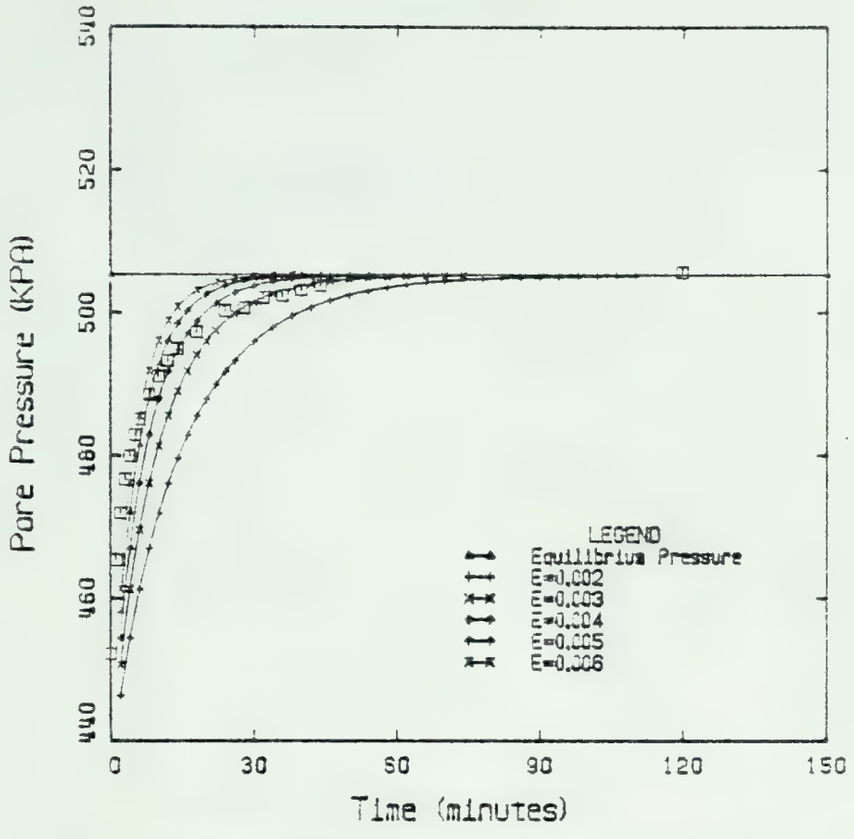


UNDRAINED ANALYSIS, TEST NO. 11D

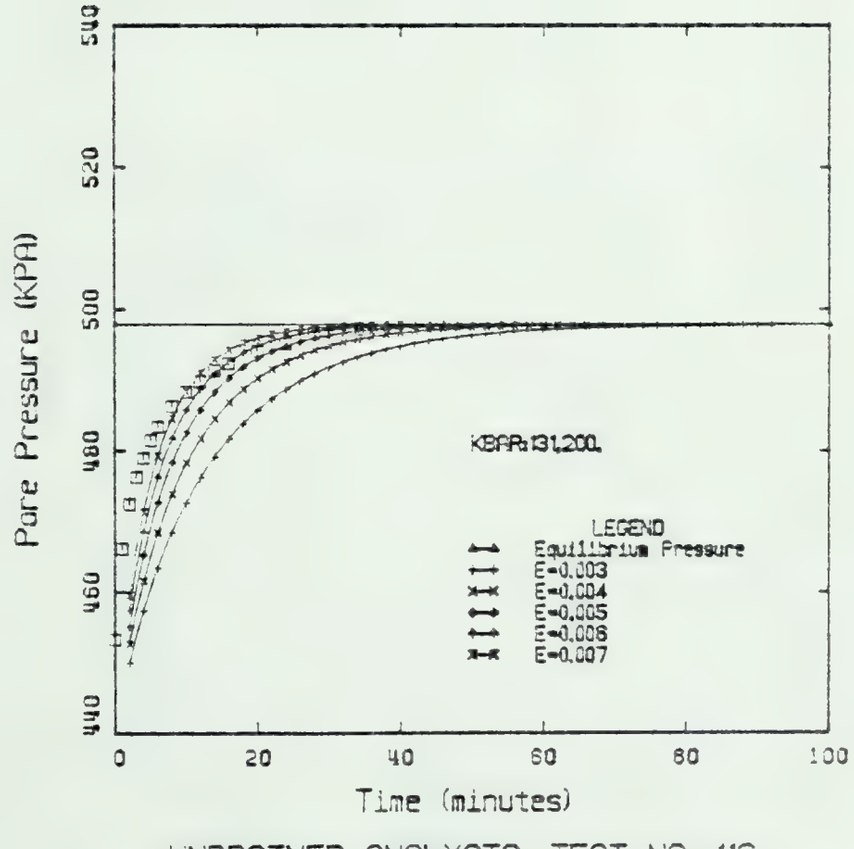


UNDRAINED ANALYSIS, TEST NO. 11E

Figures 6.4 and 6.5

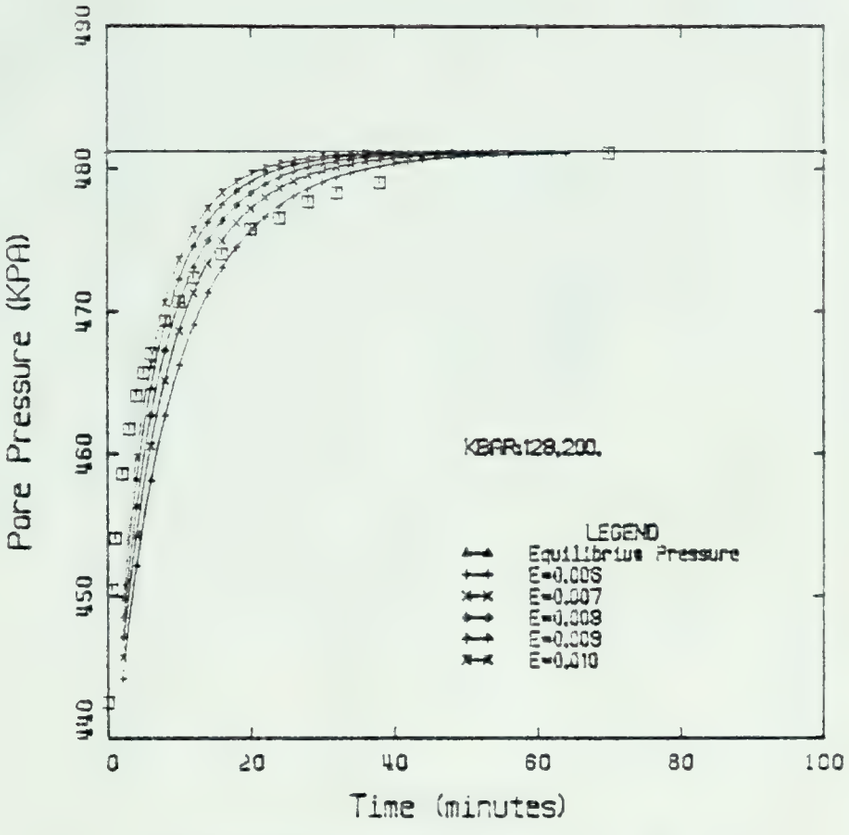


UNDRAINED ANALYSIS, TEST NO. 11F

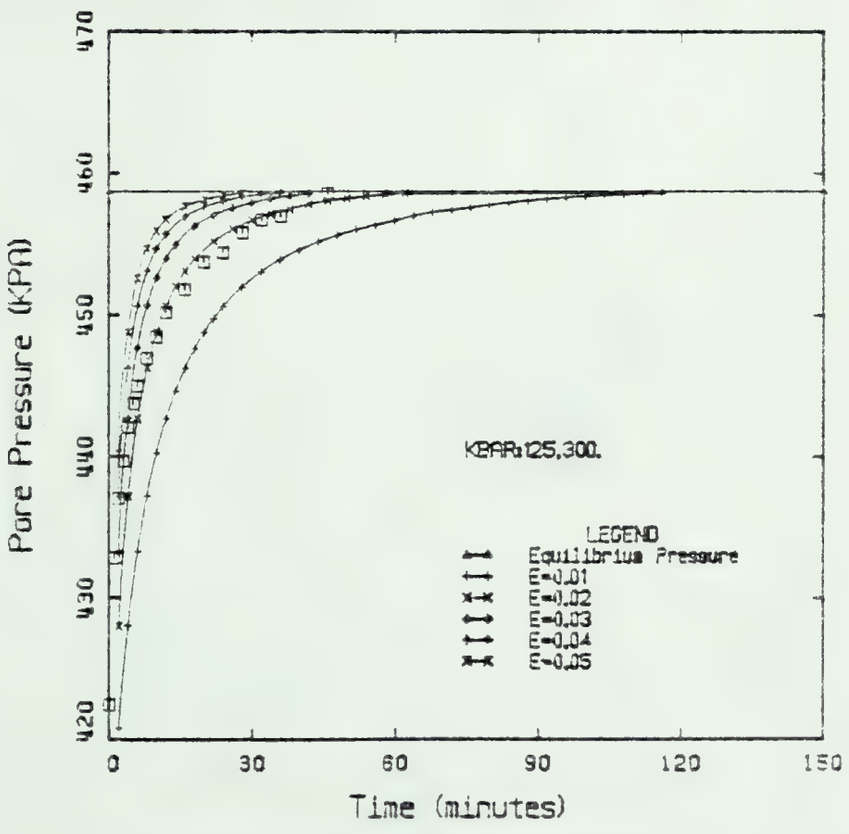


UNDRAINED ANALYSIS, TEST NO. 11G

Figures 6.6 and 6.7

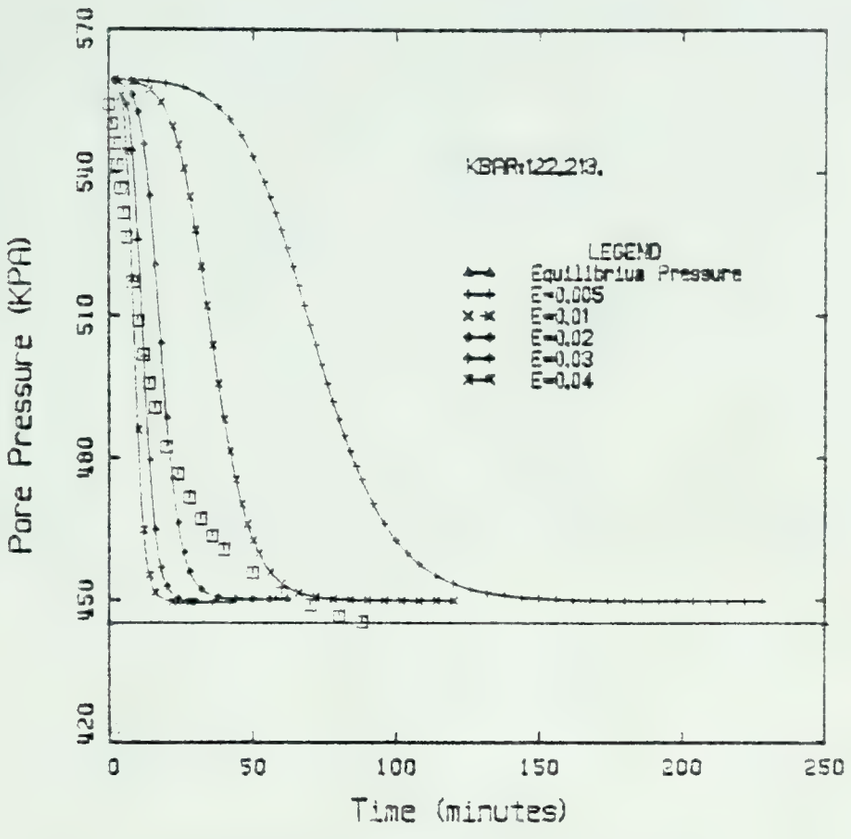


UNDRAINED ANALYSIS, TEST NO. 11H

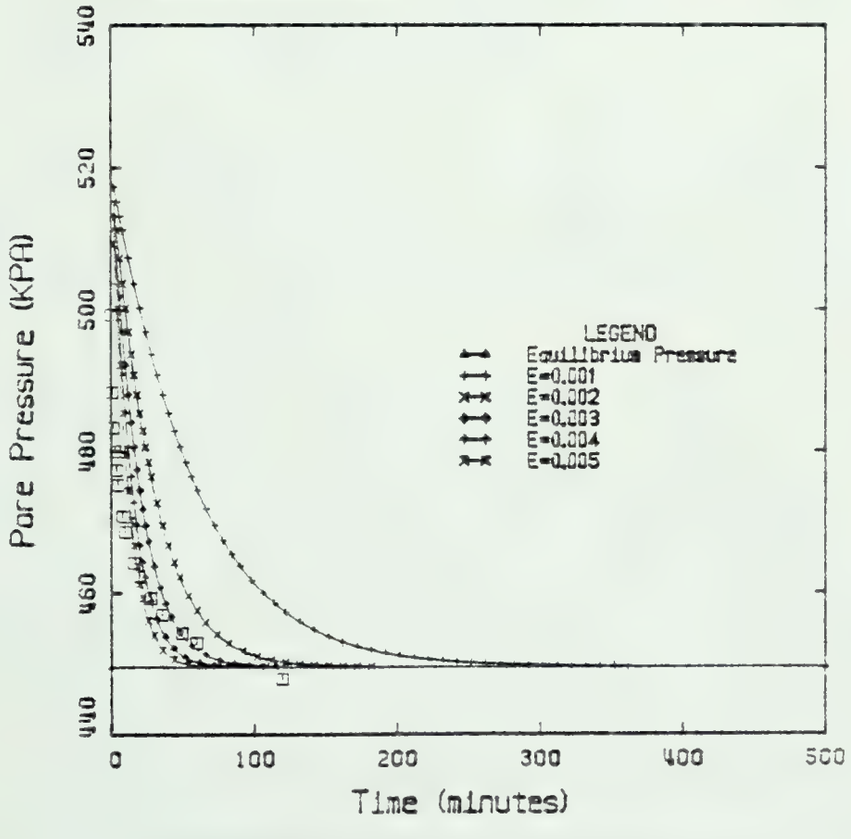


UNDRAINED ANALYSIS, TEST NO. 11J

Figures 6.8 and 6.9



UNDRAINED ANALYSIS, TEST NO. 11L



UNDRAINED ANALYSIS, TEST NO. 11M

Figures 6.10 and 6.11

(a) The fit between observed and predicted results is excellent, (except phases B & C, discussed below). This is true of both the transient predictions and the equilibrium prediction. For some phases (e.g. D or J), the fit for the transient response is almost perfect, but for most phases (E,F,G,H,L and M) the observed behaviour is somewhat flatter than the predicted response. Mathematically, this is attributable to the use of:

$$DV_{fg}/Dt = E^*(V_2-V_{fg}) \qquad (5.25a)$$

instead of:

$$DV_{fg}/Dt = (V_2-V_{fg})/(t+A) \qquad (5.24)$$

Equation 5.25a tends to overpredict the rate of change of free gas volume at longer times, as discussed at the end of Section 5.6.

(b) Physically, there is no reason to expect that $DV_{fg}/Dt = f(t)$ unless some additional process is functioning besides those of gas sorption and bubble nucleation in the pore space. It is postulated that the inclusion of t in (5.24), which produces a better fit to the psuedo-drained test results than (5.25a), is due to diffusion of gas through the sample membrane.

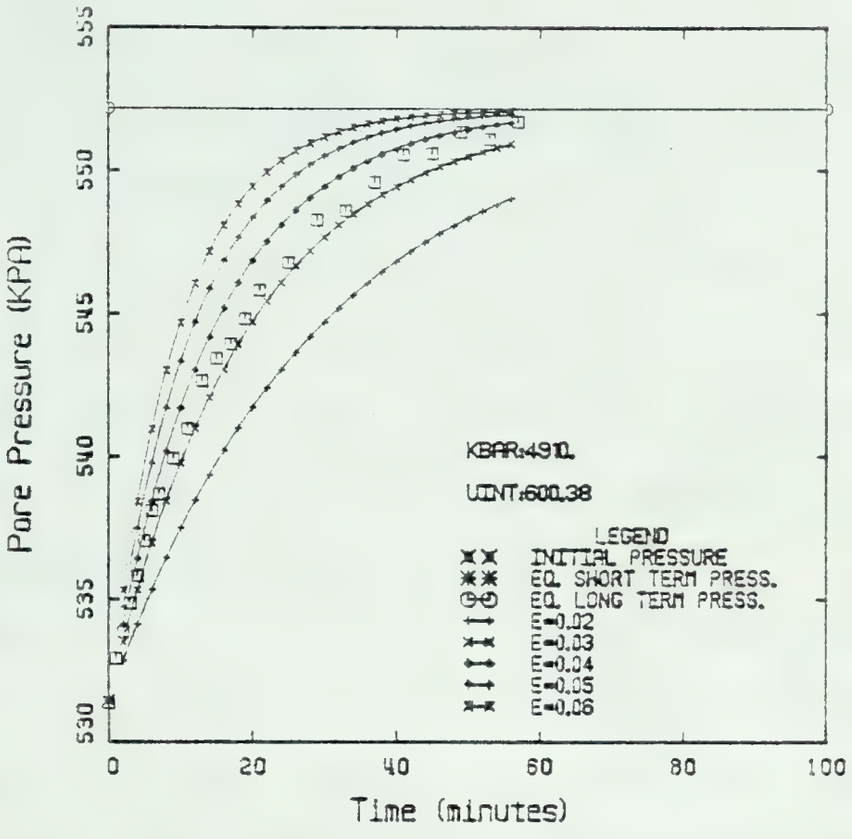
Thus, the tendency of the observed sample response to become flatter than the predicted response in the undrained tests is also attributed to this cause. It is also suggested that equation 5.25a is the more fundamentally correct expression for the "true" gas exsolution response.

(c) The predicted curves for the transient response become asymptotic after a long time to the predicted equilibrium pressure, indicating that the transient solution is converging properly. For the one analysis where this was not the case (phase L) the discrepancy (or poor convergence) was found to be due to an overly large time step.

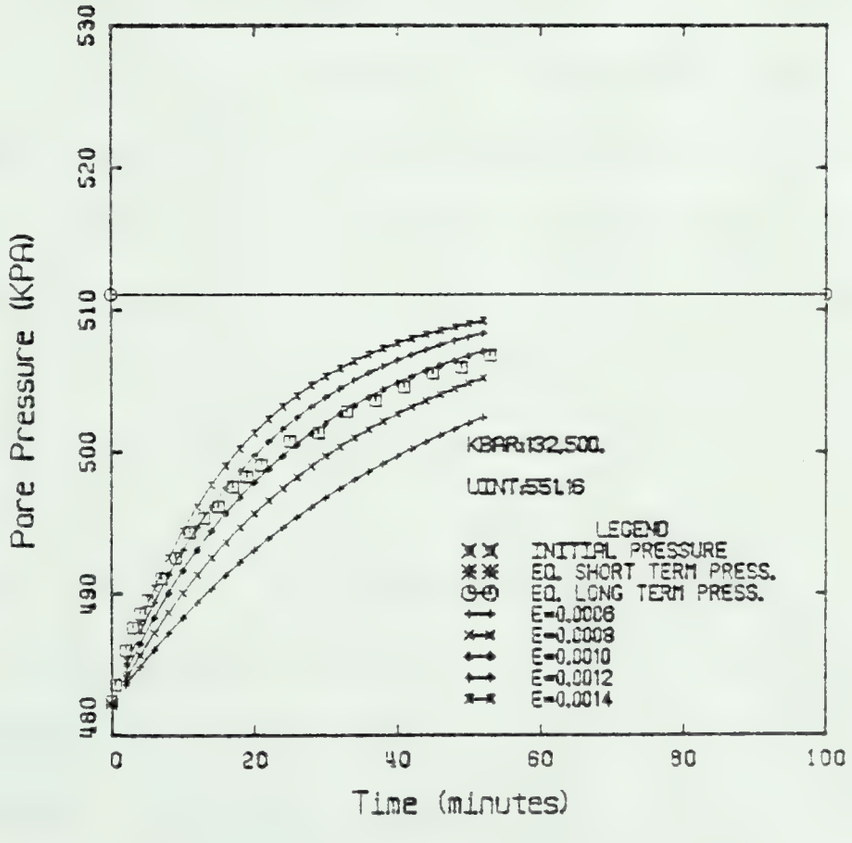
(d) As discussed in Section 3.7, B-tests performed before the commencement of phase A, and then at the beginning of phase B of Test 11 indicated that the initial saturations were actually 99.75 and 99.5% respectively. The assumption, in this analysis, of S=100% at the start of phase A, and of S=99.92% at the start of phase B, caused the initial pore pressures for phases B and C to be markedly under-predicted, (Figures 6.2 and 6.3). As the sample saturation decreased, this effect of an initial error in S became less noticeable (e.g. phases D onward). Since the predicted value of P_i was so low in phases B and C, the transient analysis also produced a poor fit to the laboratory data.

Analyses for phases B & C were rerun using S_i = 99.5% and the results are illustrated in Figures 6.12 and 6.13. The fit between observed and predicted behaviour is remarkably improved. This underlines the importance of correctly determining the initial saturation, and hence the value of P_i for the transient analysis, without which the agreement between theoretical and actual behaviour will be poor.

(e) A preliminary comment will be made here regarding the predicted behaviour in phase L of the test. Phase L represents a reloading of the sample from a condition of $\sigma'=0$. A psuedo-drained unloading test had been performed in the preceeding phase (J). The behaviour of the sample was very difficult to model at the beginning of phase L, since it was uncertain what the effective stress actually was. Using a linear e vs log σ' relationship, and the known volume of gas in the sample, an equivalent initial void ratio was calculated, and hence an initial, small value of σ'. The theoretical model predicted the response shown. The unusual characteristic of this response is the flat initial portion of the P vs t curve, due to the large volumes of free gas present at the beginning of the phase. It is significant that the actual P vs t response shows no such distinctive behaviour. This will be discussed further at the end of this section.



UNDRAINED ANALYSIS, TEST NO. 11B



UNDRAINED ANALYSIS, TEST NO. 11C

Figures 6.12 and 6.13

(f) It might also be noted that the agreement between predicted and measured volumetric strains in the sample was excellent. A comparison of the two is somewhat artificial, however, as the measured volumetric response of the soil sample has been input to the theoretical analysis via the soil compressibility β_T. Thus no presentation of these results is made here.

6.4.1 An Evaluation of Henry's constant

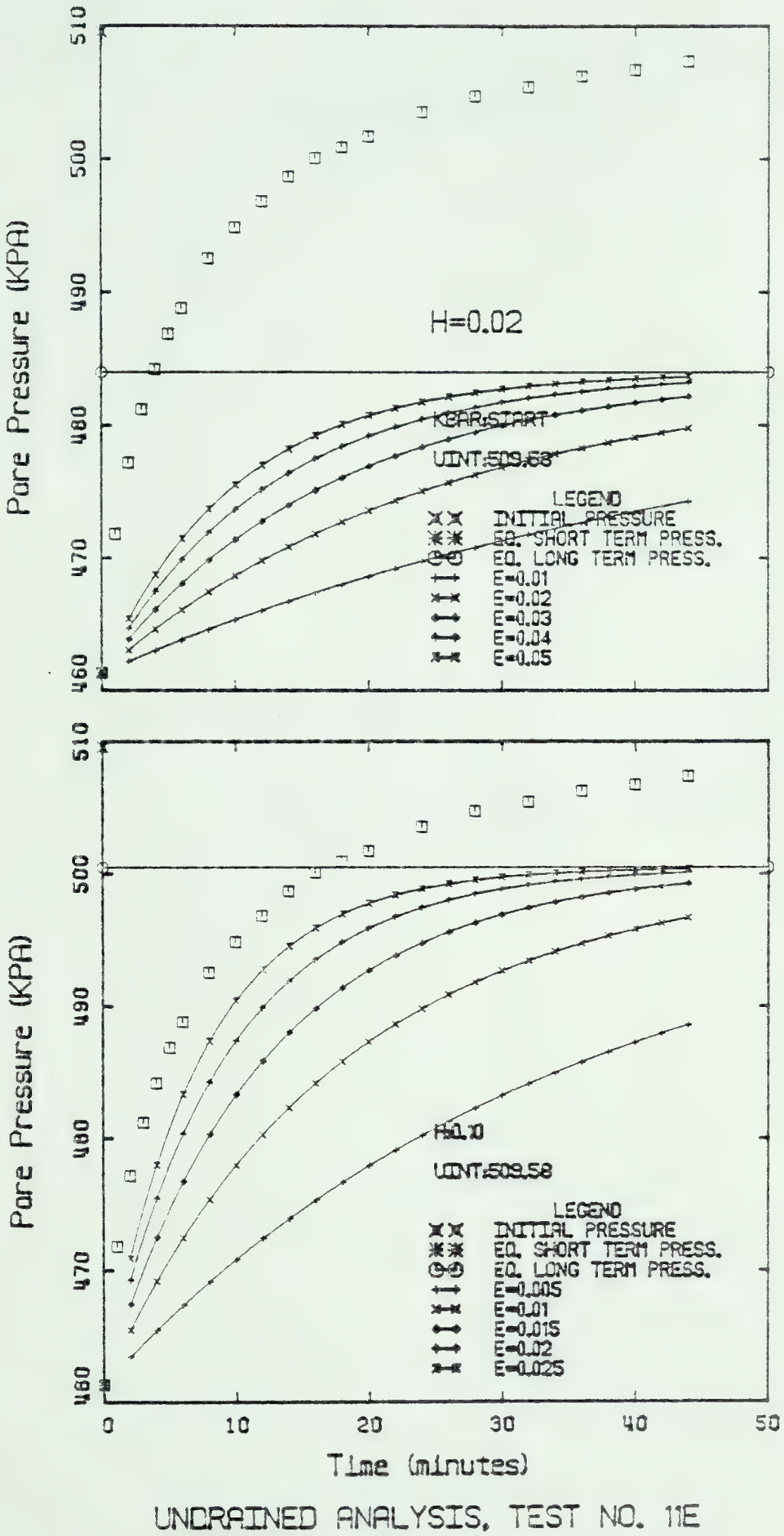
Having fully developed the analytical tools to assess the laboratory tests, it is appropriate here to investigate the manner in which Henry's constant for gas solubility influences the theoretical predictions. Up until this point, a tacit assumption has been made that the solubility of a gas in the pore liquid is equivalent to the solubility of the same gas in the pure solvent, at the same temperature. Thus it has been assumed that the existence of a particle matrix has not affected the solubility of the gas. This may be a reasonable assumption for relatively coarse-grained soils composed of chemically inert particles, but will not necessarily be true of finer-grained or more chemically active soils.

The analysis for phase E of Test No. 11 was rerun several times, using an initial saturation (99.03%) which would accurately predict its initial pressure response, and using several different values of H ranging from 0.02 (the

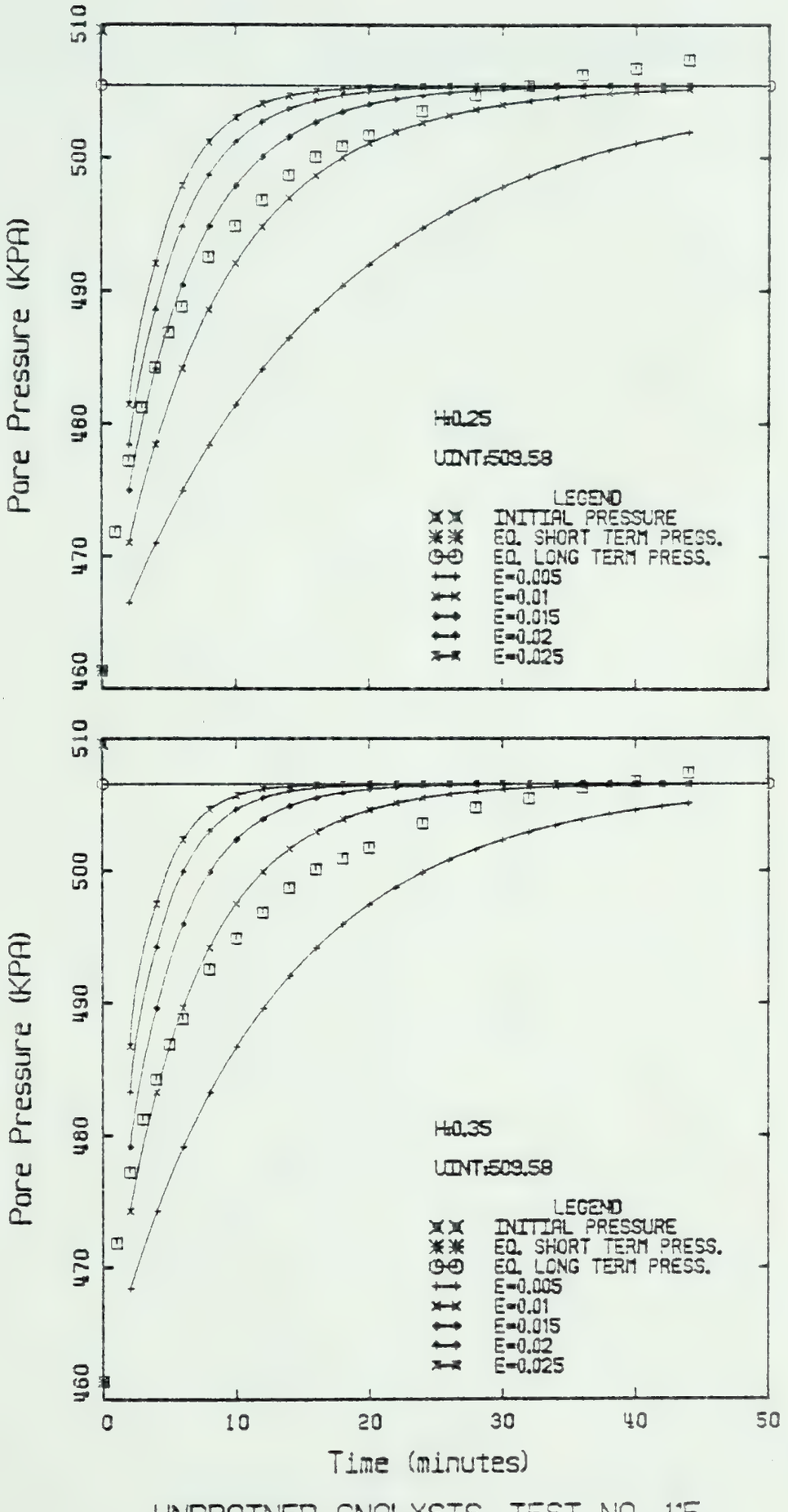
value for air in water) to 0.68, (the value for CO_2 in water, 0.86, was presented in Figure 6.5). The results are summarized in Figures 6.14 to 6.19.

It is obvious that the assumed value for H has an extreme influence on the magnitude of both the equilibrium pressure and the transient response. For this particular phase, judging by these criteria, an $H < 0.5$ would be unacceptable. Although the curves for $H = 0.5$ give a reasonable fit to the transient data at shorter times, they underpredict the equilibrium pressure. This value of H is also of questionable acceptability. It was this difference in response that allowed a differentiation between an air-saturated pore fluid (phase B) and a CO_2-saturated pore fluid (phase C).

The value of H used in the analysis also has a significant influence on the "best-fit" value of E. Consider Figure 6.20, which is a plot for an analysis of Test No. 11, Phase C, using $H = 0.02$. As discussed above, the use of $H = 0.02$ for phase C, which involved CO_2 exsolution, will seriously underestimate the equilibrium pressure. However, the predicted equilibrium pressure can be forced to match the observed value by increasing the supersaturation at the beginning of the phase through the input parameter K′, (KBAR on Figure 6.20). Given the initial conditions of phase 11C and assuming equilibrium, for air as the pore gas, K′ = 3055 KPa-cc. K′ must be increased to 4410 KPa-cc to force a fit on the observed data. When this is done, however, the

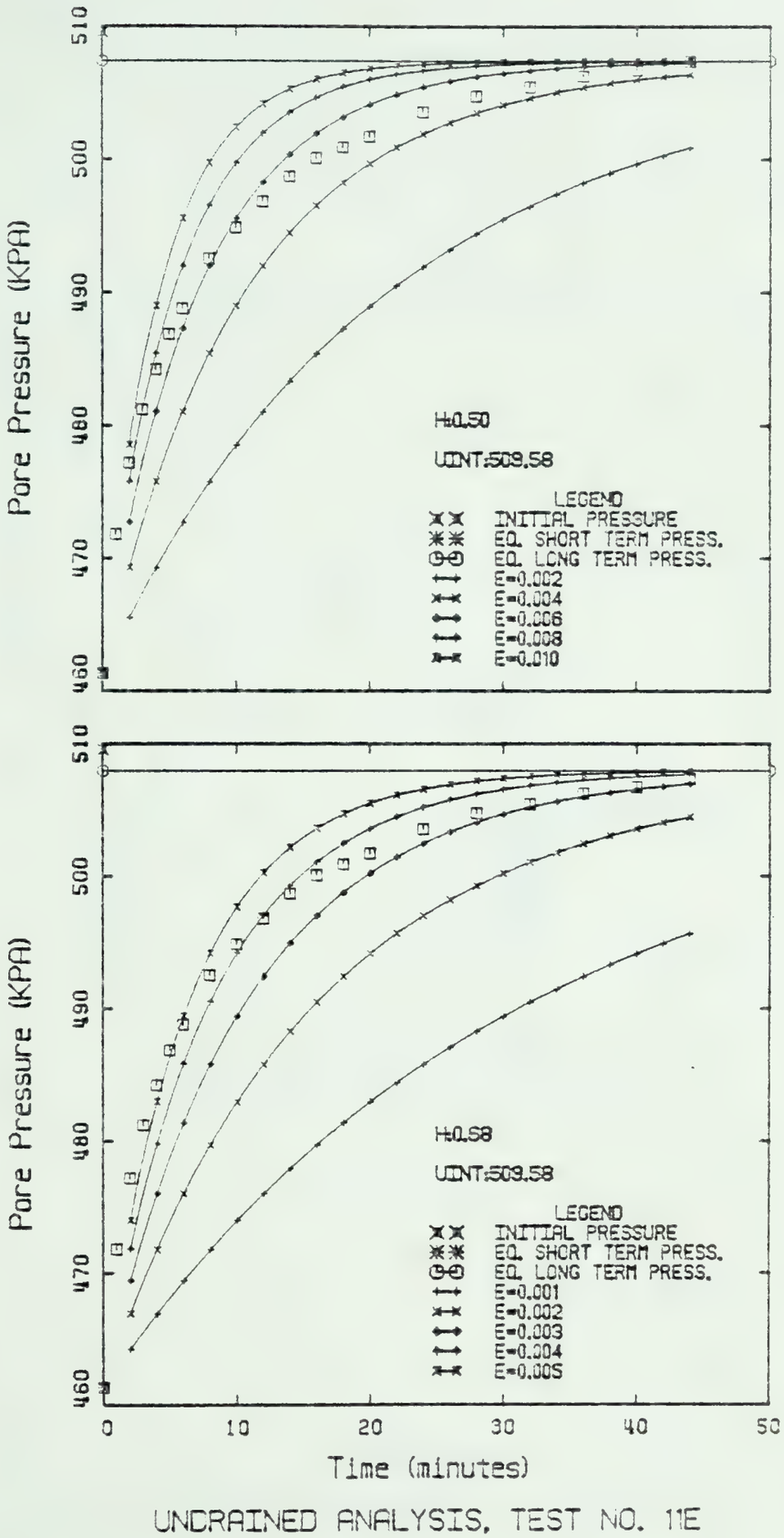


Figures 6.14 and 6.15

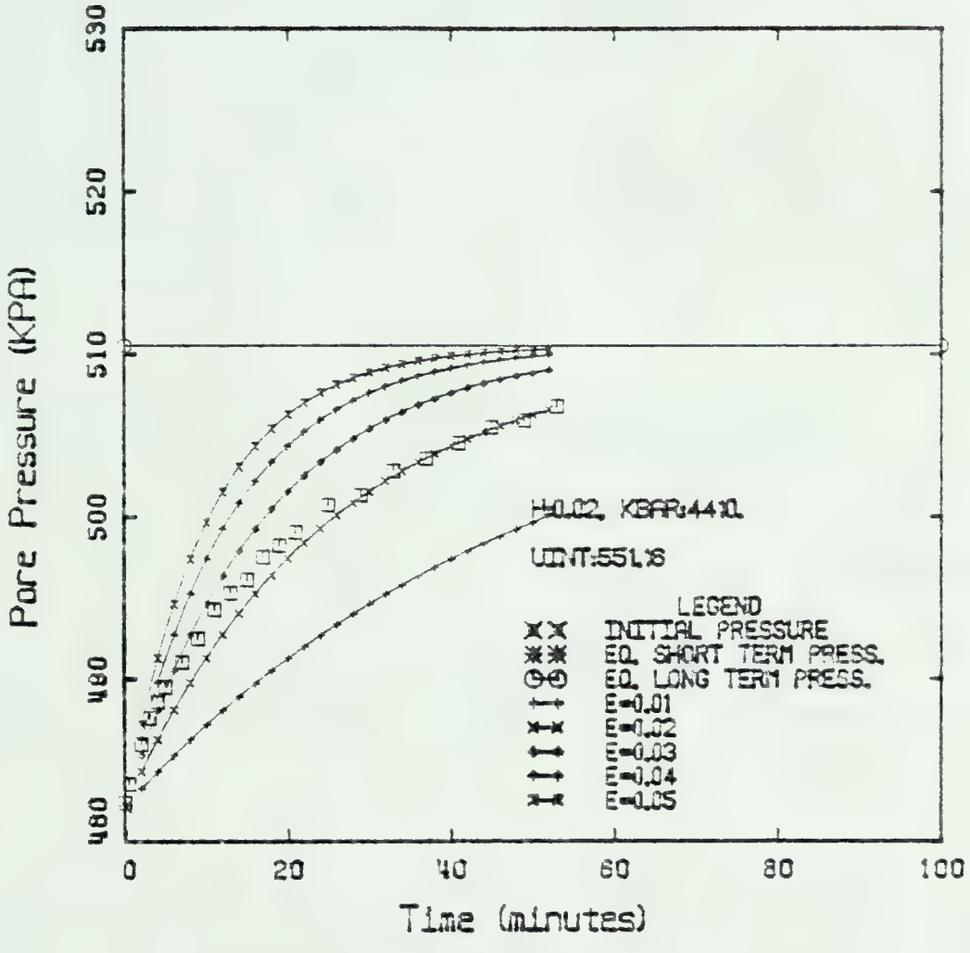


UNDRAINED ANALYSIS, TEST NO. 11E

Figures 6.16 and 6.17



Figures 6.18 and 6.19



UNDRAINED ANALYSIS, TEST NO. 11C

Figure 6.20

"best-fit" value of E for phase C is increased from 0.001 to approximately 0.025. If E is akin to k, the diffusivity of gas in a liquid, then this dependence of E on H can be easily rationalized. If a lower value of H is input in the analytical model, then a higher value of E must be necessary to match the same observed behaviour. In other words, the diffusion process has to occur more quickly to transfer the same amount of gas from the dissolved to the free state, because the gas must be brought to the bubble from a greater distance in the liquid.

6.4.2 Variation of E with initial saturation

It is clear from a survey of Figure 6.12 and Figures 6.4 to 6.11 that the gas exsolution "constant", E, is actually a function of initial gas saturation. The value of E ranges from 0.0012 (phase C) to approximately 0.02 (phase J). The larger values of E towards the end of the test indicate a quicker transient response. This was initially noted in Section 4.5, where an assessment of the transient behaviour was made purely on an empirical basis.

The "best-fit" values of the parameter E for all the isotropic and constant K tests are summarized in Table 6.1 and plotted in Figure 6.21. These were obtained by visual inspection of the plots, similar to those in Figures 6.2 to 6.9, for tests 7, 9, 11, 23, 12, 15, 21 and 22. The variation in E with gas saturation is remarkably consistent in all tests, except Test No. 9, where some problems with

TABLE 6.1 - SUMMARY OF THE GAS EXSOLUTION PARAMETER E FOR ALL TESTS

TEST → / PHASE ↓	7	9	11	23	12	15	21	22
	INITIAL GAS SATURATION (1-S) (*1) AND GAS EXSOLUTION PARAMETER E (*2)							
A							.0006 (0)	.0008 (0)
B							.001 (.03)	.001 (.07)
C	.001 (.07)		.0012 (.22)*2	.0008 (.09)	.0005 (.05)		.002 (.24)	.002 (.33)
D	.0015 (.28)		.002 (.38)	.0015 (.30)	.0012 (.17)	.0006 (0)	.003 (.59)	.003 (.68)
E	.003 (.61)		.003 (.64)	.003 (.71)	.002 (.36)	(.001) (.05)		
F	.005 (1.12)		.004 (.82)	.004 (.83)	.003 (.59)	.002 (.18)		
G		.0002 (.59)	.007 (1.13)		.004-.005 (.88)	.008 (.41)		
H		.0003 (.90)	.01 (1.48)					
I		.001 (1.30)	.02 (1.85)					
J		.003 (1.99)						
K		.02-.03 (6.0)						
L								
M								

FOOTNOTES

*1 INITIAL SATURATIONS ARE SHOWN IN PARENTHESES. (AS A%).

*2 S_i ADJUSTED TO PROVIDE BETTER MATCH FOR P_i.

*3 MORE WEIGHT WAS PLACED ON THE INITIAL RESPONSE IN DETERMINING THESE VALUES.

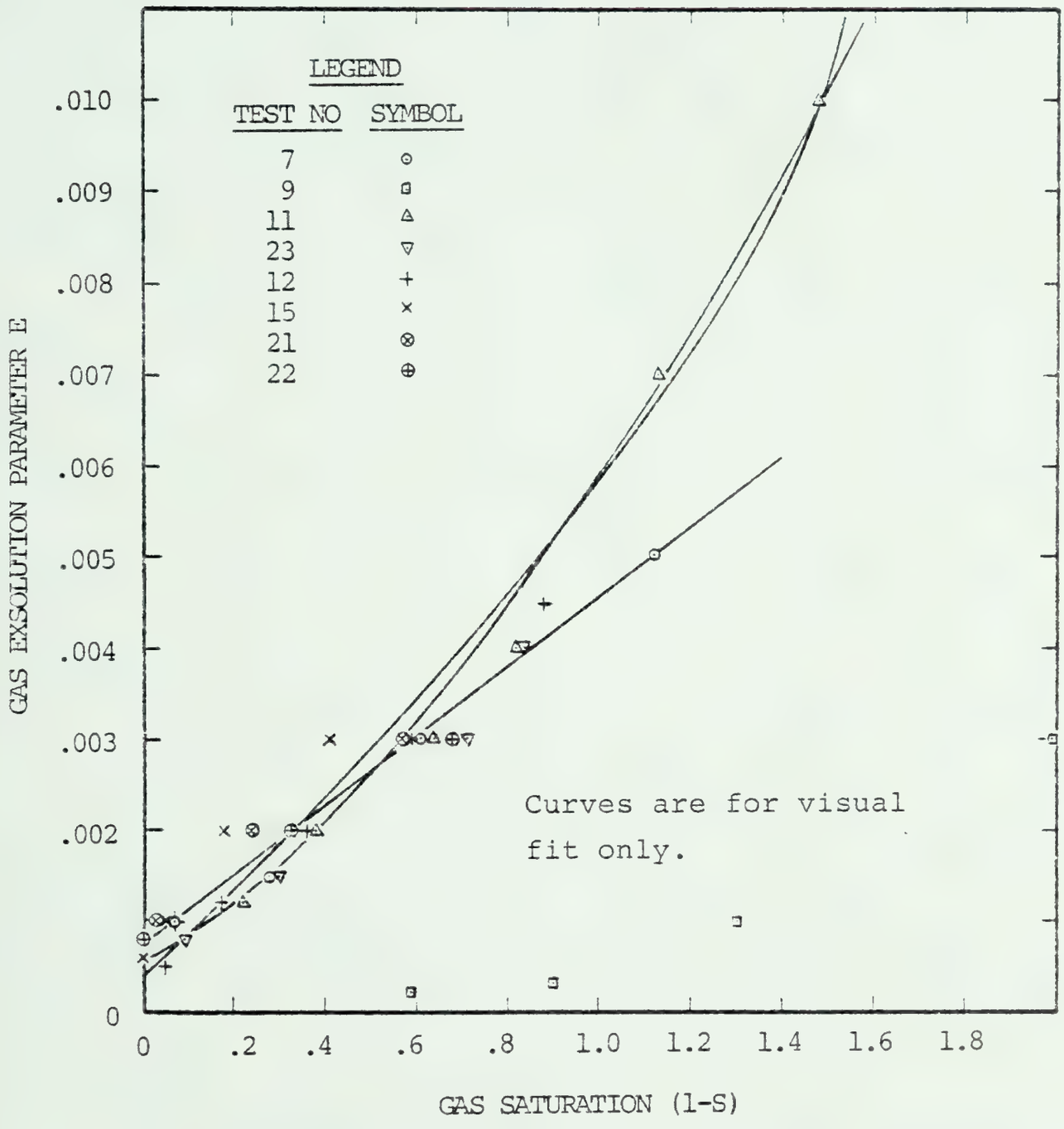


Figure 6.21 - Variation of E with Gas saturation

leakage of gas from the sample were encountered during the early stages of the test. At lower gas saturations (S_g < 1%) the E vs S_g relationship appears to be linear, but with the inclusion of data from the last three phases of Test No. 11, plus the psuedo-drained test results, it is clear that the relationship is non-linear, and that at higher gas saturations the exsolution process is even faster than would be expected from the linear relationship.

A discussion of gas exsolution was presented in Chapter 5, with mention of the two microscopic processes that are thought to dominate the behaviour, gas sorption and bubble nucleation. It is hypothesized that the increase of E with S_g is due to an increased number of bubbles in the soil sample, leading to both an increased surface area of liquid/gas contact, and to a decreased length of diffusion path. Both of these changes will increase the observable rate at which gas is produced in the soil. If such is the case, this functional relationship between E and S_g should be more pronounced upon unloading, where both bubble nucleation and growth are operative, than upon loading, where only bubble shrinkage, (aided by bubble extinction, eventually), is important.

The dependence of E on S_g may also provide some explanation for the behaviour noted in Figure 6.10 (Test 11, Phase L). The predicted pressure-time response for reloading shows an initial flat portion to the curve, indicative of the time necessary to dissolve a large volume of free gas. The

model, however, assumes an E which is constant with gas saturation. Since for this phase of the test there is a large reduction in S_g, there should also be a reduction in E, which would tend to remove the flat portion of the predicted response.

In fact, this change in E with S_g is operative during all phases of the various tests, so that an assumption of constant E is only an approximation. For phases where u is relatively high and the absolute value as well as the change in S_g is small, the approximation is reasonable. Where u is low, and S_g and S_g high, such as in Phase L of Test 11, the model is not as good at predicting the actual pressure-response.

6.5 SUMMARY

In this chapter, the empirical relationship between volume rate of free gas production and gas solubility imbalance for the drained element of soil has been incorporated in an approximate manner into a finite difference model for pressure change vs time in an undrained soil element. The laboratory test results have been reanalyzed using this model, and the model has shown excellent predictive capabilities. A minor discrepancy between observed and predicted values at longer times (the latter half of each phase of the test) is attributable to the form of the empirical relationship:

$$DV_{fg}/Dt = E * (V_2 - V_{fg}) \qquad (5.25a)$$

which was used instead of the more "accurate" equation:

$$DV_{fg}/Dt = (V_2 - V_{fg})/(t+A) \qquad (5.24)$$

The choice of equation 5.25a over equation 5.24 was made for analytical reasons, but it is felt that equation 5.25a is actually more representative of the true gas exsolution response. Equation 5.24 is more accurate at predicting the laboratory results because it is capable of accounting for diffusive gas losses from the sample.

The transient solution was found to converge on the theoretical equilibrium solution as t approached infinity, as long as small time steps were used.

The analysis of the undrained test results also revealed a relationship between E and S_g, which is thought to be due to the nucleation of a large number of bubbles in the soil element as gas exsolution progresses.

CHAPTER 7 - A COMBINED, GENERAL THEORY OF CONSOLIDATION AND GAS EXSOLUTION

7.1 INTRODUCTION

Pore pressures in soil that are time-dependent, or transient, have traditionally been recognized as due to consolidation. Consolidation is that process by which the support for an external load is transferred from the pore fluid to the soil skeleton. Pore pressures are normally reduced and effective stresses increased as the water drains from the soil mass and the volume of the soil decreases. The form of the pressure-time response is governed by the initial pore pressure distribution in the soil and the pressure or flow boundary conditions.

With the recognition of gas exsolution as another process that causes a transient pore pressure response in the soil, and with an ability to model this process, it is of interest to attempt to combine gas exsolution and consolidation in one general theory. This is particularly so when one recognizes that for most problems of geotechnical interest, these processes work to oppose each other. For example, consider any problem where a soil mass is unloaded, such as in excavating a foundation or a slope, or tunnelling in a soil mass. Because the insitu total stresses are

reduced, the undrained and immediate response[1] of a gassy soil is to cause a reduction in pore pressure. Subsequent pressure boundary conditions usually cause a further reduction in pore pressure due to consolidation, whereas, if the initial undrained response is to decrease P below $P_{l/g}$, then the tendency of gas exsolution is to cause an increase in pore pressure. At infinite time, the pressure boundary conditions must prevail, but the interim pressure response may prove to be quite unexpected, particularly if the gas exsolution process occurs more quickly than the consolidation process.

One must recognize that in those problems where gas exsolution and consolidation are acting as opposing processes, there is a limitation in the choice of a model of soil behaviour. In weighing the relative contributions of each process, the theory must consider an increase in σ', (and decrease in volume), in one case and a decrease in σ', (and increase in volume), in the other, so that the only method whereby the two can be combined is by using an elastic stress-strain model. The model need not be linear, but for simplicity the linear case will be considered here. As will be seen, the governing differential equation for the combined consolidation/gas exsolution theory is non-linear, and must be solved by numerical techniques, so that the use of a

---

[1]Recall that in talking of a gassy soil both of these terms are necessary. One does not imply the other.

non-linear stress-strain relationship should not prove to be an additional burden.

7.2 A GENERAL THEORY

In his excellent text "Principles of Soil Mechanics", R. F. Scott (1963) presented a very thorough development of the theory of consolidation, outlining clearly the assumptions and simplifications that are made in arriving at the classical one-dimensional consolidation equation:

$$c_v * D^2u/Dx^2 = Du/Dt \qquad (7.1)$$

Scott considered the effect of a Boyle's law expansion or contraction of gas, and of an immediate exsolution of gas, on the compressibility of the pore fluid. He found that the former introduced a non-linearity into the consolidation equation. In developing the theory further, these two effects were lumped together into one linear term, and given relatively little attention.

Scott's (1963) development will be followed here, except that the full, transient process of gas exsolution will be introduced into the theory, and the differential equation will be left in its non-linear form.

Continuity considerations

Consider a rectangular element of soil with sides of length dx, dy and dz. The continuity equation for this soil element states that the rate of change of water storage in the element, (i.e. of the weight of water in the element, W), is equal to the net flux of water flowing into or out of the element:

$$dW/dt = [D/Dx(\gamma_w * v_x) + D/Dy(\gamma_w * v_y) + D/Dz(\gamma_w * v_z)]dxdydz \quad (7.2a)$$

Substituting Darcy's law relating velocity to total head,

$$v_x = -K_x * Dh/Dx \quad \text{(etc.)} \quad (7.3)$$

into (7.2a), one obtains:

$$Dw/Dt = [D/Dx(\gamma_w * K_x * Dh/Dx) + D/Dy(\gamma_w * K_y * Dh/Dy) + D/Dz(\gamma_w * K_z * Dh/Dz)]dxdydz \quad (7.2b)$$

If the free gas in the pore space is assumed to be occluded and immobile, so that it does not form a part of the flowing fluid, and if the soil mass is homogeneous with respect to K_i, then:

$$DW/Dt = \gamma_w * [K_x * D^2h/Dx^2 + K_y * D^2h/Dy^2 + K_z * D^2h/Dz^2]\ dx\ dy\ dz \quad (7.2c)$$

If the body is isotropic with respect to K, then

$$DW/Dt = \gamma_w * K * (D^2h/Dx^2 + D^2h/Dy^2 + D^2h/Dz^2)\ dx\ dy\ dz \qquad (7.2d)$$

The equation will be developed for the case of a shaft or borehole (z-axis vertical) with a hydrostatic vertical distribution of pressure, so that $Dh/Dz = 0$, and, using cylindrical coordinates,[2]

$$DW/Dt = \gamma_w * K * (D^2h/Dr^2 + 1/r * Dh/Dr) dr d\theta dz \qquad (7.2e)$$

Substituting for $h = h_e + u/\gamma_w$, $Dh/Du = Dh/DP = 1/\gamma_w$,

$$DW/Dt = K * (D^2P/Dr^2 + 1/r * DP/Dr)\ dr\ d\theta\ dz \qquad (7.2f)$$

Rate of change of water storage

Consider now how the weight of water in an elemental volume of soil may vary in time:

$$DW/Dt = W_s * Dw/Dt = W_s * D/Dt(S*e*\gamma_w/\gamma_s)$$
$$= V_s * D/Dt(S*e*\gamma_w) \qquad (7.4a)$$

(assuming the soil grains are incompressible)

---

[2]This equation, which implies only radial flow, is only an approximation for a shaft or borehole in a gassy soil. This will be discussed further in Chapter 8.

The partial differentials of void ratio, density of water, and saturation with respect to time may be determined by considering the compressibilities of the soil skeleton, the liquid phase and the gaseous phase respectively. These terms are developed below.

Void ratio

Using a linear elastic constitutive relationship for the soil,

$$De/Dt = -a_v * D\sigma'/Dt \qquad (7.5a)$$

and for the case where $\Delta\sigma_T = 0$,

$$De/Dt = a_v * Du/Dt = a_v * Dp/Dt \qquad (7.5b)$$

Pore liquid

From equation 2.8,

$$\beta_l = -1/V_l * dV_l/dP$$

so that

$$\gamma_w = \gamma_{w0} * (1 + \beta_w * P) \qquad (7.6a)$$

$$D\gamma_w/Dt = \gamma_{w0} * \beta_w * DP/Dt \qquad (7.6b)$$

Pore gas

The term DS/Dt, evaluated at constant e and γ_w, may be derived from:

$$(DS/Dt)_{e,\gamma w} = 1/V_v * DV_w/Dt \qquad (7.7a)$$

For constant e and γ_w, the only way that the volume of water in the voids can change is if the free gas either compresses or goes into solution. Thus:

$$(DS/Dt)_{e,\gamma w} = -1/V_v * DV_{fg}/Dt \qquad (7.7b)$$

where DV_{fg}/Dt is composed of two terms,

$$DV_{fg}/Dt = (DV_{fg}/Dt)_{compress.} + (DV_{fg}/Dt)_{exsol.}$$

This is the same relationship as given in equation 6.3, but in the exact (rather than finite difference) form:

$$DV_{fg}/Dt = -V_{fg}/P * DP/Dt + E^*(V_2-V_{fg}) \qquad (6.3b)$$

so that

$$(DS/Dt)_{e,\gamma w} = (1-S)/P * DP/Dt - E^*(V_2-V_{fg})/V_v \qquad (7.7c)$$

The advantage of modelling the gas exsolution process with the fully drained (σ, u, σ' all constant, and thus e = constant) boundary condition instead of the undrained boundary condition is now obvious, as equation 5.25a can be

used directly in formulating the general consolidation/gas exsolution theory. As has been discussed in section 6.2.1, equation 6.3 is only approximate in its finite difference form, but becomes exact in the limit as Δt approaches 0.

Equation for rate of change of water storage

Combining equations 7.5b, 7.6b and 7.7c, 7.4a becomes:

$$DW/Dt = V_s*(S*\gamma_w*De/Dt + S*e*D\gamma_w/Dt + e*\gamma_w*DS/Dt) \quad (7.4b)$$

$$= V_s*(S*\gamma_w*a_v*DP/Dt + S*e*\gamma_{w0}*\beta_w*DP/Dt + e*\gamma_w*\{[1-S]/P * DP/Dt - E*[V_2-V_{fg}]/V_v\}) \quad (7.4c)$$

$$= V_s*\gamma_w*(DP/Dt*\{e*[(1-S)/P+S*\beta_w]+S*a_v\} - e*E*[V_2-V_{fg}]/V_v) \quad (7.4d)$$

Combined equation for consolidation and gas exsolution

Recognizing that:

$$V_s = V_T/(1+e) = drd\theta dz/(1+e) \quad (7.8)$$

equations 7.4d and 7.2f may be combined to give:

$$K*(D^2P/Dr^2 + 1/r*DP/Dr) = \gamma_w/(1+e) * \{DP/Dt[e*((1-S)/P + S*\beta_w) + S*a_v] - e*E*(V_2-V_{fg})/V_v\} \quad (7.9a)$$

or

$$D/Dr(r*DP/Dr) + r*\gamma_w*e*E/K/(1+e) * (V_2-V_{fg})/V_v = r*\gamma_w/K/(1+e) * \{e*((1-S)/P+S*\beta_w)+S*a_v\} * DP/Dt \quad (7.9b)$$

This is the general one-dimensional consolidation/gas exsolution equation for a shaft or borehole in a gassy soil. The equation is non-linear because of the 1/P multiplier in the DP/Dt term (RHS). It is referred to as being quasi-linear because the differential terms P_r, P_{rr} and P_t occur only to the first power and are not multiplied together. The equation is parabolic, and in (7.9b) has been written in self-adjoint form.

It is clear that equation 7.9b is considerably more complex than (7.1). Because of its non-linear nature, solutions for different boundary conditions are not superposable. In general, there will be no exact solution to (7.9b), and so a technique for numerical solution will be presented in the following section.

7.3 NUMERICAL SOLUTION

Ames (1965) discusses numerical methods for solving partial differential equations, and in particular, presents an implicit finite difference solution to a second-order quasi-linear partial differential equation in self-adjoint form. For an equation of the form:

$$D/Dr(f[r,t]*DP/Dr) + q[r,t,P] = s[r,t,P]*DP/Dt \quad (7.10a)$$

and defining a finite difference mesh with $h = \Delta r$, $k = \Delta t$, $r_i = r_0 + i*h$ and $t_j = j*k$, an implicit finite difference equation is:

$$1/h^2 * \{f[r_0+(i+1/2)*h,(j+1)*k]*(P_{i+1,j+1}-P_{i,j+1}) - f[r_0+(i-1/2)*h,(j+1)*k]*(P_{i,j+1}-P_{i-1,j+1})\}+ q[r_0+i*h,(j+1)*k,P_{i,j}] = s[r_0+i*h,(j+1)*k,P_{i,j}]*(P_{i,j+1}-P_{i,j})/k \qquad (7.10b)$$

Since (7.10b) contains $P_{i,j+1}$ only linearly, the algebraic problem is linear and produces a tridiagonal matrix at each time-step. Convergence of (7.10b) to that of (7.10a) has been proven for boundary value problems, (Ames, 1965). The error is $O[h^2 + k]$ and <u>no restrictions on k/h^2 occur</u>.

If equation 7.9b is rewritten as:

$$D/Dr(r*DP/Dr) + B*r = (F + D/P)*r*DP/Dt \qquad (7.9c)$$

where:

$$B = e*E*\gamma_w/K/(1+e) * (V_2-V_{fg})/V_v$$

$$F = S*\gamma_w/K/(1+e) * (e*\beta_w + a_v)$$

$$D = e*\gamma_w/K/(1+e) * (1-S)$$

then (7.10b) becomes:

$$(r_0/h+i-1/2)*P_{i-1,j+1} - (r_0/h+i)*(2+h^2/k*[F+D/P_{i,j}])*P_{i,j+1} + (r_0/h+i+1/2)*P_{i+1,j+1} = -h^2*(r_0/h+i)*(F*P_{i,j}/k + B + D/k) \qquad (7.10c)$$

The matrix form of this equation is given below for a four-point finite-difference mesh to illustrate its tridiagonal characteristic.

$$\begin{bmatrix} -\left(1+\frac{r_o}{h}\right) & \frac{r_o}{h}+\frac{3}{2} & & \\ *A_1 & & & \\ \frac{r_o}{h}+\frac{3}{2} & -\left(2+\frac{r_o}{h}\right) & \frac{r_o}{h}+\frac{5}{2} & \\ & *A_2 & & \\ & \frac{r_o}{h}+\frac{5}{2} & -\left(3+\frac{r_o}{h}\right) & \frac{r_o}{h}+\frac{7}{2} \\ & & *A_3 & \\ & & \frac{r_o}{h}+\frac{7}{2} & -\left(4+\frac{r_o}{h}\right) \\ & & & *A_4 \end{bmatrix} \begin{bmatrix} P_{1,j+1} \\ P_{2,j+1} \\ P_{3,j+1} \\ P_{4,j+1} \end{bmatrix} = -h^2 \begin{bmatrix} \left(1+\frac{r_o}{h}\right) C_1 \\ \left(2+\frac{r_o}{h}\right) C_2 \\ \left(3+\frac{r_o}{h}\right) C_3 \\ \left(4+\frac{r_o}{h}\right) C_4 \end{bmatrix} - \begin{bmatrix} \left(\frac{r_o}{h}+\frac{1}{2}\right) * P_{0,j+1} \\ 0 \\ 0 \\ \left(\frac{r_o}{h}+\frac{9}{2}\right) * P_{5,j+1} \end{bmatrix}$$

(7.10d)

where $A_i = (2+h\hat{}2/k*[F+D/P_{i,j}])$

$C_i = (F*P_{i,j}/k + B + D/k)$

and $P_{0,j+1}$ and $P_{5,j+1}$ are the pressures at the boundaries of the finite difference mesh.

Equation 7.10d can be solved by standard matrix methods, such as Gaussian elimination. However, the tridiagonal form of the square matrix in (7.10d) allows the use of a more efficient method, referred to as the Thomas Algorithm. This is summarized briefly below.

The general tridiagonal system of n equations can be written in the form:

$$
\begin{aligned}
b_1*u_1 \;+\; c_1*u_2 &= d_1 \\
a_i*u_{i-1} \;+\; b_i*u_i \;+\; c_i*u_{i+1} &= d_i \quad , \quad i=2,n-1 \\
a_n*u_{n-1} \;+\; b_n*u_n &= d_n
\end{aligned}
$$

Using Gaussian elimination this system can be transformed into upper bidiagonal form, with $a_i' = 0,(i=2,n)$; and $b_i' = 1,(i=1,n)$; where:

$$c_1' = c_1/b_1 \qquad\qquad d_1' = d_1/b_1$$

$$c_{i+1}' = c_{i+1}/(b_{i+1}-a_{i+1}*c_i')$$

$$d_{i+1}' = (d_{i+1}-a_{i+1}*d_i')/(b_{i+1}-a_{i+1}*c_i') \;;\; i=1,(n-1)$$

$$c_n = 0$$

The n^{th} equation is now $u_n=d_n'$, and working backwards with a substitution:

$$u_i = d_i - c_i'*u_{i+1} \;;\; i=(n-1),1$$

The only restrictions on this method are that $b_1 \neq 0$ and that $b_{i+1}-a_{i+1}*c_i' \neq 0$. If either of these are true, one can solve for u_{i+2} and reduce the size of the system of equations.

7.4 APPLICATION OF THE NUMERICAL SOLUTION

The application of equation 7.10c to determine an approximate solution to a gas exsolution/consolidation problem requires the input of a set of initial conditions (at t=0) on the j=0 row of the finite difference mesh, as well as a knowledge of the pressure (or flow) boundary conditions with time. In equation 7.10d these are specified as the pressures $P_{0,j+1}$ and $P_{5,j+1}$. In general, the initial pressures will be determined either from:

(a) insitu conditions

(b) insitu conditions, modified by a change in boundary total stress.

In case (a) the consolidation/gas exsolution process is initiated by a change in boundary fluid pressure. Case (b) is usually also accompanied by a change in boundary fluid pressure, but the consolidation/gas exsolution process is initiated by a change in insitu fluid pressures, which are responding to a change in boundary total stress. An example with further discussion of case (b) is given in Chapter 8. Case (a) is discussed further in section 7.4.1.

It is the intent of this section to point out several practical considerations in the use of (7.10c). It should be recognized that the input parameters V_w and V_{fg}, (and hence V_2, V_v, e and S), vary with fluid pressure, and thus also in space and with time. Their use as constants over a time

interval Δt is only an approximation. Therefore it is necessary to adjust their values from the beginning of one time step to the next. This is accomplished as follows:

(a) A set of initial conditions is established on the j=0 row using either the input values of V_w and V_{fg}, or those values modified by an undrained and immediate response to a boundary total stress change. The values of V_s, E, K, γ_w, and a_v are kept constant during the analysis. Values of V_2, V_v, e and S may vary spacially along the j=0 row.

(b) The pressures along the j=1 row, (at $t=0+\Delta t$), $P_{i,1}$, are calculated using (7.10c).

(c) $e_{i,1}$ are calculated from:

$$e_{i,1} = a_v*(P_{i,1}-P_{i,0}) + e_{i,0} \qquad (7.5b)$$

and $(V_v)_{i,1} = V_s*(e_{i,1})$

(d) From equation 7.4d :

$$\Delta V_w = \Delta P*\{V_{fg}/P+V_w*(\beta_w+a_v/e)\}-E*\Delta t*(V_2-V_{fg})$$

$$(V_w)_{i,1} = (V_w)_{i,0} + \Delta V_w \qquad (7.11)$$

$$(V_{fg})_{i,1} = (V_v)_{i,1} - (V_w)_{i,1}$$

(e) Having adjusted the values of e, S, V_{fg}, and V_v as input for the next set of calculations using (7.10c), there remains only an adjustment for V_2 in the term "B", (equation 7.9c). V_2 is a measurement of the current amount of free gas that would exist in the sample if equilibrium conditions prevailed, and thus, indirectly, indicates the total volume of gas, both free and dissolved, in the sample. Since over a time interval Δt, the pressure in the sample is changing, so is V_{Tg}. However, water is also draining out of the sample and removing some dissolved gas. The assumption is made that for Δt, the volume of water ΔV_w contains an amount of dissolved gas ΔV_{dg}, where:

$$\Delta V_{dg} = \underline{H} * \Delta V_w \qquad (7.12)$$

and $\underline{H} = (V_{dg}/V_w)$ at the beginning of the time interval. $\underline{H} \neq H$ because the pore fluid is not at equilibrium, (e.g. for a supersaturated pore fluid $\underline{H} > H$).

The total volume of gas in the sample at the end of the time interval Δt will then be:

$$(V_{Tg})_{i,1} = P_{i,0}/P_{i,1} * ([V_{Tg}]_{i,0} + \underline{H} * \Delta V_w) \qquad (7.13)$$

so that:

$$(V_2)_{i,1} = (V_{Tg})_{i,1} - H*(V_w)_{i,1} \qquad (7.14)$$

Using first equations 7.5b and 7.11 to 7.14, the values of e, S, V_{fg}, V_v and V_2 can be adjusted at the beginning of the time interval on the j=1 row, and then equation 7.10c applied to calculate the pressures $P_{i,2}$ at the end of the time interval. This process is repeated for each time step j.

One other modification is necessary during the analysis to account for gas venting upon decreasing pore fluid pressure and increasing saturation. This is accomplished by monitoring the saturation at each finite difference grid point i, for each time step j. When $S_{i,j} <$ 0.85 (or some threshold value) then the terms "B" and "D" in equation 7.10c are set equal to zero, (at that grid point), which essentially reduces (7.10c) to a form equivalent to (7.1), and renders the problem one of liquid drainage only in this zone, with no gas expansion or exsolution.

The analysis described above has been coded for computer, and a listing of this program is found in Appendix H.

7.4.1 Consolidation/gas exsolution around a borehole

The use of the consolidation/gas exsolution model will be demonstrated by analyzing the problem of change in pore pressure with time around a borehole (or shaft) in a gassy soil. The boundary conditions are somewhat artificially imposed, for the sake of simplicity. It will be assumed that a vertical shaft or borehole has been constructed such that

the surrounding stresses are kept within the elastic range and thus no volumetric strains have occurred. Furthermore, it is assumed that the shaft has been built sufficiently quickly that no drainage or gas exsolution occurs during construction.

Then at the beginning of the consolidation/gas exsolution problem, there exists a vertical borehole surrounded by a medium containing a pore fluid at some insitu pore pressure u_i. The borehole is filled with the same fluid to a particular depth, so that at any point on the borehole wall there is a pressure $u_w < u_i$. It is assumed that for a point sufficiently below the free groundwater surface, Dh/Dz = 0 both in the soil and in the borehole, resulting in a purely radial flow, and that also Dh/D = 0, (Figure 7.1).

Insitu conditions are listed in Table 7.1. The finite difference mesh employed is illustrated in Figure 7.2.

The convergence of the finite difference solution (7.10c) to the proper solution for $P_{i,j}$ may be checked against an exact solution for the case of S_0=1, E=H=0. In this case B=D=0 and (7.9c) reduces to:

$$DP/Dt = K*(1+e)/\gamma_w/(e*\beta_w+a_v)*(D^2P/Dr^2+1/r*DP/Dr) \qquad (7.9d)$$

Since $\beta_w << a_v$, (7.9d) may be recognized as (7.1) in cylindrical coordinates. Solutions to this equation for the case of a hollow cylinder (a<r<b) with the boundary conditions:

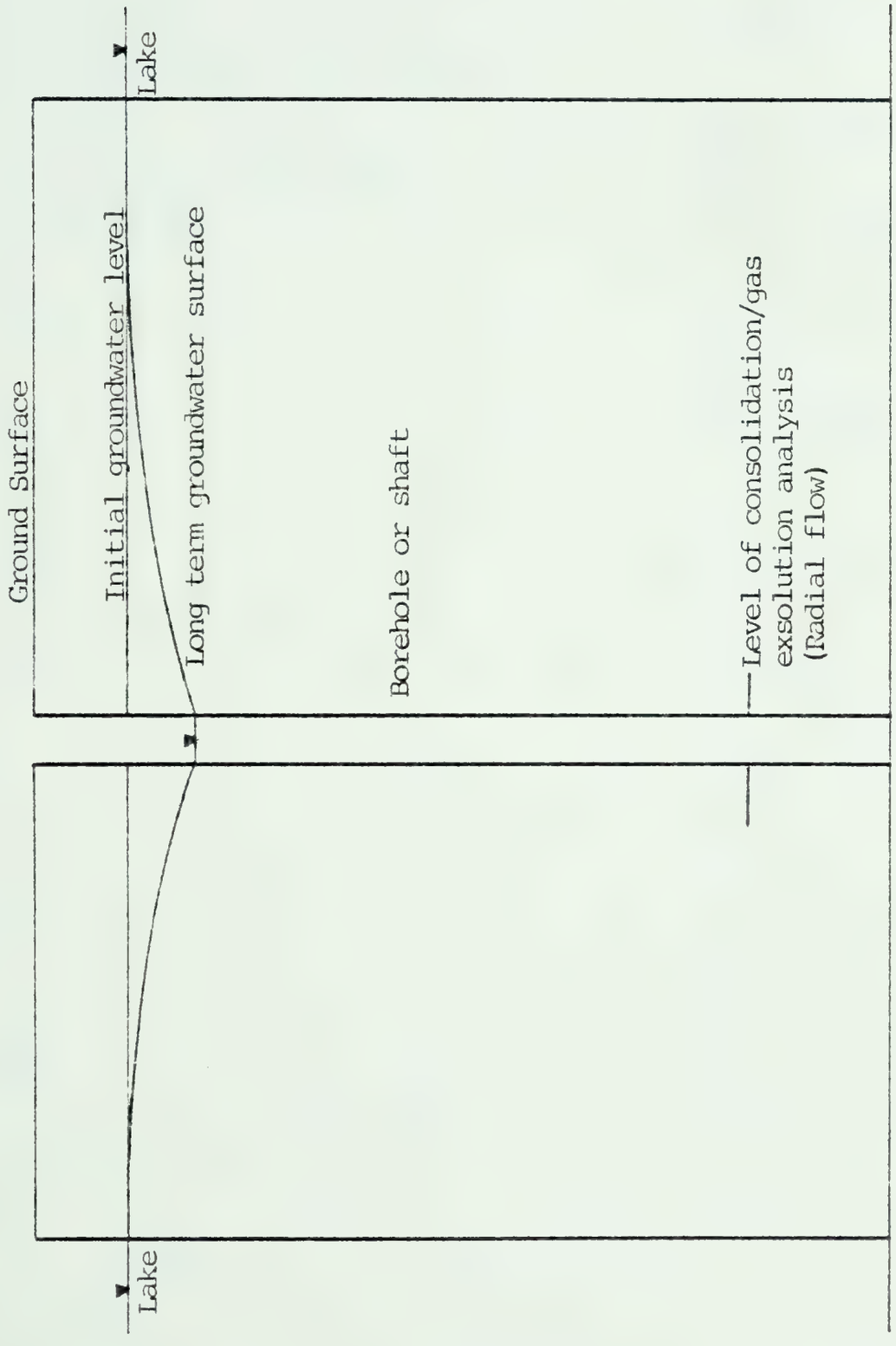


Figure 7.1 - Idealized problem for Consolidation/gas exsolution

TABLE 7.1

INSITU CONDITIONS FOR FINITE DIFFERENCE
ANALYSIS OF CONSOLIDATION/GAS EXSOLUTION PROBLEM

Radius of Borehole	0.1 meters
Radius of Influence of Consolidation/ Gas Exsolution	2.0 meters
Number of Points in F.D. Mesh	191
Time of Analysis	50,000 seconds
Time Step	100 seconds
β_w	4.5E-7 KPa^{-1}
E_{young}	240,000 KPa
μ	0.3
K	10E-10 m/sec.
e_i	0.47
S_i	0.86,0.90,0.95,1.0
E_{gas}	0, 2E-5 $sec.^{-1}$
H	0,0.86
$\sigma_{H1}=\sigma_{H2}$	2000 KPa
U_i	900 KPa
σ_{tunnel}	1500 KPa
U_W	800 KPa
$U_{l/g}$	900 KPa

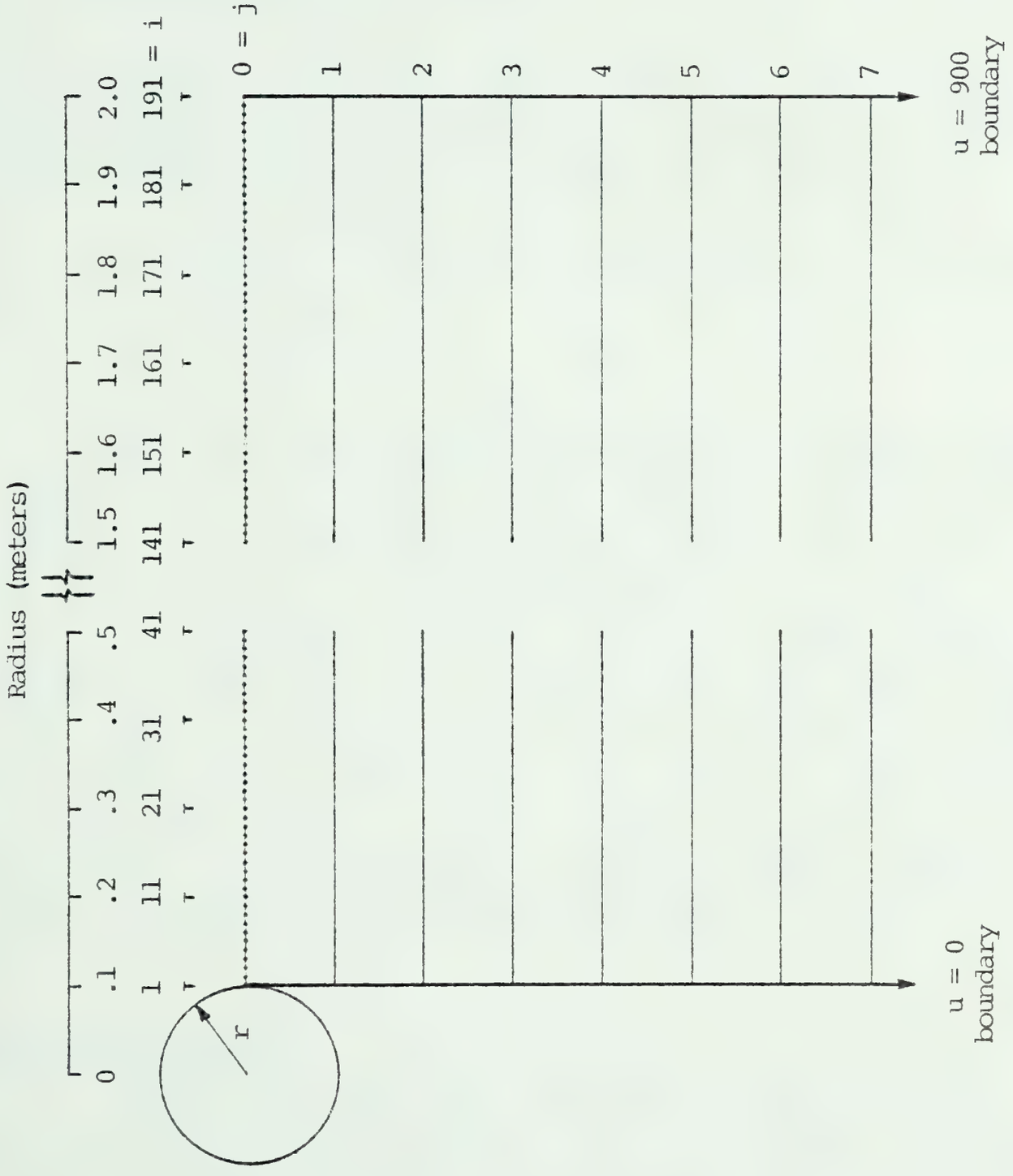


Figure 7.2 - Finite difference mesh for consolidation/gas exsolution

$$P(r,t) = P_1 \quad ; \quad r=a, \; t>0.$$

$$P(r,t) = P_2 \quad ; \quad r=b, \; t>0.$$

$$P(r,0) = P_2 \quad ; \quad a \leq r \leq b.$$

may be found, by analogy with heat flow, from Carslaw & Jaeger (1959), for the case of steady state flow, as:

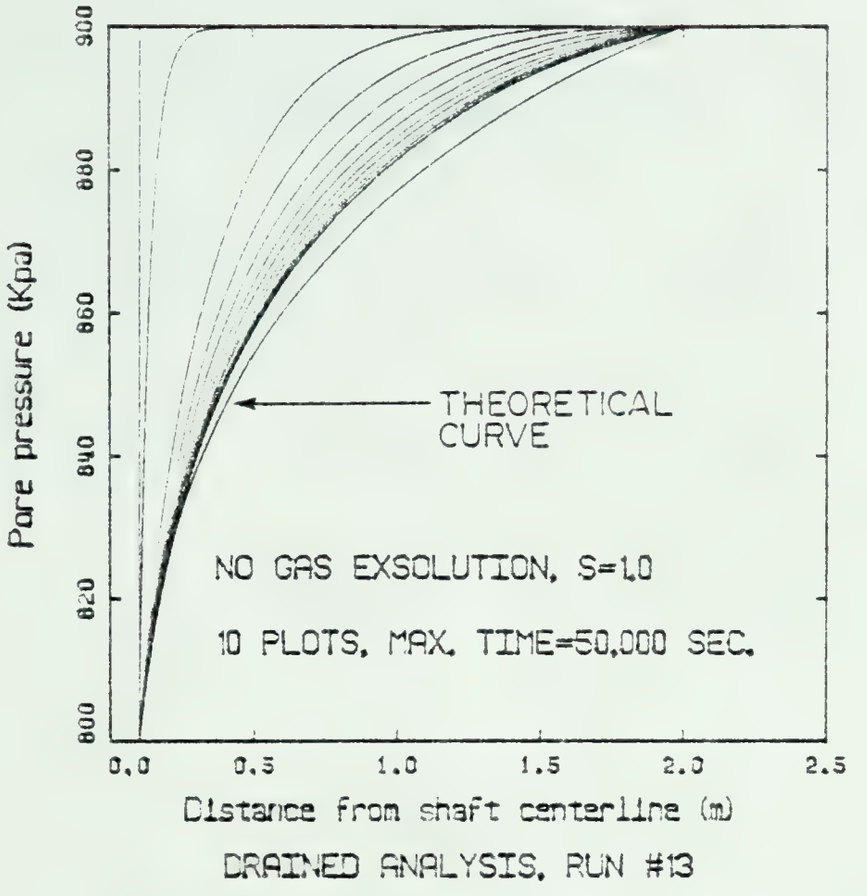
$$P = \{P_1 * \ln(b/r) + P_2 * \ln(r/a)\}/\ln(b/a) \qquad (7.15)$$

(t = infinte)

The finite difference solution to (7.9d) is then compared to (7.15) for the problem outlined in Table 7.1, and also for the case of a=100.1 m and b=102.0 m, in Figure 7.3. There is an excellent agreement for both of these solutions. It may be noted that when (b-a) is small and both b and a large, the problem approximates one dimensional flow between two parallel planes. It is expected that the pressure distribution would be linear between a and b, which is supported by both the finite difference and exact solutions.

Parametric studies

Figures 7.4 to 7.14 illustrate the transient and steady-state pressure response around a borehole for eleven different analyses. The analyses investigate the influence of varying the values of initial saturation, gas exsolution constant E, and Henry's constant H, as outlined in Table 7.2.



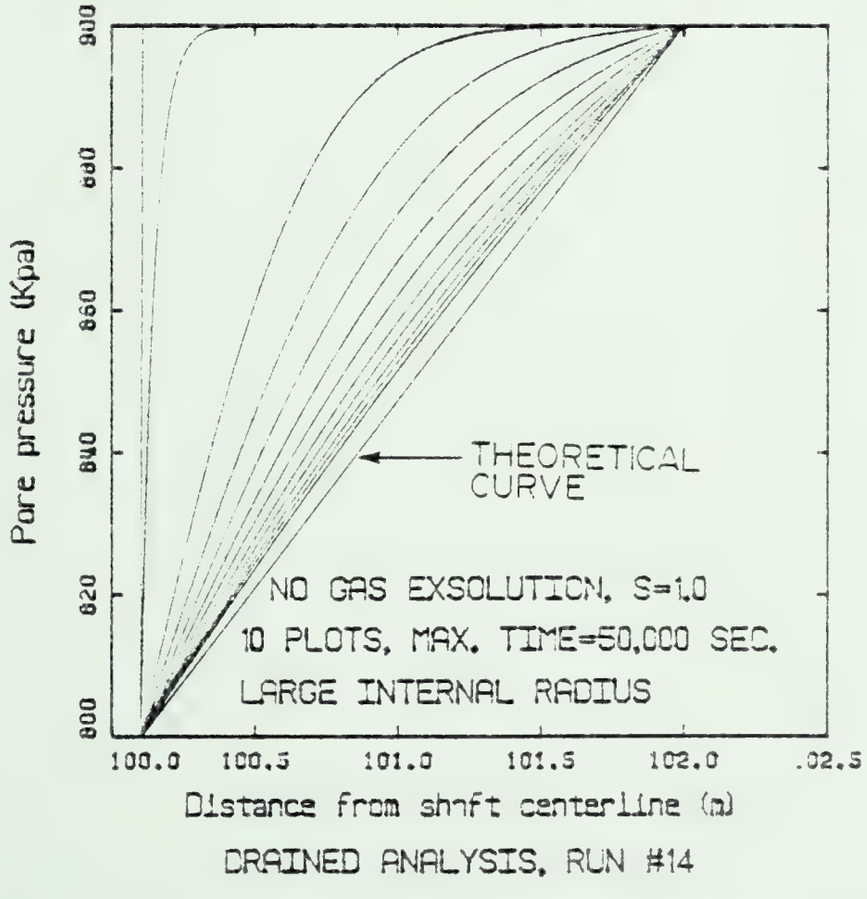
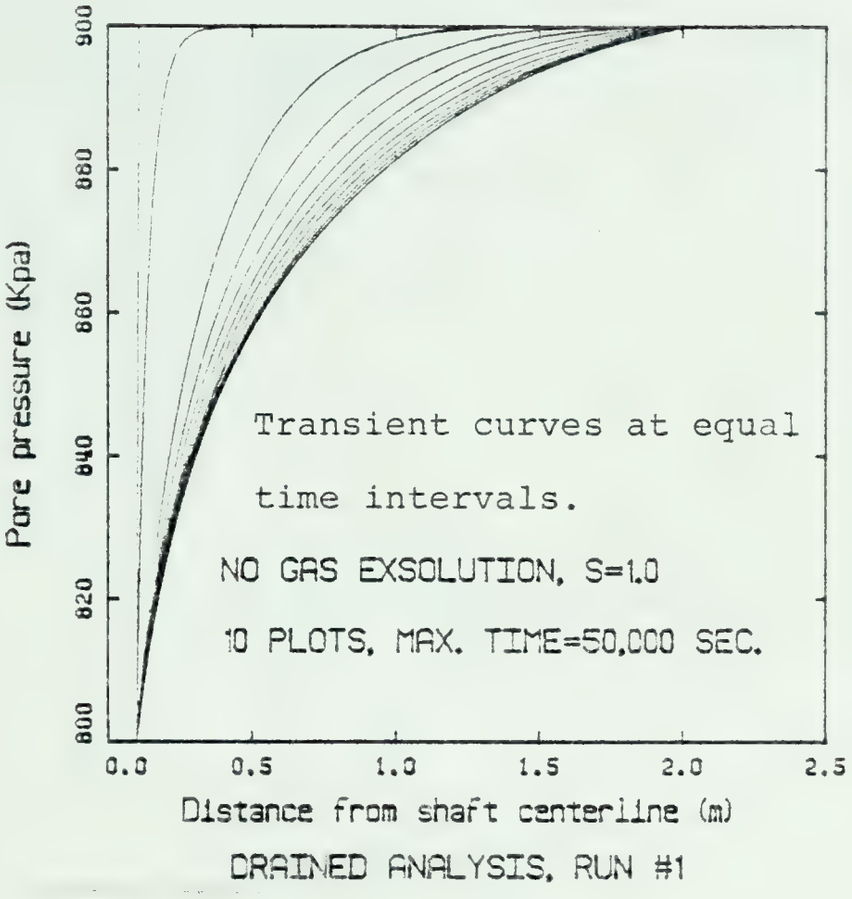


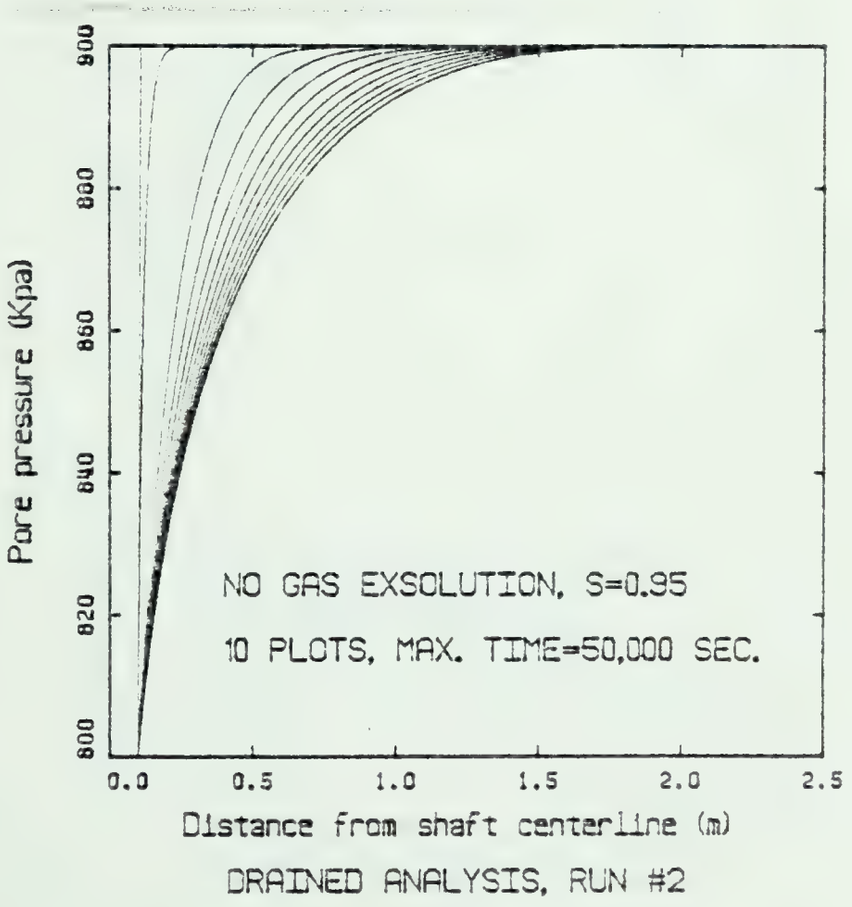
Figure 7.3 - Theoretical & F.D. solutions to consolidation problem

TABLE 7.2

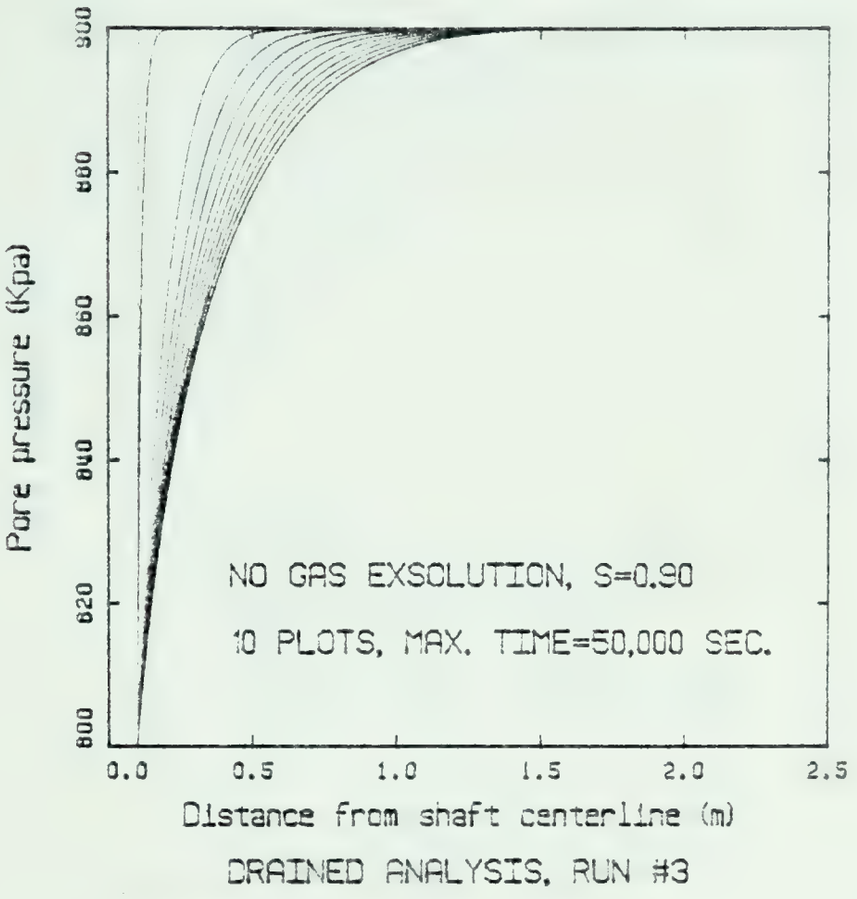
ANALYSIS OF CONSOLIDATION/GAS
EXSOLUTION AROUND A BOREHOLE

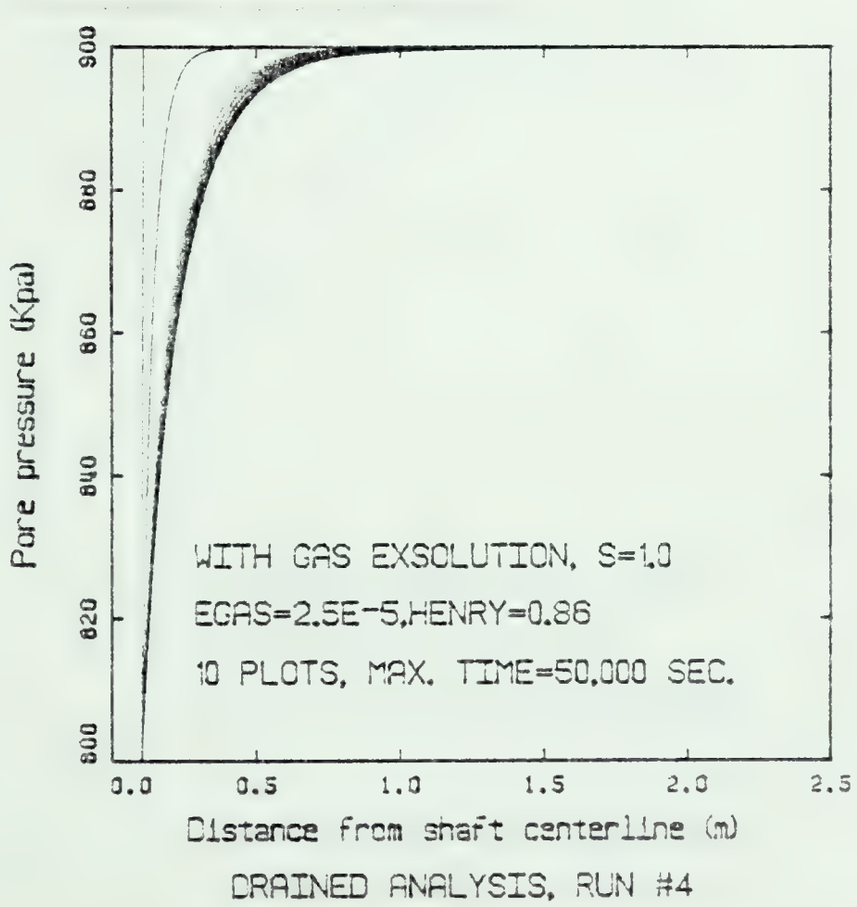
FIGURE NO.	ANALYSIS NO.	S_i	H	E ($sec.^{-1}$)	COMMENTS
7.4	1	1	0	0	
7.5	2	.95	0	0	
7.6	3	.90	0	0	
7.7	4	1	.86	2E-5	
7.8	5	.95	.86	2E-5	
7.9	6	.90	.86	2E-5	
7.10	7	1	.02	2E-5	
7.11	8	1	.02	2E-4	T_{max} = 50,000 sec.
7.12	9	1	.02	2E-4	T_{max} = 150,000 sec.
7.13	10	1	.86	2E-4	T_{max} = 150,000 sec.
7.14	11	.855	.86	2E-4	T_{max} = 150,000 sec.





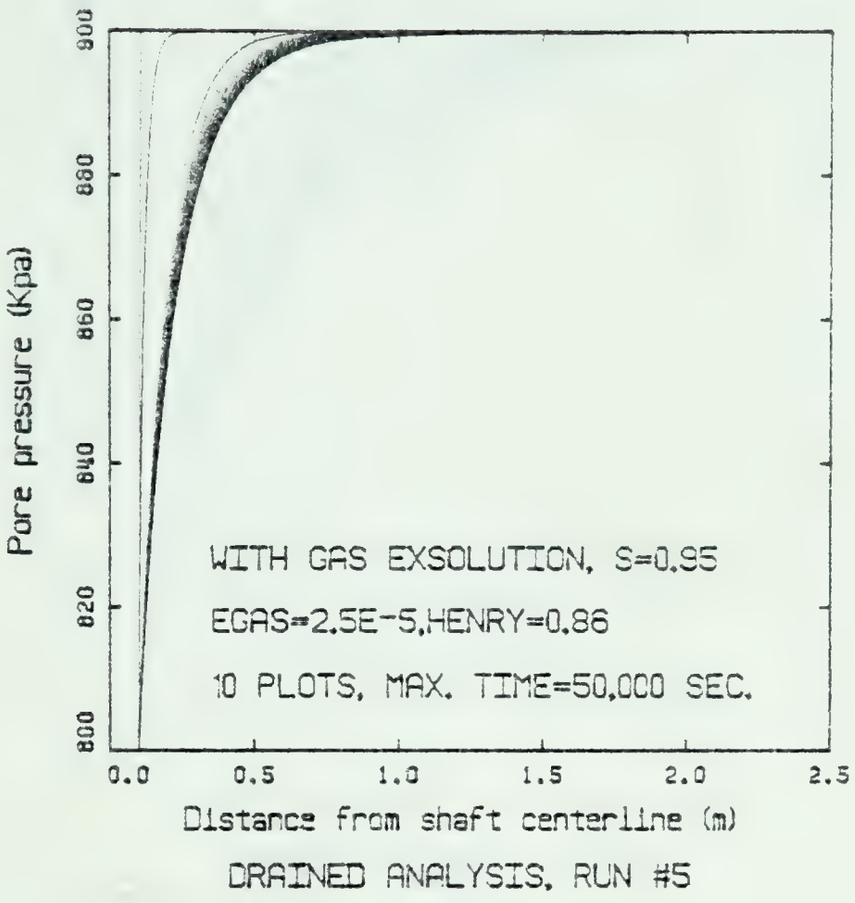
Figures 7.4 and 7.5

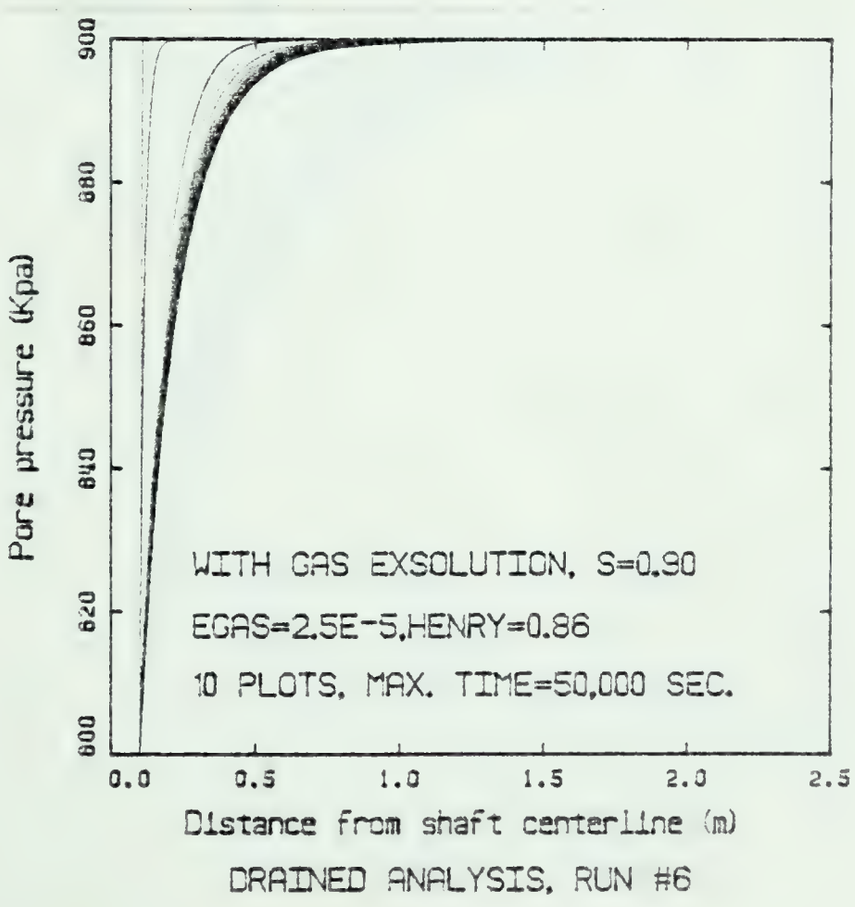




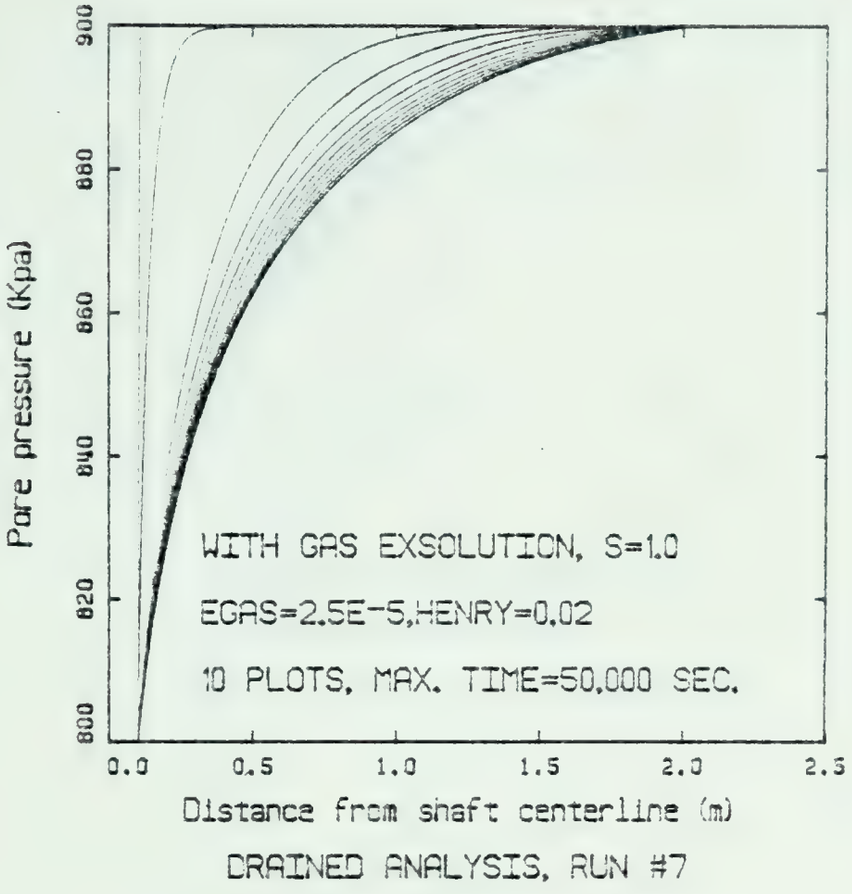
Figures 7.6 and 7.7

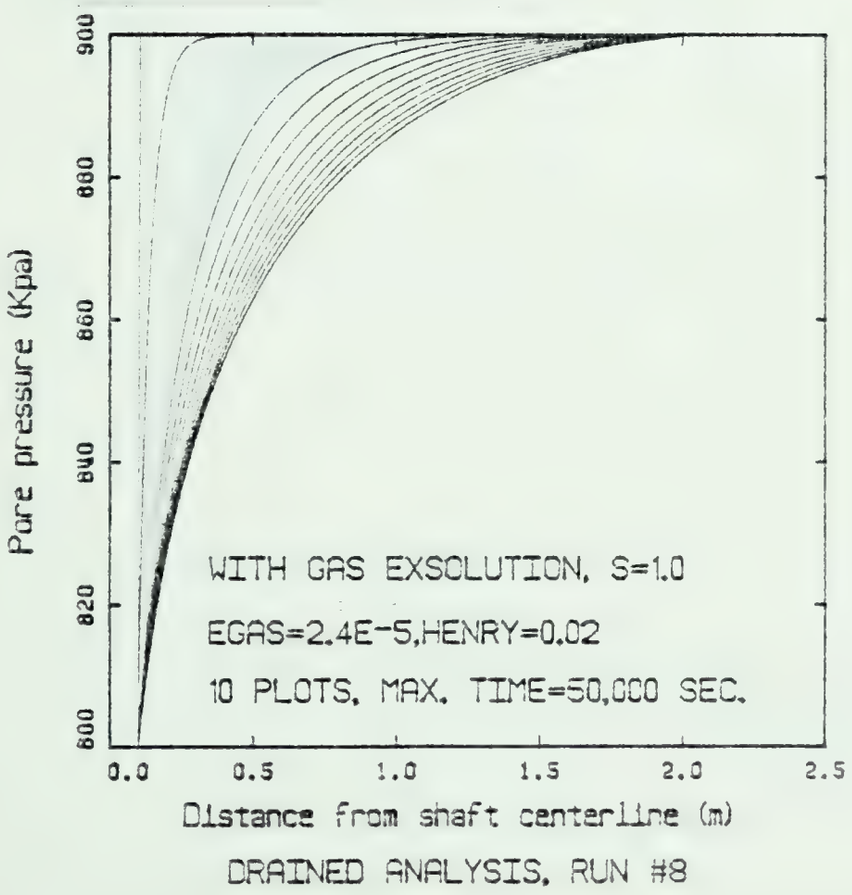




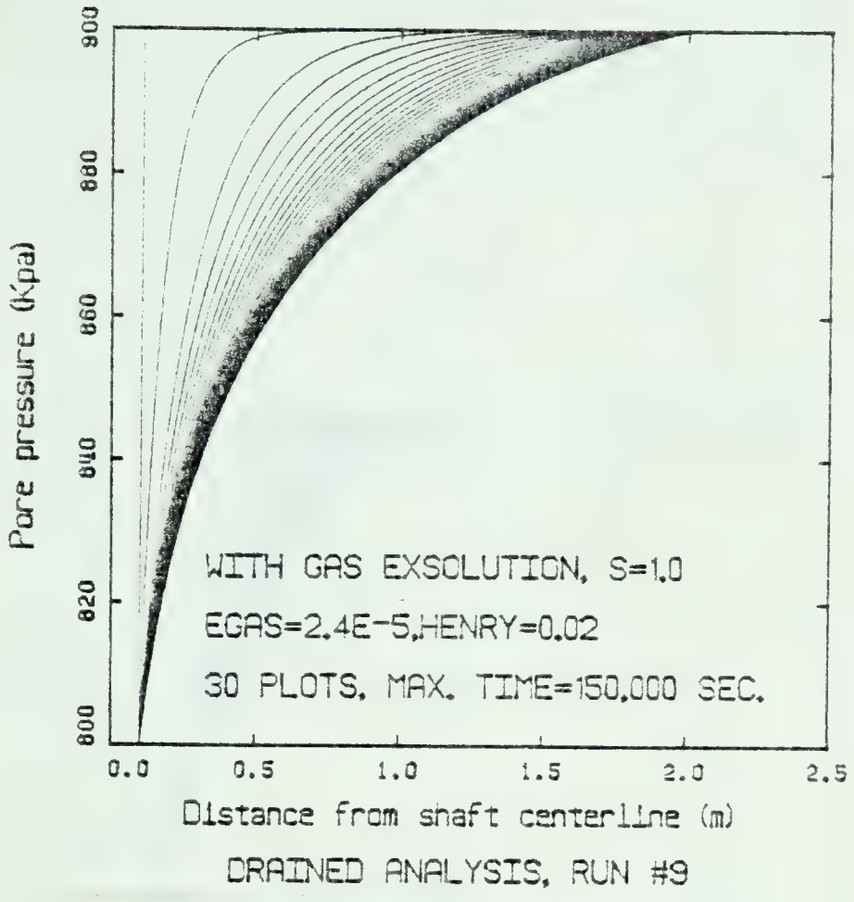


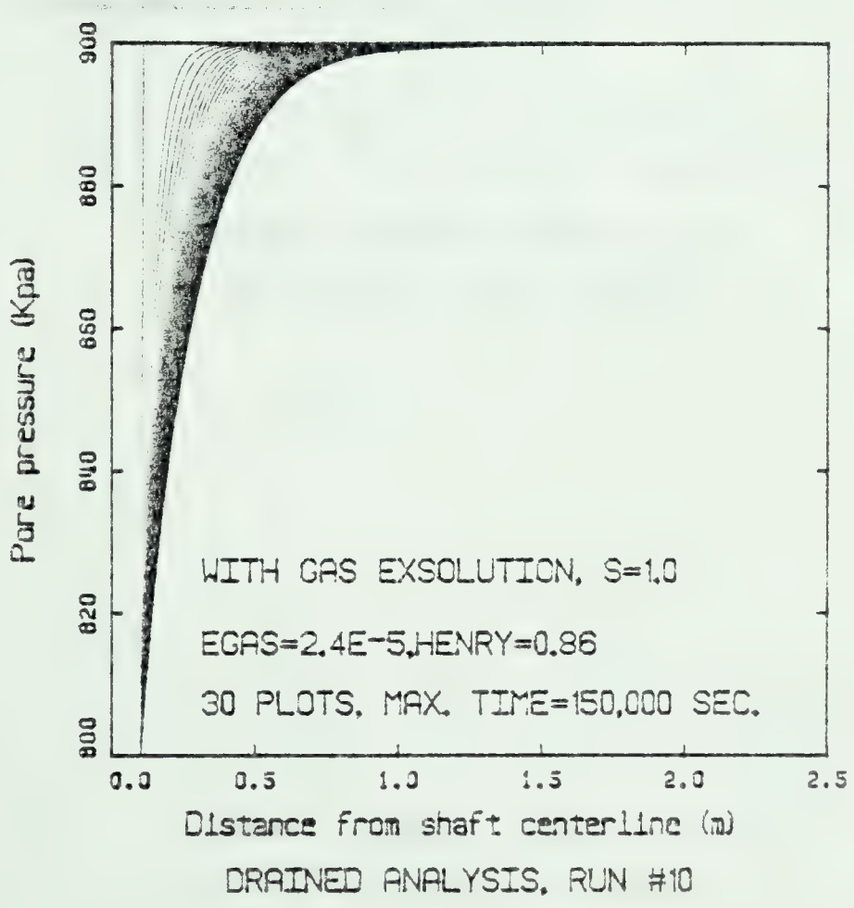
Figures 7.8 and 7.9





Figures 7.10 and 7.11





Figures 7.12 and 7.13

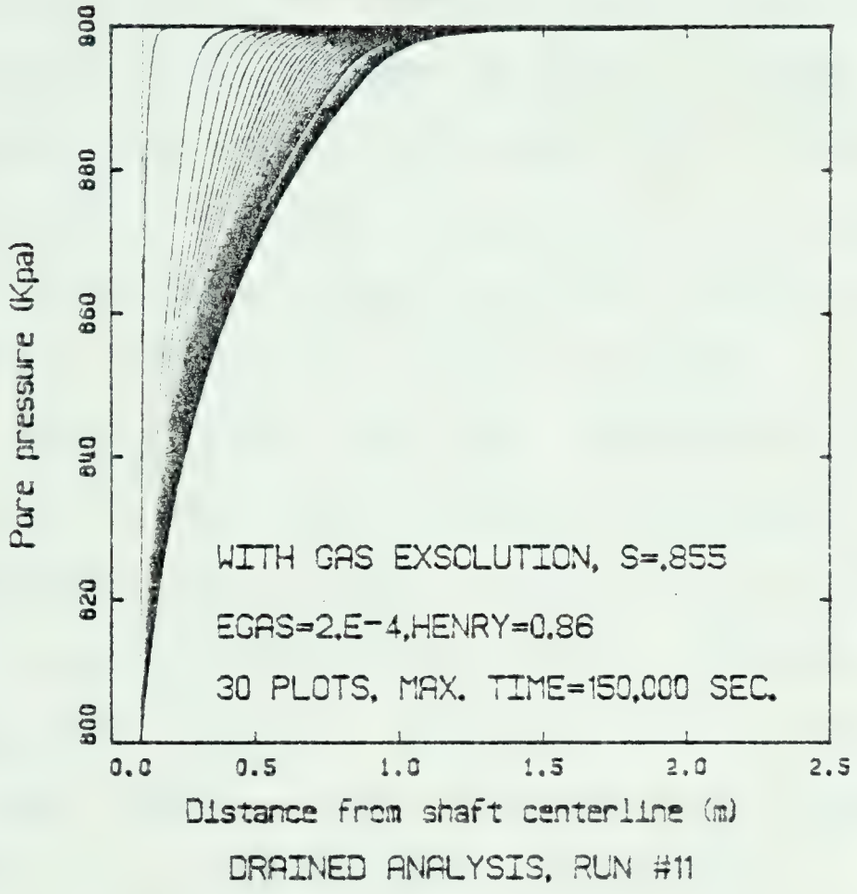

Pore pressure (Kpa)
600
620
640
660
680
700
0.0
0.5
1.0
1.5
2.0
2.5
Distance from shaft centerline (m)
WITH GAS EXSOLUTION, S=.855
EGAS=2.E-4,HENRY=0.86
30 PLOTS, MAX. TIME=150,000 SEC.
DRAINED ANALYSIS, RUN #11

Figure 7.14

All of the analyses (except Nos. 9-11) were terminated at 50,000 seconds (13.9 hours) and a family of 10 curves was plotted indicating the transient response at times of 5000, 10000, 15000 etc. seconds.

The "steady-state" pressure profile may be determined by a progressively closer spacing of curves plotted for equal time intervals. For the case of E=H=0, (Figures 7.4-6), this closer spacing of curves indicates that a true steady-state pressure profile is being established. For $E \neq H \neq 0$, (Figures 7.7-14), a grouping of transient curves may only represent an intermediate, quasi-steady pressure profile, which develops because consolidation and gas exsolution processes are temporarily of equal (and opposite) strength. With time, these pressures again change towards their true steady-state values because the amount of gas in solution in the pore fluid has been depleted. For example, in Figure 7.11, where a slightly soluble gas (H=0.02) of relatively high diffusivity ($E = 2*10^{-4}$ sec^{-1}) is exsolving, a steady-state pressure profile appears to be forming after 50,000 seconds. If this analysis is continued until 150,000 seconds, however, (Figure 7.12) it is evident that there continues to be a drop in the pressure profile as the exsolution process weakens and the consolidation process becomes more dominant. It has taken this soil 150,000 seconds to establish the same steady-state pressure profile that was reached after 40,000 seconds in Analysis #1, (H=E=0, Figure 7.4).

The parametric study shown in Figures 7.4 to 7.12 indicates the following general behaviour:

(a) For E=H=0, a decrease in S_i causes an increase in both the steady-state pressure profile, and the transient profile at any time t, (Fig. 7.4 - 7.6).

(b) For the same initial saturation, an increase in H, (E=constant), or in E, (H=constant), causes an increase in the transient pressure profile at any time t, (e.g. compare Fig. 7.4, 7.10, and 7.7, or 7.10 and 7.11).

(c) For $E \neq H \neq 0$, but constant between analyses, a decrease in S_i causes an increase in the transient pressure profile at shorter times, but appears to have a negligible effect on the quasi-steady profile.

It should be recognized that in these analyses, the pore fluid is initially at equilibrium with respect to the gas exsolution process, and it is the initiation of consolidation by a reduction of the boundary fluid pressure that causes a solubility disequilibrium. Hence the quasi-steady pressure profile is always lower than the insitu pressure. The condition of an initial disequilibrium in both the consolidation and gas exsolution processes will be treated in Chapter 8. In this case, depending upon which process dominates, the pressure at any particular radius may increase or decrease, and the quasi-steady profile (if such exists) may be higher or lower than the initial pressure profile.

7.5 SUMMARY

This chapter has presented the derivation of a general, combined theory of consolidation and gas exsolution. The theory incorporates a linear constitutive law for the soil skeleton, a linear liquid compressibility, and a gas compressibility that is caused by both a free gas compression and a time-dependent gas exsolution. It has been cast in a one-dimensional form, and the resulting differential equation is quasi-linear and parabolic.

An implicit finite difference formulation has been given for the governing differential equation, and has been applied to the case of determining the transient pressure profiles around a borehole in a gassy soil. Parametric studies have allowed the effect of varying initial saturation, Henry's constant, and gas exsolution constant, E, to be evaluated.

CHAPTER 8 - FLUID RESPONSE AROUND A BOREHOLE OR SHAFT IN A GASSY SOIL

8.1 INTRODUCTION

Having developed a general, one-dimensional theory of consolidation/gas exsolution (Chapter 7), it is desirable to investigate further practical applications of gassy soil behaviour. The response of the soil around a borehole or shaft has been chosen, because of the relative simplicity of the boundary conditions, and the applicability of the analysis to a number of problems. For example, the construction of a borehole or shaft will usually be accompanied by the establishment of transient pore pressures. The volume of fluid flowing into the shaft is often calculated on the basis of the steady state pressure profile, and yet for a gassy soil, the initial flow may be much higher. Depending upon the amount of gas in solution, the rate of exsolution, and the consolidation characteristics of the soil, higher fluid pressures and higher fluid flows may be maintained for some time after construction. Other flow-related considerations, such as the response of a borehole during a drill stem test, or the buildup of fluid pressure against an impermeable shaft lining with time, can also be modelled using the general theory. The problem of shaft wall stability, including the determination of wall closure (or ground reaction curves) and standup time may be investigated

using this theory, although as will be discussed later in the chapter, there are some practical limitations in the application of the theory at present.

The general insitu and boundary conditions shown in Table 7.1 and Figures 7.1-2, as they describe a borehole in a gassy soil, will be considered in this chapter. The behaviour predicted by the model is equally applicable to a shaft, except for the difference in scale, (both in space and time). Implications with respect to soil behaviour around a tunnel may also be made, but it must be realized that the fluid flow is in this case at least two-dimensional. It will be assumed that the construction of the borehole or shaft is very quick in relation to both the gas exsolution and consolidation processes, so that the soil behaviour can be modelled in two steps:

(a) an immediate and undrained response, which is due to a total stress change at the wall of the shaft or borehole, and which results in both pore pressure and effective stress changes in the surrounding soil.

(b) a transient response, which is due both to a change in boundary fluid pressure and to the change in fluid pressure discussed in (a).

This analysis thus differs from the one presented previously, in that at time t=0, the pore fluid may be in a disequilibrium state with respect to dissolved gas. Depending upon which transient process dominates, the pore fluid pressure at a point in the soil away from the borehole

wall may initially increase or decrease. Eventually a steady-state pressure profile must be established, but this will only occur after the gas exsolution process has ended. Intermediate fluid pressures may be much higher than expected, and may prevail for extended periods of time.

Consideration of the soil behaviour will then be treated, in this chapter, in three parts. The first part deals with the immediate and undrained response of the soil due to the construction of a shaft or borehole. A further development of theory is necessary, as in general the stresses around the shaft or borehole will be high enough to induce failure. Stress changes and volume changes in the failed zone will thus be derived, and related to the change in pore fluid pressure. For the purposes of the undrained analysis, the soil will be treated as elastic-perfectly plastic, with a non-associated flow rule and a Mohr-Coulomb ($c'=0$) failure criterion. The second part of the chapter will deal with the transient response of the soil, and will apply the theory developed in Chapter 7. Finally, the stability of the borehole wall will be discussed. Ground reaction curves will be derived for the immediate and the long-term, undrained cases, and will be examined for the transient case.

8.2 IMMEDIATE AND UNDRAINED RESPONSE

The undrained behaviour of a gassy soil with an elastic constitutive relationship has been treated previously (Chapter 2). These ideas will here be extended to the case of an elastic - perfectly plastic soil, specifically for the boundary conditions of a shaft or tunnel behaving in a plane strain manner. The condition of plane strain rather than plane stress has been chosen for the vertical shaft because it is felt that this boundary condition is more representative of behaviour at depth in a real soil, and because the stress-strain formulation is equally applicable to a shaft, or to a deeply buried tunnel.

It is the intent in this section to develop a theoretical model which will allow the prediction of the undrained (either short or long term) pore pressure profile around a shaft, given the change in total stress at the shaft wall. It will be necessary to develop expressions for stress, strain and wall displacement. The derivations are given in sections 8.2.1 and 8.2.2. Section 8.2.3 will indicate how these are combined to predict the pore pressure response.

The derivation of the appropriate stress-strain relationships follows that of Guenot (1979) with two important exceptions:

(a) The insitu state of stress is considered to be isotropic, i.e. $\sigma'_1 = \sigma'_2 = \sigma'_3 = \sigma'_h = \sigma'_v = \sigma_\infty$.

(b) The failure criterion is for a cohesionless soil, ($c' = 0$),

e.g. $\tau = \sigma_n' * \tan\phi'$

or $f = \sigma_\theta' - m * \sigma_r' = 0$ (8.1)

$m = (1+\sin\phi')/(1-\sin\phi')$

(see footnote[1])

8.2.1 Stresses

8.2.1.1 Stresses in the elastic zone

The stresses around a hole in an infinite elastic medium, with $\sigma_1 = \sigma_2 = \sigma_\infty$ and a stress σ_T, (footnote[2]), on the inside of the hole, may be found in any standard text, (e.g. Jaeger & Cook, 1979) as:

$$\sigma_r^e = \sigma_\infty - R\hat{}2/r\hat{}2 * (\sigma_\infty - \sigma_T)$$
$$\sigma_\theta^e = \sigma_\infty + R\hat{}2/r\hat{}2 * (\sigma_\infty - \sigma_T) \quad (8.2)$$
$$\tau_{r\theta} = 0$$

---

[1] Throughout this chapter it will be assumed that all stresses are effective, unless otherwise denoted by a superscript "t", and hence the prime notation will be dropped. In general, subscripts following a symbol will refer to direction, (e.g. of stress or strain), and superscripts will refer to whether the variable being described is "elastic" or "plastic", or "effective" or "total". In unusual circumstances, double subscripting is necessary - e.g. $(\sigma_r^p)_{r=I}$ refers to a radial plastic (effective) stress measured at r=I.

[2] The subscript "T" refers to stresses acting on the tunnel wall, in this case an effective stress.

where

r = distance from centerline of shaft

R = radius of hole

8.2.1.2 Stresses in the Plastic Zone

For an elastic-perfectly plastic medium, (8.2) will apply as long as $f = \sigma_\theta - m*\sigma_r < 0$. If $f = 0$, then a plastic zone will begin to develop, first at the borehole wall, and then growing in size as σ_T is decreased. Within the plastic zone (8.1) will apply.

The stresses within the plastic zone may be derived by combining the yield relationship (8.1) with the equilibrium equation:

$$D\sigma_r/Dr + 1/r*D\tau_{\theta r}/D\theta + (\sigma_r - \sigma_\theta)/r = 0 \qquad (8.3)$$

to obtain:

$$\sigma_r^p = \sigma_T * (R/r)^(1-m)$$

$$\sigma_\theta^p = m * \sigma_r^p = m * \sigma_T * (R/r)^(1-m) \qquad (8.4)$$

8.2.1.3 Radius of the Plastic Zone

The radius of the plastic zone I is found by recognizing that at r=I, $\sigma_r^e = \sigma_r^p$, $\sigma_\theta^e = m * \sigma_r^e$, and also that $\sigma_\theta + \sigma_r = 2*\sigma_\infty$. Then:

$$I = R * (2*\sigma_\infty/[\sigma_T*\{m+1\}])^(1/[m-1]) \qquad (8.5)$$

The stresses in the elastic region around the plastic zone are given by (8.2), using R=I, and $\sigma_T=(\sigma_r^p)_{r=I}$:

$$\sigma_r^e = \sigma_\infty*(1-I\hat{}2/r\hat{}2 * [m-1]/[m+1])$$
$$\sigma_\theta^e = \sigma_\infty*(1+I\hat{}2/r\hat{}2 * [m-1]/[m+1]) \qquad (8.6)$$

8.2.1.4 Stress in the z-direction

The stress in the z-direction may be obtained by considering the plane strain condition that ε_z = constant, or that $\Delta\varepsilon_z = 0$. Then in the elastic zone:

$$\Delta\sigma_z = \nu*(\Delta\sigma_r + \Delta\sigma_\theta) \qquad (8.7a)$$

and since

$$\Delta\sigma_r = -\Delta\sigma_\theta$$
$$\Delta\sigma_z = 0, \text{ hence } \sigma_z^e = \sigma_\infty \qquad (3.7b)$$

and $\sigma_r < \sigma_z < \sigma_\theta$

To develop the expression for σ_z^p, it is necessary to consider the strains in the plastic zone, ε^p. A non-associated flow rule is used of the form:

$$d\varepsilon_{ij} = Dg/D\sigma_{ij} * d\lambda \qquad g = \sigma_\theta - \alpha*\sigma_r \qquad (8.8)$$
$$1 \leq \alpha \leq m$$

from which

$$d\varepsilon_r^p + \alpha*d\varepsilon_\theta^p = 0, \quad d\varepsilon_z^p = 0 \qquad (8.9a)$$

If the unloading stress path is monotonic (no stress reversals) , and is located along the failure envelope, then:

$$\varepsilon_r^p + \alpha * \varepsilon_\vartheta^p = 0, \quad \varepsilon_z^p = 0 \tag{8.9b}$$

For a change in stress $\Delta\sigma_T$, the total strains:

$$\Delta\varepsilon_z^e + \Delta\varepsilon_z^p = 0$$

but since $\Delta\varepsilon_z^p = 0$, $\Delta\varepsilon_z^e = 0$, and hence the changes in stress in the plastic zone are still related through:

$$\Delta\sigma_z^p = \nu * (\Delta\sigma_\theta^p + \Delta\sigma_r^p) = \nu * (m+1) * \Delta\sigma_r^p \tag{8.7c}$$

The largest stress changes will always be experienced at the tunnel wall, (i.e. a point on the tunnel wall will be further along the stress path than any point with r > R). Thus for r = R,

$$\sigma_z^p = \nu * (m+1) * \sigma_T + (1-2*\nu) * \sigma_\infty \tag{8.10}$$

and hence to maintain:

$$\sigma_z^p = \sigma_2,$$

$$\sigma_T \leq [\nu * (m+1) * \sigma_T + (1-2*\nu) * \sigma_\infty] \leq m * \sigma_T \tag{8.11}$$

The left-hand inequality is satisfied for any $m \geq 1$ and $0 \leq \nu \leq 0.5$. The right-hand inequality, however, places a restriction on σ_T that:

$$\sigma_T \geq (1-2*\nu)*\sigma_\infty/[m-\nu*(m+1)] \qquad (8.12)$$

At the onset of failure, (i.e. at r = R = I), the radial stress is:

$$(\sigma_r)_{r=I} = 2 * \sigma_\infty / (1+m)$$

For $\sigma_T = (\sigma_r)_{r=I}$, equation 8.12 is always satisfied. If σ_T drops below the limiting value given in (8.12), then σ_z becomes the major principal stress. For the purposes of this thesis, (8.12) will be observed. The development of separate plastic zones with $\sigma_z \neq \sigma_2$ is discussed further in Florence & Schwer (1978).

8.2.2 Strains

The elastic strains in the plastic zone may be calculated from:[3]

$$\varepsilon_r^p = (1+\nu)/E*\sigma_T*(R/r)\hat{}(1-m)*(1-\nu*[m+1])-\nu*\varepsilon_z \qquad (8.13)$$
$$\varepsilon_\theta^e = (1+\nu)/E*\sigma_T*(R/r)\hat{}(1-m)*(m-\nu*[m+1])-\nu*\varepsilon_z$$

---

[3] In this section only, the normal solid mechanics formulation for constitutive relationships will be adopted. However, the sign convention of compressive stress positive will be maintained, which infers that compressive strain will also be positive.

The plastic strains in the plastic zone are found by combining (8.9b) with the compatibility equation for total strains:

$$r*d\varepsilon_\theta/dr + \varepsilon_\theta - \varepsilon_r = 0 \qquad (8.14)$$

then:

$$r*d\varepsilon^p_\theta/dr + \varepsilon^p_\theta*(1+\alpha) = -(r*d\varepsilon^e_\theta/dr + \varepsilon^e_\theta - \varepsilon^e_r)$$

$$= C_2*(R/r)\hat{}(1-m) \qquad (8.15b)$$

where:

$$C_2 = -(m-1)*(m+1)*(1-\nu)*(1+\nu)*\sigma_T/E$$

The differential equation 8.15b can be solved for ε^p_θ, using the boundary condition that $\varepsilon^p_\theta = 0$ at r = I to give:

$$\varepsilon^p_\theta = C_2/(m+\alpha) * (r/R)\hat{}(m-1) * \{1-[I/r]\hat{}(m+\alpha)\} \qquad (8.16a)$$

and recognizing that I is also a function of σ_T,

$$\varepsilon^p_\theta = K_1*(K_2*\sigma_T\hat{}\{[\alpha+1]/[1-m]\} - \sigma_T) \qquad (8.16b)$$

$$K_1 = (m-1)*(m+1)*(1-\nu)/(m+\alpha) * (1+\nu)/E * (r/R)\hat{}(m-1)$$

$$K_2 = (R/r)\hat{}(m+\alpha) * (2*\sigma_\infty/[m+1])\hat{}\{(m+\alpha)/(m-1)\}$$

$$\varepsilon^p_r = -\alpha * \varepsilon^p_\theta$$

8.2.2.1 Strains & displacements due to unloading

The calculation of ε_r and ε_θ in the elastic and plastic zones around the borehole or shaft are of interest insofar as they allow a calculation of the displacement at the borehole wall due to unloading, U_R. Now, consider a strain$\Delta\varepsilon'$, which is that amount of strain due to unloading only. The initial stress condition was given previously as $\sigma_{H1}=\sigma_{H2}=\sigma_v=\sigma_\infty$, and hence the initial strains in all directions are:

$$\varepsilon_r^i = \varepsilon_\theta^i = \varepsilon_z = \sigma_\infty * (1-2*\nu) / E$$

Therefore,

$$\begin{aligned}\Delta\varepsilon'_\theta &= \varepsilon_\theta^p + \varepsilon_\theta^e - \varepsilon_\theta^i \\ &= K_1*(K_2*\sigma_T\hat{}\{[\alpha+1]/[1-m]\}-\sigma_T) + \\ &\quad (1+\nu)/E*\sigma_T*(R/r)\hat{}(1-m)*[m-\nu*(m+1)] - \\ &\quad (1+\nu)*(1-2*\nu)*\sigma_\infty/E \end{aligned} \qquad (8.21a)$$

Recognizing from the definition of tangential strain that:

$$\varepsilon_\theta = 1/r * (U + DV/D\theta)$$

and since $DV/D\theta = 0$,

$$\varepsilon_\theta = U/r, \quad \text{or} \quad U = r * \varepsilon_\theta$$

The displacement at the tunnel wall, U_R, due to unloading, may then be expressed as:

$$U_R = R * (\Delta\varepsilon_\theta')_{r=R}$$
$$= R * (1+\nu)/E * \{(m-1)*(m+1)*(1-\nu)/(m+\alpha)*$$
$$[(2*\sigma_\infty/(m+1))\hat{}((m+\alpha)/(m-1))*\sigma_T\hat{}((\alpha+1)/(1-m))-\sigma_T]$$
$$+\sigma_T*[m-\nu*(m+1)]-(1-2*\nu)*\sigma_\infty\} \qquad (8.21b)$$

8.2.2.2 Volumetric strains

The calculation of ε_r and ε_θ also allows the computation of the volumetric strain ε_v, which may be used in the determination of the fluid pressure response around the borehole.

Since $\Delta\varepsilon_z = 0$,

$$\Delta\varepsilon_v = \Delta\varepsilon_r + \Delta\varepsilon_\theta \qquad (8.17a)$$

But in the elastic zone, $\Delta\varepsilon_r = -\Delta\varepsilon_\theta$, so that:

$$\Delta\varepsilon_v = 0 \qquad (8.17b)$$

In computing strains, then, and particularly in computing volumetric strain, it is useful to redefine $\Delta\varepsilon$ as that amount of strain which has occurred since the onset of failure at the borehole or shaft wall. Then,

$$\Delta\varepsilon_\theta = \varepsilon_\theta^e + \varepsilon_\theta^p - (\varepsilon_\theta^e)_{\text{at onset of failure}}$$
$$\Delta\varepsilon_r = \varepsilon_r^e + \varepsilon_r^p - (\varepsilon_r^e)_{\text{at onset of failure}} \qquad (8.18a)$$

and

$$\Delta\varepsilon_\theta = (1+\nu)/E*\{\sigma_T*(R/r)\hat{}(1-m)*(m-\nu*[m+1])\} +$$
$$K_1*\{K_2*\sigma_T\hat{}([\alpha+1]/[1-m])-\sigma_T\} -$$
$$(1+\nu)/E*\{\sigma_\infty*(1-2*\nu+R\hat{}2/r\hat{}2)-R\hat{}2/r\hat{}2*(2*\sigma_\infty/[m+1])\}$$

$$\Delta\varepsilon_r = (1+\nu)/E*\{\sigma_T*(R/r)\hat{}(1-m)*(1-\nu*[m+1])\} -$$
$$\alpha*K_1*\{K_2*\sigma_T\hat{}([\alpha+1]/[1-m]-\sigma_T\} -$$
$$(1+\nu)/E*\{\sigma_\infty*(1-2*\nu-R\hat{}2/r\hat{}2)+R\hat{}2/r\hat{}2*(2*\sigma_\infty/[m+1])\}$$

$$\Delta\varepsilon_v = (1+\nu)/E*(1-2*\nu)*\{(m+1)*\sigma_T*(r/R)\hat{}(m-1)-2*\sigma_\infty\} +$$
$$(1-\alpha)*K_1*\{K_2*\sigma_T\hat{}([\alpha+1]/[1-m])-\sigma_T\} \qquad (8.18b)$$

The first term in the expression for $\Delta\varepsilon_v$ is the elastic portion and the second term is the plastic portion. Thus it is clear that for ν=0.5, $\Delta\varepsilon_v^e = 0$, and for α=1, $\Delta\varepsilon_v^p = 0$, which is to be expected. For $\nu \neq 0.5$, $\alpha \neq 1$, and using the limit that

$$\sigma_T \leq 2*\sigma_\infty/(m+1) \qquad (8.19)$$

for a plastic zone to exist, it can be shown that:

(a) for $\sigma_T = 2*\sigma_\infty/(m+1)$ and r=R,
or for r=I, $(\sigma_r = 2*\sigma_\infty/[m+1])$,

$\Delta\varepsilon_v = 0$, and

(b) for $\sigma_T < 2*\sigma_\infty/(m+1)$ and $r < I$,

$$\Delta\varepsilon_v < 0$$

(which is expansive, using the solid mechanics sign convention).

8.2.3 Undrained, immediate pressure response

In Chapter 2, a derivation of the undrained pressure response of a gassy soil was presented using an elastic constitutive relationship, (equations 2.10, 2.8b, 2.14c and 2.15c). Equation 2.15c can be modified for an elastic perfectly-plastic soil by maintaining the expression for ΔV_T in the form (now using the convention that ΔV_T positive is an increase in volume):

$$\Delta V_T = -V_T * \varepsilon_v$$

and using (8.18b) for volumetric strains, so that the solution for Δu (2.15b) becomes:

$$A * \Delta u^2 + B * \Delta u + C = 0 \qquad (8.20)$$

$$A = n * S * \beta_l$$

$$B = n * (\beta_l*S*P_0 + 1 - S + S*H) - \varepsilon_v$$

$$C = -P_0 * \varepsilon_v$$

The immediate undrained pore pressure response is calculated with H=0. If H≠0, however, (8.20) may also be used to predict the equilibrium (long term) response in an elastic-perfectly plastic medium. Unfortunately, the transient analysis described in the following section will not converge on this equilibrium response because the elastic-perfectly plastic constitutive relationship cannot be incorporated into the consolidation/gas exsolution model, (see section 7.1).

8.3 ANALYSIS OF THE TRANSIENT FLUID PRESSURE PROFILE

Eight analyses were performed on a borehole of 0.1 m diameter, using the input variables listed in Tables 8.1 and 8.2.

Undrained response

The borehole is first unloaded in the immediate and undrained mode by decreasing the total stress at the borehole wall, and applying equations 8.18b and 8.20 to calculate the pore fluid response. It is clear from (8.4), (8.5), and (8.18b) that once the effective stress at the tunnel wall, σ_T, is known, the radius of the plastic zone I, the stress distribution $\sigma_r^p(r)$ and $\sigma_\theta^p(r)$, and ultimately the volumetric strain $\Delta\varepsilon_v(r)$ are all known. But since $(\Delta\varepsilon_v)_{r=R}$ determines the pore fluid response at R, and hence indirectly σ_T, the solution for σ_T is iterative. A flow chart illustrating the iteration technique for $\Delta\varepsilon_v$ is given in Figure 8.1.

TABLE 8.1

INPUT PARAMETERS COMMON TO ALL BOREHOLE ANALYSES

σ_∞	= 1100 KPa
Ui	= 900 KPa
No. of F.D. Points	= 191
Minimum radius	= 0.1 meters
Maximum radius	= 0.48 meters
Maximum time	= 10,000 sec. (2.8 hours)
Time Step	= 20 sec.
βw	= 4.5 E-7 KPa^{-1}
E_{young}	= 240,000 KPa
μ	= 0.3
ϕ'	= 37
K	= 10E-10 m/sec.
e_i	= 0.47
E_{gas}	= 2.0E-5 $sec.^{-1}$

TABLE 8.2 - INPUT PARAMETERS FOR BOREHOLE ANALYSES #1 - #8

Figure No.	Run No.	S_i	H	α	TOTAL STRESS IN TUNN. (KPa)	PORE PRESS. IN TUNN. (KPa)	$P_{l/g}$ (KPa)	RADIUS OF PLASTIC ZONE (m)	σ'_T (KPa)	u_T (KPa)	ZONE OF $S_g < .85$ (m)
8.3	1	0.95	0.86	2	850	800	900	.1207	248	595	0
8.4	2	0.90	0.86	2	850	800	900	.1309	194	658	0
8.5	3	0.86	0.86	2	850	800	900	.1370	169	687	.098
8.6	4	0.95	0.86	2	500	400	900	.1539	119	376	.032
8.7	5	0.95	0.86	2	100	95	900	.2572	25	74	.086
8.8	6	0.95	0.02	2	100	95	900	.2572	25	74	.028
8.9	7	0.95	0.86	2	100	95	400	.2572	25	74	.038
8.10	8	0.95	0.86	3	100	95	900	.1913	61	38	.074

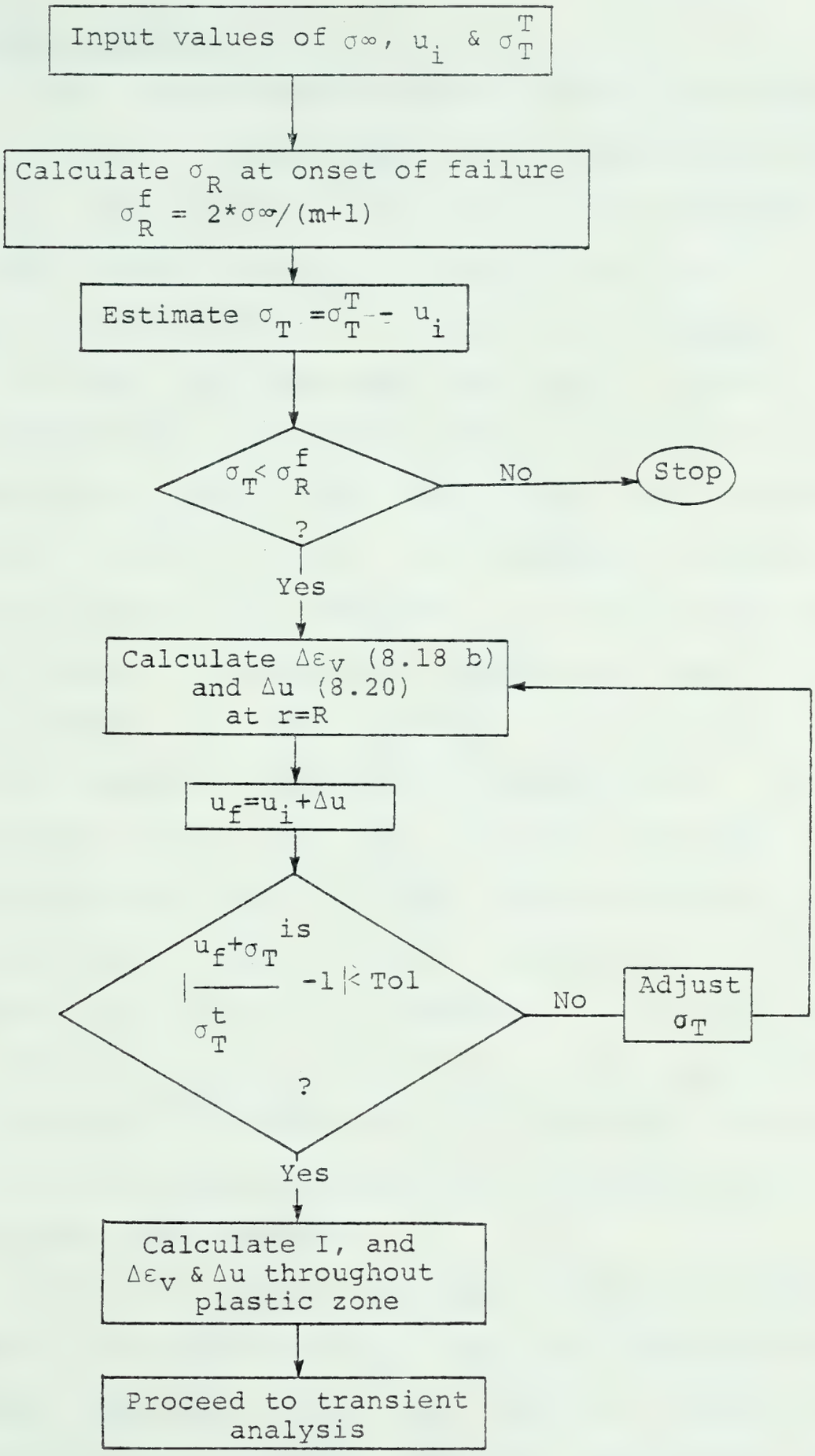


Figure 8.1 - Flow Chart for iterative solution on σ_T

Transient response

Once the undrained pressure profile is obtained, the fluid pressure at the tunnel wall is modified to its long term value and then the transient analysis is started. It is generally assumed that u_T is slightly less than σ_T^t, i.e. that a small σ_T is necessary to prevent tunnel collapse.

As has been discussed previously, (Chapter 7), the consolidation/gas exsolution theory of necessity assumes a linear elastic constitutive relationship for the soil. The transient analysis cannot (at present) incorporate the perfectly plastic soil behaviour. For those areas around the tunnel where consolidation predominates, this is a good model, since the pore pressure is decreasing and the effective stresses increasing (isotropically). The stress path moves away from the failure envelope and the elastic-perfectly plastic model predicts elastic behaviour, (Figure 8.2). The opposing contributions of the gas exsolution and consolidation processes are properly accounted for, since the volume increase due to gas exsolution, ΔV_{fg}, is independent of constitutive law, and the volume decrease due to decreasing fluid pressure is modelled correctly with the elastic relationships.

For those areas where gas exsolution predominates, however, the contribution of the soil skeleton cannot be properly predicted (using the present transient model). Increasing pore pressures and thus decreasing effective stresses require the stress path to move along the failure

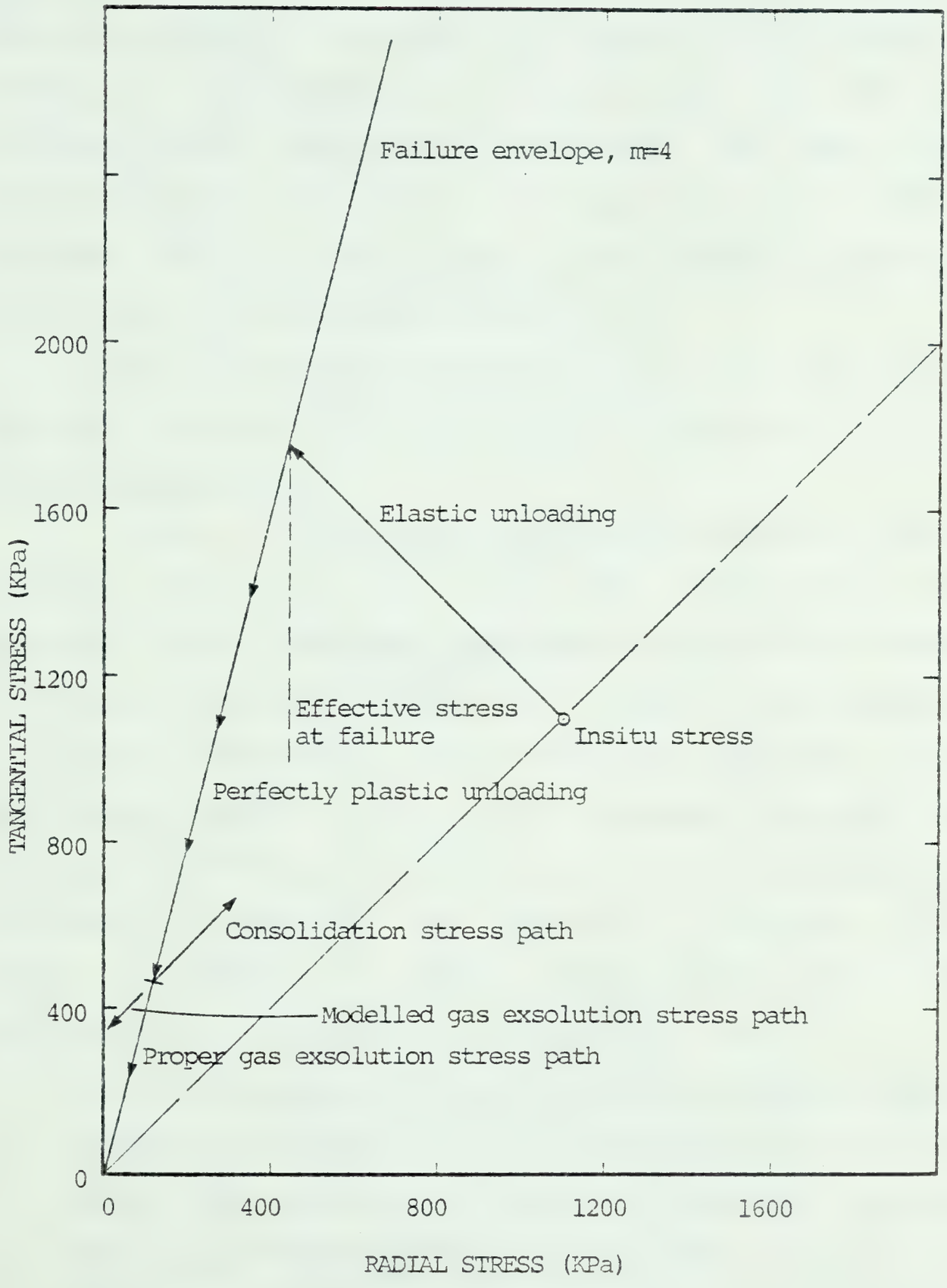


Figure 8.2 - Stress path for point on borehole wall during unloading

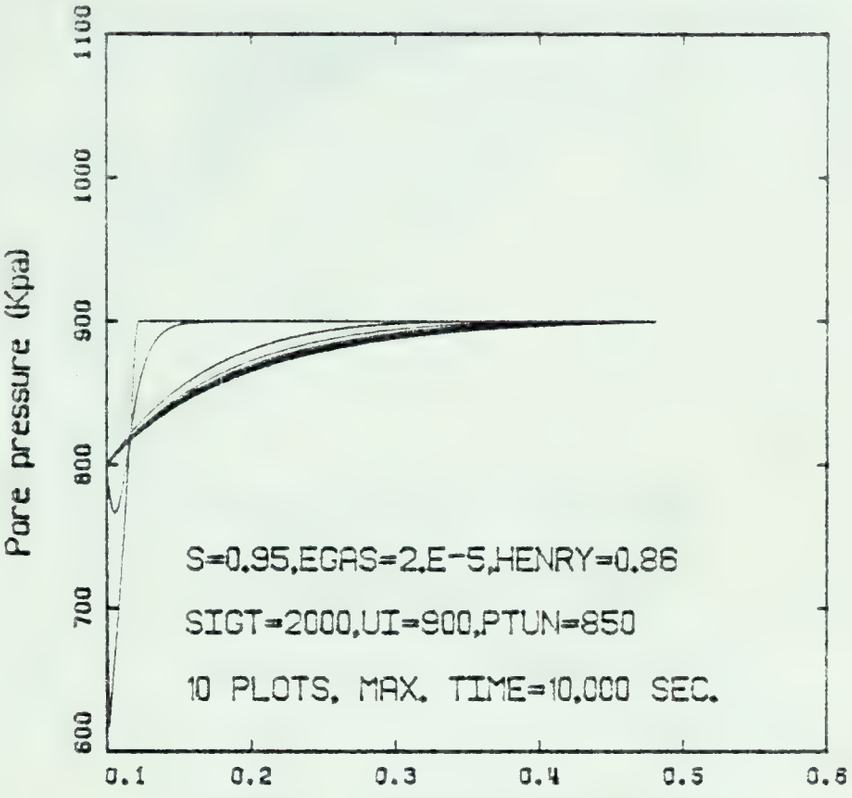
envelope, whereas the elastic model causes the stress path to move parallel to the $\sigma_1=\sigma_2=\sigma_3$ axis and thus beyond the failure envelope. The model is limited in this manner at present. Incidentally, a correct model for the soil behaviour would also have to account for some stress redistribution. The stress path must lie along the failure envelope, with $\Delta\sigma_\theta = m^*\Delta\sigma_r$, and yet the driving mechanism is an increase in u which implies $\Delta\sigma_\theta = \Delta\sigma_r$.

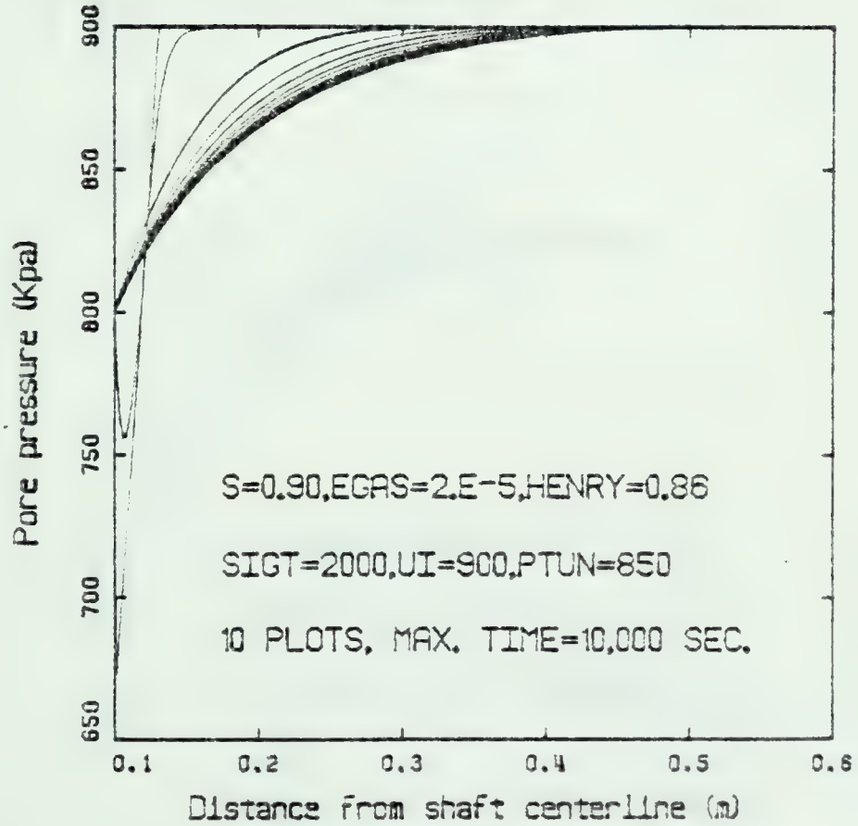
The stress paths followed during the immediate and transient responses are illustrated in Figure 8.2.

Parametric Analyses

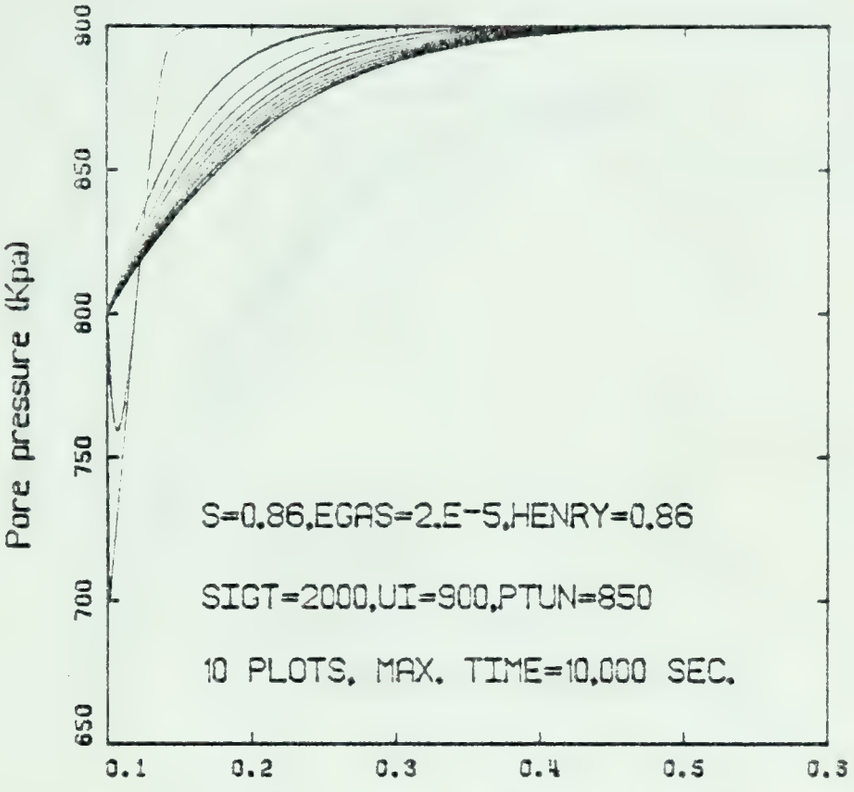
Plots of pore fluid pressure vs distance from the borehole centerline, (for t=0, 20, 1000, 2000, 3000,...10000 seconds), for the analyses described in Table 8.2 are located in Figures 8.3-8.10. These are arranged to illustrate the influence of decreasing initial saturation (Figures 8.3-.5), decreasing total stress in the borehole (Figures 8.3, 8.6-.7), decreasing H (Figures 8.7-.8), decreasing $P_{l/g}$ (Figures 8.7 and 8.9), and increasing α (Figures 8.7 and 8.10). A perusal of these figures proves to be very profitable and indicates some interesting results:

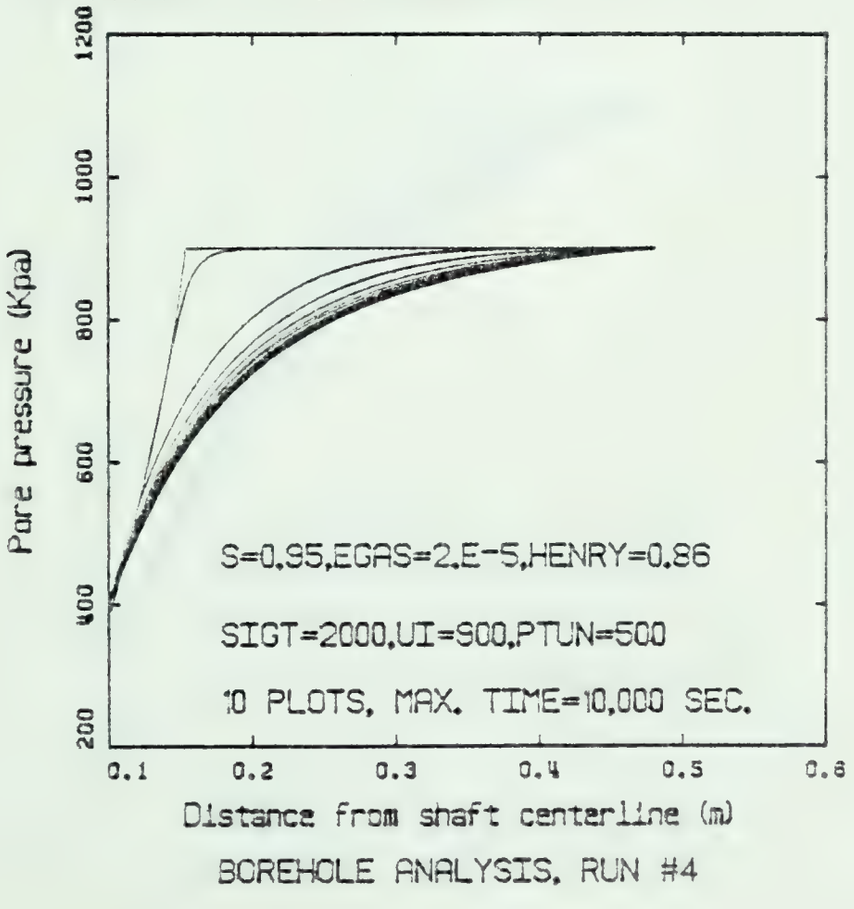
(a) It is possible for the undrained unloading phase to reduce pore pressures near the borehole wall to values below the actual fluid pressure inside the borehole. This area then experiences an increase in pressure due to both gas exsolution and swelling. The processes are



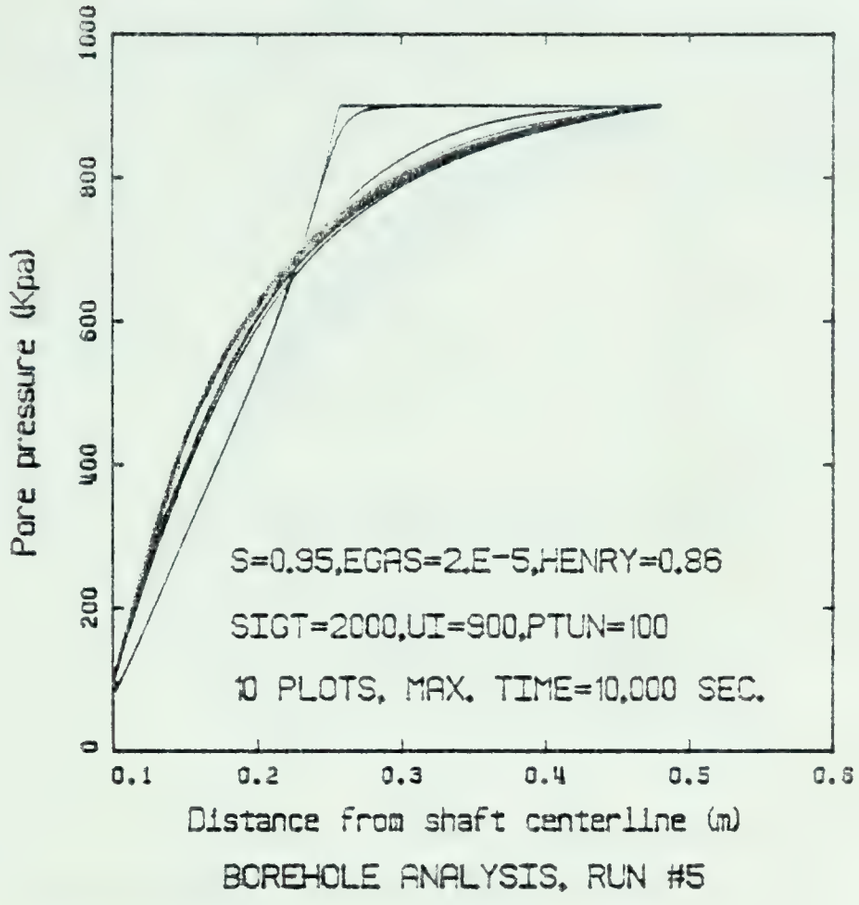


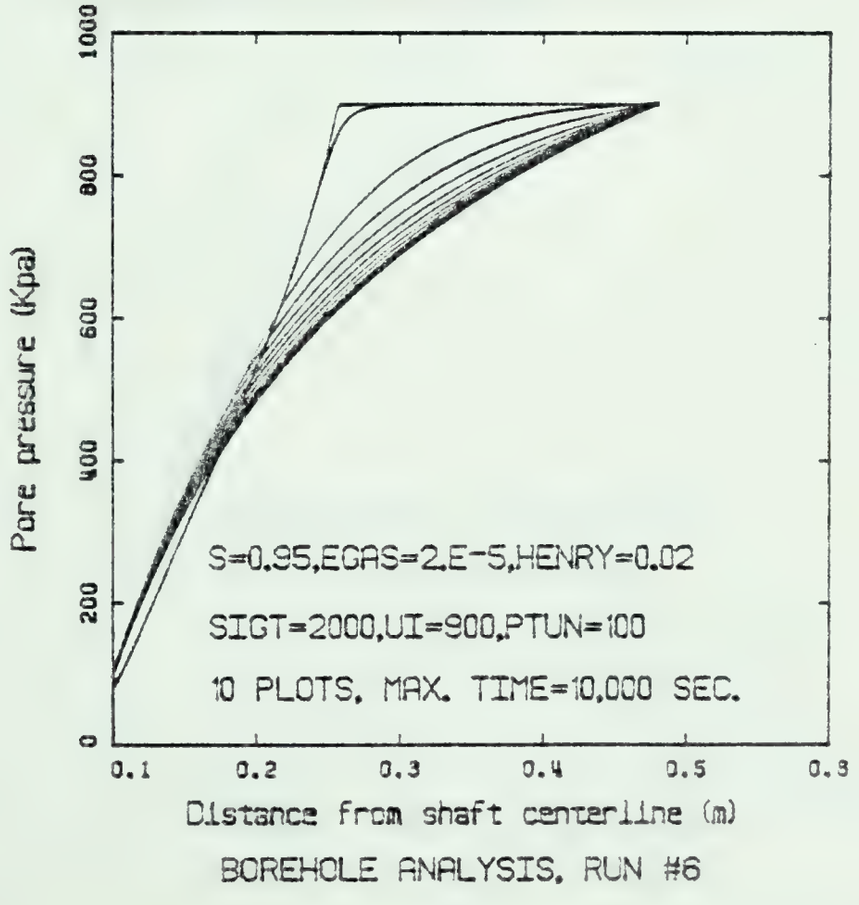
Figures 8.3 and 8.4



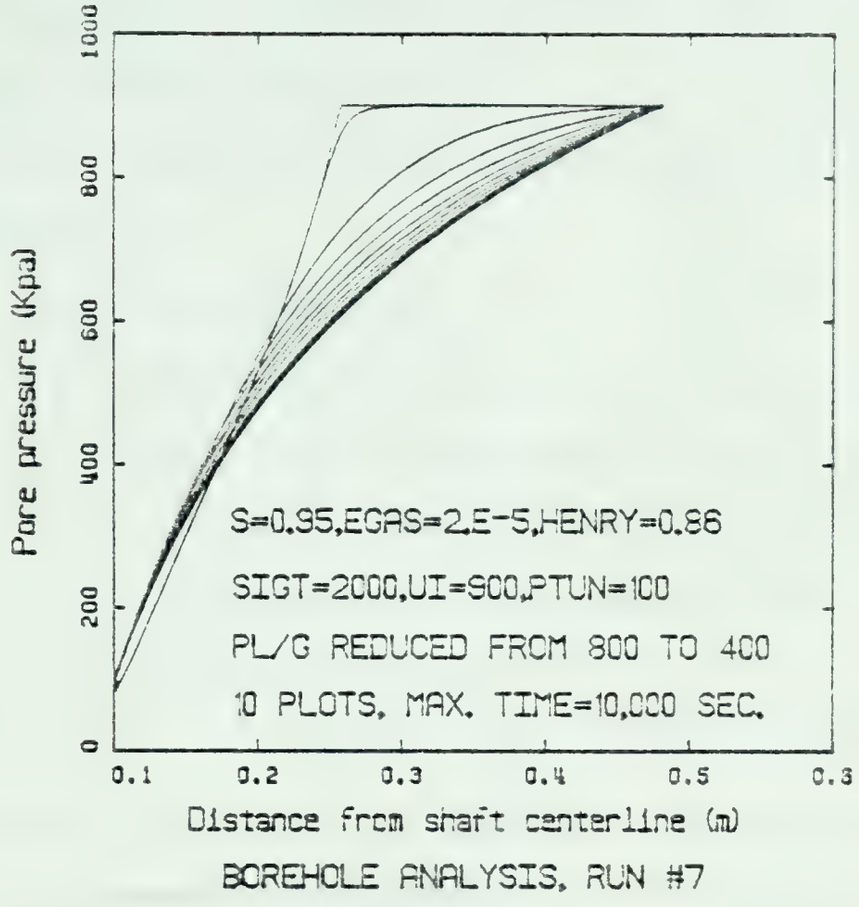


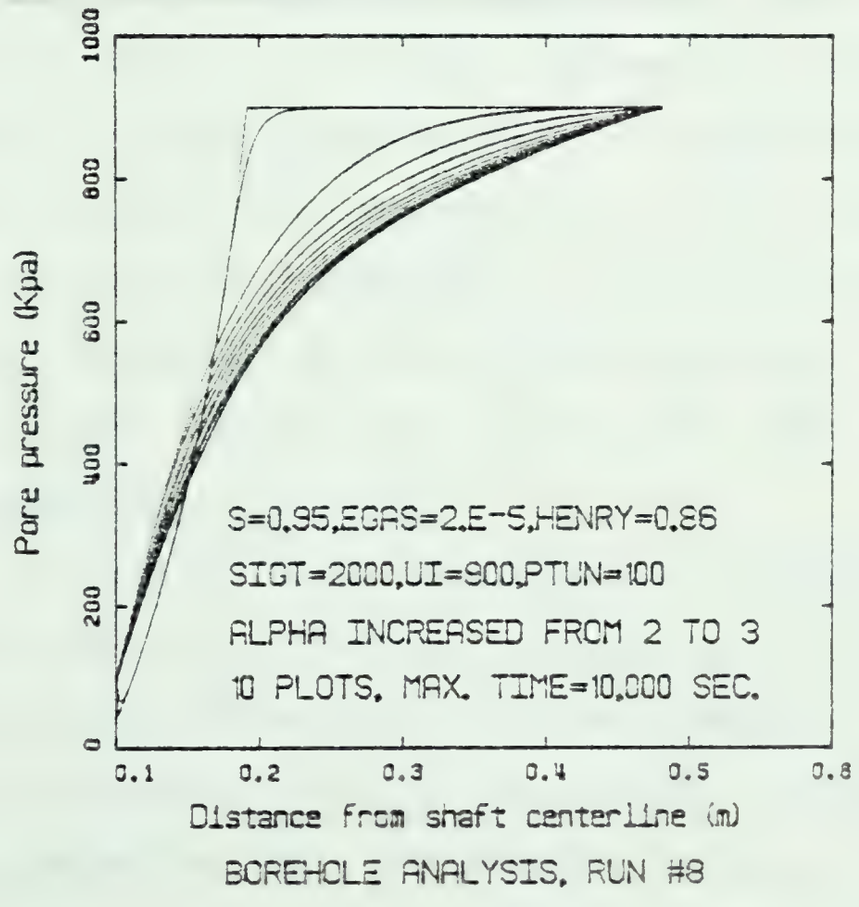
Figures 8.5 and 8.6





Figures 8.7 and 8.8





Figures 8.9 and 8.10

here working in tandem rather than opposing each other, (e.g. Figures 8.3 and 8.4).

(b) The size of the initial plastic zone may be increased by:

(i) decreasing S_i.

(ii) decreasing the total stress at the tunnel wall, σ_T^t. Note that even for values of σ_T as low as 25 KPa, the size of the plastic zone is still relatively small, (I/R = 2.57).

(iii) decreasing α.

(c) With an increase in size of the plastic zone, it is possible for the pore pressures near the borehole wall to decrease so substantially, that for a short period of time gas exsolution predominates. This behaviour is seen in Figure 8.7, where, between 0.1 and 0.25 m, the pore pressures increase for the first 3-4000 seconds, and then decrease, whereas for r > 0.25 m the pressures are continually decreasing. The extent and duration of this behaviour is also determined by the relative magnitudes of the gas exsolution and consolidation parameters.

(d) A decrease in H is seen to have a similar effect to a decrease in E (compare Figures 8.8 & 8.7), i.e. that the consolidation process is more dominant.

(e) A decrease in $P_{l/g}$ (Figure 8.9) is accompanied by the formation of a zone where $P > P_{l/g}$, (r>0.2m). In this zone, only the consolidation process is operative,

and consequently the fluid pressures are rapidly depleted. Where $P < P_{l/g}$ ($r<0.2m$) the gas exsolution process is also operative and the pore pressures are initially increased and then maintained at a relatively high level, (compare Figure 8.9 with 8.7).

(f) For analyses Nos. 3 - 8, (Figures 8.5 - .10), continued gas exsolution led to fluid saturations less than 0.85 near the borehole. This value had been chosen as the threshold at which the gas phase becomes continuous, and after which the gas exsolution process is disabled. The size of the "continuous gas" zone for the various analyses is shown in the last column of Table 8.2. A close examination of Figures 8.4 and 8.5 will disclose a wider spacing of the pressure profiles at $0.1 < r < 0.2$ in Figure 8.5 after $t \mp 2000$ seconds. This is due to the fact that the gas phase has become continuous, and thus free draining. The gas exsolution process was disabled in the analysis, and the pressures near the borehole wall decreased more rapidly.

8.4 IMPLICATIONS OF THE TRANSIENT ANALYSES

The inclusion of gas exsolution in the analysis of the transient behaviour of soils has resulted in several important changes in the expected pressure performance. Where the two transient processes oppose each other, pore fluid pressures may:

(a) decrease much more slowly than would be predicted from a normal consolidation analysis, and maintain near insitu values for prolonged periods.

(b) cause a temporary increase in pore pressures due to a large solubility disequilibrium in the pore fluid or a high gas exsolution parameter E. For the case of a borehole, shaft, or tunnel, this means that an intermediate pressure distribution may prove to be the worst from a stability point of view. A consideration of the immediate undrained, and the steady-state responses only is insufficient for stability evaluation.

This line of reasoning is just as applicable to other problems involving the unloading of a soil mass, such as the excavation of an area for a foundation to a structure, or the cutting of a slope. Depending upon the relative contributions of consolidation and gas exsolution, an intermediate pressure profile may be the more critical design parameter.

8.5 GROUND REACTION CURVES & STAND-UP TIMES

A ground reaction curve is a graphical method of illustrating the response of a tunnel wall to changes in its internal, or support, pressure. More precisely, it is a plot (or determination) of the functional relationship between the support pressure and the wall displacement, U_R. The ground

reaction curve has also been referred to as the "tunnel closure" curve, and the "convergence" curve. Ground reaction curves are useful in the design of shafts or tunnels, in determining the wall stability and standup time. Combined with the support reaction curve (or "confinement" curve) for the tunnel lining or support system, and with information on construction method and sequence, support pressures may be determined. The application of this design method to tunnels in oilsand is discussed by Smith & Byrne (1980).

Smith & Byrne distinguish between short and long term convergence curves, stating that these "will be a function of many factors which will change with time and which must be evaluated for particular situations...

(a) Time dependent strains (creep).

(b) Changes in pore fluid pressure.

(c) Changes in ground temperature."

The concepts involved in ground and support reaction curves are illustrated in Figure 8.11, which is extracted from Smith & Byrne's (1980) paper.

This section will focus mainly on the second factor, a change in pore fluid pressure, and will not deal with either item (a) or item (c). A distinction must also be made, when using the term "support" pressure, between an effective stress or a total stress applied at the tunnel wall. This is discussed further below with the consideration of boundary drainage conditions.

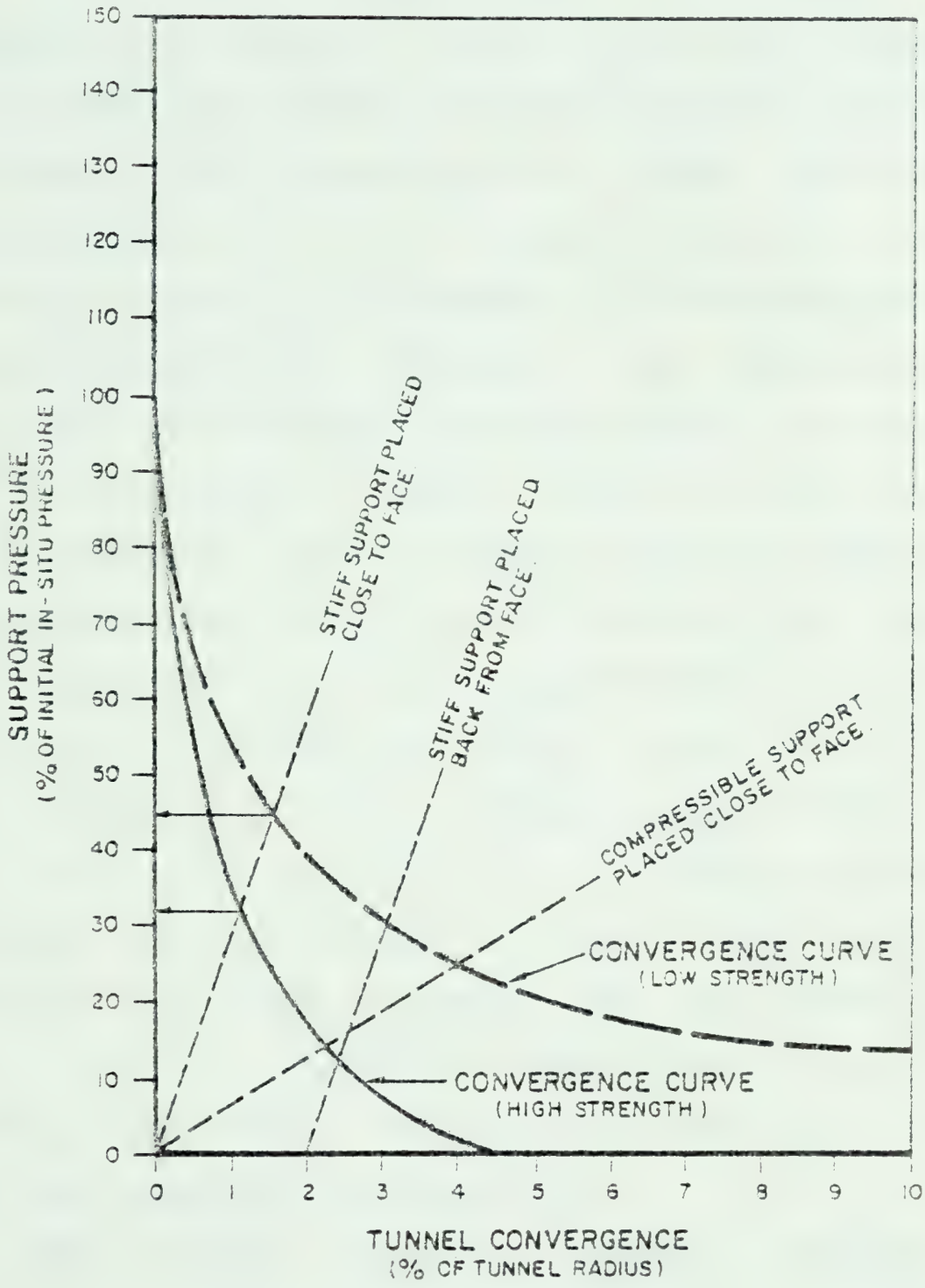


Figure 8.11 - Ground and support reaction curves
(after Smith & Byrne, 1980)

8.5.1 Drained, or undrained?

Byrne et.al. (1980) discuss the development of a two dimensional finite element program (OILSTRESS), which incorporates a non-linear constitutive law, a non-linear failure criterion, and shear dilatancy to model the behaviour of oilsand. Their analysis also includes the effects of dissolved gas, but in a limited manner, in that the exsolution process is considered to be instantaneous. The consideration of fluid drainage is also simplified to the totally drained or totally undrained boundary condition.

If the totally drained boundary condition is used, then the presence of gas in the pore fluids is superfluous to the determination of the stress distribution around the tunnel, (although it will have a marked effect on the volumes of gas and liquid draining into the tunnel or shaft). The support pressure will be an effective stress acting on the tunnel wall. In addition, if the unloading sequence is monotonic, and the strength of the material is not time dependent, then there will exist only one ground reaction curve. For the elastic-perfectly plastic model of soil behaviour used herein, this curve is defined by equation 8.21b, and illustrated in Figure 8.12.

The totally undrained boundary condition can realistically still be subdivided further into immediate and long term responses, corresponding to no gas exsolution and complete gas exsolution. This is a distinction not made by Byrne et.al. (1980). By considering the exsolution process

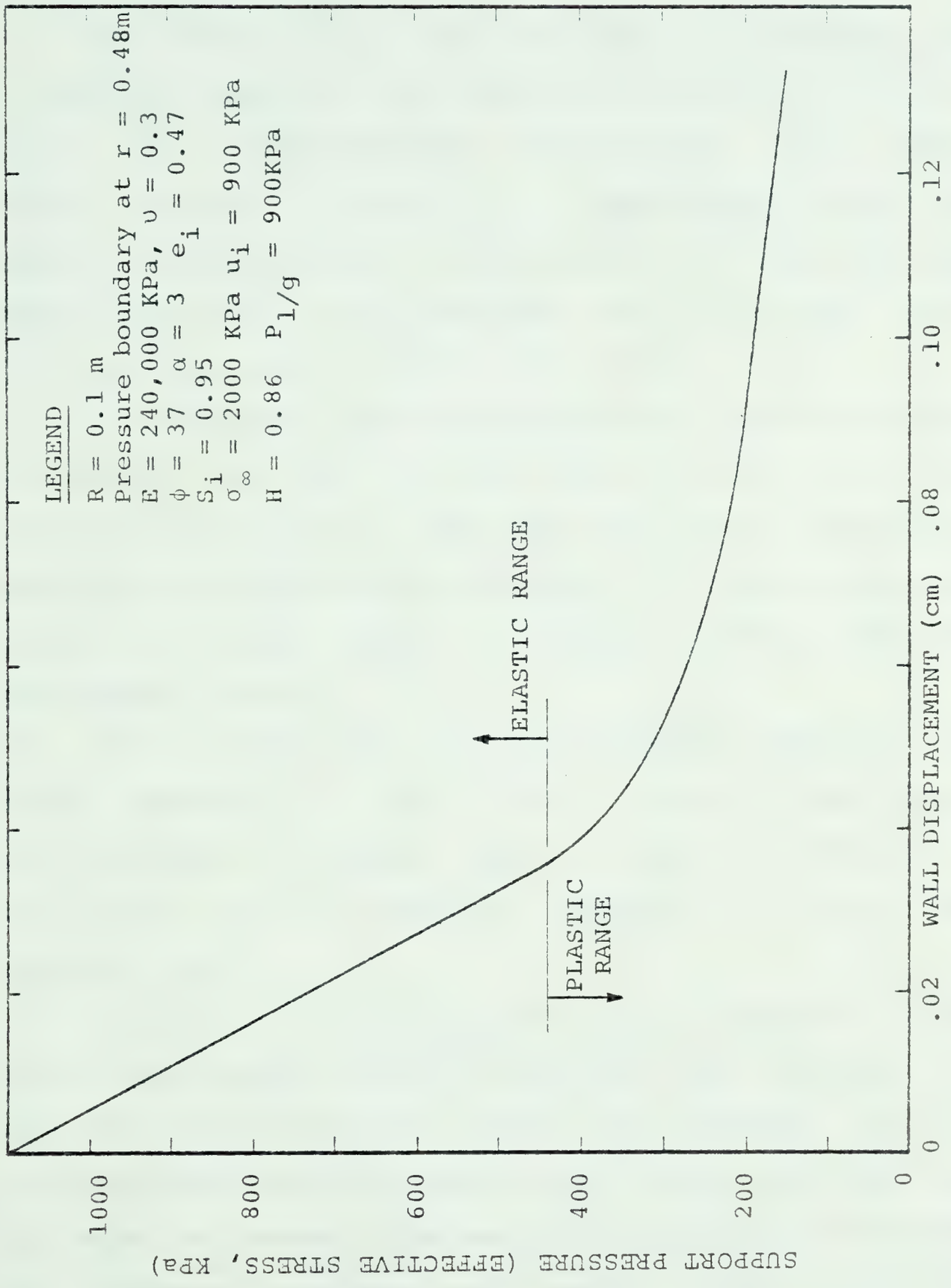


Figure 8.12 - Ground reaction curve for totally drained borehole

to be instantaneous, they have effectively compressed the two subdivisions into one.

The derivation of the theoretical relationships for the undrained behaviour was presented previously (Section 8.2 for a linear elastic-perfectly plastic soil, with a linear failure envelope). Equation 8.20, used in conjunction with equation 8.18b, allows a calculation of the undrained pressure profile. The immediate case is obtained using $H = 0$, and the long term case with $H \neq 0$.

The undrained, long term response is one that assumes no drainage not only at the shaft boundary, but also throughout the soil mass surrounding the shaft. Practically speaking, this situation is attainable if the gas exsolution process is several orders of magnitude quicker than the consolidation process.

For the completely undrained boundary condition, the support pressure is a total stress. Table 8.3 and Figure 8.13 illustrate the ground reaction curves of a shaft in a gassy soil for the immediate undrained, and long term undrained cases.

At the end of the undrained, long term example, all of the gas has exsolved from the pore fluid, but no movement of fluid has occurred anywhere in the soil profile. In both cases, the pore pressure profile on a radial line away from the tunnel is a non-equilibrium profile, and given sufficient time, these pore pressures must equalize, even if the shaft wall is maintained as a no flow boundary condition.

TABLE 8.3

UNDRAINED GROUND REACTION CURVES FOR A BOREHOLE IN A GASSY SOIL (R = 0.1 m, σ_∞ = 2000 KPa, u_i = 900 KPa)

TOTAL SUPPORT PRESS. (KPa)	U(r=R) (KPa)	EFFEC. SUPP. PRESS. (KPa)	WALL DISP. (CM)	U(r=R) (KPa)	EFFEC. SUPP. PRESS. (KPa)	WALL DISP. (CM)
	H = 0			H = 0.86		
1300	864	426	.0366	896	417	.0371
1200	789	399	.0385	878	333	.0459
1100	719	372	.0409	856	254	.0638
1000	648	342	.0446	825	184	.0993
900	581	312	.0494			
800	513	280	.0563			
700	447	248	.0658			
600	380	215	.0799			
500	317	184	.0993			

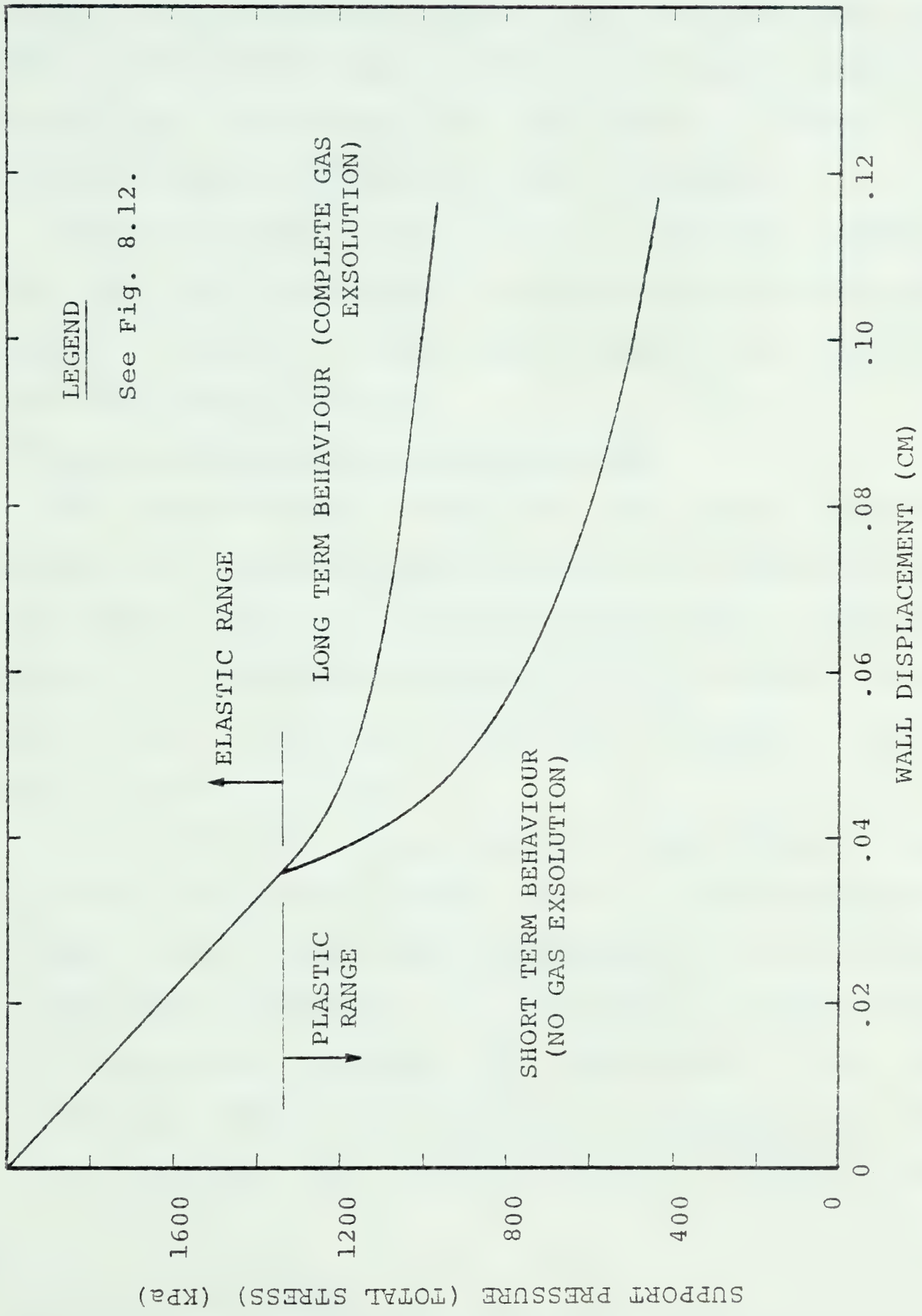


Figure 8.13 - Ground reaction curve for undrained borehole

It is apparent from Table 8.3 that the ground reaction curves for the undrained analyses are derived from the drained ground reaction curve, and thus the curves shown in Figure 8.13 are coincidental with the curve in Figure 8.12 when plotted with an "effective" support pressure.

Because of the model of soil behaviour adopted, ($c'=0$), both the fully drained (Figure 8.12) and undrained (Figure 8.13) ground reaction curves indicate an unstable wall at zero support pressure.

8.5.2 Time-dependent ground reaction curves

The time-dependent nature of the ground reaction curves can only be properly modelled when one recognizes both the drainage of fluid and the exsolution of gas as transient processes. The difficulty inherent in such a model may be appreciated by considering the possible categories of pore pressure response with time:

(a) If the consolidation process is more dominant than the gas exsolution process, then it is likely that for most of the profile the pore pressures will decrease. This type of behaviour is illustrated in Figure 8.8.[4] If the pore pressures are decreasing, then the effective stresses are increasing, isotropically, and the stress path for any element of soil is moving away

---

[4]Notice, however, that there is still a small zone near the borehole wall where pore pressures are temporarily increasing. The size of this zone will be decreased by lower values of either H or E.

from the failure envelope, (Figure 8.2, "consolidation stress path"). The borehole wall will then experience a small elastic outward movement and the stability of the wall will increase.

(b) If the gas exsolution process predominates, then the opposite is true. Pore pressures near the tunnel wall increase drastically, possibly for one to several tunnel radii, which forces a decrease of effective stress and a loss of wall stability, (Figure 8.2, "gas exsolution stress path").

The difficulty arises in calculating just what the volume changes and shaft wall displacements would be. Such a calculation is beyond the capabilities of the present model, because the consolidation/gas exsolution theory only incorporates a linear constitutive relationship for the soil. The problems associated with the use of a more realistic stress-strain law have been discussed previously. Predictions of transient ground reaction curves must await the development of a more internally consistent consolidation/gas exsolution theory.

8.6 SUMMARY

This chapter has investigated the application of the general, one-dimensional consolidation/gas exsolution theory to the problem of a borehole or shaft in a gassy soil. It has been possible to formulate the undrained (immediate or long term) fluid pressure response for an elastic-perfectly plastic soil, and to determine the wall stability in the undrained case. An approximate method of establishing the transient fluid pressure profiles has also been presented, but it has not been possible to extend the theory to an assessment of the transient ground reaction curves in more than a qualitative manner.

CHAPTER 9 - SUMMARY & CONCLUSIONS

9.1 GENERAL

It is the intent of this chapter to summarize the highlights of this research work, and point out those areas where further investigation seems warranted. This discussion is meant to focus on those aspects of the work that have made a unique contribution to our understanding of the behaviour of gassy soils.

9.2 RESTATEMENT OF OBJECTIVES

It has been the purpose of this thesis to examine and discuss the mechanics of gassy soils. Gassy soil behaviour has been divided, for convenience, into two groups, equilibrium and non-equilibrium. Both groups of behaviour have been examined in the laboratory and been given theoretical consideration, and the resulting hypotheses have been applied to field problems.

9.3 HIGHLIGHTS OF THE RESEARCH

(a) Based upon the observed equilibrium behaviour of unsaturated soils, a distinction is made between the "classical" unsaturated soil, and a gassy soil. The latter is characterized by a low hydraulic conductivity and a large volume of gas in the pore fluid.

(b) Two transient processes are identified which contribute significantly to the behaviour of a gassy soil. One is consolidation, which is well understood and has been modelled in the past. The other is gas exsolution, which is defined, in a macroscopic sense, as the ability of gas to move into or out of solution in the pore liquids. Because of the magnitude of the effects associated with gas exsolution, the exsolution process becomes an additional identifying characteristic of gassy soils.

(c) A theory combining Boyle's and Henry's laws exists, which has been applied to unsaturated soils to model behaviour. The application of such a model to an element of gassy soil, which is unloaded with an undrained boundary condition, yields an unusual prediction of behaviour:

(i) As the total stress on the element boundary decreases, the pore pressure decreases until it reaches the liquid/gas saturation pressure. Further decreases in total stress result in the production of gas in the pore space, an increase in element volume and a nearly constant pore pressure.

(ii) The pore pressure remains at a value near the liquid/gas saturation pressure, and only begins to decrease when the effective stress in the sample approaches zero.

(iii) The pore pressure parameter B for this same stress range starts at a value close to 1, decreases to a value near 0, and then increases back to 1 when the effective stress in the sample approaches 0.

(d) The behaviour predicted above for a gassy soil was verified by laboratory tests. As a consequence of the testing program, several testing techniques were developed:

(i) The use of CO_2 to displace air in partly saturated samples, which then saturated under a back pressure very quickly.

(ii) The use of direct contact LVDTs and a specially developed lateral displacement monitor to measure strains to an accuracy of $\pm$ 1 * 10^{-6}.

(iii) The use of a double latex membrane surrounded by glycerin (as a cell fluid) to limit diffusion of gas from the sample, but still permit accurate strain readings and large sample deformations.

(iv) The use of bare-wire seals to prevent leakage of the cell fluid through the electrical fittings in the cell base.

(e) The theoretical predictions and experimental observations have both demonstrated the existence and importance of the liquid/gas saturation pressure, $P_{l/g}$.

(f) The laboratory tests on undrained samples of gassy soil all portrayed a typical transient pore pressure response. Upon a step decrease in total stress, the pore pressure initially decreased, exhibiting B-values of close to

or somewhat less than 1, depending on the saturation. Decreasing pore pressure caused the pore fluid to become super-saturated with gas. As the gas exsolved, the pore pressure increased. The rate of increase was initially high, but decreased to zero as the fluid pressure became asymptotic to some maximum value. For soils of low compressibility, the maximum value of the pore pressure was only slightly less than the liquid/gas saturation pressure.

(g) The maximum value of pore pressure obtained in any one phase of an undrained unloading test could best be determined by fitting a curve to the experimental data which had the form:

$$(u - u_{min}) / (B' - u_{min}) = t / (t + A')$$

(h) It was found that the volume change vs time response of a gassy soil during a psuedo-drained test could be modelled by a relationship similar to the one mentioned above:

$$V = V_1 + (V_2 - V_1) * t / (t + A')$$

However, this relationship proved to be cumbersome to work with (theoretically). A slightly less "accurate" equation:

$$V = V_2 - (V_2 - V_1) * \exp(-E * t)$$

was preferred, because its differential with respect to time could be written in a form that did not contain t explicitly:

$$DV/Dt = E * (V_2 - V)$$

These two equations then formed the basis for a macroscopic theory of gas exsolution.

(i) The microscopic processes of gas sorption and bubble nucleation were examined and modelled, and the theoretical relationships for both bore a remarkable resemblance in form to the two latter equations. Although it was not certain that these two processes were the sole contributors, it was thought that they played a dominant role in the observed gas exsolution behaviour.

(j) As an offshoot of (i), the concept of interfacial tension was examined and found to have a viable application to the problem of occluded gas bubbles. This was contrary to recently published information in the geotechnical literature.

(k) The macroscopic theory of gas exsolution derived for the drained case was further developed for the undrained case. The resulting model was found to predict the observed transient pore pressure behaviour extremely well. The model allowed an assessment to be made of the relative importance of such parameters as initial saturation, Henry's constant, and the gas exsolution parameter E.

(l) The gas exsolution parameter E was found to be dependent upon the initial gas saturation, (1-S). This was attributed to the effect of an increased number of gas bubbles in the soil element.

(m) Using an elastic constitutive relationship, the consolidation and gas exsolution processes were combined into one general theory of transient soil behaviour. The resulting differential equation was non-linear, due to the presence of the free gas compressibility term. It was solved using an implicit finite difference scheme.

(n) The problem of gassy soil behaviour around a borehole or shaft due to a decreasing pore fluid pressure at the shaft wall was examined. In comparison to the consolidation only solution, the pore pressures for the gassy case were seen to decrease much more slowly. High pore pressures were encouraged by low values of the initial saturation, or high value of H or E.

(o) Further responses of a gassy soil around a shaft due to total stress unloading at the shaft wall were examined. Both the immediate soil response and the transient response were modelled. In the former case, an elastic - perfectly plastic model of soil behaviour was used. In the latter case, the model was restricted to an elastic constitutive relationship, which was sufficient for those analyses where the consolidation process dominated the soil behaviour.

(p) A parametric analysis of the shaft problem indicated that:

(i) It was possible for pore pressures near the shaft wall to increase in the short term due to a predominance of the gas exsolution process.

(ii) The size of this zone was influenced by Henry's constant, the gas exsolution parameter E, and the liquid/gas saturation pressure $P_{l/g}$.

(iii) Gas exsolution may lead to the formation of a zone of continuous gas near the tunnel wall. This introduces two-phase fluid flow into the problem, which was incorporated in the model in an approximate manner. The permeability of the soil to gas was assumed to be much higher than that for the water, so that gas pressures were relieved almost instantaneously.

(q) The behaviour of the shaft wall was examined in light of the "ground reaction curve" concept. It was possible to develop ground reaction curves for both the short and long term undrained cases. The latter case was the least stable. Ground reaction curves for the transient case were not developed due to the present limitations of the consolidation/gas exsolution theory.

9.4 SUGGESTIONS FOR FURTHER RESEARCH

(a) It was apparent to the author, after some time, that the development of a general model of gas exsolution would have to be based on observed data and indirect theoretical inferences. This was due to the "immature" development of the theory for the gas sorption process, and the near total ignorance with regard to bubble nucleation in soils. It is believed that a major step in modelling gas exsolution in soils has been taken, in that an hypothesis describing observed behaviour has been formulated. However, much like the development of the effective stress equation, there is almost unlimited potential for research to increase our understanding of the fundamental processes. It is suggested that work should be pursued in studying the role of bubble nucleation in soils. This is a vast topic, one that could comfortably accomodate the work of several researchers, both in the experimental and the theoretical arenas.

(b) Further work could also be directed to the less critical areas of:

(i) improving the model of gas sorption in soils.

(ii) identifying other transient processes contributing to gas exsolution at the microcsopic level.

(iii) developing a theory of gas exsolution from the microscopic processes, rather than directly from the observed behaviour.

(c) The other major area of the thesis which needs further development is the question of formulating a consolidation - gas exsolution theory which incorporates a more realistic model of soil behaviour. The elastic - perfectly plastic model seems to contain some inherent disadvantages, and it may be that a non-linear elastic constitutive relationship could be more effectively used.

BIBLIOGRAPHY

The following abbreviations have been used in this bibliography:

ASCE JSMFD	American Society of Civil Engineers. Journal of the Soil Mechanics and Foundation Division.
ICSMFE	International Conference on Soil Mechanics and Foundation Engineering.
ASTM STP	American Society for Testing and Materials Standard Testing Procedures.
CGJ	Canadian Geotechnical Journal.
ASCE JGED	American Society of Civil Engineers, Journal of the Geotechnical Engineering Division.
ASME	American Society of Mechanical Engineers.
AIME	American Institute of Mining and Metallurgical Engineers.

Adam, Bloomsburg, & Corey, (1969) "Diffusion of Trapped Gas From Porous Media." Water Resources Research, V5, p.840.

Agar, J., (1982) "Personal Communication Regarding Laboratory Tests of Oilsand at Elevated Temperatures and Pressures", University of Alberta.

Allam, M. M. & Sridharan, Asuri, (1980) "Influence of the Back Pressure Technique on the Shear Strength of Soils." Geotechnical Testing Journal, GTJODJ, Vol. 3, No. 1, pp.35-40.

Ames, W. F., (1965) "Non-linear Partial Differential Equations in Engineering." Academic Press, Vols. I & II

Ames, William, F., (1969) "Numerical Methods for Partial Differential Equations." T. Nelson & Sons Ltd.

Balla, (1957) "Stress Conditions in the Triaxial Compression Test." Proc. 4th ICSMFE V.1, p.140.

Bankoff, S. G., (1966) "Diffusion - Controlled Bubble Growth", Advances in Chemical Engineering, Edited by Drew, Hoopes, & Vermeulen, Vol. 6, Academic Press.

Barden, L., (1965) "Consolidation of Compacted and Unsaturated Clays", Geotechnique, Vol. XV, N3, pp.267-285.

Barden, Madedor & Sides, (1969) "Volume Change Characteristics of Unsaturated Clay, ASCE JSMFD 95 (SM1) pp.33-51.

Barden & Sides, (1967) "The Diffusion of Air Through the Pore Water of Soils." Proc. 3rd Asian Reg. Conf., Vol 1, pp.135-138.

Barden, L., and Sides, G. R., (1970) "Engineering Behaviour and Structure of Compacted Clay", JSMFD, ASCE, SM4, pp.1171-1200.

Barlow, E. J. & Langlois, W. E., (1962) "Diffusion of Gas From a Liquid Into An Expanding Bubble." I.B.M. Journal of Research, V6, p.329.

Bear, J., (1972) "Dynamics of Fluids in Porous Media", American Elsevier, N. Y.

Bhatnagar, S. S., (1920) "The Effect of Absorbed Gases on the Surface Tension of Water." J. Phy. Chem. V24, p.716-35.

Biot, M. A., (1941a), "General Theory of 3-D Consolidation." Journal of Applied Physics, V12, p.155.

Birkhoff, Margulies & Horning, (1958) "Spherical Bubble Growth", The Physics of Fluids, V1, N3, pp.201-4.

Bishop, A. W., (1954) "The Use of Pore Pressure Coefficients in Practice." Geotechnique V4 N4 pp.148-152.

Bishop, A. W., (1957) "Some Factors Controlling the Pore Pressures Set Up During the Construction of Earth Dams", Proceedings, Fourth International Conference on Soil Mechanics and Foundation Engineering, London, Vol. II, pp.294-300.

Bishop, A. W., (1973) "The Influence of an Undrained Change in Stress on the Pore Pressure in Porous Media of Low Compressibility." Geotechnique, V23, N3, pp.435-442.

Bishop, A. W., (1976) "The Influence of System Compressibility on the Observed Pore-Pressure Response to an Undrained Change in Stress in Saturated Rock." Geotechnique, V26, pp.371-375.

Bishop, Alpan, Blight, & Donald, (1960) "Factors Controlling the Strength of Partially Saturated Cohesive Soils" Research Conference on the Shear Strength of Cohesive Soils, (1960) pp.503-532.

Bishop & Blight, (1963) "Some Aspects of Effective Stresses in Saturated and Partially Saturated Soils" Geotechnique V13, pp.177-197 .

Bishop & Donald, (1961) "The Experimental Study of Partially Saturated Soil in the Triaxial Apparatus", Proc. 5th ICSMFE Vol.1, pp.13-21.

Bishop, A. W., and Eldin, G., (1950) "Undrained Triaxial Tests on Saturated Sands and Their Significance in the General Theory of Shear Strength", Geotechnique, Vol. II, pp. 13-32.

Bishop, A. W., & Gibson, R. E., (1963) "The Influence of the Provisions for Boundary Drainage on Strength and Consolidation Characteristics of Soils Measured in the Triaxial Apparatus", ASTM STP 361, pp.435-451.

Bishop, A. W., & Hight, D. W., (1977) "The Value of Poisson's Ratio in Saturated Soils and Rocks Stressed Under Undrained Conditions." Geotechnique, V27, N3, pp.369-384.

Bishop, Kumapley, & El-Ruwayih, (1975) "The Influence of Pore-Water Tension on the Strength of Clay." Philosophical Transactions of the Royal Society, London, A, V278, p.511-554.

Black, D. K., & Lee, K. L., (1973) "Saturating Laboratory Samples by Back Pressure." ASCE JSMFD SM1, V. 99, p.75.

Blight, (1965) "A Study of Effective Stresses for Volume Change" in Moisture Equilibrium and Moisture Changes in Soils Beneath Covered Areas, Butterworth, Australia, pp.259-269.

Burcik, (1956) "Properties of Petroleum Reservoir Fluids", International Human Resources Development Corporation, Boston, 190 pages.

Burland, J. B., (1965) "Some Aspects of the Mechanical Behaviour of Partly Saturated Soils" in: Moisture Equilibrium and Moisture Changes in Soils Beneath Covered Areas, Butterworth, Australia, pp.270-278.

Byrne, Smith, Grigg and Stewart, (1980) "A Computer Model for Stress-Strain and Deformation Analysis of Oil Sands", Applied Oilsands Geoscience, Edmonton, Alberta.

Cable, M., (1967) "The Dissolving of Stationary Gas Bubbles in a Liquid." Chem. Eng. Science V22, pp.1393-98.

Cable, M. & Evans, D. J., (1967) "Spherically Symmetrical Diffusion-controlled Growth or Dissolution of a Sphere." Journal of Applied Physics, V38 N7, p.2899

Campanella & Mitchell, (1968) "Influence of Temperature Variations on Soil Behaviour." ASCE J.SMFD SM3, V94, p.709.

Carrigy, M. A., (1967) "The Physical and Chemical Nature of a Typical Tar Sand: Bulk Properties and Behaviour". Proceedings of the Seventh World Petroleum Congress, Mexico City, V3, Tar Sands Section, pp.573-581.

Carslaw, H. S., and Jaeger, J. C., (1959) "Conduction of Heat in Solids", Oxford University Press, Second Edition.

Castro, G., (1969) "Liquefaction of Sands", Ph. D. Thesis, Harvard University, 112 pages.

Chaplin, T. K., (1961) "Compressibility of Sands and Settlements of Model Footings and Piles in Sand." Proc. 5th ICSMFE, Vol.II p.33.

Chaplin, T. K., (1965) "A Fundamental Stress-Strain Pattern in Granular Materials Sheared with Small or No Volume Change." Proc. 6th ICSMFE, Vol.1, p.193.

Chopra, P. S., & Saxena, S. K. (1979), "Geo-science Related Aspects of Geopressure Energy." ASCE, J. Energy Div., EY2, p.213.

Coleman, J. D., (1962) "Stress/Strain Relations for Partly Saturated Soil." Corresp. Geotechnique V12 N4 pp.348-350.

Corapcioglu, M. Y., (1979) "Diffusion of Dissolved Gas in Consolidating Porous Media", Water Resources Research, V15, N3, pp.563-8.

Cornforth, D. H., (1964) "Some Experiments on the Influence of Strain Conditions on the Strength of Sand", Geotechnique, Vol. XVI, p.193.

D'Appolonia, (1981) "ENEL VI and VIII Nuclear Power Plant, Alto Lazio, Italy, Report on Site Performance, July 1978 through December 1980", Unpublished Report, Project 77-500.

Danckwerts, P. V., (1970) "Gas-Liquid Reactions", McGraw-Hill (Chemical Eng. Series).

Danchwerts & Kennedy, (1958) "The Kinetics of Absorption of CO_2 into Neutral and Alkaline Solutions." Chem. Eng. Sci. V8 N3/4. p.201.

Davies, J. T. & Rideal, E. K., (1961) "Interfacial Phenomena", Academic Press.

Davies, Robert (Editor), (1964) "Cavitation in Real Liquids", Elsevier Publishing Co.

Dixon, W. J., and Brown, M. B., (1979) "BMDP-79: Biomedical Computer Programs, P-Series", University of California Press.

Dorsey, N. E., (1968) "Properties of Ordinary Water-Substance." American Chemical Society, Monograph, No. 81, Hafner Publishing Co., N. Y.

Dresser-Titan, T300 CO_2 Engineering, T310 N_2 Engineering

Duda, J. L. & Vrentas, J. S., (1969) "Mathematical Analysis of Bubble Dissolution." A.I. Chemical Eng., Journal, V15, N3, pp.351-56.

Duda, J. L., & Vrentas, J. S., (1971) "Heat or Mass Transfer-controlled Dissolution of an Isolated Sphere." Int. Journal of Heat & Mass Transfer, V.14, p.395.

Dunn, (1964) "Developments in the Design of Triaxial Equipment for Testing Compacted Soils", Pro. Symposium on the Economic Use of Soil Testing in Site Investigationn, pp. 3:19-25, Birmingham.

Dusseault, M. B., (1975), "Stress State & Hydraulic Fracturing in the Athabasca Oil Sands." Can. Journal Pet. Tech., V16, N3, pp.19-27.

Dusseault, M., (1977) "The Geotechnical Characteristics of the Athabasca Oil Sands", Ph. D. Thesis, Department of Civil Engineering, University of Alberta, 472 pages.

Dusseault, M., (1979) "Undrained Volume and Stress Change Behaviour of Unsaturated Very Dense Sands." CGJ, V16, N4, pp.627-640.

Dusseault, M. B., (1980) "Sample Disturbance in Athabasca Oil Sands." Journal of Canadian Petroleum Technology, V19, N2.

Dusseault & Morgenstern (1978a), "Characteristics of Natural Slopes in the Athabasca Oil Sands." CGJ, V15, N2, pp.202-215.

Dusseault & Morgenstern (1978b), "Shear Strength of Athabasca Oil Sands." CGJ, V15, N2, pp.216-238.

Dusseault & Morgenstern (1978c), "Locked Sands." University of Alberta, Civil Eng. Dept., Internal Memo.

Eigenbrod, Kurt, D., (1975) "Analysis of the Pore Pressure Changes Following the Excavation of a Slope." CGJ, V12, p.429.

El-Ruwayih, A. A., (1976) "Design Manufacture and Performance of a Lateral Strain Device", Geotechnique, Vol. XXVI, p.215.

El-Sohby, M. A., (1969) "Deformation of Sands Under Constant Stress Ratios." Proc. 7th ICSMFE Mexico, Vol.1, pp. 111-119.

Ells, S. C., (1926) "Bituminous Sands of Northern Alberta; Occurence and Economic Possibilities; Report on Investigations to End of 1924". Canada Mines Branch Report 632, 239 pages.

Epstein, D., (1975) "Effect of a Dense Gas Equation of State on the Expansion and Contraction of An Underwater Gas Bubble." J. Acoustic Soc. Am., V57, N6, p.1427.

Epstein, E. P. & Plesset, M. S., (1950) "On the Stability of Gas Bubbles in Liquid Solutions." Journal of Chemical Physics V18 N11, p.1505.

Fahrenwald, A. W., (1924) "Surface Reactions in Flotation", Transactions, AIME, V70, N.1283M, 90 pages.

Florence, A. L., & Schwer, L. E., (1978) "Axisymmetric Compression of a Mohr-Coulomb Medium Around a Circular Hole." Int. Journal for Numerical & Analytical Methods in Geomechanics. V2, pp.367-79.

Fogler, H. S., & Verma, V. K., (1971) "Solubility Inversion Effects on Diffusion from Collapsing Bubbles." Chemical Eng. Science, V26, pp.1391-1400.

Forest, T. W., & Ward, C. A., (1977) "Effect of a Dissolved Gas on the Homogeneous Nucleation Pressure of a Liquid", Journal of Chemical Physics, V66, N6, pp.2322-2330.

Forest, T. W., & C. A. Ward, (1978) "Homogeneous Nucleation of Bubbles in Solutions at Pressures Above the Vapour Pressure of the Pure Liquid", Journal of Chemical Physics, V69, N5, pp.2221-30.

Forsythe & Wasow, (1960) "Finite Difference Methods for Partial Differential Equations." John Wiley & Sons.

Fredlund, D. G., (1973) "Volume Change Behaviour of Unsaturated Soils." Ph. D. Thesis, University of Alberta - Dept of Civil Eng.

Fredlund, (1974) "Engineering Approach to Soil Continua" Proc. 2nd Symposium on the Applications of Solid Mechanics, Hamilton, Ont. Vol. 1, pp.46-59.

Fredlund, (1975) "A Diffused Air Volume Indicator for Unsaturated Soils." CGJ V12 N4 pp.533-539.

Fredlund, D. G., (1976) "Density and Compressibility Characteristics of Air-Water Mixtures." CGJ V13, N4, p.386

Fredlund, (1977) "Stress State Variables for Unsaturated Soils." ASCE JGED 107 (GT5) pp.447-466.

Fredlund, D. G., (1979) "Appropriate Concepts and Technology for Unsaturated Soils." Second Canadian Geotechnical Colloquim, CGJ, V16, N1, pp.121-139.

Fredlund, D. G., & Morgenstern, N. R., (1976) "Constitutive Relations for Volume Change in Unsaturated Soils." CGJ V13, N3, p.261.

Fredlund & Morgenstern, (1977) "Stress State Variables for Unsaturated Soils." ASCE GT5, V.103, p.447.

Fredlund, Morgenstern & Widger, (1978) "The Shear Strength of Unsaturated Soils." CGJ V.15, N3, p.313.

Frydman, S., & Zeitlen, J. G., (1969) "Some Pseudo-Elastic Properties of Granular Media." Proc. 7th ICSMFE, Mexico, V.1, pp.135-141.

Geertsma, J., (1957) "The Effect of Fluid Pressure Decline on Volumetric Changes of Porous Rocks." Petroleum Transactions, AIME, V210, p.331-338.

Gerrard, W., (1976) "Solubility of Gases & Liquids", Plenum Press, New York.

Guenot, A., (1979) "Investigation of Tunnel Stability by Model Tests", MSc. Thesis, University of Alberta.

Hardy, R. M., and Hemstock, R. A., (1963) "Shearing Strength Characteristics of Athabasca Oil Sands", K. A. Clark Volume, Research Council of Alberta, Information Series No. 45, p. 109.

Harris, M. C., and Sobkowicz, J. C., (1977), "Engineering Behaviour of Oil Sand", The Oil Sands of Canada-Venezuela, CIM Special Volume 17, Edited by Redford & Winestock.

Harris, M.C., Poppen, S., & Morgenstern, N. R., (1979) "Tunnels in Oil Sands", Journal of Canadian Petroleum Technology, V8, N4, pp.34-40.

Hartland & Hartley, (1976) "Axisyminetric Fluid-Liquid Interfaces." Elsevier Publishing Co.

Harvey, E. A. & Smith, W., (1959) "The Absorption of CO_2 by a Quiescent Liquid." Chemical Engineering Science, V10, pp.275-80.

Hasan, J. V., and Fredlund, D. G., (1980) "Pore Pressure Parameters for Unsaturated Soils", CGJ, V17, N3, pp.395-404.

Haxby, W. F., & Turcotte, D. L., (1976) "Stresses Induced by the Addition or Removal of Overburden and Associated Thermal Effects." Geology, pp.181-184.

Hilf, J. W., (1948) "Estimating Construction Pore Pressures in Rolled Earth Dams", Proceedings, 2nd International Conference on Soil Mechanics and Foundation Engineering, Rotterdam, Vol. III, pp.234-240.

Himmelblau, D. M., (1964) "Diffusion of Dissolved Gases in Liquids", Chemical Reviews, V64, pp.527-549.

Holstein, T., (1951) Westinghouse Electric Corp. Research Report, 60-94411-9-D.

Holubec, Igor, (1968) "Elastic Behaviour of Cohesionless Soil." ASCE, J. SMFD, V94, No. SM6, p.1215.

Hough, Heuer & Walker, (1959) "An Improved Pendant Drop, Interfacial Tension Apparatus and Data for CO_2 and Water." J. Pet. Tech., V11, p.77.

Hughes, J. M. O., Wroth, C. P., & Windle, D., (1977) "Pressuremeter Tests in Sands." Geotechnique V27, N4, pp.455-477.

Hulbert, M. H., and Bennett, R. H., (1981) "Anomalous Pore Pressures in Mississippi Delta Sediments: gas and Electrochemical Effects", Marine Geotechnology, V5, N1, pp.51-62.

Hunt, E. B. Jr., & Berry, V. J. Jr., (1956) "Evolution of Gas from Liquids Flowing Through Pourous Media." American Institute of Chemical Engineers, Journal, V.2 N4, p.560-567.

International Association for Hydraulic Research. (1972) "Fundamentals of Transport Phenomena in Porous Media." Elsevier Publishing Co.

Irwin, W. P. & Barnes, I., (1980) "Tectonic Relations of CO_2 Discharges and Earthquakes." J. Geoph. Res., V85, N.B6, pp.3115-3121.

Izydorczyk, J., Podkowka, J., & Salwinski, J., (1977) "Application of McInnes's Electrode for the Determination of Carbon Dioxide Diffusion Coefficients Through Polymer Membranes." Journal of Membrane Science, V2, N3, p.235.

Jaeger, J. C., and Cook, N.G.W., (1979) "Fundamentals of Rock Mechanics", Chapman and Hall, Third Edition.

Jakobson, B., (1957) "Some Fundamental Properties of Sand." Proc. 4th ICSMFE, Vol.1, pp.140-167.

Janbu, N., & Hjeldnes, E. I., (1965) "Principal Stress Ratios and Their Influence on the Compressibility of Soils." Proc. 6th ICSMFE V1. p.249.

Jenike & Shield, (1959) "On the Plastic Flow of Coulomb Solids Beyond Original Failure." Trans. ASME Series E., Journal of Applied Mechanics, p.599.

Jennings, & Burland, (1962) "Limitations to the Use of Effective Stresses in Partially Saturated Soils." Geotechnique V12, pp.125-144.

Kamiyama, S., & Yamasaki, T., (1977) "Theory on Charged Bubble Growth", Cavitation & Polyphase Flow Forum, pp.3-6.

Kennedy & Olson, (1952) "Bubble Formation in Supersaturated Hydrocarbon Mixtures." AIME, Trans, Vol. 195, pp.271-78.

Kezdi, A., & Horvath, G. Y., (1977) "Stress and Strains in Sand in Axially Symmetrical Case." Proc. IX ICSMFE Tokyo, V.1, pp.161-164.

Ko, H. Y., & Scott, R. F., (1967) "Deformation of Sand in Hydrostatic Compression." ASCE J. SMFD, V93, NSM3, p.137.

Ko, H. Y., & Scott, R. F., (1967) "Deformation of Sand in Shear." ASCE J. SMFD, V.93, N.SM5, Part I, p.283.

Krieger, I. M., Mulholland, G. W., & Dickey, C. S., (1967) "Diffusion Coefficients for Gases in Liquids from the Rates of Solution of Small Gas Bubbles." Journal of Phys. Chem. V.71 N4, p.1123.

Lachenbruch, A. H., (1980) "Frictional Heating, Fluid Pressure and the Resistance to Fault Motion." Journal of Geophysical Research, V85, N.B11, pp.6097-6112.

Law (1975) "Deformation of Earth Dams During Construction", Ph. D., Thesis, Dept. of Civil Engineering, University of Alberta.

LeBlond, P. H., (1969) "Gas Diffusion from Ascending Gas Bubbles." J. Fluid Mechanics, V35, pp.711-719.

Lee, Kenneth, L., & Black, David K., (1972) "Time to Dissolve Air Bubble in Drain Line." JSMFD ASCE SM2, p.181.

Lowe & Johnson, (1960) "Use of Back Pressure to Increase Degree of Saturation of Triaxial Test Specimens." ASCE Research Conf. on Shear Strength of Cohesive Soils Boulder, Colo. p.819-36.

Makhlouf, H. M., & Stewart, J. J. (1965) "Factors Influencing the Modulus of Elasticity of Dry Sand." Proc. 6th ICSMFE, V.1, p.298.

Manley, D. M. J. P., (1960) "Change of Size of Air Bubbles in Water Containing A Small Dissolved Air Content." British Journal of Applied Physics. V.11, p.39.

Matyas & Radhakrishna, (1968) "Volume Change Characteristics of Partially Saturated Soils." Geotechnique, V18 pp.432-448.

May, J. C., "So What's A Bubble?", (1979) SciQuest, V52, N8, pp.16-20.

McWhorter, Corey, & Adam, (1973) "The Elimination of Trapped Gas from Porous Media by Diffusion." Soil Science, V116, N1, p.18.

Mendelson, Alexander,(1968) "Plasticity: Theory & Application." MacMillan Co., N.Y.

Menzies, B. K., (1976) Correspondence regarding "Design Manufacture and Performance of a Lateral Strain Device", Geotechnique, Vol. XXVI, p.542.

Mesri, Adachi & Ullrich, (1976) "Pore Pressure Response in Rock to Undrained Change in all Round Stress." Geotechnique, V26, N2, pp.317-330.

Misniakiewicz and Pokrzyk, (1969) "Effect of the Gas Phase on Surface Tension of Water", (Polish), Zeszyty Naukowe Politechniki Slaskiej, Chemia, N47, pp.103-10.

Mitchell & Griffiths, (1980) "The Finite Difference Method in Partial Differential Equations." John Wiley & Sons.

Mori, Y., Hijikata, K., & Nagatani, T., (1977) "Fundamental Study of Bubble Dissolution in Liquid", International Journal of Heat & Mass Transfer, V20 p.41.

Muskat, M., (1937) "The Flow of Homogeneous Fluids Through Porous Media." McGraw-Hill, NY.

Newland, P. L., & Allely, B. H., (1959) "Volume Changes in Drained Triaxial Tests on Granular Materials." Geotechnique, V7, p.17.

Newman, G. H., (1973) "Pore Volume Compressibility of Consolidated, Friable, and Unconsolidated Reservoir Rocks Under Hydrostatic Loading." Journal of Petroleum Technology, V25, N2, pp.129-134.

Nur, A., & Byerlee, J. D., (1971) "An Exact Effective Stress Law for Elastic Deformation of Rock with Fluids." Journal of Geophysical Research, V76, N26, pp.6414-19.

Okumura, T., (1977) "Stress Change in Soil Sample Taken from Sea Floor." 9th ICSMFE, Specialty Session 2, Soil Sampling, Tokyo, pp.141-145.

Plum & Esrig, (1969) "Some Temperature Effects on Soil Compressibility and Pore Water Pressure", in: Effects of Temperature & Heat on Engineering Behaviour of Soils, Highway Research Board, Special Report 103, p.231.

Readey, D. W. & Cooper, A. R., (1966) "Molecular Diffusion with a Moving Boundary and Spherical Symmetry." Chemical Engineering Science, V21, p.917.

Richards, B. G., (1974) "Behaviour of Unsaturated Soils". Chap. 4 in Soil Mechanics - New Horizons. Ed. Lee, J. K., American Elsevier, pp.112-157.

Roesner & Poppen, (1978) "Shaft Sinking & Tunnelling in the Oil Sands of Alberta." AOSTRA Seminar on Underground Excavation in Oil Sands.

Rosner, D. E., & Epstein, M., (1970) "Lifetime of a Soluble Sphere of Arbritrary Density." Journal of Phys. Chem. V74, N22, p.4001.

Rosner, D. E., & Epstein, M., (1972) "Effects of Interface Kinetics, Capillarity & Solute Diffusion on Bubble Growth Rates in Highly Super-saturated Liquids." Chem. Eng. Sci., V27, p.69.

Rowe, P. W., (1962) "The Stress-Dilatancy Relation for Static Equilibrium of An Assembly of Particles in Contact." Royal Society of London Proceedings, Series A, Vol. 269, pp.500-527.

Rowe, P. W., (1971) "Theoretical Meaning and Observed Values of Deformation Parameters for Soil", in: Stress-Strain Behaviour of Soils, Proceedings of the Roscoe Memorial Symposium Cambridge, pp.143-194.

Saxena, S. K., (1980) "Geotechnical and Environmental Aspects of Geopressure Energy", Proceedings of a Conference by the same name, sponsored by Engineering Foundation, N.Y.

Scheidegger, A. E., (1974) "The Physics of Flow Through Porous Media." University of Toronto Press.

Schultze, & Moussa, (1961) "Factors Affecting the Compressibility of Sand." Proc. 5th ICSMFE V.1, p.335.

Schuurman, I. E., (1966) "The Compressibility of an Air/Water Mixture and a Theoretical Relation Between the Air and Water Pressures." Geotechnique, V16, p.269.

Schwen, K., (1970) "Effect of Atmospheric CO_2 on the Surface Tenstion of Conductive Water" (German), Tenside, V7, N1, pp.21-2.

Scott, R. F., (1963) "Principles of Soil Mechanics", Addison-Wesley.

Scott, Tung, & Drickamer, (1951) "Diffusion Through an Interface", Journal of Chemical Physics, V19 N9, p.1075.

Scriven, L. E., (1959) "On the Dynamics of Phase Growth." Chemical Engineering Science. V.10 N1, pp.1-13.

Sides, G. R. & Barden, L., (1970) "The Time Required for the Attainment of Air-Water Equilibrium in Clay Soils." Journal of Soil Science, V.21 N1, p.50.

Skempton, A. W., (1954) "The Pore Pressure Coefficients A and B. in Geotechnique Vol. IV, N4 pp.143-147.

Smith, L. B., and Byrne, P. M., (1980) "Convergence-confinement Method of Design for Shafts and Tunnels in Oilsands", Applied Oilsands Geoscience, Edmonton, Alberta.

Stephen, H. & Stephen, T., (1963) "Solubilities of Inorganic & Organic Compounds." Vol. 1 Binary Systems.

Sterne, K. B., (1981) "Hollow Cylinder Testing of Oil Sands", MSc. Thesis, University of Alberta.

Stewart, Hunt, Schneider, Geffen & Berry, (1954) "The Role of Bubble Formation in Oil Recovery by Solution Gas Drives in Limestone". AIME, Trans, Vol. 201, pp.294-301.

Stewart, P. B., & Munjal, P., (1970) "Solubility of CO_2 In Pure H_2O, Snythetic Sea Water & Synthetic Sea Water Concentrates at -5^{o} to 25^{o} C and 10 - 45 Atm. Pressure." Journal of Chemical & Engineering Data, V.15, N1, pp.67-71.

Szekely, J. & Martins, G. P., (1971) "Non-equilibrium Effects in the Growth of Spherical Gas Bubbles Due to Solute Diffusion." Chem. Eng. Science, V26, p.147.

Szekely, J., & Fang, S. D., (1973) "Non-equilibrium Effects in the Growth of Spherical Gas Bubbles Due to Solute Diffusion - II." Chem. Eng. Science, V28, pp.2127-40.

Tao, L. N., (1978) "Dynamics of Growth or Dissolution of A Gas Bubble", Journal of Chemical Physics, V69, N9, pp.4189-94.

Tao, L. N., (1979) "The General Solution and its Analyticity for Growth or Dissolution of a Gas Bubble", Journal of Chemical Physics, V71, N8, pp.3455-61.

Terzaghi, K., (1943) "Theorectical Soil Mechanics", John Wiley & Sons, N.Y.

Timoshenko & Goodier, (1970) "Theory of Elasticity" (Engineering Monograph Series) 3rd Ed. McGraw Hill

Tucker, A. S., (1974) "Measurement of Dissolved Gas and Diffusion Coefficients in Liquids Using the Unstable Equilibrium State of Bubbles", Ph. D. Thesis, University of Toronto, 130 pages.

Tucker, A. S., & Ward, C. A., (1975) "Critical State of Bubbles in Liquid-Gas Solutions." Journal of Applied Physics, V46, N11, p.4801.

Verma, N. S., (1976) "One Dimensional Compression and Pore Pressure Characteristics of Compacted Soils." Ph. D. Thesis, University of Ottawa - Dept. of Civil Eng.

Walker, F. C., and Daehn, W. W., (1948) "Ten Years of Pore Pressure Measurements", Proceedings, Second International Conference on Soil Mechanics and Foundation Engineering, Rotterdam, Vol. III, pp.245-250.

Walker, J., (1981) "Reflections on the Rising Bubbles in a Bottle of Beer", Scientific American, December, pp.172-176.

Ward, Balakrishnan & Hooper, (1970) "On the Thermodynamics of Nucleation in Weak Gas-Liquid Solutions." Trans. ASME V92 p.695. (Journal of Basic Engineering).

Ward, Tikuisis and Venter (1982) "Stability of Bubbles in a Closed Volume of Liquid-gas Solution", Paper submitted to the Journal of Applied Physics, Dec. 10, 1981, 37 pages.

Ward, C. A. & Tucker, A.S., (1975) "Thermodynamic Theory of Diffusion-controlled Bubble Growth or Dissolution & Experimental Examination of the Predictions." Journal of Applied Physics, V.46, N1, p.233.

Ward, C. A., & Tucker, & So., (1979) "A Bubble Evolution Method for Diffusion Coefficient Measurements Utilizing the Critical Size Concept", J. Physical Chemistry, V83, N4, pp.543-50.

Ward, C. A. et al., (1982) "Comparison of Stress Produced by Bubble Nucleation Within a Bone Cell and the Stress Necessary to Fracture a Semi-circular Canal of the Inner Ear", Proceedings, Canadian Congress on Ocean Technology.

Wedlake, G. D., & Robinson, D. B., (1979) "Solubility of CO_2 in Silicone Oil." Journal of Chemical & Engineering Data, V24, N4, p.305-6.

White, et al., (1970) "Physics of Desaturation in Porous Materials" ASCE IR2, Vol. 96, p.165.

Wilson, G., & Sutton, J. L. E., (1948) "A Contribution to the Study of the Elastic Properties of Sand." Proc. 2nd ICSMFE, V1, p.197.

Wissa, A. E. Z., (1969) "Pore Pressure Measurement in Saturated Stiff Soils." J. SMFD JGED ASCE SM4, p.1063.

Withiam & Kulhawy, (1976) "Undrained Volume Changes in Compacted Cohesive Soil", ASCE GT10, V.102, p.1029.

Wood, D. M. (1979) "The Behaviour of Partly Saturated Soils: A Review" Univ. of Cambridge, Dept. of Civil Engineering, CUED/D - Soils/TR 69.

Wyckoff & Botset, (1936) "The Flow of Gas-Liquid Mixtures Through Unconsolidated Sands." Physics V7, p.325.

Yang, Wen-jei., (1972) "Stability of Gas Bubbles in a Deformable Material Containing Dissolved Gases." Journal of Chem. Phys. V56 N4, p.1610.

APPENDIX A

GAS EXSOLUTION IN AN UNDRAINED ELEMENT OF SOIL

COMPUTER PROGRAM

APPENDIX A

GAS EXSOLUTION IN AN UNDRAINED ELEMENT OF SOIL

COMPUTER PROGRAM

```
100: "B":USING:INPUT "POROSITY(%)=";N,"SATURATION(%)=";S:
     N=N/100:S=S/100
110: INPUT "HENRYS CONSTANT(CC/CC)=",H,"COMPRESS INDEX=",W
120: INPUT "INITIAL PP(KPA)=",U:E=N/(1-N):P=U+101.33:L=0
130: INPUT "INIT.TOT.STRESS(KPA)=",T,"DEL.TOTAL STRESS(KPA)=
     ",X:X=-ABS(X)
132: INPUT "BUBBLE PRESS(KPA)=",I
135: Q=0:Y=4.5E-7
136: IF T>0 GOTO 140
137: Z=W: GOSUB 500: GOTO 210
140: R=T-U
142: PRINT "EFF.STRESS=",R
143: IF R>ABS(X) GOTO 145
144: INPUT "DEL.TOT.STRESS(KPA)=",X:X=-ABS(X)
145: Z=W*LOG(1+.1*X/R)/(1+E)/.1/X
150: GOSUB 500
160: O=X-U:D=W*LOG(1+O/R)/(1+E)/O:M=ABS(Z/D-1)
170: IF M<=.05 GOTO 200
180: Z=D: GOTO 150
200: IF L=1 GOTO 250
205: IF H=0 GOTO 250
210: Q=H:L=1:G=U/X:PRINT "SHORT DELU=",U:PRINT "B=",G
211: IF T>0 GOTO 145
212: GOSUB 500
250: L=0:G=U/X:PRINT "LONG DELU=",U:PRINT "B=",G
260: P=P+U:U=P-101.33:T=T+X
261: IF T>0 LET F=E+W*LOG(R/(R+O))
262: IF T<=0 LET F=E-(1+E)*W*O
270: S=S/(1+(F-E)/E):E=F:N=E/(1+E):Q=0
280: GOTO 136
500: A=Z+N*S*Y:B=Z*(P-X)+N*(Y*S*P+1-S+S*Q):C=-Z*X*P
501: IF I=0 GOTO 510
502: IF L=0 GOTO 510
503: C=C+N*P*(1-S)+N*S*Q*(P-I-101.33)
510: J=√(B*B-4*A*C):U=(-B+J)/(2*A):V=(-B-J)/(2*A)
520: IF V>=X GOTO 550
530: RETURN
550: PAUSE "TWO SOLUTIONS FOR DELU":U=V:RETURN
```

VARIABLES USED IN PROGRAM

A	Parameter A in quadratic solution for Δu
B	Parameter B " "
C	Parameter C in " "
D	New value of compressibility β_T
E	Void ratio
F	New void ratio
G	"B" parameter, $\Delta u/\Delta\sigma$
H	Henry's constant
I	Bubble pressure. (If D=0, assume equilibrium at start)
L	Counter
M	Check value for tolerance for iterative solution on Δu
N	Porosity
O	Change in effective stress, X-U
P	Pore pressure (absolute)
Q	Current value of H
R	Effective stress
S	Saturation
T	Total stress. Also indicator for W. If T>0, W=C_c If T=0, W=β_T
U	On input, U is gauge pore pressure. Later, U is the change in pore pressure.
V	Alternate solution for change in pore pressure
W	Compression index or compressibility, depending on value of T
X	Change in total stress
Y	Compressibility of water
Z	Old value of compressibility

APPENDIX B

PLOTS FOR GAS DIFFUSION THROUGH SAMPLE MEMBRANE

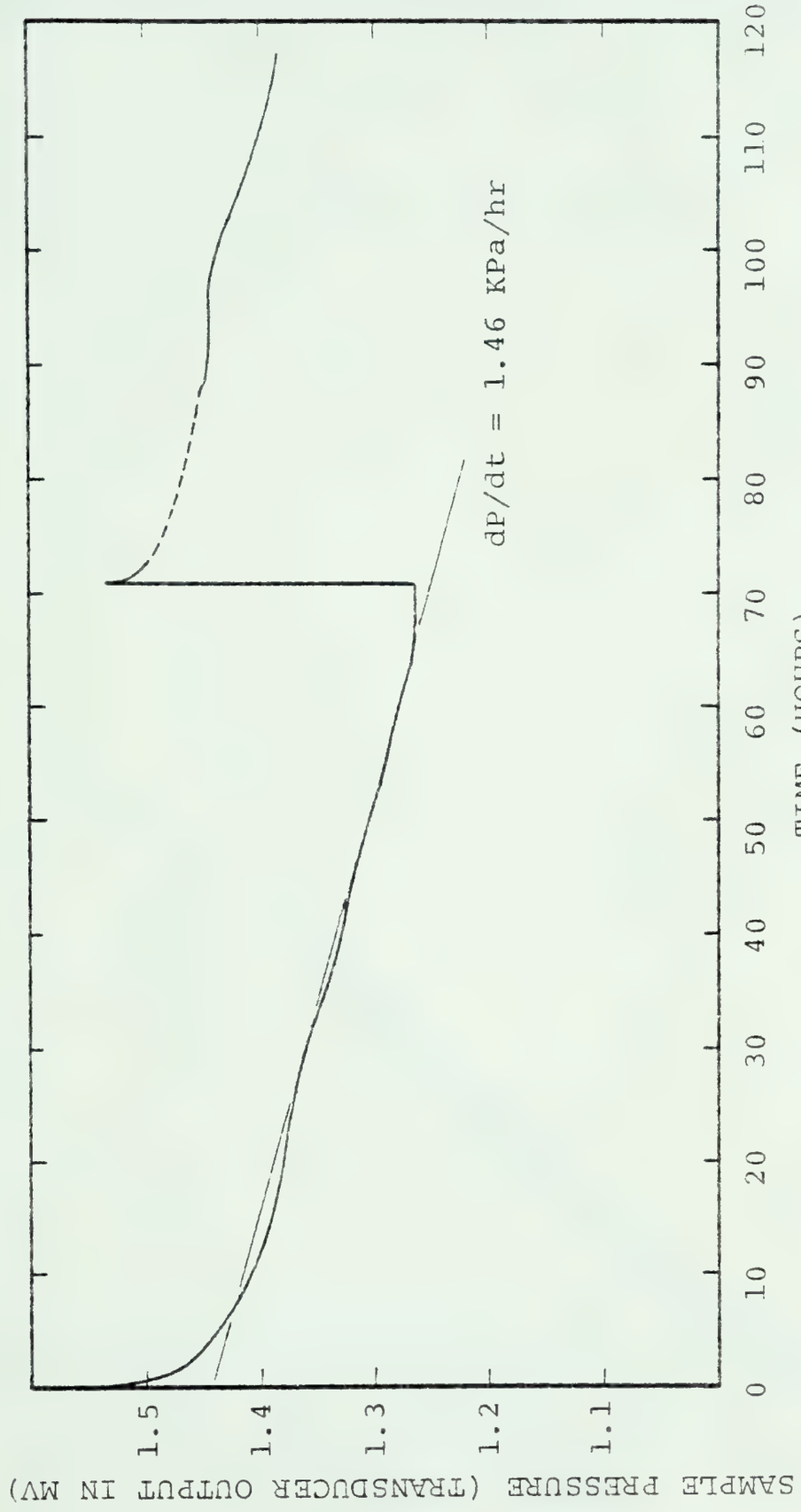


Figure B.1 - Diffusion test for Sample 4

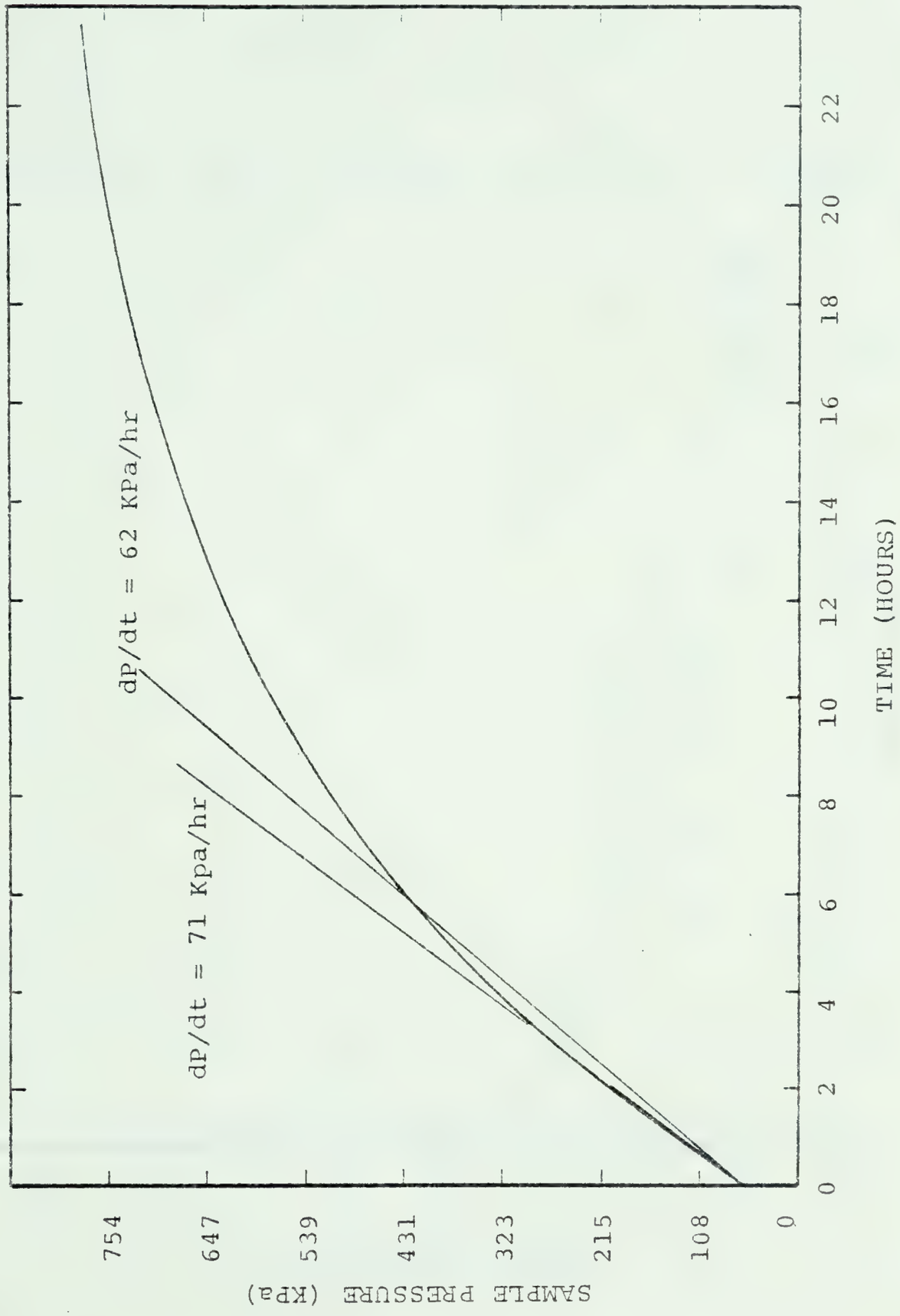


Figure B.2 - Diffusion Test for Sample 5

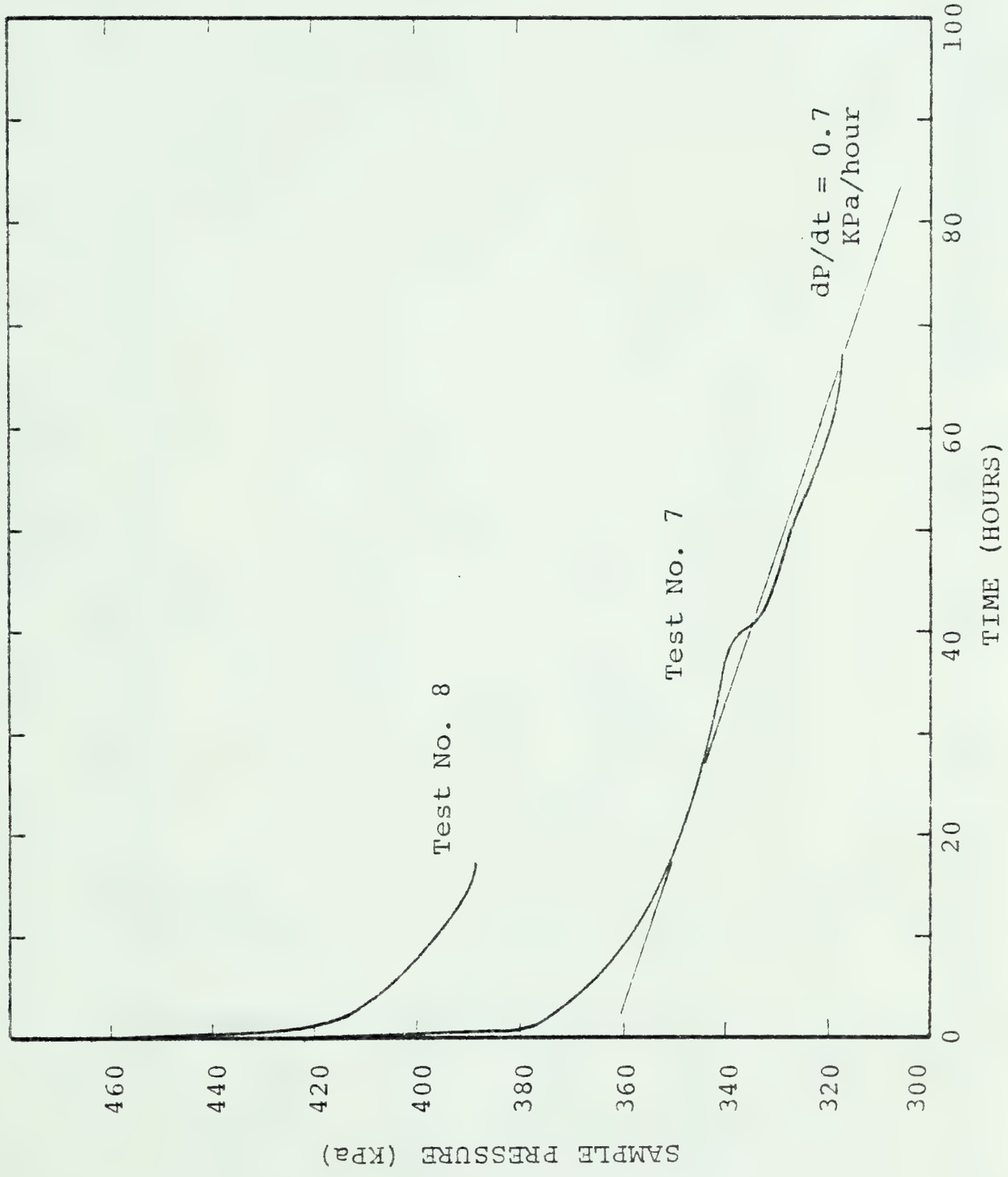


Figure B.3 - Diffusion test for Sample 7 and 8

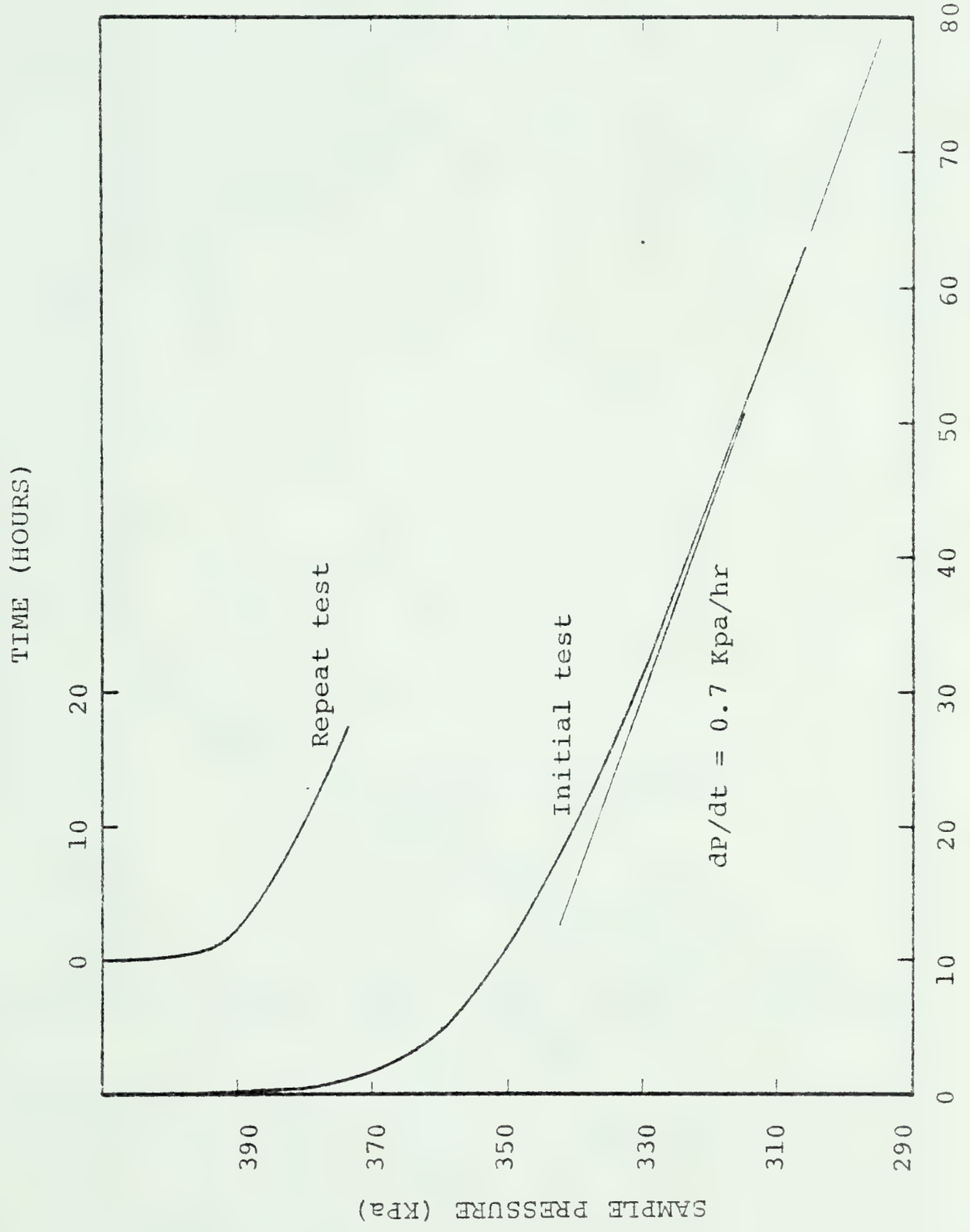


Figure B.4 - Diffusion Test for Sample 10G

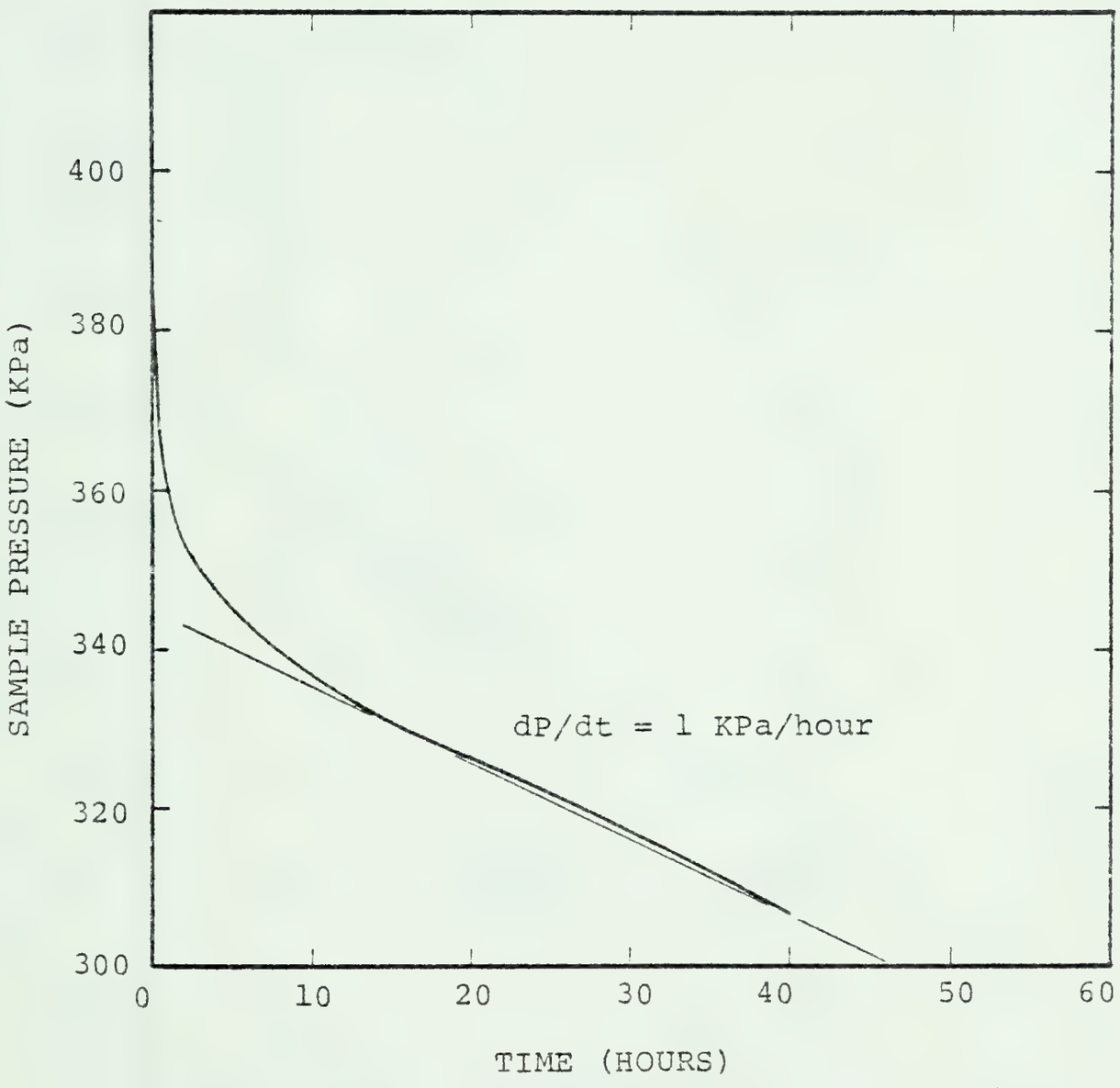


Figure B.5 - Diffusion test for Sample 11

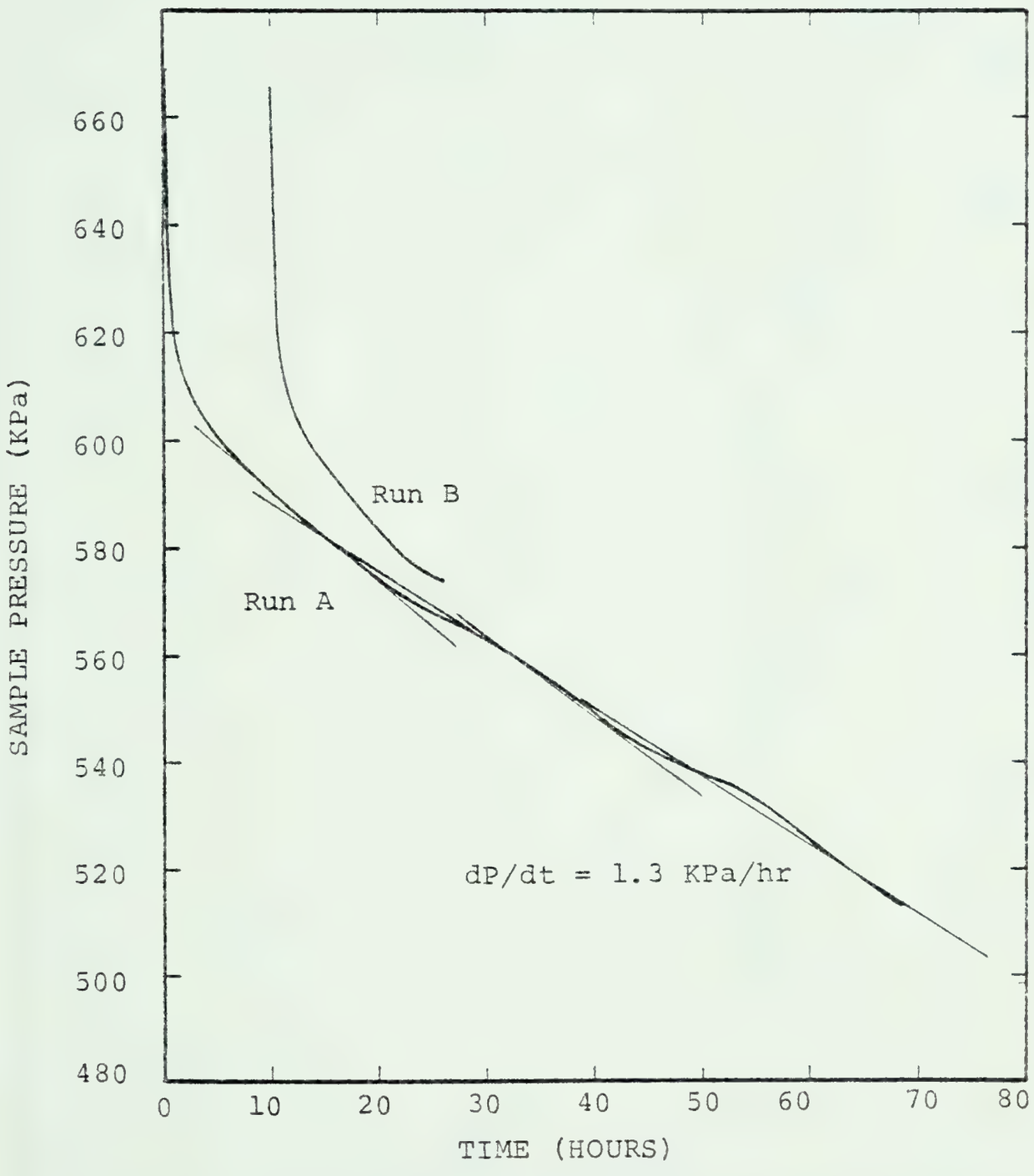


Figure B.6 - Diffusion test for Sample 12

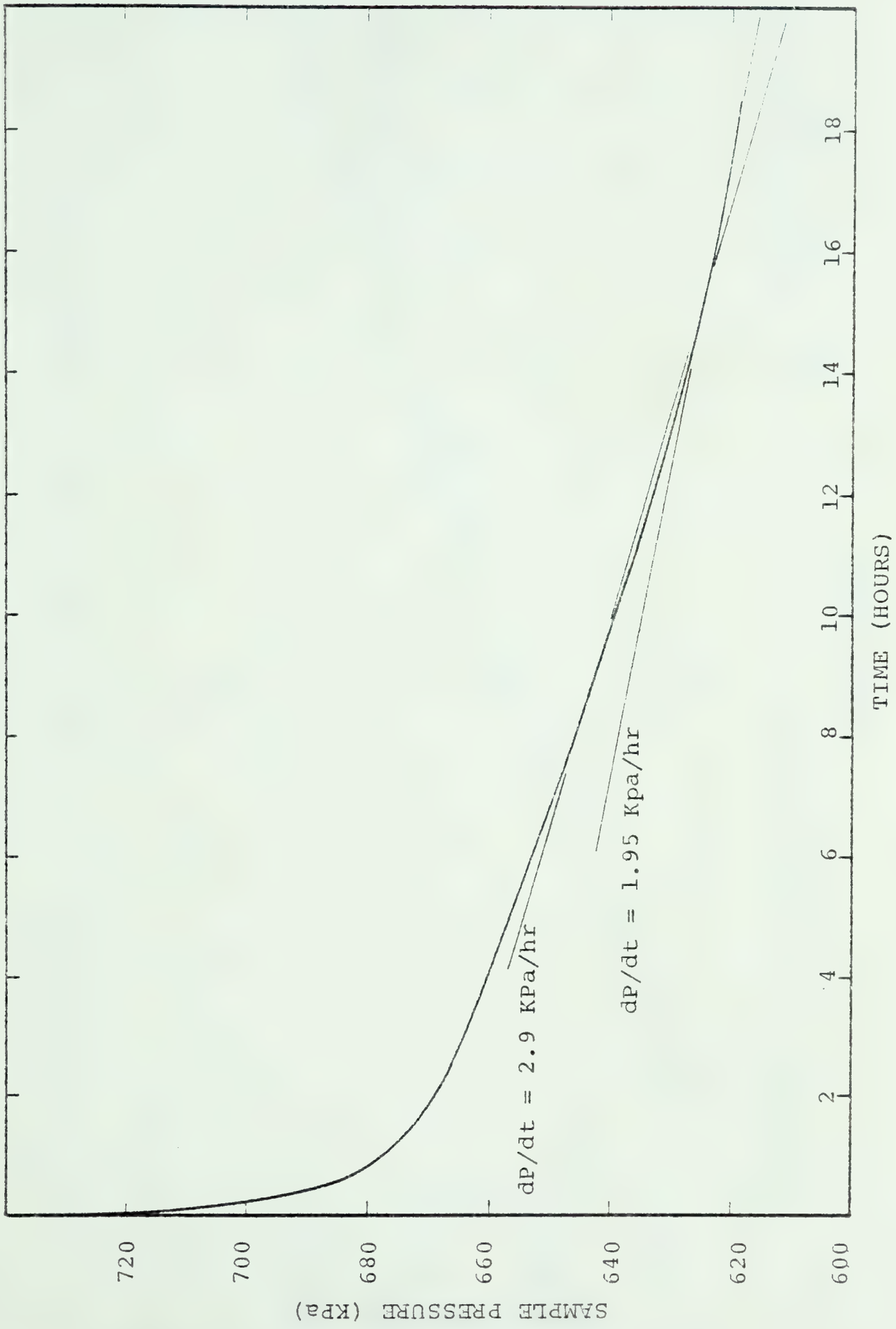


Figure B.7 - Diffusion Test for Sample 15

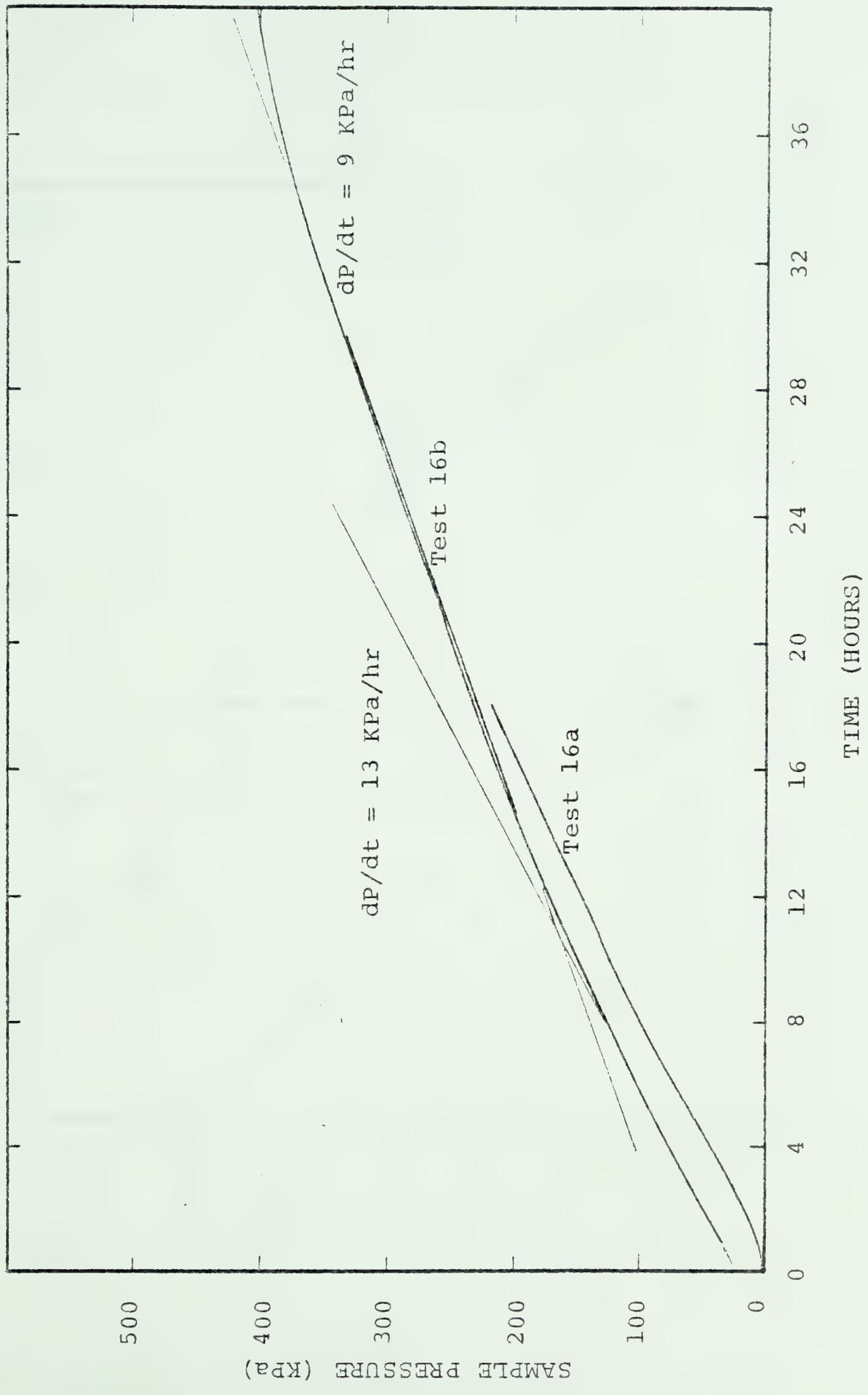


Figure B.8 - Diffusion test for Sample 16

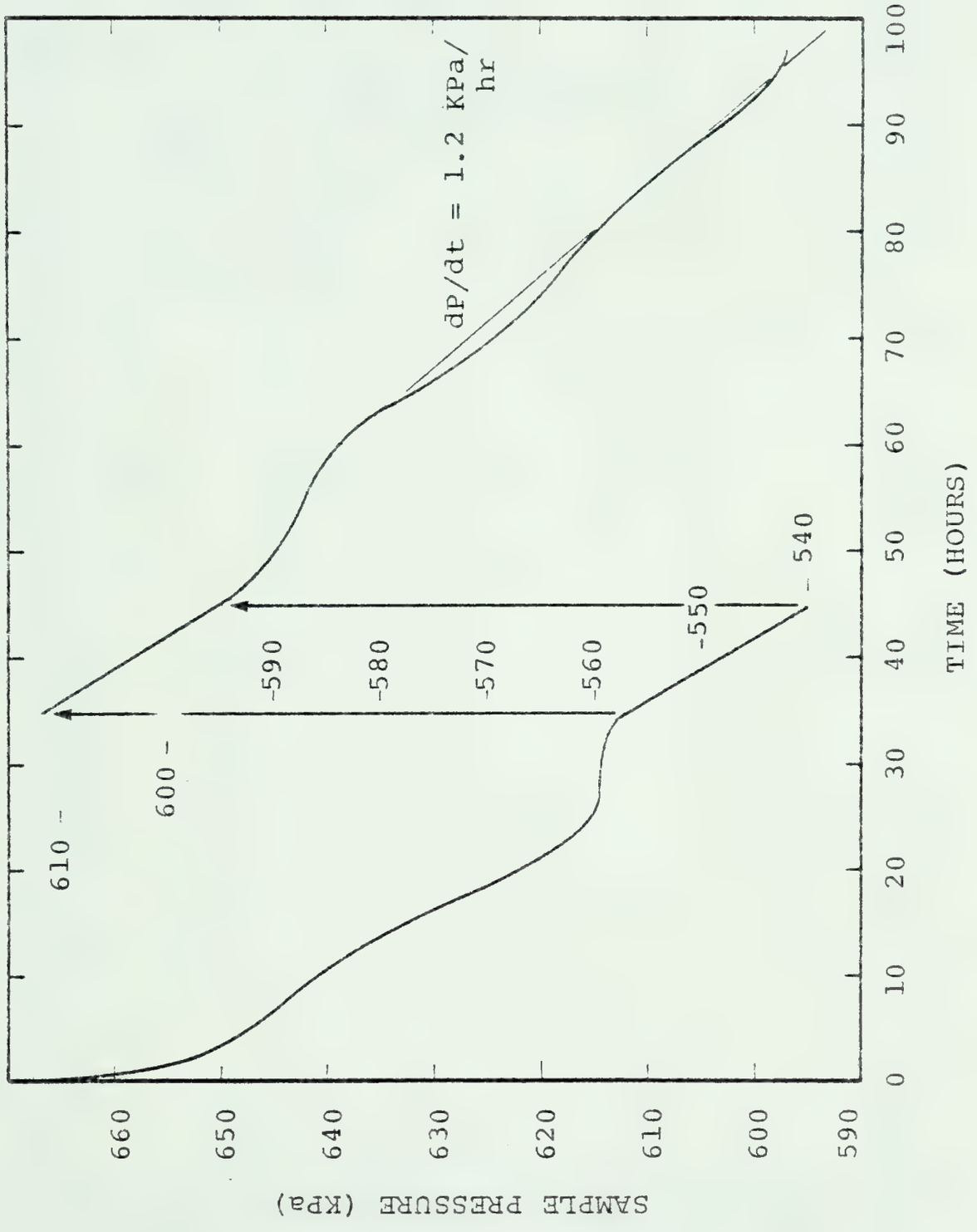


Figure B.9 - Diffusion Test for Sample 17

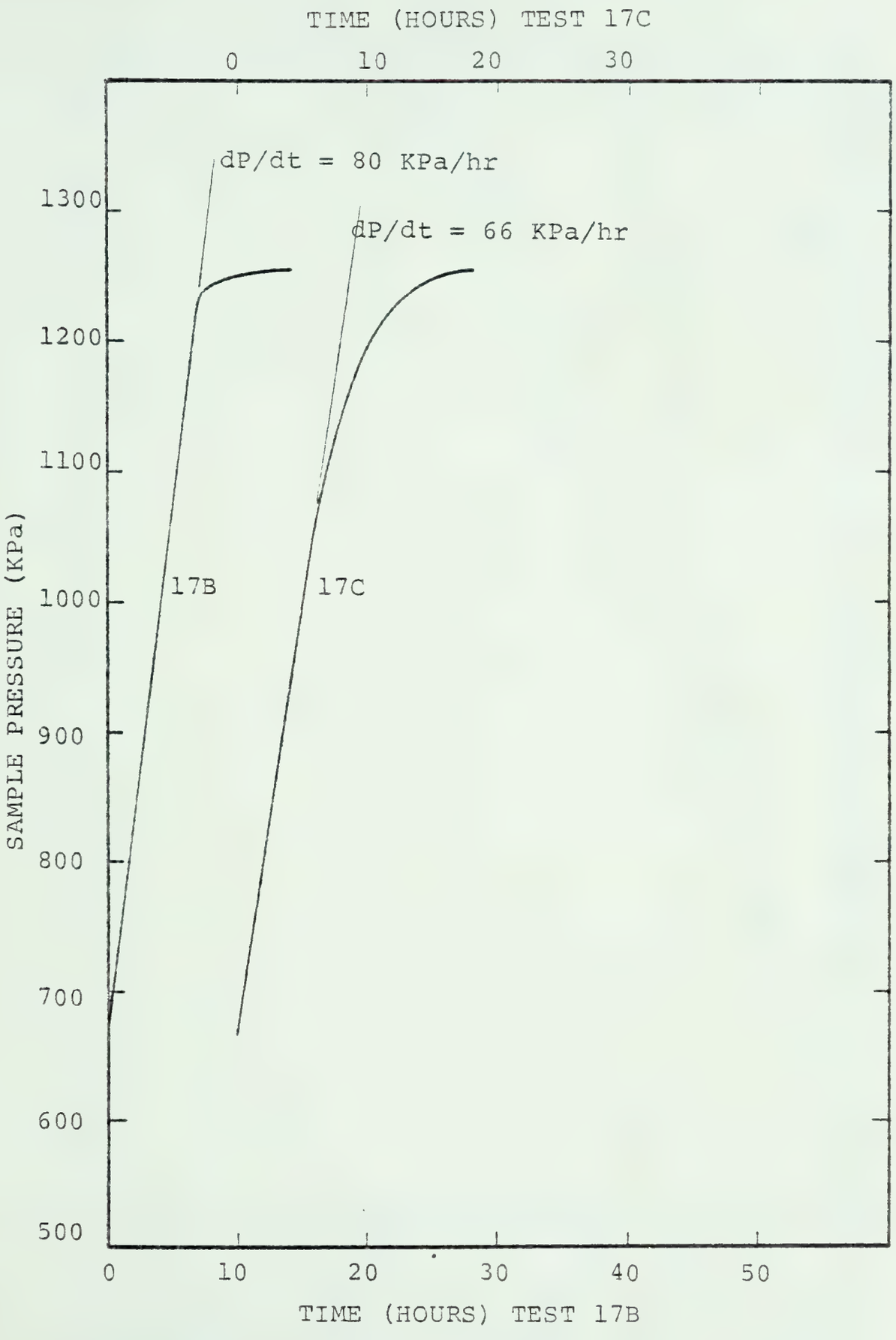


Figure B.10 - Diffusion test for Sample 17

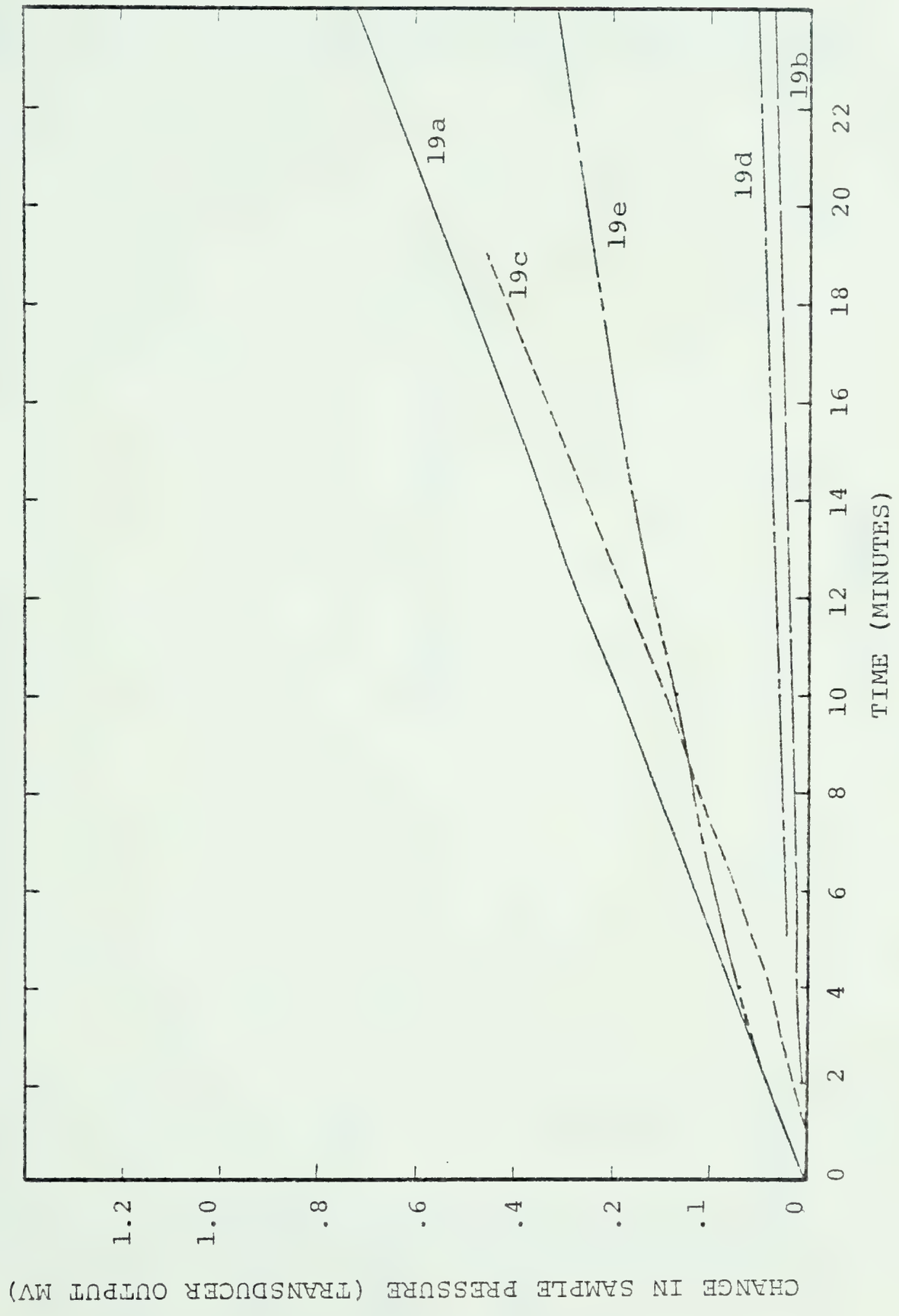


Figure B.11 - Diffusion test for Sample No. 19

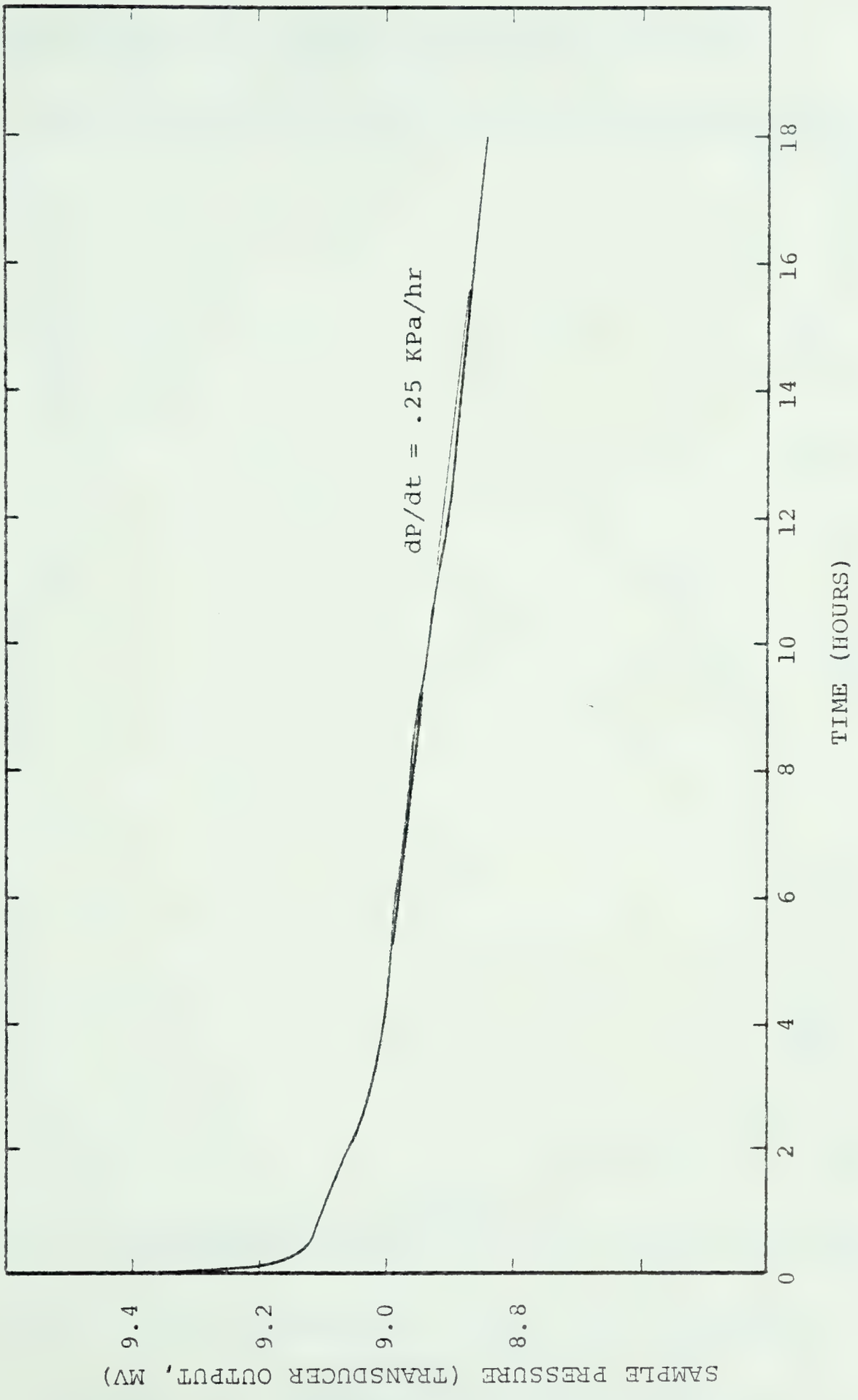


Figure B.12 - Diffusion test for Sample No. 19f

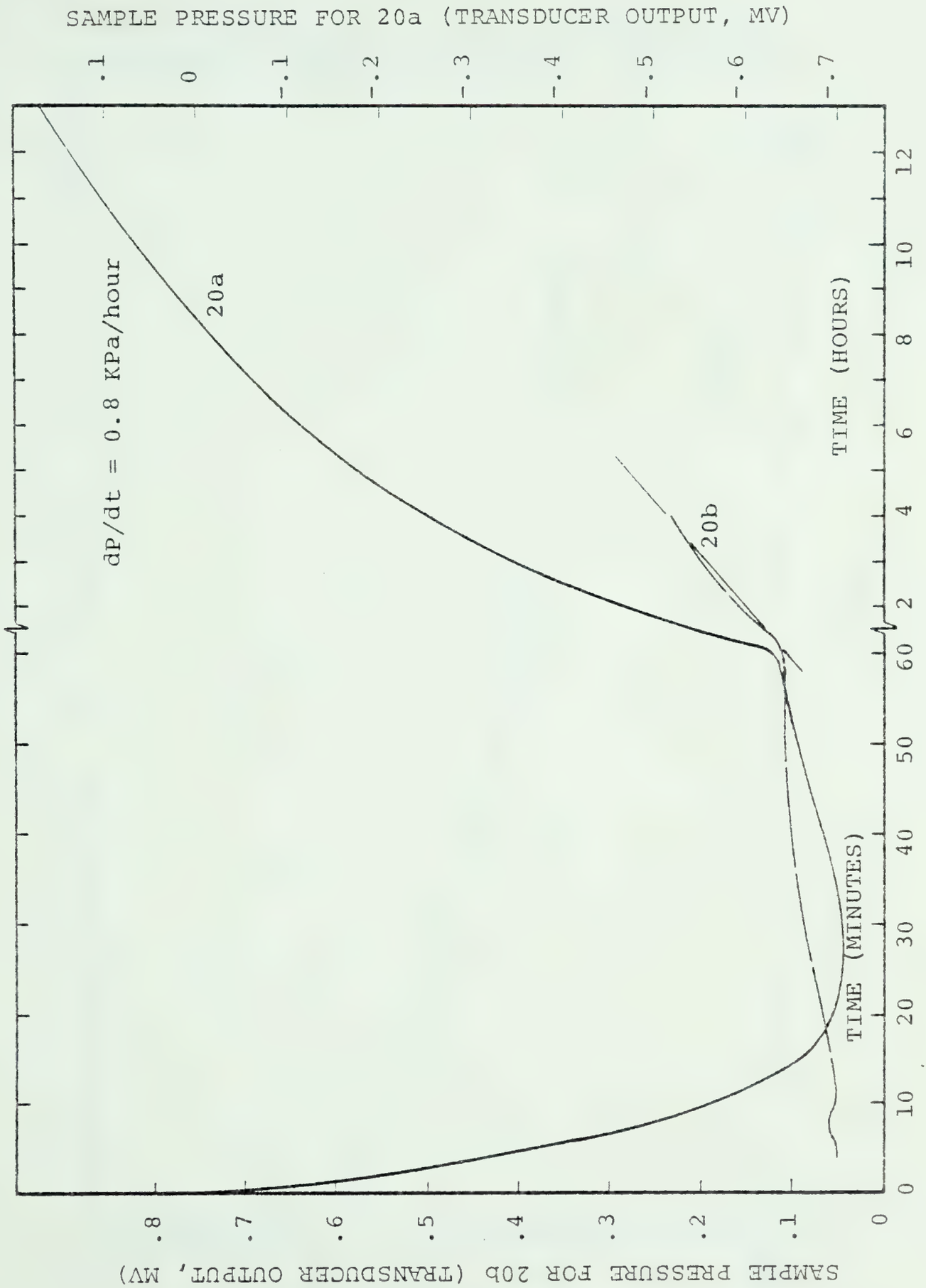


Figure B.13 - Diffusion Test for Sample No. 20

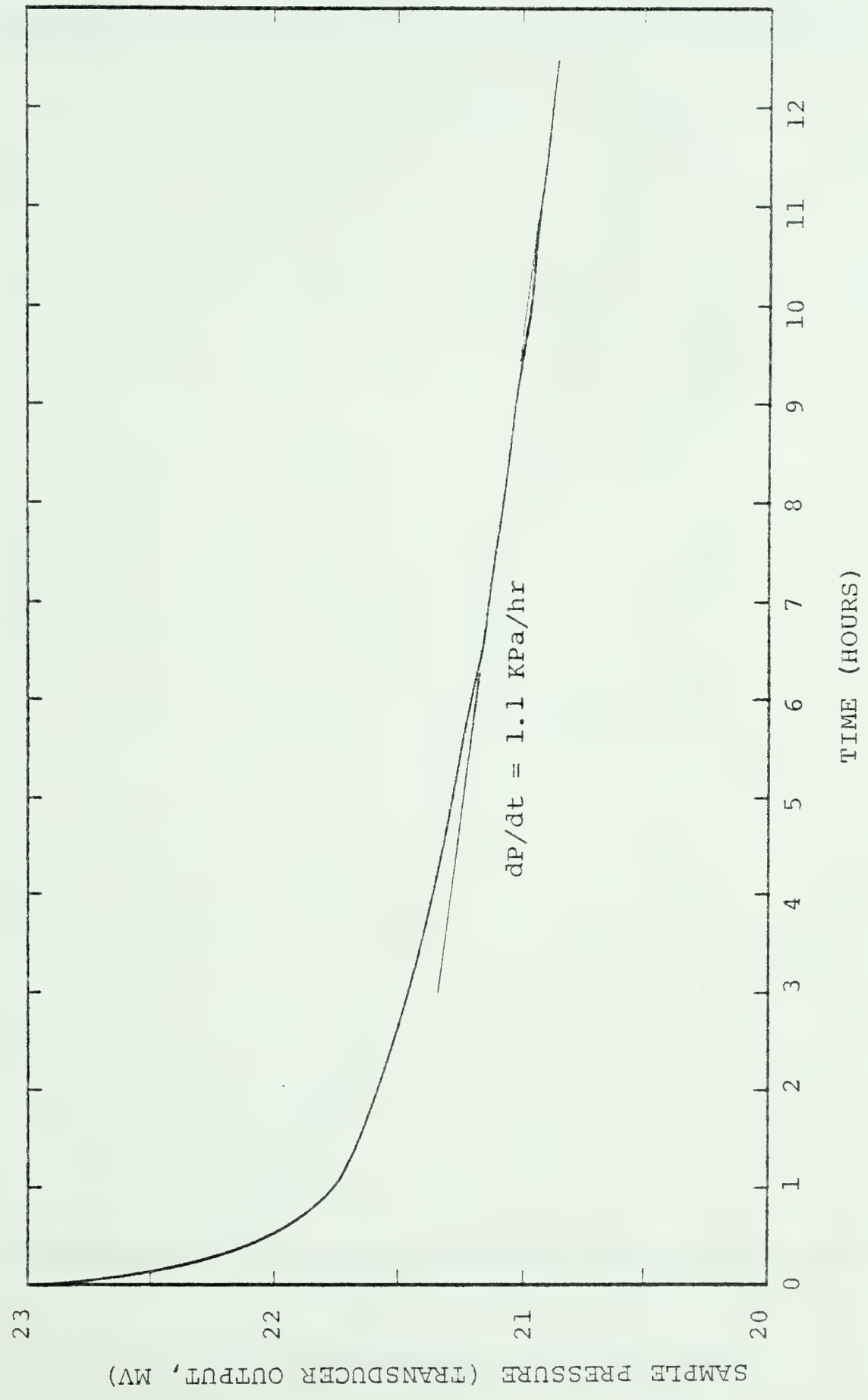


Figure B.14 - Diffusion test for Sample No. 20c

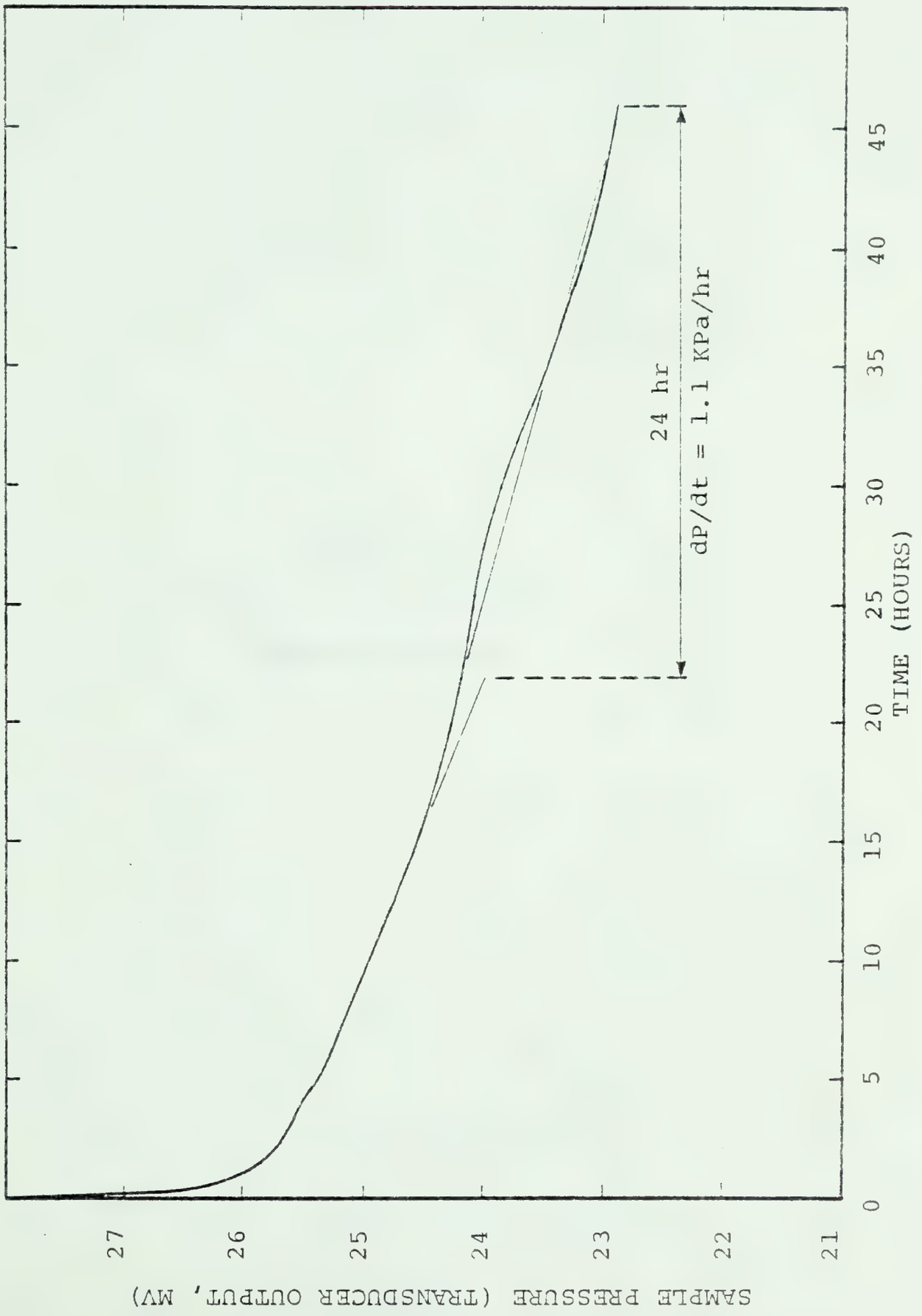


Figure B.15 - Diffusion Test for Sample No. 21

APPENDIX C

ISOTROPIC TEST RESULTS

TESTS 7, 9, 23

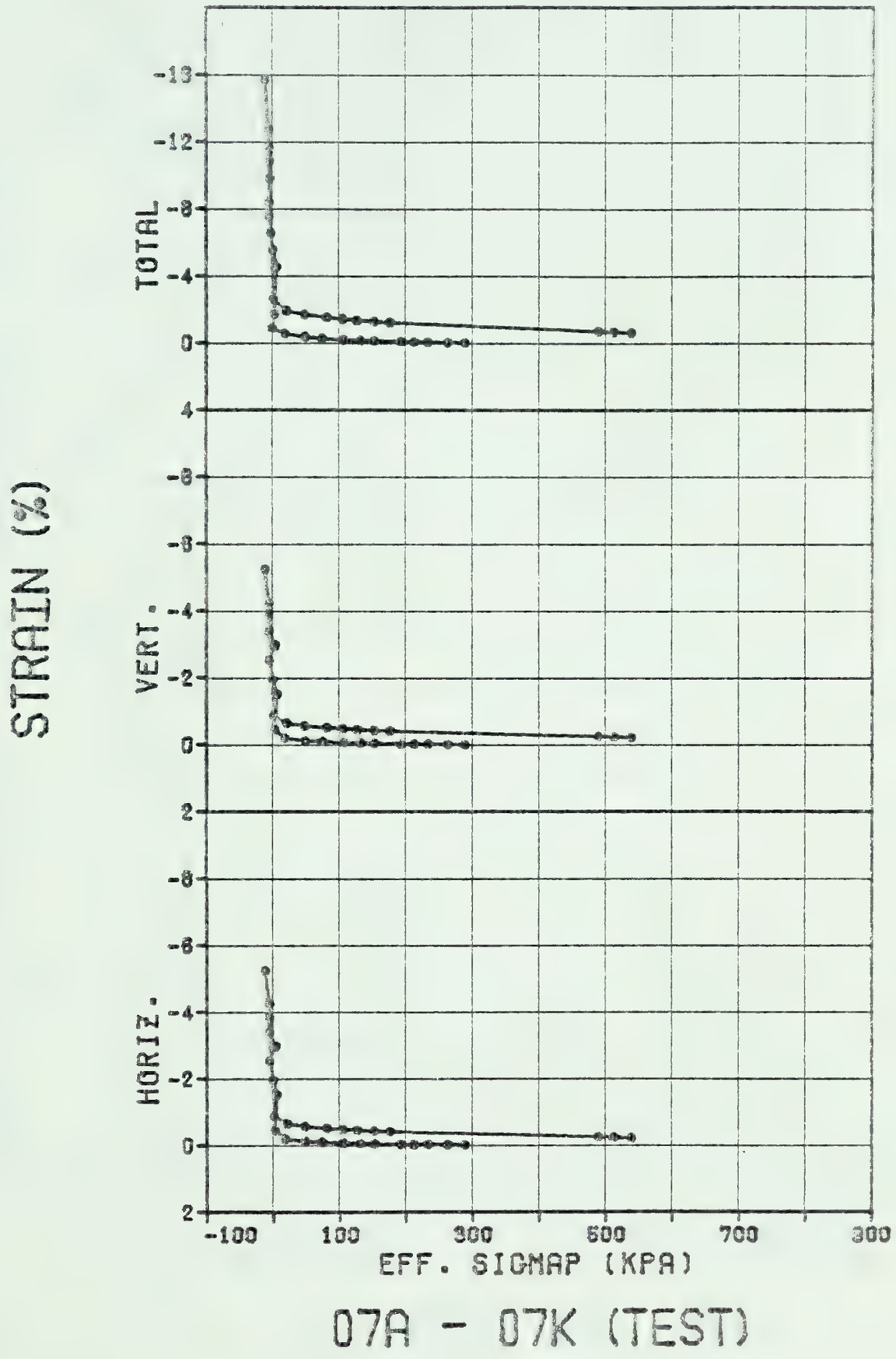

STRAIN (%)
TOTAL
VERT.
HORIZ.
-12
-8
-4
0
4
-8
-8
-4
-2
0
2
-8
-8
-4
-2
0
2
-100
100
300
500
700
900
EFF. SIGMAP (KPA)
07A - 07K (TEST)

Figure C.1

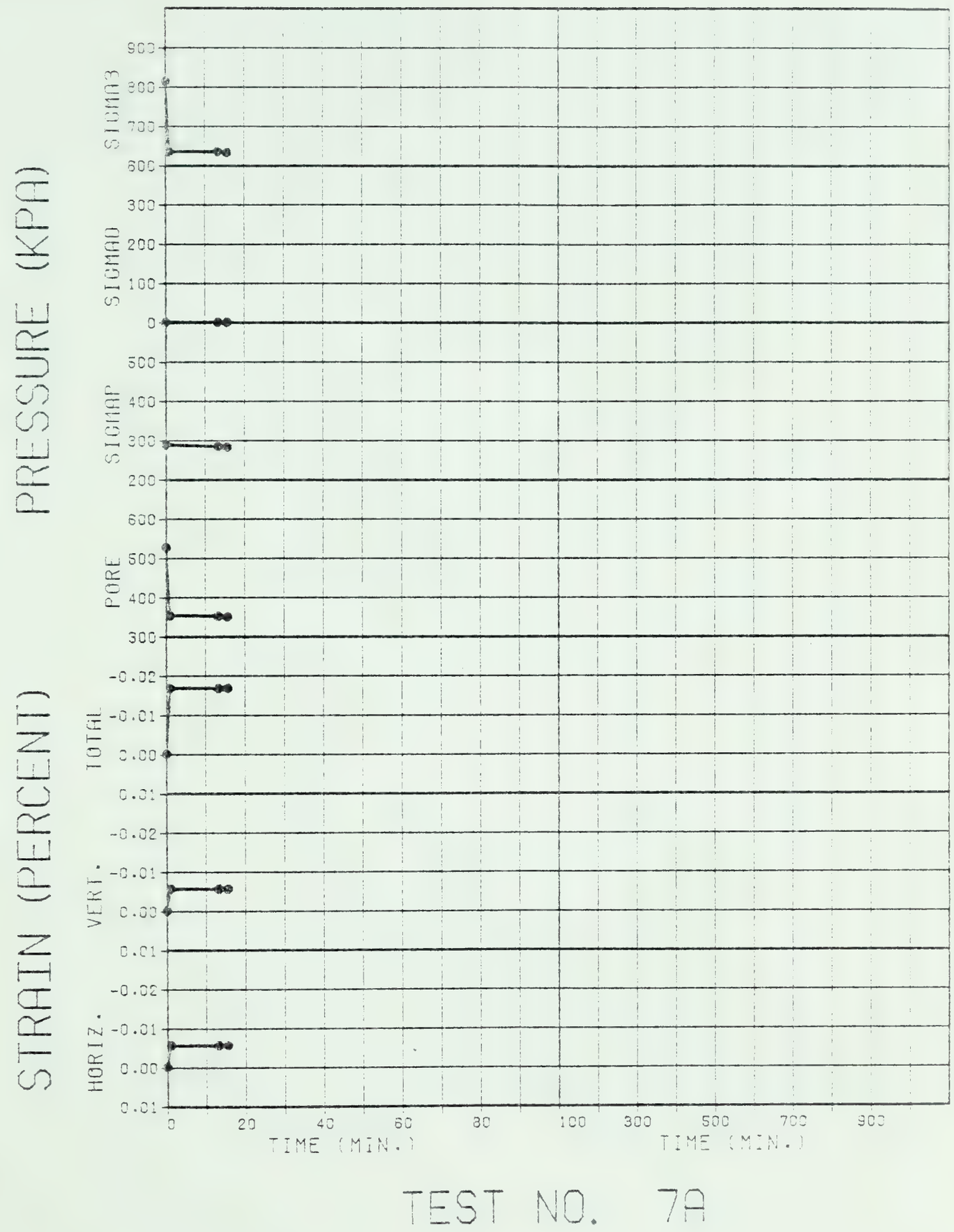

PRESSURE (KPA)
STRAIN (PERCENT)
SIGMA3
SIGMAD
SIGMAP
PORE
TOTAL
VERT.
HORIZ.
900
800
700
600
300
200
100
0
500
400
300
200
600
500
400
300
-0.02
-0.01
0.00
0.01
-0.02
-0.01
0.00
0.01
-0.02
-0.01
0.00
0.01
0
20
40
60
80
100
300
500
700
900
TIME (MIN.)
TIME (MIN.)
TEST NO. 7A

Figure C.2

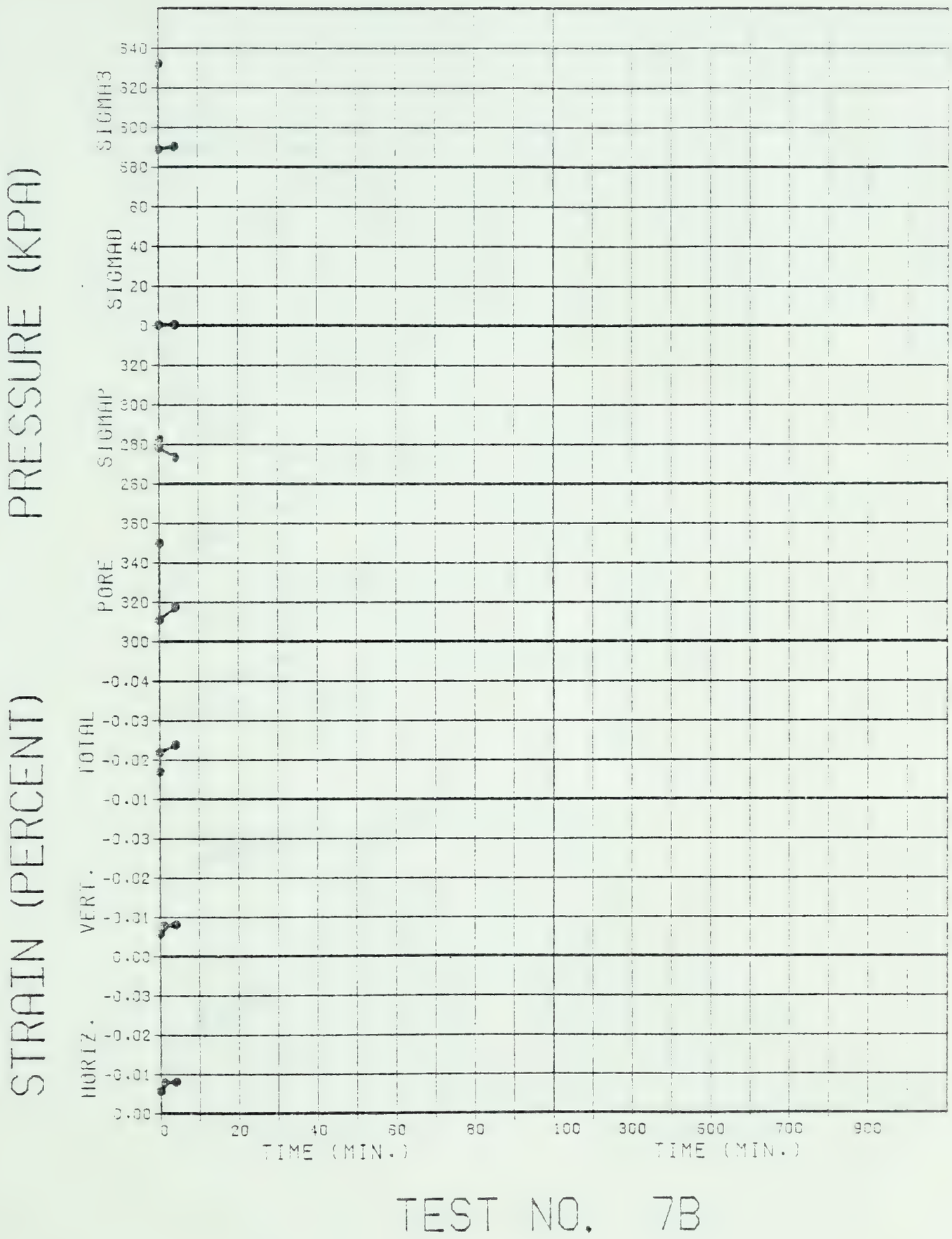

PRESSURE (KPA)
STRAIN (PERCENT)
SIGMA3
SIGMAD
SIGMAP
PORE
TOTAL
VERT.
HORIZ.
TIME (MIN.)
TIME (MIN.)
TEST NO. 7B

Figure C.3

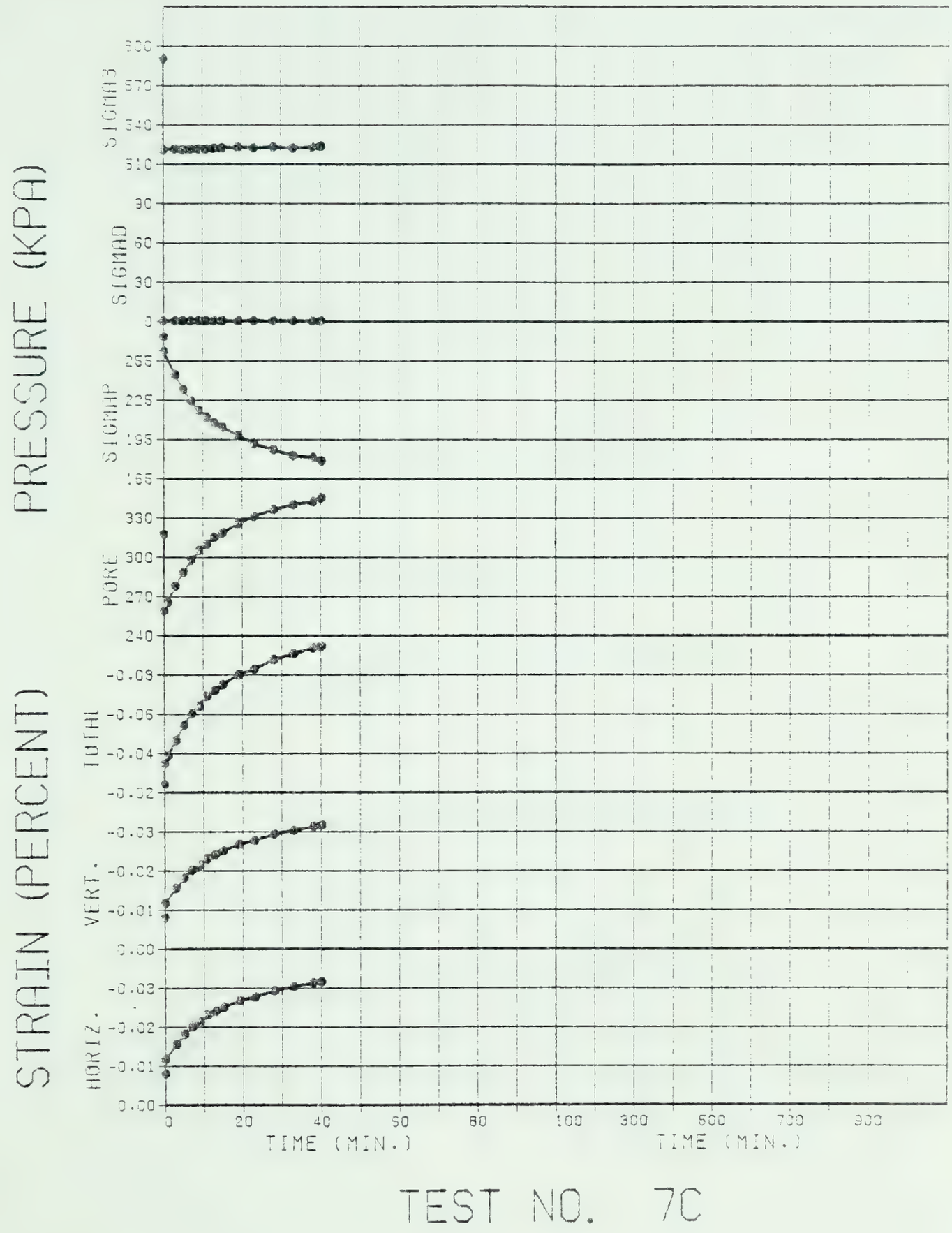

PRESSURE (KPA)
STRAIN (PERCENT)
SIGMA3
SIGMAD
SIGMAP
PORE
TOTAL
VERT.
HORIZ.
TIME (MIN.)
TIME (MIN.)
TEST NO. 7C

Figure C.4

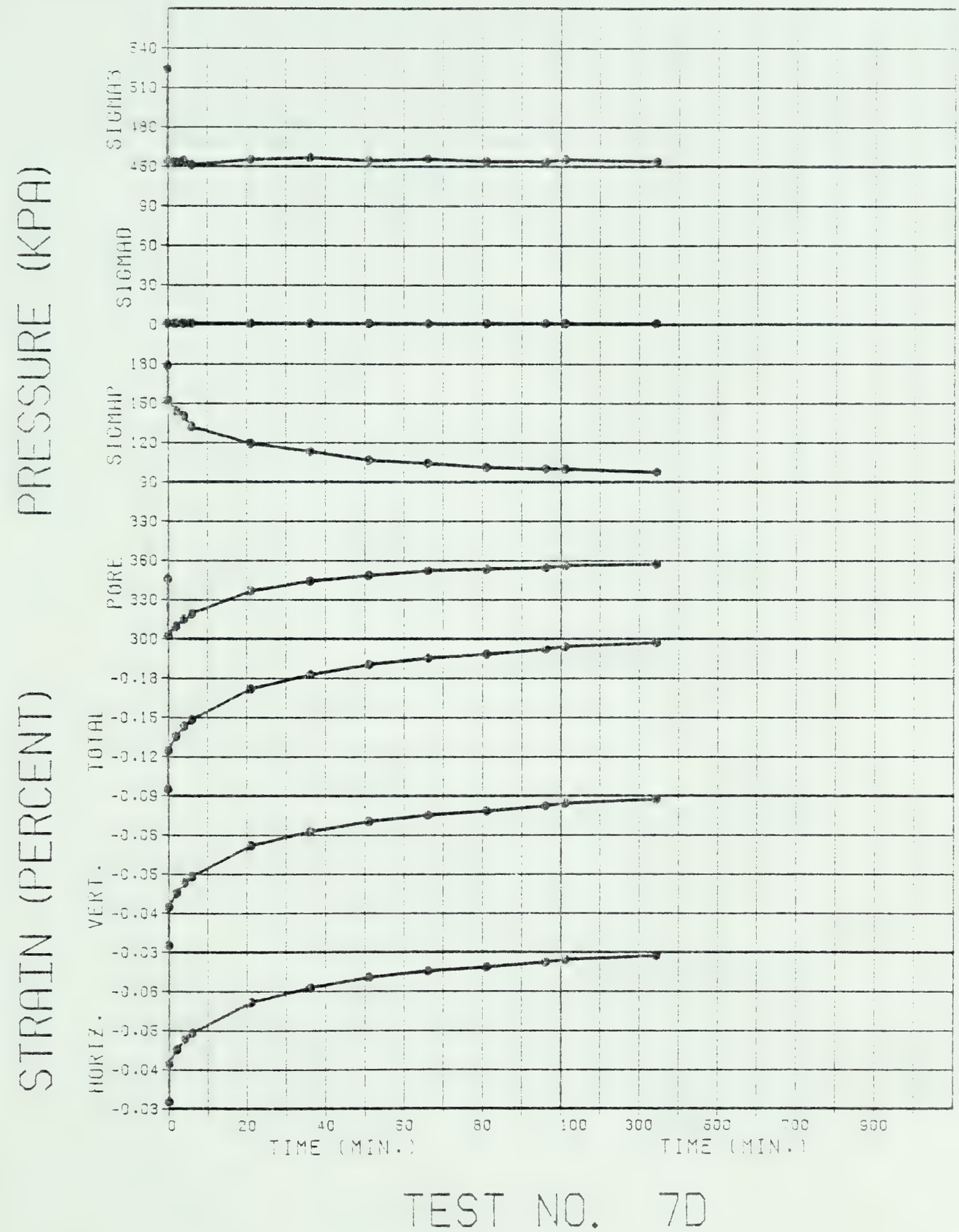

STRAIN (PERCENT)
PRESSURE (KPA)
SIGMA3
SIGMAD
SIGMAP
PORE
TOTAL
VERT.
HORIZ.
TIME (MIN.)
TIME (MIN.)
TEST NO. 7D

Figure C.5

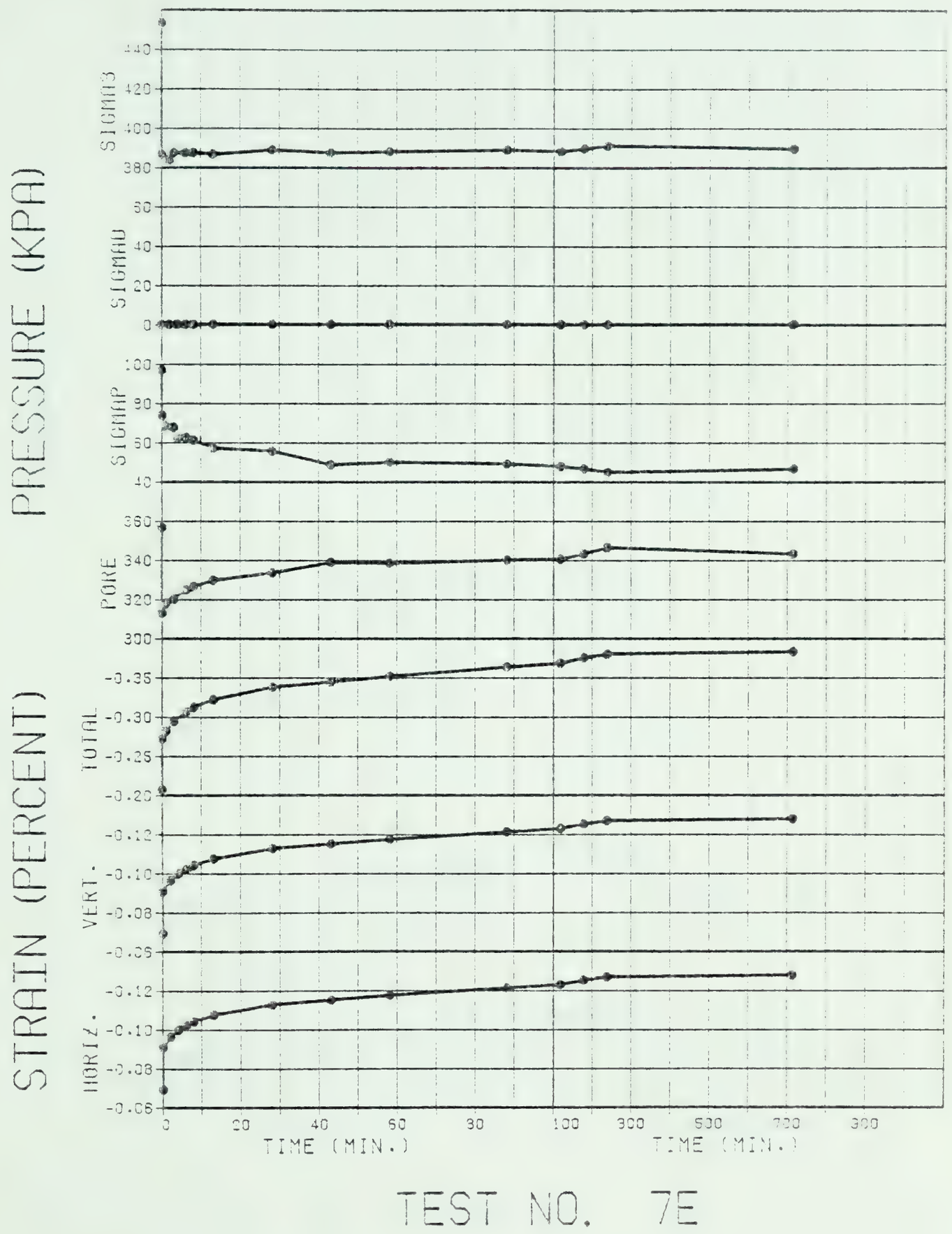

PRESSURE (KPA)
STRAIN (PERCENT)
SIGMA3
SIGMAD
SIGMAP
PORE
TOTAL
VERT.
HORIZ.
TIME (MIN.)
TIME (MIN.)
TEST NO. 7E

Figure C.6

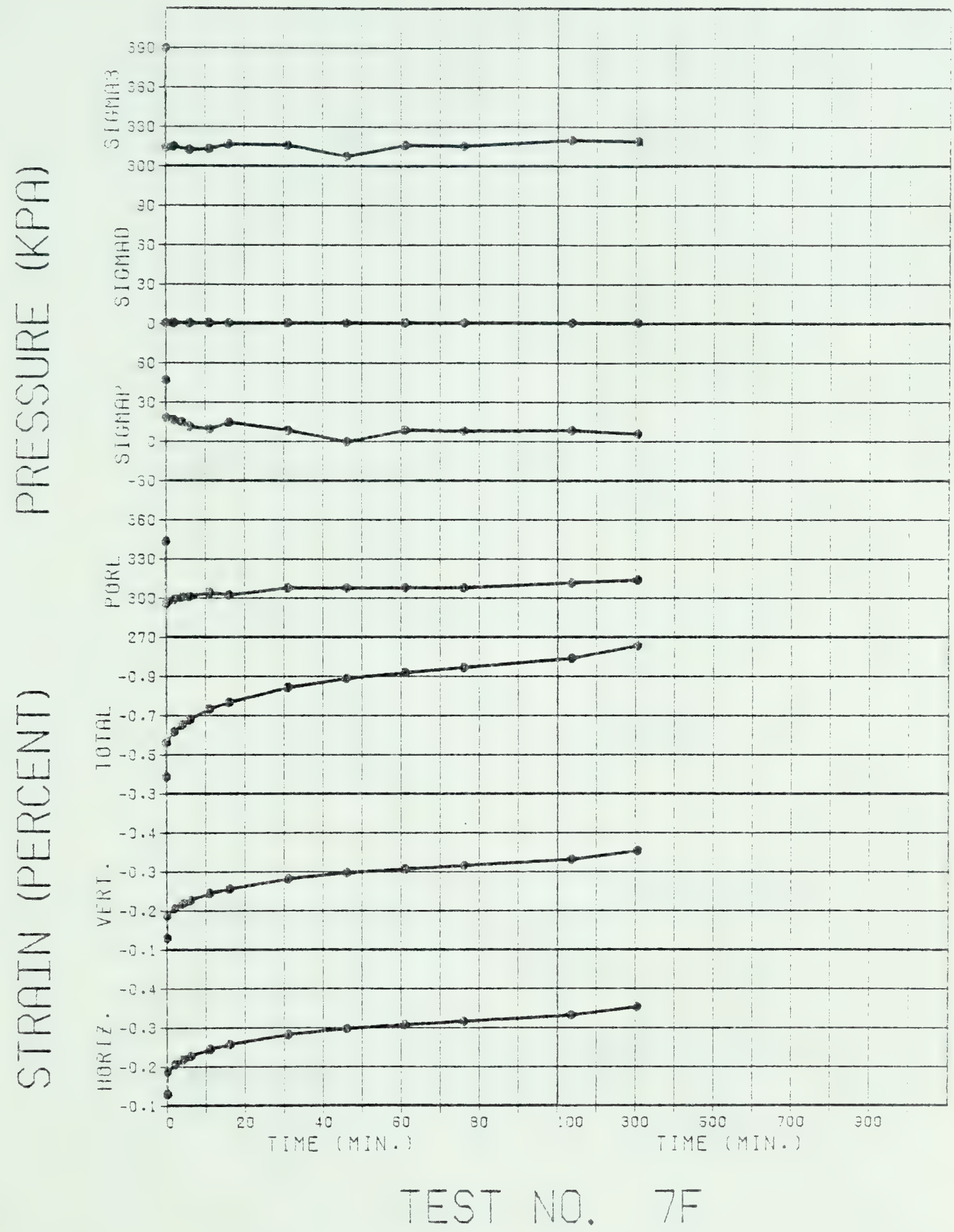

PRESSURE (KPA)
STRAIN (PERCENT)
SIGMA3
SIGMAD
SIGMA1
PORE
TOTAL
VERT.
HORIZ.
TIME (MIN.)
TIME (MIN.)
TEST NO. 7F

Figure C.7

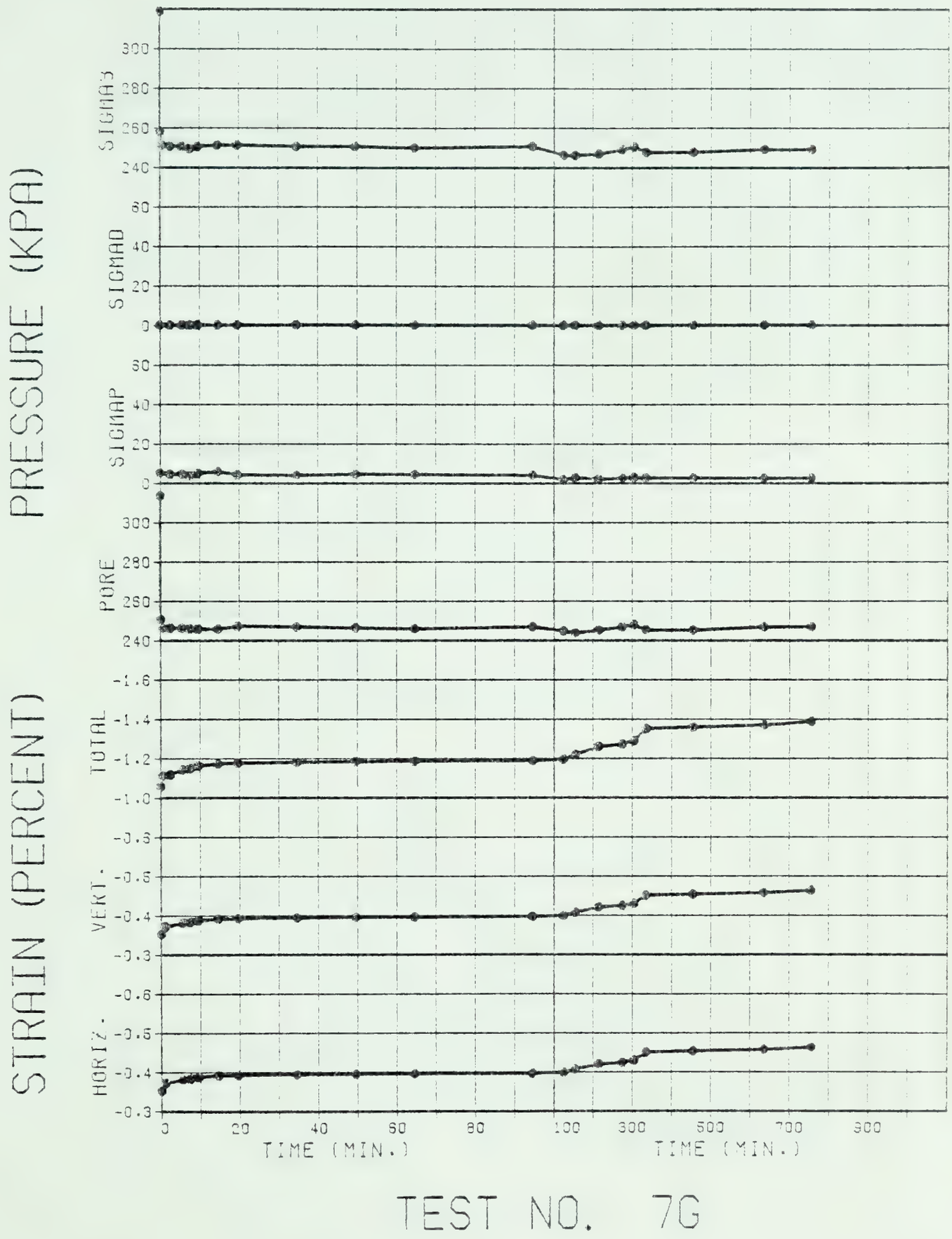

PRESSURE (KPA)
STRAIN (PERCENT)
SIGMA3
SIGMAD
SIGMAP
PORE
TOTAL
VERT.
HORIZ.
TIME (MIN.)
TIME (MIN.)
TEST NO. 7G

Figure C.8

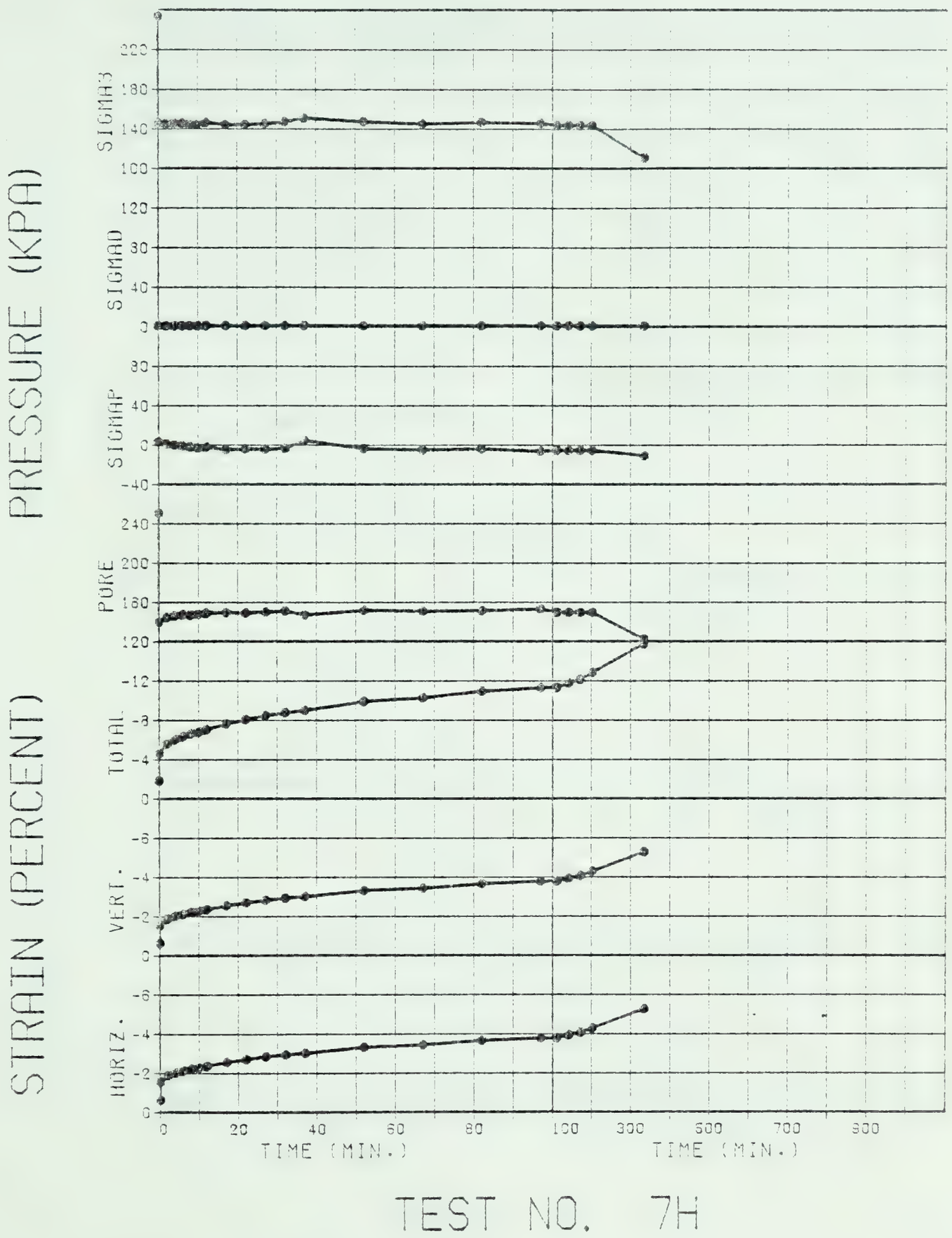

PRESSURE (KPA)
STRAIN (PERCENT)
SIGMA3
SIGMAD
SIGMAP
PORE
TOTAL
VERT.
HORIZ.
TIME (MIN.)
TIME (MIN.)
TEST NO. 7H

Figure C.9

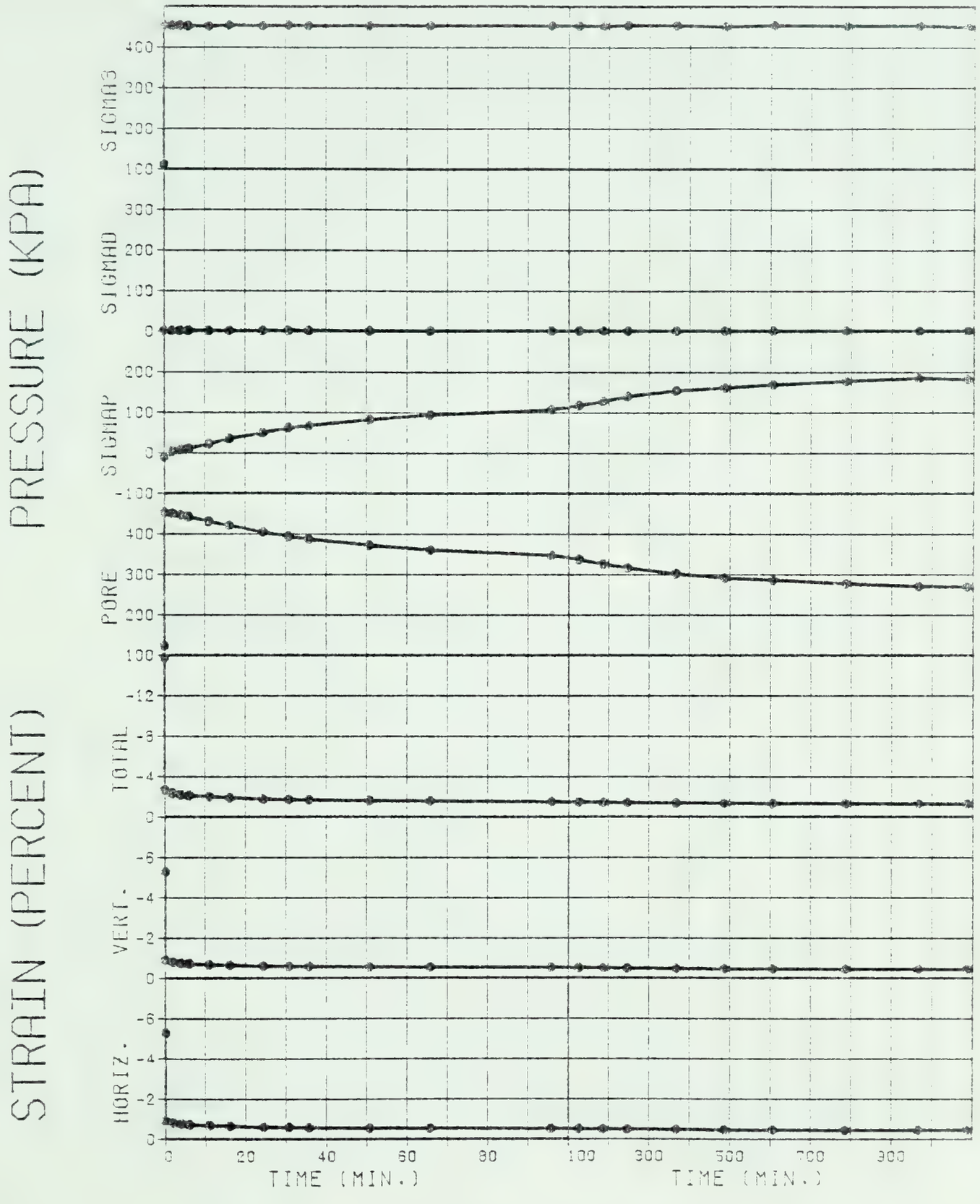

PRESSURE (KPA)
STRAIN (PERCENT)
SIGMA3
SIGMAD
SIGMAP
PORE
TOTAL
VERT.
HORIZ.
TIME (MIN.)
TIME (MIN.)
TEST NO. 7J

Figure C.10

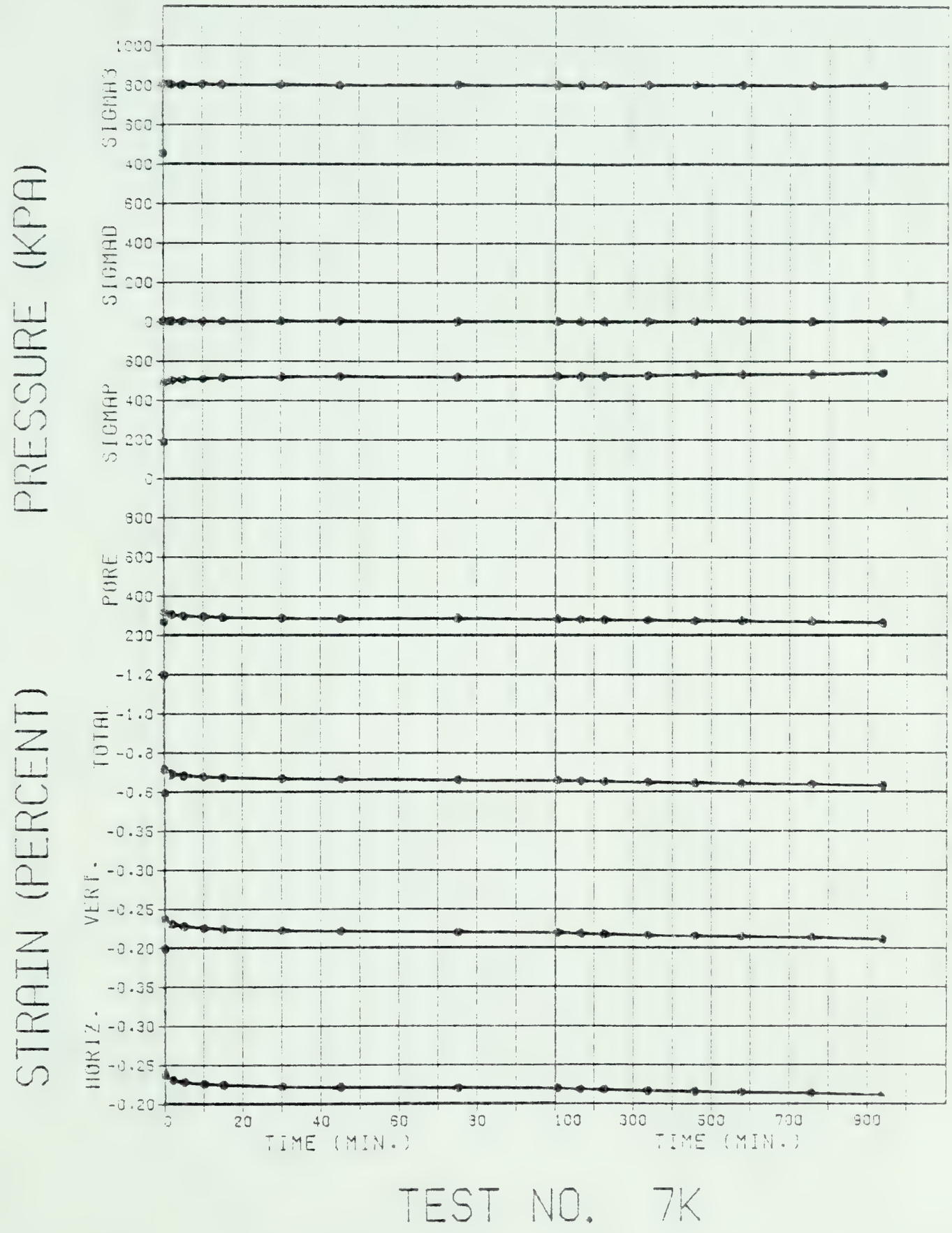
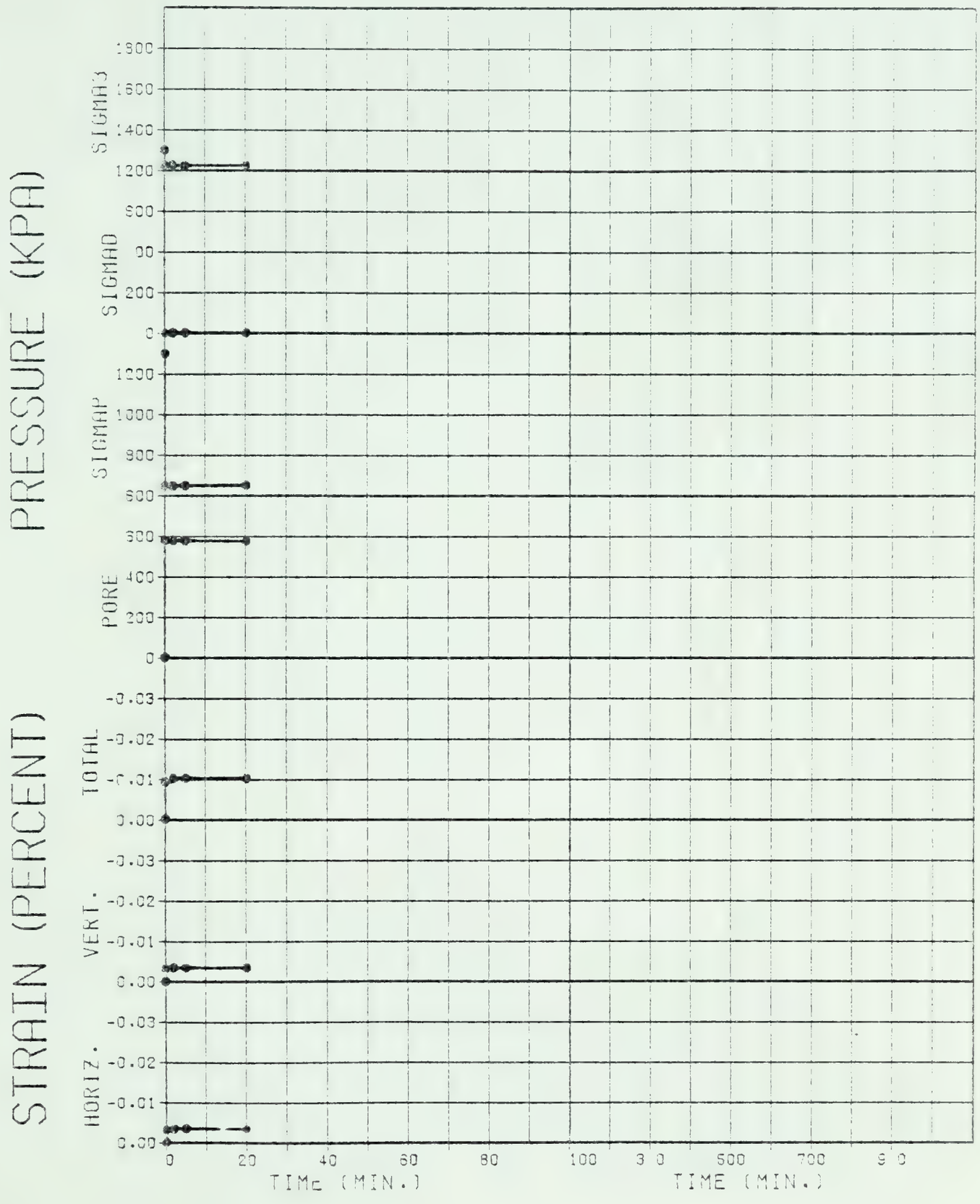
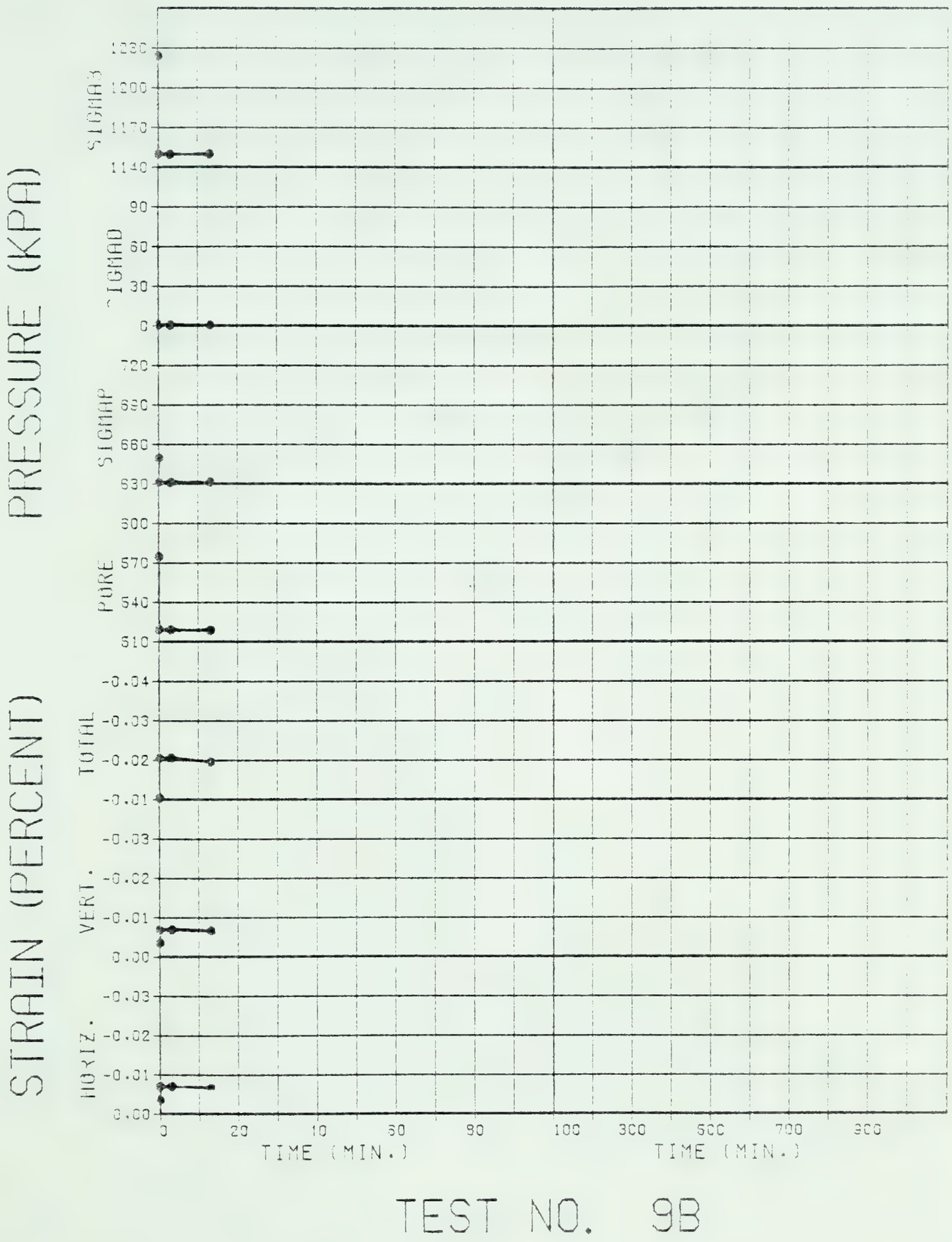

PRESSURE (KPA)
STRAIN (PERCENT)
SIGMA3
SIGMAD
SIGMAP
PORE
TOTAL
VERT.
HORIZ.
TIME (MIN.)
TIME (MIN.)
TEST NO. 7K

Figure C.11



TEST NO. 9A

Figure C.12



TEST NO. 9B

Figure C.13

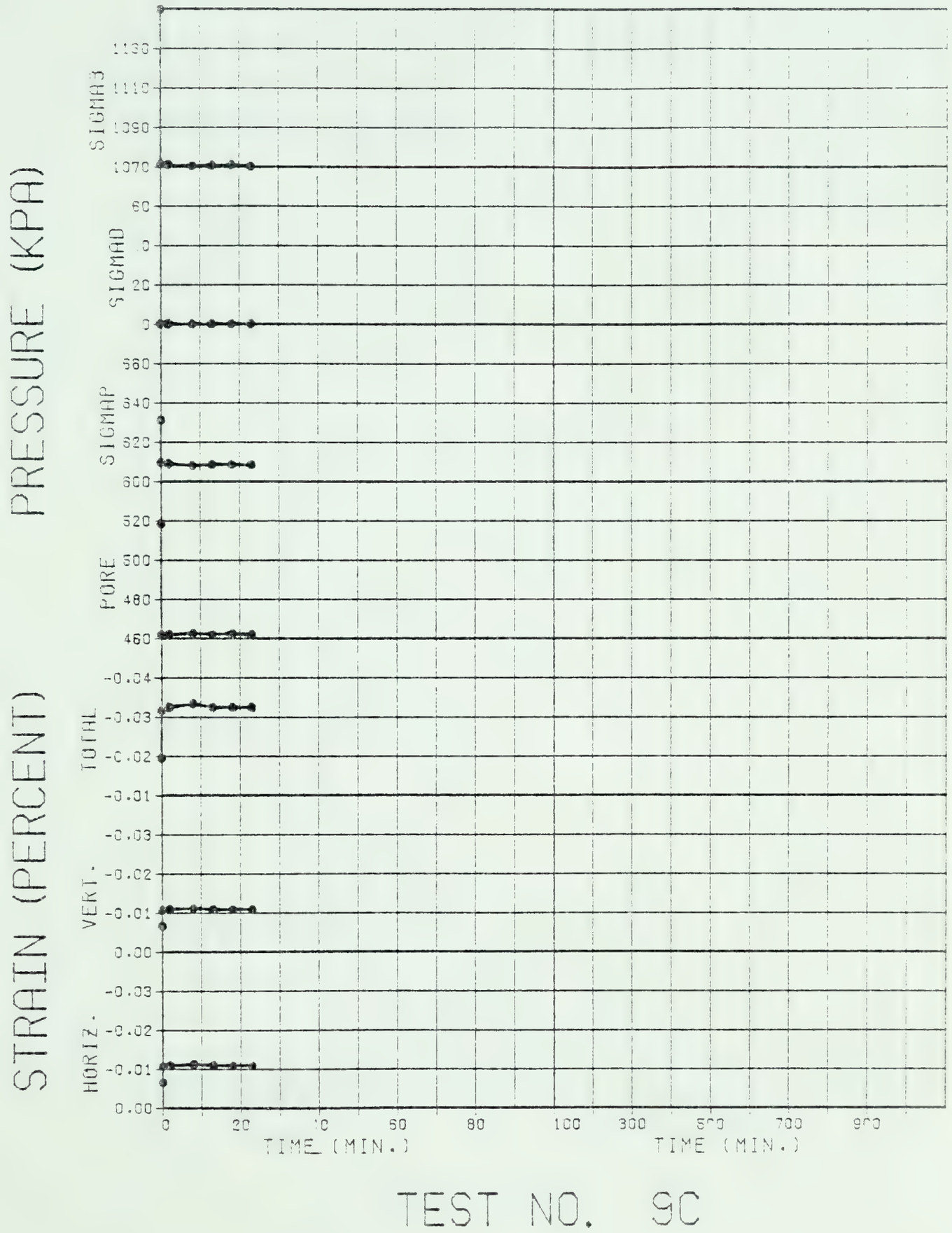

PRESSURE (KPA)
STRAIN (PERCENT)
SIGMA3
SIGMAD
SIGMAP
PORE
TOTAL
VERT.
HORIZ.
TIME (MIN.)
TIME (MIN.)
TEST NO. 9C

Figure C.14

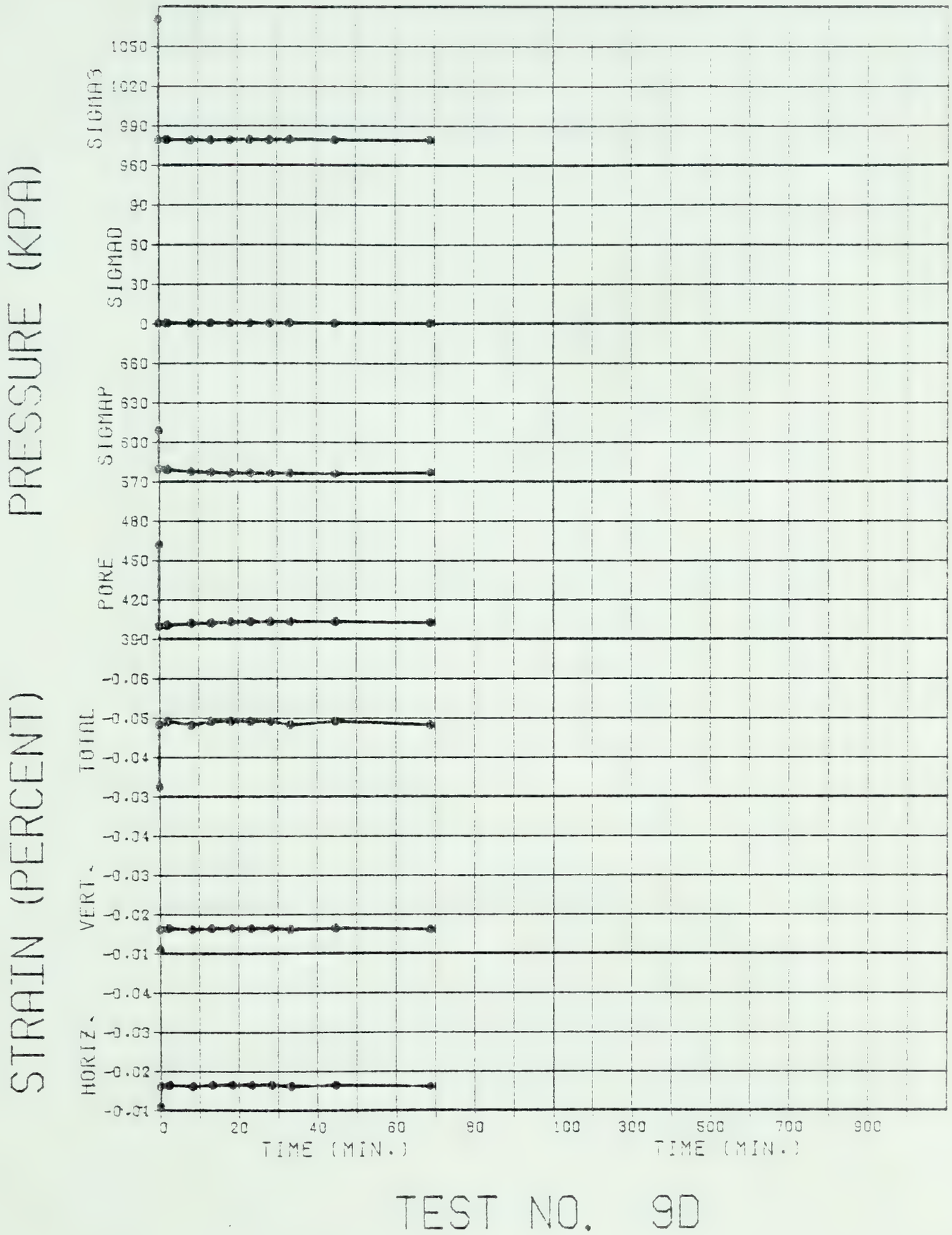

PRESSURE (KPA)
STRAIN (PERCENT)
SIGMA3
1050
1020
990
960
SIGMAD
90
60
30
0
SIGMAP
660
630
600
570
PORE
480
450
420
390
TOTAL
-0.06
-0.05
-0.04
-0.03
VERT.
-0.04
-0.03
-0.02
-0.01
HORIZ.
-0.04
-0.03
-0.02
-0.01
0
20
40
60
80
100
300
500
700
900
TIME (MIN.)
TIME (MIN.)
TEST NO. 9D

Figure C.15

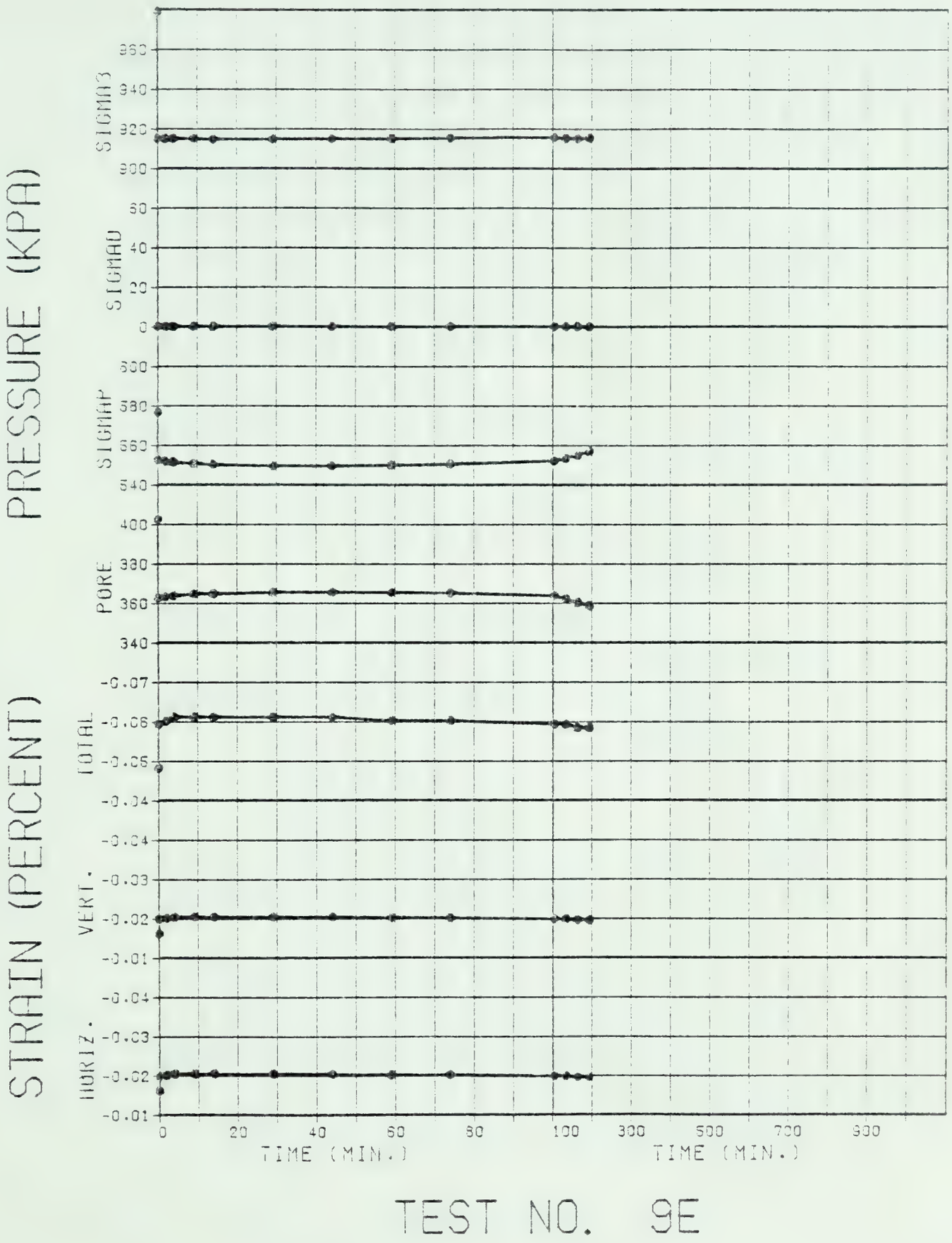
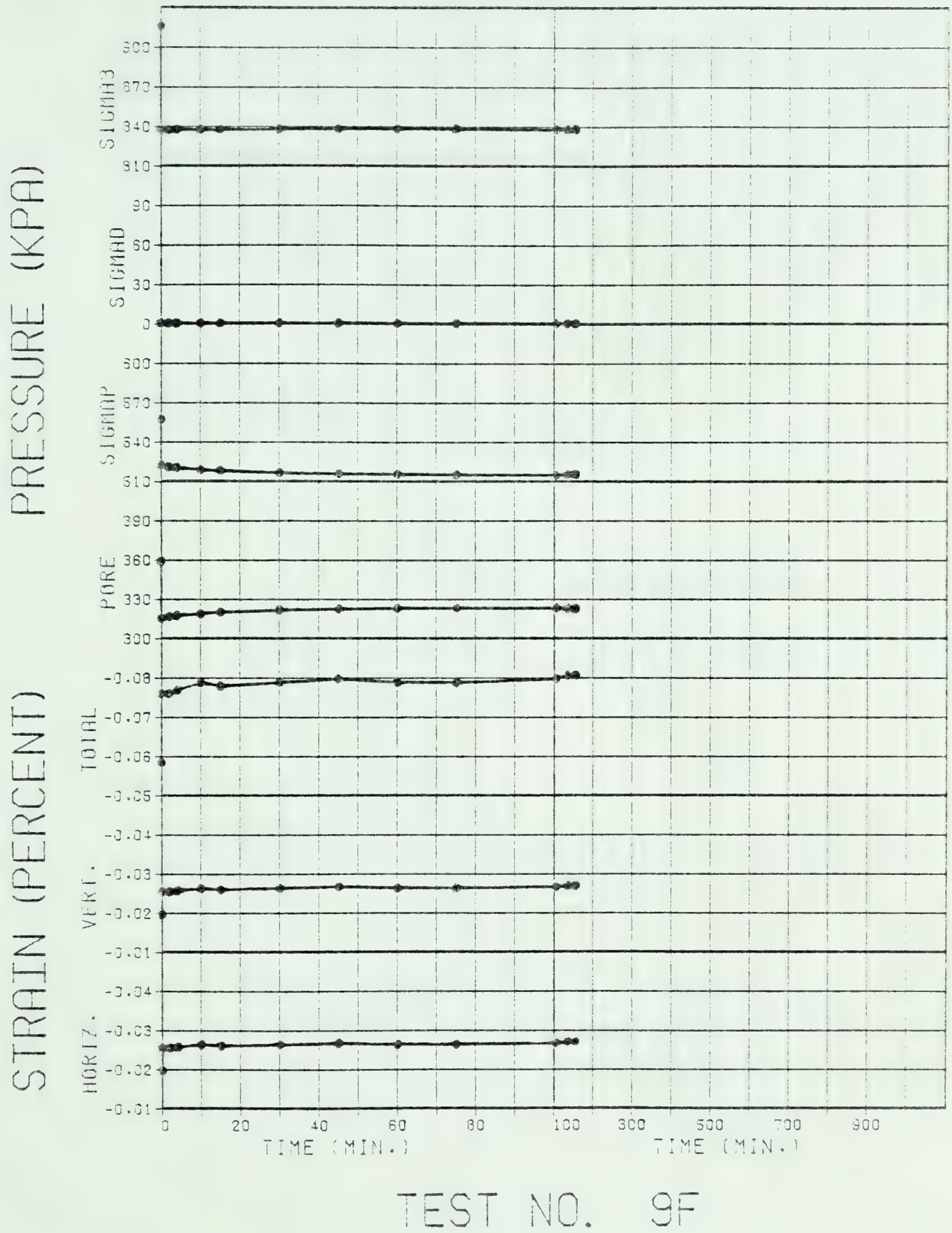
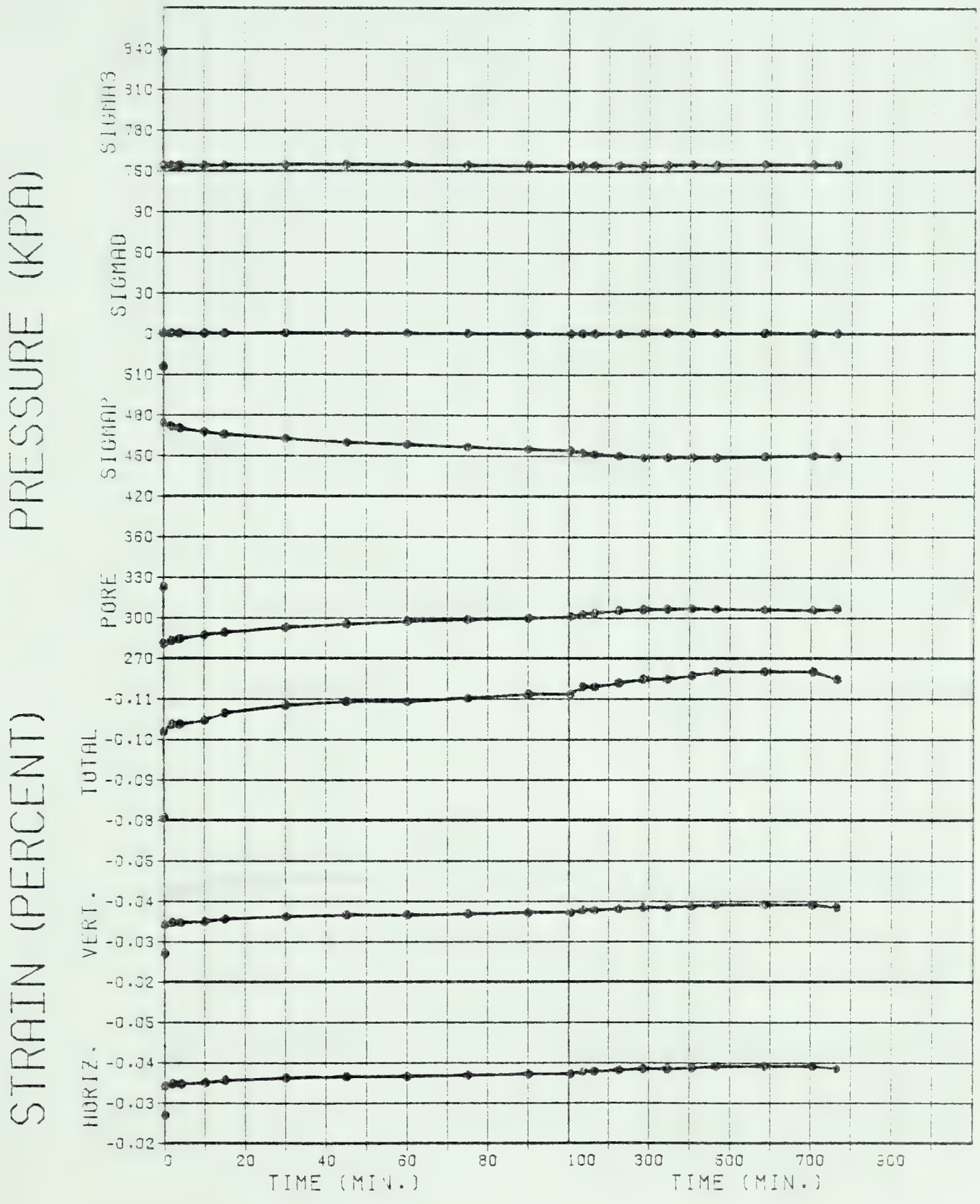

PRESSURE (KPA)
STRAIN (PERCENT)
SIGMA3
SIGMAD
SIGMAP
PORE
TOTAL
VERT.
HORIZ.
TIME (MIN.)
TIME (MIN.)
TEST NO. 9E

Figure C.16



TEST NO. 9F

Figure C.17



TEST NO. 9G

Figure C.18

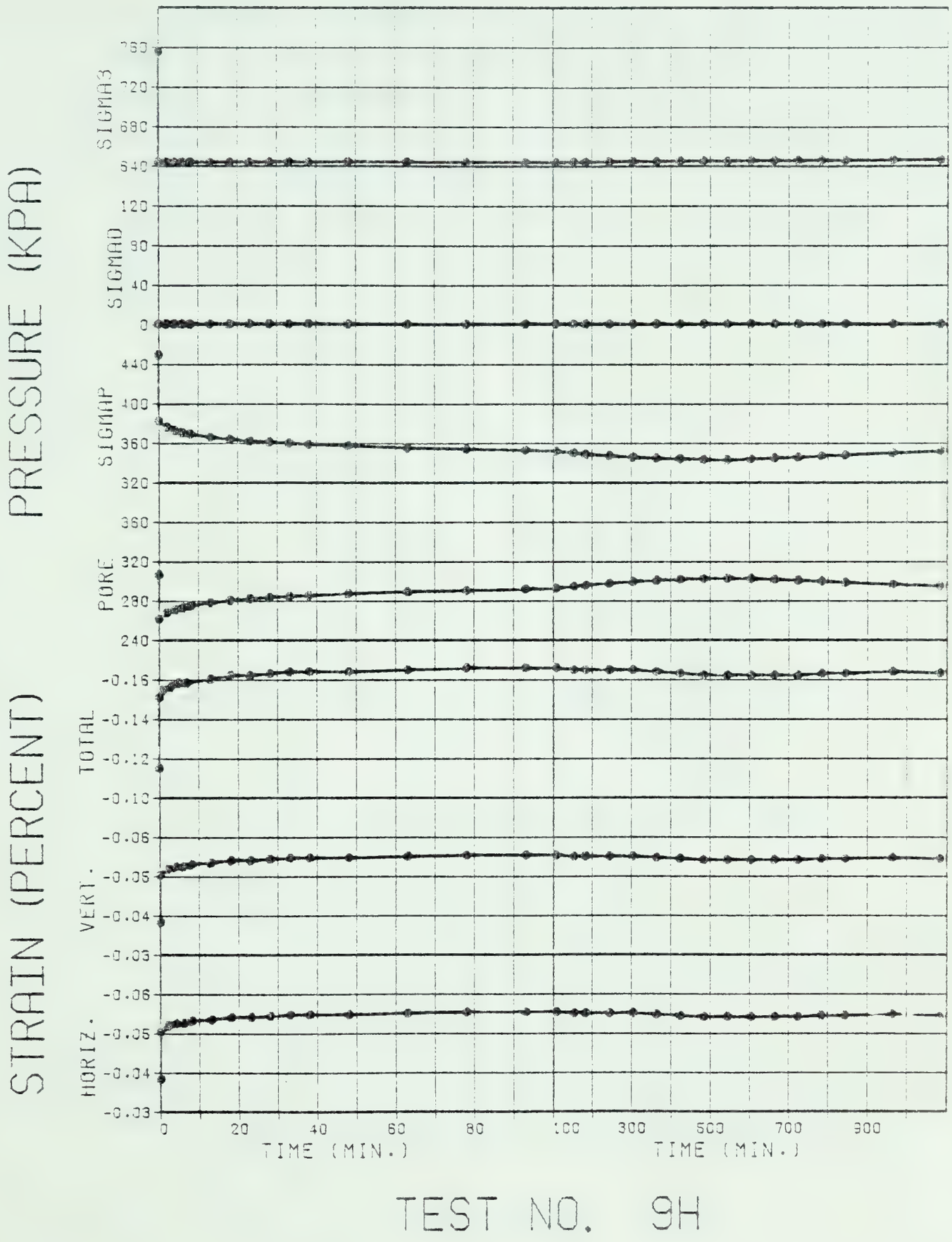

PRESSURE (KPA)
STRAIN (PERCENT)
SIGMA3
SIGMAD
SIGMAP
PORE
TOTAL
VERT.
HORIZ.
TIME (MIN.)
TIME (MIN.)
TEST NO. 9H

Figure C.19

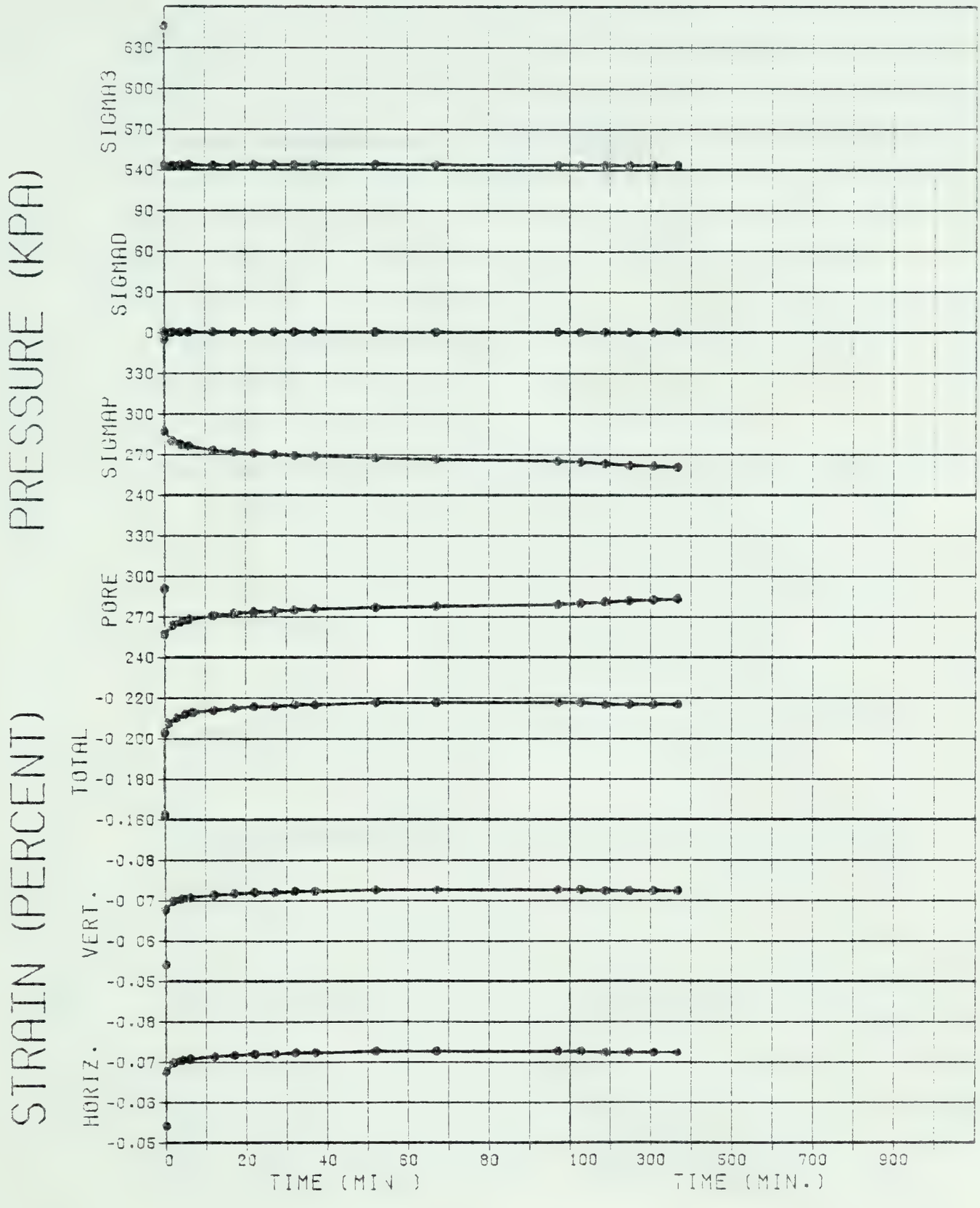

PRESSURE (KPA)
STRAIN (PERCENT)
SIGMA3
630
600
570
540
SIGMAD
90
60
30
0
SIGMAP
330
300
270
240
PORE
330
300
270
240
TOTAL
-0 220
-0 200
-0 180
-0.160
VERT.
-0.08
-0 07
-0 06
-0.05
HORIZ.
-0.08
-0.07
-0.06
-0.05
0
20
40
60
80
100
300
500
700
900
TIME (MIN)
TIME (MIN.)
TEST NO. 9I

Figure C.20

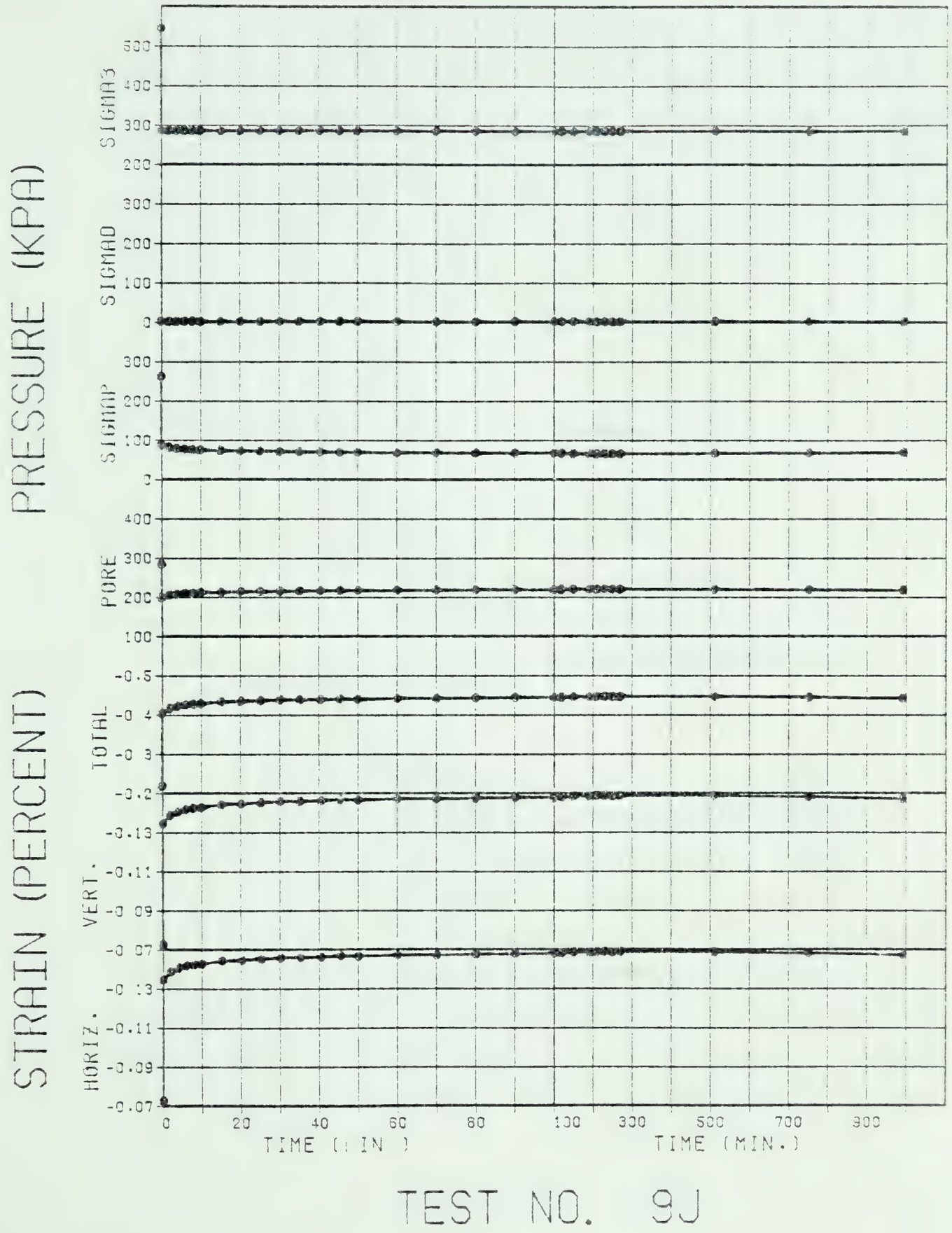

PRESSURE (KPA)
STRAIN (PERCENT)
SIGMA3
SIGMAD
SIGMAP
PORE
TOTAL
VERT.
HORIZ.
TIME (: IN)
TIME (MIN.)
TEST NO. 9J

Figure C.21

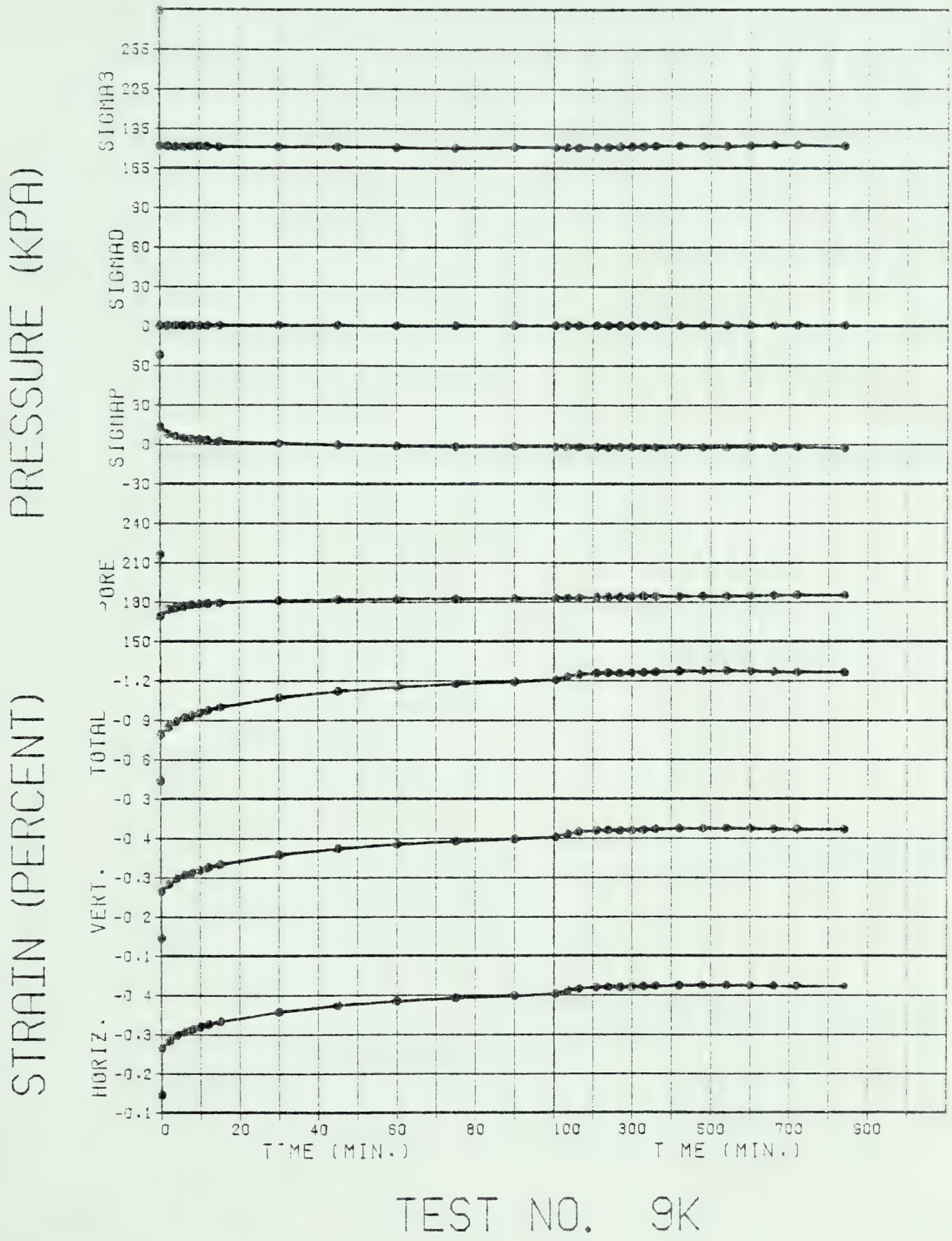

PRESSURE (KPA)
STRAIN (PERCENT)
SIGMA3
SIGMAD
SIGMAP
PORE
TOTAL
VERT.
HORIZ.
TIME (MIN.)
TIME (MIN.)
TEST NO. 9K

Figure C.22

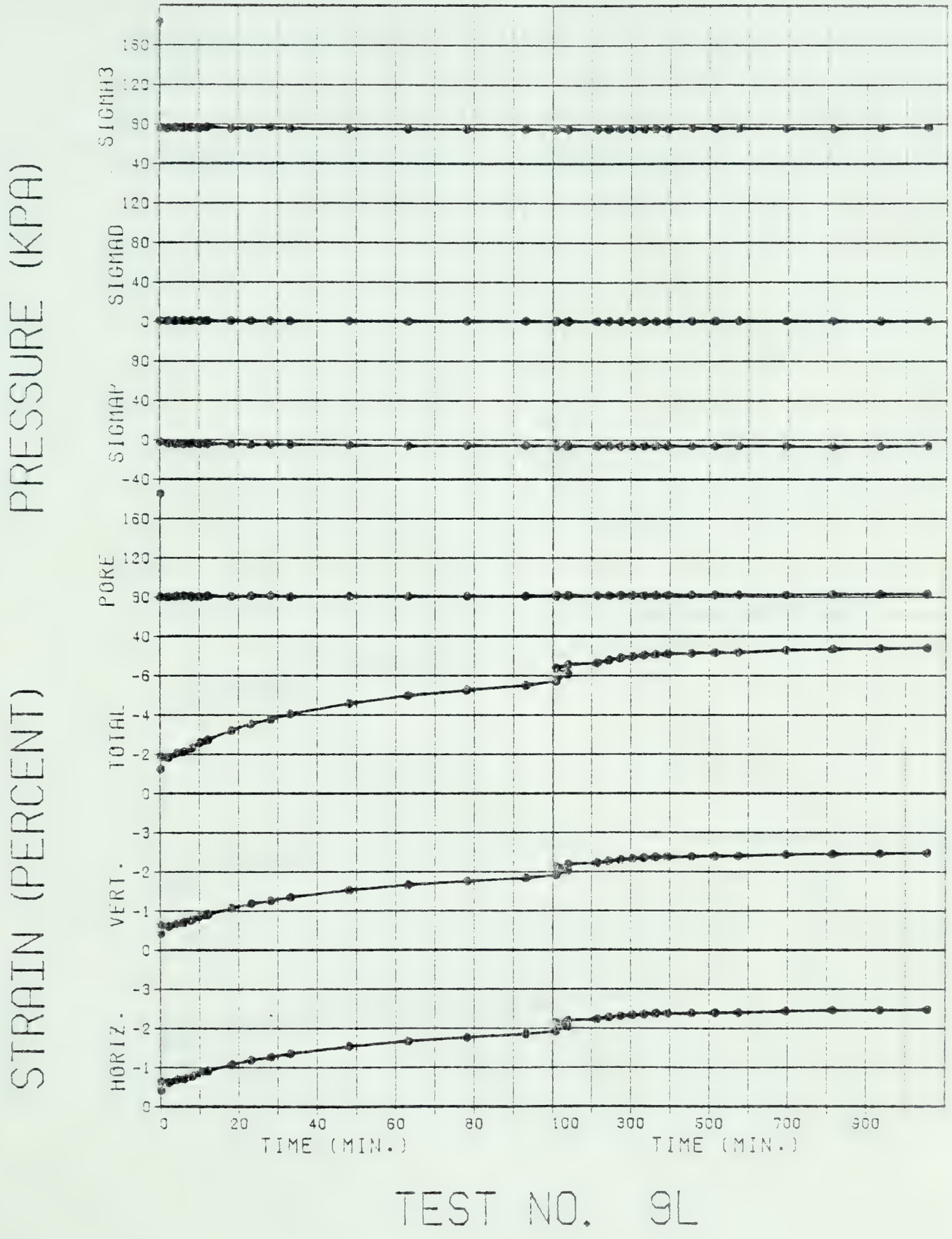

PRESSURE (KPA)
STRAIN (PERCENT)
SIGMA3
SIGMAD
SIGMAP
PORE
TOTAL
VERT.
HORIZ.
TIME (MIN.)
TIME (MIN.)
TEST NO. 9L

Figure C.23

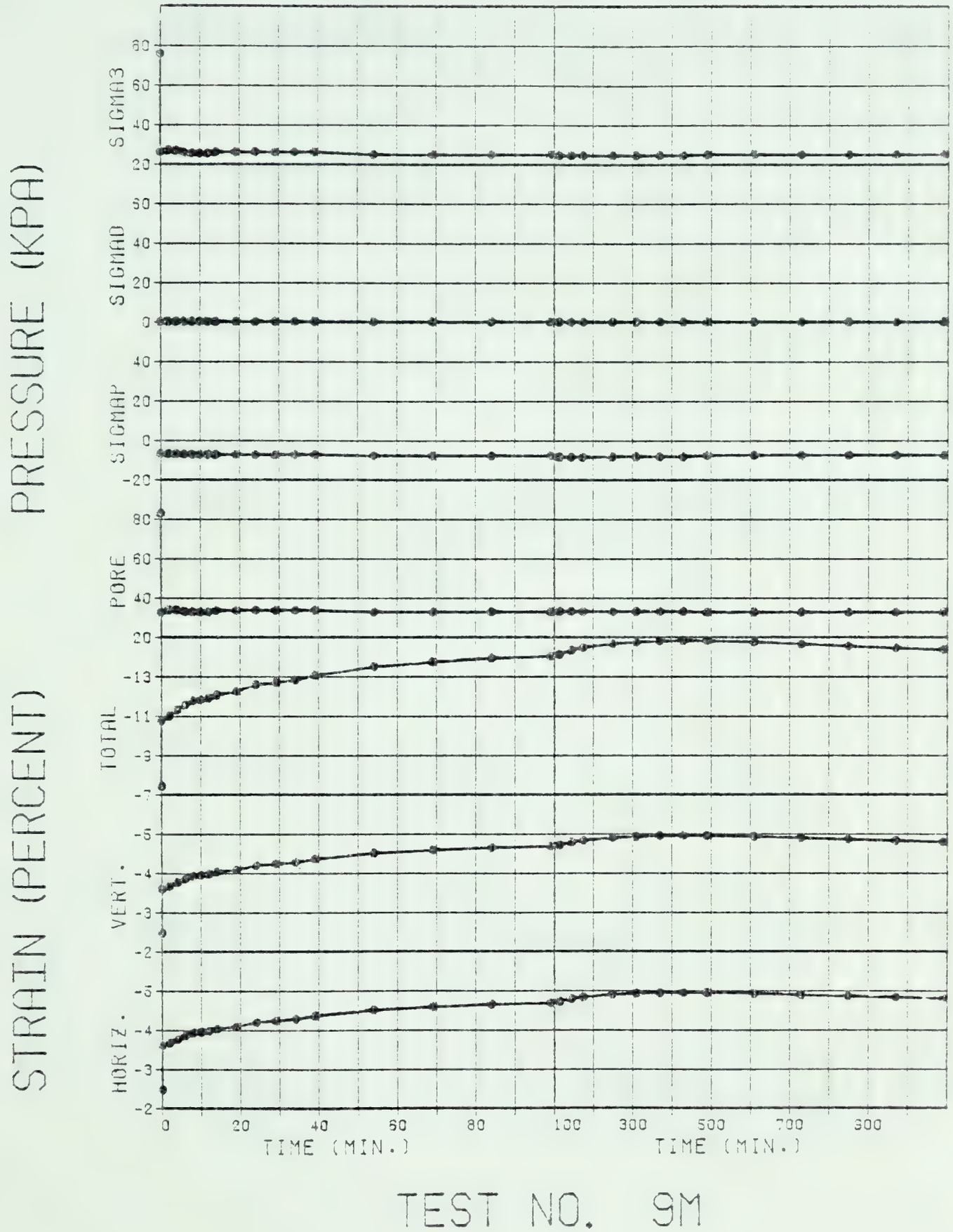

PRESSURE (KPA)
STRAIN (PERCENT)
SIGMA3
SIGMAD
SIGMAP
PORE
TOTAL
VERT.
HORIZ.
TIME (MIN.)
TIME (MIN.)
TEST NO. 9M

Figure C.24

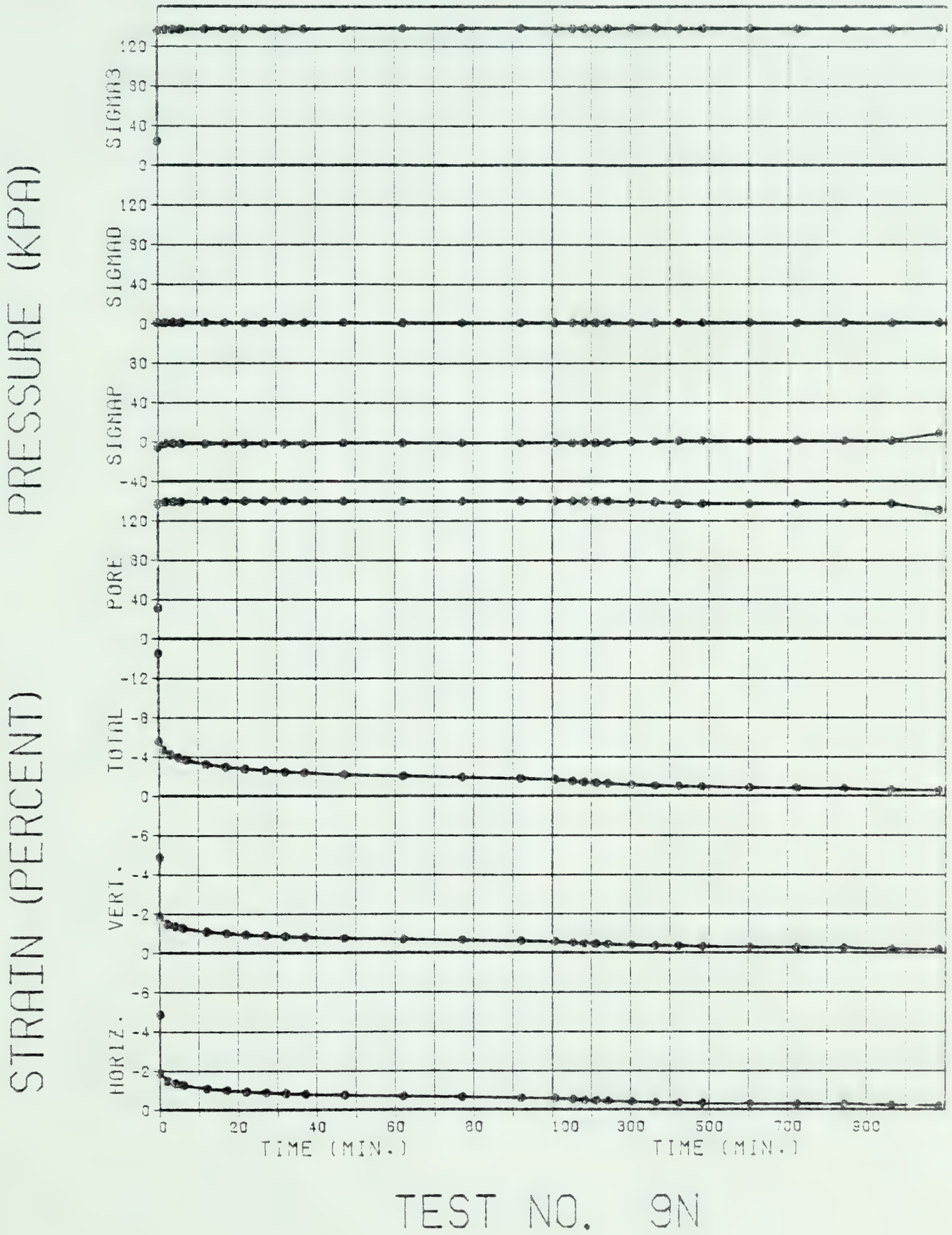

PRESSURE (KPA)
STRAIN (PERCENT)
SIGMA3
SIGMAD
SIGMAP
PORE
TOTAL
VERT.
HORIZ.
120
80
40
0
-40
-12
-8
-4
-6
-2
0
20
40
60
80
100
300
500
700
900
TIME (MIN.)
TIME (MIN.)
TEST NO. 9N

Figure C.25

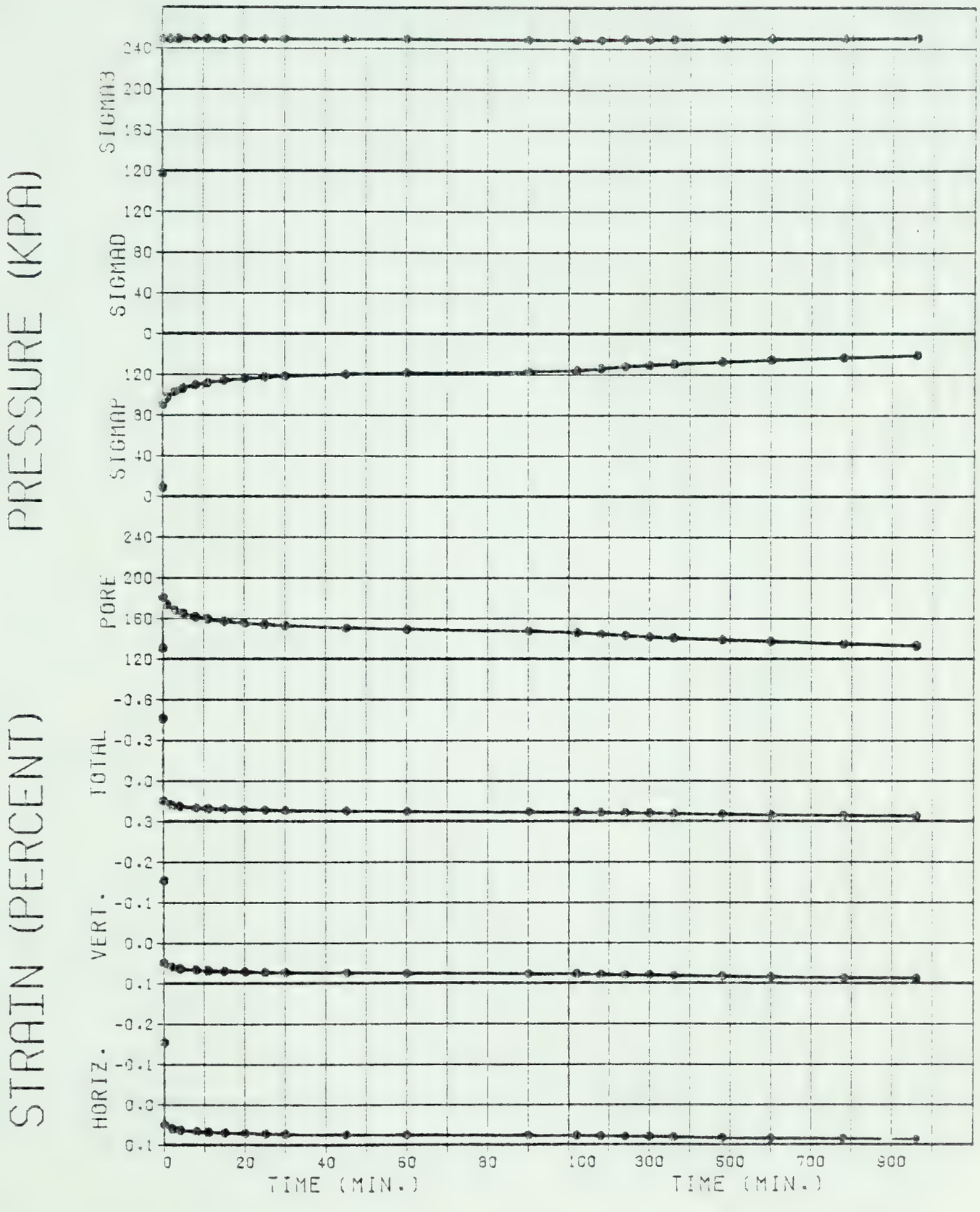

PRESSURE (KPA)
STRAIN (PERCENT)
SIGMA3
SIGMAD
SIGMAP
PORE
TOTAL
VERT.
HORIZ.
TIME (MIN.)
TIME (MIN.)
TEST NO. 90

Figure C.26

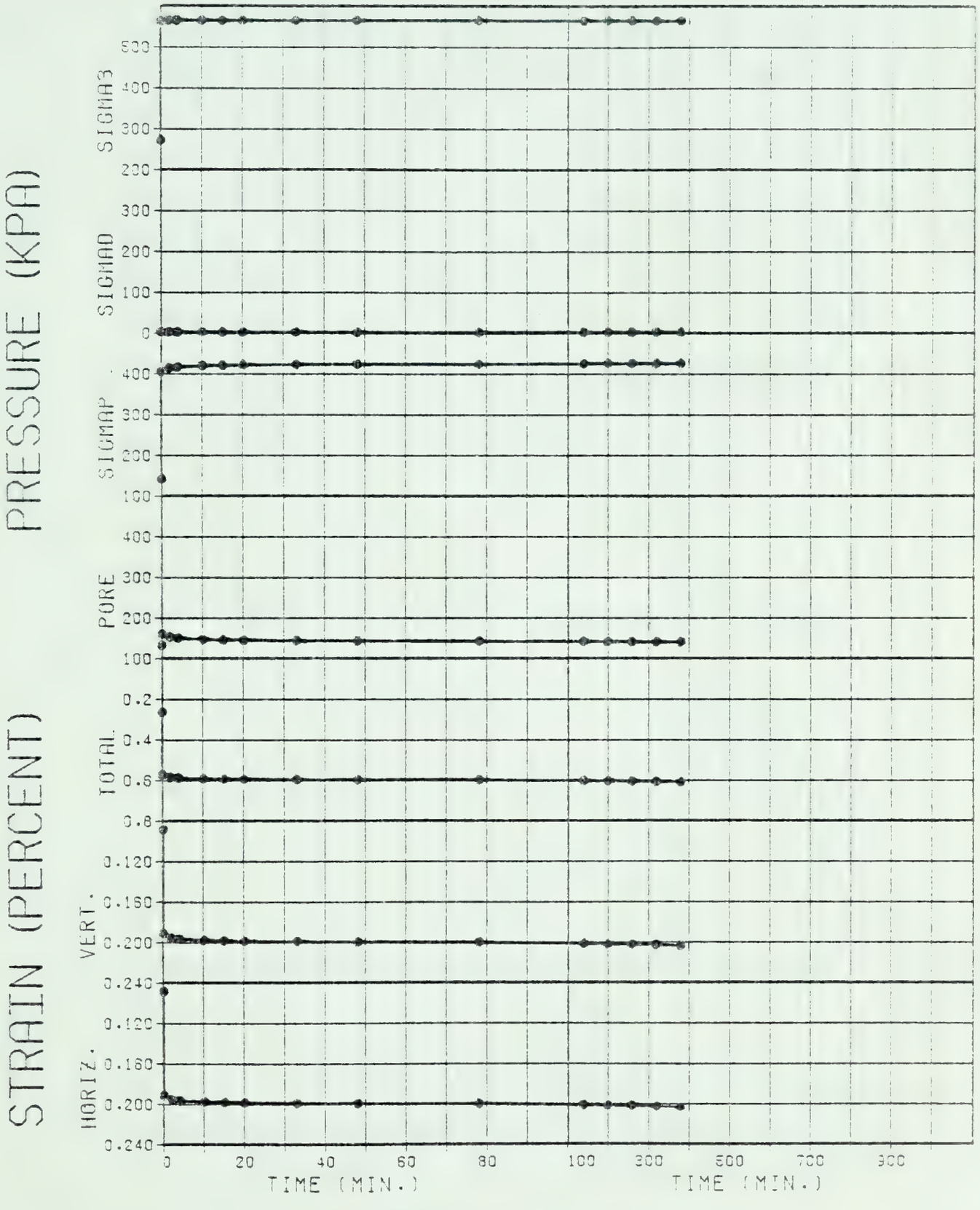
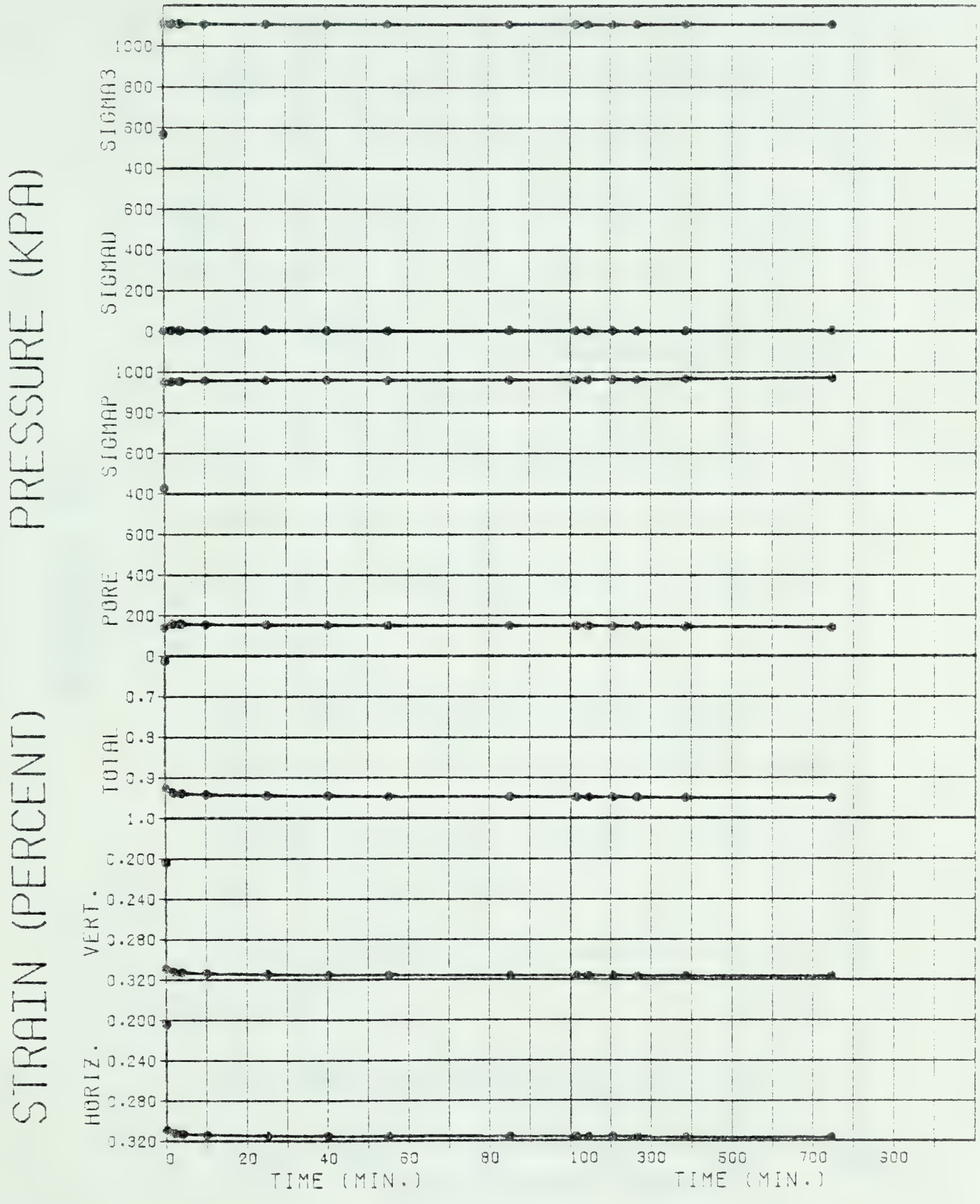

PRESSURE (KPA)
STRAIN (PERCENT)
SIGMA3
SIGMAD
SIGMAP
PORE
TOTAL
VERT.
HORIZ.
TIME (MIN.)
TIME (MIN.)
TEST NO. 9P

Figure C.27



TEST NO. 90

Figure C.28

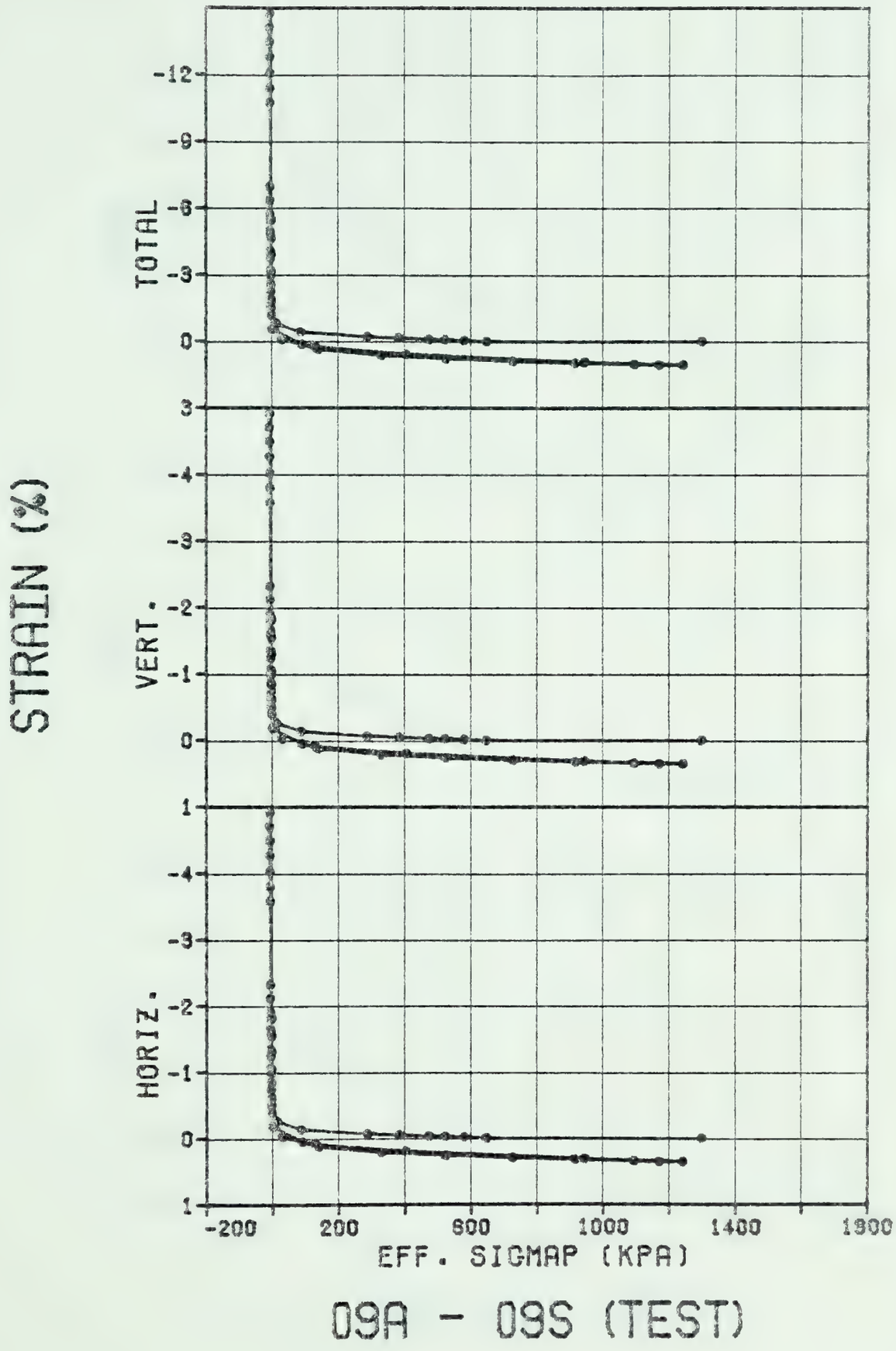

STRAIN (%)
TOTAL
VERT.
HORIZ.
-12
-9
-6
-3
0
3
-4
-3
-2
-1
0
1
-4
-3
-2
-1
0
1
-200
200
600
1000
1400
1800
EFF. SIGMAP (KPA)
09A - 09S (TEST)

Figure C.29

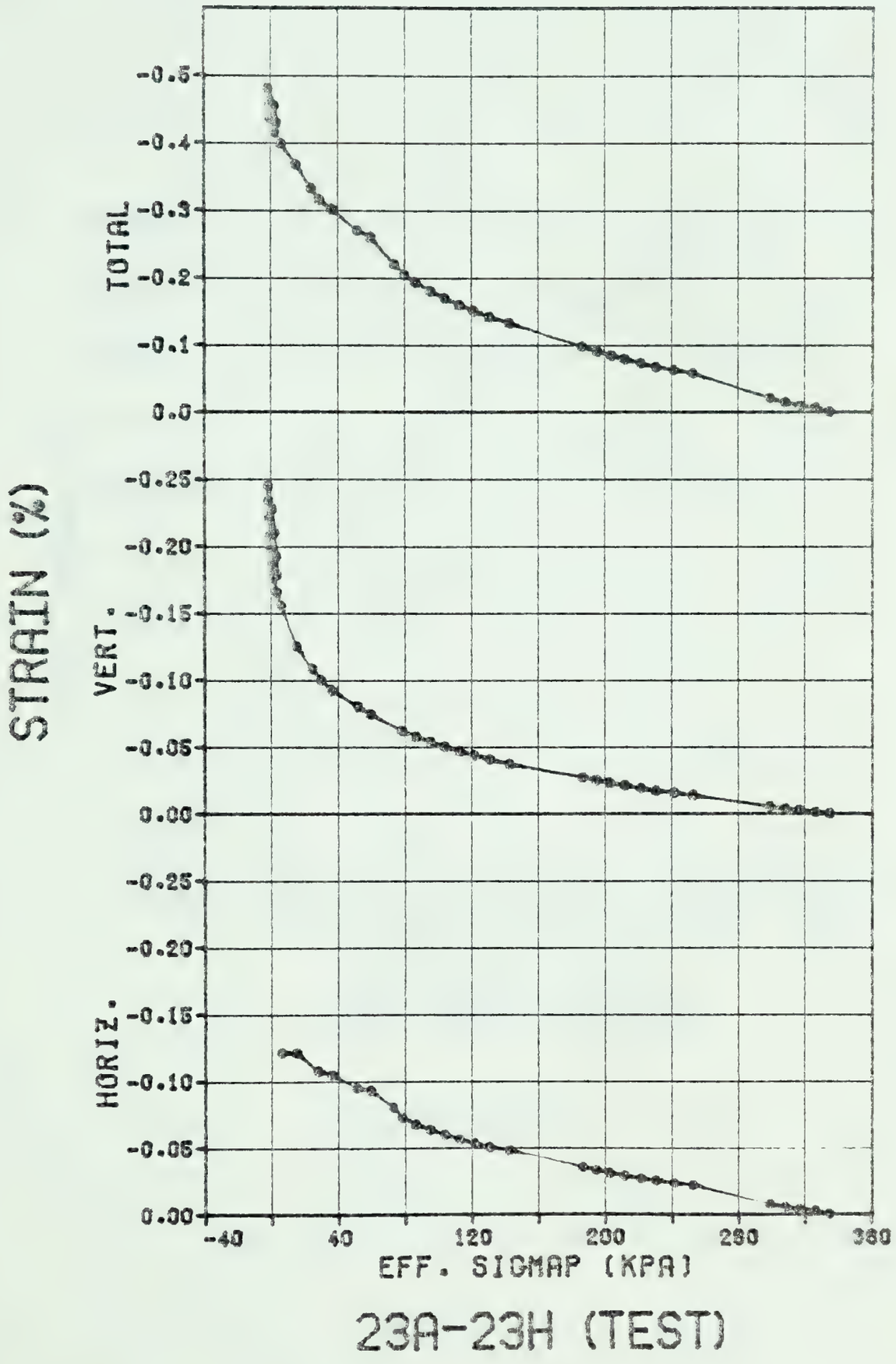

STRAIN (%)
TOTAL
VERT.
HORIZ.
-0.5
-0.4
-0.3
-0.2
-0.1
0.0
-0.25
-0.20
-0.15
-0.10
-0.05
0.00
-0.25
-0.20
-0.15
-0.10
-0.05
0.00
-40
40
120
200
280
360
EFF. SIGMAP (KPA)
23A-23H (TEST)

Figure C.30

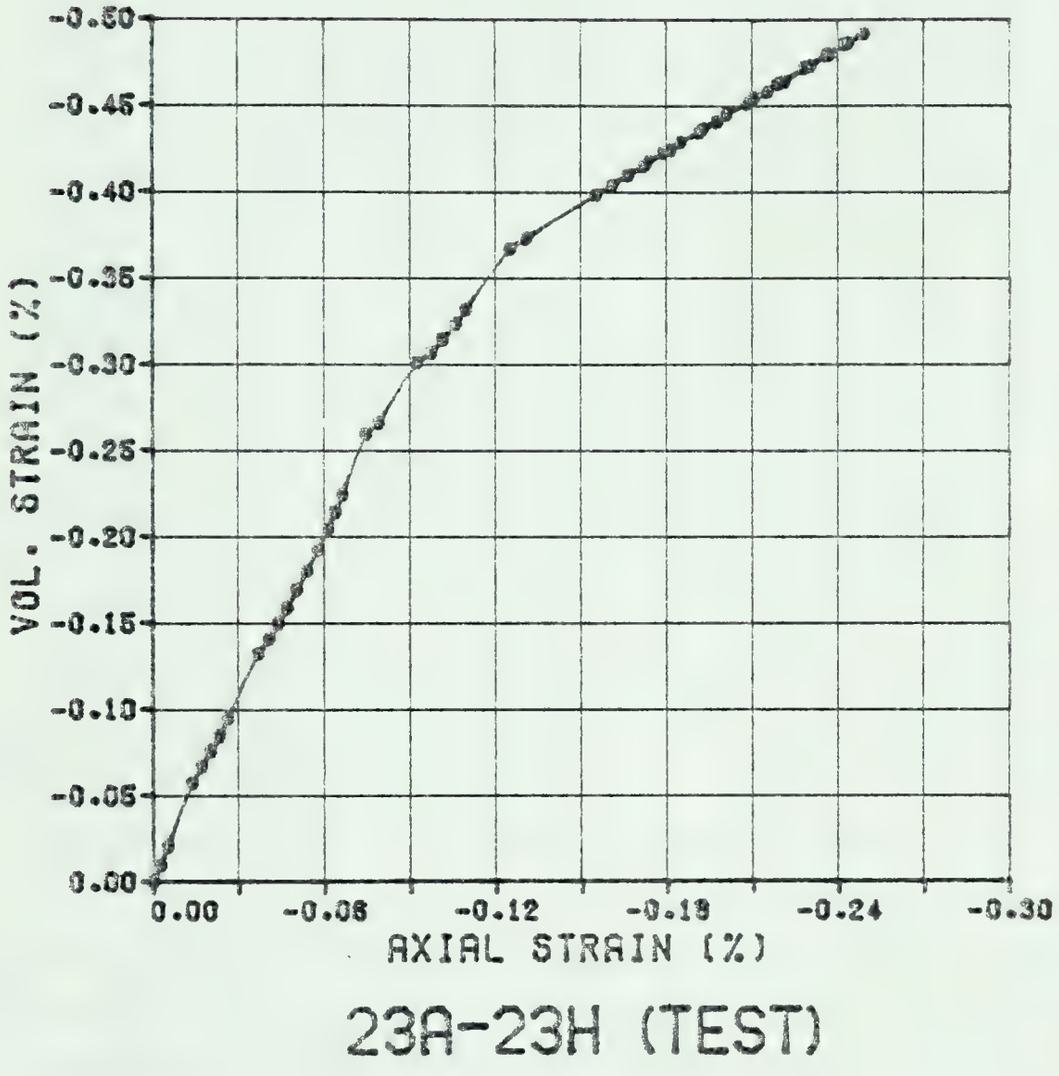
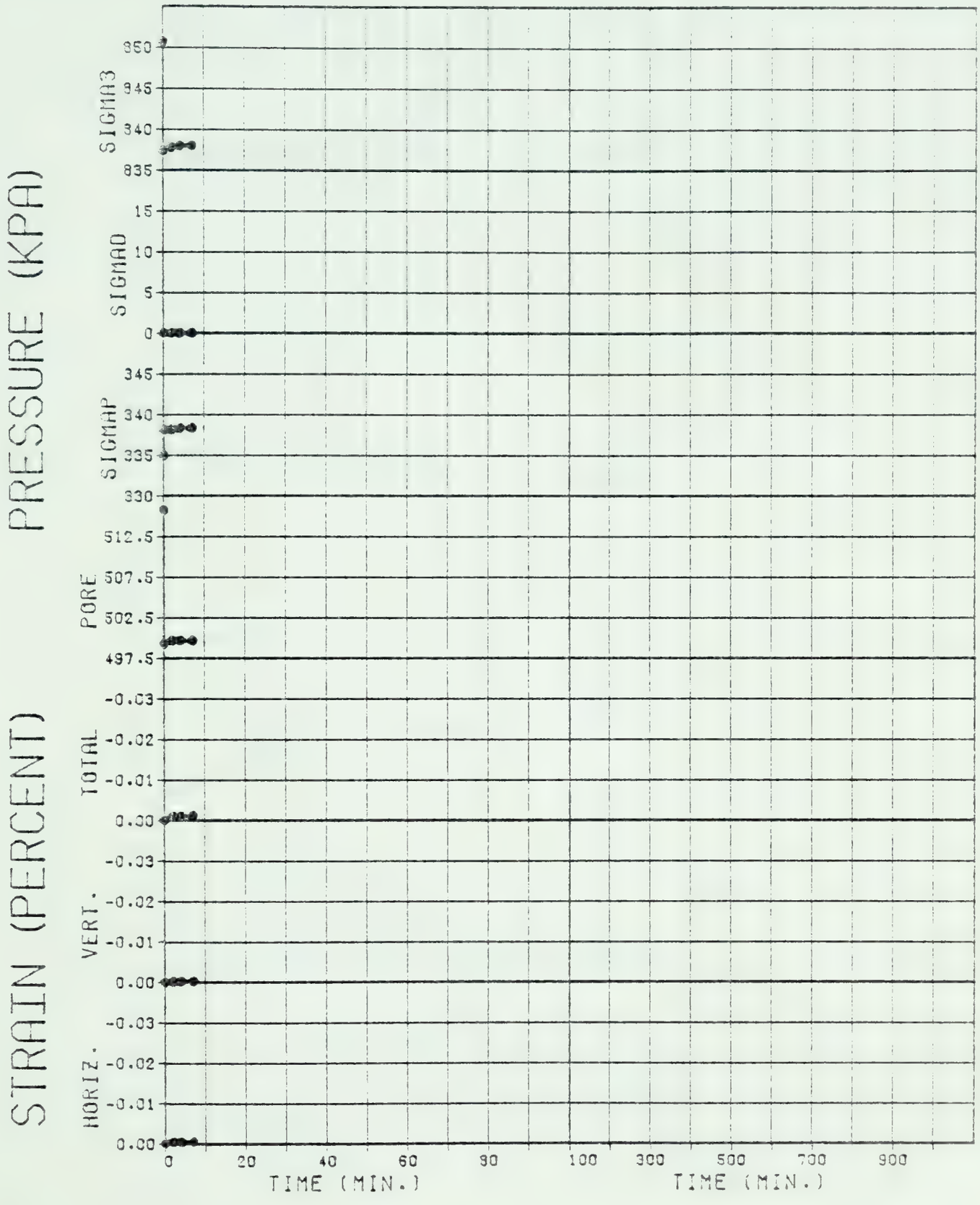

-0.50
-0.45
-0.40
-0.35
-0.30
-0.25
-0.20
-0.15
-0.10
-0.05
0.00
VOL. STRAIN (%)
0.00
-0.06
-0.12
-0.18
-0.24
-0.30
AXIAL STRAIN (%)
23A-23H (TEST)

Figure C.31



TEST NO. 23A

Figure C.32

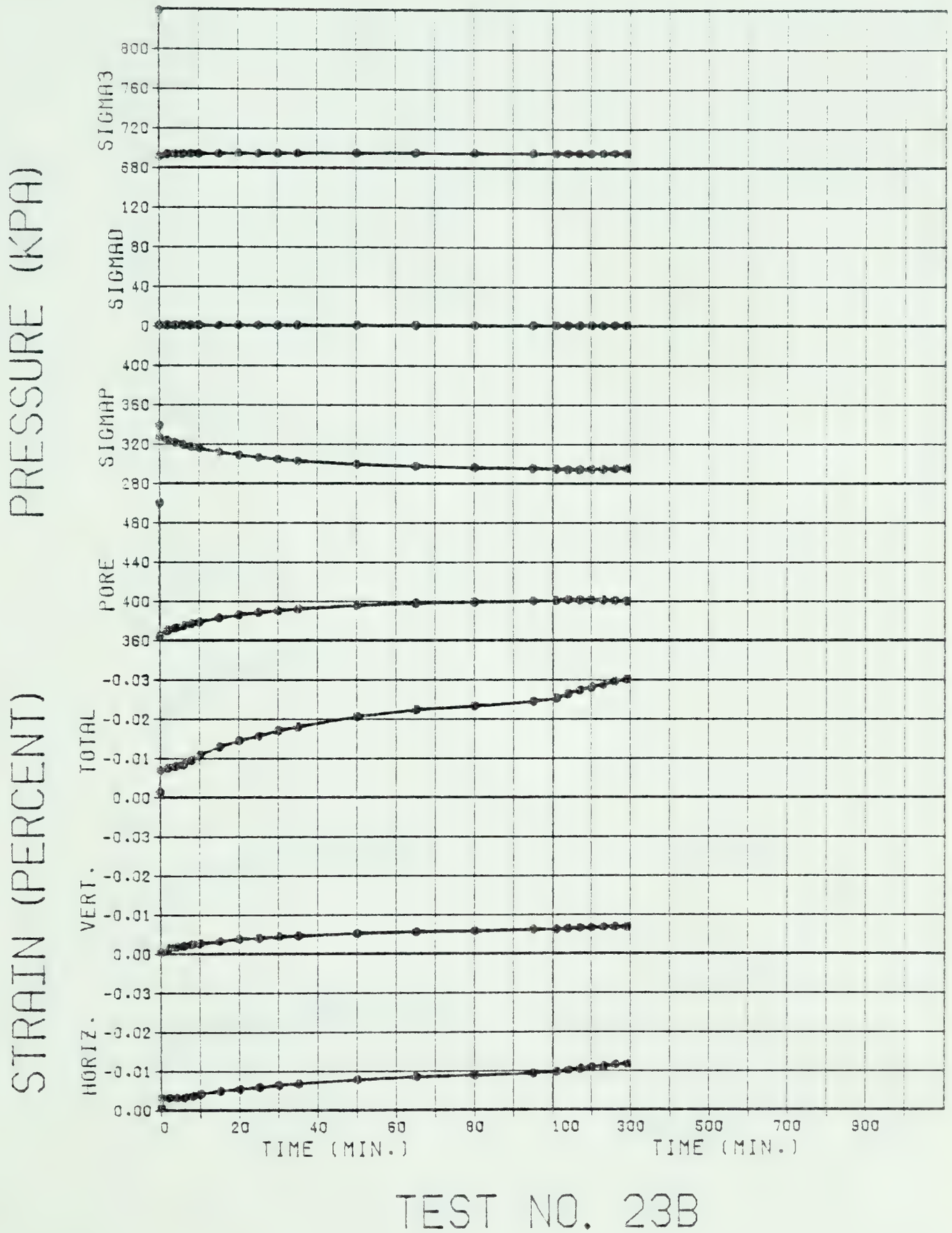

PRESSURE (KPA)
SIGMA3
800
760
720
680
SIGMAD
120
80
40
0
SIGMAP
400
360
320
280
PORE
480
440
400
360
STRAIN (PERCENT)
TOTAL
-0.03
-0.02
-0.01
0.00
VERT.
-0.03
-0.02
-0.01
0.00
HORIZ.
-0.03
-0.02
-0.01
0.00
0
20
40
60
80
100
300
500
700
900
TIME (MIN.)
TIME (MIN.)
TEST NO. 23B

Figure C.33

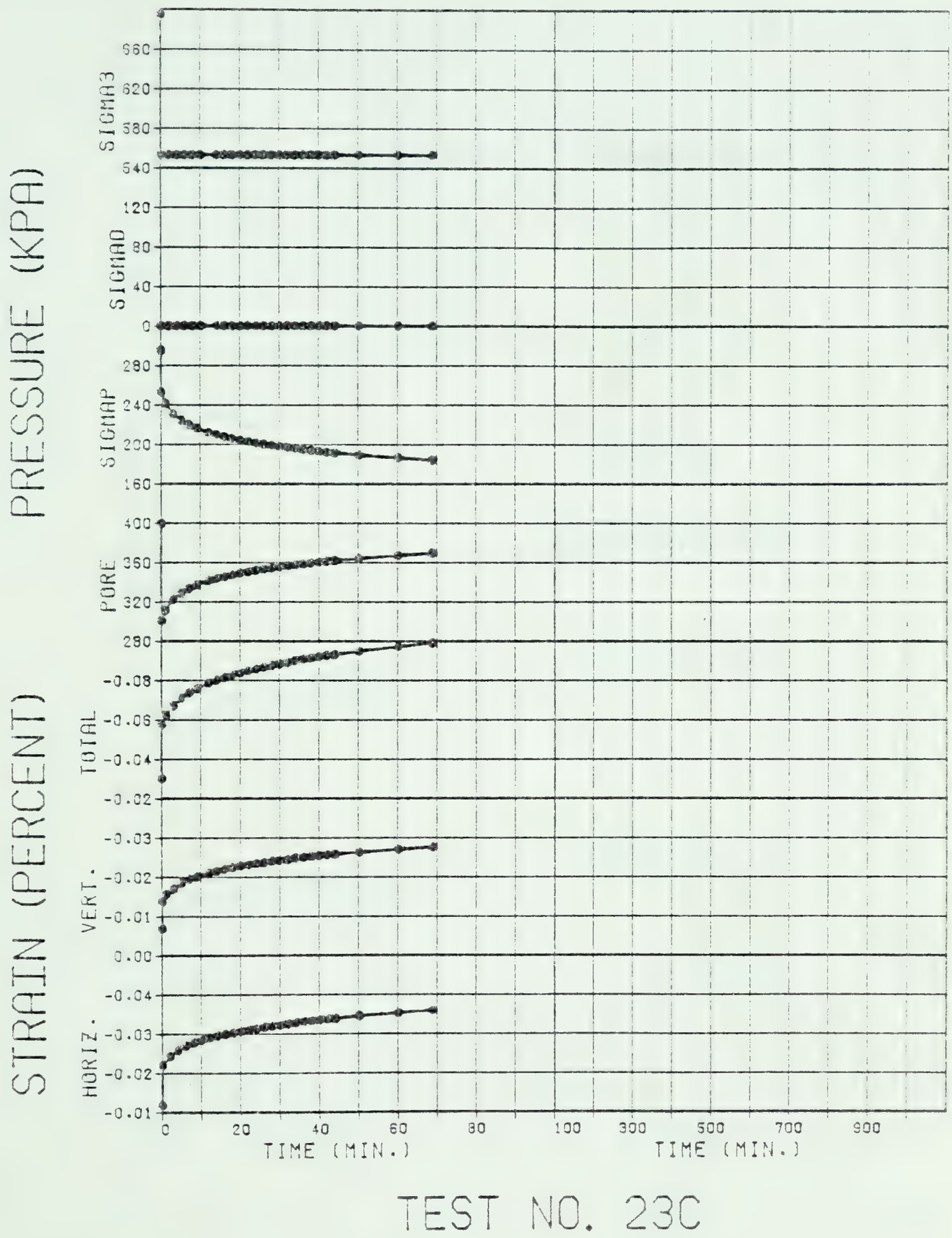

PRESSURE (KPA)
STRAIN (PERCENT)
SIGMA3
SIGMAD
SIGMAP
PORE
TOTAL
VERT.
HORIZ.
TIME (MIN.)
TIME (MIN.)
TEST NO. 23C

Figure C.34

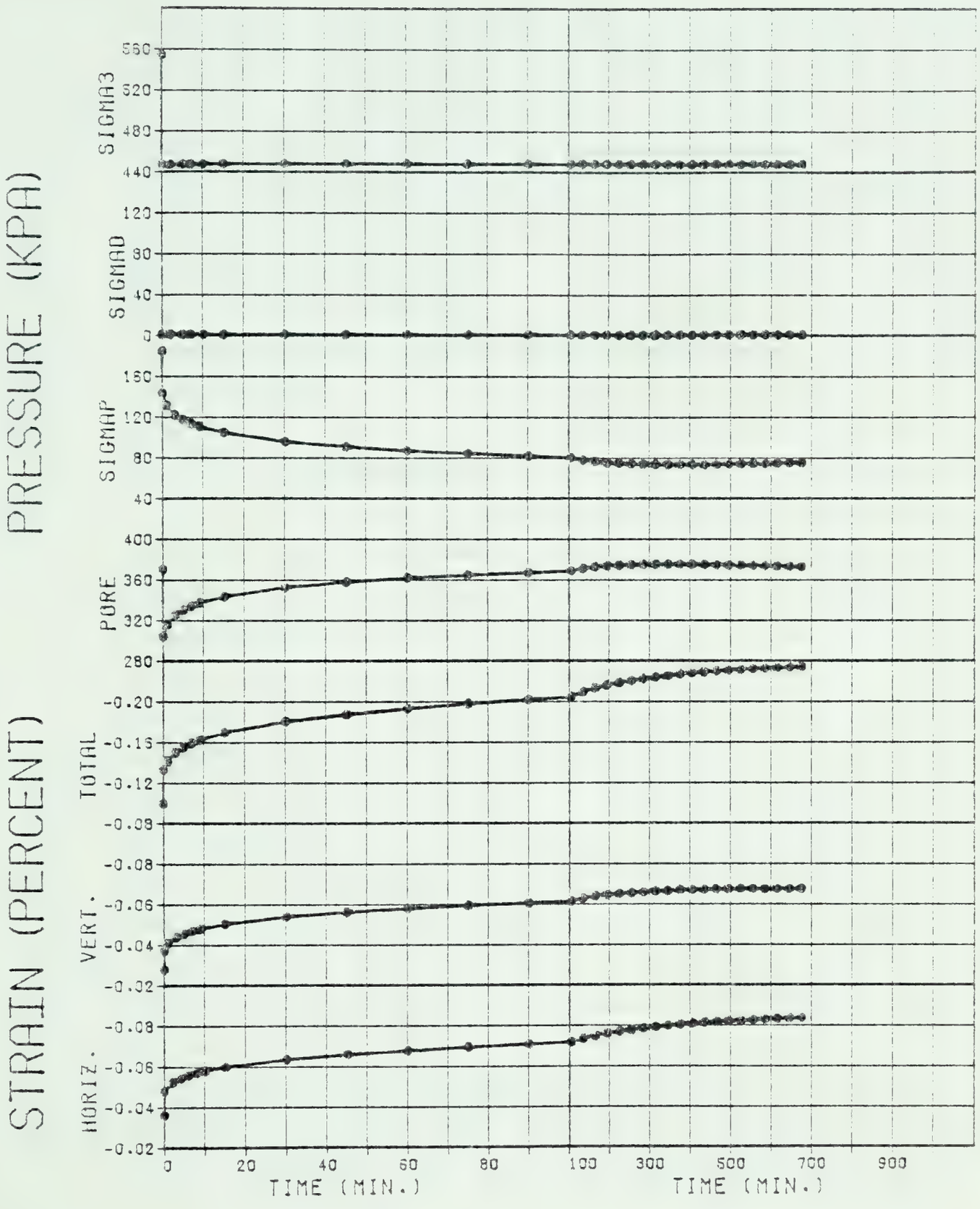

PRESSURE (KPA)
STRAIN (PERCENT)
SIGMA3
SIGMAD
SIGMAP
PORE
TOTAL
VERT.
HORIZ.
TIME (MIN.)
TIME (MIN.)
TEST NO. 23D

Figure C.35

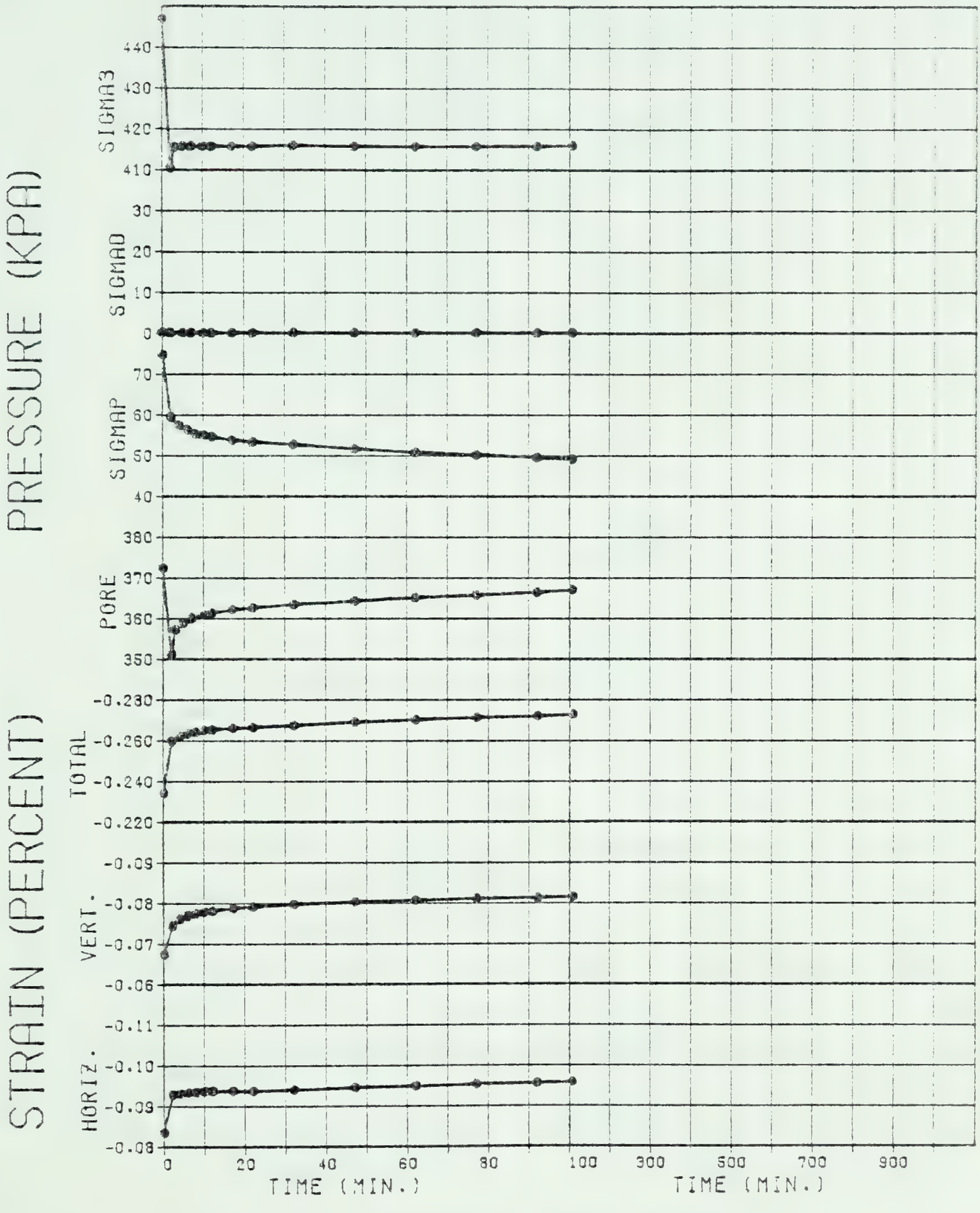
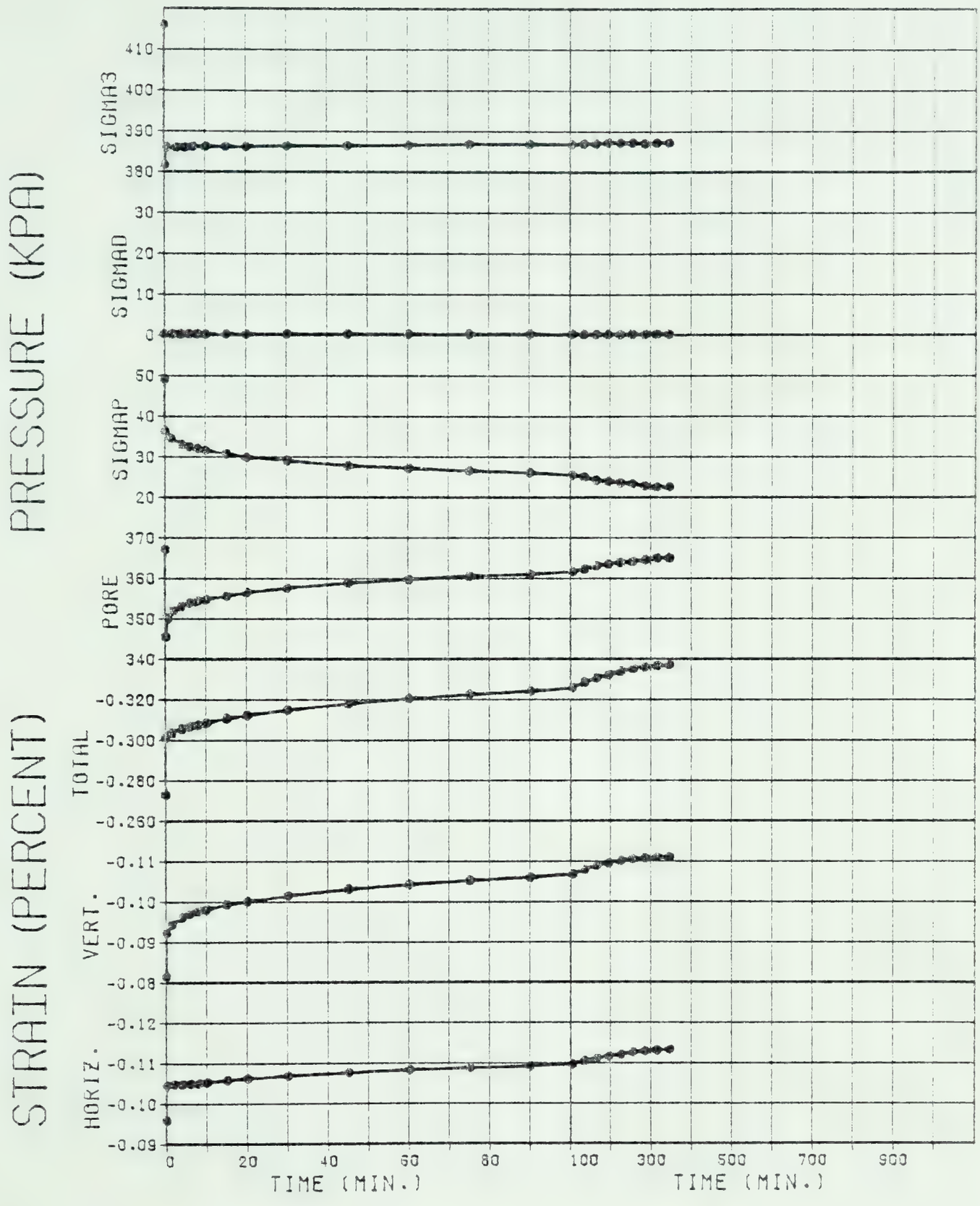
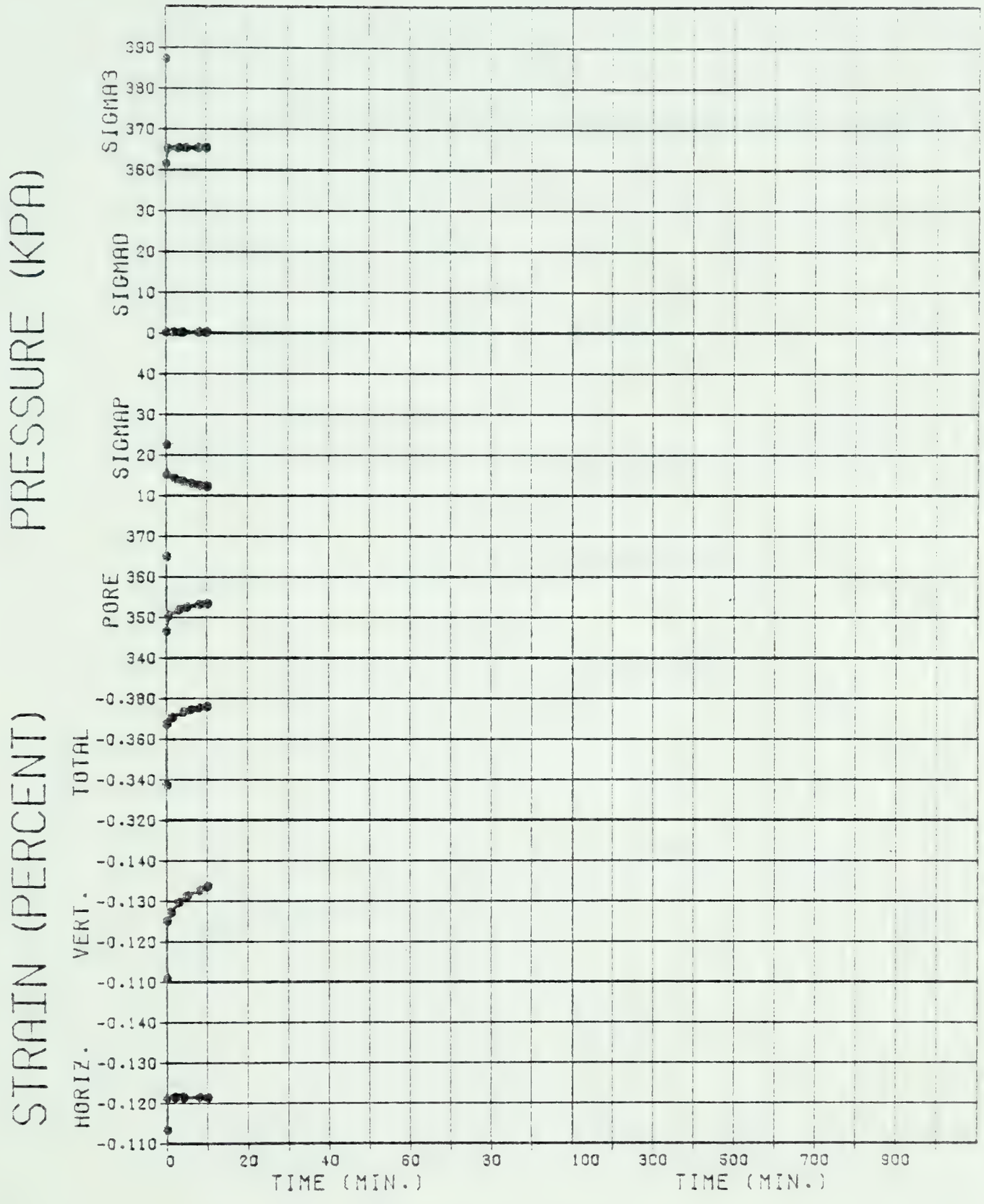

PRESSURE (KPA)
SIGMA3
SIGMAD
SIGMAP
PORE
STRAIN (PERCENT)
TOTAL
VERT.
HORIZ.
TIME (MIN.)
TIME (MIN.)
TEST NO. 23E

Figure C.36



TEST NO. 23F

Figure C.37



TEST NO. 23G

Figure C.38

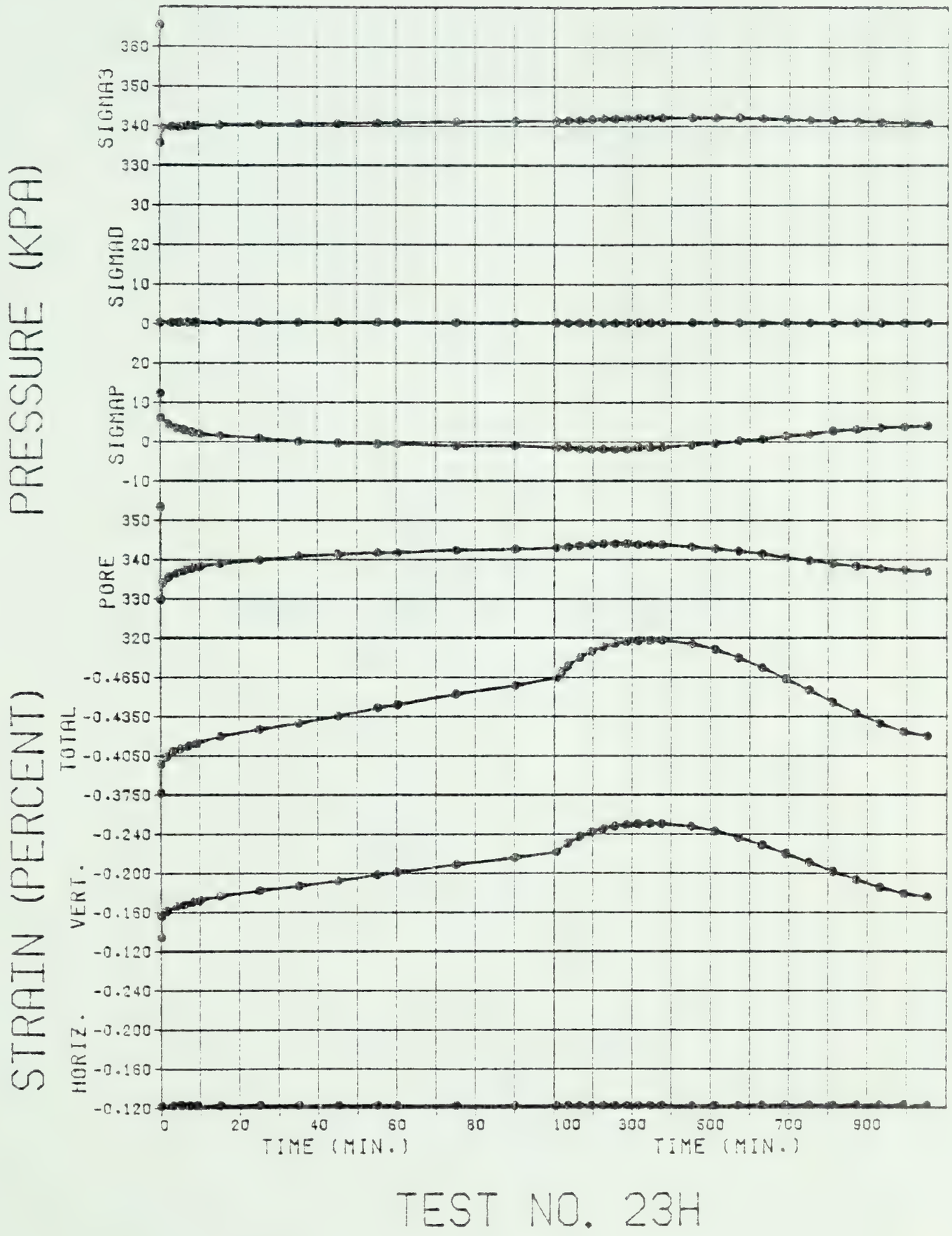
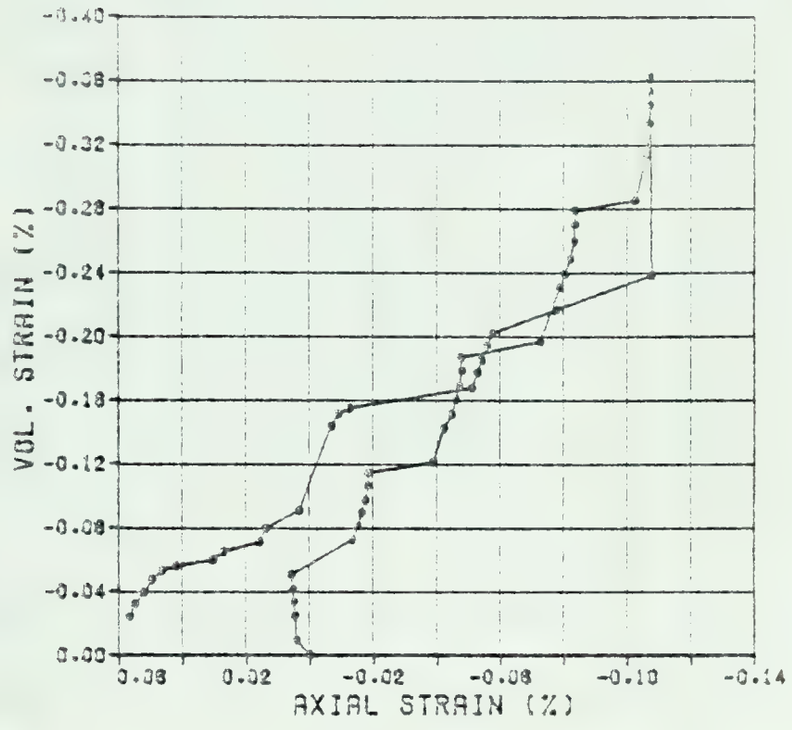

PRESSURE (KPA)
SIGMA3
SIGMAD
SIGMAP
PORE
STRAIN (PERCENT)
TOTAL
VERT.
HORIZ.
TIME (MIN.)
TIME (MIN.)
TEST NO. 23H

Figure C.39

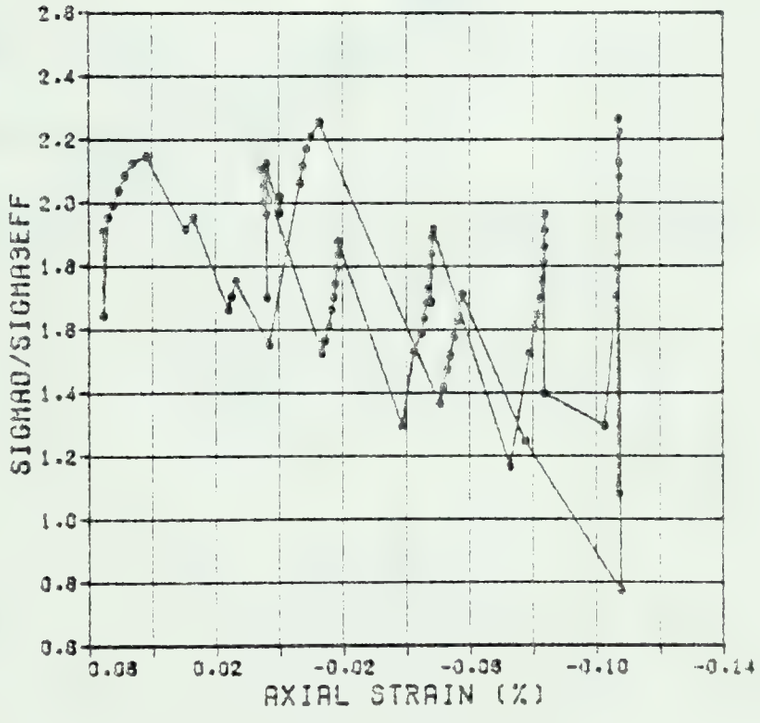
APPENDIX D

CONSTANT STRESS RATIO TEST RESULTS

TESTS 12, 15, 22



12A-12J (TEST)



12A-12J (TEST)

Figures D.1 & D.2

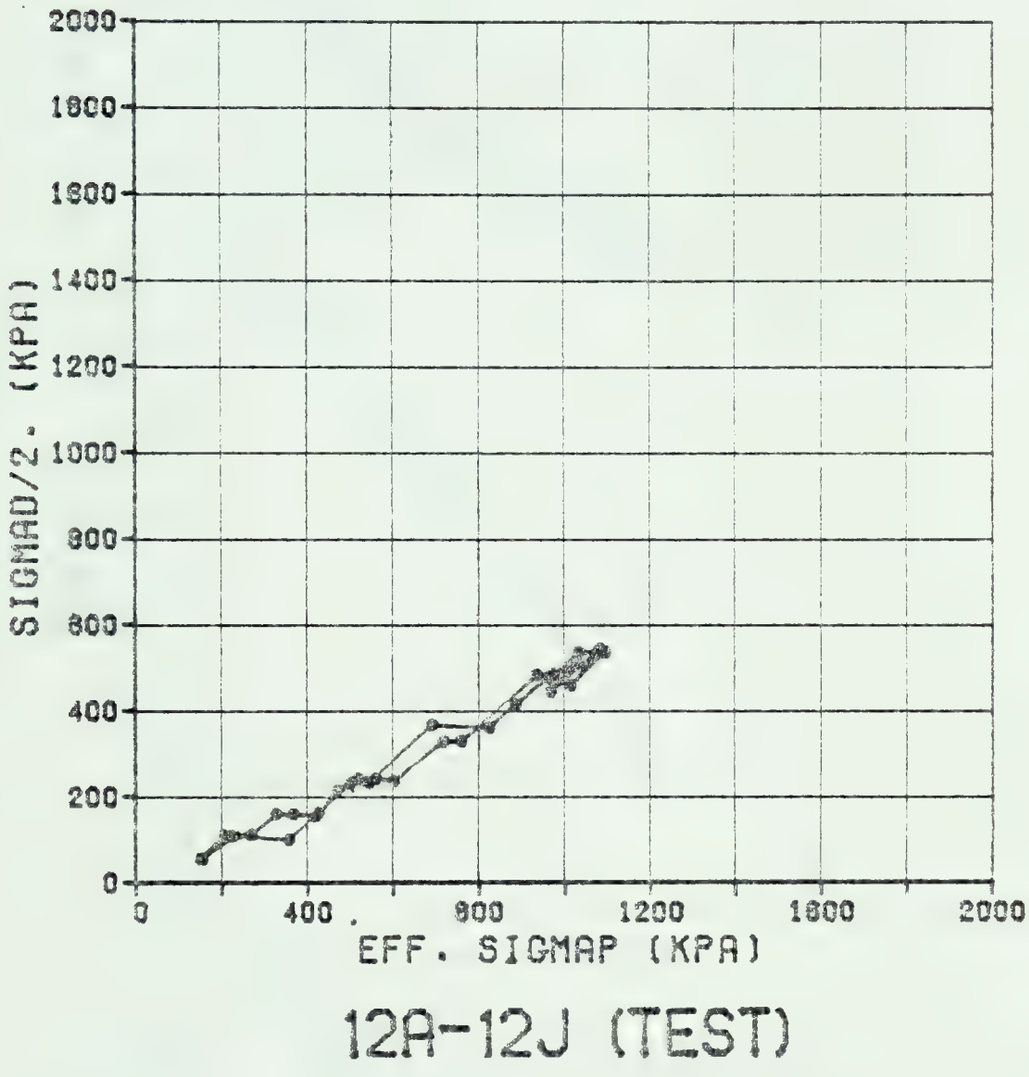

2000
1800
1600
1400
1200
1000
800
600
400
200
0
SIGMAD/2. (KPA)
0
400
800
1200
1600
2000
EFF. SIGMAP (KPA)
12A-12J (TEST)

Figure D.3

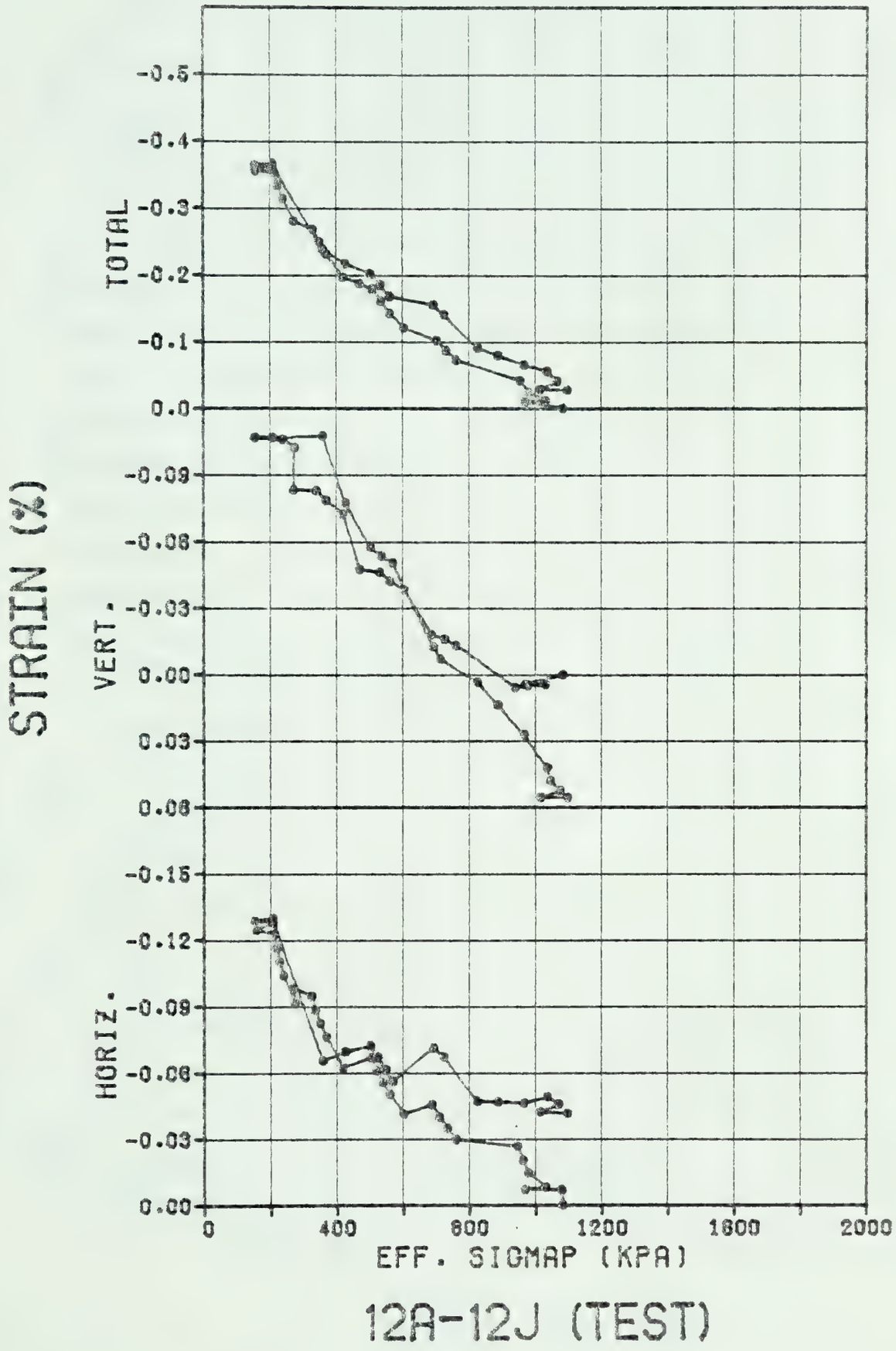

STRAIN (%)
TOTAL
VERT.
HORIZ.
-0.5
-0.4
-0.3
-0.2
-0.1
0.0
-0.09
-0.06
-0.03
0.00
0.03
0.06
-0.15
-0.12
-0.09
-0.06
-0.03
0.00
0
400
800
1200
1600
2000
EFF. SIGMAP (KPA)
12A-12J (TEST)

Figure D.4

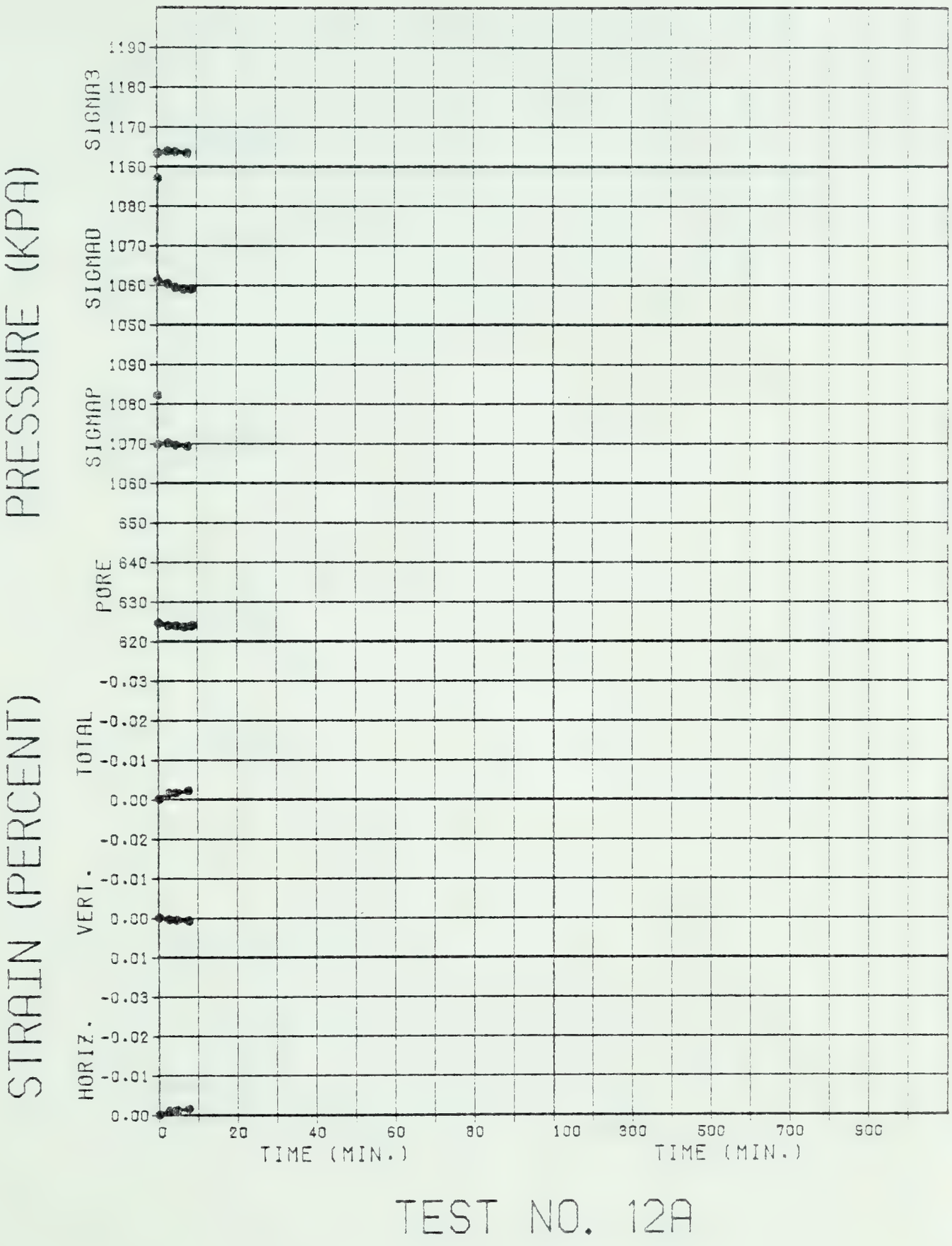

PRESSURE (KPA)
STRAIN (PERCENT)
SIGMA3
SIGMAD
SIGMAP
PORE
TOTAL
VERT.
HORIZ.
1190
1180
1170
1160
1080
1070
1060
1050
1090
1080
1070
1060
650
640
630
620
-0.03
-0.02
-0.01
0.00
-0.02
-0.01
0.00
0.01
-0.03
-0.02
-0.01
0.00
0
20
40
60
80
100
300
500
700
900
TIME (MIN.)
TIME (MIN.)
TEST NO. 12A

Figure D.5

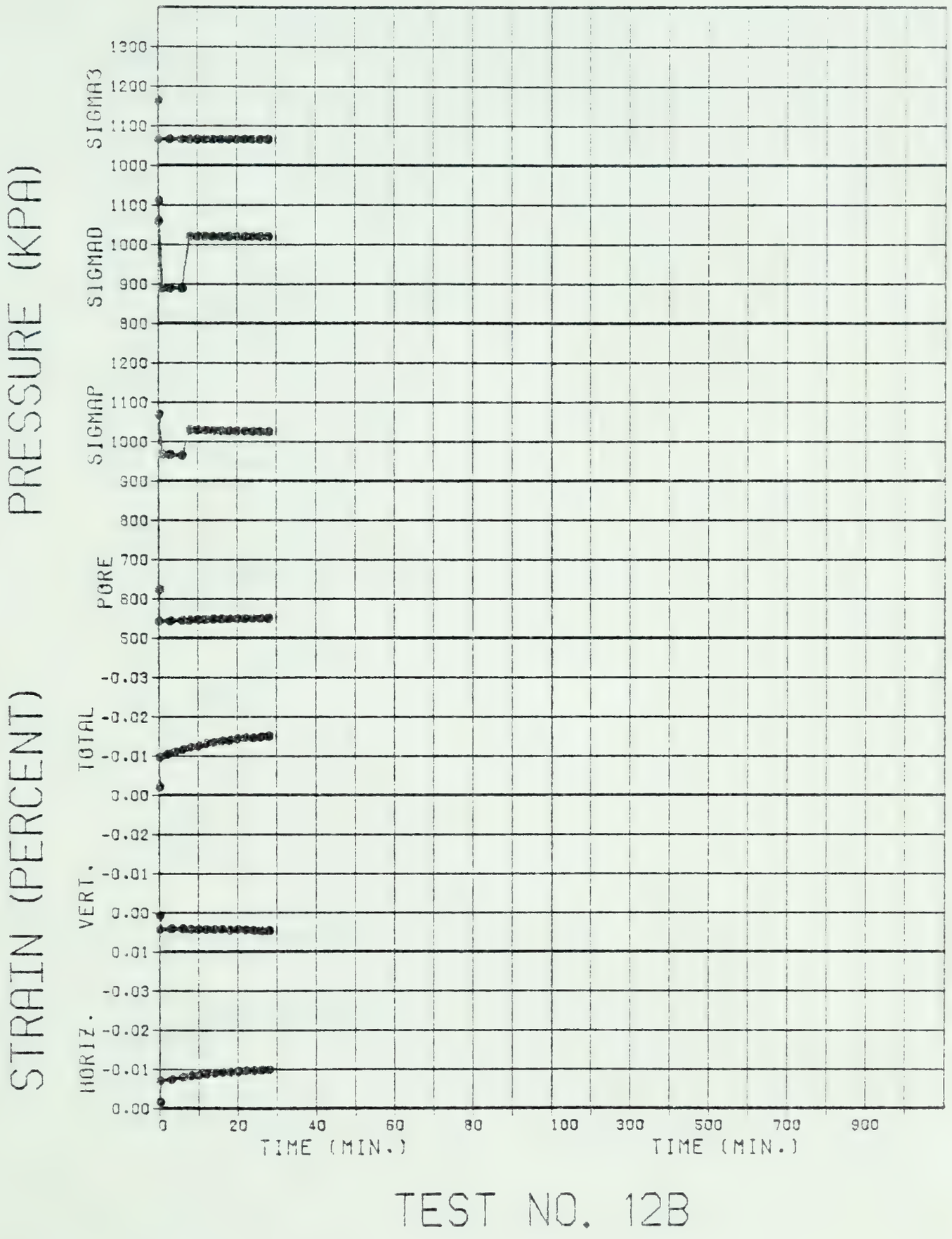

PRESSURE (KPA)
STRAIN (PERCENT)
SIGMA3
SIGMAD
SIGMAP
PORE
TOTAL
VERT.
HORIZ.
TIME (MIN.)
TIME (MIN.)
TEST NO. 12B

Figure D.6

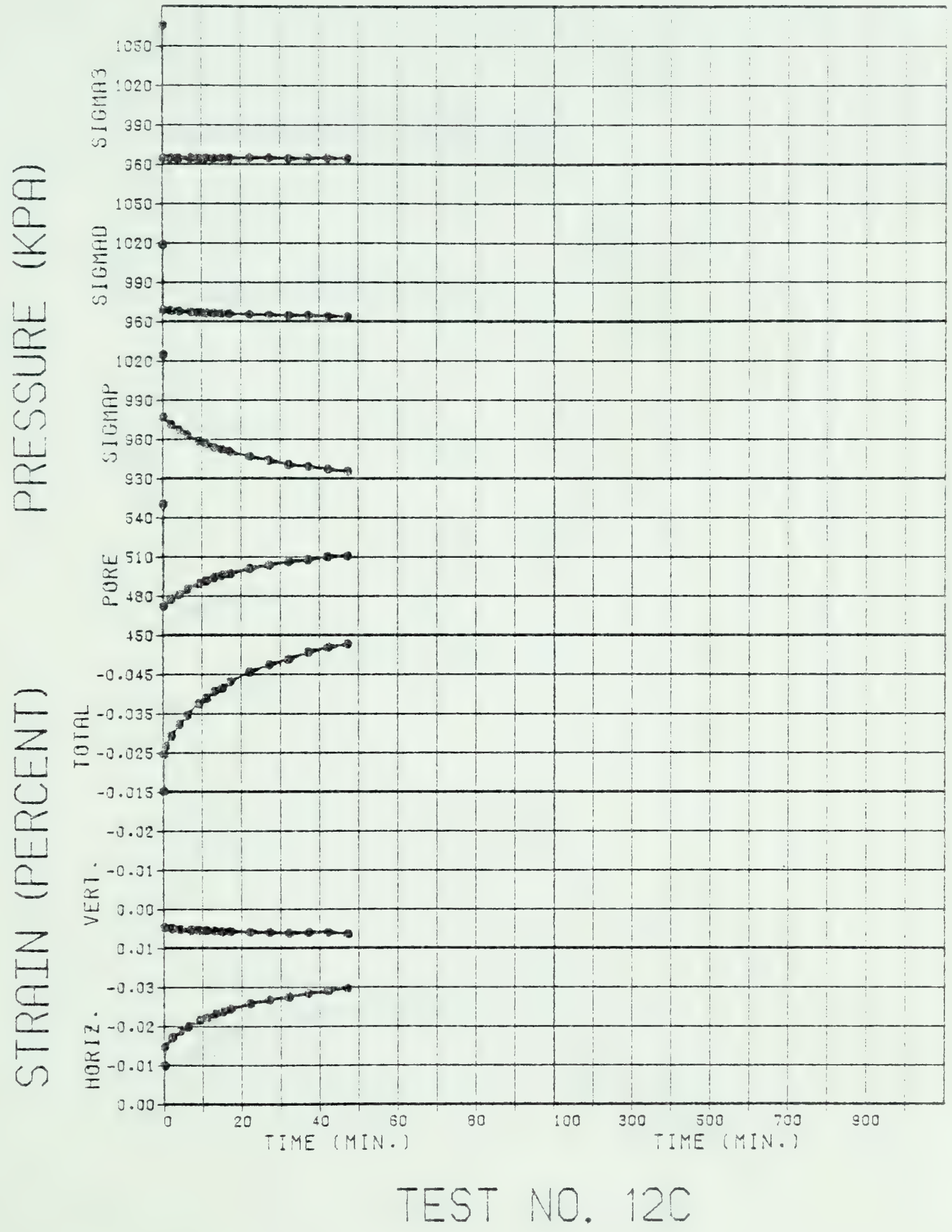

PRESSURE (KPA)
STRAIN (PERCENT)
SIGMA3
SIGMAD
SIGMAP
PORE
TOTAL
VERT.
HORIZ.
1050
1020
990
960
930
540
510
480
450
-0.045
-0.035
-0.025
-0.015
-0.02
-0.01
0.00
0.01
-0.03
-0.02
-0.01
0.00
0
20
40
60
80
100
300
500
700
900
TIME (MIN.)
TIME (MIN.)
TEST NO. 12C

Figure D.7

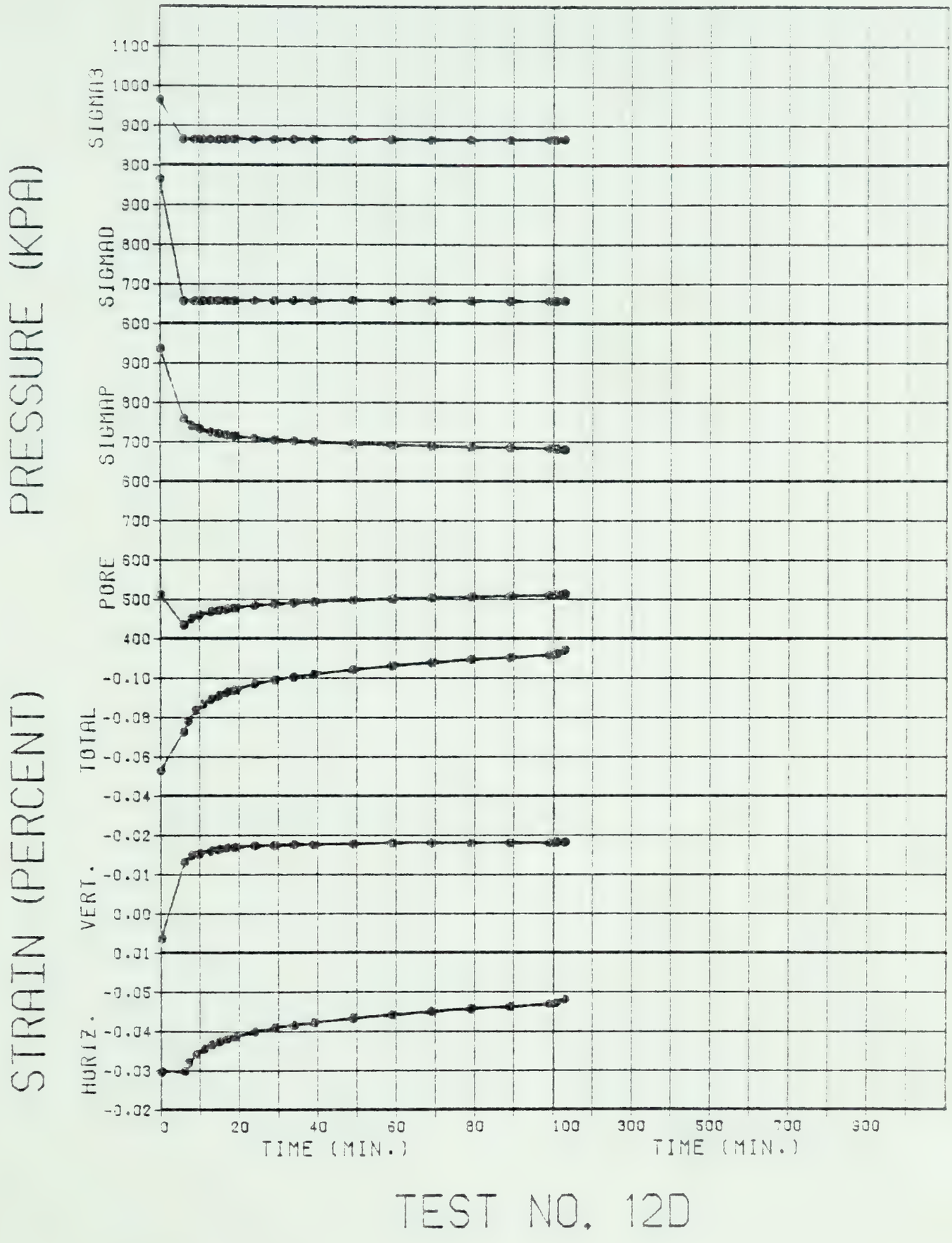

PRESSURE (KPA)
STRAIN (PERCENT)
SIGMA3
SIGMAD
SIGMAP
PORE
TOTAL
VERT.
HORIZ.
TIME (MIN.)
TIME (MIN.)
TEST NO. 12D

Figure D.8

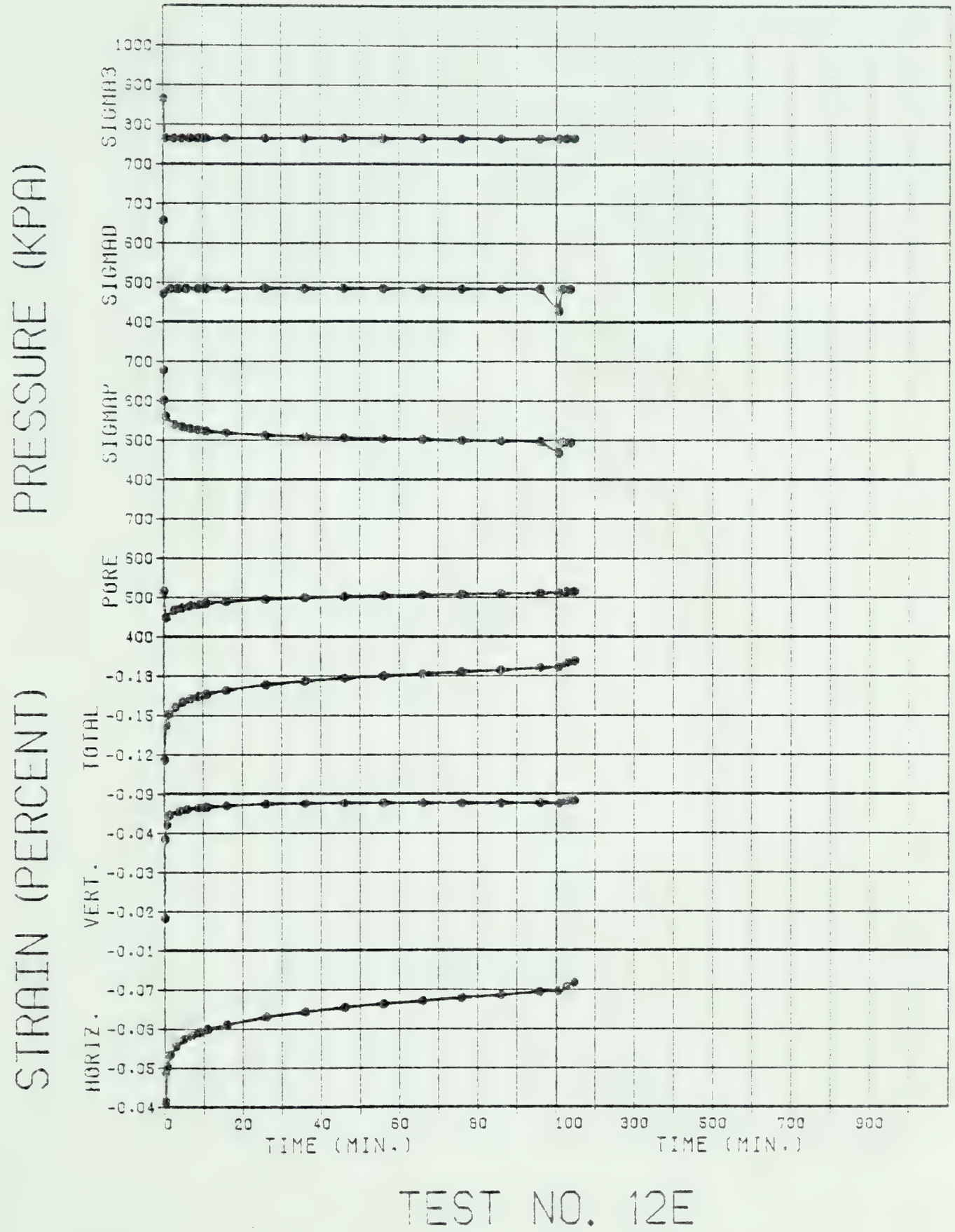
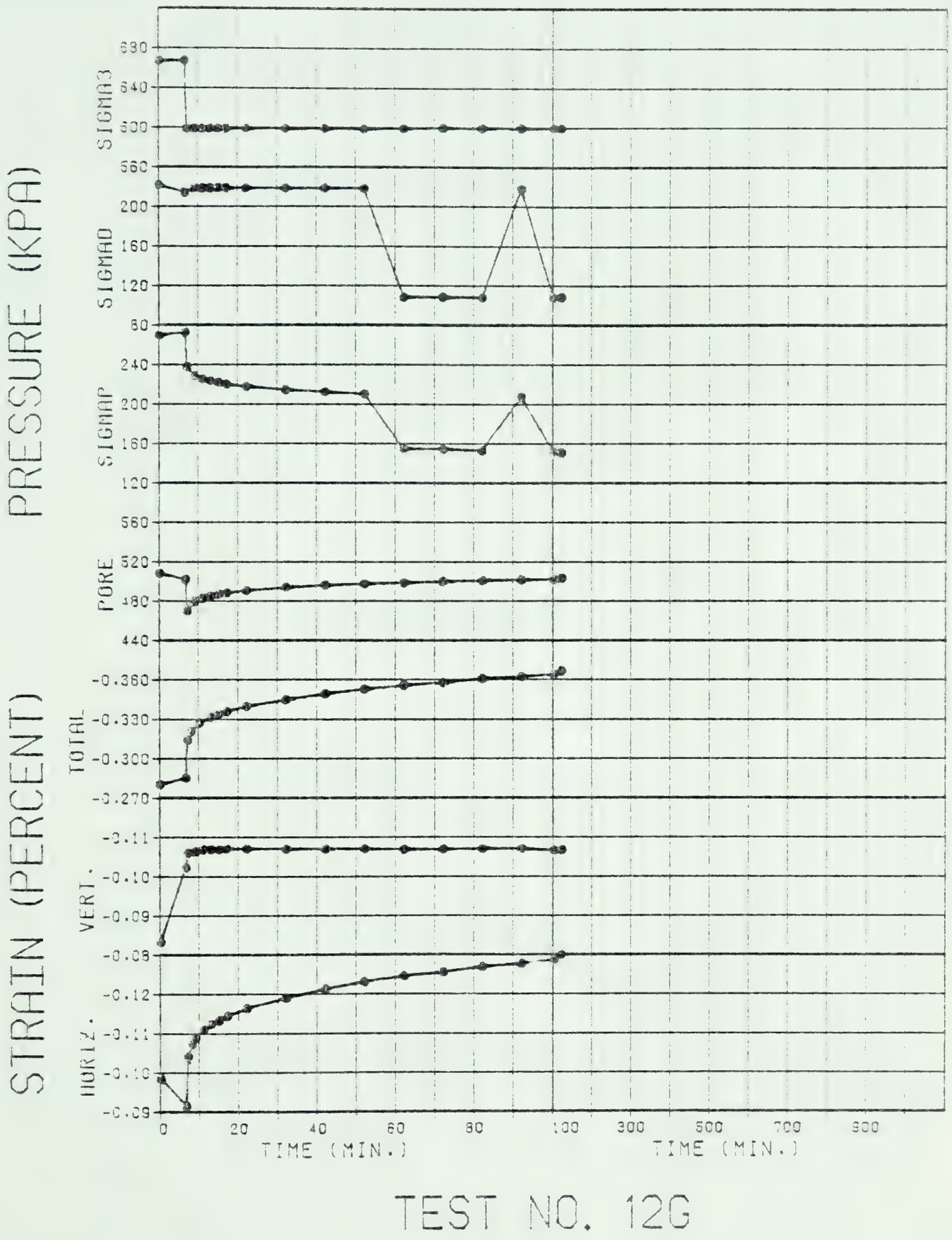

PRESSURE (KPA)
STRAIN (PERCENT)
SIGMA3
SIGMAD
SIGMAP
PORE
TOTAL
VERT.
HORIZ.
1000
900
800
700
600
500
400
-0.18
-0.15
-0.12
-0.09
-0.04
-0.03
-0.02
-0.01
-0.07
-0.06
-0.05
-0.04
0
20
40
60
80
100
300
500
700
900
TIME (MIN.)
TIME (MIN.)
TEST NO. 12E

Figure D.9



TEST NO. 12F

Figure D.10



TEST NO. 12G

Figure D.11

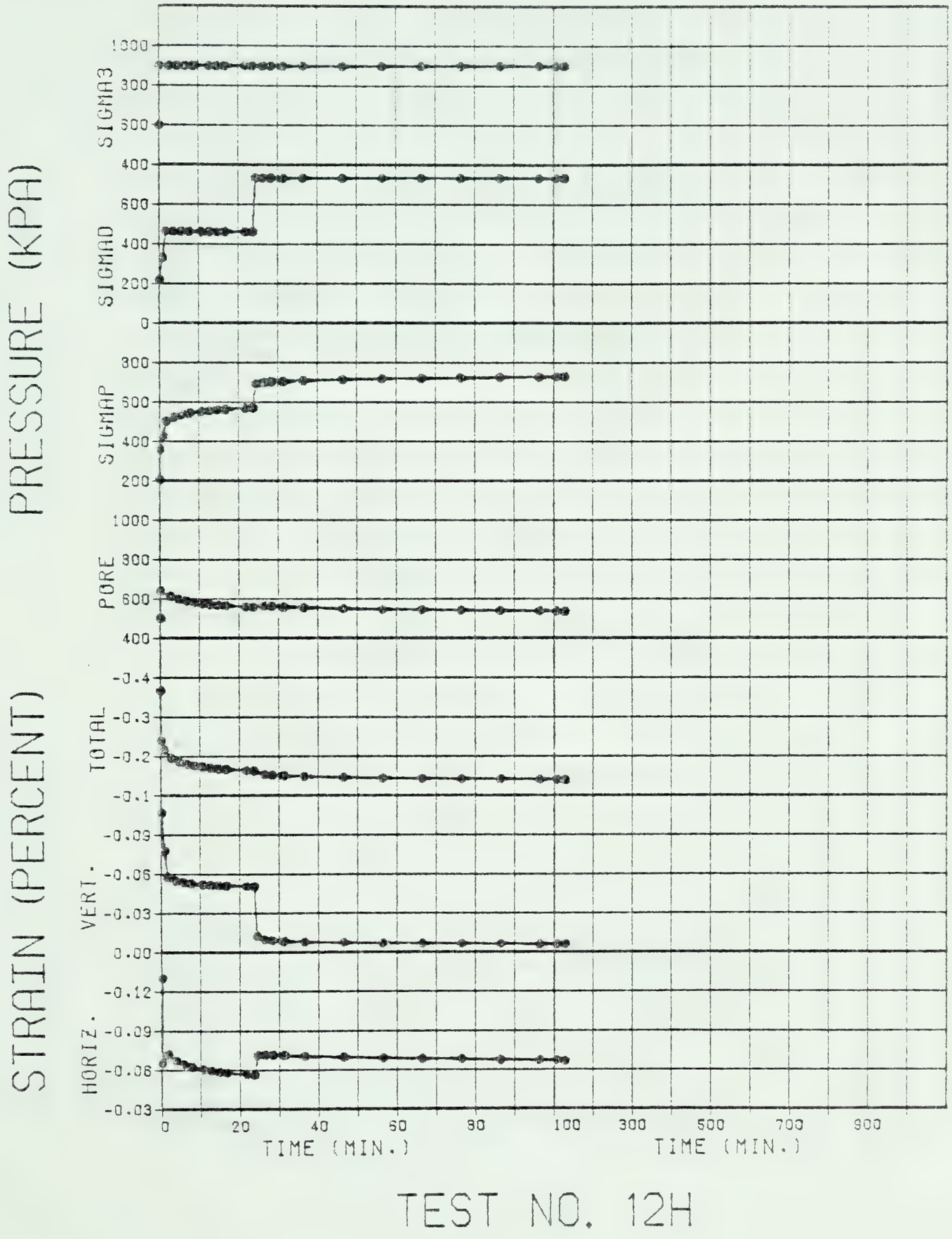
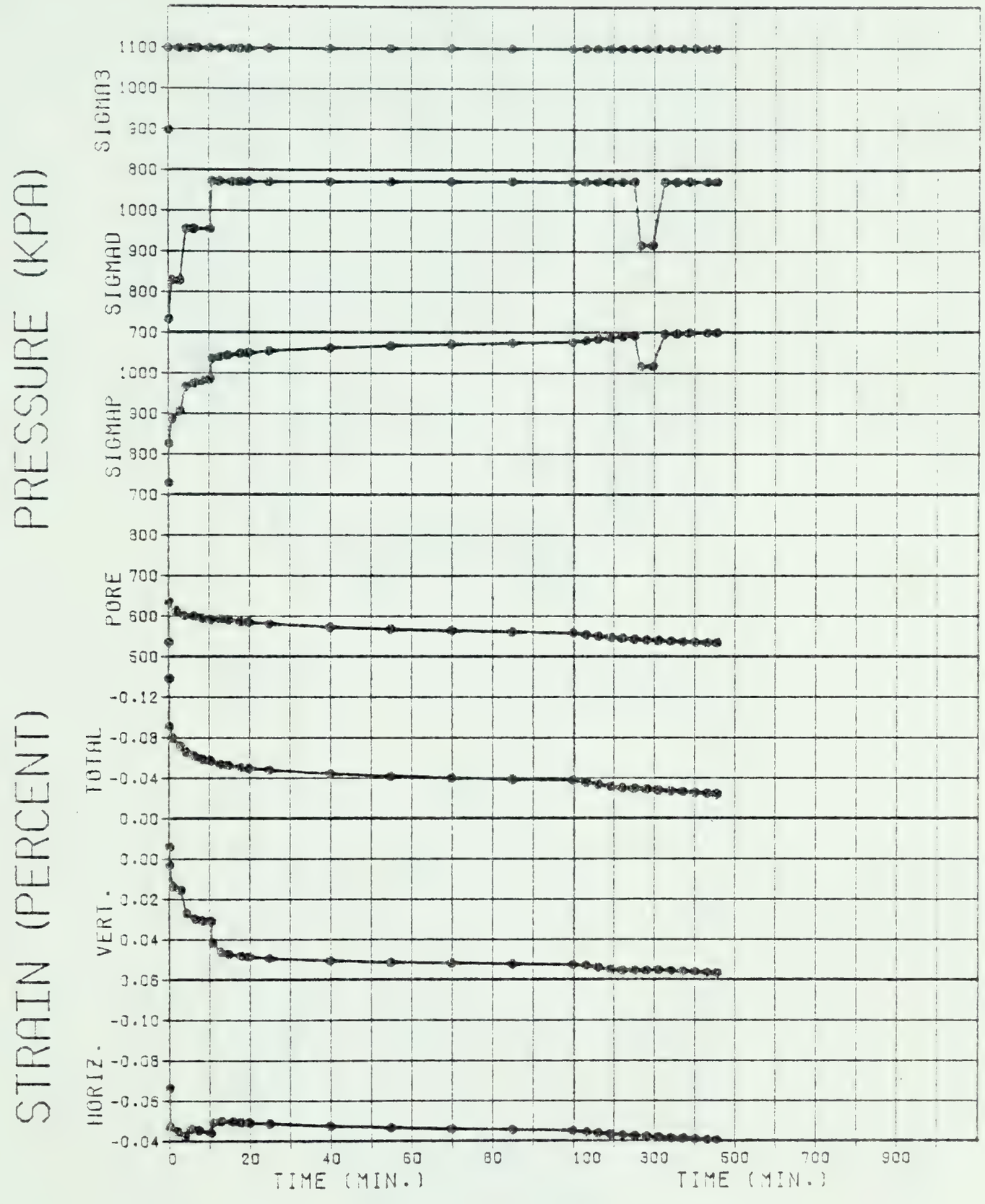
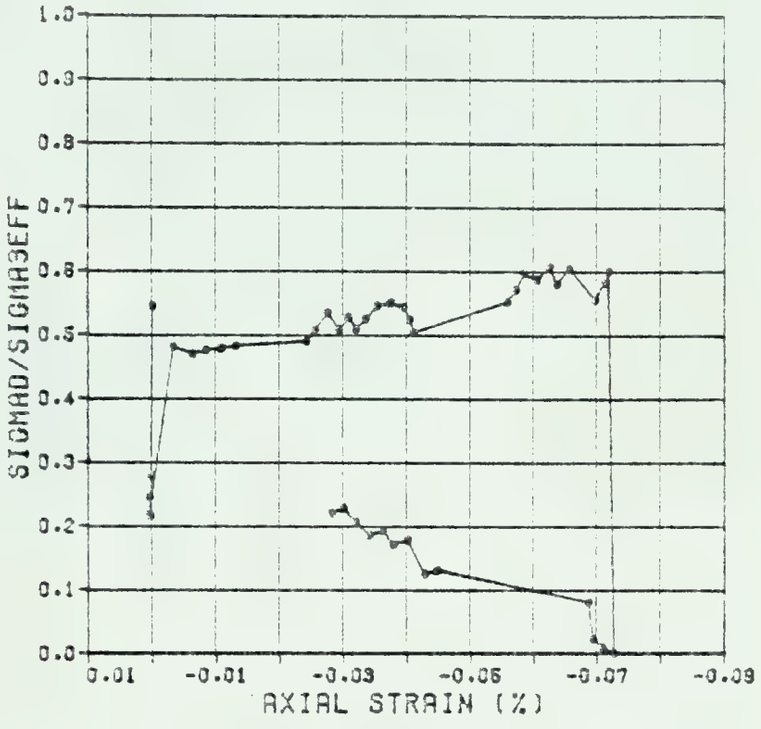

PRESSURE (KPA)
STRAIN (PERCENT)
SIGMA3
SIGMAD
SIGMAP
PORE
TOTAL
VERT.
HORIZ.
1000
800
600
400
200
0
-0.4
-0.3
-0.2
-0.1
-0.09
-0.06
-0.03
0.00
-0.12
-0.09
-0.06
-0.03
0
20
40
60
80
100
300
500
700
900
TIME (MIN.)
TIME (MIN.)
TEST NO. 12H

Figure D.12

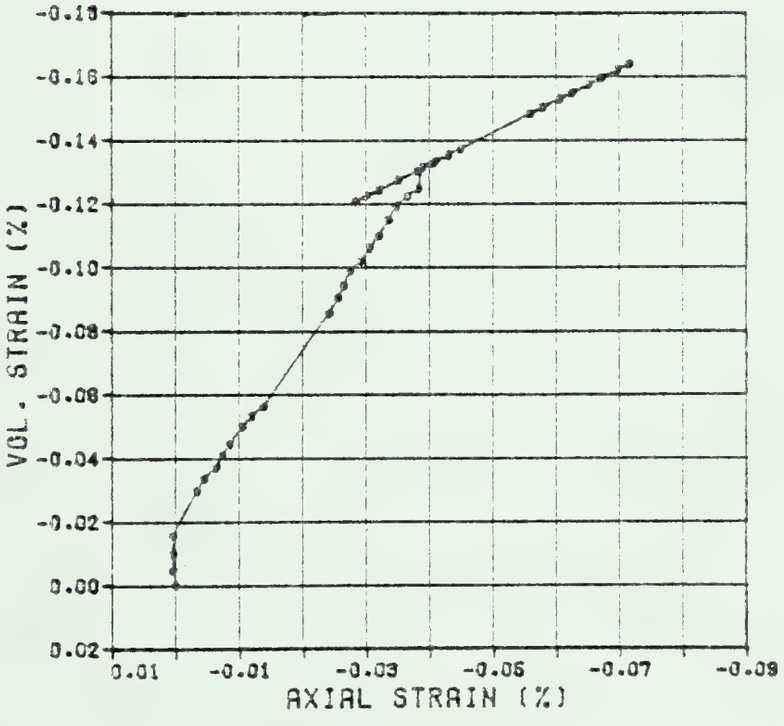


TEST NO. 12J

Figure D.13

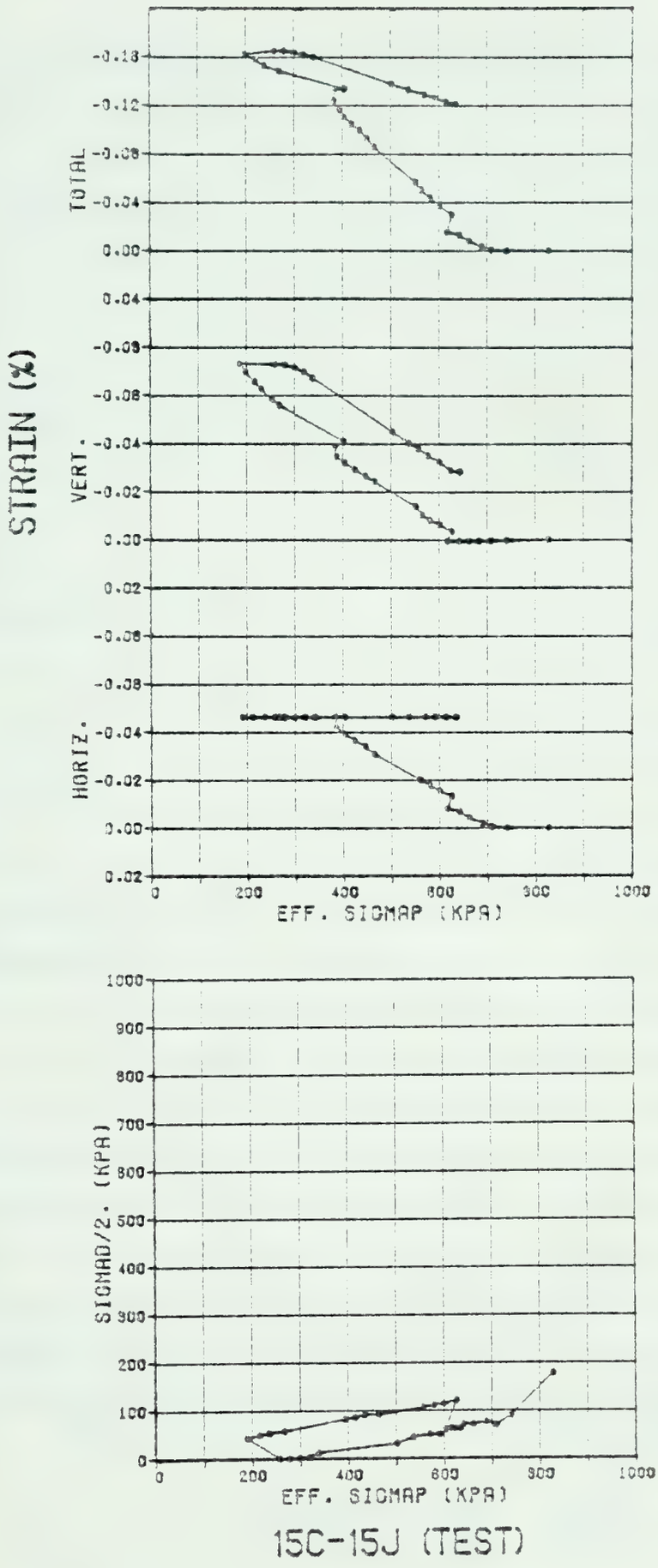


15C-15J (TEST)

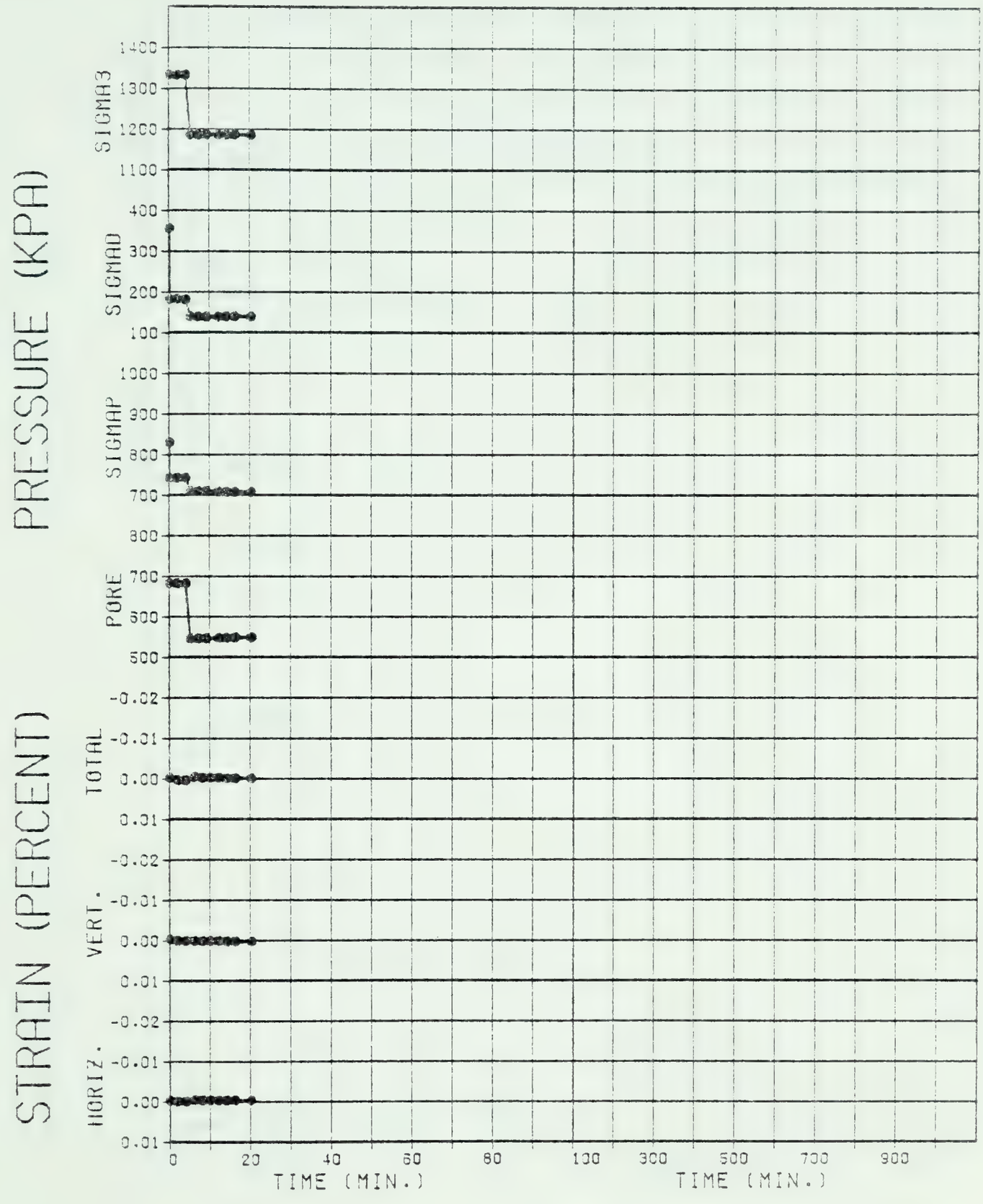


15C-15J (TEST)

Figures D.14 & D.15



Figures D.16 & D.17



TEST NO. 15C

Figure D.18

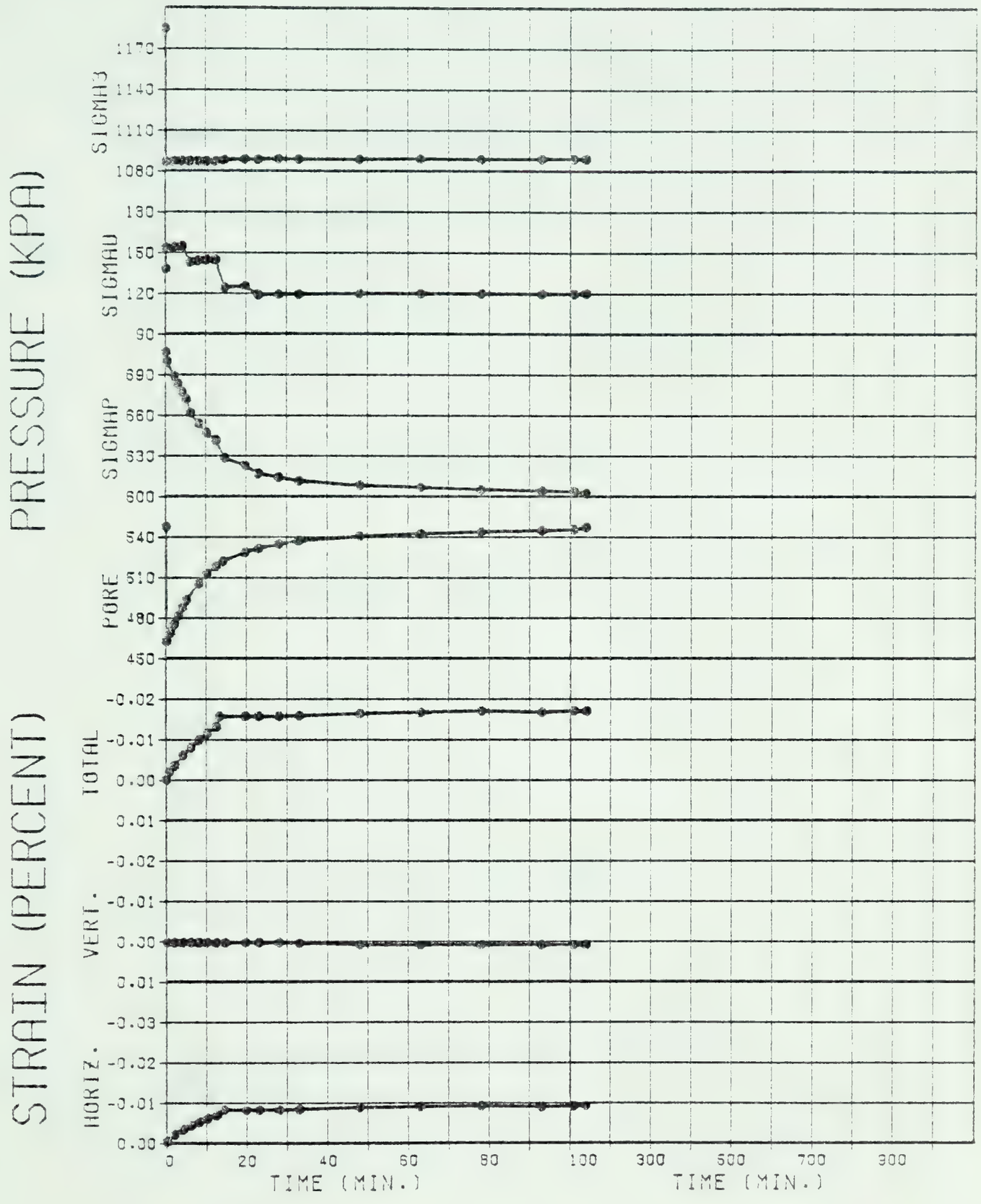

PRESSURE (KPA)
STRAIN (PERCENT)
SIGMA3
SIGMAD
SIGMAP
PORE
TOTAL
VERT.
HORIZ.
TIME (MIN.)
TIME (MIN.)
TEST NO. 15D

Figure D.19

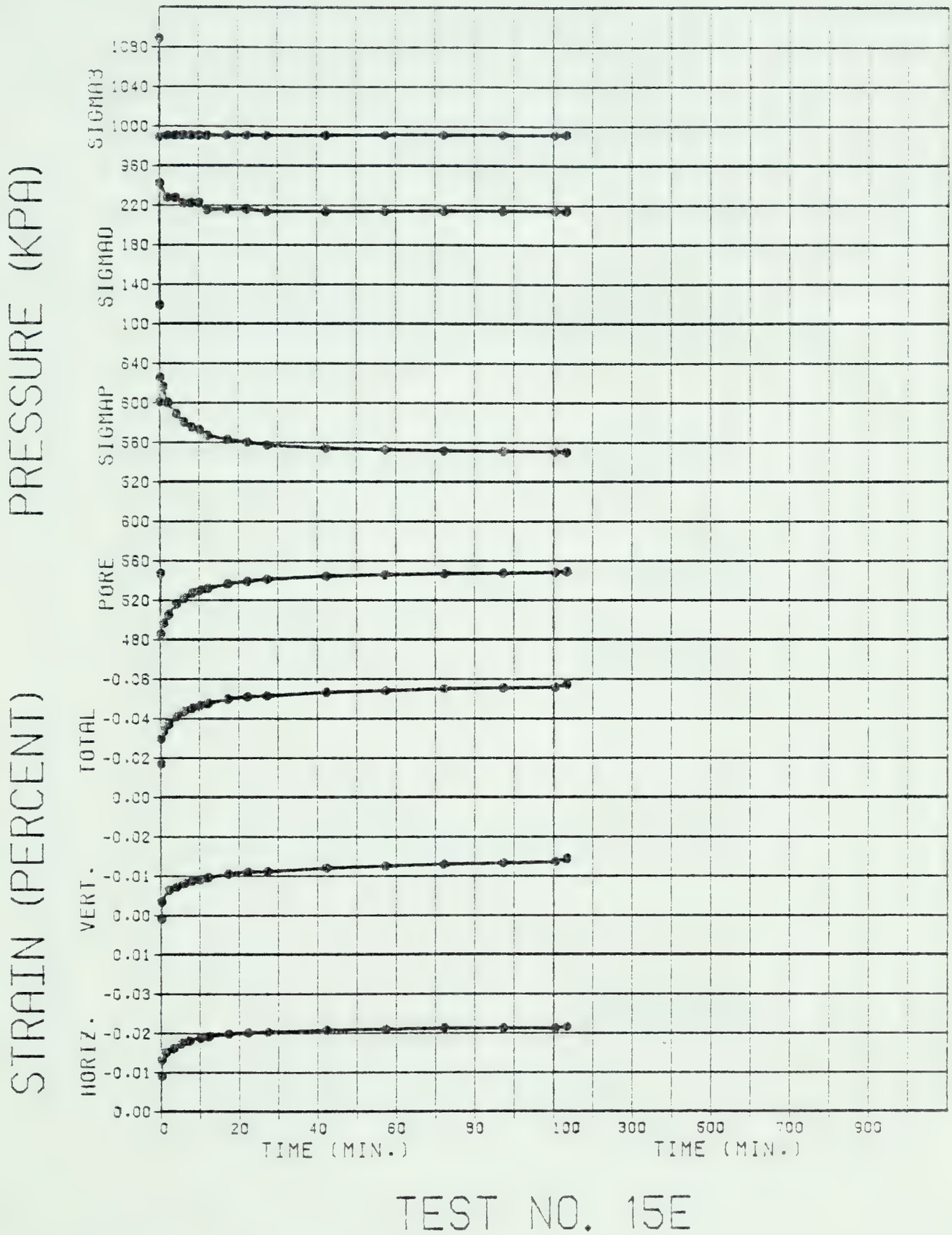
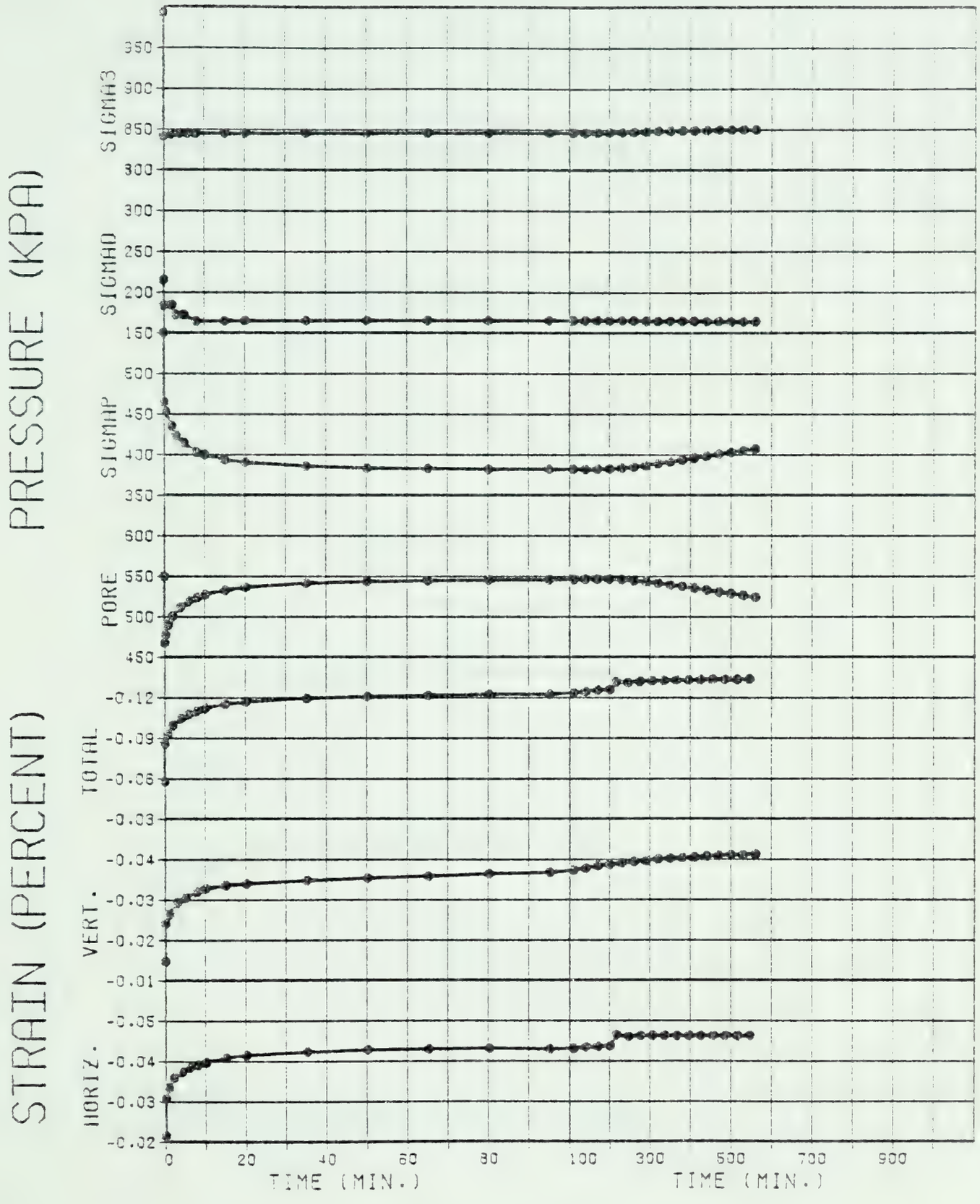
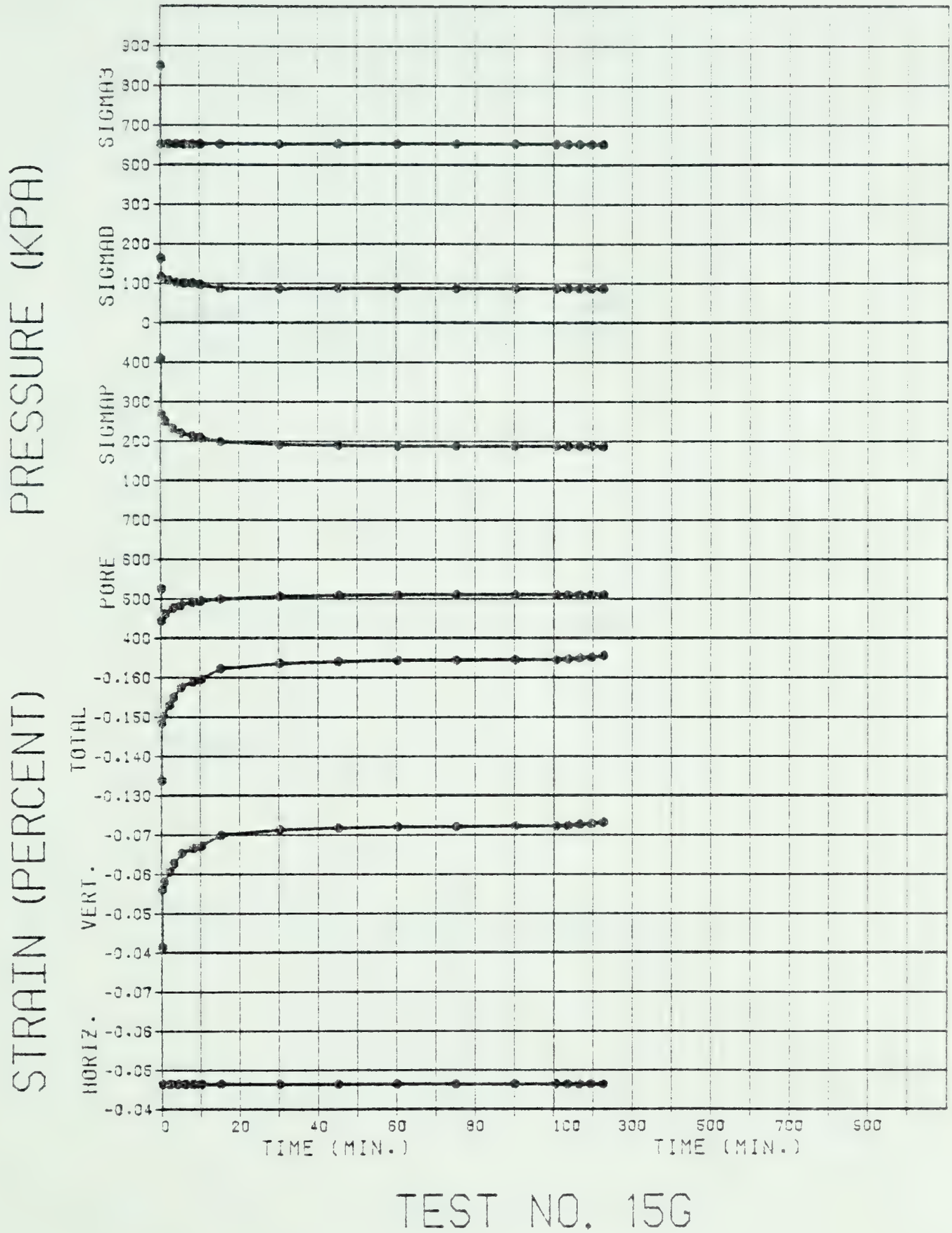

PRESSURE (KPA)
STRAIN (PERCENT)
SIGMA3
SIGMAD
SIGMAP
PORE
TOTAL
VERT.
HORIZ.
TIME (MIN.)
TIME (MIN.)
TEST NO. 15E

Figure D.20



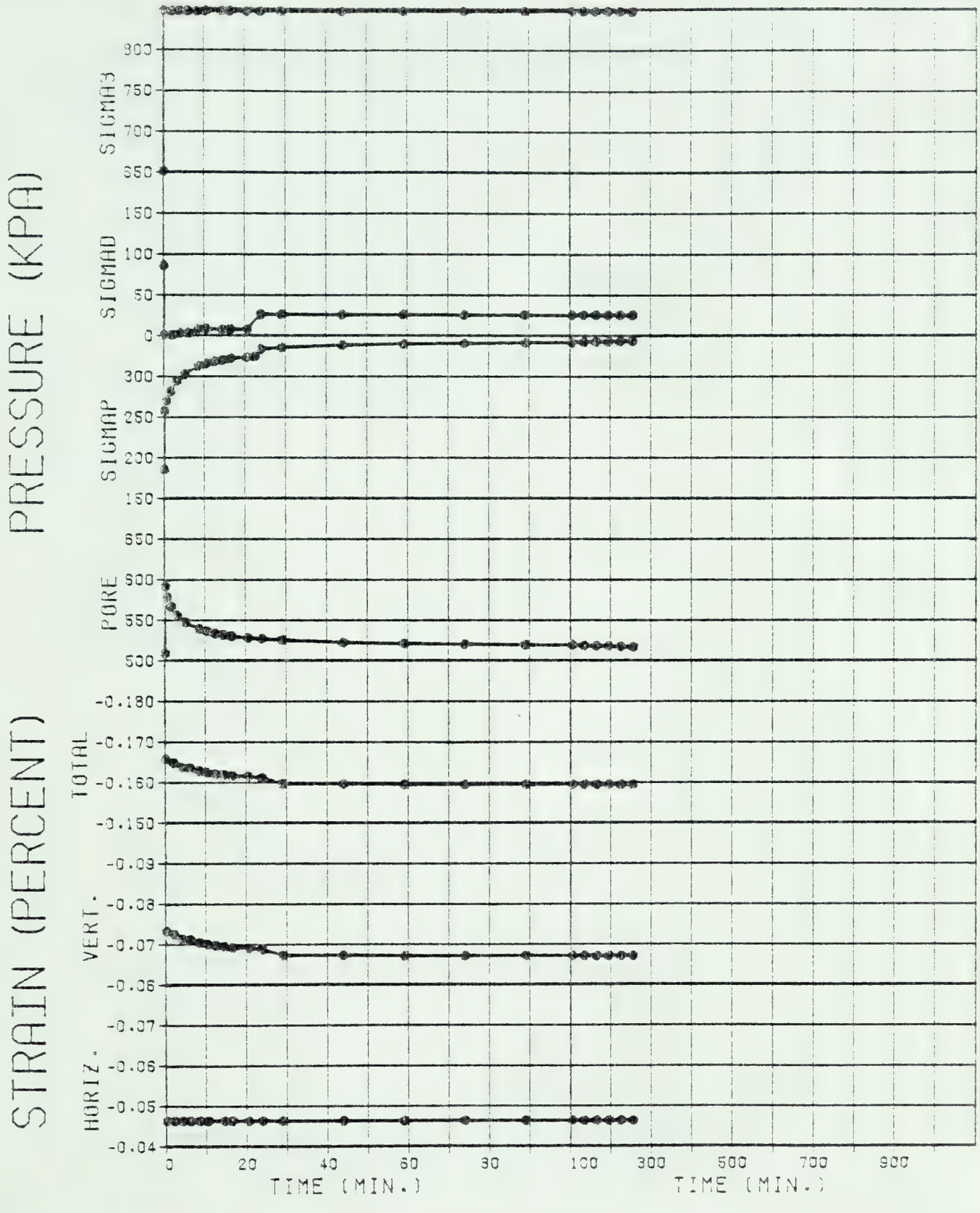
TEST NO. 15F

Figure D.21



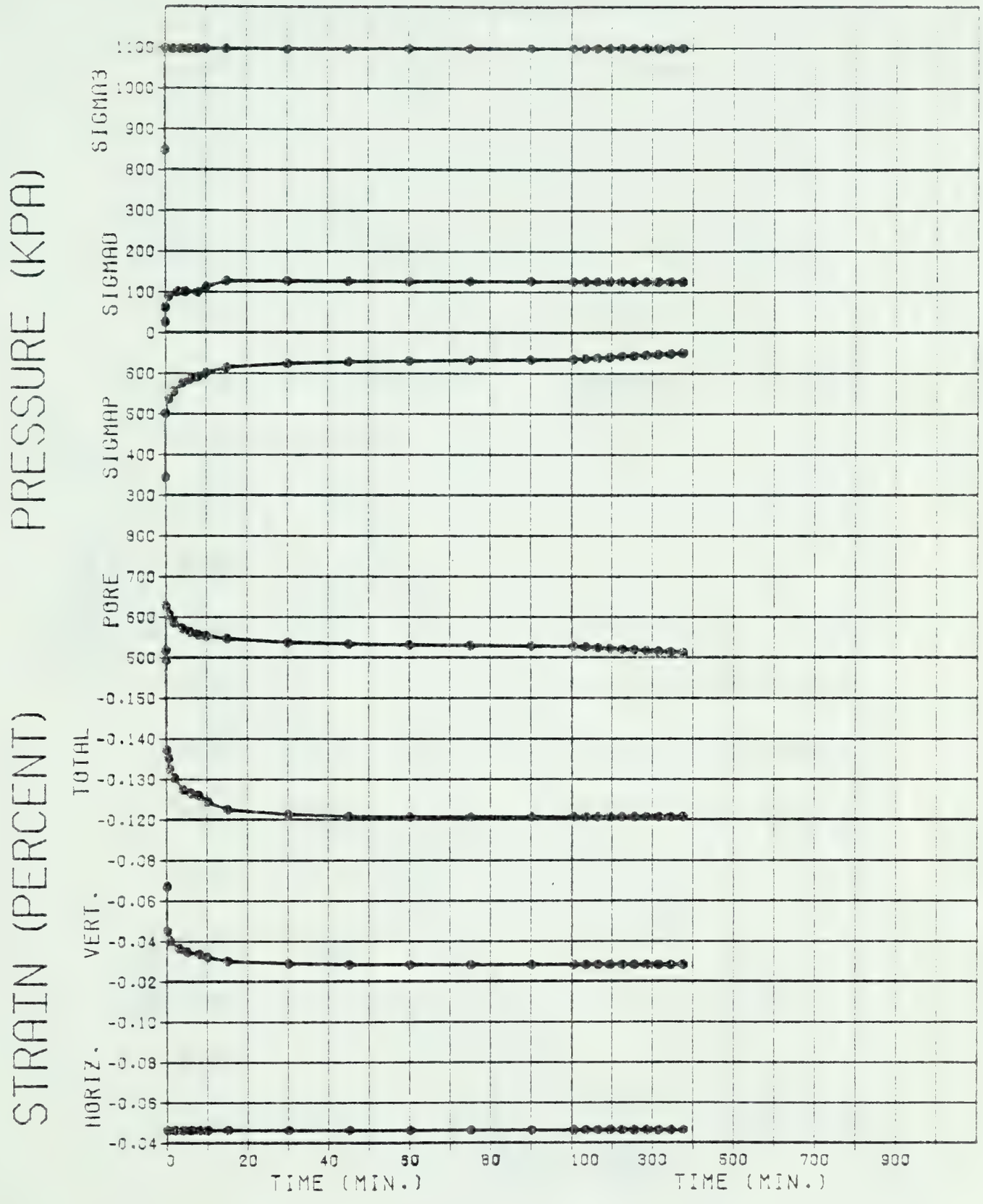
TEST NO. 15G

Figure D.22



TEST NO. 15H

Figure D.23



TEST NO. 15J

Figure D.24

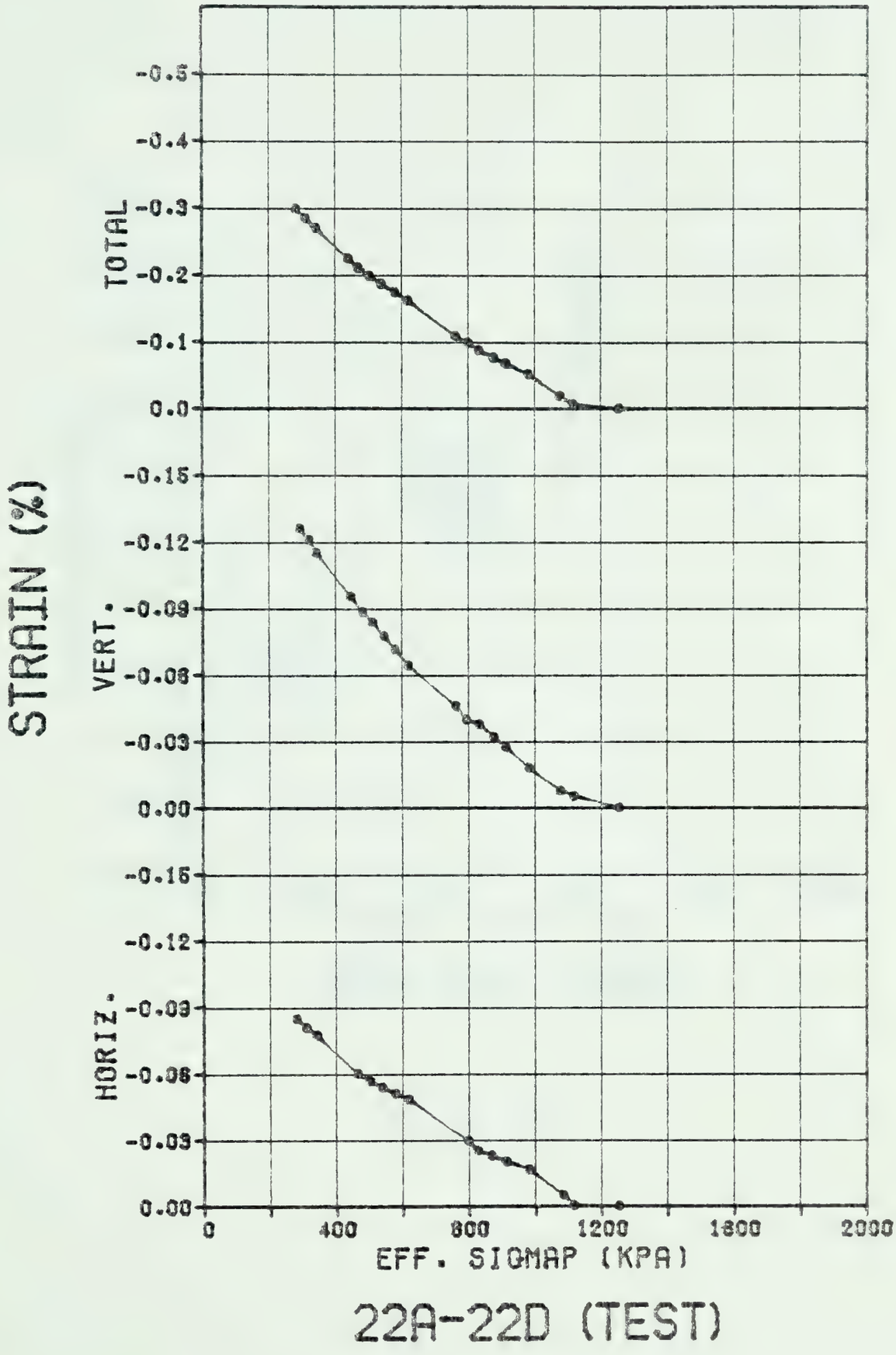

STRAIN (%)
TOTAL
VERT.
HORIZ.
-0.5
-0.4
-0.3
-0.2
-0.1
0.0
-0.15
-0.12
-0.09
-0.06
-0.03
0.00
-0.15
-0.12
-0.09
-0.06
-0.03
0.00
0
400
800
1200
1600
2000
EFF. SIGMAP (KPA)
22A-22D (TEST)

Figure D.25

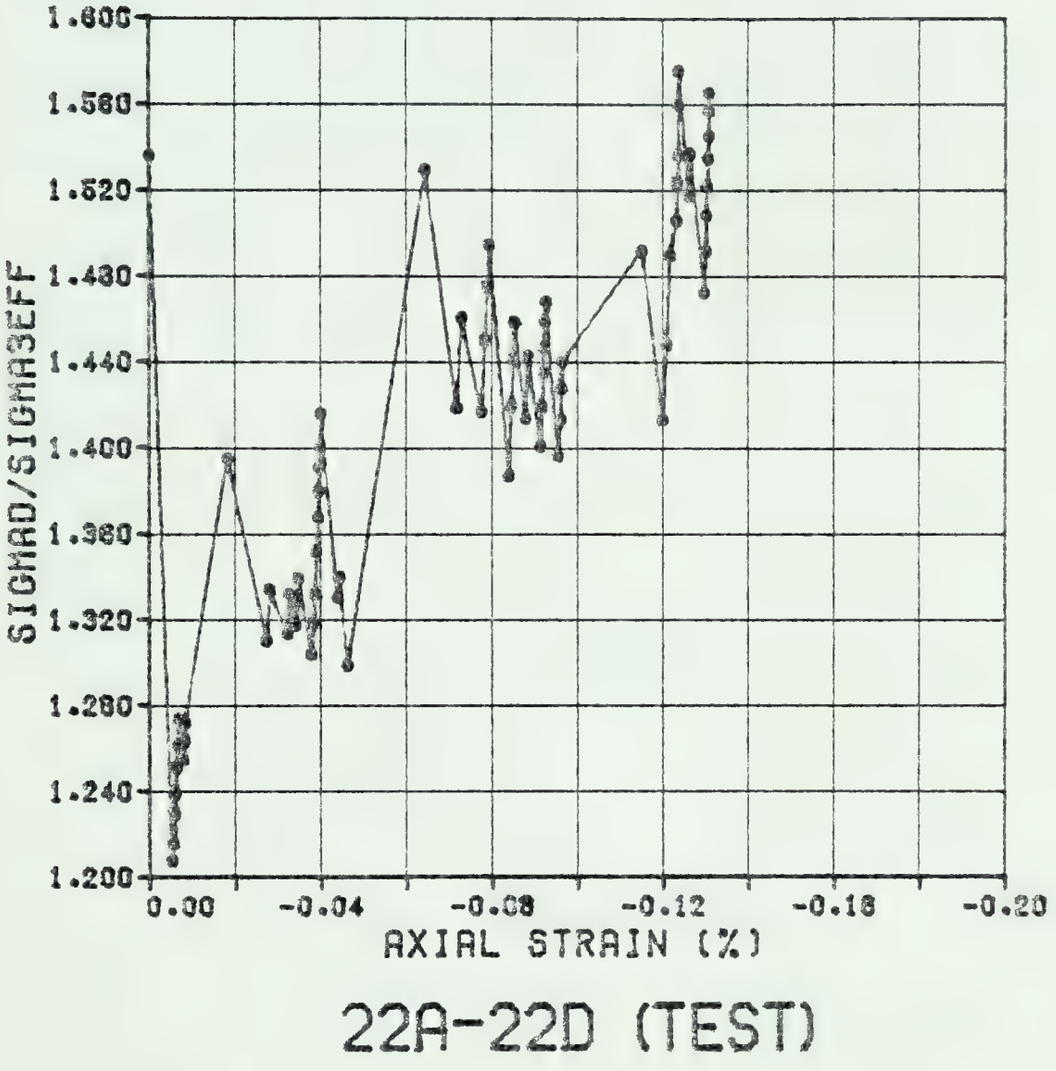

1.600
1.560
1.520
1.480
1.440
1.400
1.360
1.320
1.280
1.240
1.200
SIGMAD/SIGMA3EFF
0.00
-0.04
-0.08
-0.12
-0.16
-0.20
AXIAL STRAIN (%)
22A-22D (TEST)

Figure D.26

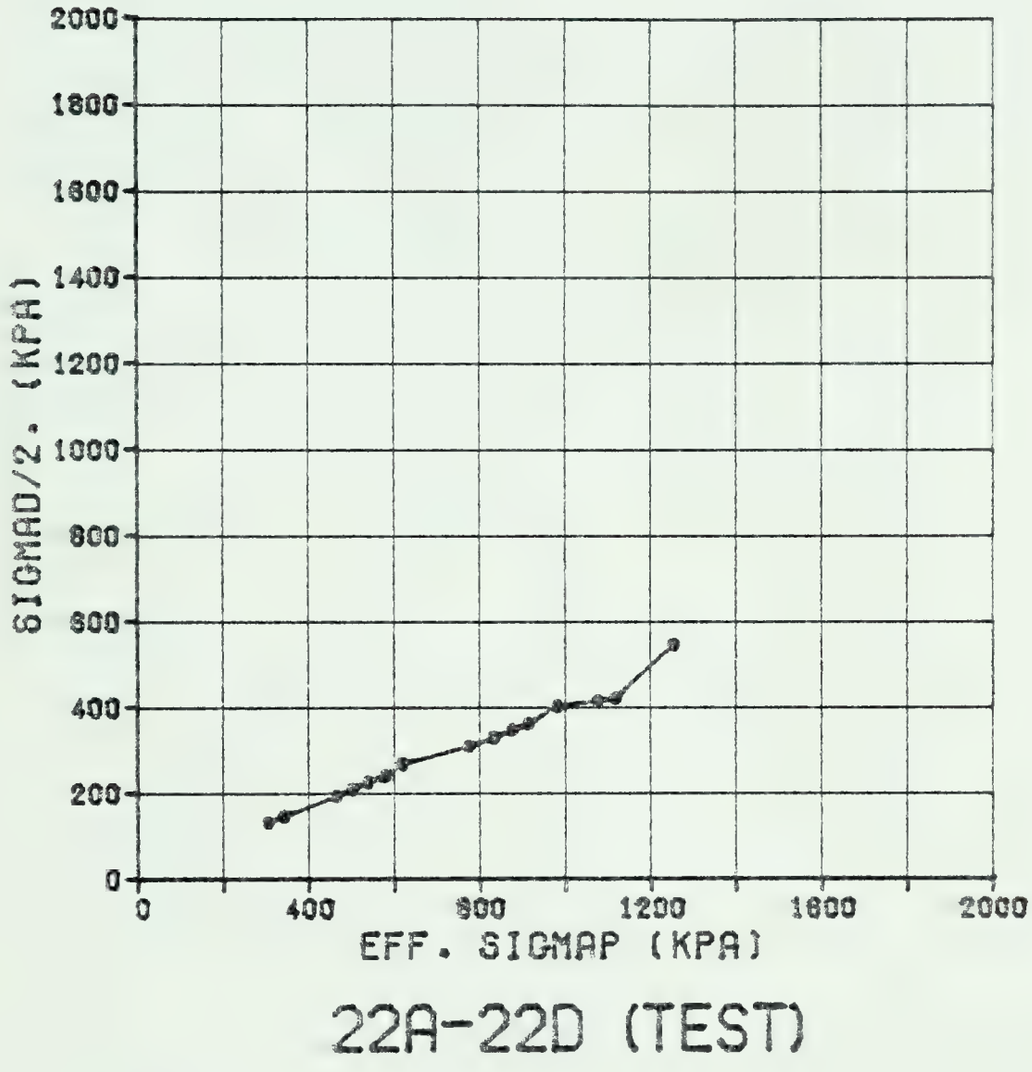

2000
1800
1600
1400
1200
1000
800
600
400
200
0
SIGMAD/2. (KPA)
0
400
800
1200
1600
2000
EFF. SIGMAP (KPA)
22A-22D (TEST)

Figure D.27

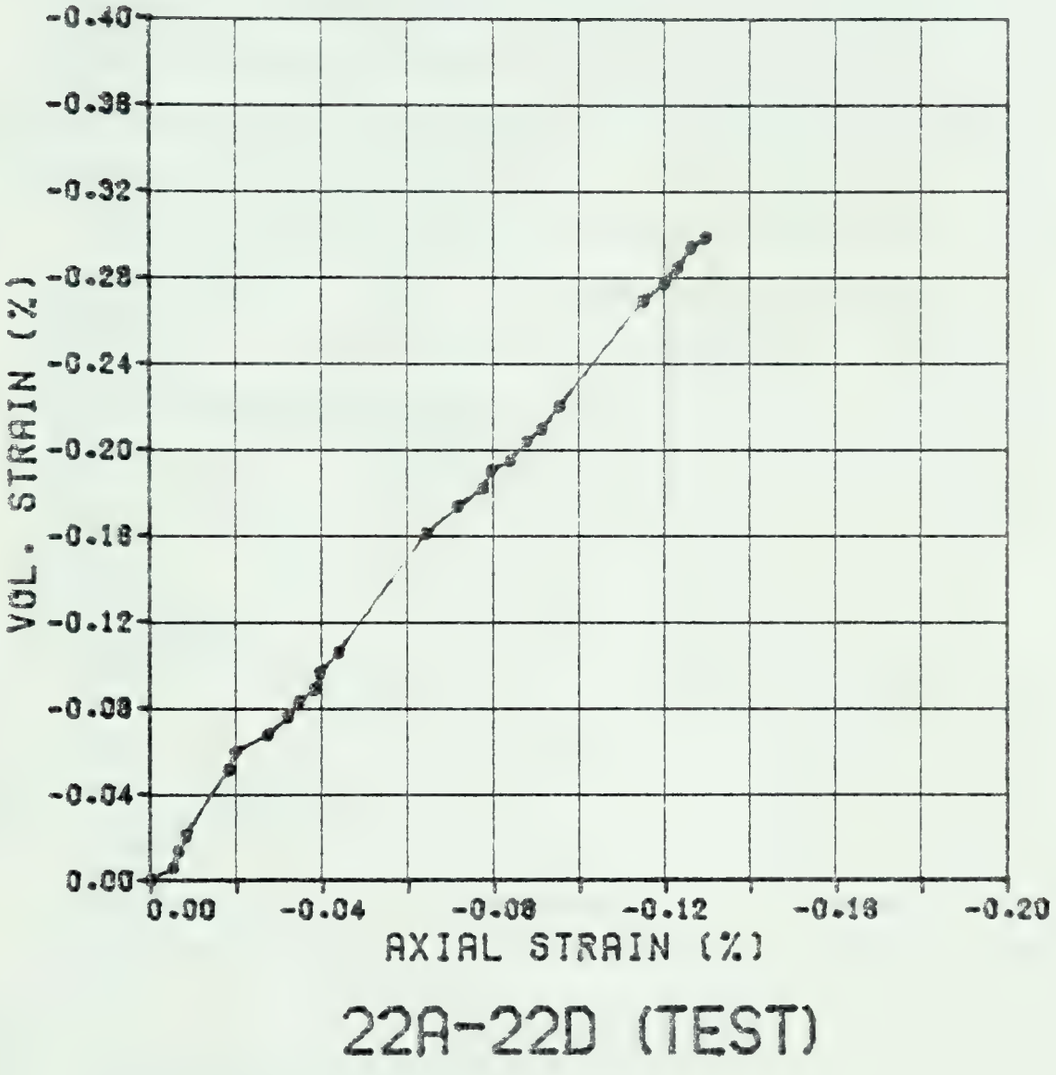
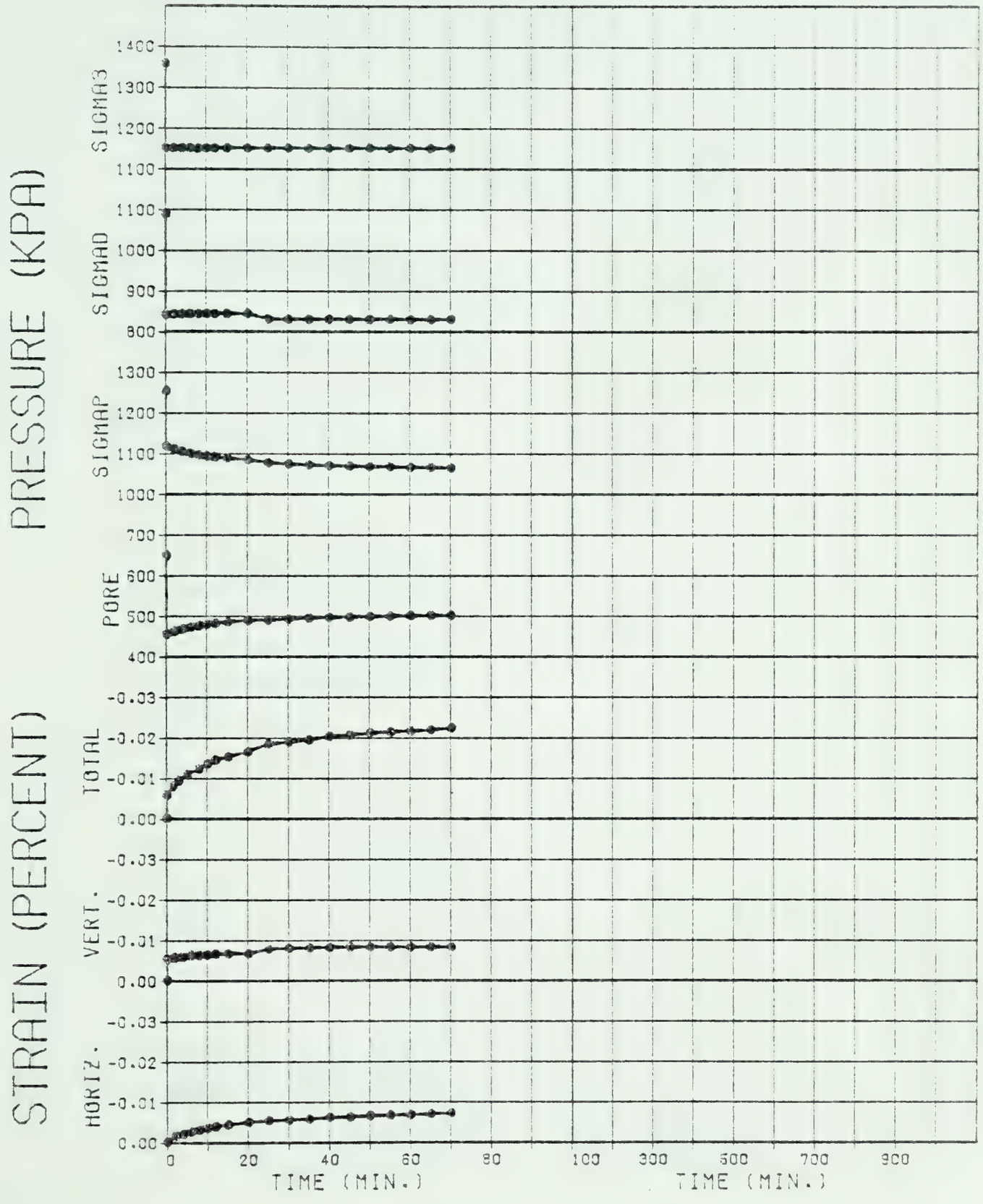

-0.40
-0.36
-0.32
-0.28
-0.24
-0.20
-0.16
-0.12
-0.08
-0.04
0.00
VOL. STRAIN (%)
0.00
-0.04
-0.08
-0.12
-0.16
-0.20
AXIAL STRAIN (%)
22A-22D (TEST)

Figure D.28



TEST NO. 22A

Figure D.29

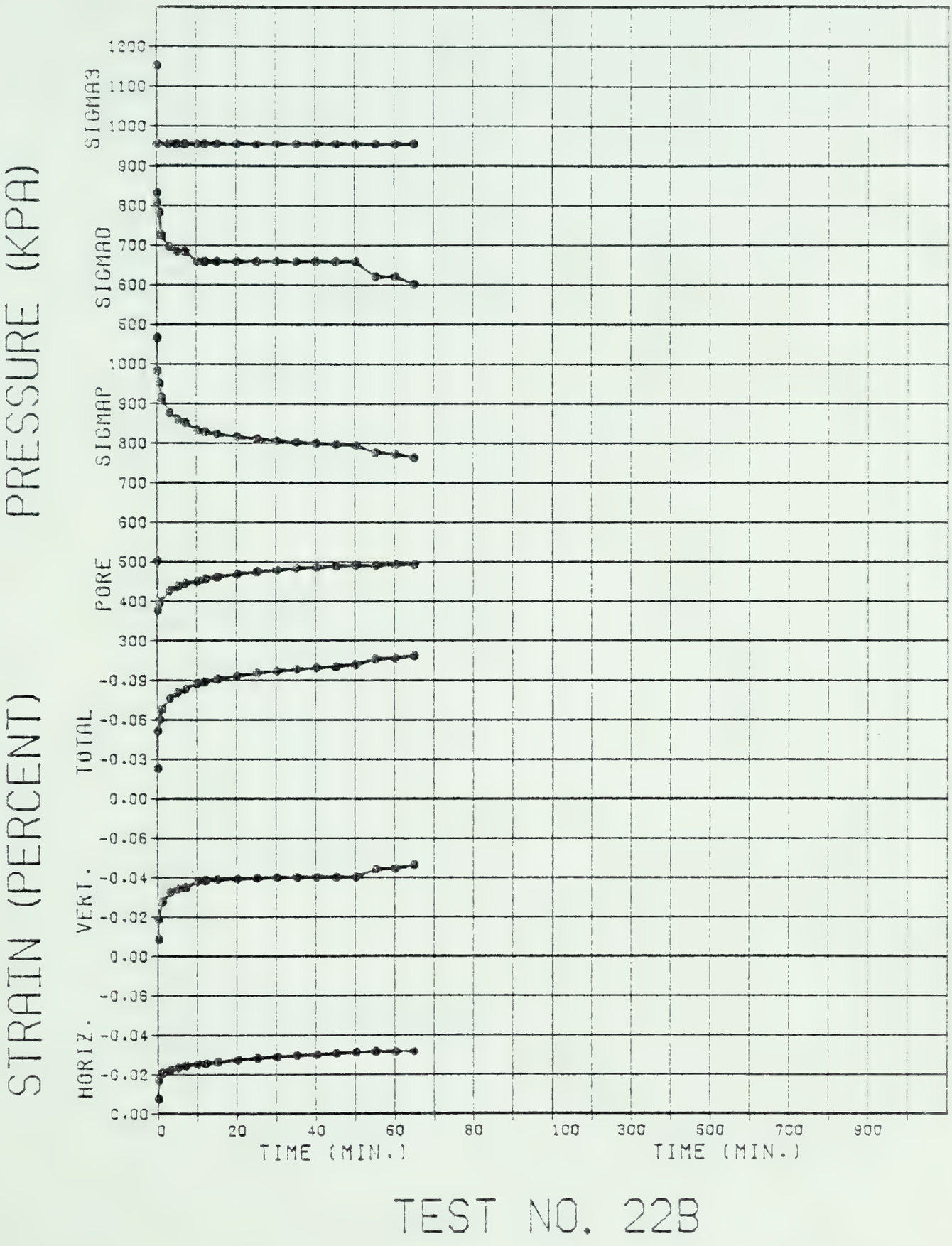

PRESSURE (KPA)
STRAIN (PERCENT)
SIGMA3
SIGMAD
SIGMAP
PORE
TOTAL
VERT.
HORIZ.
TIME (MIN.)
TIME (MIN.)
TEST NO. 22B

Figure D.30

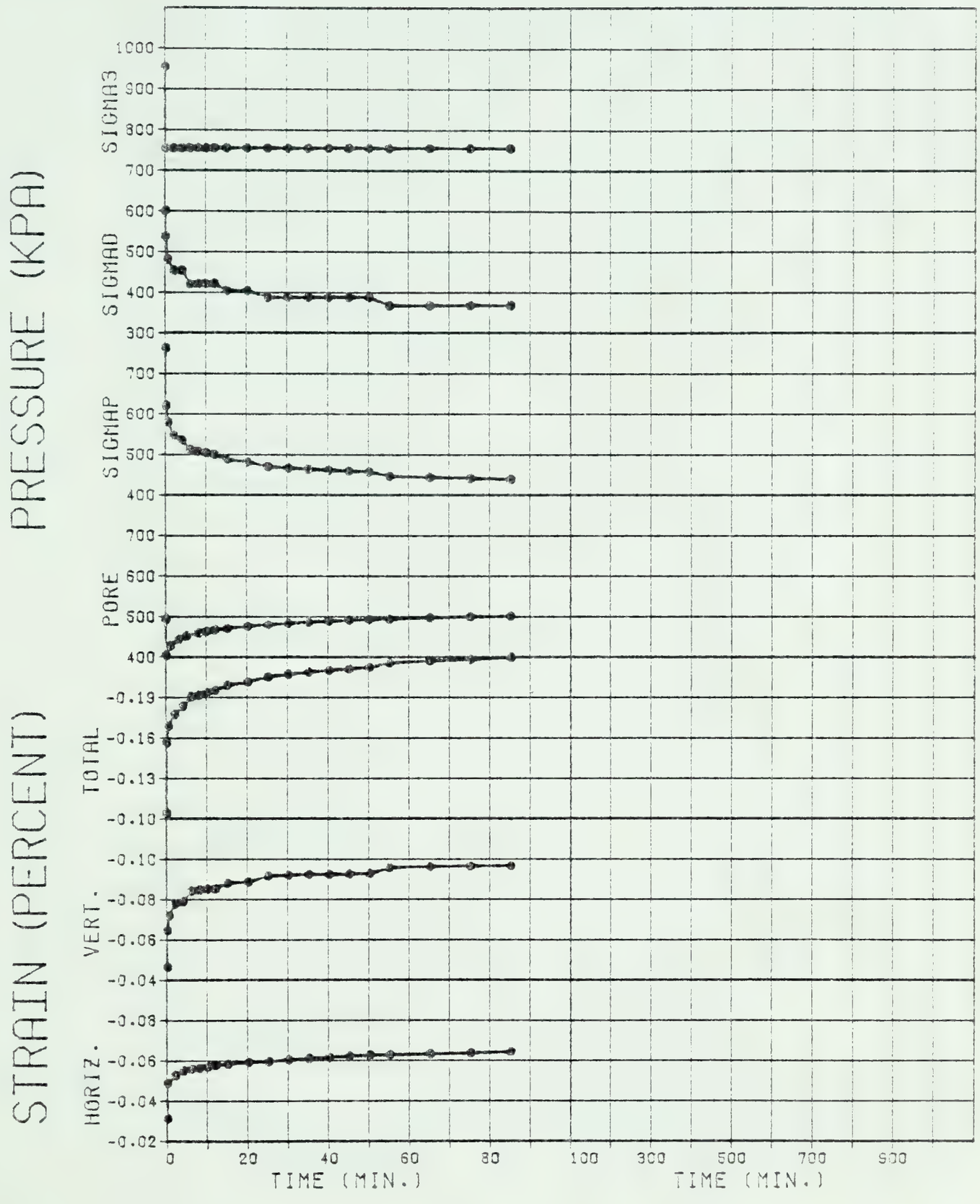

PRESSURE (KPA)
STRAIN (PERCENT)
SIGMA3
SIGMAD
SIGMAP
PORE
TOTAL
VERT.
HORIZ.
1000
900
800
700
600
500
400
300
-0.19
-0.16
-0.13
-0.10
-0.10
-0.08
-0.06
-0.04
-0.08
-0.06
-0.04
-0.02
0
20
40
60
80
100
300
500
700
900
TIME (MIN.)
TIME (MIN.)
TEST NO. 22C

Figure D.31

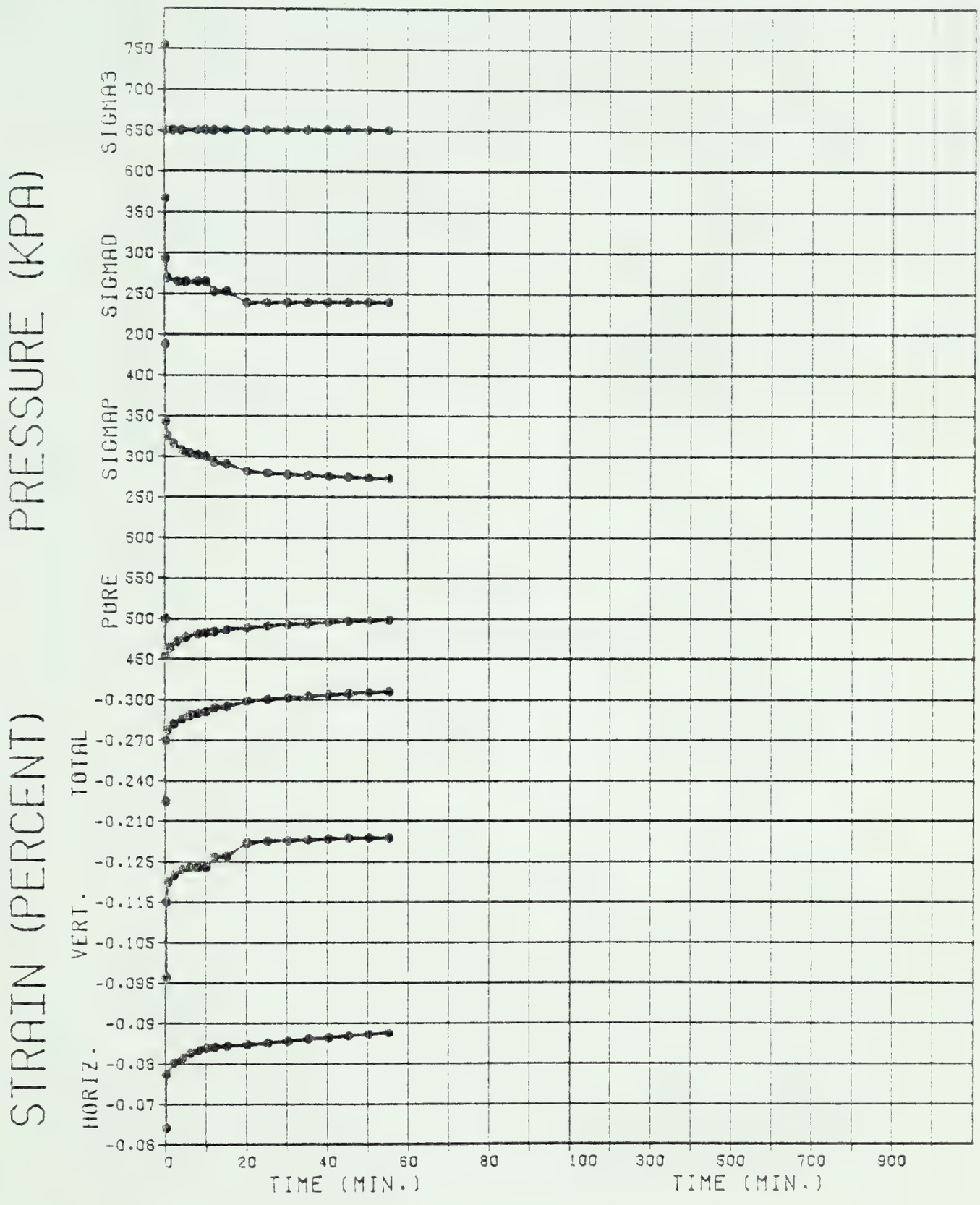

PRESSURE (KPA)
SIGMA3
SIGMAD
SIGMAP
PORE
STRAIN (PERCENT)
TOTAL
VERT.
HORIZ.
TIME (MIN.)
TIME (MIN.)
TEST NO. 22D

Figure D.32

APPENDIX E

TESTS TO FAILURE

TESTS 12, 22, 13, 14

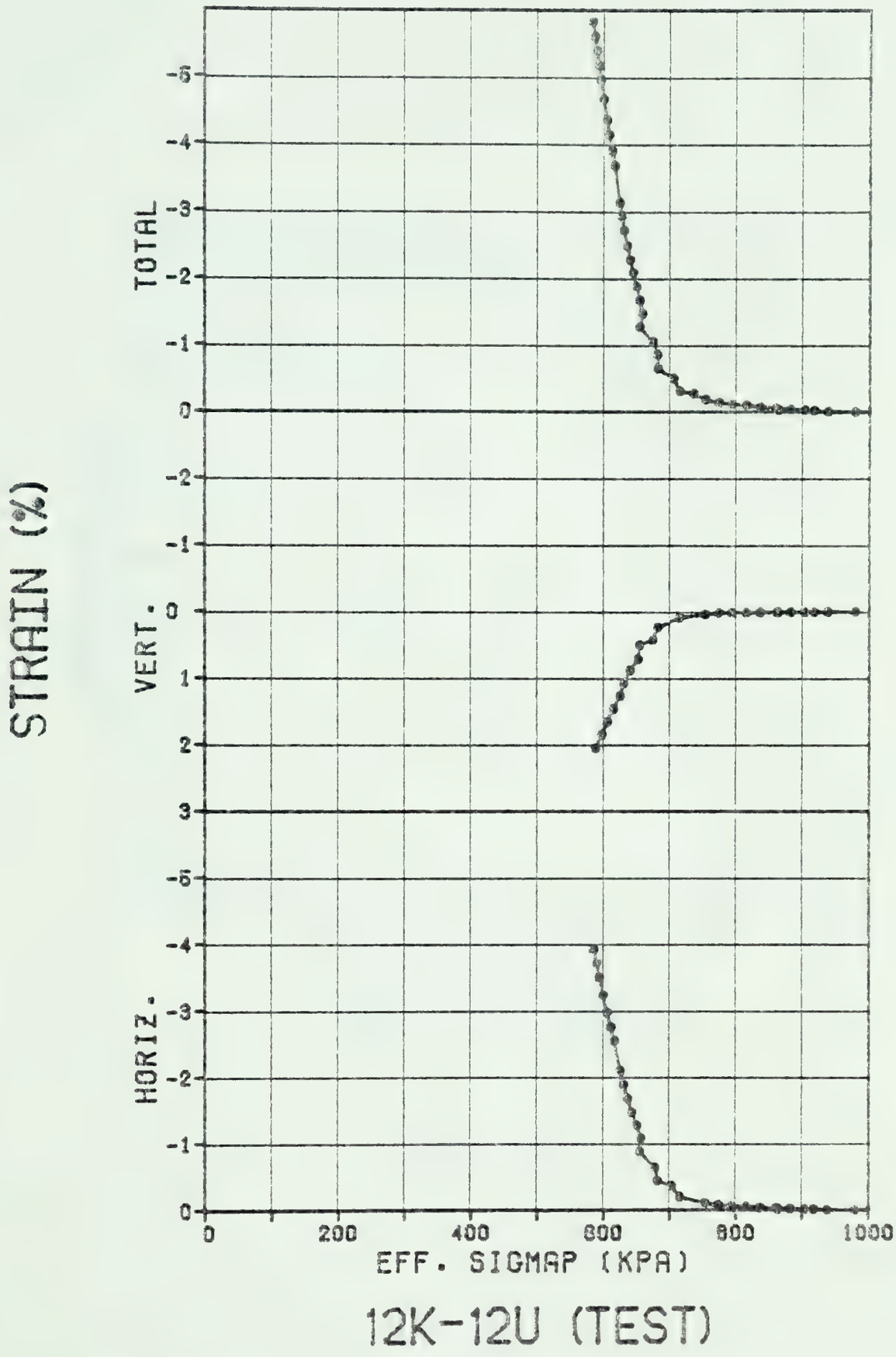

STRAIN (%)
TOTAL
VERT.
HORIZ.
-6
-4
-3
-2
-1
0
-2
-1
0
1
2
3
-6
-4
-3
-2
-1
0
0
200
400
600
800
1000
EFF. SIGMAP (KPA)
12K-12U (TEST)

Figure E.1

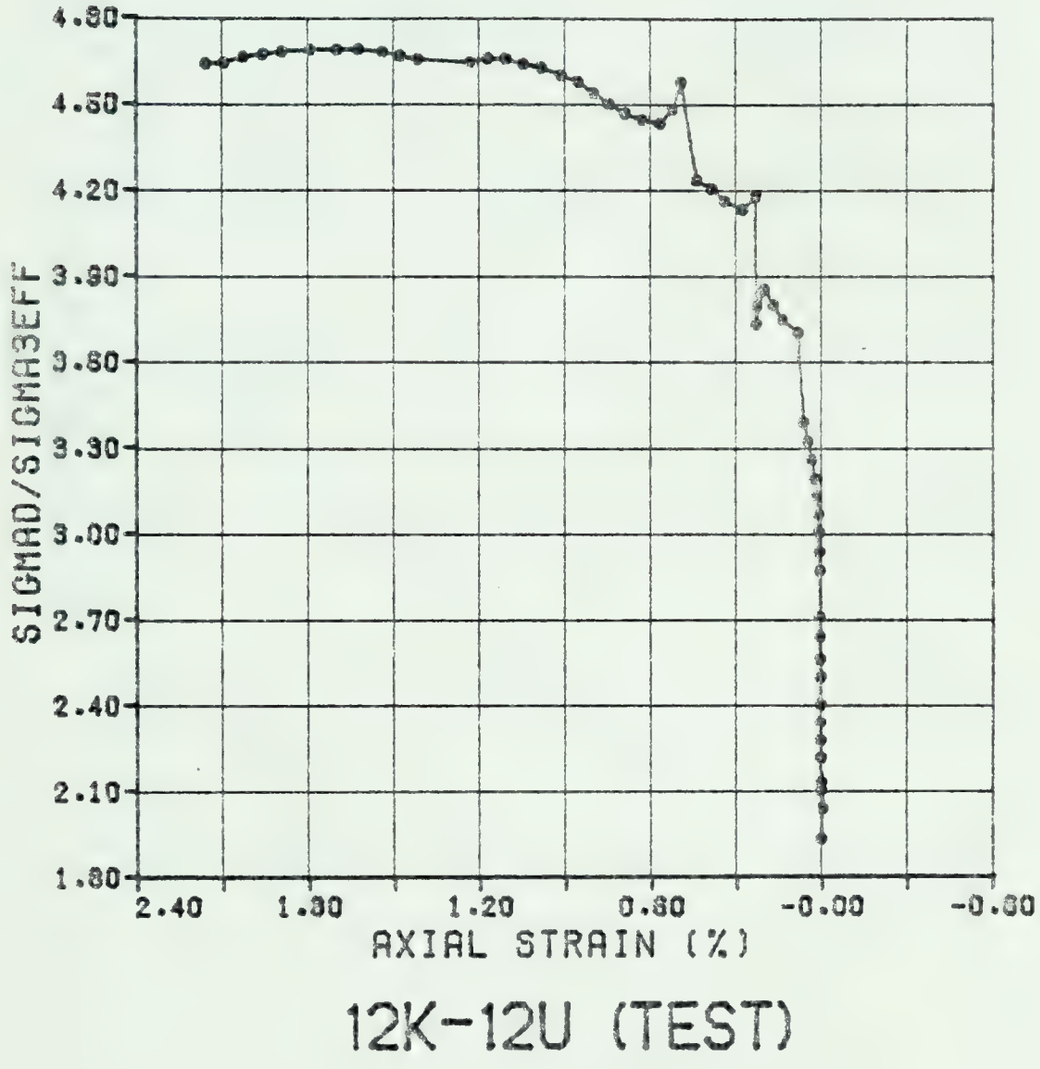

4.80
4.50
4.20
3.90
3.60
3.30
3.00
2.70
2.40
2.10
1.80
SIGMAD/SIGMA3EFF
2.40
1.80
1.20
0.60
-0.00
-0.60
AXIAL STRAIN (%)
12K-12U (TEST)

Figure E.2

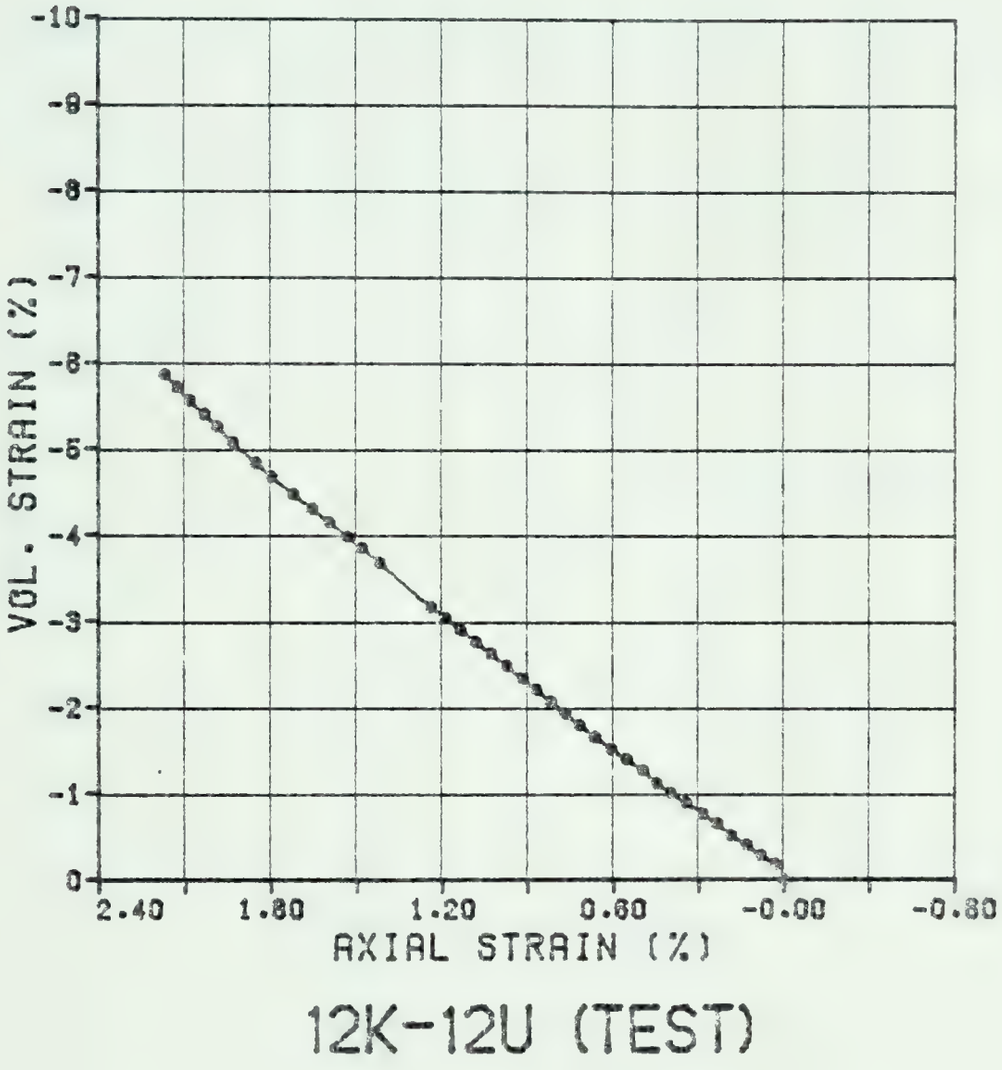

-10
-9
-8
-7
-6
-5
-4
-3
-2
-1
0
VOL. STRAIN (%)
2.40
1.80
1.20
0.60
-0.00
-0.60
AXIAL STRAIN (%)
12K-12U (TEST)

Figure E.3

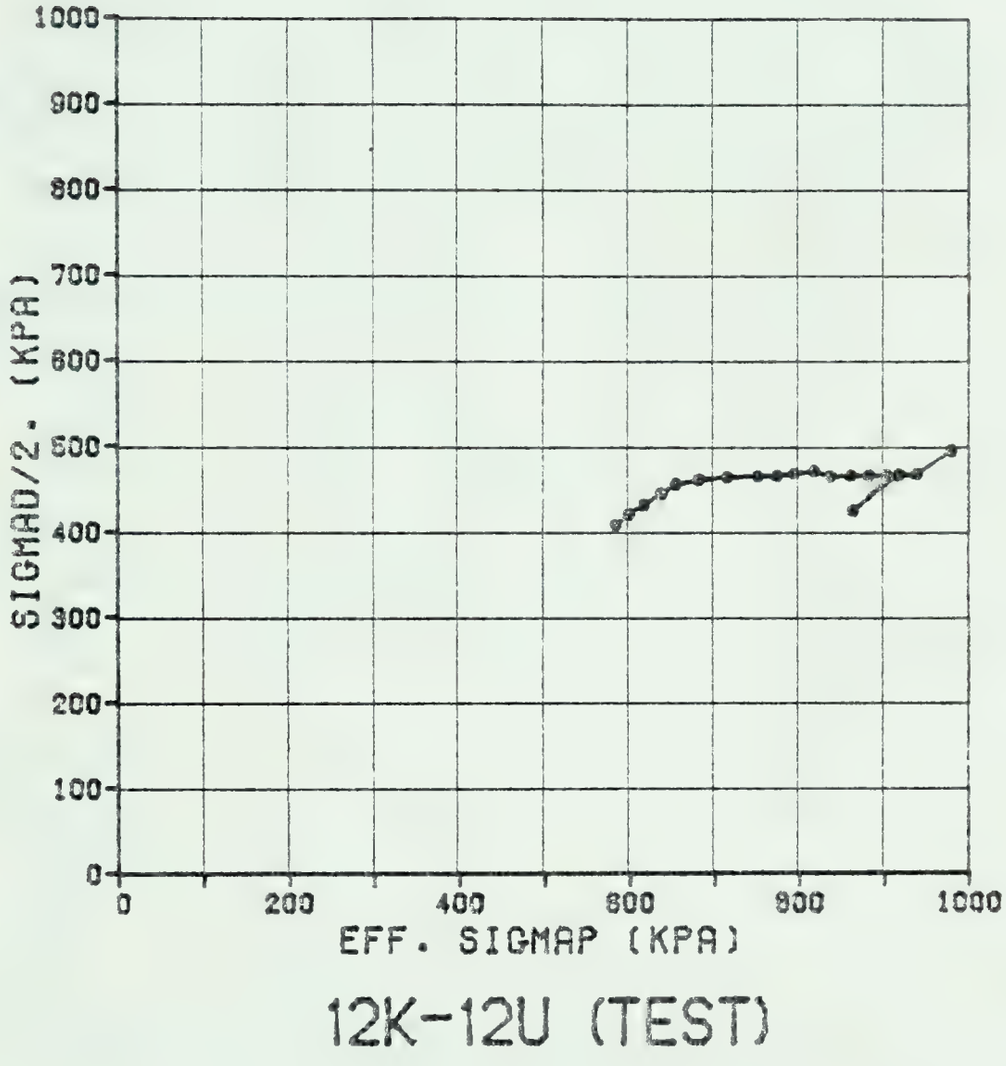

1000
900
800
700
600
500
400
300
200
100
0
SIGMAD/2. (KPA)
0
200
400
600
800
1000
EFF. SIGMAP (KPA)
12K-12U (TEST)

Figure E.4

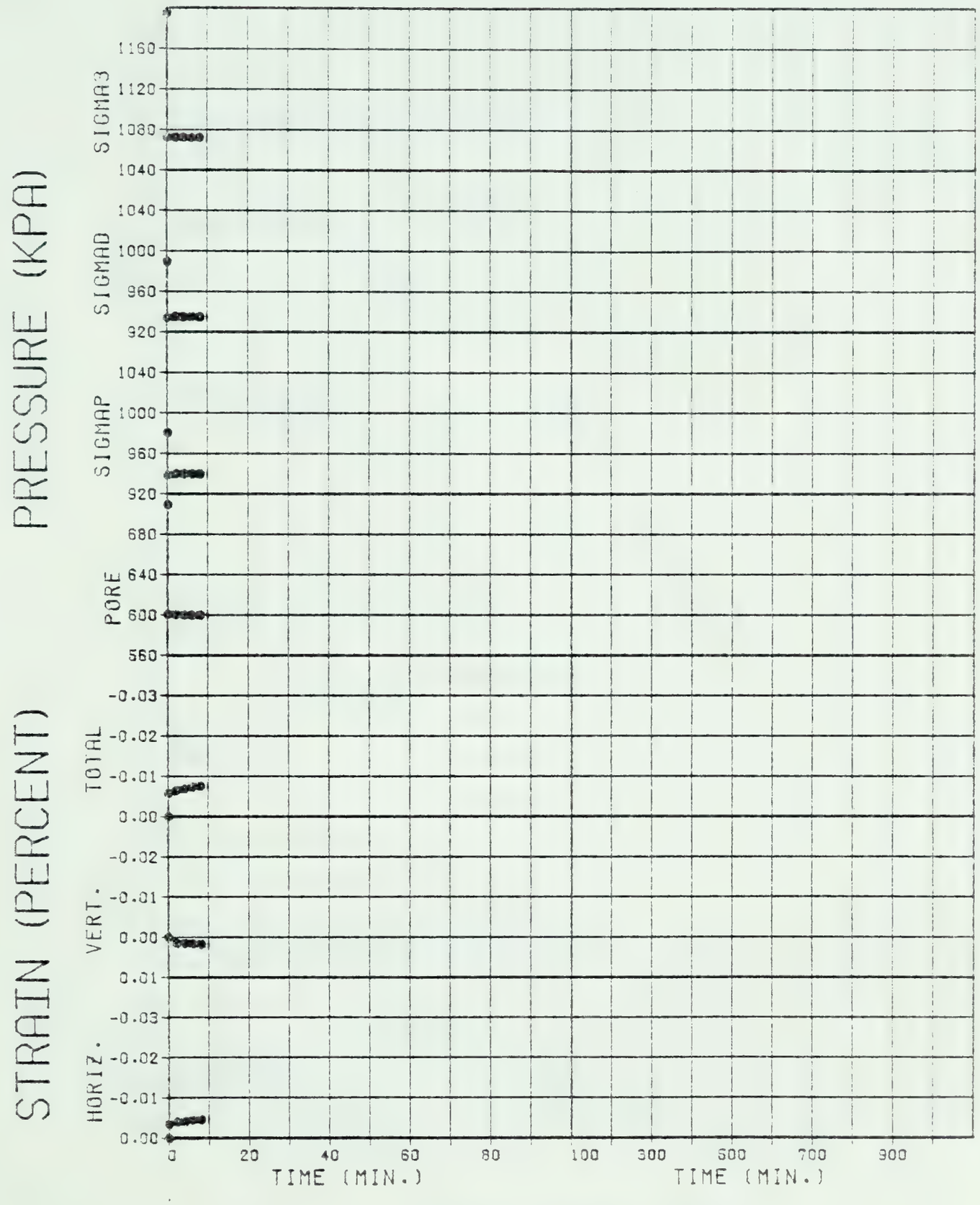

PRESSURE (KPA)
STRAIN (PERCENT)
SIGMA3
SIGMAD
SIGMAP
PORE
TOTAL
VERT.
HORIZ.
1160
1120
1080
1040
1040
1000
960
920
1040
1000
960
920
680
640
600
560
-0.03
-0.02
-0.01
0.00
-0.02
-0.01
0.00
0.01
-0.03
-0.02
-0.01
0.00
0
20
40
60
80
100
300
500
700
900
TIME (MIN.)
TIME (MIN.)
TEST NO. 12K

Figure E.5

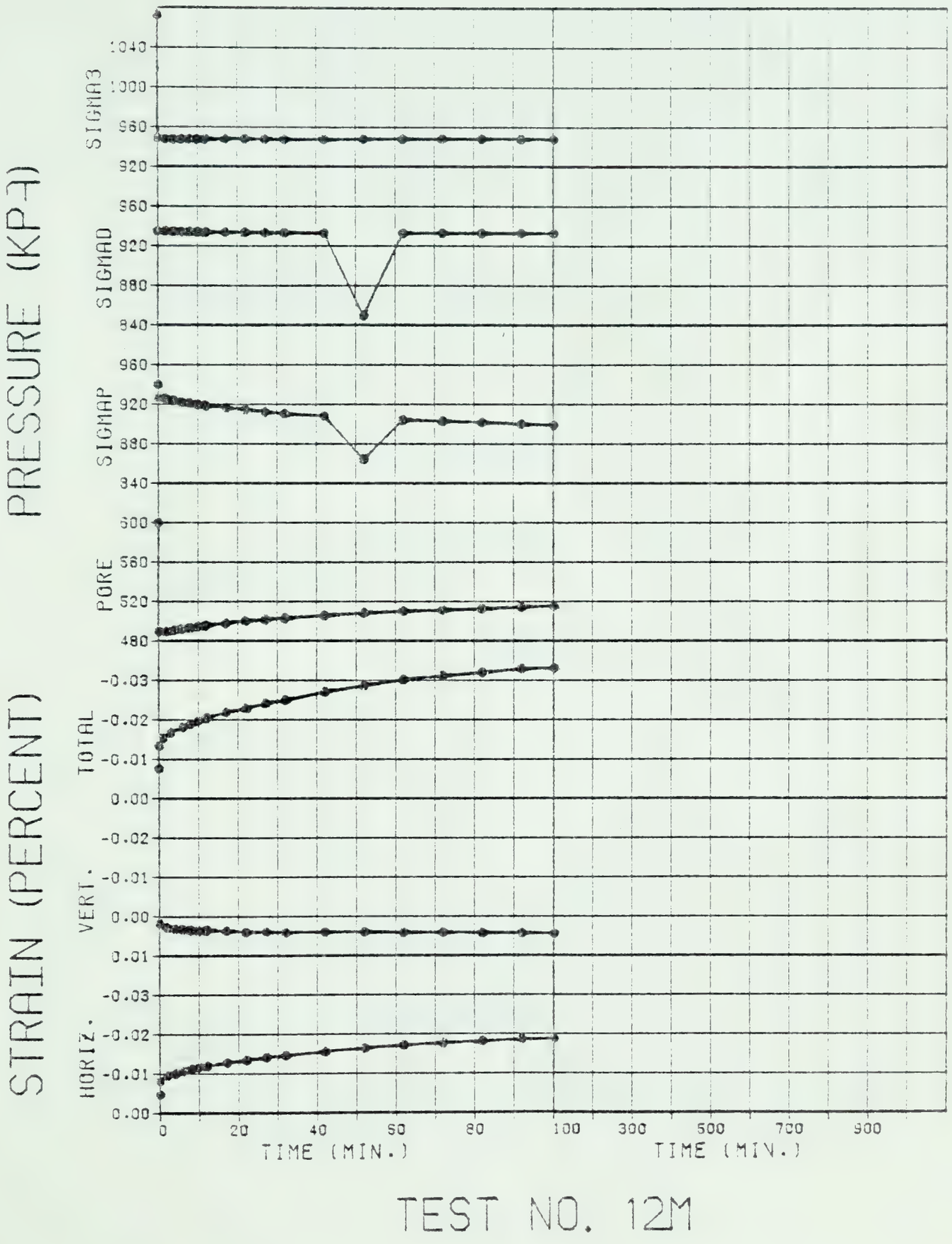
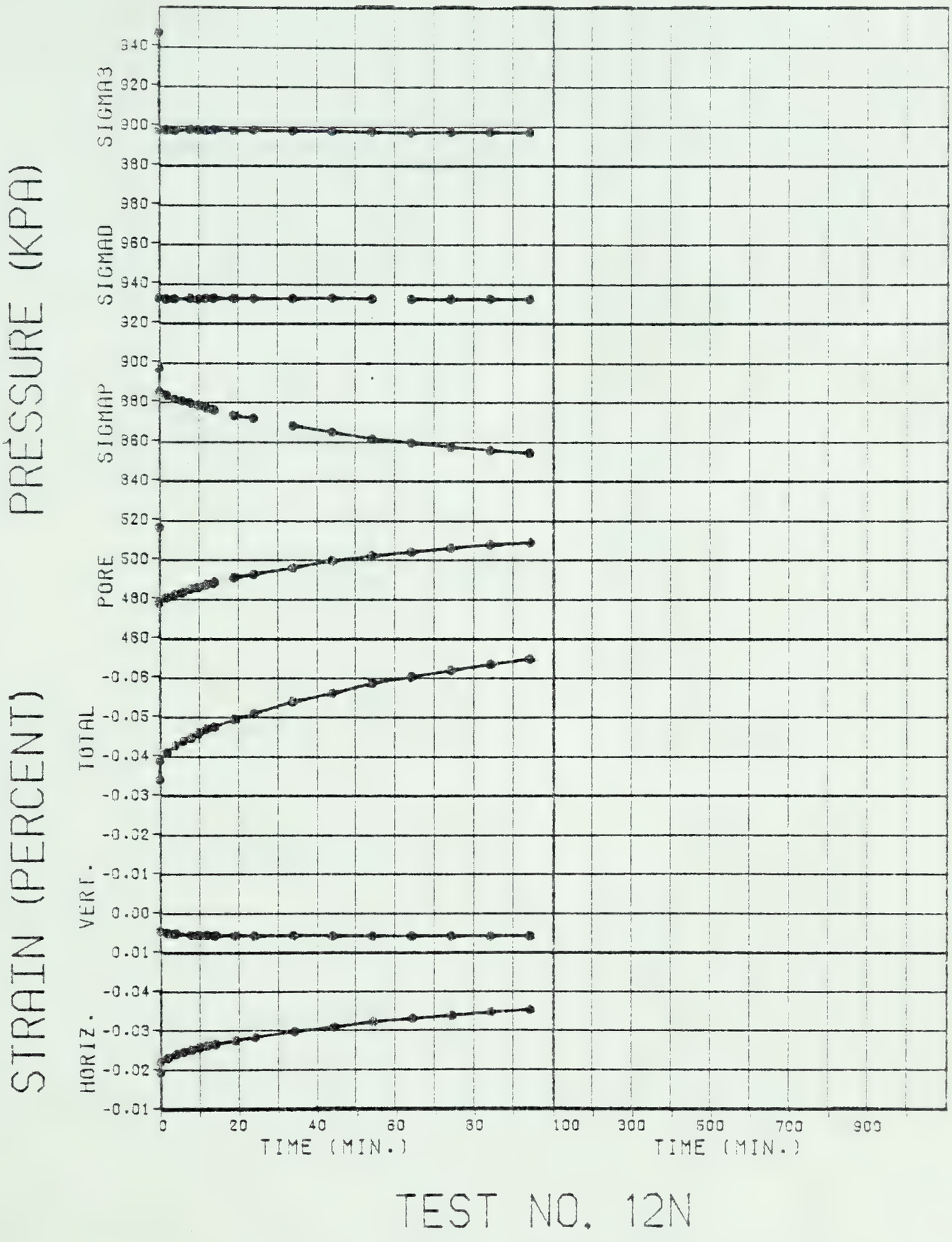

PRESSURE (KPA)
STRAIN (PERCENT)
SIGMA3
SIGMAD
SIGMAP
PORE
TOTAL
VERT.
HORIZ.
1040
1000
960
920
960
920
880
840
960
920
880
840
600
560
520
480
-0.03
-0.02
-0.01
0.00
-0.02
-0.01
0.00
0.01
-0.03
-0.02
-0.01
0.00
0
20
40
60
80
100
300
500
700
900
TIME (MIN.)
TIME (MIN.)
TEST NO. 12M

Figure E.6



TEST NO. 12N

Figure E.7

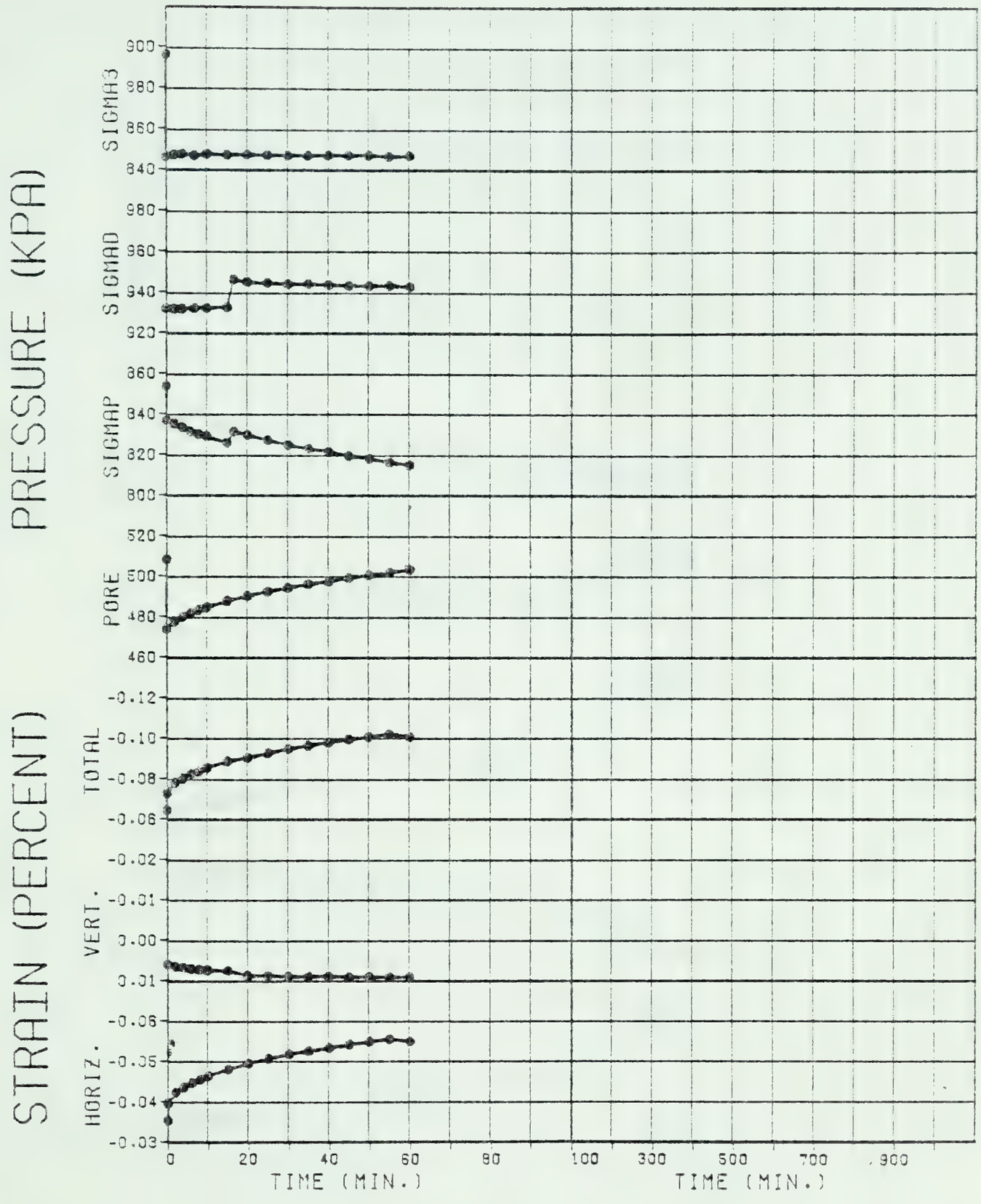
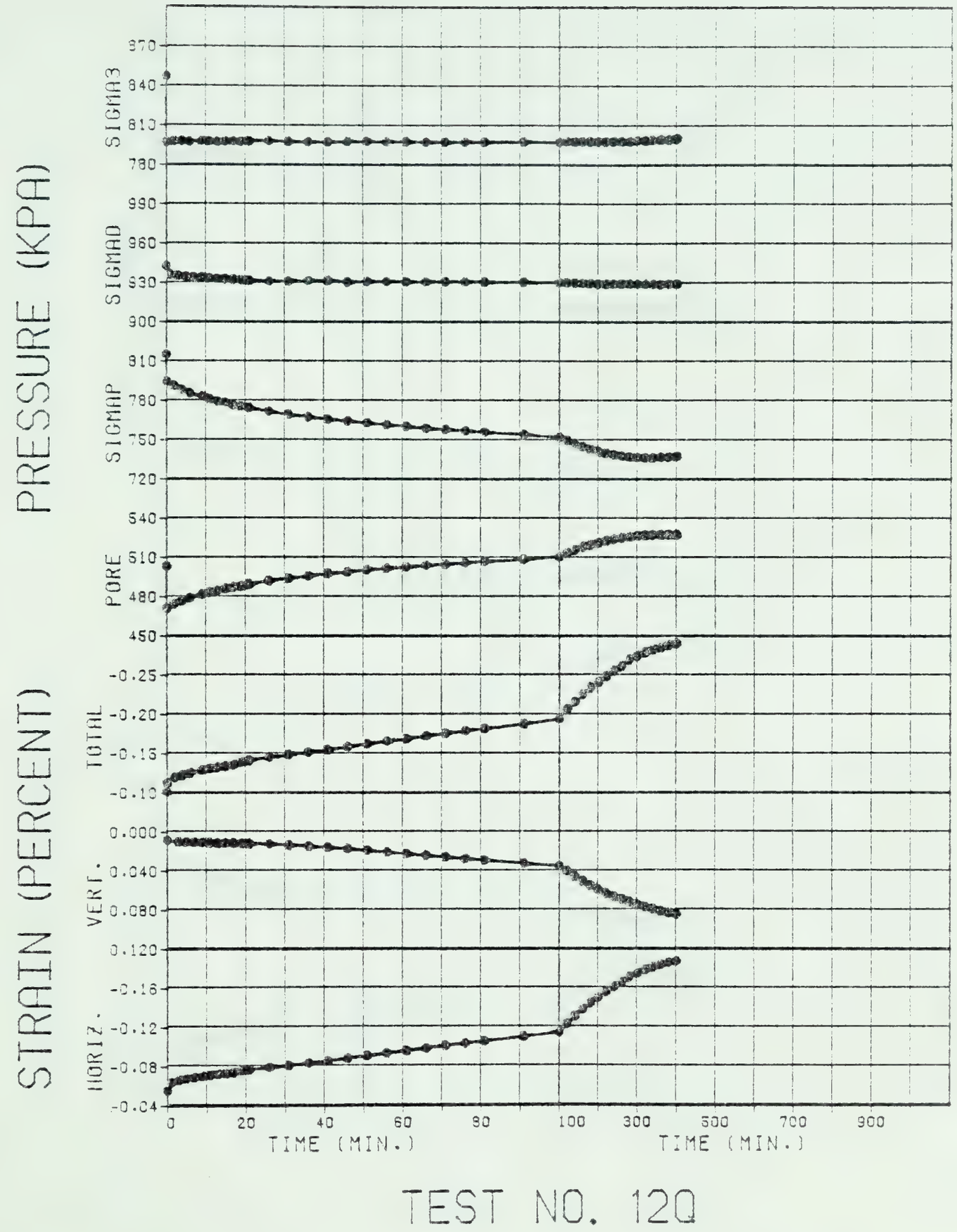

PRESSURE (KPA)
SIGMA3
900
880
860
840
SIGMAD
980
960
940
920
SIGMAP
860
840
820
800
PORE
520
500
480
460
STRAIN (PERCENT)
TOTAL
-0.12
-0.10
-0.08
-0.06
VERT.
-0.02
-0.01
0.00
0.01
HORIZ.
-0.06
-0.05
-0.04
-0.03
0
20
40
60
80
100
300
500
700
900
TIME (MIN.)
TIME (MIN.)
TEST NO. 12P

Figure E.8



TEST NO. 120

Figure E.9

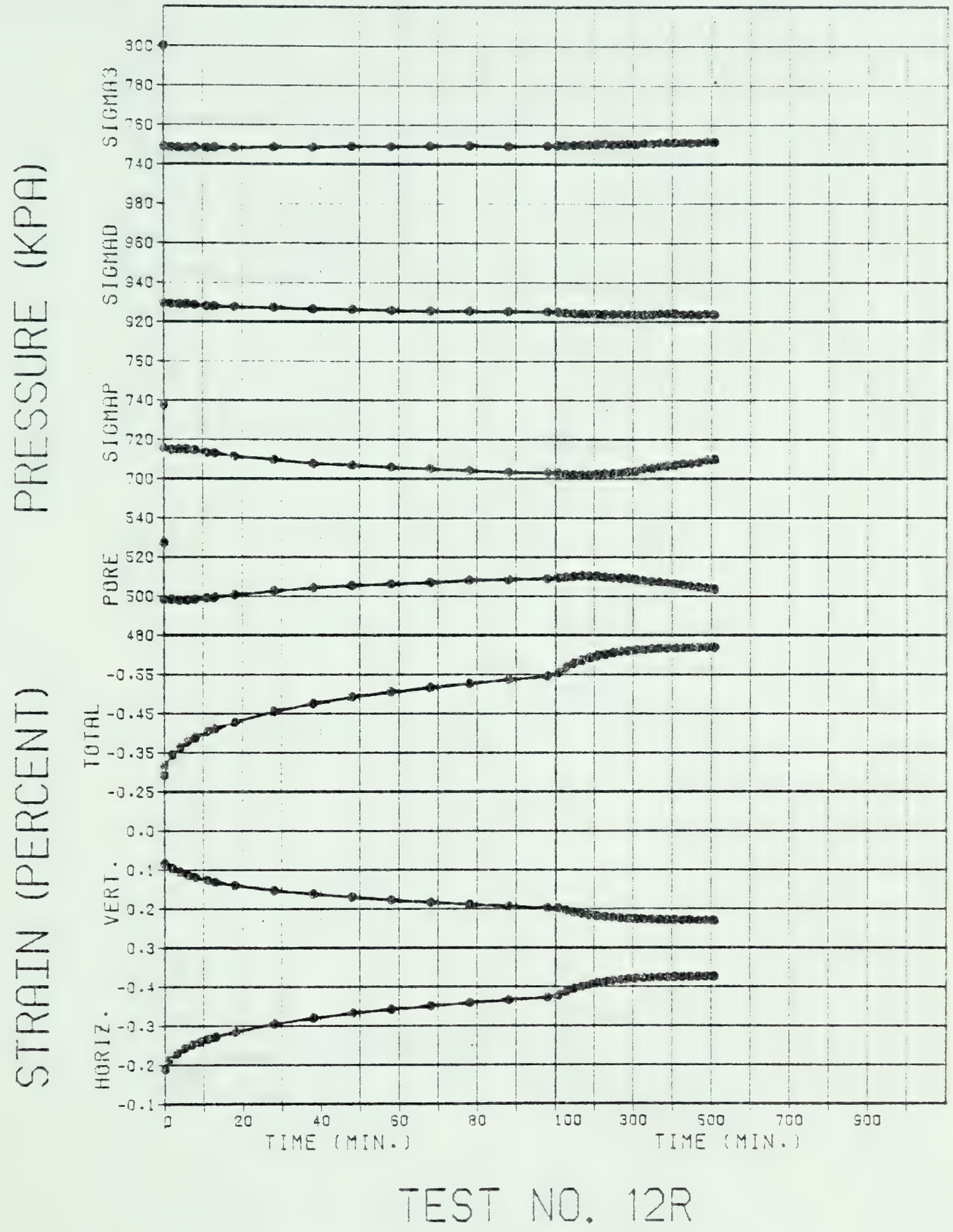

PRESSURE (KPA)
STRAIN (PERCENT)
SIGMA3
SIGMAD
SIGMAP
PORE
TOTAL
VERT.
HORIZ.
TIME (MIN.)
TIME (MIN.)
TEST NO. 12R

Figure E.10

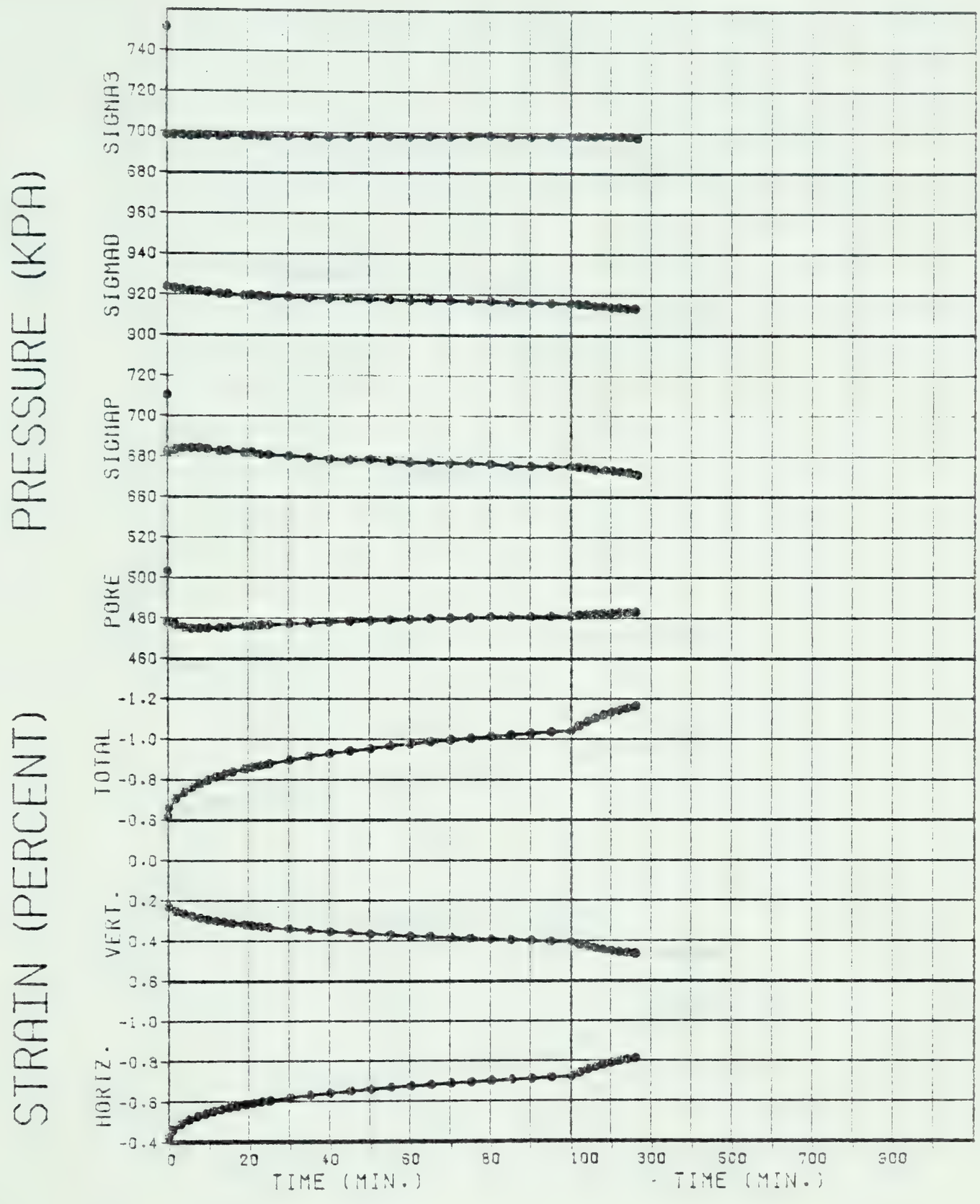

PRESSURE (KPA)
STRAIN (PERCENT)
SIGMA3
740
720
700
680
SIGMAD
960
940
920
900
SIGMAP
720
700
680
660
PORE
520
500
480
460
TOTAL
-1.2
-1.0
-0.8
-0.6
VERT.
0.0
0.2
0.4
0.6
HORIZ.
-1.0
-0.8
-0.6
-0.4
0
20
40
60
80
100
300
500
700
900
TIME (MIN.)
TIME (MIN.)
TEST NO. 12S

Figure E.11

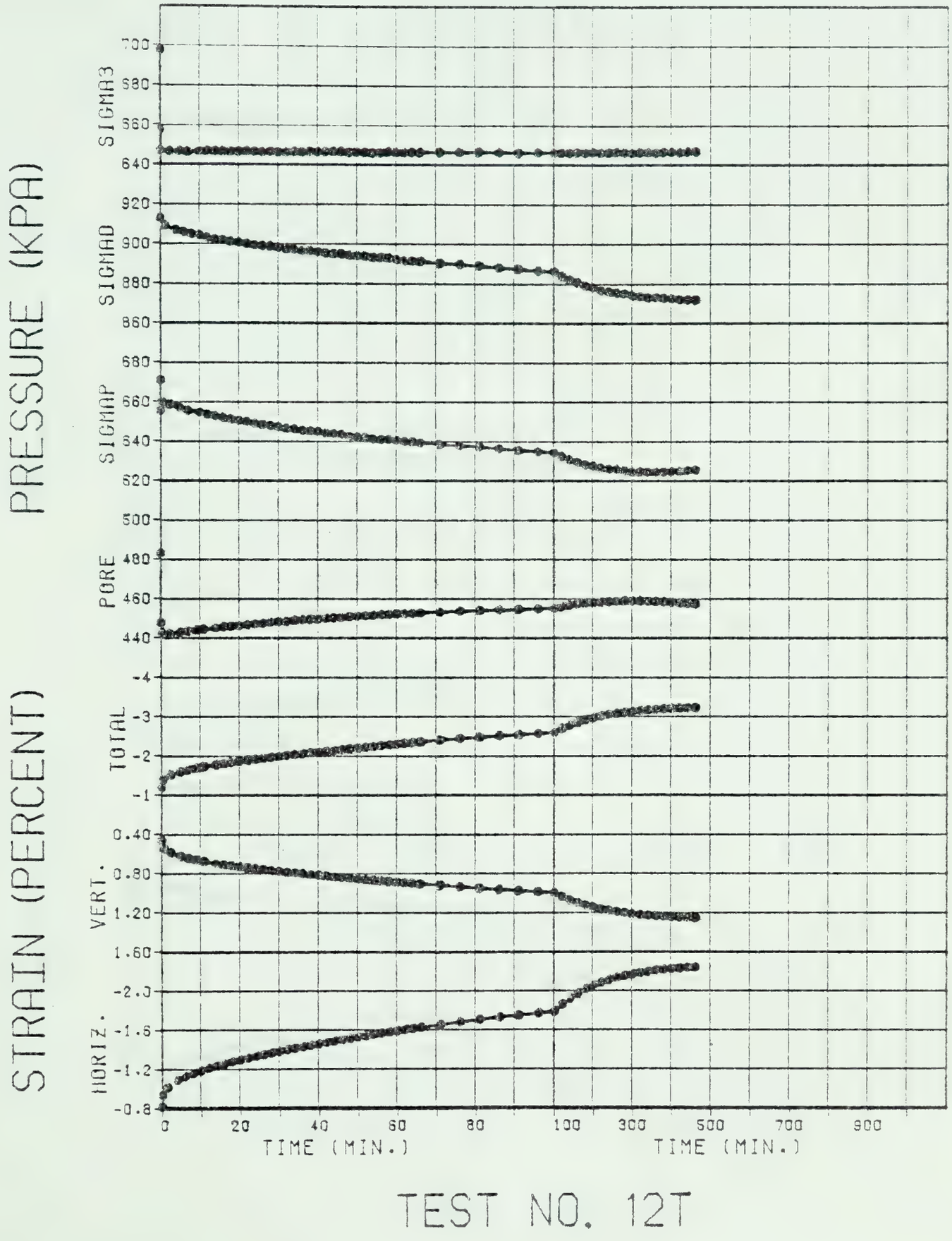

PRESSURE (KPA)
STRAIN (PERCENT)
SIGMA3
SIGMAD
SIGMAP
PORE
TOTAL
VERT.
HORIZ.
TIME (MIN.)
TIME (MIN.)
TEST NO. 12T

Figure E.12

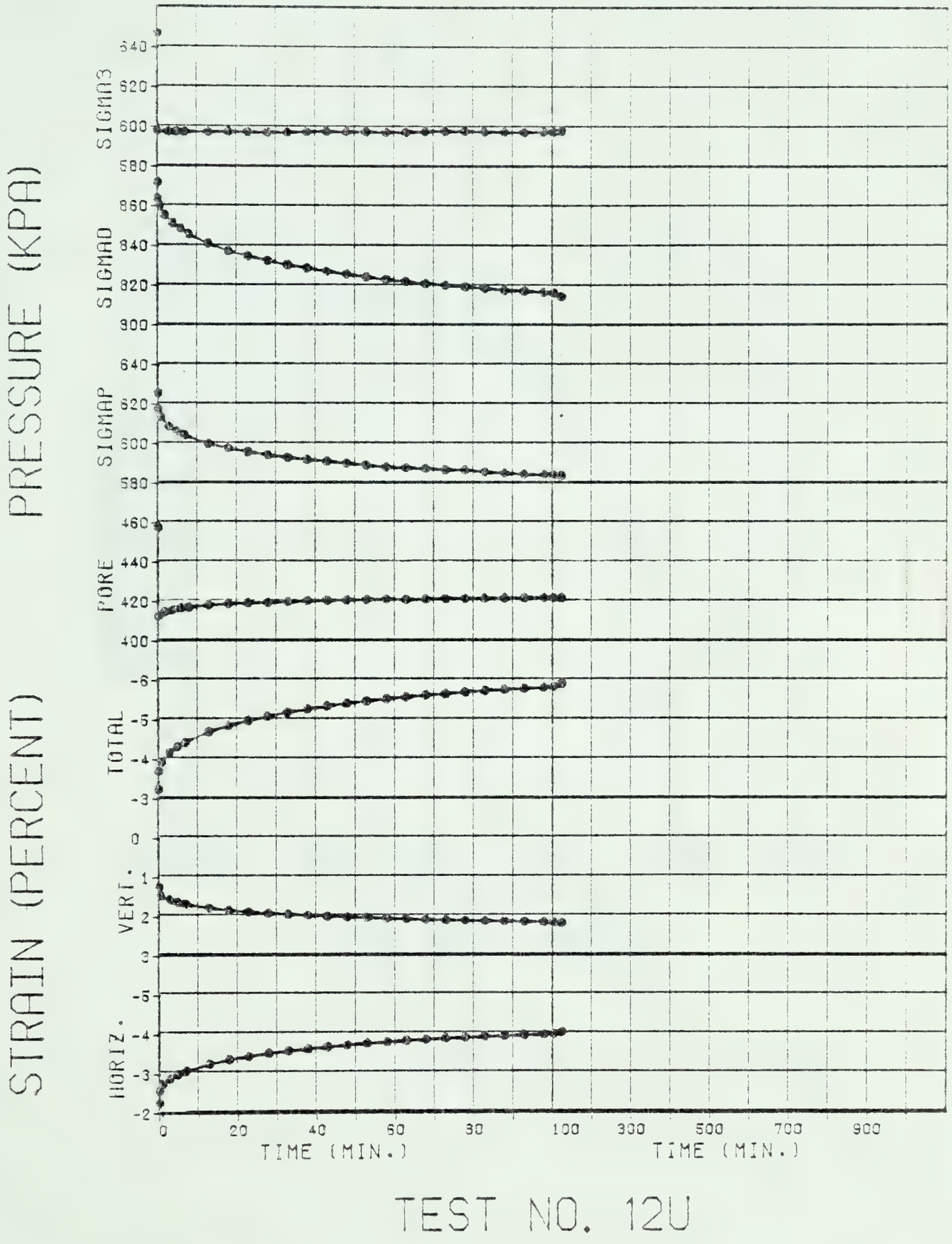

PRESSURE (KPA)
SIGMA3
SIGMAD
SIGMAP
PORE
STRAIN (PERCENT)
TOTAL
VERT.
HORIZ.
TIME (MIN.)
TIME (MIN.)
TEST NO. 12U

Figure E.13

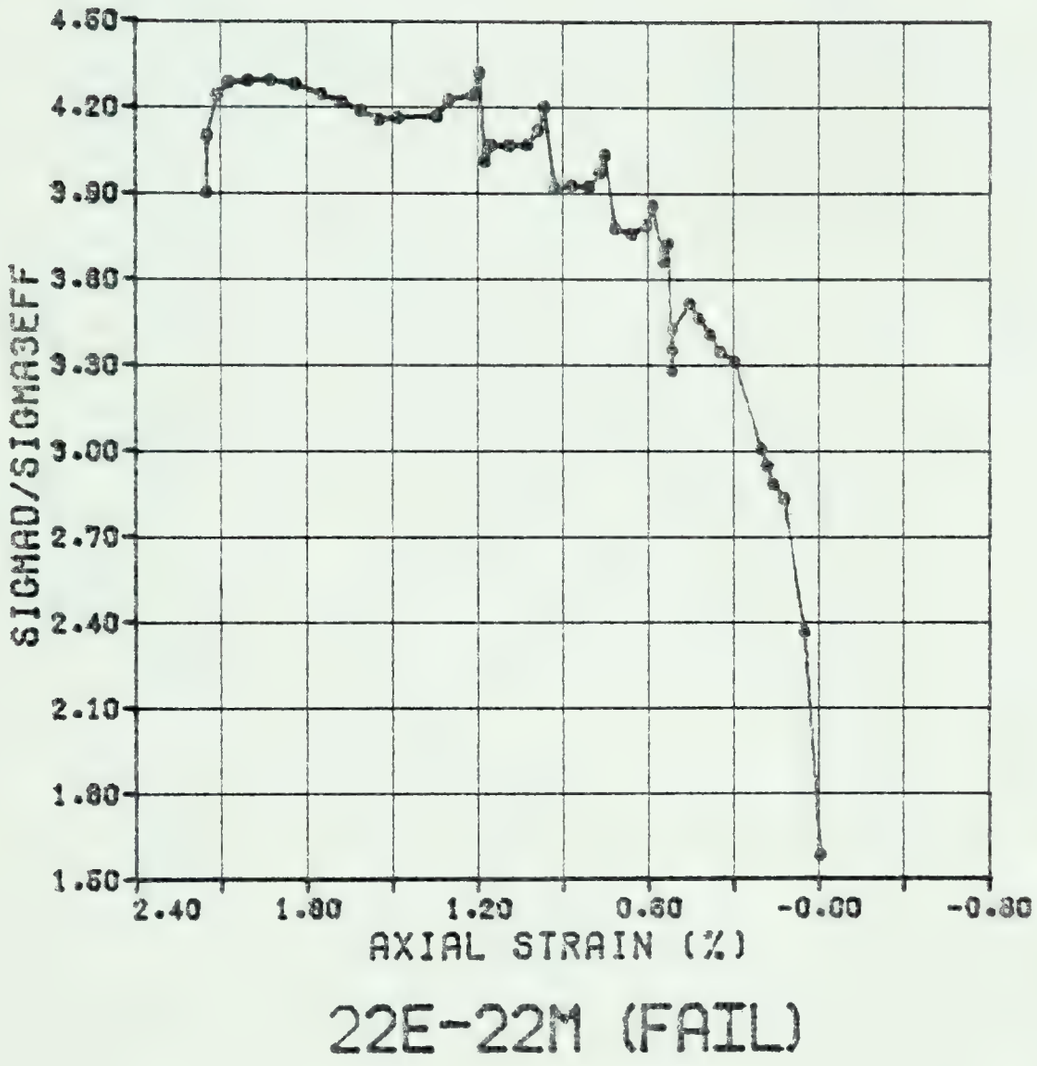

4.60
4.20
3.90
3.60
3.30
3.00
2.70
2.40
2.10
1.80
1.50
SIGMAD/SIGMA3EFF
2.40
1.80
1.20
0.60
-0.00
-0.60
AXIAL STRAIN (%)
22E-22M (FAIL)

Figure E.14

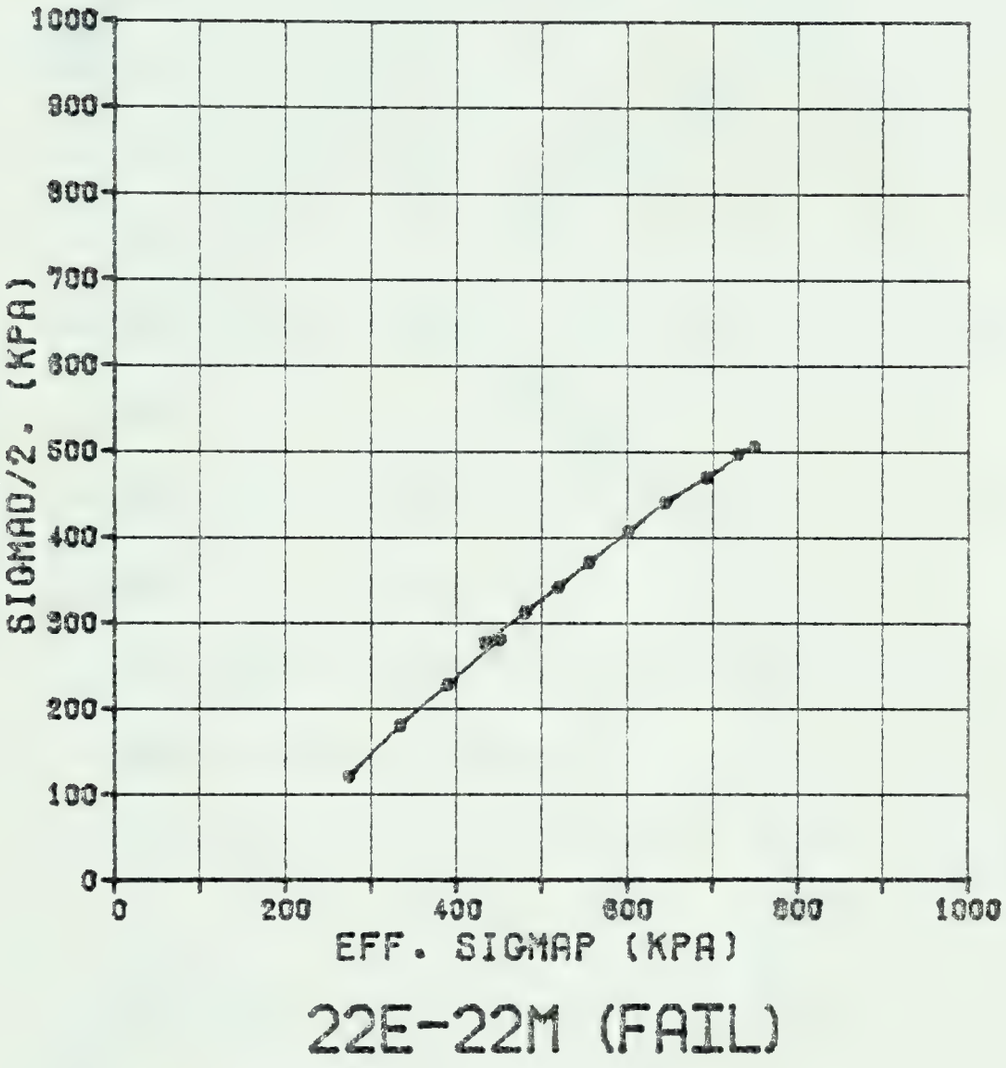

1000
900
800
700
600
500
400
300
200
100
0
SIGMAD/2. (KPA)
0
200
400
600
800
1000
EFF. SIGMAP (KPA)
22E-22M (FAIL)

Figure E.15

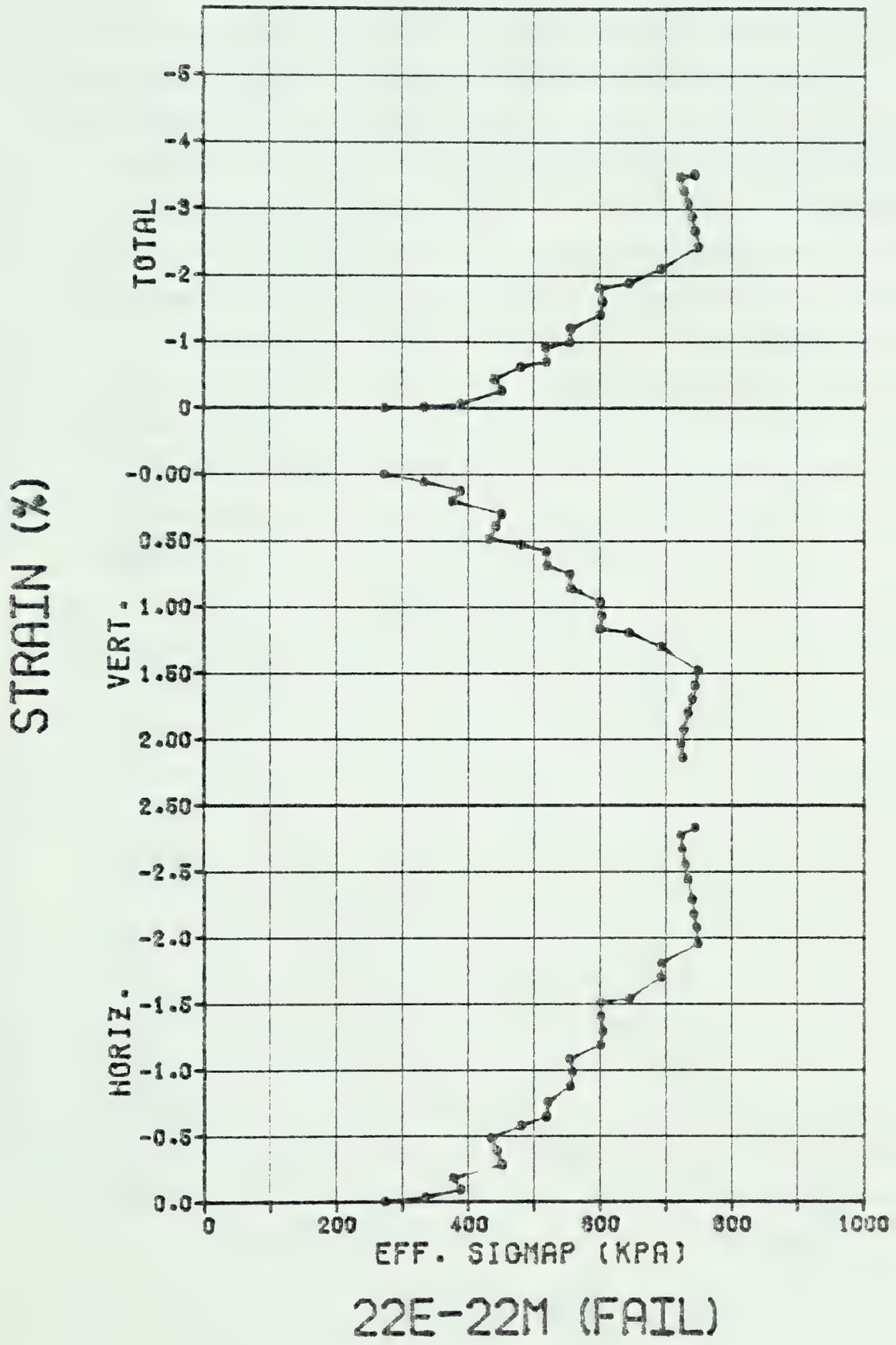
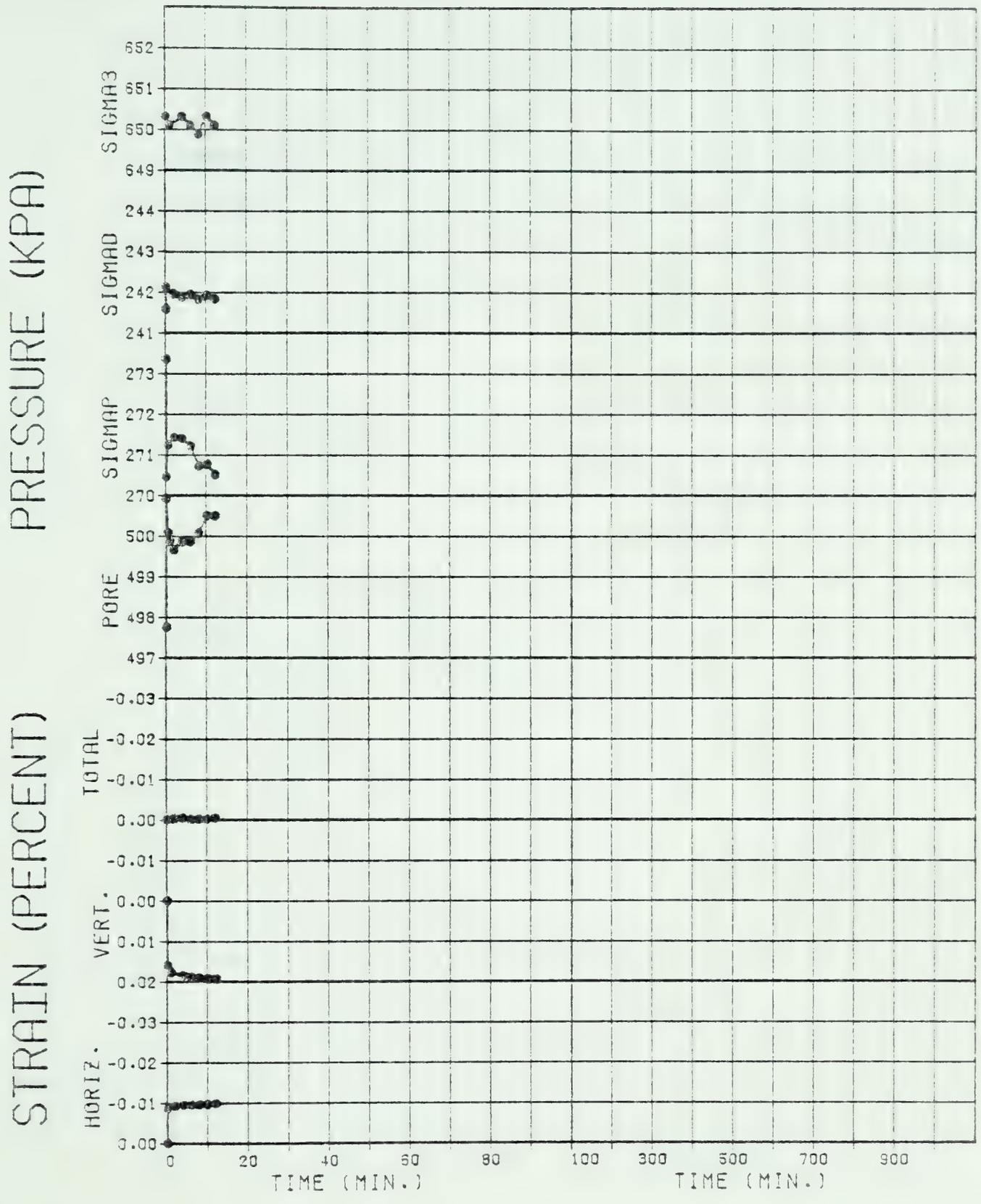

STRAIN (%)
TOTAL
VERT.
HORIZ.
-5
-4
-3
-2
-1
0
-0.00
0.50
1.00
1.50
2.00
2.50
-2.5
-2.0
-1.5
-1.0
-0.5
0.0
0
200
400
600
800
1000
EFF. SIGMAP (KPA)
22E-22M (FAIL)

Figure E.16



TEST NO. 22E

Figure E.17

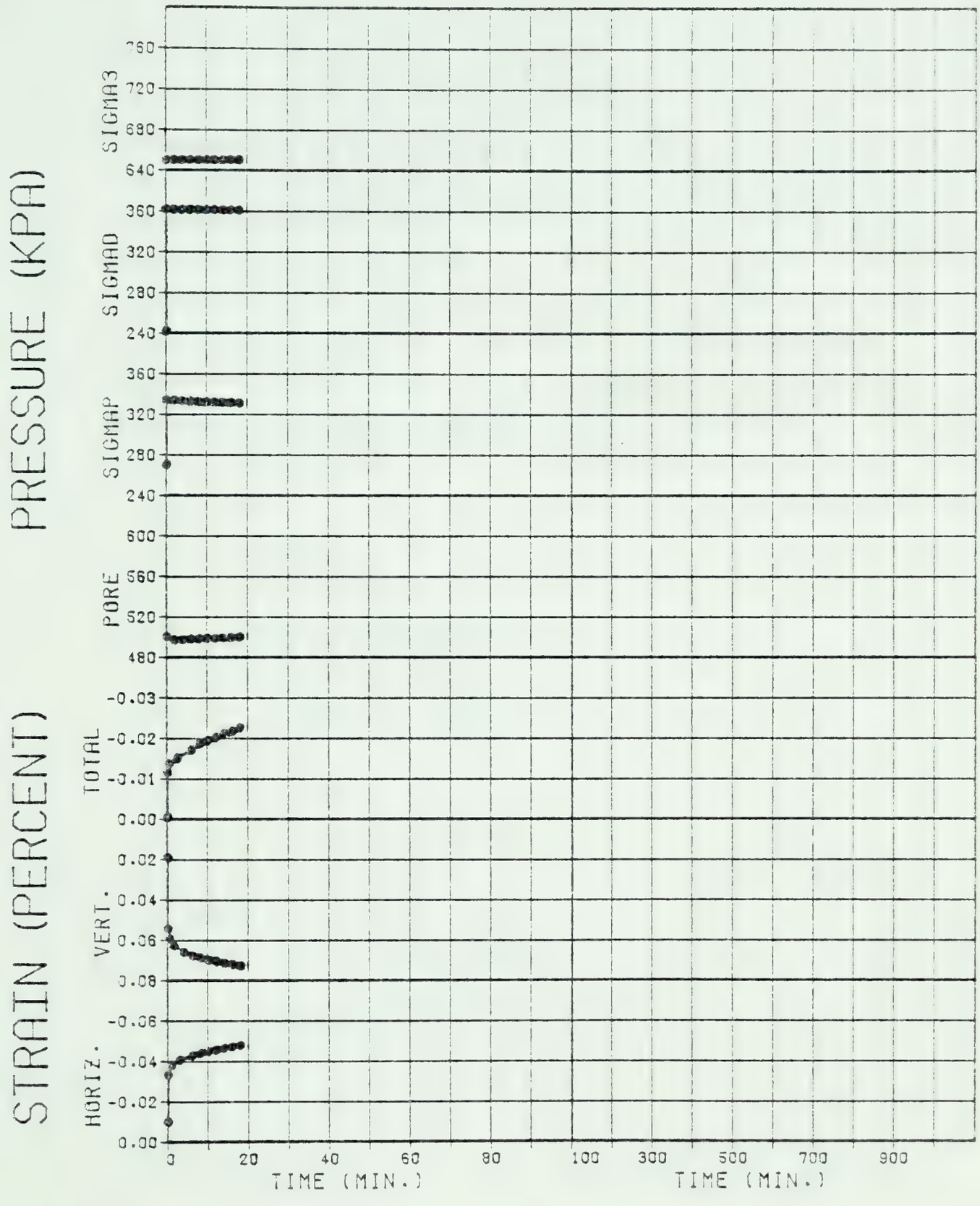

PRESSURE (KPA)
STRAIN (PERCENT)
SIGMA3
SIGMAD
SIGMAP
PORE
TOTAL
VERT.
HORIZ.
TIME (MIN.)
TIME (MIN.)
TEST NO. 22F

Figure E.18

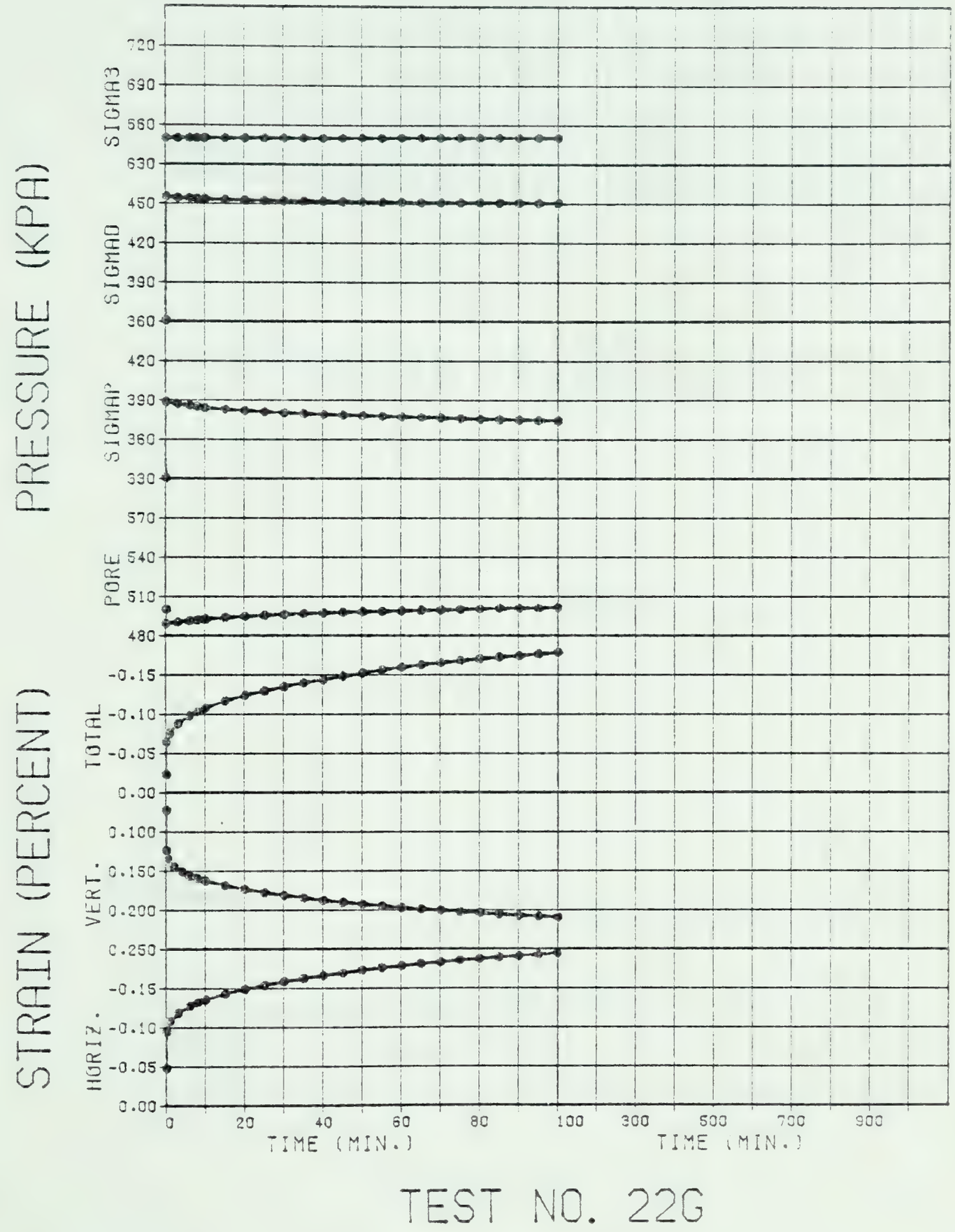
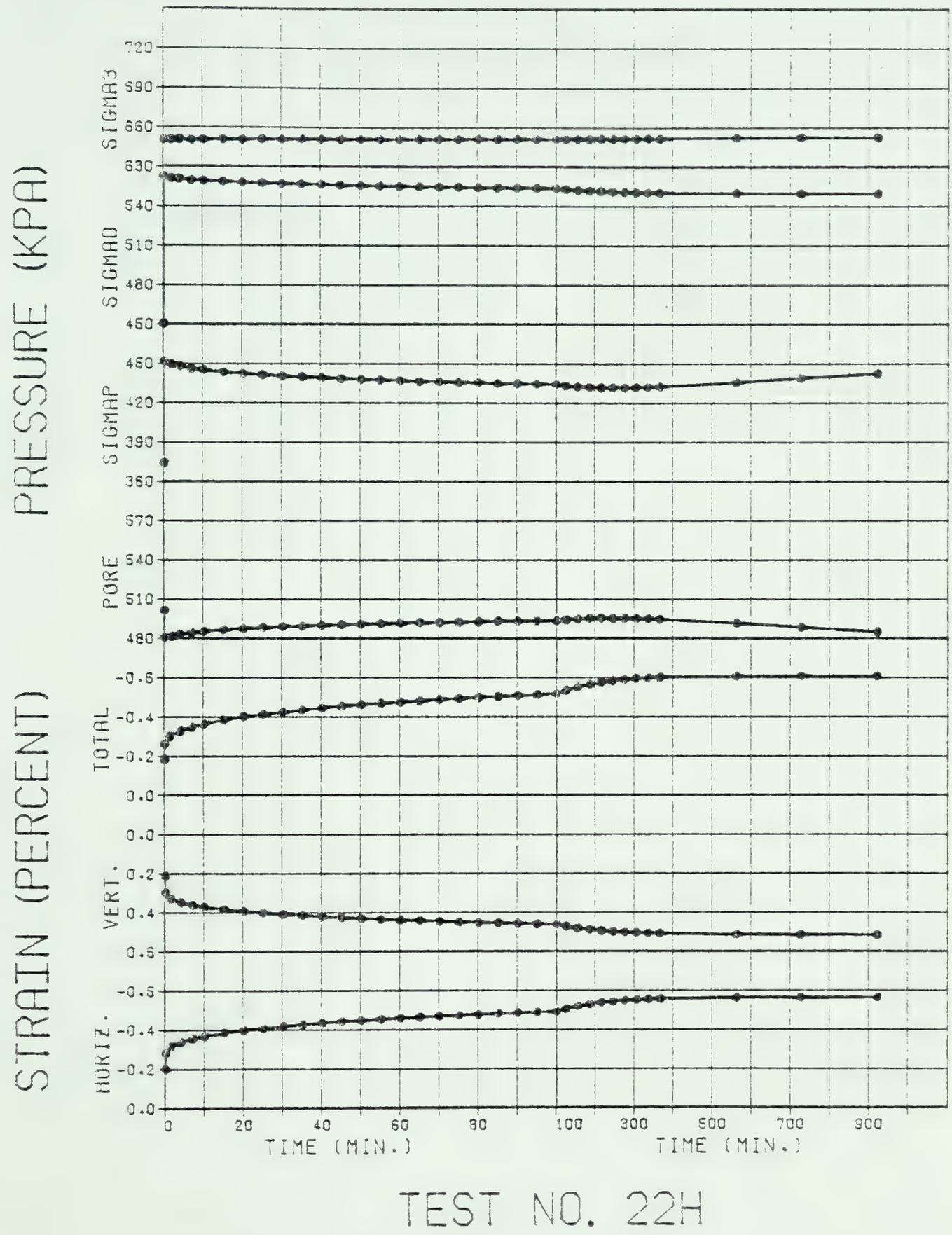

PRESSURE (KPA)
STRAIN (PERCENT)
SIGMA3
SIGMAD
SIGMAP
PORE
TOTAL
VERT.
HORIZ.
720
690
660
630
450
420
390
360
420
390
360
330
570
540
510
480
-0.15
-0.10
-0.05
0.00
0.100
0.150
0.200
0.250
-0.15
-0.10
-0.05
0.00
0
20
40
60
80
100
300
500
700
900
TIME (MIN.)
TIME (MIN.)
TEST NO. 22G

Figure E.19



TEST NO. 22H

Figure E.20

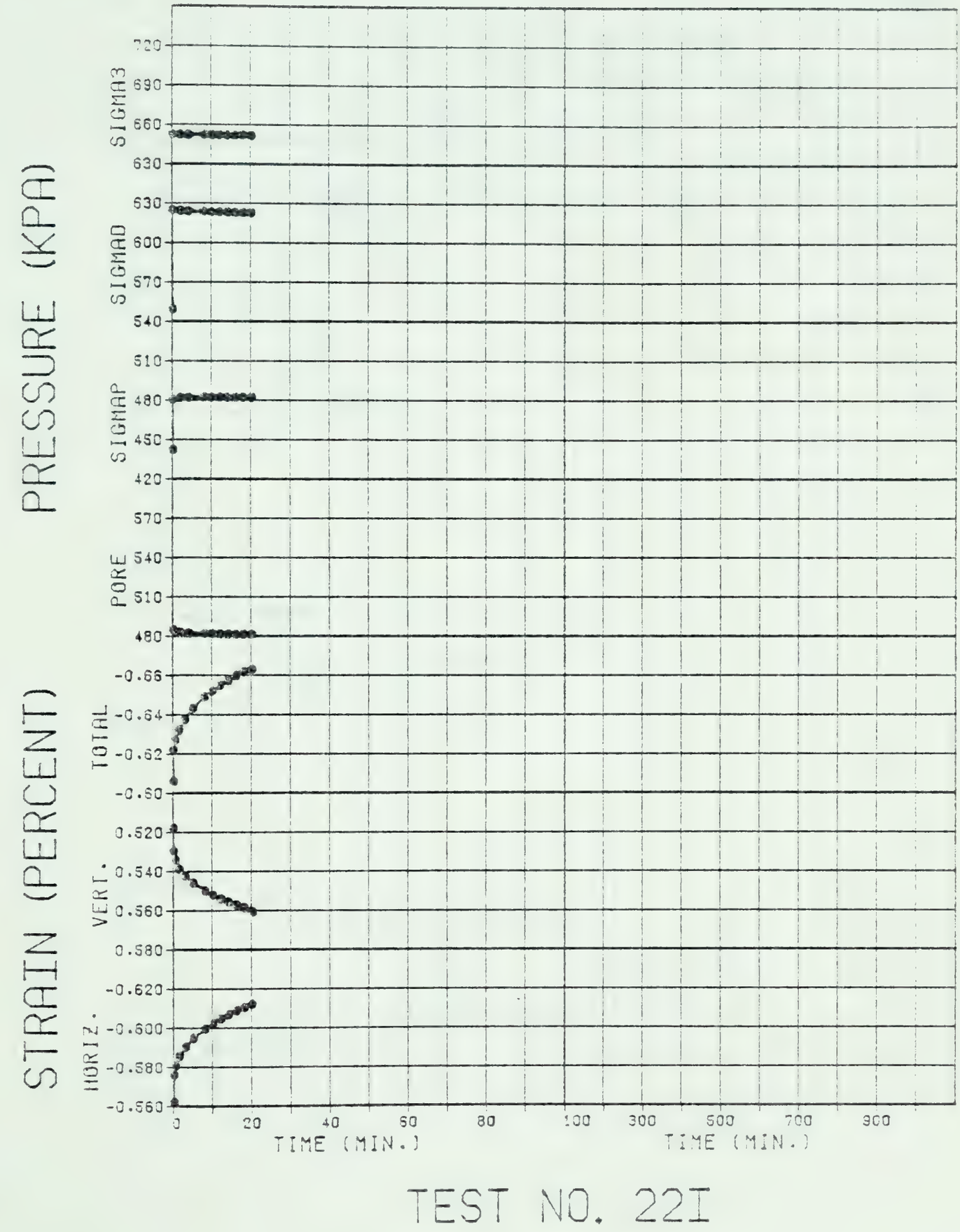

PRESSURE (KPA)
STRAIN (PERCENT)
SIGMA3
SIGMAD
SIGMAP
PORE
TOTAL
VERT.
HORIZ.
TIME (MIN.)
TIME (MIN.)
TEST NO. 22I

Figure E.21

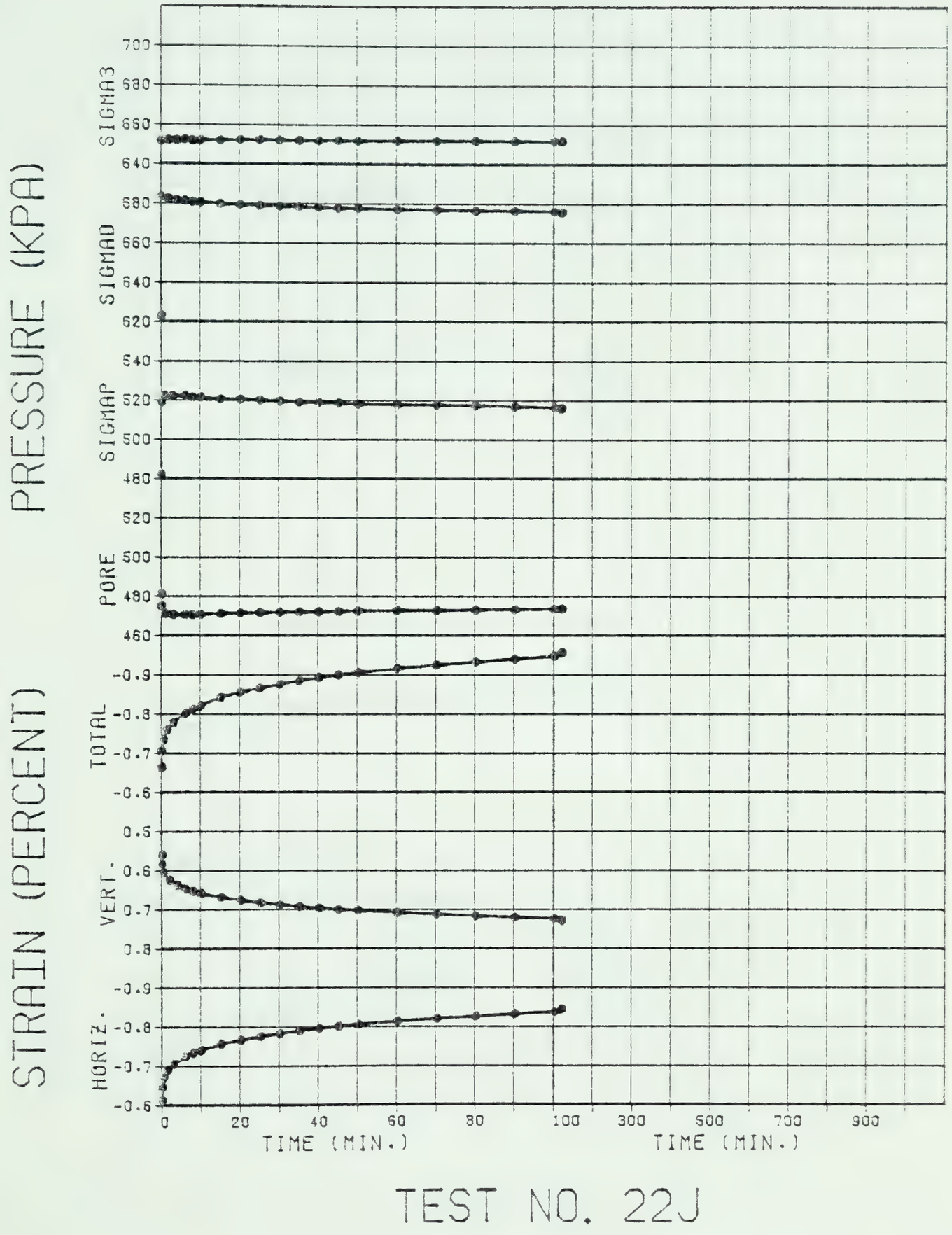

PRESSURE (KPA)
STRAIN (PERCENT)
SIGMA3
SIGMAD
SIGMAP
PORE
TOTAL
VERT.
HORIZ.
TIME (MIN.)
TIME (MIN.)
TEST NO. 22J

Figure E.22

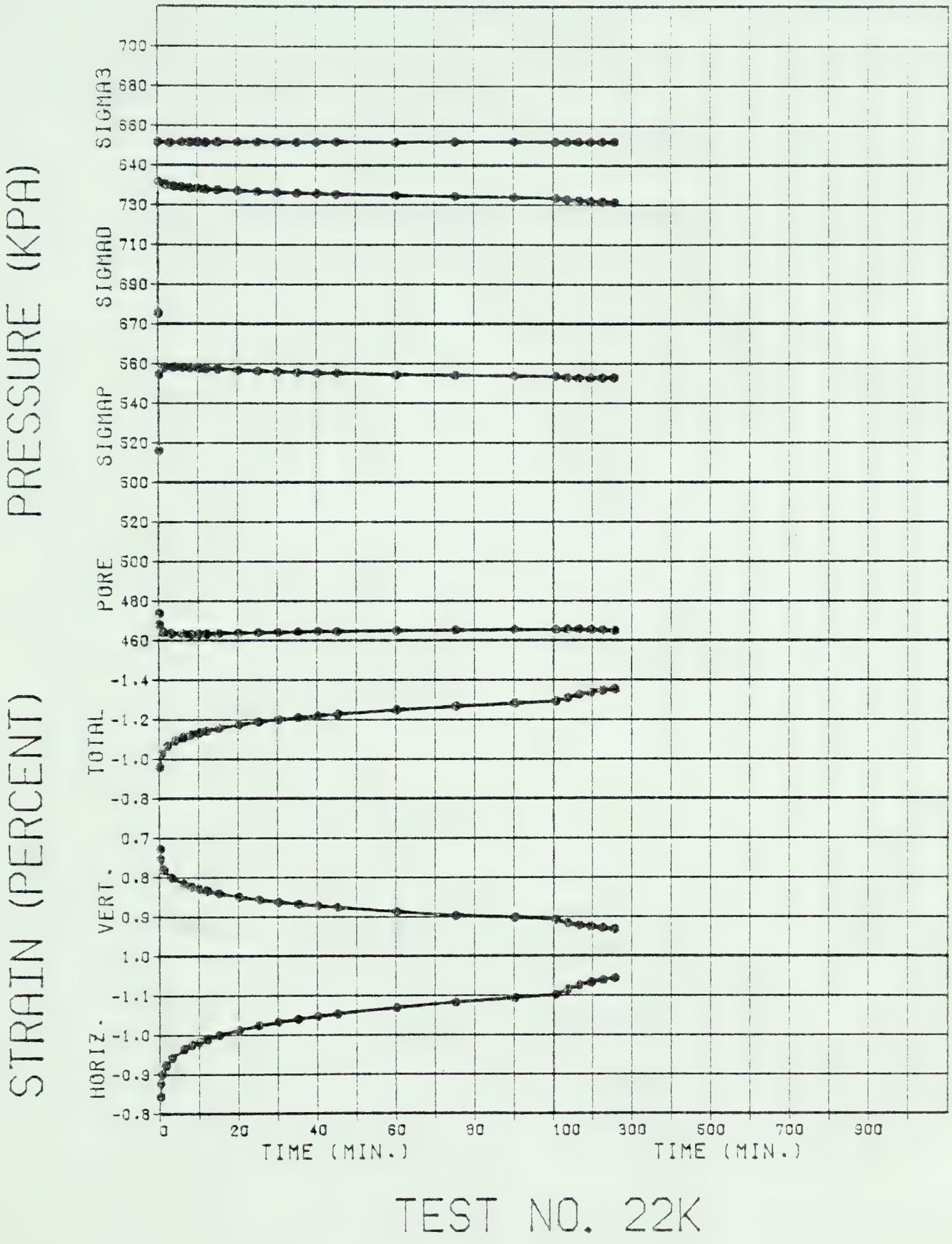
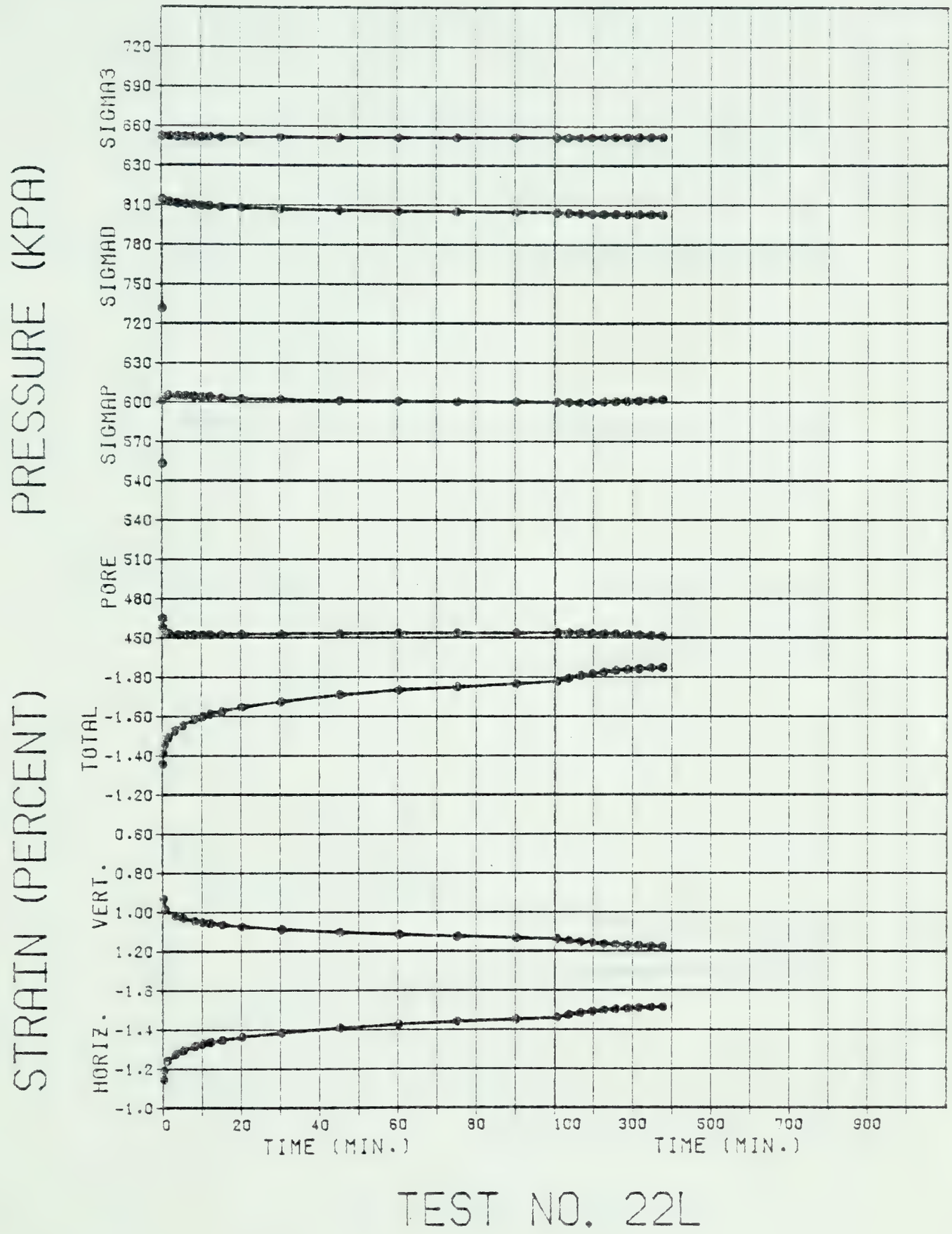

PRESSURE (KPA)
STRAIN (PERCENT)
SIGMA3
SIGMAD
SIGMAP
PORE
TOTAL
VERT.
HORIZ.
700
680
660
640
730
710
690
670
560
540
520
500
520
500
480
460
-1.4
-1.2
-1.0
-0.8
0.7
0.8
0.9
1.0
-1.1
-1.0
-0.9
-0.8
0
20
40
60
90
100
300
500
700
900
TIME (MIN.)
TIME (MIN.)
TEST NO. 22K

Figure E.23



TEST NO. 22L

Figure E.24

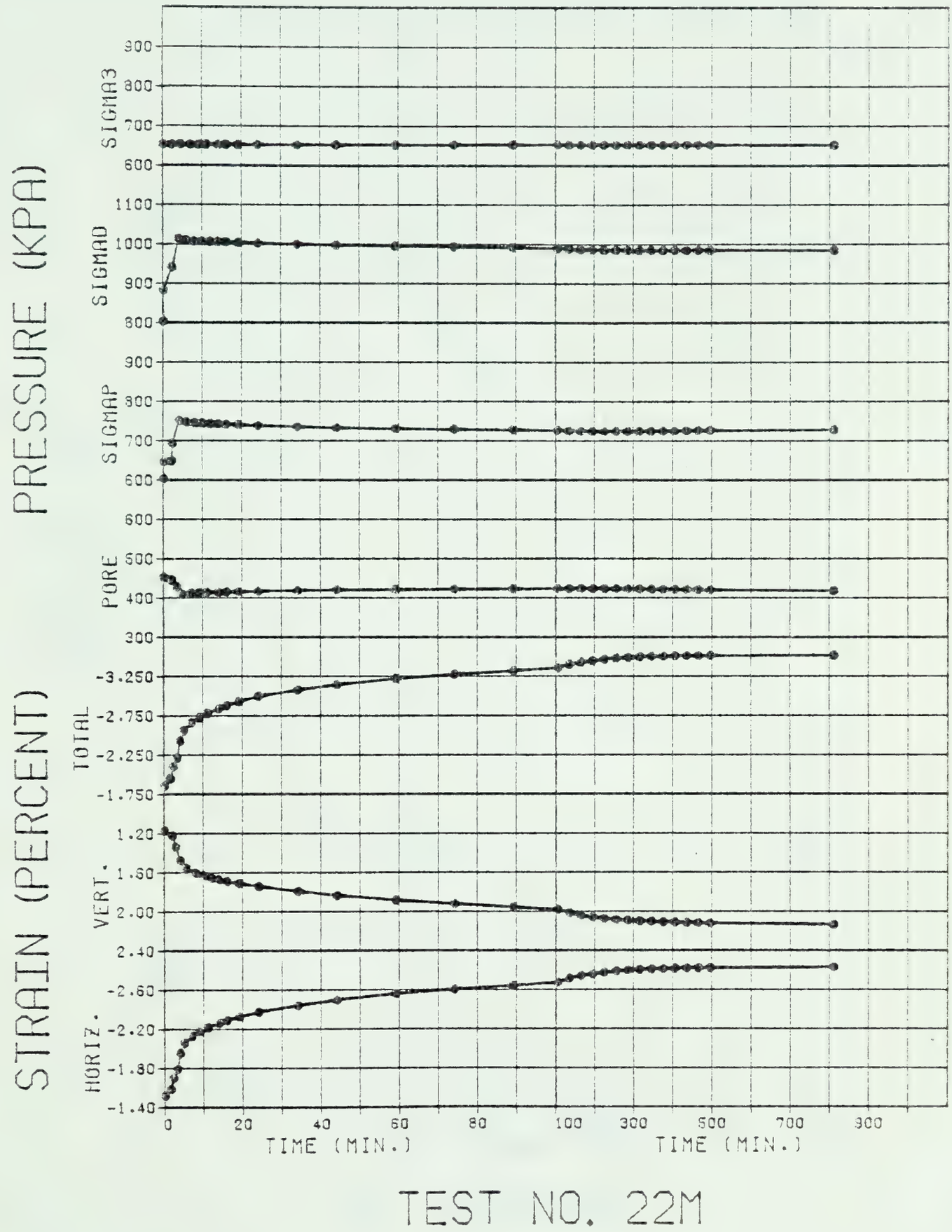

PRESSURE (KPA)
SIGMA3
SIGMAD
SIGMAP
PORE
STRAIN (PERCENT)
TOTAL
VERT.
HORIZ.
TIME (MIN.)
TIME (MIN.)
TEST NO. 22M

Figure E.25

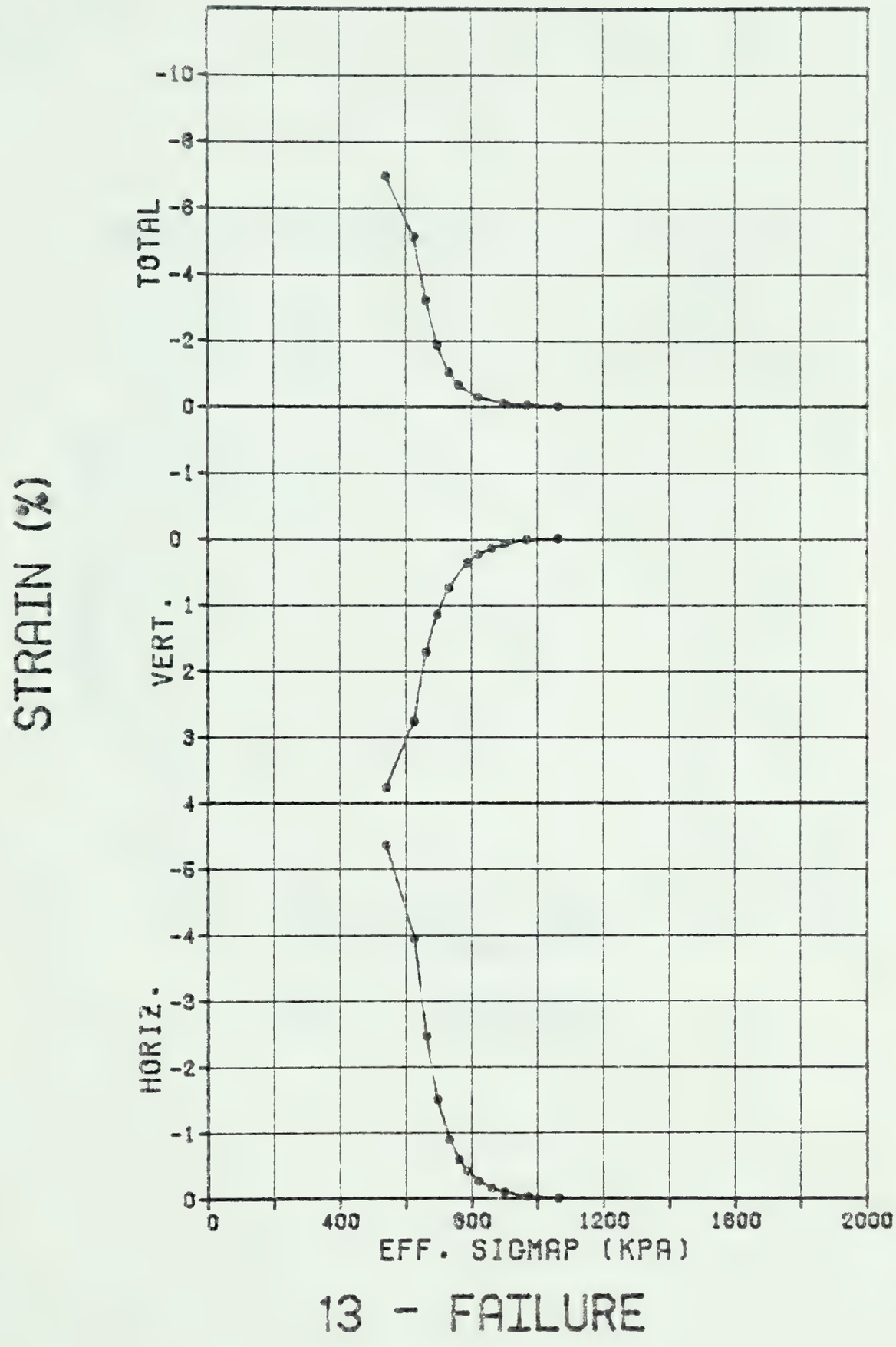

STRAIN (%)
TOTAL
VERT.
HORIZ.
-10
-8
-6
-4
-2
0
-1
0
1
2
3
4
-5
-4
-3
-2
-1
0
0
400
800
1200
1600
2000
EFF. SIGMAP (KPA)
13 - FAILURE

Figure E.26

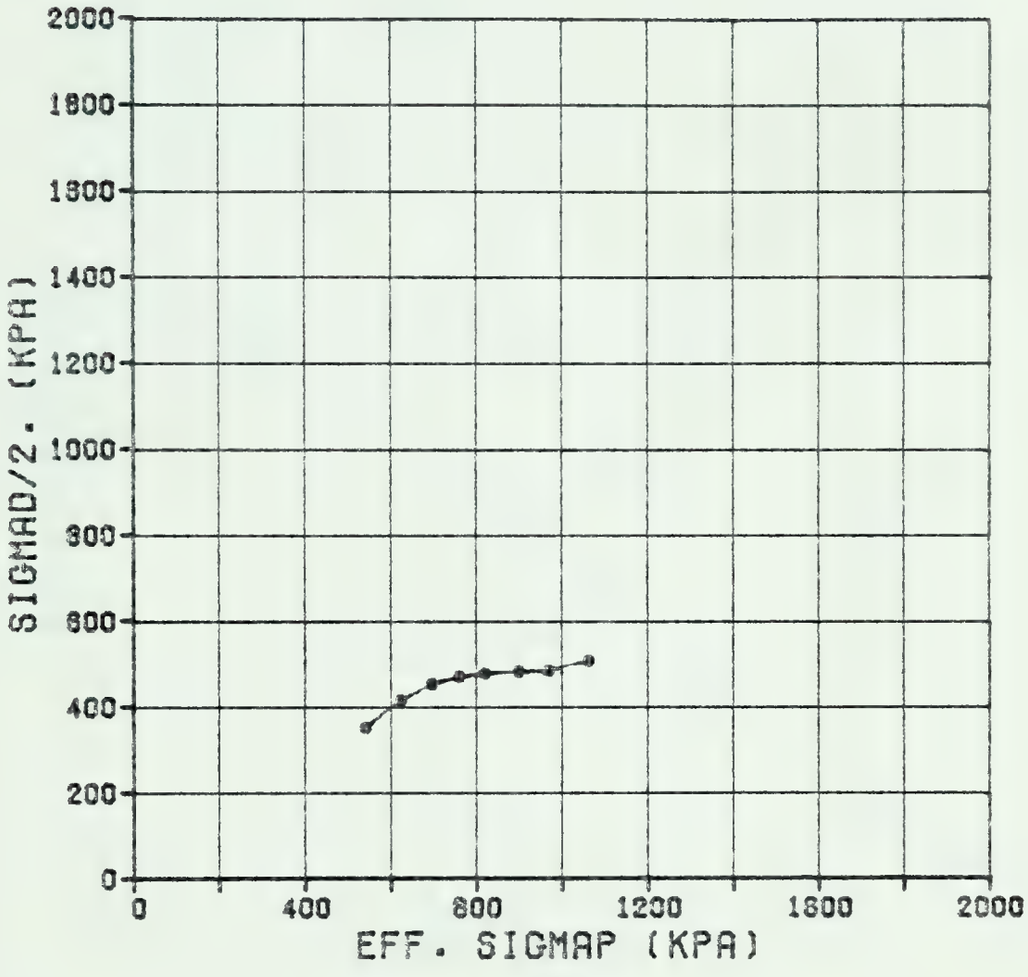

2000
1800
1600
1400
1200
1000
800
600
400
200
0
SIGMAD/2. (KPA)
0
400
800
1200
1600
2000
EFF. SIGMAP (KPA)
13 - FAILURE

Figure E.27

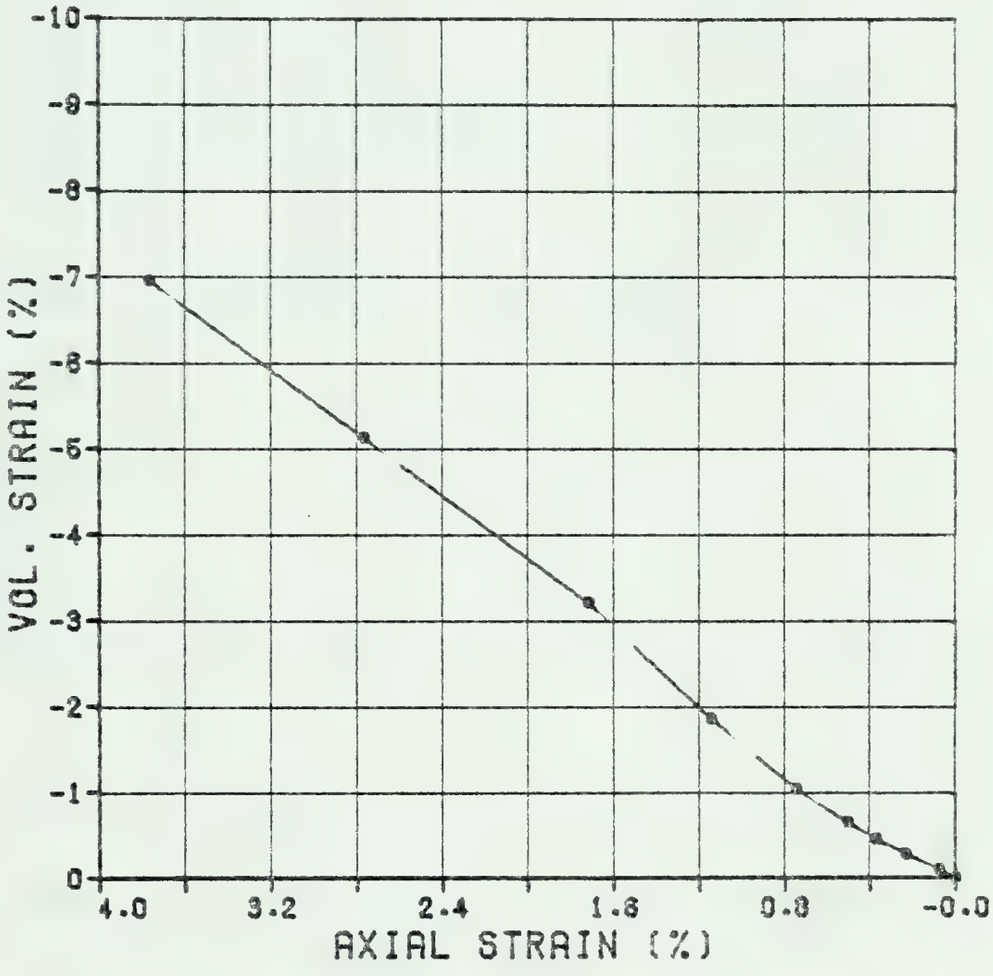

-10
-9
-8
-7
-6
-5
-4
-3
-2
-1
0
VOL. STRAIN (%)
4.0
3.2
2.4
1.6
0.8
-0.0
AXIAL STRAIN (%)
13 - FAILURE

Figure E.28

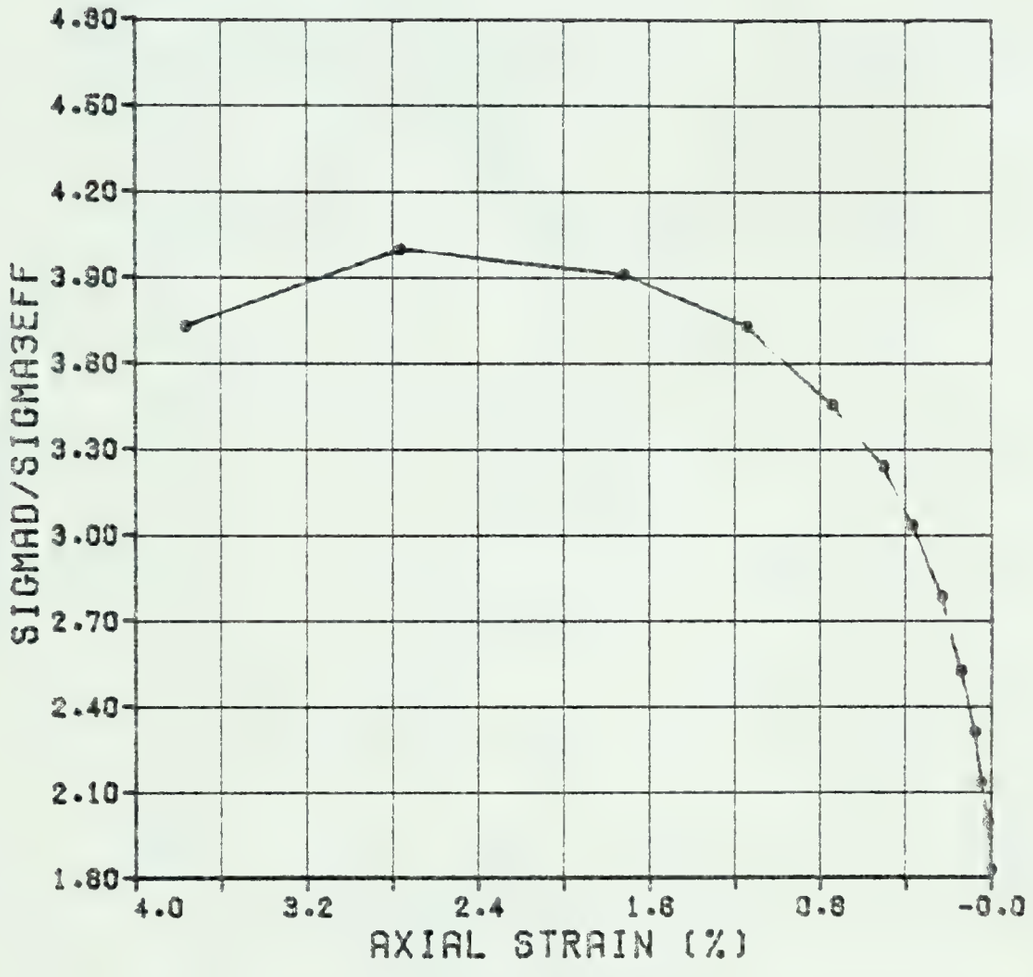

4.80
4.50
4.20
3.90
3.60
3.30
3.00
2.70
2.40
2.10
1.80
SIGMAD/SIGMA3EFF
4.0
3.2
2.4
1.6
0.8
-0.0
AXIAL STRAIN (%)
13 - FAILURE

Figure E.29

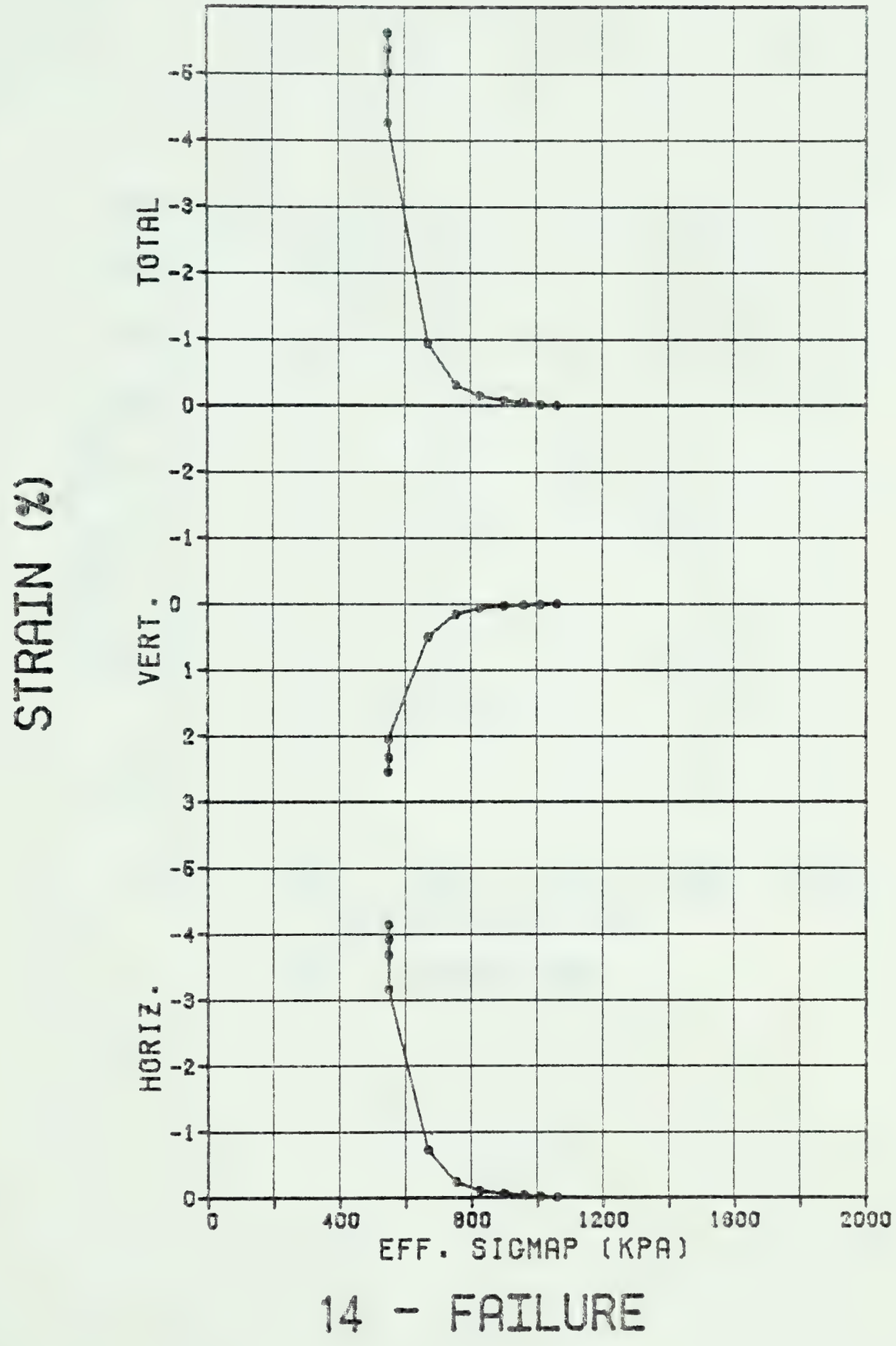

STRAIN (%)
TOTAL
VERT.
HORIZ.
-6
-4
-3
-2
-1
0
-2
-1
0
1
2
3
-6
-4
-3
-2
-1
0
0
400
800
1200
1600
2000
EFF. SIGMAP (KPA)
14 - FAILURE

Figure E.30

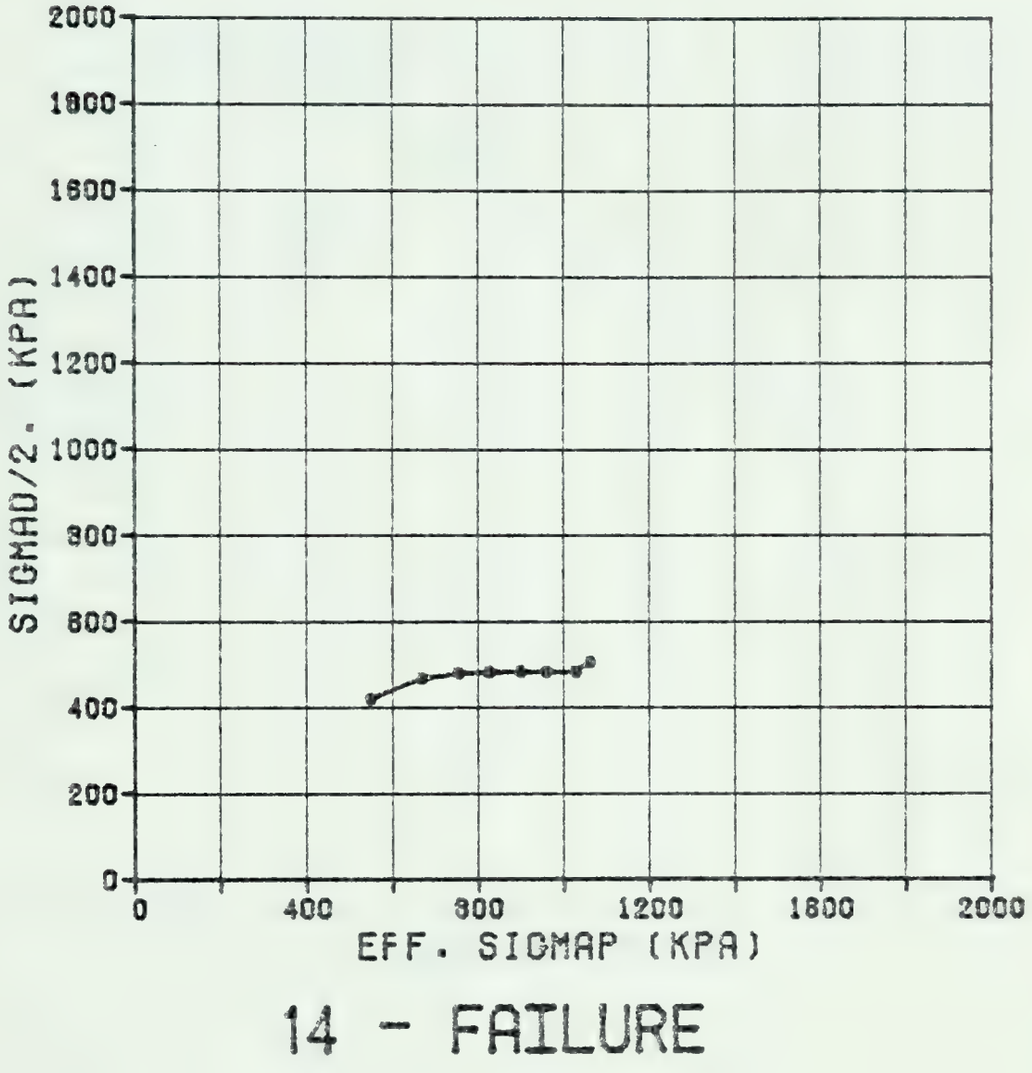

2000
1800
1600
1400
1200
1000
800
600
400
200
0
SIGMAD/2. (KPA)
0
400
800
1200
1600
2000
EFF. SIGMAP (KPA)
14 - FAILURE

Figure E.31

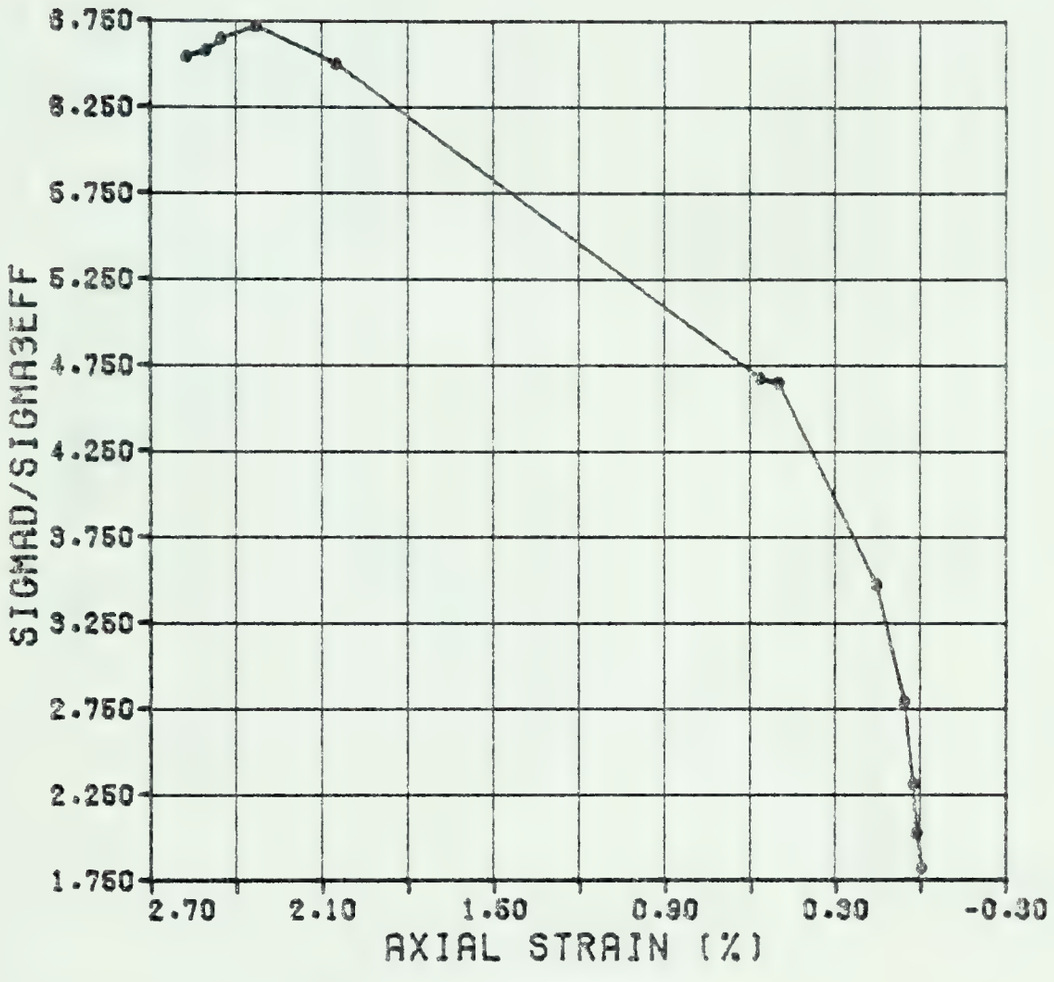

8.750
8.250
5.750
5.250
4.750
4.250
3.750
3.250
2.750
2.250
1.750
SIGMAD/SIGMA3EFF
2.70
2.10
1.50
0.90
0.30
-0.30
AXIAL STRAIN (%)
14 - FAILURE

Figure E.32

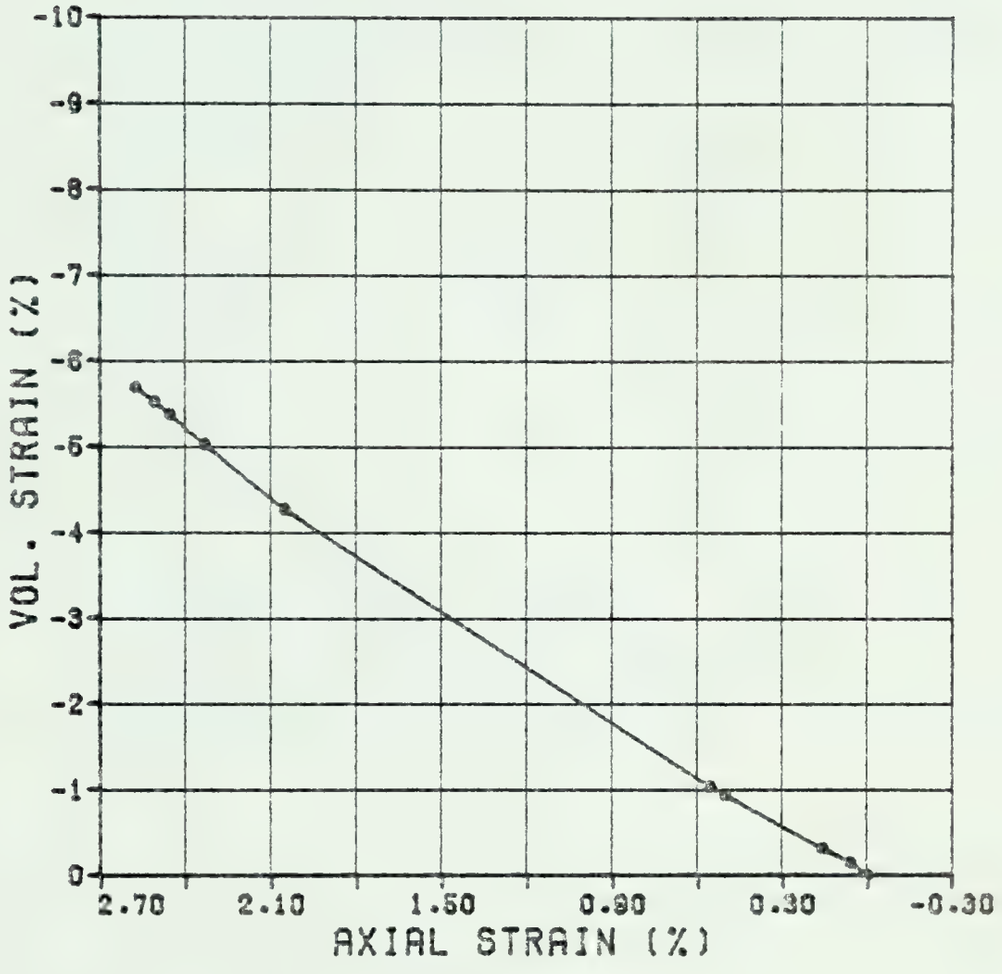

-10
-9
-8
-7
-6
-5
-4
-3
-2
-1
0
VOL. STRAIN (%)
2.70
2.10
1.50
0.90
0.30
-0.30
AXIAL STRAIN (%)
14 - FAILURE

Figure E.33

APPENDIX F

COMPUTER PROGRAM TO MODEL UNDRAINED LABORATORY TESTS

```
 1      C      PROGM8 FEB 15,1982.  JOHN SOBKOWICZ
 2      C      FINITE DIFFERENCE PROGRAM TO PREDICT THE UNDRAINED RESPONSE
 3      C      OF A GAS-SATURATED SOIL DUE TO GAS SORPTION.
 4      C
 5      C      DIMENSIONING
 6      C
 7             REAL KBAR,NO
 8             DIMENSION TITLE(10),E(10),X1(500),Y1(500)
 9             DIMENSION TIME(500,10),PRESS(500,10),ATIME(100),APRESS(100)
10             INTEGER NSTEPS(10)
10.5           REAL MAX,MIN
11             COMMON MAX,MIN,PLOTSZ
12             PLOTSZ=5.
13     C
14     C      READ INITIAL DATA
15     C
16             READ(5,16)(TITLE(I),I=1,10)
17          16 FORMAT(10A4)
18             READ(5,101)VGO,VWO,VS,H,KBAR,KSTAR
18.2       101 FORMAT(5F10.2,I10)
19           1 FORMAT(10F10.2)
20             VTI=VGO+VWO+VS
21             VTI2=VWO+VS
22             READ(5,1)PO,TSO,DELTS
23             PO=PO+101.3
24             READ(5,1)CC,CW
25             READ(5,1)DELTM,TOL
26             READ(5,2)NE,(E(I),I=1,NE)
27           2 FORMAT(I10,10F10.2)
27.1           READ(5,46)NRGS,(ATIME(I),APRESS(I),I=1,NRGS)
27.2           IF(NRGS.LE.100)GOTO 50
27.3        46 FORMAT(I2/(T27,F7.2,T58,F6.2))
27.4           WRITE(6,51)
27.5        51 FORMAT('1***ERROR*** ARRAY DIMENSIONS ONLY ALLOW 100 (MAXIMUM)',
27.6          1' ACTUAL PRESSURE READINGS')
27.65          STOP
27.7        50 CALL MAXMIN(0.,100.,MAX,MIN,ATIME,NRGS)
27.8           IF(MAX.GT.500.)MAX=500.
28     C
29     C      CALCULATE IMMEDIATE AND LONG TERM RESPONSE
30     C
30.5           IF(KBAR.GE.1.)GOTO 91
31             KBAR=(VGO+H*VWO)*PO
32          91 VVO=VGO+VWO
33             SWO=VWO/VVO
34             SGO=1-SWO
35             NO=VVO/VTI
36             ESO=TSO-PO+101.3
37             VOIDR=VVO/VS
38             H1=0.
39             CTO=0.4342944819*CC/(1+VOIDR)/ESO
40           8 IFIRST=0
41             ISEC=0
42             CT=CTO
43             DELUC=0.0
44             NTRLS=0
45          14 A=CT+CW*NO*SWO
46             IF(H1.LE.0.0001)C=-1.*PO*CT*DELTS
46.5           IF(H1.GT.0.0001)C=PO*(-CT*DELTS+NO*(SGO+H1*SWO))-KBAR/VTI
47             B=CT*(PO-DELTS)+NO*(SGO+SWO*(H1+CW*PO))
```

```
48            DELU1=(-B+SQRT(B*B-4*A*C))/(2*A)
49            DELU2=(-B-SQRT(B*B-4*A*C))/(2*A)
49.1          IF(H1.LE.0.0001)GOTO 96
49.2          IF(KSTAR.EQ.1)DELTS=-DELTS
50         96 SIGN1=DELTS*DELU1
51            SIGN2=DELTS*DELU2
52         11 IF(SIGN1.LE.0.0.AND.SIGN2.LE.0.0)GOTO 3
53            IF(SIGN1.LE.0.0)GOTO 30
54            IF(SIGN2.LE.0.0)GOTO 5
55         95 DG=ABS(DELTS)+0.01
56         12 IF(ABS(DELU1).GT.DG.AND.ABS(DELU2).GT.DG)GOTO 4
56.5       98 IF(ABS(DELU1).LE.DG.AND.ABS(DELU2).LE.DG)GOTO 97
57            IF(ABS(DELU2).GT.ABS(DELTS))GOTO 5
58         30 DELU=DELU2
59            GOTO 6
60          5 DELU=DELU1
60.5        6 IF(H1.LE.0.0001)GOTO 100
60.7          IF(KSTAR.EQ.1)DELTS=-DELTS
61        100 IF(ABS(DELU-DELUC).LE.TOL)GOTO 13
62            IF(NTRLS.GT.100)GOTO 66
63            ESF=ESO+DELTS-DELU
64            IF(IFIRST.EQ.1)GOTO 70
65            IF(ESF.GT.0.0)GOTO 65
66            IFIRST=1
67            NTIMES=1
68         71 ESF=0.1**NTIMES
69            ALL=ESF
70            AUL=ESF
71            GOTO 65
72         70 IF(ISEC.EQ.1)GOTO 72
73            IF(ESF.GT.AUL)GOTO 73
74            NTIMES=NTIMES+1
75            GOTO 71
76         73 ISEC=1
77         74 ESF=ALL+0.1**NTIMES
78            AUL=ESF
79            GOTO 65
80         72 IF(ESF.GT.AUL)GOTO 75
81            NTIMES=NTIMES+1
82            GOTO 74
83         75 ALL=AUL
84            GOTO 74
85         65 CT=CC*ALOG10(ESF/ESO)/(1+VOIDR)/(ESF-ESO)
86            DELUC=DELU
87            NTRLS=NTRLS+1
88            GOTO 14
89         66 IF(H1.GT.0.0001)GOTO 69
90            WRITE(6,67)
91            GOTO 13
92         69 WRITE(6,68)
93         67 FORMAT('0***WARNING***NO CONVERGENCE FOR SHORT TERM',
94           1' UNDRAINED EQUILIBRIUM RESPONSE')
95         68 FORMAT('0***WARNING***NO CONVERGENCE FOR LONG TERM',
96           1' UNDRAINED EQUILIBRIUM RESPONSE')
97         13 IF(H1.GT.0.0001)GOTO 7
98            DELUST=DELU
99            H1=H
100           CTS=CT
101           GOTO 8
101.1      97 WRITE(6,99)
```

```
101.2       99 FORMAT('1STOP AT STATEMENT 98')
101.3          STOP
102             3 WRITE(6,9)
103               STOP
104             4 WRITE(6,10)
105               STOP
106             9 FORMAT('1STOP AT STATEMENT 11')
107            10 FORMAT('1STOP AT STATEMENT 12')
108             7 DELULT=DELU
109       C
110       C       CALCULATE END-OF-SHORT TERM QUANTITIES
111       C
112               P1=PO+DELUST
113               TS1=TSO+DELTS
114               ES1=TS1-P1+101.3
115               VG1=VGO*PO/P1
116               VW1=VWO*(1-CW*DELUST)
117               VT1=(VTI)*(1-CTS*(DELTS-DELUST))
118       C
119       C       PRINT OUT INFO ON SHORT AND LONG TERM RESPONSE
120       C
121               WRITE(6,15)TITLE
122            15 FORMAT('1',T10,10A4//T10,'SHORT AND LONG TERM PRESSURE RESPONSE',
123              1//T29,'INITIAL',T48,'FINAL'/)
124               WRITE(6,17)VGO,VG1
125            17 FORMAT(' VOLUME OF FREE GAS=',T30,F10.4,T50,F10.4)
126               WRITE(6,18)VWO,VW1
127            18 FORMAT(' VOLUME OF WATER=',T30,F10.4,T50,F10.4)
128               WRITE(6,19)VS
129            19 FORMAT(' VOLUME OF SOLIDS=',T30,F10.4)
130               VTN1=VS+VG1+VW1
131               WRITE(6,20)VTI,VTN1,VT1
132            20 FORMAT(' TOTAL VOLUME=',T30,F10.4,T50,F10.4/T50,F10.4)
133               PLT=PO+DELULT
134               Z1=PO-101.3
135               Z2=P1-101.3
136               Z3=PLT-101.3
137               WRITE(6,21)Z1,Z2,Z3
138            21 FORMAT(' WATER PRESSURE=',T30,F10.4,T50,F10.4/T50,F10.4)
139               WRITE(6,22)TSO,TS1
140            22 FORMAT(' TOTAL STRESS=',T30,F10.4,T50,F10.4)
141               WRITE(6,23)ESO,ES1
142            23 FORMAT(' EFFECTIVE STRESS=',T30,F10.4,T50,F10.4)
143               WRITE(6,52)CTS,CT
144               WRITE(6,24)H,CC,CW
145            24 FORMAT(' H=',E12.5,', CC=',E12.5,', CW=',E12.5)
146            52 FORMAT(' COMPRESSIBILITY=',T28,E12.5,T48,E12.5)
147               WRITE(6,25)DELTM,TOL,(E(I),I=1,NE)
148            25 FORMAT(' DELTM=',E12.5,', TOL=',E12.5,', E=',10(1X,F5.4,','))
148.1             WRITE(6,90)KBAR
148.2          90 FORMAT(/' KBAR=',E12.5)
149       C
150       C       START TRANSIENT RESPONSE CALCS
151       C
152               F1=(KBAR/P1-H*VW1-VG1)
153               DO 26 I=1,NE
154               VOIDP=(VG1+VW1)/VS
155               WRITE(6,27)TITLE,E(I)
156            27 FORMAT('1',T10,10A4//T10,'TRANSIENT PRESSURE RESPONSE FOR E=',
157              1F7.5//' STEP   TIME   NO. OF   PORE   EFFEC.  TOTAL    GAS',
```

```
158           2'    WATER    VOL.    VOID     AVERAGE'/' NO.  (MIN.)   SUB',
159           6'-   PRESS.',
160           3' STRESS  VOLUME  VOLUME  VOLUME  STRAIN  RATIO    COMPRESS.'/,
161           4T16,'STEPS   **BOTH IN KPA*  ******ALL IN CM3******   (%)',T82,
162           5'KPA(-1)'/)
163            VSTRN=(VT1-VTI2)/VTI2*100.
164            WRITE(6,40)Z2,ES1,VT1,VG1,VW1,VSTRN,VOIDP
165         40 FORMAT(T5,'0     0.0',T24,2(F6.2,2X),F6.1,2X,2(F6.2,2X),
166           1F6.3,2X,F5.4)
167            VG2=VG1
168            VW2=VW1
169            P2=P1
170            ES2=ES1
171            VT2=VT1
172            NTSTEP=MAX/DELTM
173            IF(NTSTEP.LE.500)GOTO 43
173.5          AZMAX=MAX/500.
174            WRITE(6,44)E(I),AZMAX
175         44 FORMAT('0**ERROR**FOR E=',F6.5,', TIME STEP MUST BE',
175.5         1' GREATER THAN ',F5.2)
176            STOP
177         43 DO 28 J=1,NTSTEP
178            F2=(KBAR/P2-H*VW2-VG2)
181            IF((F1*F2).GT.0.0)GOTO 31
186         60 WRITE(6,32)E(I),J
187         32 FORMAT(' FOR E=',F7.5,', AND AT THE BEGINNING OF STEP NO.',
188           1I4,', GAS SORPTION COMPLETE.')
189            GOTO 26
190         31 DELUC=0.0
191            DO 29 K=1,10
192            NITS=2**(K-1)
193            DM=DELTM/NITS
194            VG3=VG2
195            VW3=VW2
196            P3=P2
197            ES3=ES2
198            VT3=VT2
199            DO 33 L=1,NITS
200            VOID=(VG3+VW3)/VS
201            F=(KBAR/P3-H*VW3-VG3)
202            CT=CC*ALOG10((ES3+10.)/ES3)/(1+VOID)/10.
203            DUC=0.0
204            DO 34 M=1,100
205            A=CT*VT3+CW*VW3
206            D=E(I)*DM*F
207            C=-1.*P3*D
208            B=VG3+P3*A+E(I)*DM*H*VW3/2
209            DU=(-B+SQRT(B*B-4*A*C))/(2*A)
210         36 IF(ABS(DU-DUC).LE.TOL)GOTO 35
211            CT=CC*ALOG10((ES3-DU)/ES3)/(1+VOID)/(-DU)
212            DUC=DU
213         34 CONTINUE
214            WRITE(6,37)E(I),J,NITS,L
215         37 FORMAT(' FOR E=',F7.5,', STEP NO.',I4,', NO OF SUBSTEPS=',I3,
216           1', AND SUBSTEP NO.',I3/' NO CONVERGENCE FOR DELTAU AND SOIL',
217           2' COMPRESSIBILITY')
218            STOP
219         35 VG3=(P3/(P3+DU))*(VG3+D-E(I)*DM*H*VW3*DU/(2*P3))
220            VW3=VW3*(1-CW*DU)
221            VT3=VT3*(1+CT*DU)
```

```
222            P3=P3+DU
223            ES3=ES3-DU
224          33 CONTINUE
225            DELU=P3-P2
226            IF(ABS(DELU-DELUC).LE.TOL)GOTO 38
227            DELUC=DELU
228          29 CONTINUE
229            WRITE(6,39)E(I),J
230          39 FORMAT(' FOR E=',F7.5,', AND STEP NO.',I4,', THERE IS NO',
231           2' CONVERGENCE',
232           1' ON DECREASING DELTA TIME, EVEN WITH 512 SUBSTEPS')
233            STOP
234          38 VG2=VG3
235            VW2=VW3
236            P2=P3
237            VT2=VT3
238            VOIDN=(VG2+VW2)/VS
239            VOIDAV=(VOIDN+VOIDP)/2.
240             IF(ABS(ES3-ES2).LT.0.1)GOTO 55
241            CT=CC*ALOG10(ES3/ES2)/(1+VOIDAV)/(ES3-ES2)
242            GOTO 56
243          55 CT=0.4342944819*CC/(1+VOIDAV)/ES3
244          56 VOIDP=VOIDN
245            ES2=ES3
246            NSTEPS(I)=J
247            TIME(J,I)=J*DELTM
248            PRESS(J,I)=P2-101.3
249            VSTRN=(VT2-VTI2)/VTI2*100.
250            TJCS=J*DELTM
251            IJ=IFIX(FLOAT(J)/50.)*50
252            IF(IJ.NE.J)GOTO 41
253            WRITE(6,27)TITLE,E(I)
254          41 WRITE(6,42)J,TJCS,NITS,PRESS(J,I),ES2,VT2,VG2,VW2,VSTRN,VOIDP,CT
255          42 FORMAT(1X,I4,2X,F6.1,3X,I3,4X,2(F6.2,2X),F6.1,2X,2(F6.2,2X),
256           1F6.3,2X,F5.4,2X,E12.5)
257          28 CONTINUE
258            WRITE(6,45)
259          45 FORMAT('0 *WARNING* EQUILIBRIUM FOR GAS SORPTION HAS NOT BEEN',
260           1' ACHIEVED AFTER 500 MINUTES')
261          26 CONTINUE
262       C
263       C      PLOT RESULTS
264       C
265            CALL GPEP5(1,2,3)
266            CALL GPEP8(0.25,0.3)
276            CALL GRAPH(XA,XB,1.,1)
277            CALL MAXMIN(0.,1000.,MAX,MIN,APRESS,NRGS)
277.1          Y1(1)=Z2
277.2          Y1(2)=Z3
277.4          CALL MAXMIN(MAX,MIN,MAX,MIN,Y1,2)
278            DO 48 I=1,NE
279          48 CALL MAXMIN(MAX,MIN,MAX,MIN,PRESS(1,I),NSTEPS(I))
280            CALL GRAPH(YA,YB,1.,1)
281            CALL SORT(ATIME,APRESS,XB,YB,NRGS,K,X1,Y1,0)
282            CALL PLOTIT(X1,Y1,K,1,1,1,1,XA,XB,PLOTSZ,YA,YB,PLOTSZ,7)
283            NP=132
284            DO 49 I=1,NE
285            CALL SORT(TIME(1,I),PRESS(1,I),XB,YB,NSTEPS(I),K,X1,Y1,0)
286            CALL PLOTIT(X1,Y1,K,NP,1,1,3,XA,XB,PLOTSZ,YA,YB,PLOTSZ,7)
287            NP=NP+1
```

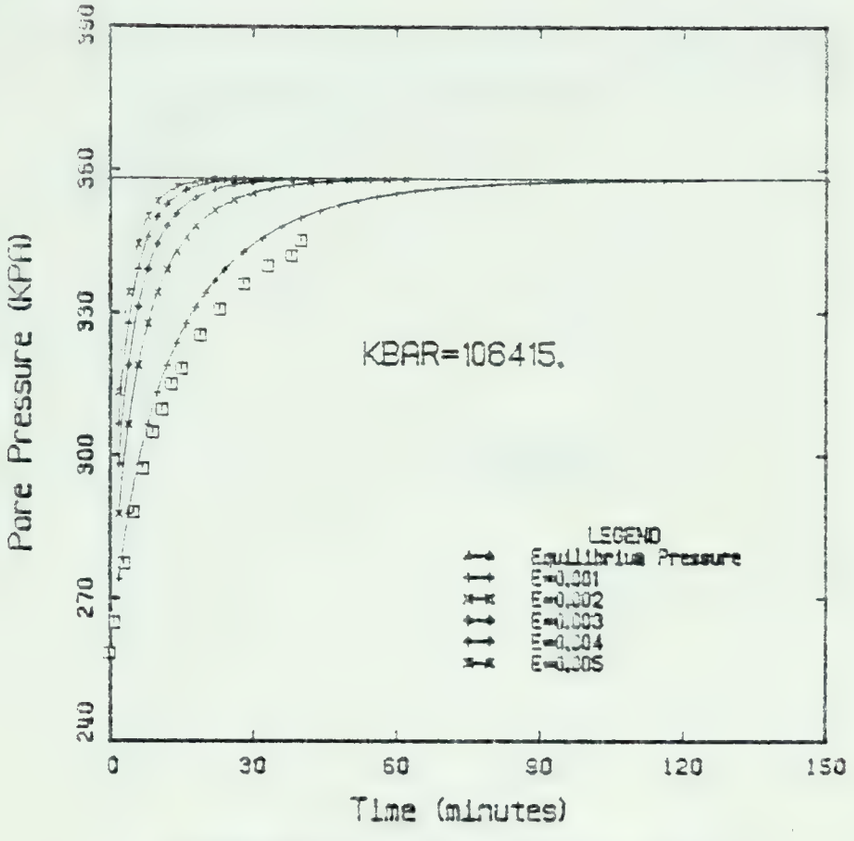
```
288         49 CONTINUE
289            X1(1)=0.0
290            X1(2)=PLOTSZ*XB
291            Y1(1)=Z3
292            Y1(2)=Z3
293            CALL PLOTIT(X1,Y1,2,2,1,1,2,XA,XB,PLOTSZ,YA,YB,PLOTSZ,7)
293.2          Y1(1)=Z2
293.4          CALL PLOTIT(X1,Y1,1,12,1,1,1,XA,XB,PLOTSZ,YA,YB,PLOTSZ,7)
293.7          Y1(1)=Z1
293.8          CALL PLOTIT(X1,Y1,1,11,1,1,1,XA,XB,PLOTSZ,YA,YB,PLOTSZ,7)
294            CALL PLOTIT(X1,Y1,2,0,1,1,1,XA,XB,PLOTSZ,YA,YB,PLOTSZ,7)
295            STOP
296            END
297            SUBROUTINE MAXMIN(SMAX,SMIN,FMAX,FMIN,Z,K)
298            DIMENSION Z(500)
299            FMAX=SMAX
300            FMIN=SMIN
301            DO 1 I=1,K
302            IF(Z(I).GT.FMAX)FMAX=Z(I)
303            IF(Z(I).LT.FMIN)FMIN=Z(I)
304          1 CONTINUE
305            RETURN
306            END
307            SUBROUTINE GRAPH(ZERO,SCALE,SINT,IDIR)
308            REAL MAX,MIN,FAC(16)
309            COMMON MAX,MIN,PLOTSZ
310            DIFF=MAX-MIN
311            SCALE=DIFF/PLOTSZ
312            Q=1.
313            FAC(1)=1.
314            DO 2 I=2,12,5
315            FAC(I)=Q*2.
316            FAC(I+1)=Q*3.
317            FAC(I+2)=Q*4.
318            FAC(I+3)=Q*5.
319            FAC(I+4)=Q*10.
320            Q=Q*10.
321          2 CONTINUE
322            DO 1 I=1,16
323            TEST=FAC(I)*SINT
324            IF(SCALE.GT.TEST)GOTO 1
325            SCALE=TEST
326            GOTO 5
327          1 CONTINUE
328            ENTRY GRAPH2(ZERO,SCALE,SINT,IDIR,I)
329            SCALE=ABS(SCALE)
330          5 ICHECK=0
331            IF(IDIR.GT.0)GOTO 3
332            TZERO=MAX
333            IF(TZERO.GT.0.)TZERO=TZERO+SCALE
334            GOTO 4
335          3 TZERO=MIN
336            IF(TZERO.LT.0.)TZERO=TZERO-SCALE
337          4 M=IFIX(TZERO/SCALE)
338            ZERO=FLOAT(M)*SCALE
339         11 IF(IDIR.GT.0)GOTO 6
340            SIMUL=ZERO-PLOTSZ*SCALE
341            IF(SIMUL.LE.MIN)GOTO 7
342         10 IF(ICHECK.EQ.1)GOTO 8
343            M=IFIX(2.*TZERO/SCALE)
```

```
   344            ZERO=FLOAT(M)*SCALE/2.
   345            ICHECK=1
   346            GOTO 11
   347          8 IF(I.LT.16)GOTO 9
   348             SCALE=SCALE*10.
   349             GOTO 5
   350          9 SCALE=FAC(I+1)*SINT
   351            GOTO 5
   352          6 SIMUL=ZERO+PLOTSZ*SCALE
   353            IF(SIMUL.GE.MAX)GOTO 7
   354            GOTO 10
   355          7 IF(IDIR.LT.0)SCALE=-SCALE
   356            RETURN
   357            END
   358            SUBROUTINE SORT(X,Z,SCALEX,SCALEY,ND,K,X1,Y1,IPLOT)
   359            REAL X(500),Z(500),X1(500),Y1(500)
   360            K=1
   361            X1(K)=X(1)
   362            Y1(K)=Z(1)
   363            J=1
   364          3 DO 1 I=2,ND
   365            IF(IPLOT.GE.1)GOTO 2
   366            IF(X(I).LE.500.)GOTO 2
   367            RETURN
   368          2 A=(X(I)-X(J))/SCALEX
   369            B=(Z(I)-Z(J))/SCALEY
   370            DIST=SQRT(A**2+B**2)
   371            IF(DIST.LT.0.1)GOTO 1
   372            K=K+1
   373            J=I
   374            X1(K)=X(I)
   375            Y1(K)=Z(I)
   376          1 CONTINUE
   377            RETURN
   378            END
End of file
```

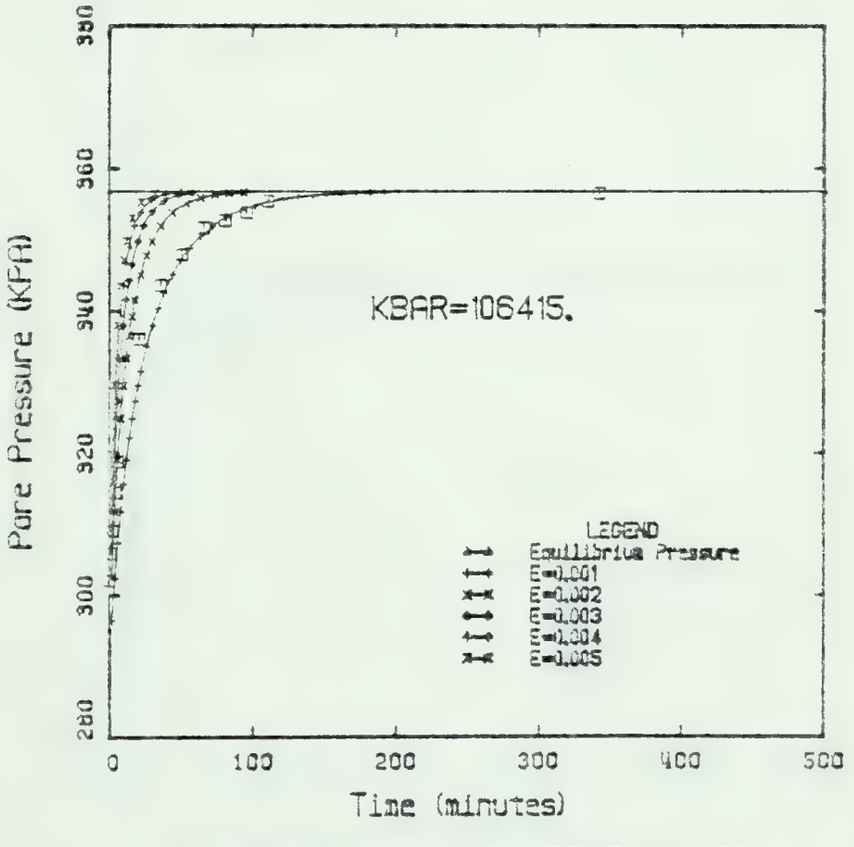
APPENDIX G

P vs t BEHAVIOUR FOR ALL UNDRAINED TESTS

COMPARISON OF ACTUAL AND PREDICTED BEHAVIOUR

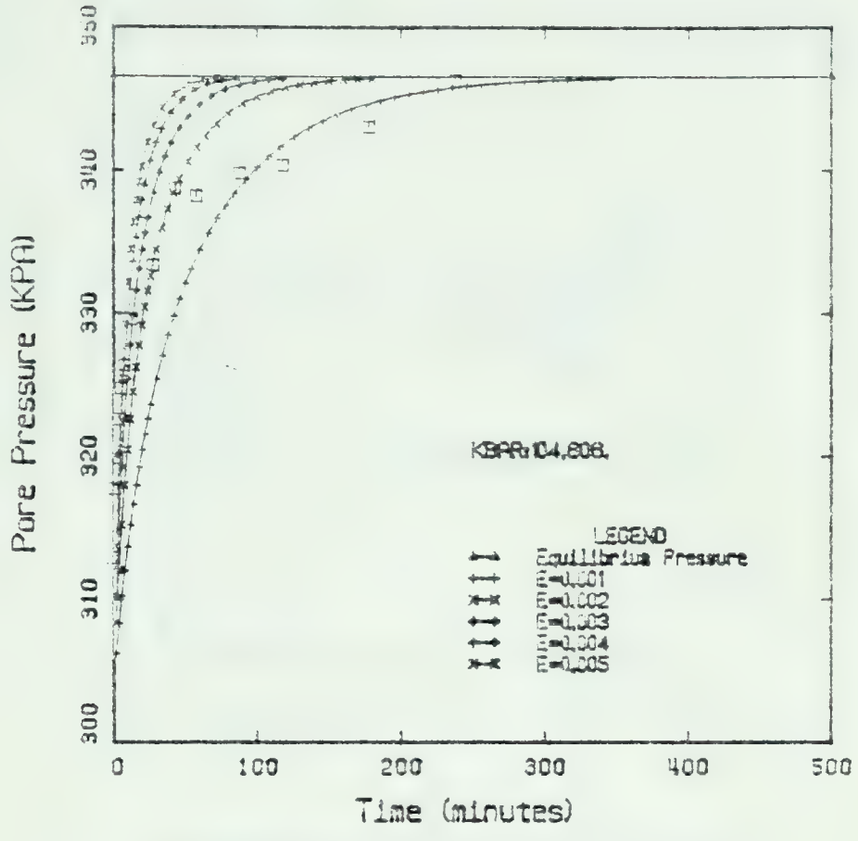


UNDRAINED ANALYSIS, TEST NO. 7C

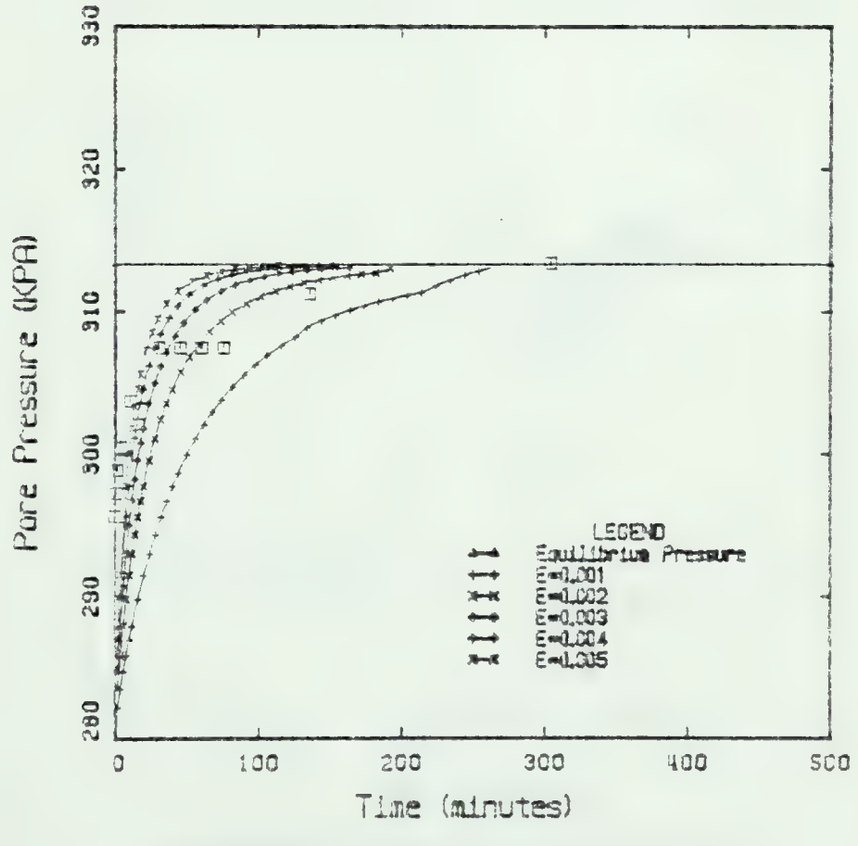


UNDRAINED ANALYSIS, TEST NO. 7D

Figures G.1 and G.2

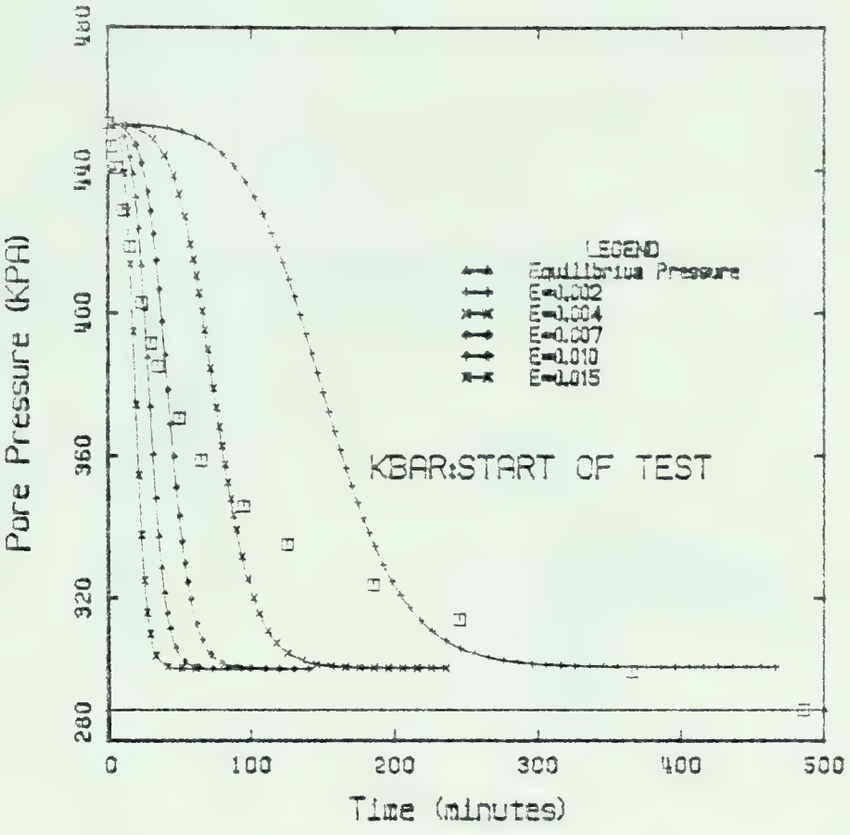


UNDRAINED ANALYSIS, TEST NO. 7E

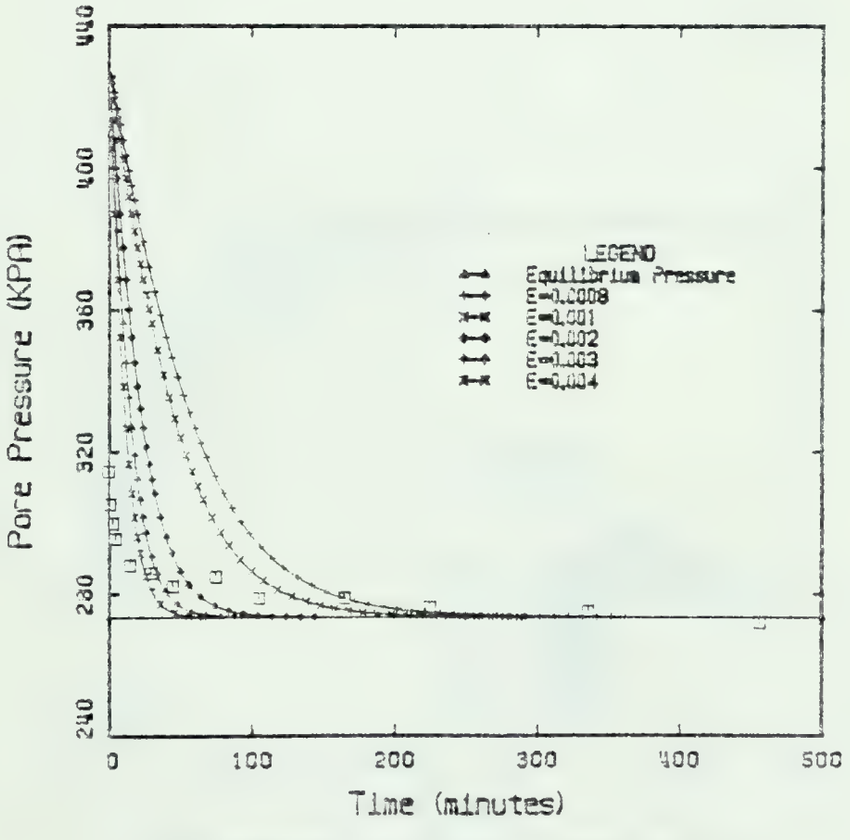


UNDRAINED ANALYSIS, TEST NO. 7F

Figures G.3 and G.4

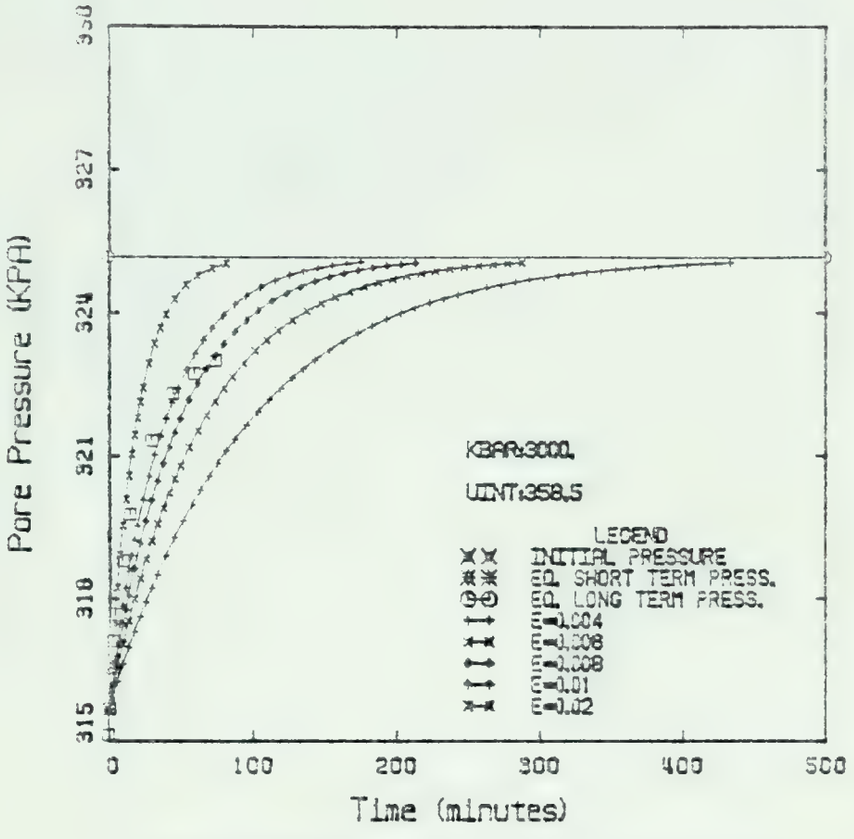


UNDRAINED ANALYSIS, TEST NO. 7J

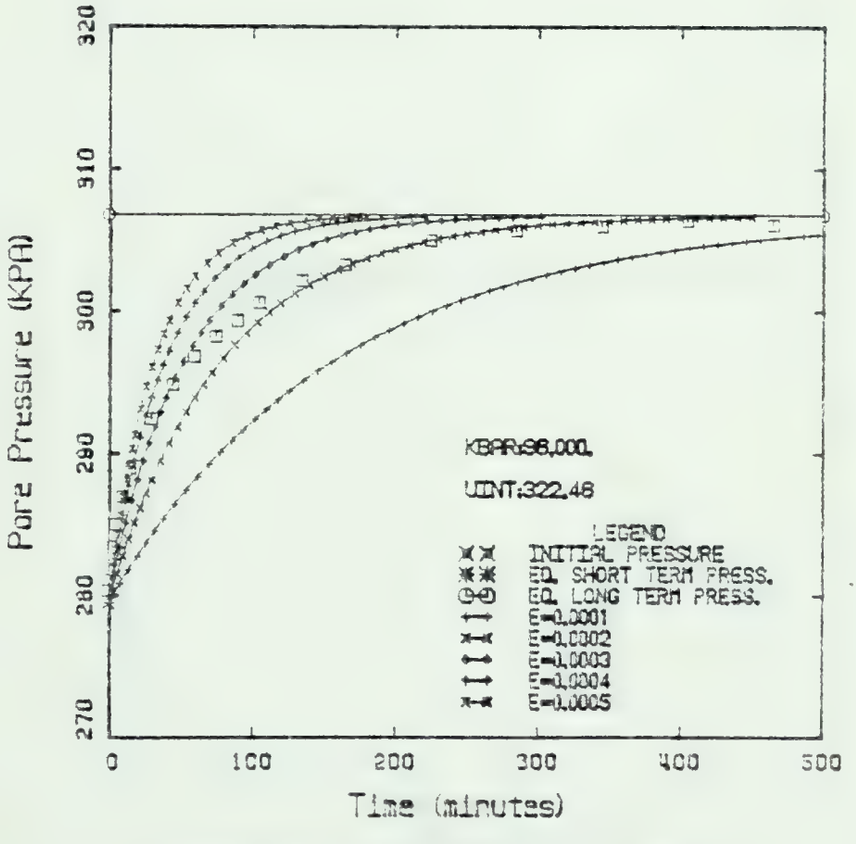


UNDRAINED ANALYSIS, TEST NO. 7K

Figures G.5 and G.6

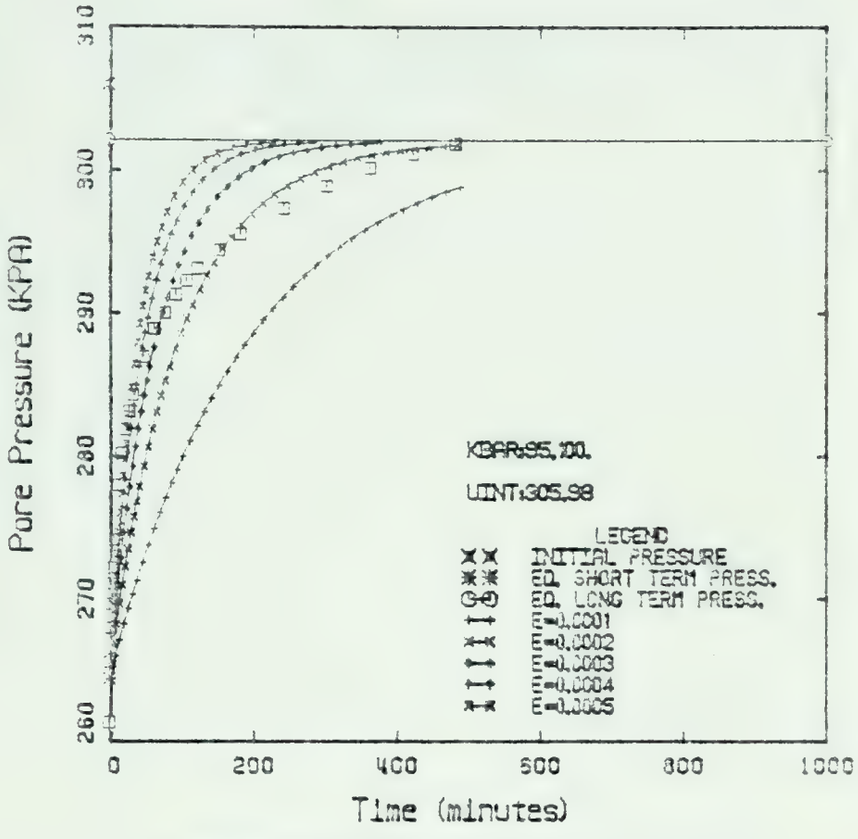


UNDRAINED ANALYSIS, TEST NO. 9F

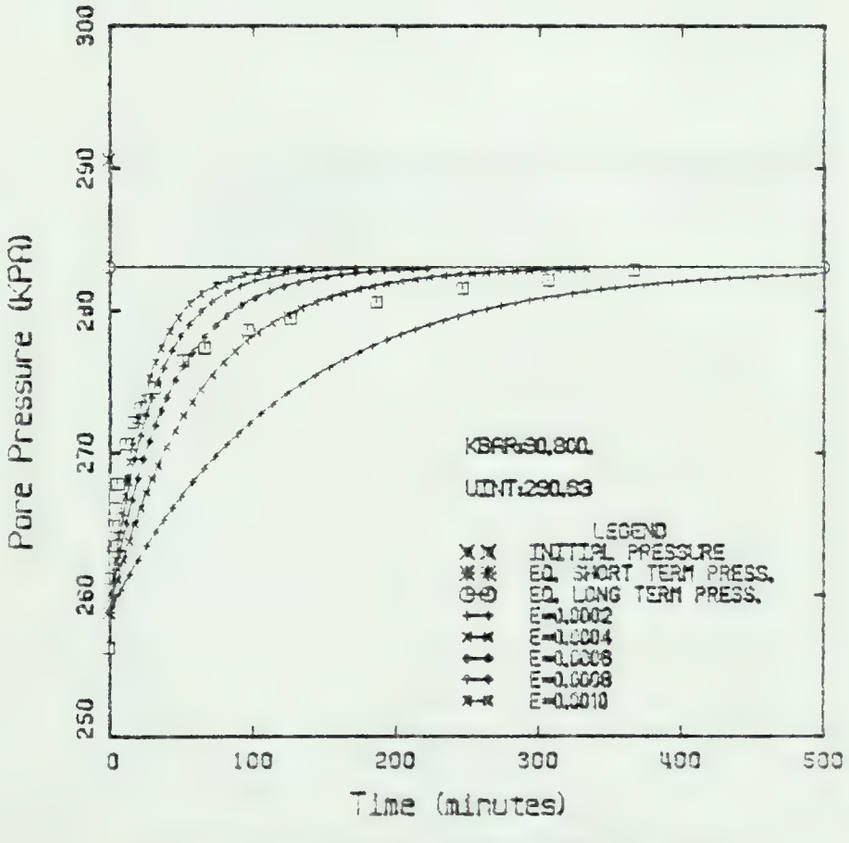


UNDRAINED ANALYSIS, TEST NO. 9G

Figures G.7 and G.8

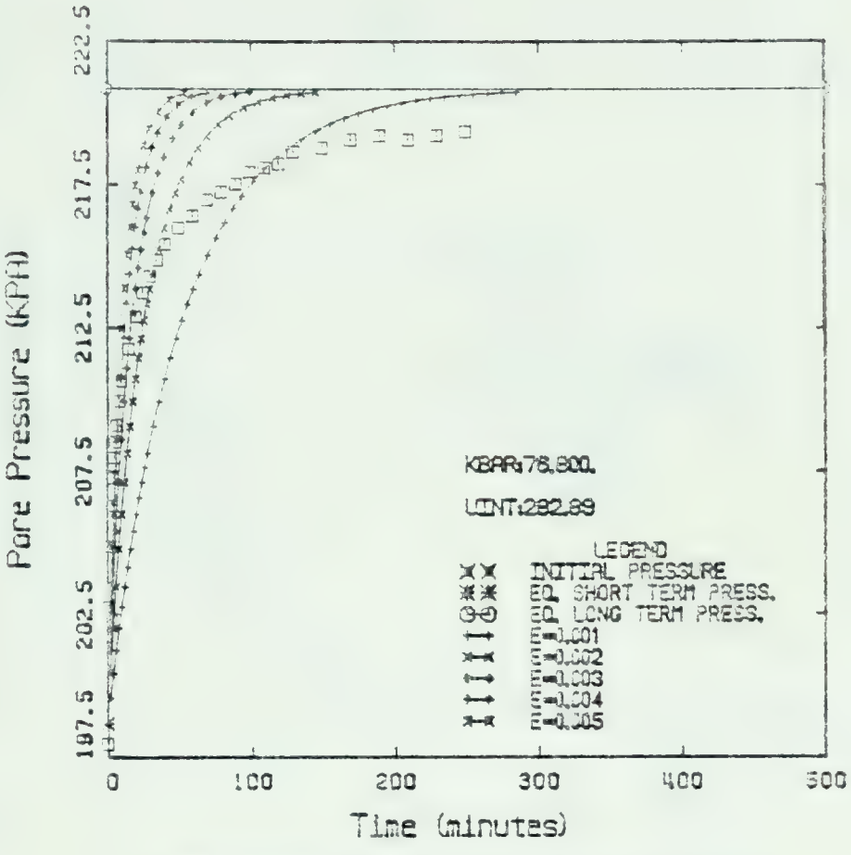


UNDRAINED ANALYSIS, TEST NO. 9H

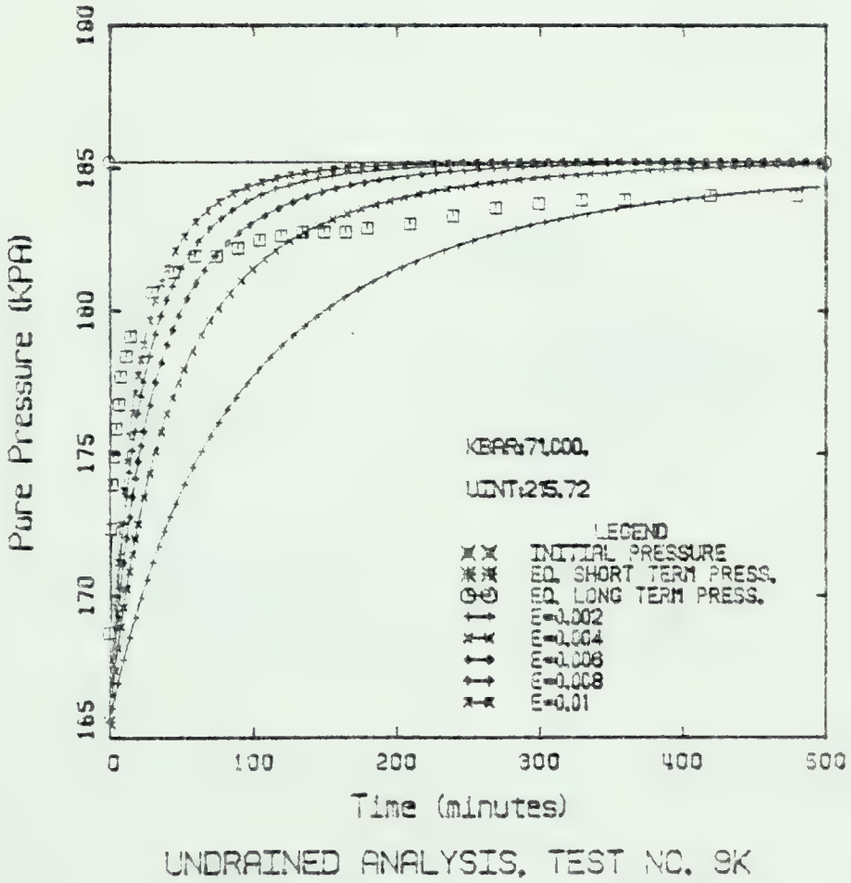


UNDRAINED ANALYSIS, TEST NO. 9I

Figures G.9 and G.10

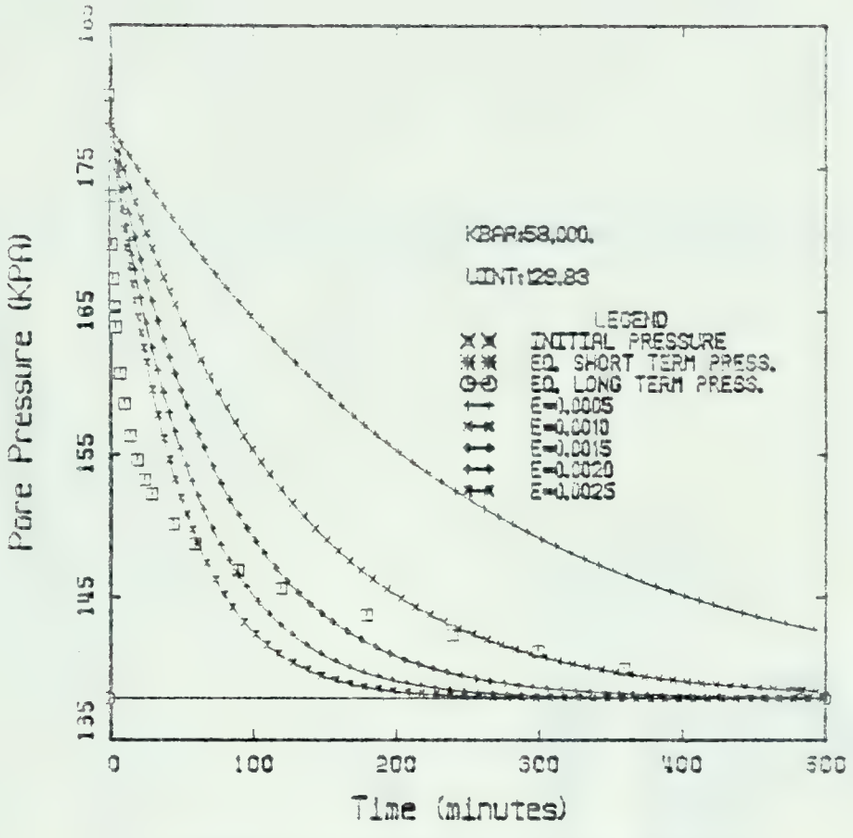


UNDRAINED ANALYSIS, TEST NO. 9J

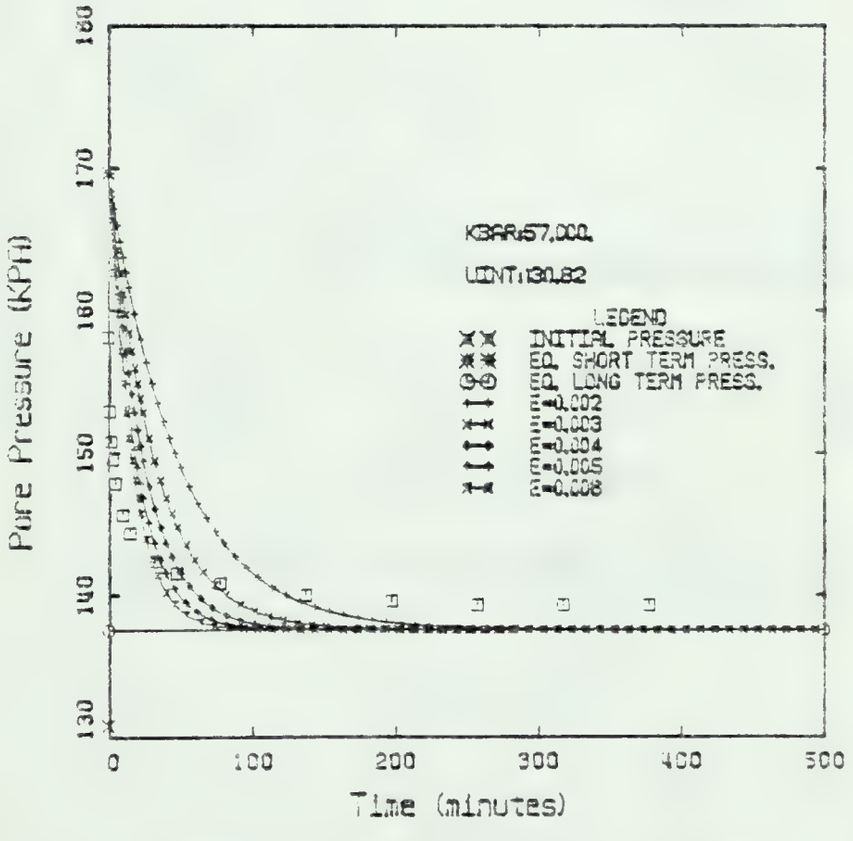


UNDRAINED ANALYSIS, TEST NO. 9K

Figures G.11 and G.12



UNDRAINED ANALYSIS, TEST NO. 9D



UNDRAINED ANALYSIS, TEST NO. 9P

Figures G.13 and G.14

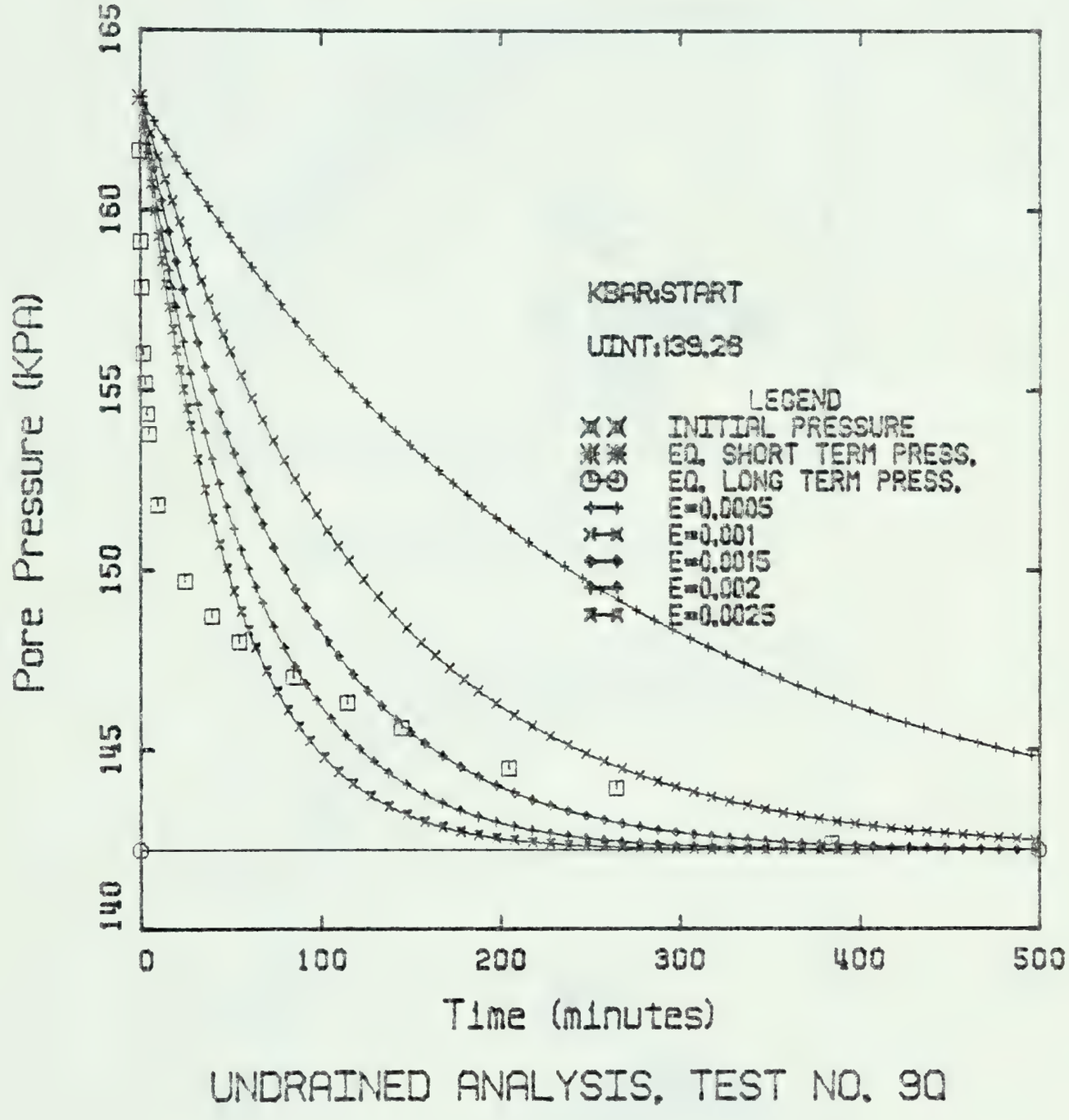
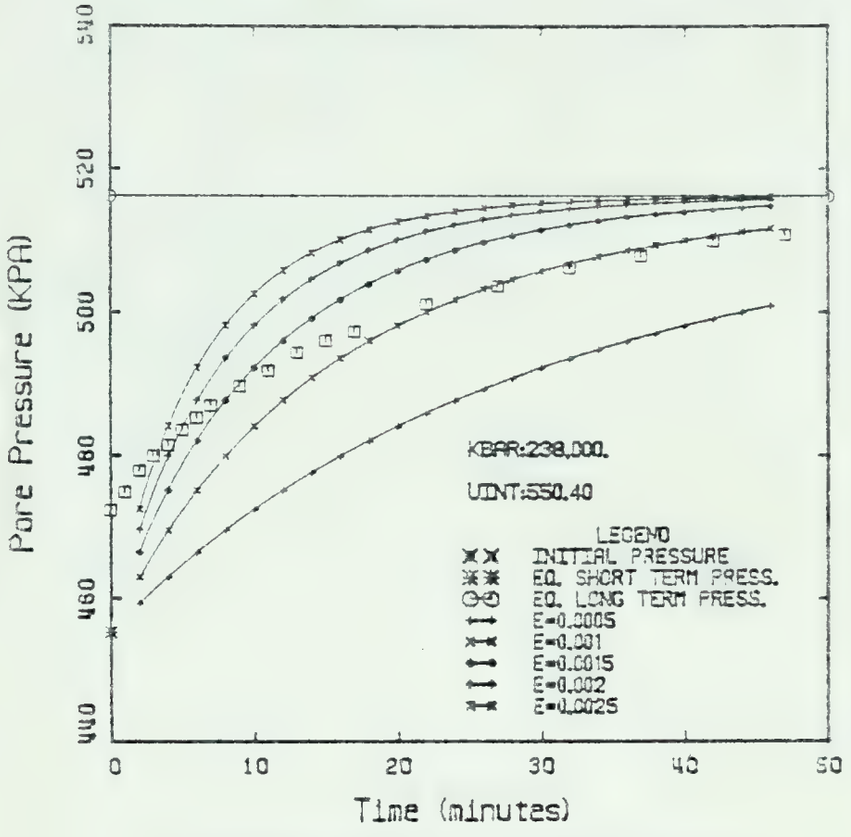
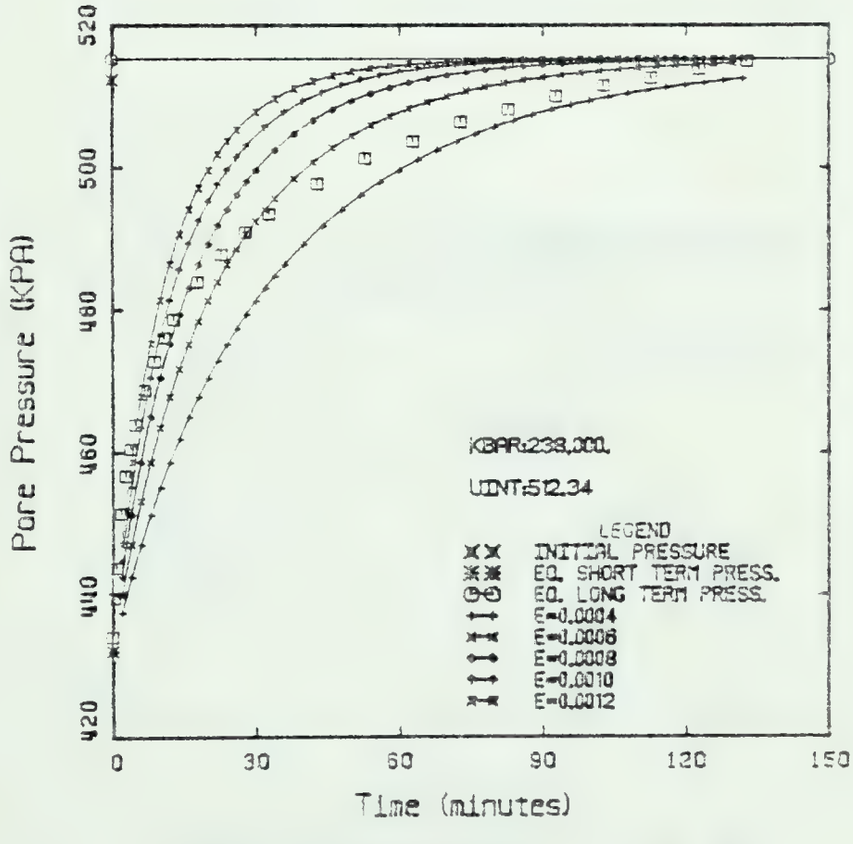

Pore Pressure (KPA)
165
160
155
150
145
140
0
100
200
300
400
500
Time (minutes)
KBAR:START
UINT:139.28
LEGEND
INITIAL PRESSURE
EQ. SHORT TERM PRESS.
EQ. LONG TERM PRESS.
E=0.0005
E=0.001
E=0.0015
E=0.002
E=0.0025
UNDRAINED ANALYSIS, TEST NO. 90

Figure G.15

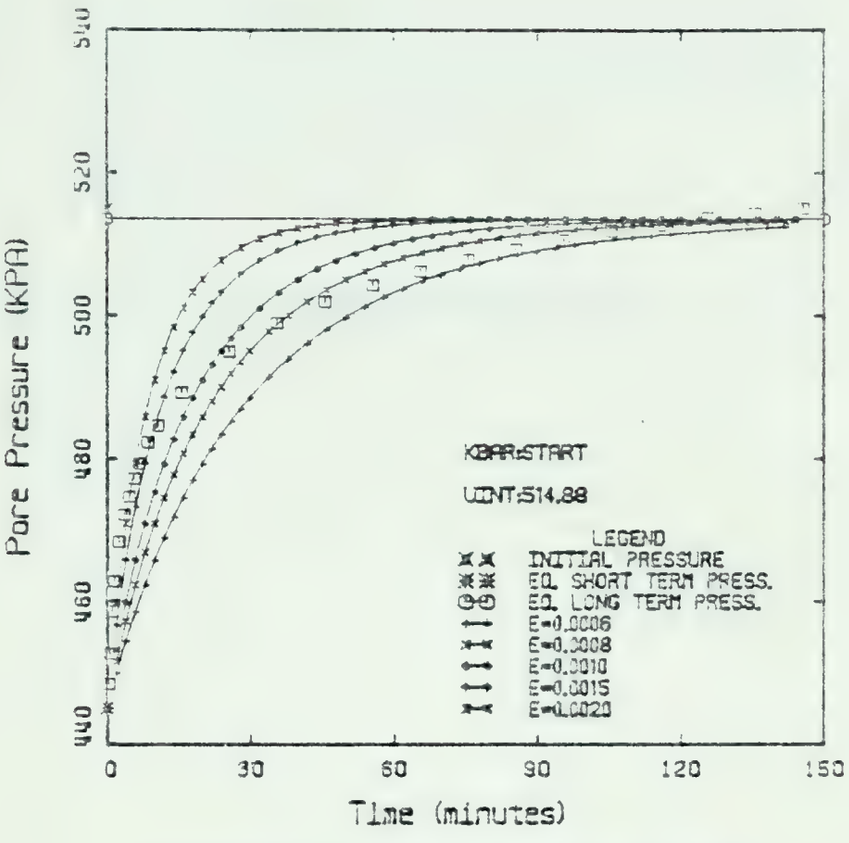


UNDRAINED ANALYSIS, TEST NO. 12C

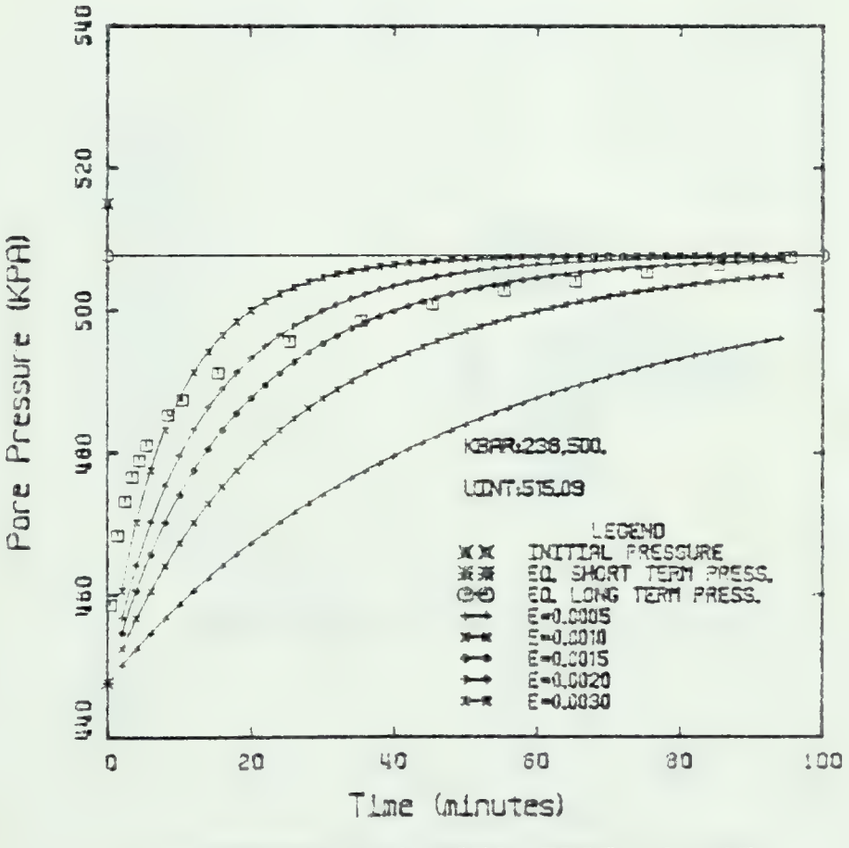


UNDRAINED ANALYSIS, TEST NO. 12D

Figures G.16 and G.17

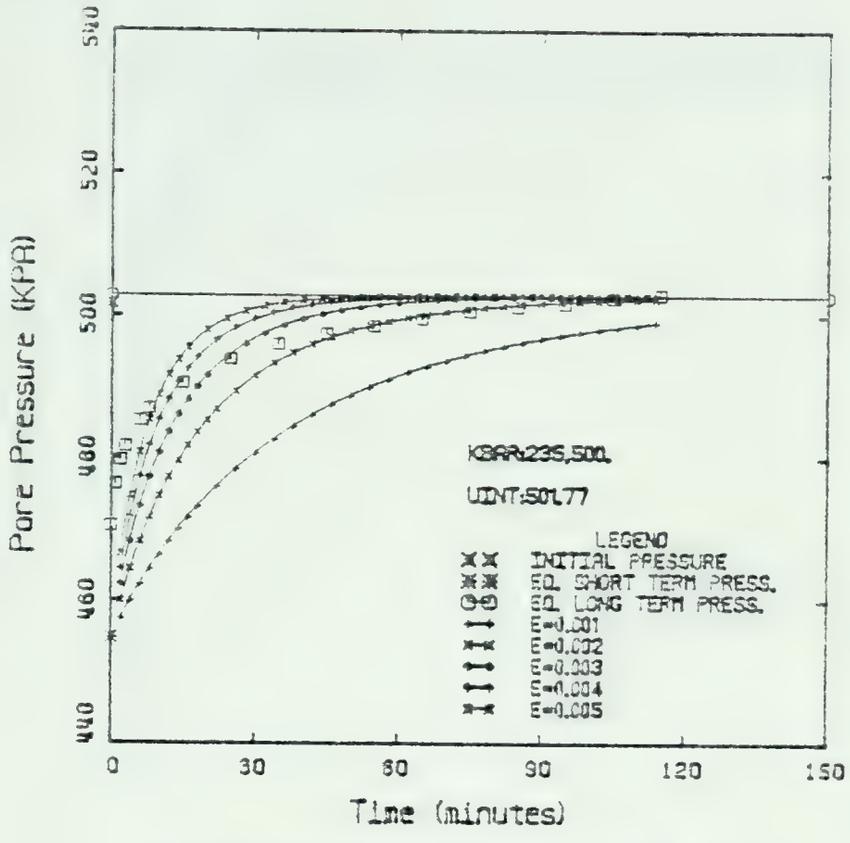


UNDRAINED ANALYSIS, TEST NO. 12E

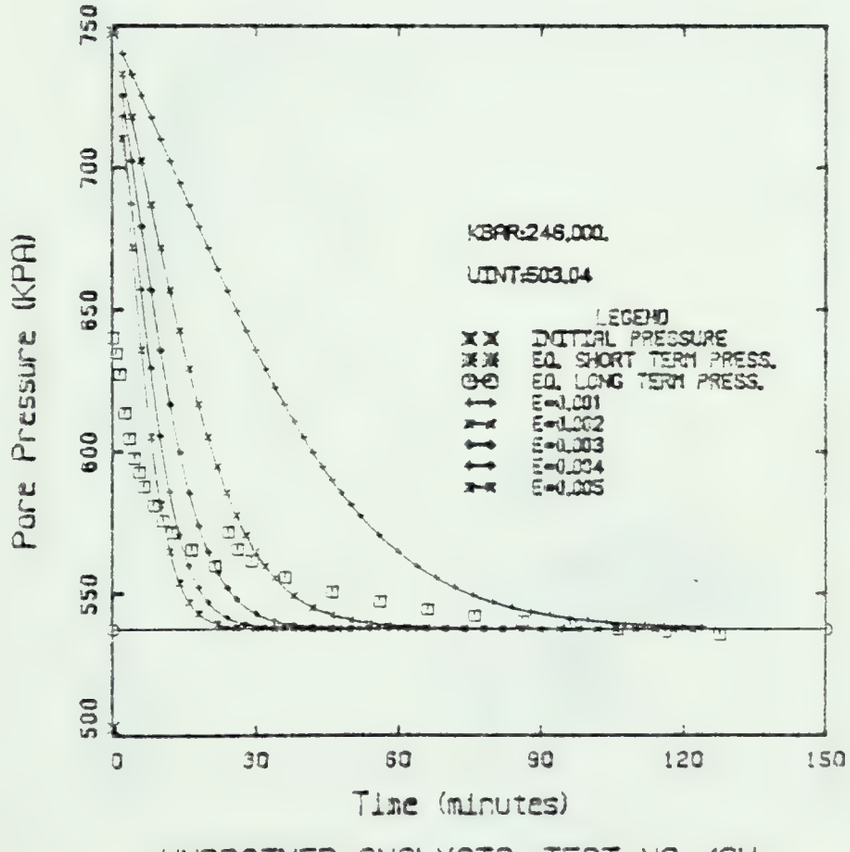


UNDRAINED ANALYSIS, TEST NO. 12F

Figures G.18 and G.19

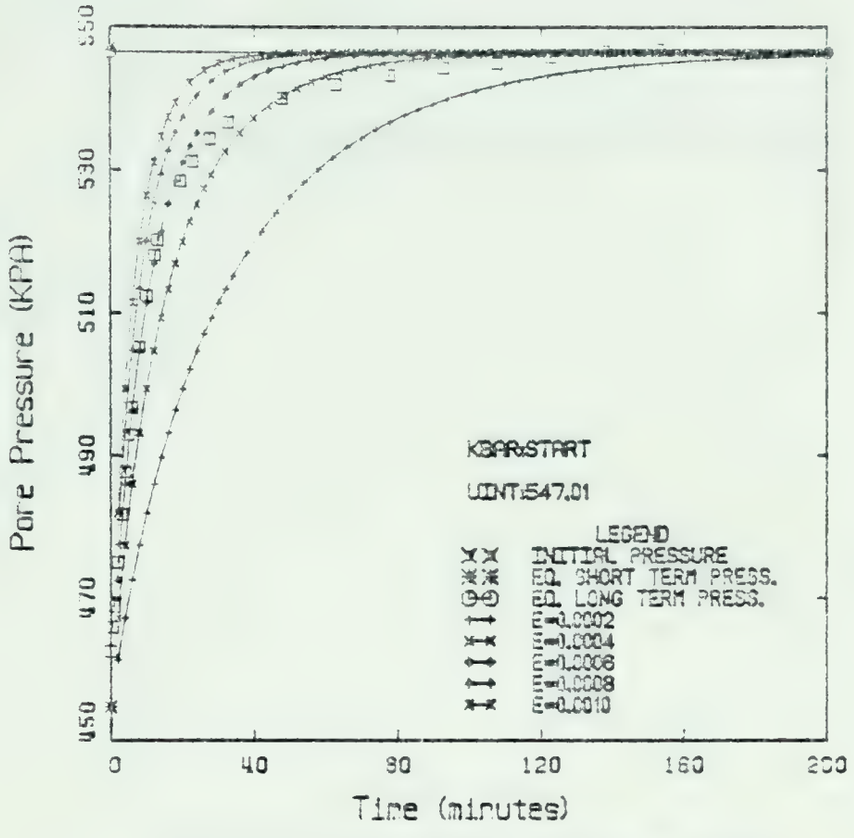


UNDRAINED ANALYSIS, TEST NO. 12G

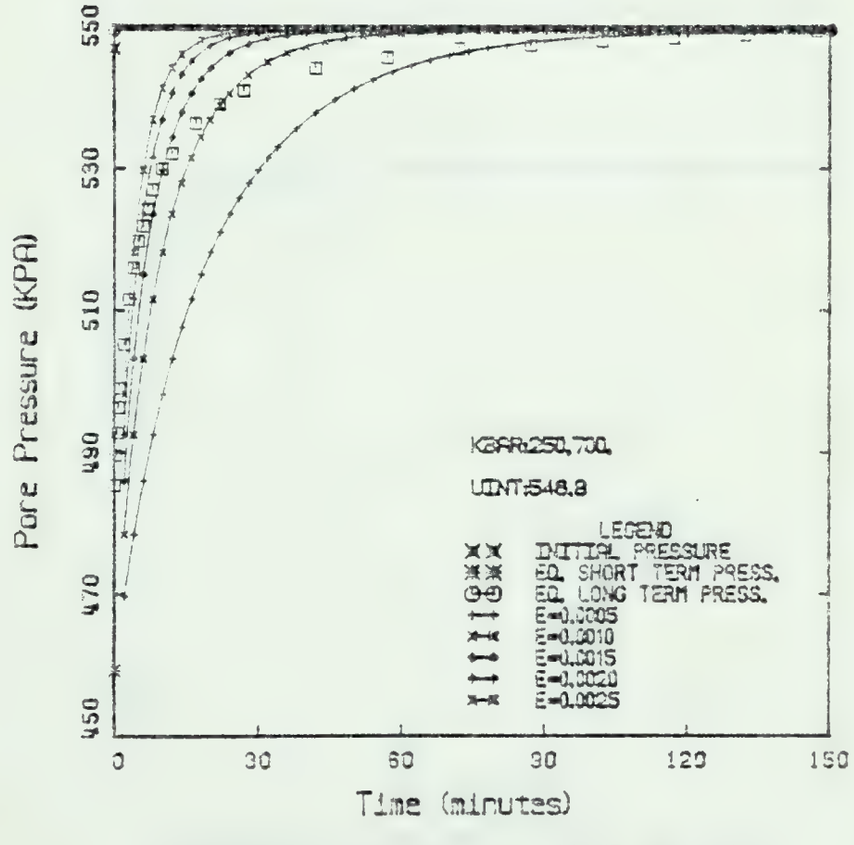


UNDRAINED ANALYSIS, TEST NO. 12H

Figures G.20 and G.21

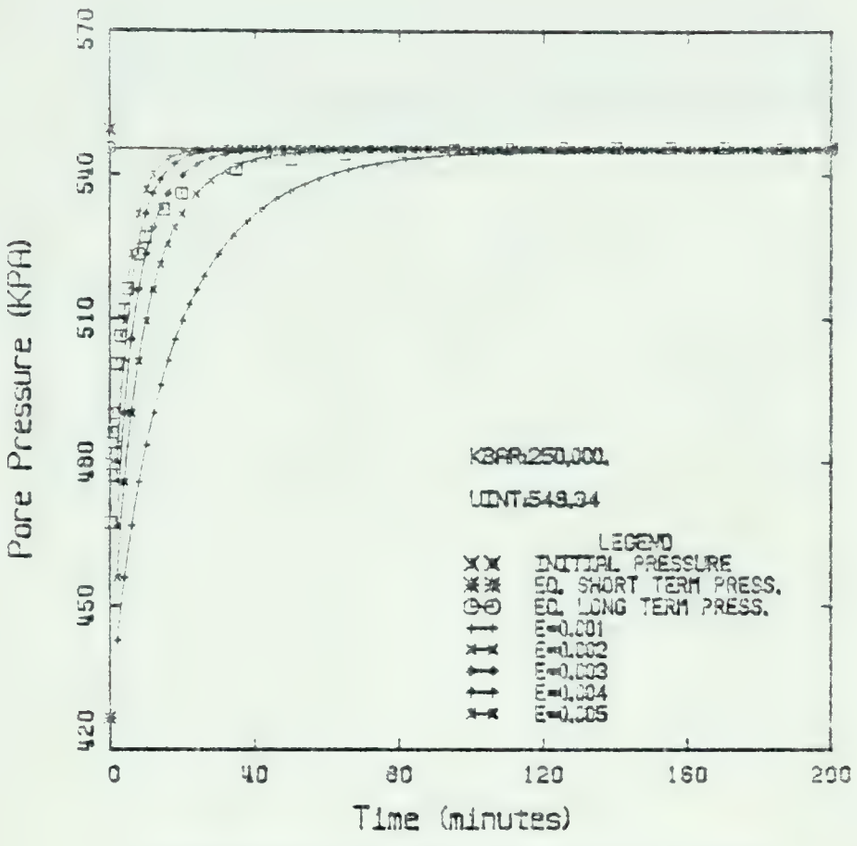


UNDRAINED ANALYSIS, TEST NO. 15D

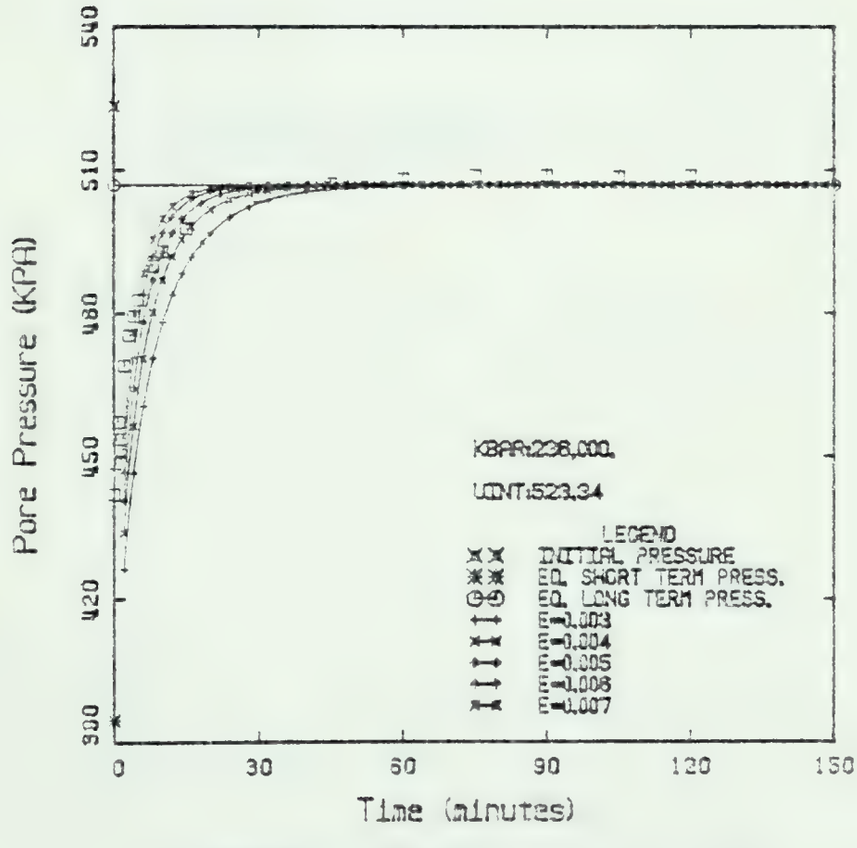


UNDRAINED ANALYSIS, TEST NO. 15E

Figures G.22 and G.23

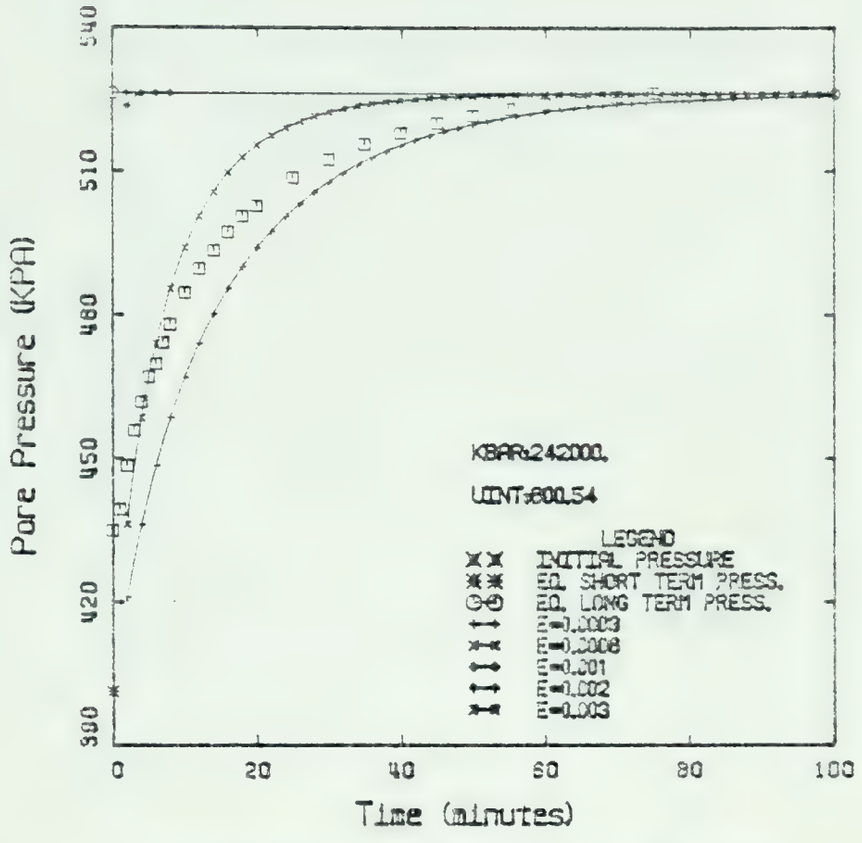


UNDRAINED ANALYSIS, TEST NO. 15F

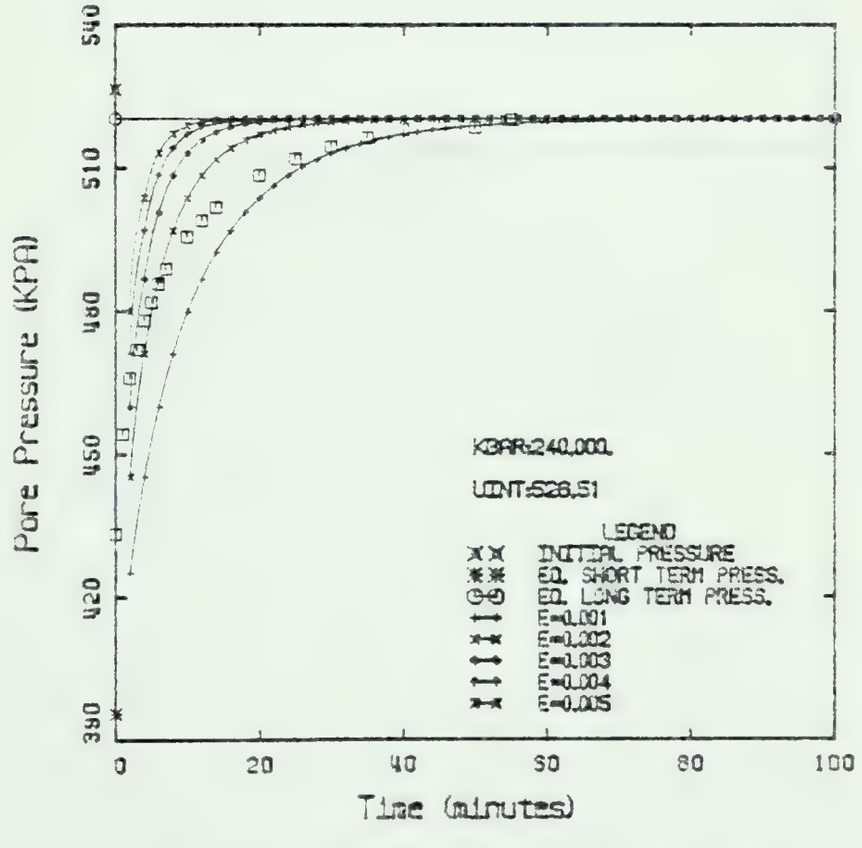


UNDRAINED ANALYSIS, TEST NO. 15G

Figures G.24 and G.25

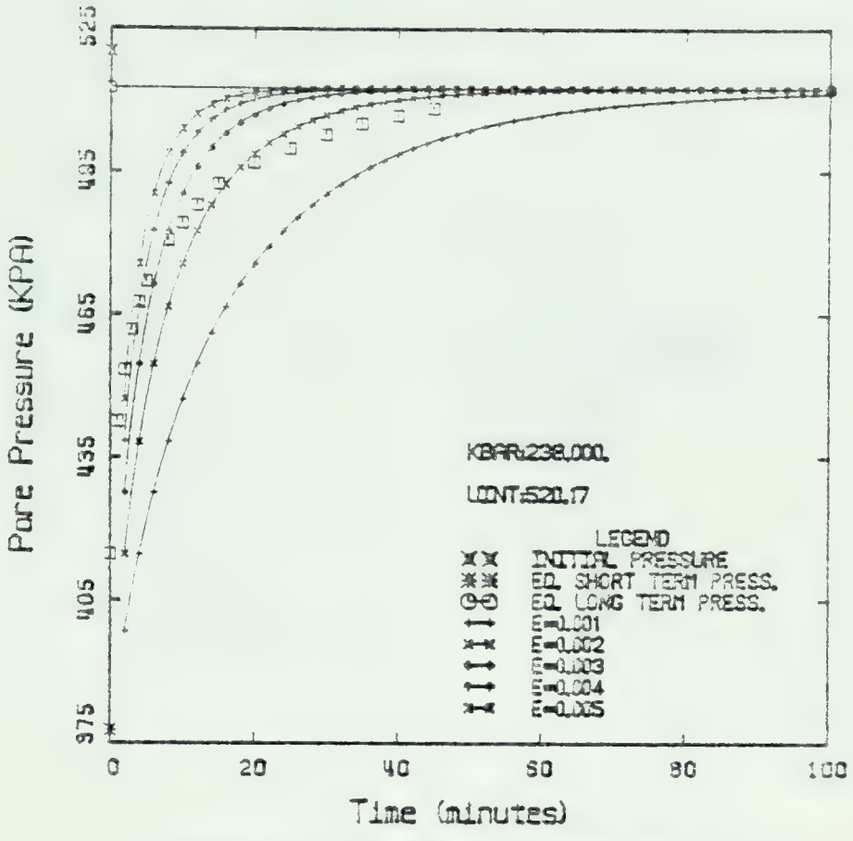


UNDRAINED ANALYSIS, TEST NO. 21A

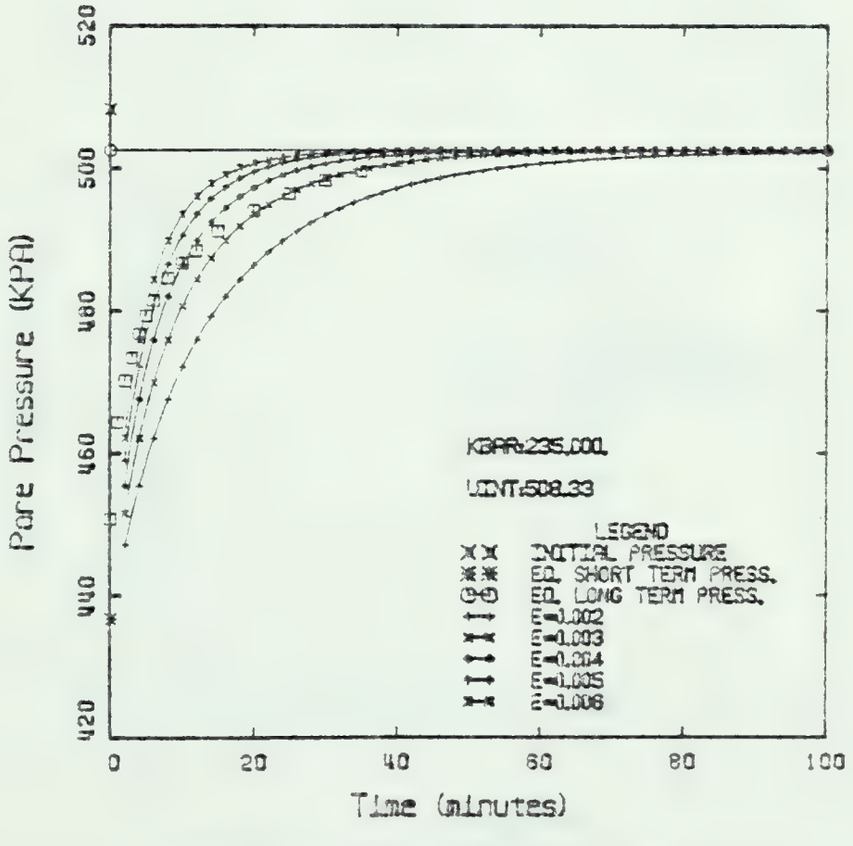


UNDRAINED ANALYSIS, TEST NO. 21B

Figures G.26 and G.27

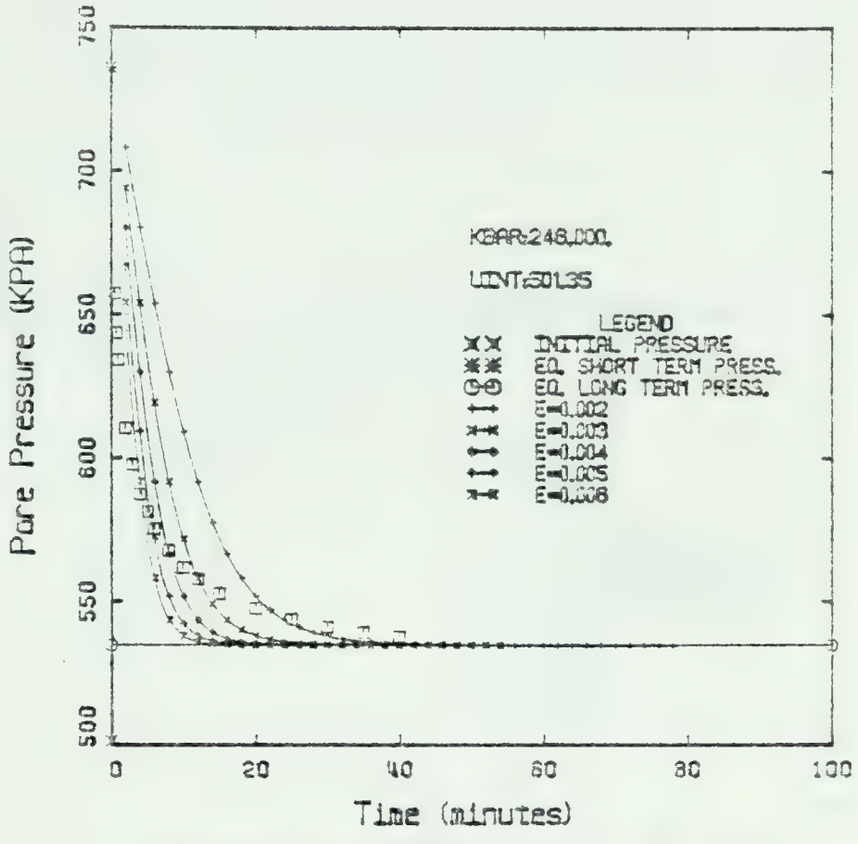


UNDRAINED ANALYSIS. TEST NO. 21C

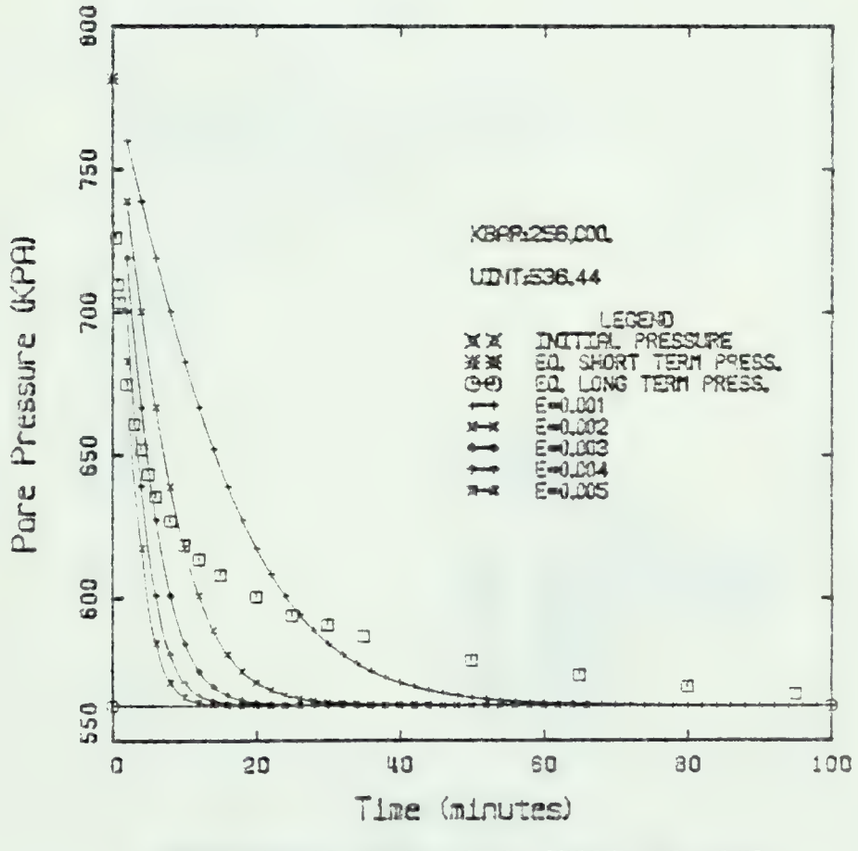


UNDRAINED ANALYSIS. TEST NO. 21D

Figures G.28 and G.29

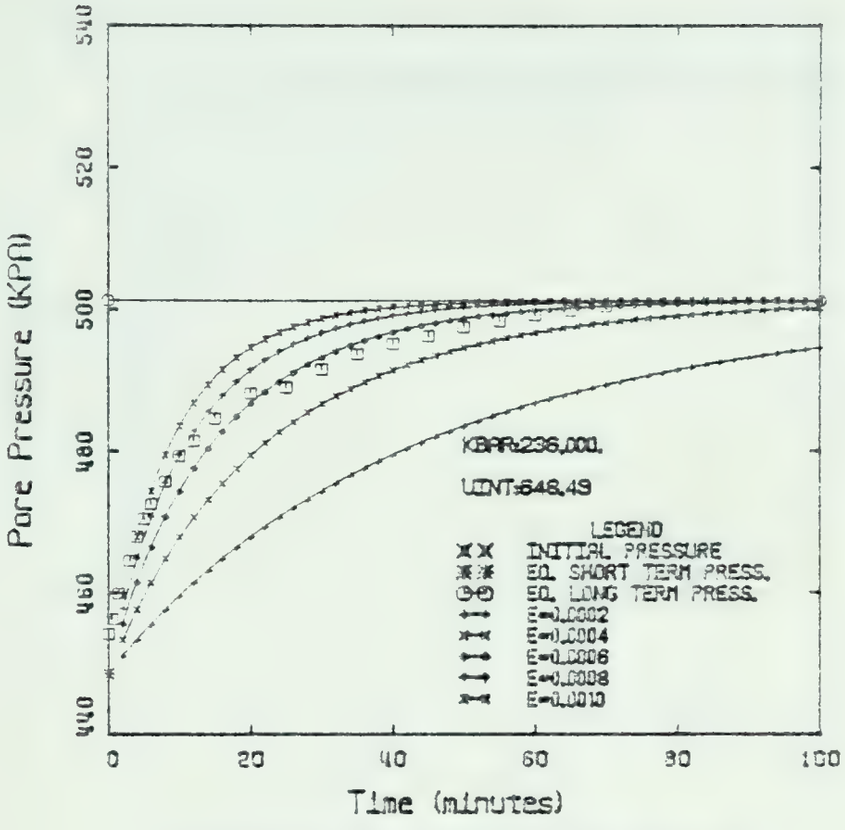


UNDRAINED ANALYSIS, TEST NO. 21E

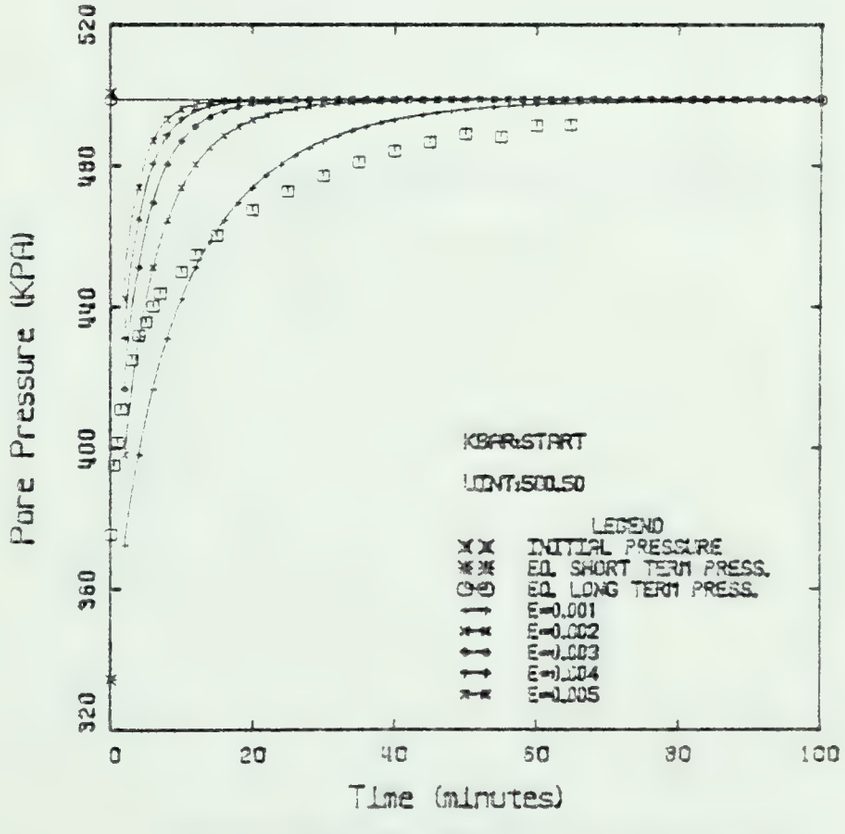


UNDRAINED ANALYSIS, TEST NO. 21F

Figures G.30 and G.31

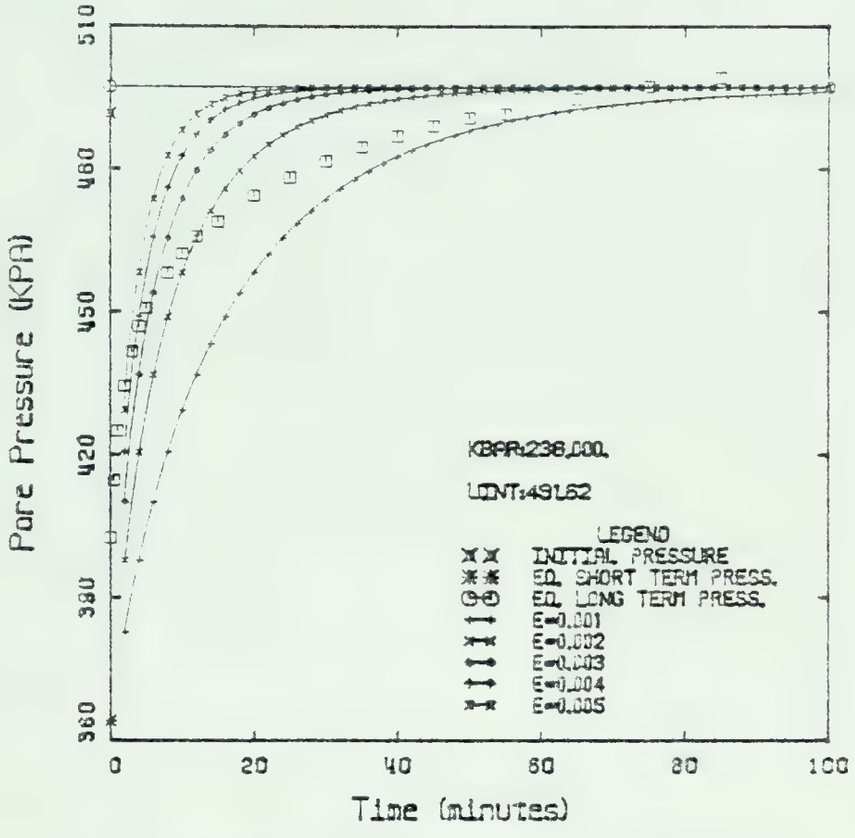


UNDRAINED ANALYSIS, TEST NO. 22A

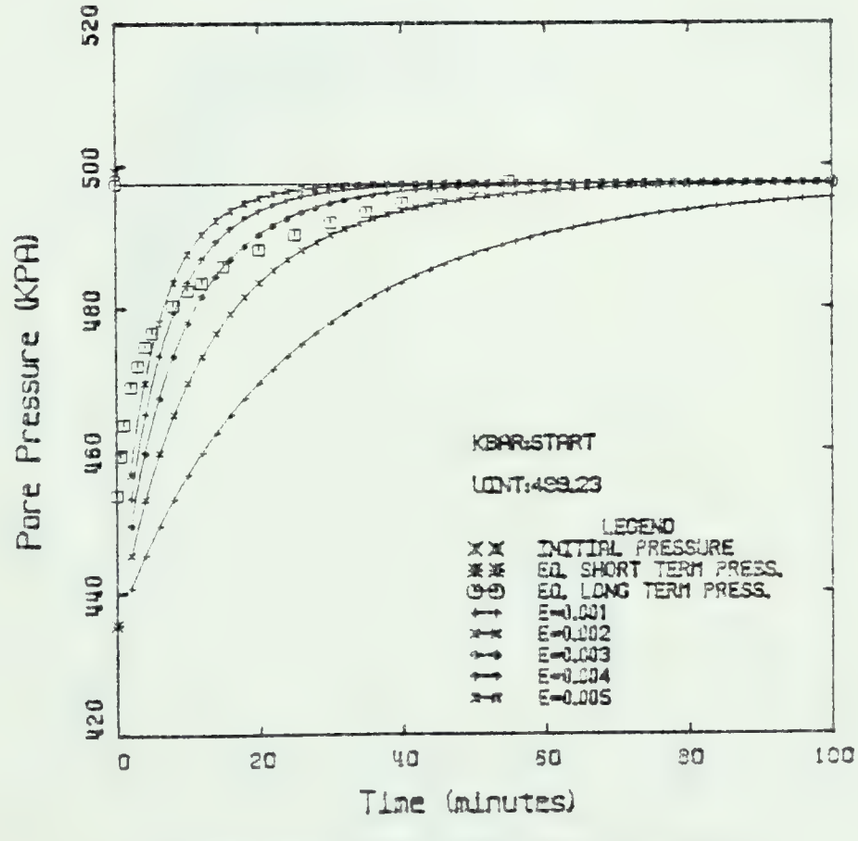


UNDRAINED ANALYSIS, TEST NO. 22B

Figures G.32 and G.33

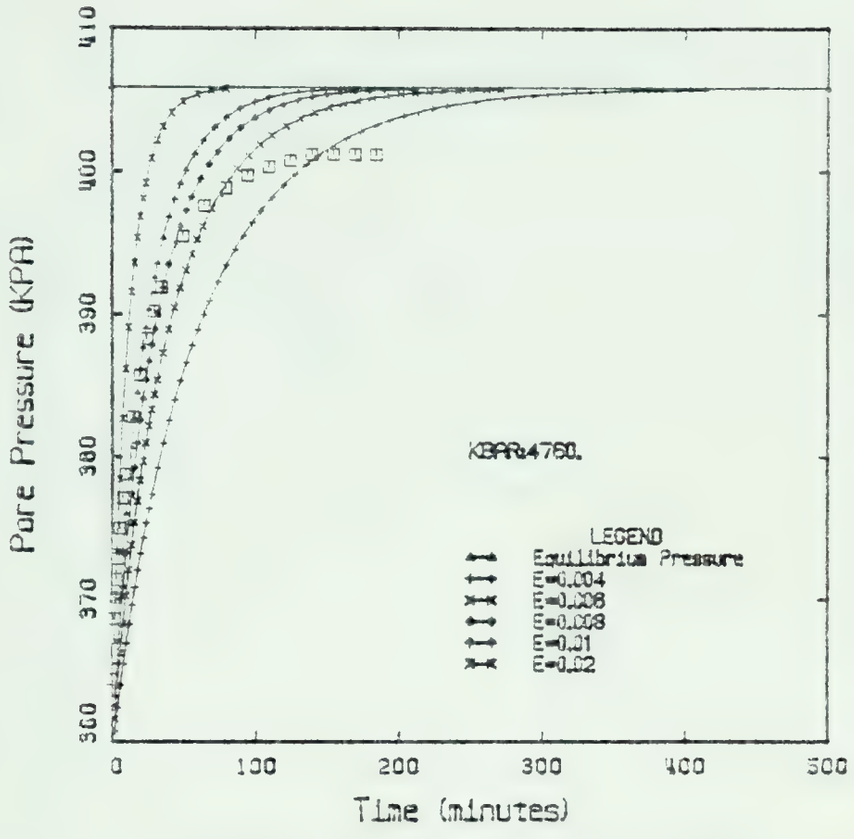


UNDRAINED ANALYSIS, TEST NO. 22C

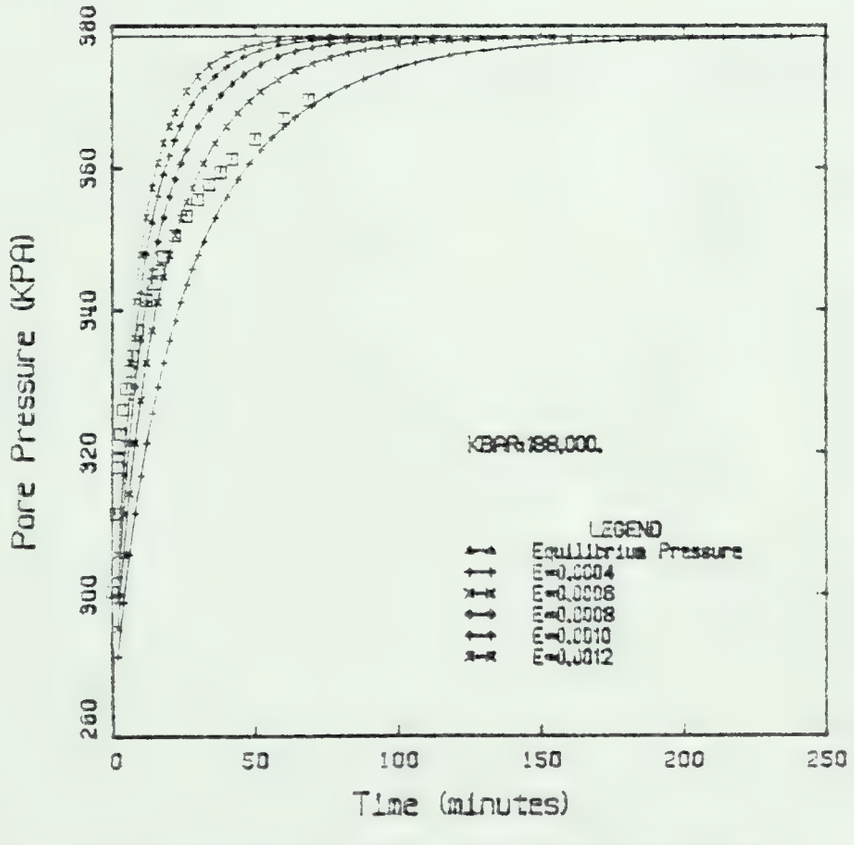


UNDRAINED ANALYSIS, TEST NO. 22D

Figures G.34 and G.35

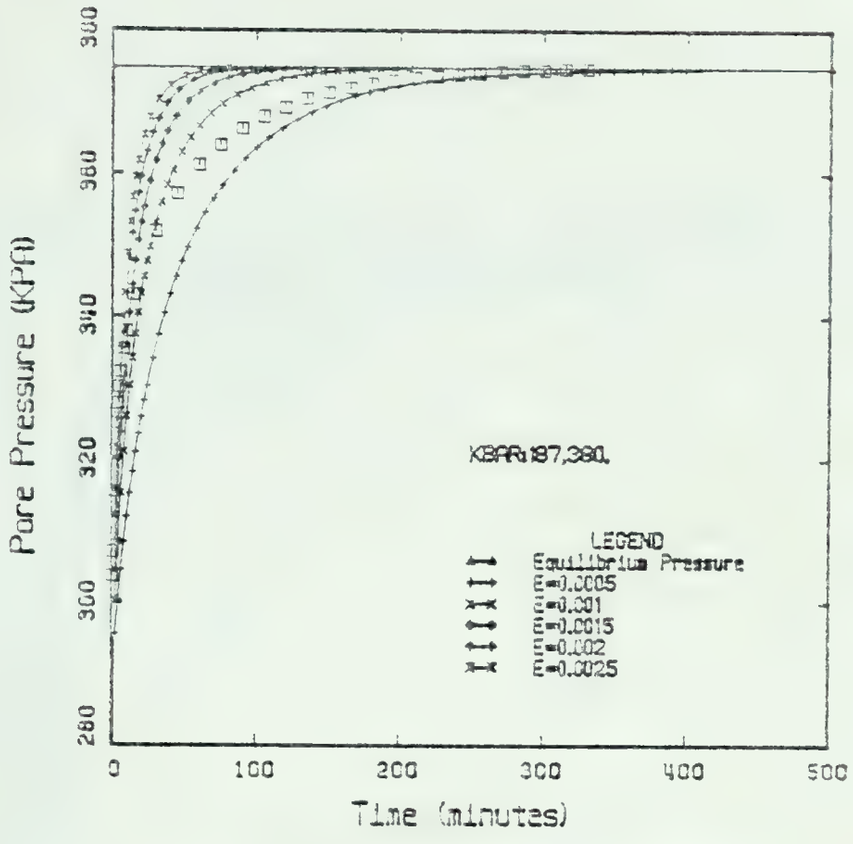


UNDRAINED ANALYSIS, TEST NO. 23B

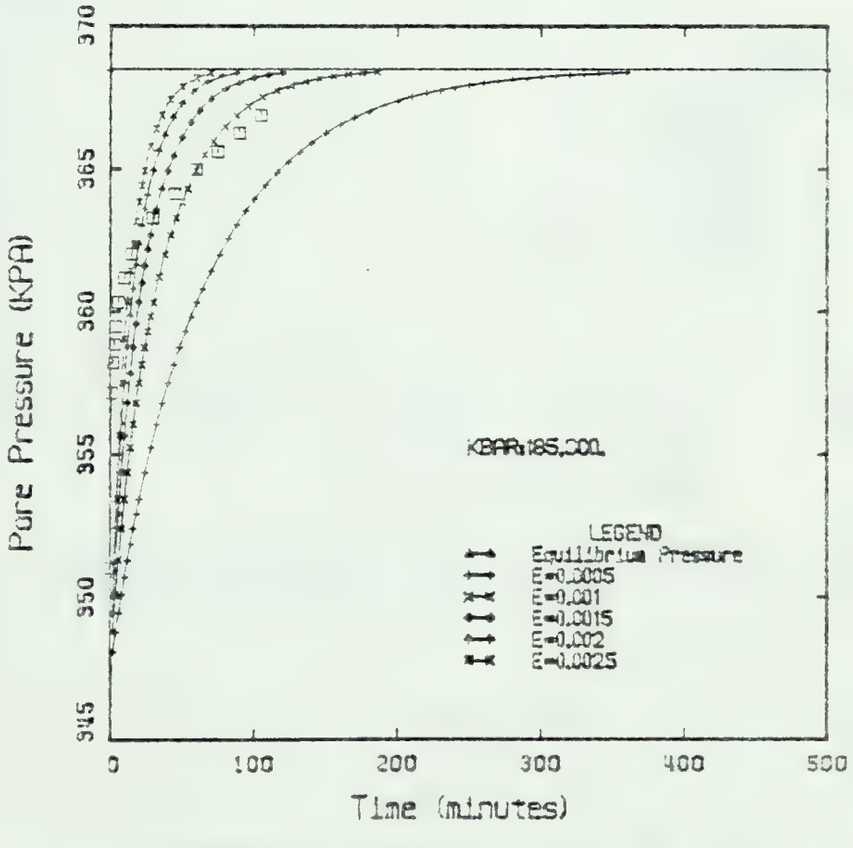


UNDRAINED ANALYSIS, TEST NO. 23C

Figures G.36 and G.37



UNDRAINED ANALYSIS, TEST NO. 23D



UNDRAINED ANALYSIS, TEST NO. 23E

Figures G.38 and G.39

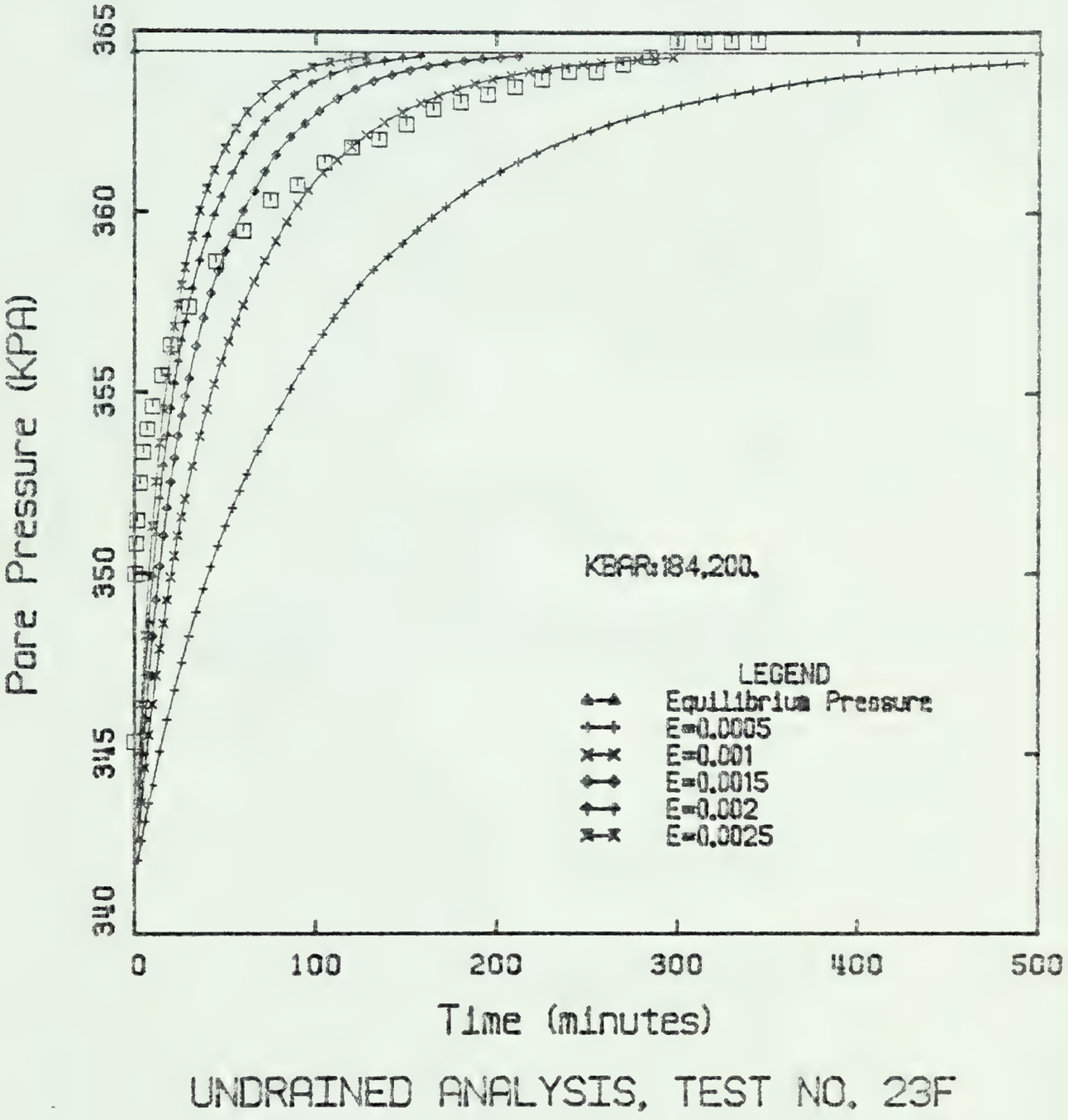

Pore Pressure (KPA)
340
345
350
355
360
365
0
100
200
300
400
500
Time (minutes)
KBAR:184.200.
LEGEND
Equilibrium Pressure
E=0.0005
E=0.001
E=0.0015
E=0.002
E=0.0025
UNDRAINED ANALYSIS, TEST NO. 23F

Figure G.40

APPENDIX H

COMPUTER PROGRAM FOR

CONSOLIDATION/GAS EXSOLUTION MODEL

```
      C FINITE DIFFERENCE PROGRAM FOR CONSOLIDATION/GAS EXSOLUTION
      C PROBLEMS.  THIS PROGRAM CONSIDERS THE ONE-DIMENSIONAL PROBLEM
      C OF FLOW TO A BOREHOLE OR SHAFT IN WHICH THERE EXISTS A
      C HYDROSTATIC GRADIENT (RADIAL FLOW).
      C ALLOWANCE IS MADE FOR FREE GAS EXPANSION AND ALSO FOR THE
      C SORPTION OF DISSOLVED GAS.
      C THE GAS BUBBLES ARE ASSUMED TO BE IMMOBILE BUT TO CONTRIBUTE
      C TO THE COMPRESSIBILITY OF THE PORE FLUIDS.
      C THE PARTIAL DIFFERENTIAL EQUATION GOVERNING THE PHYSICAL PROCESS
      C IS DEVELOPED IN A THESES BY J. SOBKOWICZ, U. OF ALBERTA, 1982.
      C IT IS QUASILINEAR AND OF SECOND ORDER.
      C FINITE DIFFERENCE APPROXIMATION IS DISCUSSED IN:
      C "NUMERICAL METHODS FOR PARTIAL DIFFERENTIAL EQNS." BY
      C W.F.AMES (1969, PP. 82-85)
      C THIS PROCEDURE IS IMPLICIT AND THE RESULTING LINEAR SYSTEM
      C OF EQUATIONS PRODUCES A SYMMETRIC TRIDIAGONAL MATRIX WHICH IS
      C SOLVED USING THE THOMAS ALGORITHM.
      C INITIAL STRESS DISTRIBUTION IS GIVEN ON THE BASIS OF PLANE-
      C STRAIN UNLOADING OF A TUNNEL IN AN INITIALLY ISOTROPIC STRESS
      C FIELD TO A KNOWN INTERNAL TOTAL PRESSURE, MODELLING THE SOIL
      C AS ELASTIC, PERFECTLY PLASTIC, WITH A NON-ASSOCIATED FLOW RULE,
      C AND ALLOWING SOME DILATION IN THE PLASTIC ZONE.
      C THE ELASTIC, PERFECTLY PLASTIC MODEL ONLY APPLIES TO THE INITIAL
      C UNDRAINED RESPONSE, I.E. TO THE INITIAL DISTRIBUTION OF STRESSES.
      C THE CONSOLIDATION/GAS EXSOLUTION PROCESS BY NECESSITY INCORPORATES
      C AN ELASTIC MODEL FOR SOIL BEHAVIOUR.
      C CODED IN APRIL 1982 BY J. SOBKOWICZ.
      C ALL RIGHTS RETAINED BY THE AUTHOR.
      C
      C
      C
            DIMENSION TITLE(20),R(200),U(200),EV(200),SW(200),UEX(200)
            DIMENSION B3(200),IS(200),D3(200),F3(200),B4(200),D4(200)
            DIMENSION F4(200),TOTGAS(200),UGAS(200),DU(200)
            DIMENSION A9(800)
            REAL MAX,MIN,HBAR(200)
            COMMON MAX,MIN,PLOTSZ
            COMMON/ONE/DELX,DELT,F3,D3,B3,UOJ1,UOJN,RMIN
      C
      C STATEMENT FUNCTION FOR THE VOLUMETRIC STRAIN IN THE
      C PLASTIC ZONE AROUND A TUNNEL
      C
            DELV1(A,B,C,D,E,H,Z)=(1+A)/B*((1-2*A)*((E+1)*C*
           1(Z/H)**(E-1)-2*D))
44.5        DELV2(A,B,C,D,E,F,H,Z)=(1+A)/B*
44.7       1((1-F)*(E-1)*(E+1)*(1-A)/(E+F)*
           2(Z/H)**(E-1)*((H/Z)**(E+F)*(2*D/(E+1))**
           3((E+F)/(E-1))*C**((F+1)/(1-E))-C))
            PLOTSZ=5.
            PAT=101.33
      C
      C READ IN INITIAL DATA
      C
            READ(5,2) NPTS,RMIN,RMAX,TMAX,DELT,TOL
            READ(5,2) NPLOTS
          2 FORMAT(I10,5F10.0)
            IF(NPTS.LE.200)GOTO 3
            WRITE(6,4)
          4 FORMAT('1PROGRAM ONLY DIMENSIONED FOR 200 POINTS.')
            STOP
```

```
 59          3 NSTEPS=TMAX/DELT
 60            DELX=(RMAX-RMIN)/(NPTS-1)
 61            DO 7 I=1,NPTS
 62            R(I)=(I-1)*DELX+RMIN
 63          7 CONTINUE
 64            READ(5,8)COMPW,EYOUNG,EMU,PHI,ALPH
 65            PHI=PHI/360.*2*3.14159
 66            PM=(1+SIN(PHI))/(1-SIN(PHI))
 67          8 FORMAT(10F10.0)
 68            READ(5,8)PERM,VOID,SAT
 69            READ(5,8)EGAS,HENRY
 70            READ(5,2)ISAT,SIGTOT,UINT,PTUN,UGASAT,UINTUN
 71            POROS=VOID/(1+VOID)
 72      C
 73      C SET INITIAL VALUES FOR LATER PLOTS
 74      C
 75            CALL GPEP5(1,2,3)
 76            CALL GPEP8(0.25,0.3)
 77            MIN=RMIN
 78            MAX=RMAX
 79            CALL GRAPH(XA,XB,.1,1)
 80            MAX=UINT
 81            MIN=UINTUN
 82            CALL GRAPH(YA,YB,1.,1)
 83      C
 84      C CALCULATE INTERNAL PRESSURE AT ONSET OF FAILURE
 85      C AND ESTIMATE ACTUAL INTERNAL PRESSURE
 86      C
86.1           HENRY1=HENRY
86.2           GOTO 41
86.3         40 HENRY1=0.0
 87          41 P1=SIGTOT-UINT
 88             DI=2*P1/(PM+1)
 89             DF=PTUN-UINT
 90             DINC=1.
 91             IPDIR=0
 92             IF(DF.LT.DI)GOTO 37
 93             WRITE(6,38)
 94          38 FORMAT('OPTUN IS TOO HIGH : GROUND AROUND TUNNEL',
 95            1' STILL IN ELASTIC RANGE.')
 96             IPLP1=1
 97             GOTO 100
 98      C
 99      C CALCULATE MINIMUM EFFECTIVE INTERNAL PRESSURE
100      C TO MAINTAIN SIGMAZ=SIGMA2
101      C
102          37 DF=(DF+DI)/2.
103             IF(DF.LE.0.0)GOTO 37
104             PMIN=P1*(1-2*EMU)/(PM-EMU*(PM+1))
105      C
106      C ESTIMATE SIZE OF PLASTIC ZONE
107      C
108          10 RPLAS=RMIN*(2*P1/(DF*(PM+1)))**(1/(PM-1))
109      C
110      C SOLVE FOR VOLUMETRIC STRAIN AT BOREHOLE WALL
111      C THEN FOR PORE PRESSURE CHANGE, THEN CHECK THAT
112      C PEFFICTIVE + POREPRESS = PTOTAL AT WALL.
113      C IF NOT, ITERATE ON SOLUTION FOR RADIUS OF PLASTIC ZONE.
114      C
114.5          DELVT1=DELV1(EMU,EYOUNG,DF,P1,PM,RMIN,RMIN)
```

```
115            DELVT2=DELV2(EMU,EYOUNG,DF,P1,PM,ALPH,RMIN,RMIN)
115.5          DELVTR=-(DELVT1+DELVT2)
116            A=POROS*SAT*COMPW
117            B=DELVTR+POROS*(SAT*(COMPW*(UINT+PAT)-1+HENRY1)+1)
118            C=DELVTR*(UINT+PAT)
119            DELU=(-B+SQRT(B*B-4*A*C))/(2*A)
120            IF(ABS(DELU).LT.UINT)GOTO 90
121            DF=(DF+DI)/2.
122            GOTO 10
123         90 UFIN=UINT+DELU
124            PTOT=DF+UFIN
125            CHECK=ABS(1.-PTOT/PTUN)
126            IF(CHECK.LE.TOL)GOTO 9
127            IF(IPDIR.NE.0)GOTO 91
128            IF(PTOT.GT.PTUN)GOTO 92
129            DF=DF+DINC
130            IPDIR=1
131            GOTO 10
132         92 DF=DF-DINC
133            IPDIR=-1
134            GOTO 10
135         91 IF(PTOT.GT.PTUN)GOTO 93
136            IF(IPDIR.EQ.1)GOTO 94
137            DINC=DINC/10.
138            IPDIR=1
139         94 DF=DF+DINC
140            GOTO 10
141         93 IF(IPDIR.EQ.-1)GOTO 95
142            DINC=DINC/10.
143            IPDIR=-1
144         95 DF=DF-DINC
145            GOTO 10
146      C
147      C CHECK TO SEE THAT SIGMAZ IS STILL SIGMA2
148      C
149             9 IF(DF.GE.PMIN)GOTO 15
150               WRITE(6,13)
151            13 FORMAT('1***WARNING*** WITH CHOSEN VALUE OF PTUN,',
152              1' DF IS SO SMALL THAT SIGMAZ IS NO LONGER SIGMA2.')
153      C
154      C CALCULATE VOLUMETRIC STRAINS AND PP CHANGE THROUGHOUT
155      C PLASTIC ZONE AT F.D. NODES. CALCULATE NEW VALUES OF
156      C VOID RATIO AND SATURATION AS WELL.
157      C
157.5          15 IF(HENRY1.NE.0.0)GOTO 40
158               IPLAS=IFIX((RPLAS-RMIN)/DELX)+1
159               JCS=NPTS/2
160               IF(IPLAS.LT.JCS)GOTO 17
161               JCS=0.8*NPTS
162               IF(IPLAS.LT.JCS)GOTO 12
163               WRITE(6,19)
164            19 FORMAT('0***ERROR*** PLASTIC ZONE GREATER THAN',
165              1' 80% OF F.D. MESH SIZE. STOP.')
166               STOP
167            12 WRITE(6,18)
168            18 FORMAT('0***WARNING***PLASTIC ZONE GREATER THAN',
169              1'HALF THE F.D. MESH SIZE')
170            17 DO 11 I=1,IPLAS
170.5             DELVT1=DELV1(EMU,EYOUNG,DF,P1,PM,RMIN,R(I))
171               DELVT2=DELV2(EMU,EYOUNG,DF,P1,PM,ALPH,RMIN,R(I))
```

```
171.5          DELVT=-(DELVT1+DELVT2)
172            EV(I)=VOID*(1+DELVT)+DELVT
173            SW(I)=SAT*POROS/(POROS+DELVT)
174            B=DELVT+POROS*(SAT*(COMPW*(UINT+PAT)-1)+1)
175            C=DELVT*(UINT+PAT)
176            DELU=(-B+SQRT(B*B-4*A*C))/(2*A)
177            U(I)=UINT+DELU
178         11 CONTINUE
179            IPLP1=IPLAS+1
180        100 DO 16 I=IPLP1,NPTS
181            EV(I)=VOID
182            SW(I)=SAT
183            U(I)=UINT
184         16 CONTINUE
185            U(1)=UINTUN
186            QMIN=MIN
187            DO 200 I=1,NPTS
188            IF(U(I).LT.QMIN)QMIN=U(I)
189        200 CONTINUE
190            IF (QMIN.GE.MIN)GOTO 201
191            MIN=QMIN
192            CALL GRAPH(YA,YB,1.,1)
193        201 CALL PLOTIT(R,U,NPTS,1,1,1,4,XA,XB,PLOTSZ,YA,YB,PLOTSZ,7)
194      C
195      C CALCULATE FINITE DIFFERENCE 'CONSTANTS' FOR T=0 ROW
196      C
197            UOJ1=UINTUN+PAT
198            UOJN=UINT+PAT
199            ICS=NPTS-1
200      C
201      C PLANE STRAIN AV
202      C
203            AV=(1+VOID)*2.*(1.-2.*EMU)*(1.+EMU)/EYOUNG
204            DO 20 I=2,ICS
205            A3=9.807/PERM/(1+EV(I))
206            D4(I)=EV(I)*(1-SW(I))
207            D3(I)=A3*D4(I)
208            F4(I)=SW(I)*(EV(I)*COMPW+AV)
209            F3(I)=A3*F4(I)
210            IF(ISAT.EQ.1)GOTO 21
211            IS(I)=0
212            TOTGAS(I)=(SAT*(HENRY-1)+1)*VOID*(UINT+PAT)/(U(I)+PAT)
213            VDIFF=TOTGAS(I)/EV(I)-(SW(I)*(HENRY-1)+1)
214            GOTO 22
215         21 IF(U(I).LE.UGASAT)GOTO 23
216            VDIFF=0.
217            IS(I)=1
218            GOTO 22
219         23 IS(I)=0
220            TOTGAS(I)=HENRY*VOID*(UGASAT+PAT)/(U(I)+PAT)
221            VDIFF=HENRY*((UGASAT+PAT)/(U(I)+PAT)-1.)
222         22 B4(I)=VDIFF*EGAS*EV(I)
223            HBAR(I)=VDIFF/SW(I)+HENRY
224            B3(I)=B4(I)*A3
225         20 CONTINUE
226      C
227      C ESTABLISH PP FOR T=1 ROW
228      C
229            NM2=NPTS-2
230            CALL THOM(U(2),UEX(2),NM2,DU(2),A9(1),A9(201),A9(401),A9(601))
```

```
231           DO 50 I=2,ICS
232          50 U(I)=UEX(I)-PAT
233           CALL PLOTIT(R,U,NPTS,2,1,1,4,XA,XB,PLOTSZ,YA,YB,PLOTSZ,7)
234           NPLOT=NSTEPS/NPLOTS
235           NPP=3
236           NINC=NPLOT
237      C
238      C ITERATE SOLUTION FOR EACH TIME STEP
239      C
240           IDRAIN=1
241           DO 33 I=2,ICS
242           UGAS(I)=UGASAT
243          33 CONTINUE
244           DO 24 J=2,NSTEPS
245      C
246      C CALCULATE VOID RATIO,SATURATION AND TOTAL GAS VOLUME
247      C AT BEGINNING OF EACH TIME STEP
248      C
249           DO 25 I=2,ICS
250           DMULT=1.
251           DVW=DU(I)*(D4(I)/(U(I)+PAT)+F4(I))-B4(I)*DELT
252           EOLD=EV(I)
253           EV(I)=EV(I)+AV*DU(I)
254           SW(I)=(SW(I)*EOLD+DVW)/EV(I)
255           IF(SAT.EQ.1.0.AND.EGAS.EQ.0.0.AND.HENRY.EQ.0.0)SW(I)=SAT
256           IF(IS(I).EQ.1)GOTO 26
257      C
258      C NEXT 12 STATEMENTS ALLOW FOR LOSS OF GAS IF SG<.85
259      C
260           IF(SAT.EQ.1.0.AND.EGAS.EQ.0.0.AND.HENRY.EQ.0.0)GOTO 110
261          32 IF(I.GT.IDRAIN)GOTO 30
262         110 VDIFF=0.
263           DMULT=0.
264           GOTO 27
265          30 IF(I.GT.IDRAIN+1)GOTO 31
266           IF(SW(I).GE.0.85)GOTO 31
267           IDRAIN=I
268           VDIFF=0.
269           DMULT=0.
270           WRITE(6,35) J,I
271          35 FORMAT('0IDRAIN NOW AT POINT',I5,', AT STEP NO.',I5)
272           GOTO 27
273          31 PNEW=U(I)+PAT
274           POLD=PNEW-DU(I)
275           RATIO=POLD/PNEW
276           TOTGAS(I)=RATIO*(TOTGAS(I)+HBAR(I)*DVW)
277           VDIFF=TOTGAS(I)/EV(I)-(SW(I)*(HENRY-1)+1)
278           GOTO 27
279          26 IF(U(I).LE.UGAS(I))GOTO 28
280          81 VDIFF=0.
281           GOTO 27
282          28 IS(I)=0
283           TOTGAS(I)=HENRY*EV(I)*(UGAS(I)+PAT)/(U(I)+PAT)
284           VDIFF=HENRY*((UGAS(I)+PAT)/(U(I)+PAT)-1.)
285      C
286      C CALCULATE F.D. CONSTANTS FOR STEP
287      C
288          27 A3=9.807/PERM/(1.+EV(I))
289           D4(I)=EV(I)*(1-SW(I))*DMULT
290           D3(I)=A3*D4(I)
```

```
291           F4(I)=SW(I)*(EV(I)*COMPW+AV)
292           F3(I)=A3*F4(I)
293           B4(I)=VDIFF*EGAS*EV(I)
294           B3(I)=B4(I)*A3
295           HBAR(I)=VDIFF/SW(I)+HENRY
296        25 CONTINUE
297     C
298     C PLOT VALUES AT BEGINNING OF STEP IF DESIRED
299     C
300           IF(J.EQ.NSTEPS)GOTO 36
301           IF(J.LT.NPLOT)GOTO 29
302        36 NPLOT=NPLOT+NINC
303           CALL PLOTIT(R,U,NPTS,NPP,1,1,4,XA,XB,PLOTSZ,YA,YB,PLOTSZ,7)
304           NPP=NPP+1
305     C
306     C CALCULATE PP FOR END OF TIME STEP
307     C
308        29 CALL THOM(U(2),UEX(2),NM2,DU(2),A9(1),A9(201),A9(401),A9(601))
309           DO 51 I=2,ICS
310           U(I)=UEX(I)-PAT
311           IF(U(I).GT.UINT)U(I)=UINT
312        51 CONTINUE
313        24 CONTINUE
314           CALL PLOTIT(R,U,NPTS,0.,1,1,5,XA,XB,PLOTSZ,YA,YB,PLOTSZ,7)
315           STOP
316           END
317           SUBROUTINE THOM(U1,U2,N,DU,A,B,C,D)
318     C
319     C SUBROUTINE CODING THOMAS' ALGORITHM FOR SOLVING
320     C TRIDIAGONAL MATRICES
321     C
322           DIMENSION U1(N),U2(N),DU(N),A(N),B(N),C(N),D(N)
323           DIMENSION F(200),D3(200),B3(200)
324           REAL K
325           COMMON/ONE/H,K,F,D3,B3,X,Y,RO
326           PAT=101.33
327           DO 1 I=1,N
328           A(I)=(2.*I-1)/2.+RO/H
329           C(I)=(2.*I+1)/2.+RO/H
330           B(I)=-(I+RO/H)*(2.+H*H/K*(F(I+1)+D3(I+1)/(U1(I)+PAT)))
331           D(I)=-H*H*(I+RO/H)*(F(I+1)/K*(U1(I)+PAT)+B3(I+1)+D3(I+1)/K)
332         1 CONTINUE
333           D(1)=D(1)-A(1)*X
334           D(N)=D(N)-C(N)*Y
335           IF(ABS(B(1)).GT.0.0001)GOTO 2
336           WRITE(6,6)
337         2 C(1)=C(1)/B(1)
338           D(1)=D(1)/B(1)
339           DO 3 I=2,N
340           DENOM=B(I)-A(I)*C(I-1)
341           IF(ABS(DENOM).GT.0.0001)GOTO 4
342           WRITE(6,6)
343         4 C(I)=C(I)/DENOM
344           D(I)=(D(I)-A(I)*D(I-1))/DENOM
345         3 CONTINUE
346           U2(N)=D(N)
347           NNN=N-1
348           DO 5 L=1,NNN
349           I=N-L
350           U2(I)=D(I)-C(I)*U2(I+1)
```

```
    5 CONTINUE
      DO 7 I=1,N
      DU(I)=U2(I)-U1(I)-101.33
    7 CONTINUE
    6 FORMAT('0***WARNING*** THOMAS ALGORITHM : DENOMINATOR',
     1' IS LESS THAN 0.0001')
      RETURN
      END
      SUBROUTINE GRAPH(ZERO,SCALE,SINT,IDIR)
      REAL MAX,MIN,FAC(16)
      COMMON MAX,MIN,PLOTSZ
      DIFF=MAX-MIN
      SCALE=DIFF/PLOTSZ
      Q=1.
      FAC(1)=1.
      DO 2 I=2,12,5
      FAC(I)=Q*2.
      FAC(I+1)=Q*3.
      FAC(I+2)=Q*4.
      FAC(I+3)=Q*5.
      FAC(I+4)=Q*10.
      Q=Q*10.
    2 CONTINUE
      DO 1 I=1,16
      TEST=FAC(I)*SINT
      IF(SCALE.GT.TEST)GOTO 1
      SCALE=TEST
      GOTO 5
    1 CONTINUE
      ENTRY GRAPH2(ZERO,SCALE,SINT,IDIR,I)
      SCALE=ABS(SCALE)
    5 ICHECK=0
      IF(IDIR.GT.0)GOTO 3
      TZERO=MAX
      IF(TZERO.GT.0.)TZERO=TZERO+SCALE
      GOTO 4
    3 TZERO=MIN
      IF(TZERO.LT.0.)TZERO=TZERO-SCALE
    4 M=IFIX(TZERO/SCALE)
      ZERO=FLOAT(M)*SCALE
   11 IF(IDIR.GT.0)GOTO 6
      SIMUL=ZERO-PLOTSZ*SCALE
      IF(SIMUL.LE.MIN)GOTO 7
   10 IF(ICHECK.EQ.1)GOTO 8
      M=IFIX(2.*TZERO/SCALE)
      ZERO=FLOAT(M)*SCALE/2.
      ICHECK=1
      GOTO 11
    8 IF(I.LT.16)GOTO 9
       SCALE=SCALE*10.
       GOTO 5
    9 SCALE=FAC(I+1)*SINT
      GOTO 5
    6 SIMUL=ZERO+PLOTSZ*SCALE
      IF(SIMUL.GE.MAX)GOTO 7
      GOTO 10
    7 IF(IDIR.LT.0)SCALE=-SCALE
      RETURN
      END
End of file
```

B30360